

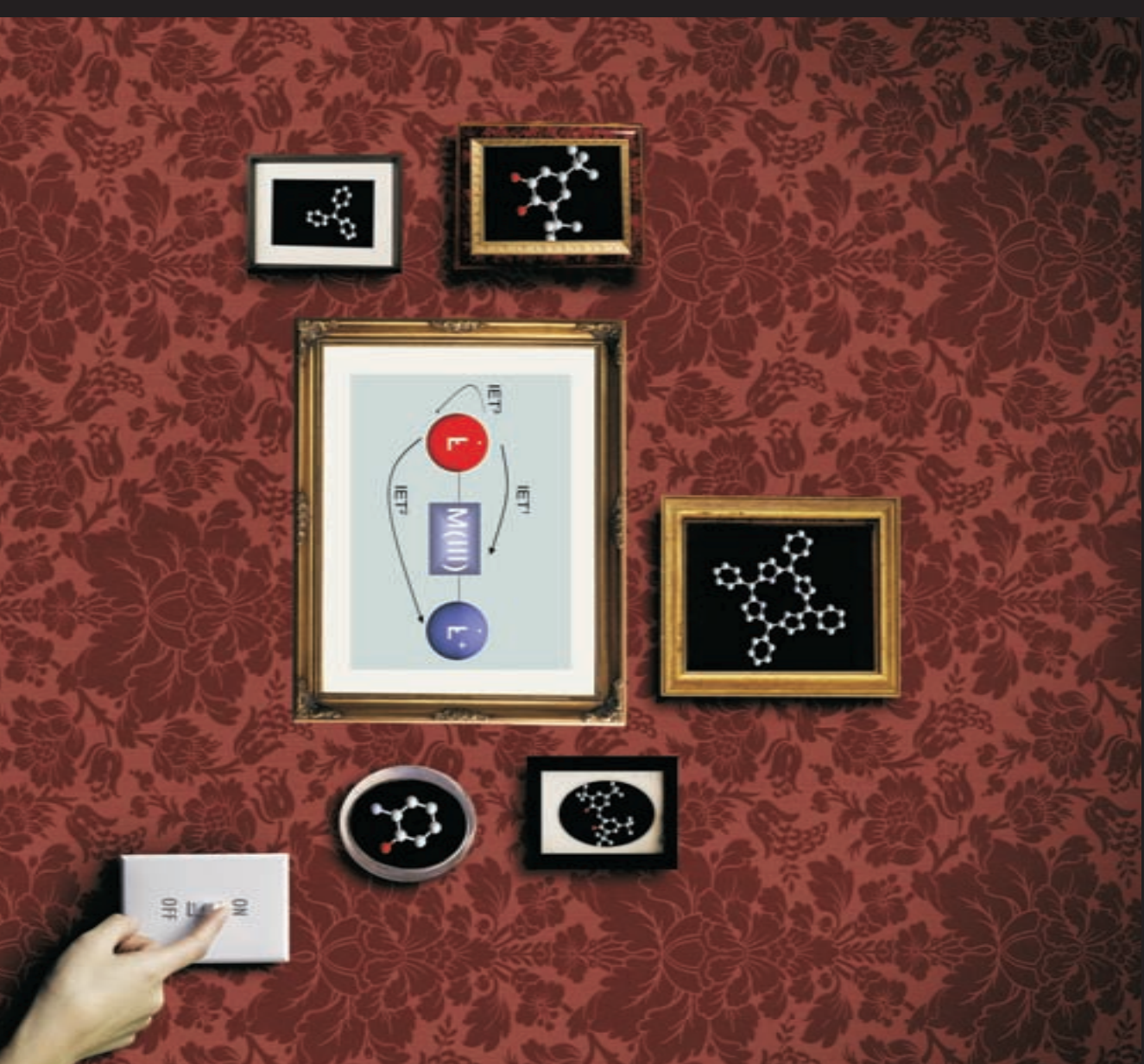


Emi Evangelio Castells

IET
Intramolecular Electron Transfer
**In Phenoxyate and Catecholate
Based Molecular Systems**

Emi Evangelio Castells
Institut de Ciència dels Materials de Barcelona
Centre d'Investigació en Nanociència i Nanotecnologia
Juliol 2008

Intramolecular Electron Transfer
In Phenoxyate and Catecholate Based Molecular Systems



Daniel Ruiz-Molina, com a Investigador del Consell Superior d'Investigacions Científiques del Centre d'Investigació en Nanociència i Nanotecnologia (CIN2)

CERTIFICA

Que Emi Evangelio Castells, llicenciada en Ciències Químiques, ha dut a terme sota la seva direcció el treball que porta per títol "Intramolecular Electron Transfer in Phenoxyate and Catecholate based Molecular Systems", i que queda recollit en aquesta memòria per optar al Grau de Doctor en Ciència dels Materials.

I perquè així consti, signa el present certificat.

Dr. Daniel Ruiz-Molina

Bellaterra, 1 de Juny del 2008

CON LAS FUERZAS PRIMERAS

....
La vida es terrible, atroz en su belleza,
pero yo la acepto -los dientes apretados,
los puños apretados y mis ojos
de tan claros quiero que parezcan feroces.
La inocencia es espanto. La desnudez florece
con una violencia demasiado alegre.
Pero yo quiero esto. Callad, callad vosotros,
blancos profesores de melancolías.
Sois demasiado sabios
para un mundo que es joven, que sigue siendo joven
en el amor, en las olas, en el viento,
en su alegre rebeldía sin sentido.
Mil dolores pequeños a veces me anonadan.
La noche me recoge fatigado y me abraza;
pero vuelvo, y aún vuelvo, y vuelvo todavía
violento y desnudo, joven con el día.
La vida me alimenta; yo quemo la alegría.
La luz es resplandor de espadas que combaten
y creo en la ráfaga, en los gritos
que aún no han muerto en pensamientos.
No importan mis angustias, no voy a confesarlas.
Basta para vencerlas la inocencia dorada
de las fuerzas primeras que crean y destruyen.

...

Gabriel Celaya
Cuadernos de poesía "Norte"

...i arriba el gran moment, el moment d'agrair l'esforç de totes aquelles persones que directa o indirectament han fet possible la realització d'aquesta Tesi Doctoral. En primer lloc vull expressar el meu agraïment al meu director de Tesi, el Dr. Daniel Ruiz-Molina, per motivar-me, il·lusionar-me i obrir-me noves fronteres en la recerca interdisciplinària de la Ciència dels Materials. Per altre banda donar-li les gràcies també per escoltar-me, entendre'm i fer-me entendre què vol dir ser un científic en tota la amplitud de la paraula. El seu esforç i dedicació, sobretot aquests darrers anys han establert un respecte no sols en el terreny laboral, sinó en l'àmbit personal del qual me'n sento molt orgullosa.

De la mateixa manera, agraeixo al grup dels Professors Jaume Veciana i Concepció Rovira, per haver-me permès entrar en el seu grup. La seva experiència en tots aquests anys m'ha fet possible viatjar i conèixer altres maneres de treballar en ciència a través de col·laboracions, així com la possibilitat d'anar a diversos congressos.

En l'apartat de col·laboracions m'agradaria agrair en primer lloc l'hospitalitat rebuda per part del Dr. José Ángel Martín Gago, així com a la resta de gent del seu grup de recerca al Instituto de Ciencia de Materiales de Madrid. Vaig aprendre moltíssimes coses d'STM i AFM entre d'altres. Especialment, al Gonzalo Otero, qui no sols em va aconsellar i explicar la física involucrada en els experiments que vàrem fer, si no que va ser el meu guia a Madrid. Al Professor Andrea Dei, de la Università di Firenze per les mesures d'EPR realitzades sobre alguns dels compostos presentats en aquesta Tesi, així com per les productives discussions científiques al voltant del tautomerisme de valència. A la Clara Rodríguez i al Dr. Javier Campo per les mesures magnètiques de bona part dels compostos presentats, de les quals em consta que algunes han estat un bon mal de cap. Al Dr. Klaus Wurst de la Universitat d'Innsbruck, per la resolució de la majoria d'estructures cristal·lines que apareixen en aquest treball. Al Dr. Motohiro Nakano, de Osaka University per l'ajuda en el desenvolupament de la Metodologia d'Evans. A la Marie Laure Bonet i al Dr. Vincent Robert pels càlculs teòrics en els sistemes de valència mixta. Al Dr. Jordi Hernando, per l'ajuda en la realització e interpretació de les mesures de fluorescència així com pels càlculs DFT realitzats en dos dels lligands presentats en aquest treball. M'agradaria destacar les discussions realitzades, tant amb el Dr. Vincent Robert com amb el Dr. Jordi Hernando, de les quals he après i refrescat moltíssima física-química, imprescindible en aquest treball. Al Dr. Jean-Pascal Sutter i a tot el grup del Laboratoire de Chimie de la Coordination a Toulouse, voldria agrair la hospitalitat rebuda durant els tres mesos que vaig estar al seu laboratori. Especialment a la Julie Milon, per l'ajuda i el bon humor prestats en tot moment. L'estància a Toulouse em va permetre establir el contacte amb una química nova, i fer mesures espectroscòpiques a baixes temperatures que han estat molt importants al llarg del desenvolupament d'aquest treball. Molt especialment al Jean-François Meunier i al Dr. Yannick Coppel per les mesures espectroscòpiques. Al Dr. Miquel Cabañas, de la Universitat Autònoma, per la dedicació i realització de tots els espectres d'RMN realitzats a molts dels compostos presentats, sense els quals aquesta Tesi no hauria estat possible. A la Gisela Bardají, al Javier Saiz i al Dr. Félix Busqué, de la Universitat Autònoma de Barcelona, per tota la síntesi orgànica dels lligands. De l'Institut de Ciència de Materials de Barcelona, A la Dra. Vega Lloveras i al Dr. José Vidal, per les mesures d'EPR realitzades als darrers compostos sintetitzats. Aquesta recerca ha resultat una de les més engrescadores, segurament perquè encara estem als inicis d'entendre el comportament d'aquests complexos. Al Francisco Javier Campos per la difracció de Raigs-X en pols. Finalment a l'Amable Bernabé i al José Manuel Pérez per les mesures espectroscòpiques i magnètiques dels compostos que es presenten en aquesta Tesi, així com pel somriure que sempre dedicaven a qualsevol de les idees que podien sorgir durant la recerca. Al Dr. Inhar Imaz i al Dr. Daniel MasPOCH del Centre d'Investigació en Nanociència i Nanotecnologia, per la resolució d'algunes de les estructures cristal·lines que es presentaran més endavant. Al Xavi Giol i a la

Joana Casals pel disseny de la portada d'aquesta Tesi. Finalment al CIN2 i al seu director, al Dr. Jordi Pascual per cedir-me un espai i preocupar-se constantment per l'estat de la Tesi.

Òbviament, després de tants anys, res de tot això no hagués estat possible sense la gent que m'he trobat pel camí, i que ha omplert els espais de somriures, xerrades, cafès, lluites i plors, aguantant-me, impulsant-me endavant i fent-me créixer cada dia. El Fernando, la Chiara, la Mireia, el Pascal, el Luis, l'Ana, l'Oscar i la Carole van fer que la meua estància a Toulouse fos un record importantíssim i una amistat que ha perdurat més enllà de Toulouse. "Ya os podéis ir preparando, que vuelvo...". Després de tres anys a l'Institut de Ciència de Materials, hi quedarà sempre el record de molta gent. Començant per administració, la gent de la Biblioteca, la Palmira i tots aquells que fan que la nostre estància allà sigui una mica més fàcil i l'esforç dels quals tantes vegades es veu poc reconegut. Moltes gràcies també, al grup de Nanociència Molecular i Materials Orgànics del ICMA. L'ajuda constant i els somriures de la gent que el forma han fet que tot plegat fos més fàcil. Especialment al Christian, al Xavi, al Santi i al Daniel amb qui començava els matins dels primers anys. Els cafès han continuat amb la Núria i la Mary, que han estat les meves companyes de fatigues, "nenes, brindo perquè ens haguem trobat!". A la Liber, l'Aitor, la Cecília, la Mónica, el David, i al Roberto, per ser un "rumberos" i estar al meu costat en moments realment difícils, "David, quan gravem el disc?". Al Jordi i al Félix de la UAB, moltes, moltíssimes gràcies per aportar la dosi de "buen rollito" necessària per passar-ho bé de debó i aprendre en tot moment. A l'Aitor, al Gustavo, al Sebastian, al Cornelius, a la Rosa i al Juanjo, entre d'altres, per passar a formar part d'una nova família al CIN2. Finalment, al meu grup "Nanosfun" del CIN2, els quals han estat qui més han patit aquesta tesi (nanos us tocava el moment final). l'Inhar, en Daniel, l'Alberto, l'Elena, el Carles, el Javi, la Irene, el Sergio i la Neus. La veritat és que sols donar les gràcies queda curt, però no es pot fer de cap més manera, així que en certa manera aquesta tesi va dedicada a vosaltres, per estar allà, per escoltar-me i entendre'm i fer-me somriure més d'una i de dues vegades. Voldria fer una menció especial per l'Inhar i en Daniel, els quals m'han prestat una dedicació absoluta aquestes dues setmanes (així com a les seves respectives dones que no deuen saber perquè no arriben a casa a hores raonables). "Nens, brindo un altre cop per haver-vos trobat".

Aquesta tesi també va dedicada a la gent del Poblenou, al Víctor, la Pati, el Ferran, el Marc, l'Anna, els Jordis i l'Estefania, la Eva, la Gemma, el David i la Montse, entre d'altres, gent que amb la seva lluita constant del dia a dia, m'impulsa endavant a ser més crítica amb la societat i a construir un espai millor pels altres. Especialment, a l'Ignasi, el qual m'ha donat un suport constant abans i després de la Tesi. A la Maria i al José Miquel, per estar al meu costat i sense els quals no hagués conegut la meitat de bars de Barcelona on toquen en directe. A la Mariajo per guiar-me en el magnífic món de D-Recerca i Precarios, i pels cafès i les xerrades. Finalment als meus pares, sense els quals res de tot això s'hagués pogut fer. Al seu recolzament constant, a la seva motivació i a la seva estimació dec la persona que sóc. I... nombrar a tothom és una tasca difícil, i segurament impossible, així que a tots moltíssimes gràcies de nou per estar amb mi,

" i la propera aventura serà...;" menys mal que sereu allà per sentir-la.

Abbreviations

MV	Mixed-valence
IET	Intramolecular electron transfer
IVT	Intervalence transition
VT	Valence tautomerism
EA	Electro-active
UV-Vis	Ultraviolet-visible
NMR	Nuclear magnetic resonance
EPR	Electron paramagnetic resonance
Near-IR	Near-infrared
MLCT	Metal-to-ligand charge transfer
PET	Photo induced electron
PTM	Polichlotriphenylmethyl
TPP	Tetraphenylporphyrin
DTBQ	Di- <i>tert</i> -butyl-benzoquinone
DTBSQ/DTBSQ ⁻	Di- <i>tert</i> -butyl-semiquinone / di- <i>tert</i> -butyl-semequinonate
DTBCat/DTBCat ²⁻	Di- <i>tert</i> -butyl-catechol / di- <i>tert</i> -butyl-catecholate
TBA	Tetrabutylammonium hydroxide
Bu ₄ NPF ₆	Tetrabutylammonium hexafluorophosphate
Bpy	2,2'-Bipyridine
Phen	1,10-Phenanthroline
pyz	Pyrazine
Terpy	2,2';6',2''-Terpyridine
Tppz	2,3,5,6-tetrakis(2-pyridyl)pyrazine
HOMO	Highest occupied molecular orbital
LUMO	Lowest occupied molecular orbital
DFT/TD-DFT	Density functional theory / time-dependent functional theory
CASPT2	Complete active space with second order perturbation theory

Index

CHAPTER 1: General Introduction	1
1.1 Intramolecular electron transfer (IET)	3
1.1.1 Mixed-valence systems	4
1.2. Intramolecular electron transfer in mixed-valence complexes bearing “non-innocent” redox-active ligands and a transition metal ion: valence tautomerism	7
1.2.1. Redox-active ligands	7
1.2.1.1 Catecholate complexes	8
1.2.1.2 Phenoxylate complexes	9
1.2.2. Valence tautomerism: IET between a redox-active ligand and a metal ion	11
1.3. Thesis context	15
OBJECTIVES	21
RESULTS AND DISCUSSION	25
CHAPTER 2: Valence tautomerism: Metal Ion and Environmental Effects	27
2.1. Introduction	30
2.1.1. Principal actors: metal and electroactive ligand	30
2.1.1.1 Catecholate complexes.	30
2.1.1.2 Phenoxylate-like complexes	32
2.1.2. Secondary actors	33
2.1.2.1 Counter-ligand effect	34
2.1.2.2 Charge-induced effect	36
2.1.2.3 Environmental effects	38
2.1.3. Summary	39
2.2. Results	39
2.2.1. Metal ion influence: VT on the series of complexes [M(Cat-N-SQ)(cat-N-BQ)]; M = Fe (24), Co (25), Ni (26)	39
2.2.1.1 Variable –temperature UV-visible spectroscopy	40
2.2.1.2 Magnetic measurements in solution: Evans Method	42
2.2.1.3 Solid magnetic measurements	45
2.2.1.4 Discussion	45
2.2.2. Solvent effects on VT: a comparison between the interconversion in solution and solid state	47
2.2.2.1 VT in solution	47
2.2.2.2 VT in solid state	51
2.2.2.3 VT in polymeric matrix	54
2.3. Conclusions	55

CHAPTER 3: Ligand-to-Ligand Intramolecular Electron Transfer	59
3.1. Introduction	62
3.1.1. Pure organic mixed-valence systems	62
3.1.2. IET between organic units mediated through a metal ion	64
3.1.3. Summary	68
3.2. Results	69
3.2.1. Ligand-to-ligand IET in complex [Co(3,5-DTBCat)(3,5-DTBSQ)]; 14	69
3.2.1.1 <i>Electrochemistry</i>	69
3.2.1.2 <i>Magnetism</i>	70
3.2.1.3 <i>Electronic and vibrational spectroscopy</i>	71
3.2.2. Ligand-to-ligand IET in the series of complexes [M(Cat-N-SQ)(Cat-N-BQ)]; M = Fe (24) and Co(25)	73
3.2.2.1 <i>¹H-NMR experiments</i>	74
3.3. Conclusions	78
CHAPTER 4: New Optically-Active Catecholate and Phenoxylate Based Ligands	81
4.1. Introduction	84
4.1.1. Multifunctional VT systems	84
4.1.2. Molecular optical chemosensors	86
4.1.3. Summary	87
4.2. Results	89
4.2.1. Catechol derivatives as fluorescent chemosensors for wide range pH detection	89
4.2.1.1 <i>X-ray structure</i>	89
4.2.1.2 <i>Acid-base equilibriums of ligands 27 and 28</i>	90
4.2.1.3 <i>pH modulated fluorescence</i>	94
4.2.1.4 <i>Fluorescence pH-sensing</i>	96
4.2.1.5 <i>Complexation ability of 28</i>	98
4.2.2. Synthesis, X-Ray structure and reactivity of a sterically protected azo bisphenol ligand (29): on the quest for new multifunctional active ligands	98
4.2.2.1 <i>Synthesis and X-ray structure</i>	99
4.2.2.2 <i>Acid-base equilibrium of 29</i>	99
4.2.2.3 <i>Complexation ability of 29</i>	101
4.2.2.4 <i>Three-states switching array</i>	104
4.2.3. Cobalt complexes based on the azo bisphenol ligand 29	106
4.2.3.1 <i>Synthesis, X-ray structure and molecular geometry</i>	106
4.2.3.2 <i>Magnetic and spectroscopic characterization</i>	109
4.2.3.3 <i>Spectroelectrochemistry</i>	111

4.2.3.6	Synthesis, X-ray structure and physico-chemical characterization of the neutral complex $[\text{Co}(\text{Cat-N=N-Cat})(\text{Cat-N=N-SQ})]$; 74	116
4.3.	Conclusions	121
CHAPTER 5: Experimental Section		125
5.1.	Instruments	127
5.1.1.	Physical measurements	127
5.2.	Synthesis and characterization	130
5.2.1.	General procedure	130
5.2.1.1	Synthesis of $[\text{Co}(3,5\text{-DTBCat})(3,5\text{-DTBSQ})\text{N-N}]$ where N-N = bipyridine (14) or phenanthroline (17)	130
5.2.1.2	Synthesis of $[\text{Co}(\text{Cp})_2][\text{Co}(3,5\text{-DTBCat})_2(\text{bpy})]$; (14 ·CoCp ₂)	130
5.2.1.3	Synthesis of $[\text{Co}(3,5\text{-DTBSQ})_2(\text{bpy})]\cdot\text{Cl}$; (20 ·Cl)	130
5.2.1.4	Synthesis of $M(\text{Cat-N-SQ})(\text{Cat-N-BQ})$ M = Fe (24) or Co (25) and $[M(\text{cat-N-BQ})_2]$ M=Ni (26)	131
5.2.1.5	Synthesis of $[\text{Co}(\text{Cat-N=N-Cat})(\text{H}_2\text{O})_3]\cdot\text{Cl}$; (69)	131
5.2.1.6	Synthesis of $[\text{Co}(\text{Cat-N=N-Cat})(\text{py})(\text{H}_2\text{O})_2]\cdot\text{Cl}$; (70)	132
5.2.1.7	Synthesis of $[\text{Co}(\text{Cat-N=N-Cat})(\text{phen})(\text{H}_2\text{O})]\cdot\text{Cl}$; (71)	132
5.2.1.8	Synthesis of $[\text{Co}(\text{Cat-N=N-Cat})(\text{terpy})]\cdot\text{Cl}$; (72)	132
5.2.1.9	Synthesis of $[\text{Co}(\text{Cat-N=N-Cat})(\text{tppz})]\cdot\text{Cl}$; (73)	132
5.2.1.10	Synthesis of $[\text{Co}(\text{Cat-N=N-Cat})(\text{Cat-N=N-SQ})]$; (74)	133
5.2.1.11	Synthetic approaches for the obtaining of cobalt complexes derived of ligand 28 ·HCl	133
5.3.	Crystallographic data	134
5.3.1.	(E)-2-[(3-bromo-4,5-dihydroxyphenyl)-1-ethenyl]pyridinium chloride; (28 ·HCl)	134
5.3.2.	2,2'-dihydroxy-4,3,4',3'-tetra-tert-butylazobenzene; (29)	135
5.3.3.	$[\text{Co}(\text{Cat-N=N-Cat})(\text{H}_2\text{O})_3]\cdot\text{Cl}$; (69)	136
5.3.4.	$[\text{Co}(\text{Cat-N=N-Cat})(\text{py})(\text{H}_2\text{O})_2]\cdot\text{Cl}$ and $[\text{Co}(\text{Cat-N=N-Cat})(\text{H}_2\text{O})_3]\cdot\text{Cl}$; (70)	137
5.3.5.	$[\text{Co}(\text{Cat-N=N-Cat})(\text{phen})(\text{H}_2\text{O})]\cdot\text{Cl}$; (71)	138
5.3.6.	$[\text{Co}(\text{Cat-N=N-Cat})(\text{terpy})]\cdot\text{Cl}$; (72)	139
5.3.7.	$[\text{Co}(\text{Cat-N=N-Cat})(\text{tppz})]\cdot\text{Cl}$; (73)	140
5.3.8.	$[\text{Co}(\text{Cat-N=N-Cat})(\text{Cat-N=N-SQ})]$; 74	141
5.3.9.	Selected bond lengths and angles for 29 and 69-74	142
Annex I: Self Exchange Intramolecular Electron Transfer		145
I.1.	Mechanisms for the intramolecular electron transfer (IET)	147
I.1.1	Self exchange Intramolecular Electron Transfer (IET)	148

Annex II: ¹H-NMR Spectroscopy	153
II.1. Evan Method	155
II.1.1 Equations development	155
<i>II.1.1.1 Variations of the equation by using the molar mass</i>	156
II.1.2 Sample preparation	157
II.1.3 Experiment realised with complex 25	158
Annex III: Organic Synthesis	163
III.1. Organic synthesis	165
III.1.1 Synthesis of catecholate-based ligands	165
<i>III.1.1.1 Synthesis of 3-Bromo-4,5-dihydroxybenzaldehyde; (76)</i>	166
<i>III.1.1.2 Synthesis of 3-Bromo-4,5-bis(tert-butyl)diphenylsilyloxy)benzaldehyde; (77)</i>	166
<i>III.1.1.3 Synthesis of (E)-3-bromo-5-(2-phenyl-1-ethenyl)-1,2-di(tert-butyl)diphenylsilyloxy)benzene; (78)</i>	167
<i>III.1.1.4 Synthesis of (E)-3-bromo-5-(2-phenyl-1-ethenyl)-1,2-benzenediol; (27)</i>	167
<i>III.1.1.5 Synthesis of (E)-2-[3-bromo-4,5-di(tert-butyl)diphenylsilyloxy)phenyl]-1-ethenyl]pyridine; (79)</i>	168
<i>III.1.1.6 Synthesis of (E)-2-[(3-bromo-4,5-dihydroxyphenyl)-1-ethenyl]pyridinium chloride; (28·HCl)</i>	168
III.1.2 Synthesis of phenoxyate-based ligands	168
<i>III.2.1.1 Synthesis of Synthesis of 2,2'-dihydroxy-4,6,4',6'-tetra-tert-butylazobenzene; (29)</i>	169
Annex IV: Complexes with Valence Tautomerism Phenomena	171
IV.1. Table of complexes presenting VT phenomena induced by temperature	173
IV.2. Table of complexes presenting VT phenomena induced by irradiation	189
IV.3. Table of complexes presenting VT phenomena induced by pressure	192
CHAPTER 6: Articles	193
6.1. Articles Revised by the Doctoral Commission	195
6.1.1 Article I: Valence Tautomerism: New Challenges for Electroactive Ligands	197
6.1.2 Article II: Solvent effects on valence tautomerism: A comparison between the interconversion in solution and solid state.	199
6.1.3 Article III: Intramolecular electron transfer in the mixed-valence [Co(3,5-DTBCat)(3,5-DTBSQ)(bpy)] complex: Beyond Valence tautomerism.	201

6.1.4 Article IV: Synthesis, X-Ray Structure and Reactivity of Sterically Protected Azobisphenol Ligand: On the Quest for New Multifunctional Active Ligands	203
6.2. Articles After the Doctoral Commission	205
6.2.1 Article V: Catechol Derivatives as Fluorescent Chemosensors for Wide range pH Detection	207
6.2.2 Article VI: Intramolecular Electron Transfer in the Series of Mixed-Valence Complexes [MIII(Cat-N-SQ)(Cat-N-BQ)] (M=Fe, Co, Ni) bearing Non-Innocent Ligands: a Combined Experimental and Theoretical Study	209
6.2.3 Article VII: Valence Tautomerism: More Actors than Just Electroactive Ligands and Metal Ions	211

Chapter | 1

General Introduction

1.1 Intramolecular electron transfer (IET)

Considerable interest is being devoted to the obtaining of molecular systems that exhibit intramolecular electron transfer (IET) phenomena.¹ The interest arises from the **potential use of such systems on integrated molecular devices and the technical advantages** that can be derived from them. A first advantage is an ever-increasing miniaturization of the architectural components in the chips that reverts in the size reduction of computational systems,² thanks to the manipulation of the electronic wavefunction of the metallic electrodes through a molecule rather than through a semiconductor material.³ However, the design of functional devices based on this approach remains a challenge, even though several groups are working nowadays to face this problem. For instance, Feringa *et al.*⁴ and Lindsay *et al.*⁵ succeeded in contacting diarylarenes by the break junction technique where the molecule is effectively connected in between two small electrodes. The second advantage derived from using such molecular systems is that the time for an electron to travel through the circuit can be minimized using molecular-scale electronic architectures, which operate at greater speeds.⁶ The main drawbacks are the high conformational requirements that the molecule must fulfil, such as the rotation of the structure.⁷ All these problems encouraged the scientific community to realise studies in model systems to **understand and therefore control such requirements** before any real application becomes a reality.⁸

Mixed-valence systems (MV)⁹ are excellent candidates for such studies since they contain at least two redox sites with different oxidation states linked by a bridge that mediates the transfer of electrons from one site to the other. In these systems, the IET can be monitored and quantified through the study of an intervalence band transition (IVT) that usually appears in the near-infrared (near-IR) region of the electronic spectrum. Indeed, the electronic interaction between the two redox sites is characterized by the V_{ab} parameter that has the dimension of energy and can be experimentally determined from the position, intensity and width of the IVT band. A more detailed explanation about the origin of this band from this type of MV systems is developed in Annex I.¹⁰ A schematic representation of a MV system bearing two electro-active units (a donor and an acceptor unit) connected through a bridge is shown in Figure 1.1.



Figure 1.1. General representation of a MV system characterised by two electro-active-sites (EA_{site}) linked by a bridge that allows the electron transfer.

1.1.1 Mixed-valence systems

Depending on the strength of the interaction between the redox centres, Robin and Day classified the MV systems into three main different groups.¹¹ The potential energy curves for the three types of MV compounds, which represent the systems at any geometry along the nuclear coordinate, are shown in Figure 1.2. In the **Class I** MV systems, the interaction between the redox centres is null or extremely weak and, therefore, the system only exhibits the properties of the isolated redox units. Even if the molecule acquires sufficient activation energy to reach the intersection region, the probability of electron exchange would be negligible. On the contrary, in **Class III** MV systems, the electronic interaction is so intense that the electron is completely delocalised all over the molecule. Then, the properties of each isolated unit are not any longer observed, and new properties associated to the delocalised species appear. Finally, the interaction between the redox centres is moderate for **Class II** systems. In such systems, the electronic interaction has almost no effect on the potential energy curves in the vicinity of the equilibrium geometries, but causes mixing in the vicinity of the crossing point. In other words, the electron is vibrationally localised in one of the redox centres due to the presence of an activation energy barrier (ΔG). However, such a barrier may be overcome by an external stimulus, such as optical or thermal energy, to promote an IET process.

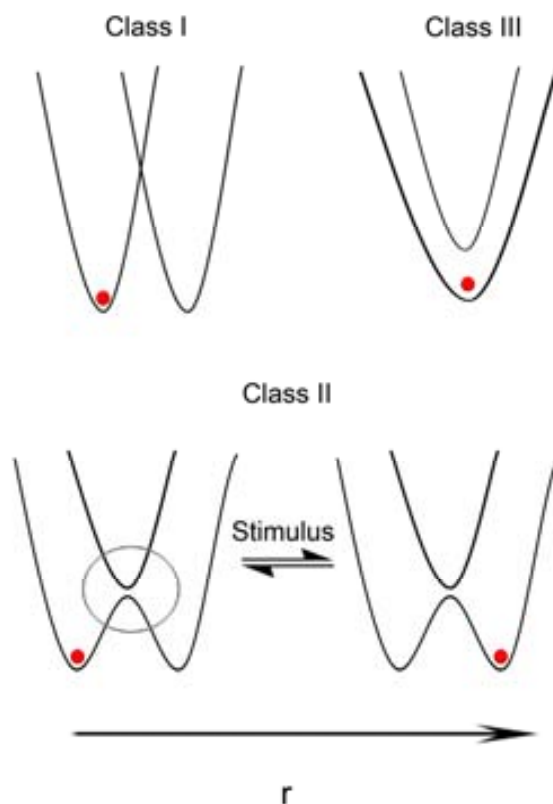


Figure 1.2. Schematic representation of the potential energy curves for the three categories of MV systems according to the classification of Robin and Day (1967).¹¹

The study of molecular MV Class II systems was initiated by Taube's seminal work on $[(\text{NH}_3)_5\text{Ru-bridge-Ru}(\text{NH}_3)_5]^{5+}$ (**1**) compounds.¹² The odd configuration of the "Creutz-Taube" ion results in an electron hole localised on one of the metal atoms and a charge localisation. Within this type of complexes, one of the metals stays as a Ru(II) and the other as a Ru(III). The historical importance of this first system is explained as it provides the first example of an inorganic MV ion, especially if we consider that forty years ago it was really difficult to discern between the localised or delocalised postulations of a given molecular system. Since then, most of the MV complexes shown to exhibit IET phenomena are homo and heteronuclear metallic complexes, (Figure 1.3a) where the two metal atoms with different oxidation states are connected through an organic bridging ligand. From them, ruthenium complexes and ferrocene moieties have been widely used thanks to their great stability, easy of oxidation and their kinetic inertness.¹³

In addition to their relevance and implication in future devices, IET have also an important relevance in biological processes. For this reason, several groups developed systematic studies focused upon measurements between metal centres over long distances in proteins or protein pairs. These studies clarified new insights into the distance, the driving force and the intervening medium. Interesting results were observed in the DNA helix, considered as a rigid, aromatic and water-soluble polymer, which provides a great medium through which to examine electron transfer process. For instance, Murphy *et al.*¹⁴ showed a rapid photoinduced electron transfer (PET) over distances bigger than 40 Å (comparable to biological systems) between metallointercalators: $[\text{Ru}(\text{phenanthroline})_2(\text{dppz})]^{2+}$ complex **2**, where dppz is dipyrrophenazine, that is acting as a donor and $[\text{Rh}(9,10\text{-phenanthrenequinonediimine})_2\text{phen}]^{3+}$ complex **3**, where phen is phenanthroline, that is acting as an acceptor unit. Such complexes are linked to one of the base-pair termini of a DNA duplex, which is acting as the spacer, demonstrating its efficiency as long-range mediator. However, it must be emphasised that the use of DNA as a molecular wire is still controversial.

An elegant alternative to metal ion based MV systems lies on the use of pure organic electro-active units (Figure 1.3b). One of the main advantages of these systems is the possibility to fine-tune intramolecular electron transfer in a more precise way thanks to the flexibility of organic synthesis. However, the number of examples described so far is considerably smaller than those based on metal ions, mostly due to their higher instability.¹⁵ The synthetic flexibility applies not only to the organic electrode units but also to the connection with the organic bridge, which is most often used through covalent bonds. The first pure organic MV compound studied was the bis(indanone) (**4**).¹⁶ Since then, only a few examples of pure organic MV compounds showing IET phenomena have been described. For example, some of these systems are radicals derived from quinones¹⁷ or tetrathiafulvalenes.¹⁸ A more complete revision of these pure organic MV systems is given in Chapter 3.

Finally, another type of Class II MV systems are heterogeneous complexes combining both redox-active ligands and transition metal ions. The IET between them has been named

with the generic term of **valence tautomerism** (VT, Figure 1.3c). Complexes showing this phenomenon are known to exhibit two nearly degenerated electronic states (tautomers) with localised electronic structures. The IET between both redox active units, that is activated by an external stimulus, such as photons, temperature and/or pressure, brings to a reversible interconversion between the degenerated electronic states. Moreover, since both electronic states present different optical and/or magnetic properties, these complexes are excellent candidates to be used as molecular components in future electronic devices.^{1,19} Examples of electronic labile complexes are also the spin-crossover²⁰ systems. The comprehension of the characteristic features for all these complexes has been developed in parallel over the last decades, rising out a large interest in the scientific community as demonstrated by the large amount of examples developed for each case.

A schematic representation of the three families of Class II MV systems is shown in Figure 1.3. As a general approximation, such systems should present two electro-active sites (transition metal ions or stable organic radicals) and a bridge that could mediate the pass of electrons (organic π -system or, in some cases, an specific metal ion),

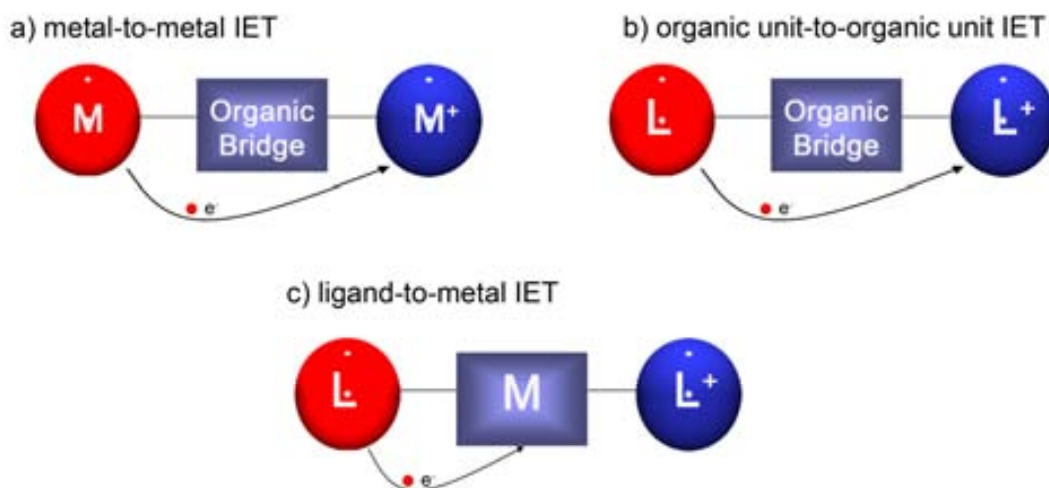


Figure 1.3. Schematic representation of the three possible approaches used for designing Class II MV systems. M stands for metal ion and L for an organic electro-active unit.

From the three different families of MV previously described, the last family of complexes (VT) has been less studied in spite of their enormous interest. Indeed, these complexes not only are excellent models to study IET in transition metal complexes but also are excellent candidates to be used in the near future in molecular-based devices. In the following sections, these complexes are revised more in detail.

1.2. Intramolecular electron transfer in mixed-valence complexes bearing “non-innocent” redox-active ligands and a transition metal ion: valence tautomerism

1.2.1 Redox-active ligands

The term of non-innocent ligand was directly related to the role and the influence of certain ligands on the final electronic distribution of transition metal complexes. For example, firstly pointed out by Jørgensen,²¹ this concept can be used when both, the metal-centred and ligand-centred electronic frontier orbitals, are similar in energies. Within such scenario, the final oxidation state of the complex and the internal electronic distribution may be modulated becoming a great subject of investigation by theoretical²² and experimental means.²³ This investigation is of interest not only for the field of electron-transfer (nanotechnology and materials-science) but also for several other fields including the study of complexes bearing non-innocent ligands that perform physiological functions on biological systems. For instance, transition metal complexes, in which at least one of the ligands is a phenoxyl radical, have attracted much interest due to their broad occurrence in technical processes²⁴ and enzymatic metalloproteins, such as galactose oxidase (**5**) (GAO)²⁵ or glyoxal oxidase (**6**) (GLO).²⁶ A schematic representation of the active site of both metalloproteins is shown in Figure 1.4.

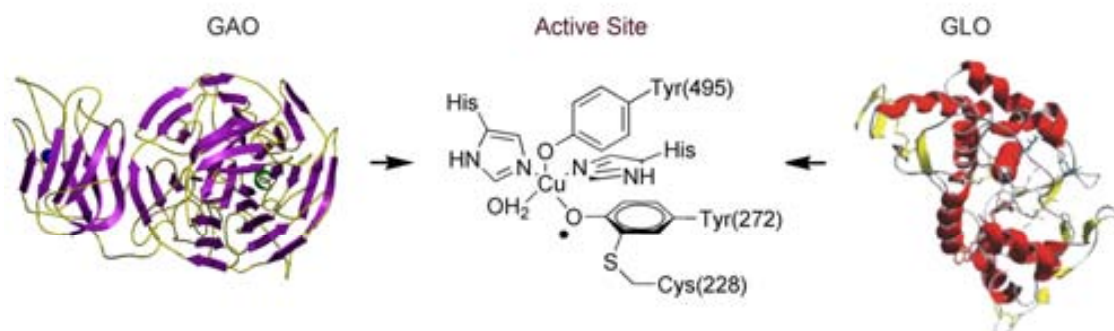


Figure 1.4. Representation of the phenoxyl radical acting as an active site in enzymatic metalloproteins such as galactose oxidase (**5**, GAO) and glyoxal oxidase (**6**, GLO). Pictures of the proteins were extracted from personal scientific web page of Prof. Mike McPherson: www.astbury.leeds.ac.uk/gallery/leedspix.html and *Int. Microbiol.*, 8, (2005), 195. Rights authorised by ©International Microbiology.

Thus far, many different types of redox-active ligands have been described in the literature.²⁷ Some important examples are quinone-type, crown-ethers²⁸ and tetrathiafulvalene derivatives.²⁹ Another example is the family of π -conjugated polymers and/or oligomers bearing coordinating sites, such as polyanilines and polythiophenes.³⁰ However, the number of redox-active ligands exhibiting VT is rather limited. For this to take place, two main conditions must be satisfied simultaneously: first the degree of covalency in the interaction between metal ion and the electro-active ligand must be low. And second, the energy of their frontier orbitals must be similar. In other words, it is necessary that these complexes exhibit localised electronic structures, low orbital mixing and a small energy difference between the two electronic

tautomers. Ligands such as polychlorotriphenylmethyl radicals (PTM)³¹ and tetraphenylporphyrin (TPP)³² have been shown to exhibit VT as is presented in Figure 1.5. However, most of the VT complexes reported so far are based on catecholates and phenoxylates ligands. A complete revision of the different complexes so far described in the literature to exhibit VT, was given in Chapter 3. The characteristics of these two families of ligands (catecholate and phenoxylate) are explained next, whereas a review of the VT complexes formed from these ligands is given in Chapter 2.

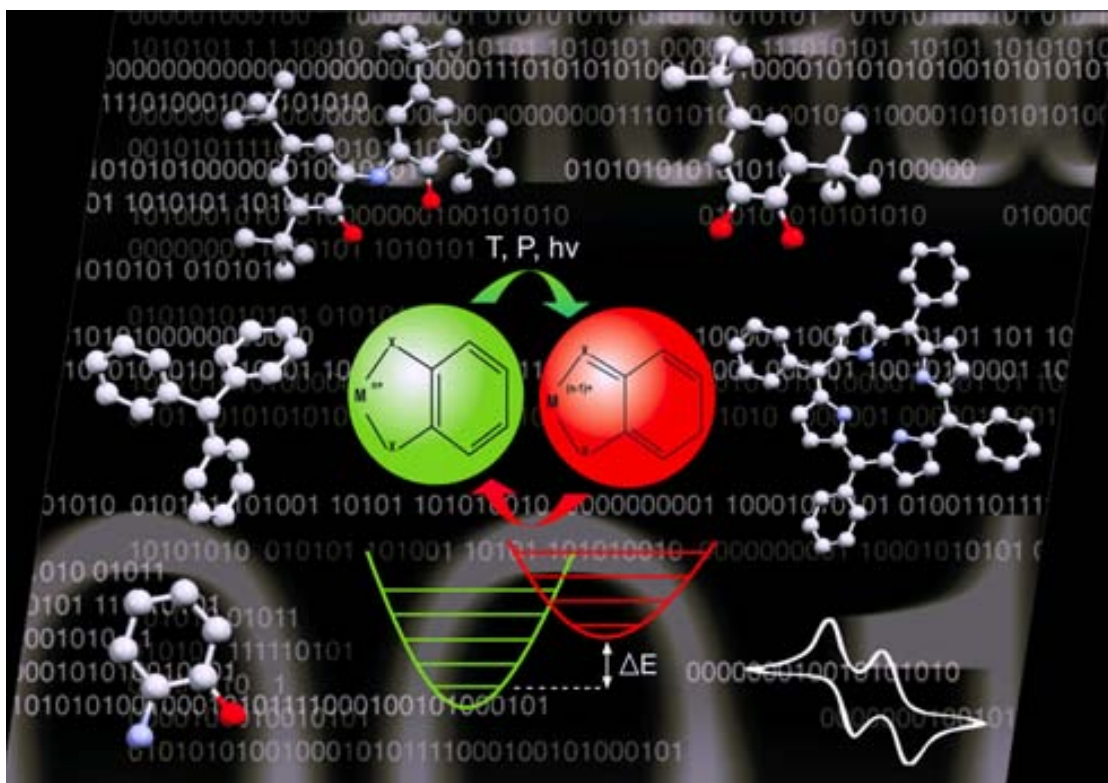


Figure 1.5. Figurative representation of the different families of ligands that have been participated in VT processes.

1.2.1.1 Catecholate complexes

The transition metal coordination chemistry of ligands derived from catechols and o-benzoquinones has been developed over the past twenty five years with interesting and surprising results.³³ Initial interest in these complexes was associated with the redox activity of the quinone ligands (1,2-benzoquinone, **7**) showed in Figure 1.6, and the potential for synthesising coordination complexes that may exist in a number of electronic states.³⁴ The magnetic properties of complexes prepared with metals of the first transition series subsequently revealed that the partially-reduced radical semiquinone (SQ) form was stabilised upon coordination. This stability allowed the observation of metal-SQ magnetic couplings if the metal ion is paramagnetic. In the cases of diamagnetic metal ion and more than one SQ ligand, a metal-mediated SQ–SQ exchange coupling was also obtained.^{27a} Charge delocalisation within

the metal–quinone chelate ring was also found to be much less significant than for related complexes of the 1,2-dithiolene (**8**) and diimine ligands, leading to the view that quinone-derived ligands may be described in one of the three charge–localised electronic forms shown in Figure 1.6.

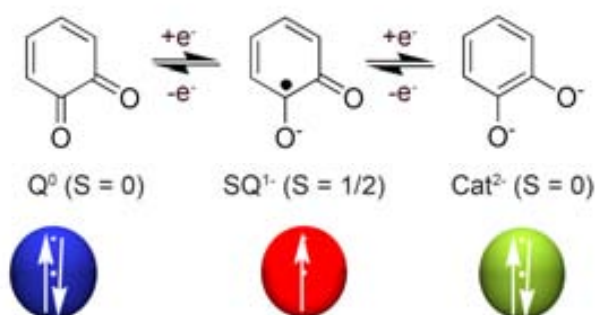


Figure 1.6. Different oxidation states of the 1,2-benzoquinone (**7**).

A feature unanticipated at the outset of this research thanks to such a localisation is the close separation in energy between metal and quinone electronic levels. This has led to discoveries on IET between redox isomers differing in charge distribution under equilibrium conditions in a process that we described as an example of VT in analogy with Prussian blue analogues.³⁵ In addition to exhibit electron transfer phenomena, several other interesting features, such as the design of paramagnetic molecules with predetermined spin topologies and activation of small molecules like O₂ and N₂, have also been described for catechol based complexes.³⁶

1.2.1.2 Phenoxylate complexes

Phenoxyl radicals are monovalent oxygen radical species that exhibit delocalisation of the unpaired electron over the aromatic ring. In most of the cases, *ortho* and *para* substituents give steric protection to the molecule.³⁷ For instance, it has been shown that *tert*-butyl substituents at the *ortho* and *para* positions of the phenolates facilitate one-electron oxidation to the corresponding phenoxyl radicals because these substituents decrease the oxidation potential of the phenolates, and provide enough steric bulkiness to suppress bimolecular decay reactions of the generated phenoxyl radicals.³⁸ Several groups have studied metal-phenoxyl complexes giving new insights into the chemical factors that govern the generation and stability of this type of radicals;³⁹ among them worth to mention the work directed by Prof. K. Wieghardt. For instance, they have established that bidentate *O,N*-coordinated *o*-aminophenolato ligands (**9**) can be found in one of the following different protonation and oxidation levels bounded to a transition metal ion: *o*-imidophenolate (**9**²⁻) anions, *o*-iminobenzosemiquinonate (**9**¹⁻) π radical monoanions or even *o*-iminobenzoquinone (**9**). All these forms can exist in coordination

compounds, as confirmed by high quality X-ray crystallography studies at low temperatures.⁴⁰ In addition, *o*-iminobenzosemiquinonate (9^{1-}) anions are paramagnetic ($S=1/2$) ligands that couple either ferro- or antiferromagnetic fashion to the respective paramagnetic transition metal ion, depending on the symmetry of the symmetry of magnetic *d* orbital of the metal ion and the π radical according to the Goodenough-Kanamori rules.⁴¹ Following this approximation, a large number of new complexes bearing non-innocent ligands have been reported, not only in the aminophenolate case (O,N-)⁴² or N,N- case⁴³ but also with other donor atoms such as S (S,N-, S,S- or S,O-)⁴⁴ and different metal ions.⁴⁵

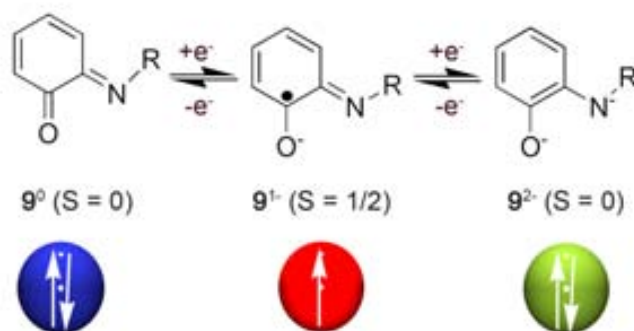


Figure 1.7. Different oxidation states of the *o*-aminophenol ligand (**9**).

A further step has been the study and characterization of *O,N,O*-coordinated type ligands containing two phenolate donor groups, such as ligand BQ-N-SQ (**10**, Figure 1.8).⁴⁶ These ligands, in addition to producing phenoxyl radicals in the presence of air, exhibit better chelating capabilities and good π -donor atoms that stabilize higher oxidation states.⁴⁷ The synthesis and mechanical features for the obtaining of ligand BQ-N-SQ was first described in 1975 by Girgis and Balch,^{46c} treating the 3,5-di-*tert*-butyl-catechol (**11**) with aqueous ammonia in the presence of a divalent metal ion under aerobic conditions. Since then, a considerable interest for this family of complexes has increased in the scientific community. Thanks to their rich redox activity, such ligands may exist at least in four different oxidation states (Figure 1.8) although structural and magnetic characterisation of the complexes bearing this ligand suggest that they can be mostly found as $M^{IV}(\text{Cat-N-SQ})_2$, $M^{III}(\text{Cat-N-SQ})(\text{Cat-N-BQ})$ and $M^{II}(\text{Cat-N-BQ})_2$.

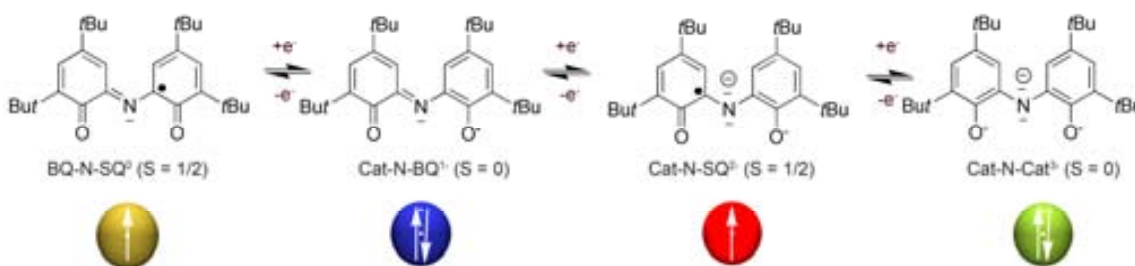


Figure 1.8. Different oxidation states of the Schiff-base ligand **10**.

Other unusual interesting trends of the electronic distribution along different members of this family of complexes have also been found.⁴⁸ Recently, Wiegardt *et al.*⁴⁹ showed the stabilization of the trianionic (Cat-N-Cat)³⁻ form in a Cu(II) metal complex (**12**). Moreover, on the quest for dinuclear M^{II}-phenoxyl radical complexes playing an active role on the aerobic catalysis of alcohols, a new zinc-complex⁵⁰ with the paramagnetic form [Zn(Cat-N-SQ)(BQ-N-SQ)] (**13**) have been published. In spite of its poor stability, this complex is the first example where the oxidation levels of the two coordinated ligands (**10**) differs formally by two electrons.

1.2.2 Valence tautomerism: IET between a redox-active ligand and a metal ion

Once the concept of a redox-active ligand has been defined, the next step is to introduce their role into a VT complex. VT metal complexes combine a transition metal ion, which can exist at least in two different oxidation states, and an electro-active ligand, both with well-defined charge localisation. An external stimulus may induce a reversible IET between the metal ion and the redox-active ligand, leading to the existence of two electronic isomers (valence tautomers) with different charge distributions, and consequently, different optical, electric and magnetic properties.⁵¹ A schematic representation of VT together with the corresponding potential energy curve plotted as a function of the nuclear coordinate is shown in Figure 1.9. A more detailed information of this family of complexes is given in Article I.

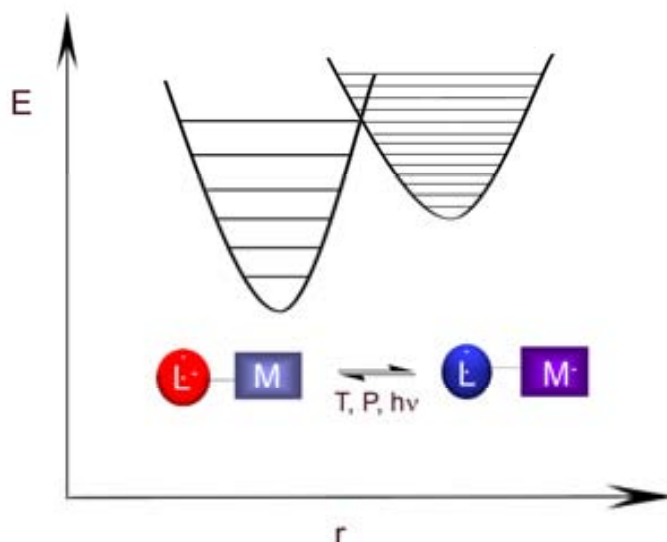
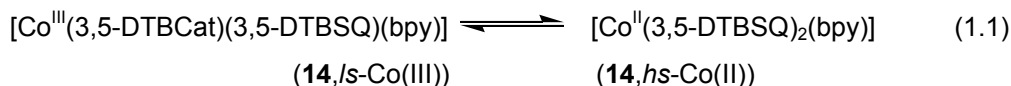


Figure 1.9. Schematic representation of VT involving a redox active ligand and a transition metal ion together with the corresponding potential energy curve plotted in function of the nuclear coordinate.

In the literature, one of the first complexes showing VT was the cobalt bis(quinone) complex [Co^{III}(3,5-DTBCat)(3,5-DTBSQ)(bpy)] (**14**),⁵² where 3,5-DTBCat²⁻ and 3,5-DTBSQ⁻ refer to the catecholate (DTBCat²⁻) and semiquinonate (DTBSQ⁻) forms of 3,5-di-tert-butyl-o-

quinone (**15**) respectively, and bpy is 2,2'-bipyridine (Figure 1.10). In solution, this complex can exist in two electronic isomers. Indeed, by inducing changes in the temperature, both isomers follow the equilibrium showed in Eq. 1.1. This equilibrium can be monitored by magnetic measurements and spectroscopic techniques such as UV–VIS, NMR and/or EPR.



Taking the UV-Vis spectroscopy as the monitoring technique, a solution of complex **14** in dichloromethane at low temperatures shows an UV-Vis spectrum with a band around 580 nm characteristic of the $[\text{Co}^{\text{III}}(3,5\text{-DTBCat})(3,5\text{-DTBSQ})(\text{bpy})]$ (**14**,*ls*-Co(III)) tautomer. An increase of the temperature promotes an IET so **14**,*ls*-Co(III) converts into **14**,*hs*-Co(II) as one of the ligands is reduced by one electron from a DTBSQ⁻ to a DTBCat²⁻ ligand. As a consequence, the intensity of this previous band decreases and a band at 770 nm characteristic of the **14**,*hs*-Co(II) tautomer increases in intensity (see Figure 1.10). Importantly, accompanying the optical changes, variations of the magnetic response were also observed.

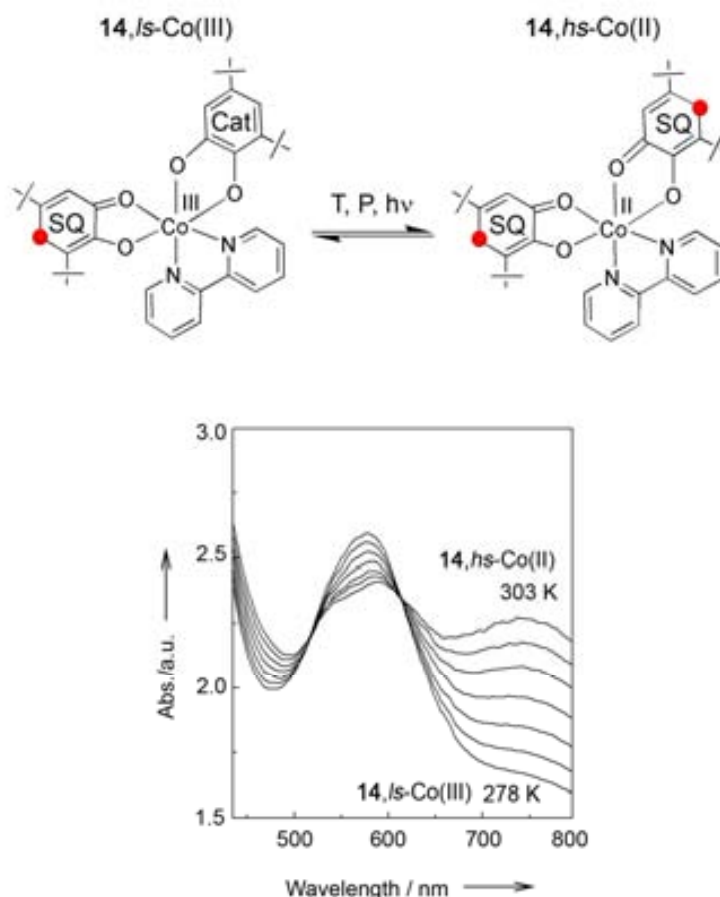


Figure 1.10. Valence tautomeric transformation of complex **14** under the influence of temperature (T), pressure (P) and light ($h\nu$) (top). Temperature dependence of the electronic absorption spectrum of a CH_2Cl_2 solution of complex **14** in the temperature range 278–303 K (bottom).

Valence tautomerism is an entropy-driven process, in analogy to the extensively studied low-spin to high-spin crossover phenomena.²⁰ The large entropy gain arises from: first a gain in electronic entropy due to the higher spin state degeneracy of the *hs*-Co(II) form and second the higher density of vibrational states of the *hs*-Co(II) form due its longer metal-ligand bond lengths.⁵³ Thus, thermal population of tautomeric states is dictated by the Gibbs free energy expression shown in Eq. 1.2. At low temperatures, $T\Delta S$ is negligible compared to ΔH , and consequently, if $\Delta H > kT$ only the *ls*-Co(III) state is populated. An increase of the temperature will increase the $T\Delta S$ contribution, making it non negligible and favouring the population of the *hs*-Co(II) state up to a critical temperature T_c where $\Delta G = 0$ and $\Delta H = T\Delta S$. A further increase of the temperature will change the sign of ΔG , and consequently, will promote the population of the *hs*-Co(II) form.

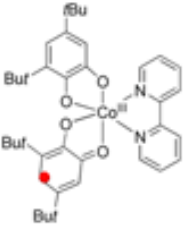
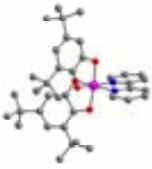
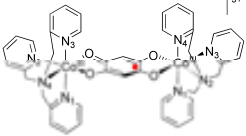
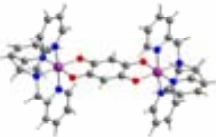
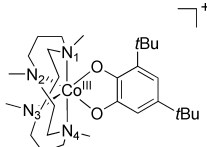
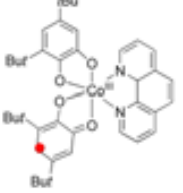
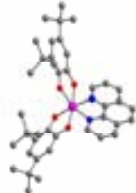
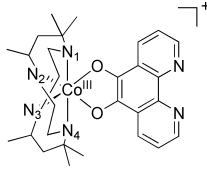
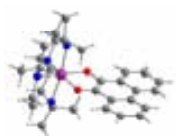
$$\Delta G = \Delta G_{hs-Co(II)} - \Delta G_{ls-Co(III)} = \Delta H - T\Delta S \quad (1.2)$$

Moreover, since valence tautomeric complexes are electronically labile, they exhibit significant vibronic interactions, and therefore, an appreciable sensitivity to the environment. As a consequence, IET can be induced not only by temperature variations but also by irradiation or pressure. Relevant examples of VT complexes in which the electronic equilibrium is allowed by light stimulus, are given next. For instance, Hendrickson *et al.* have reported results of the first picosecond time-resolved optical experiments on VT complexes in solution.⁵⁴ Literature examples where the VT transition occurs in solid state at low temperatures promoted by light as external stimuli have been reported,^{55,56,57} even for polynuclear complexes. Sato *et al.*⁵⁸ reported not only photoswitching but also hysteresis effects around room temperature (310 and 297 K) for complex $[\{Co(tpa)\}_2(DHBQ)](PF_6)_3$ (**15**), (where DHBQ is the deprotonated 2,5-dihydroxy-1,4-benzoquinone), for which intermolecular interactions are enhanced by the presence of significant π - π interactions. Some years before, Dei *et al.*⁵⁹ realised additional femtosecond spectroscopic experiments in a simple cobalt-dioxolene derivative, $[Co(Me_4Cyclam)DTBSQ]^+ Me_4Cyclam = 1,4,8,11$ -tetramethyl-1,4,8,11-tetraazacyclotetradecane (**16**), showing the involvement of at least three states in a two-step VT process in solution.

Examples of pressure-induced VT have also been reported although in less extent than thermally-driven or light-induced transitions, mainly due to experimental difficulties.⁶⁰ In these experiments, the increase of the molecular size on passing from the low to the high-spin isomer due to the population of antibonding orbitals is used to favour the low-spin isomer after applying pressure. The first example of a pressure-driven solid state valence tautomeric transformation was reported by Verdaguer and Hendrickson,⁶¹ who studied the non-solvated complex $[Co^{II}(3,5-DTBSQ)_2(phen)]$ (**17**) and its related solvated form $17 \cdot C_6H_5CH_3$ by EXAFS and XANES. Recently, pressure-induced VT has also been monitored by changes on the magnetic response.⁶² An interesting example is complex $[Co(cth)(Phendiox)]PF_6 \cdot H_2O$ (**18**· PF_6), where *cth* is a macrocycle and *phendiox* corresponds to the dioxolene neutral form of 9,10-dihydroxyphenanthrene. X-ray experiments referred on this complex showed that the size of the

unit cell decreases (up to 4%) along the VT process.⁶³ A schematic representation of the representative complexes **14** to **18** as well as a brief summary of their VT characteristics is shown in Table 1.1.

Table 1.1. Representative examples of complexes bearing VT induced by different external stimuli and their interconversion characteristics

Ext. Stimuli	Representative Compounds	Crystal Structure	Charact. Techniques	*T _C /P _C or Temperature Range		Medium
T	 14-Is		Magnetism EPR X-Ray Diffraction	310 K		Solid (ref. 52a)
			Spectroscopic (UV-Vis, NMR, EPR) Magnetism	273 K		Liquid (ref. 52b)
hv	 15-Is		Magnetism	hv 532 nm		Solid (ref. 58)
	 16-Is	—	Spectroscopic	hv 400 nm		Liquid (ref. 59)
P	 17-Is		Diamond Cell XANES EXAFS	17	0.37 GPa	Solid (ref. 61)
				17.C ₆ H ₅ CH ₃	1.1 GPa	
	 18-Is		Hydrostatic Pressure Cell. Magnetism X-Ray diff.	1 bar – 7.4 Kbar 10 ⁻⁷ GPa- 0.74 GPa		Solid (ref. 62)

*T_C(critical temperature), λ_{exc}, and P_C (critical pressure), defined as the temperature and pressure at which the equilibrium is best represented by the presence of equal amounts of both electronic isomers. T_C sometimes is defined as a temperature range due to the lack of the thermodynamic parameters ΔH and ΔS.

A complete revision of the majority of complexes bearing VT phenomena is given in Annex IV. Complexes were located at each table depending on the external stimuli (temperature, pressure or irradiation) that induce the equilibrium. In these tables, complexes were also ordered depending on the metal ion involved in the VT transition (Co, Mn, Cu, Fe and Ni). Therefore, a historical evolution of such molecular materials can be followed. Also, the new examples recently published in this field show a tendency towards the design of new systems based on dimers, polymers and gold nanoparticles.

1.3. Thesis context

By the beginning of this Thesis, several examples of heterogeneous complexes bearing a transition metal ion and a redox-active ligand that exhibit VT had already been described. A completed and updated revision of such systems is given in Chapter 2 and Annex I and IV. The interest for such systems is twofold. First, they are unique model systems that provide insight into the basic factors affecting IET between a ligand and a metal ion. And second the large changes in the optical, structural and magnetic properties associated with these systems provide them excellent characteristics to be used as bistable molecular materials with their subsequent integration into devices. However, before any potential application of these systems becomes a reality, the development of systematic studies that help to determine how is the electronic distribution localised on a given complex and tune it, is highly required. For instance, observation of VT has been traditionally associated to the matching of the redox-active ligand and transition metal ion electronic orbitals. However, a detailed revision and study of the nature of the metal ion on VT was missing. Moreover, the study of other factors such as the network environment must be developed. Indeed, due to the electronic lability of this family of complexes, they exhibit significant vibronic interactions, and therefore, an appreciable sensitivity to the environment. For this reason, the equilibrium in which the VT molecule is localised, is highly dependent of the medium, i.e., whether if the molecule is found as a crystalline material, solution or embedded in a polymer. Therefore, its understanding was crucial. A detailed information on the different studies so far developed on VT is shown in Chapter 2 and Article VII.

Another important question that has risen for this family of VT systems is whether in those complexes bearing more than one redox-active ligand we may have intramolecular ligand-to-ligand (IET^{LL}) electron transfer in addition to the previously described VT also termed from now on as intramolecular ligand-to-metal electron transfer (IET^{LM}). A schematic representation of such multielectron transfer processes is shown Figure 1.11. For example, complexes with the general formula [M(DTBCat)(DTBSQ)(N-N)] containing mixed-charge ligands are analogous of classical Taube's MV systems where the situation has been inverted. In this case, instead of two metal ions with different oxidation states, where IET takes place through an organic bridge, two ligands with different oxidation state are connected through a metal ion that is acting as a bridge. In this sense Prokofev *et al.*⁶⁴ have shown the dynamic exchange of charge between

ligands on the complexes $[P(3,5\text{-DTBSQ})(3,5\text{-DTBCat})_2]$ (**19**) and for the $[M(3,6\text{-DTBSQ})(3,6\text{-DTBCat})_2]^{2-}$ ($M = \text{Si}$ (**20**), Sn (**21**)) anions. Among transition metal compounds, Pierpont *et al.*⁶⁵ showed by EPR that the radical spin in $[\text{Ga}(\text{tmeda})(3,6\text{-DTBSQ})(3,6\text{-DTBCat})]$ (**22**) is equally distributed over both ligands. A more detailed explanation of this multielectron transfer process is given in Chapter 3 and Articles III and VI

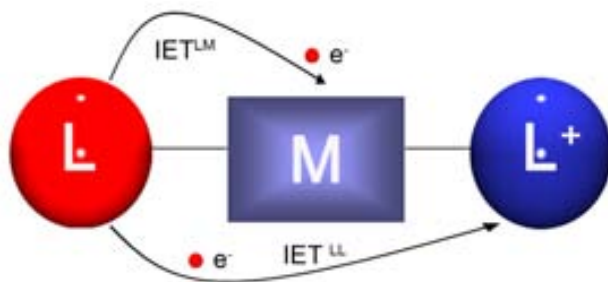


Figure 1.11. General Representation of a MV system, characterized in general trends as two electro-active sites ligands linked by a metal bridge, which can allow the electron transfer.

From a scientific point of view this complexes could present an excellent scenario to gain insight into the IET mechanisms. And from an applied perspective the possibility to combine, control and gate the electron transfer open several possibilities. For this reason a detailed study was highly convenient.

Finally, a completely new approach that was not explored by the beginning of this Thesis and even nowadays, is the combination of VT with an additional property inherent to the ligand, on the quest to multifunctional systems. Only a few examples have been focused into this objective. For instance Awaga *et al.*⁶⁶ reported VT in the spin-labeled complex $[\text{Co}(\text{nnbpy})(3,5\text{-DTBSQ})_2]$ (**23**), where nnbpy is a bipyridine substituted by a nitronyl nitroxide radical. In spite this pioneering example on the quest for synergism and multifunctional properties, this remains an open issue that deserves much attention due to its enormous interest. A detailed analysis is given in Chapter 4 and Article IV.

References

- [1] (a) P. Gütllich, Y. Garcia, T. Woike, *T. Coord. Chem. Rev.*, **219**, **2001**, 839. (b) A. Hauser, *Coord. Chem. Rev.* **111**, **1991**, 275. (c) O. Kahn, J. P. Launay, *Chemtronics* **3**, **1988**, 140.
- [2] As an alternative way, some improvements are done with single-walled carbon nanotubes (SWNTs). Combination of excellent electrical and mechanical properties may provide an accessible route to advancing in new areas, thanks to its characteristic electronic noise with decreasing size. New studies focused into this field could bring, in a near future (around 10-15 years), to the replacement of silicon by carbon nanotubes. As one of the examples we can cite: D. B. Suyatin, J. Sun, A. Fuhrer, D. Wallin, L. E. Fröberg, L. S. Karlsson, I. Maximov, L. R. Wallenberg, L. Samuelson, H. Q. Xu, *Nanoletters*, DOI: 10.1021/nl073193y, and references cited herein
- [3] M. A. Row, C. Zhou, C. J. Muller, T. P. Burgin, J. M. Tour, *Science*, **278**, **1997**, 252.
- [4] N. Dulic, S. J. van der Molen, T. Judernac, H. T. Jonkman, J. J. D. de Jongm T. N. Bowden, J. van Esch, B. L. Feringa, B. J. Wees, *Phys. Rev. Lett.*, **91**, **2003**, 207402.
- [5] J. He, F. Chem, P. A. Liddell, J. Andreasson, S. D. Straight, D. Gust, T. A. Moore, A. L. Moore, J. Li, O. F. Sankey, S. M. Lindsay, *Nanotechnology*, **16**, **2005**, 695 and references cited herein.
- [6] Typical molecular sized systems would permit the use of approximately 10^{13} logic gates per cm^2 compared with the present capacity of a microchip of less than 10^6 gates per cm^2 , thereby offering a 10^5 decrease in required size. In addition, the response times of molecular devices can be in the range of femtoseconds, while the fastest current devices operate in the nanosecond regime. (a) J. M. Tour, M. Kozaki, J. M. Seminario, *J. Am. Chem. Soc.*, **120**, **1998**, 8486. (b) J. M. Seminario, J. M. Tour in *Molecular Electronic-Science and Technology* (Eds.: A. Aviram, M. A. Ratner, New York Academy of Science, New York, **1988**, 69. (c) A. P. de Silva, S. S. K. de Silva, N. C. W. Goonesekera, H. Q. N. Gunaratne, P. L. M. Lynch, K. R. Nesbitt, S. T. Patuwathavithana and N. L. D. S. Ramyalal, *J. Am. Chem. Soc.*, **129**, **2007**, 3050, and references cited herein.
- [7] A. Gourdon, *Atomic and Molecular Wires* (Ed.) C. Joachim and S. Roth, NATO ASI Series, Dordrecht, The Netherlands, **1997**, 89.
- [8] (a) F. Moresco, A. Gourdon, *Proc. Natl. Acad. Sci. USA*, **102**, **2005**, 8809. (b) S. R. Vázquez, M. C. R. Rodríguez, M. Mosquera, F. Rodríguez-Prieto, *J. Phys. Chem., A*, **111**, **2007**, 1814. (c) S. Nikolau, H. E. Toma, *Eur. J. Inorg. Chem.*, **2008**, DOI: 10.1002/ejic.20080079.
- [9] J. J. P. Fackler, *Encyclopedia of Inorganic compounds*, **15**, **2006**, 2270.
- [10] (a) C. Creutz, *Prog. Inorg. Chem.*, **30**, **1983**, 1. (b) R. J. Crutchley, *Adv. Inorg. Chem*, **41**, **1994**, 273.
- [11] M. B. Robin, P. Day, *Adv. Inorg. Chem. Radiochem.*, **10**, **1967**, 247.
- [12] C. Creutz, H. Taube, *J. Am. Chem. Soc.*, **91**, **1969**, 3988.
- [13] For ruthenium complexes: (a) M. D. Ward, *Chem. Ind.*, **1996**, 568. (b) R. Ziessel, M. Hissler, A. El-Ghayoury, A. Harriman, *Coord. Chem. Rev.*, **178**, **1998**, 1251. (c) M. N. Paddon-Row, *Acc. Chem. Res.* **27**, **1994**, 18. (d) M. R. Wasielewski, *Chem. Rev.* **92**, **1992**, 435. (e) J. P. Launay, *Chem. Soc. Rev.* **30**, **2001**, 386. For metallocene examples: (a) T. M. Figueira-Duarte, V. Lloveras, J. Vidal-Gancedo, A. Gégout, B. Delavaux-Nicot, R. Welter, J. Veciana, C. Rovira, J.-F. Nierengarten, *Chem. Commun.*, **2007**, 4345. (b) S. Barlow, D. O'Hare, *Chem. Rev.*, **97**, **1997**, 637, and references therein
- [14] C. J. Murphy, M. R. Arkin, Y. Jenkins, N. D. Ghatlia, S. H. Bossmann, N. J. Turro, J. K. Barton, *Science*, **262**, **1993**, 1025.
- [15] For a general review on pure organic mixed-valence systems, see: D. Ruiz-Molina, J. Sedó, C. Rovira, J. Veciana in *Handbook of Advanced Electronic Materials and Devices* (Ed. H. S. Nalwa), **2001**, 303, and references cited therein.
- [16] (a) S. Mazur, C. Sreekumar, A. H. Schroeder, *J. Am. Chem. Soc.* **98**, **1976**, 6713. (b) A. H. Schroeder, S. Mazur, *J. Am. Chem. Soc.*, **100**, **1978**, 7339.
- [17] (a) S. F. Rak and L. L. J. Miller, *J. Am. Chem. Soc.*, **114**, **1992**, 1388. (b) L. L. Miller and C. A. Liberko, *Chem. Mater.*, **2**, **1990**, 339 and references cited therein.
- [18] K. Lahlil, A. Moradpour, C. Bowlas, F. Menou, P. Cassoux, J. Bonvoisin, J. P. Launay, G. Dive, D. Dehareng, *J. Am. Chem. Soc.*, **117**, **1995**, 9995.
- [19] N. Sutin, *Acc. Chem. Res.*, **15**, **1982**, 275.
- [20] P. Gütllich, H. A. Goodwin, *Spin Crossover in Transition Metal Complexes I, II, and III*. Topics Curr. Chem. (Ed.) Springer-Verlag, Heidelberg, **233**, **234**, **235**, **1994**.

- [21] C. K. Jørgensen, *Coord. Chem. Rev.*, **1**, **1966**, 164
- [22] S. Messaoudi, V. Robert, N. Guihéry, D. Maynau, *Inorg. Chem.*, **45**, **2006**, 3212, and references cited herein.
- [23] W. Kaim, B. Schwederski, *Pure Appl. Chem.*, **76**, **2004**, 351, and references cited therein.
- [24] B. A. Jazdzewski, W. B. Tolman, *Coord. Chem. Rev.*, **200-262**, **2000**, 633.
- [25] J. W. Whittaker, *Chem. Rev.*, **103**, **2003**, 2347.
- [26] M. M. Whittaker, P. J. Kersten, D. Cullen, J. W. Whittaker, *J. Biol. Chem.*, **274**, **1999**, 36226.
- [27] (a) C. G. Pierpont, C. W. Lange, *Prog. Inorg. Chem.*, **41**, **1994**, 331. (b) A. M. Costero, C. Andreu, R. Martínez-Mañez, J. Soto, L. E. Ochando, J. M. Amigó, *Tetrahedron* **54**, **1998**, 8159. (c) T. Hirao, *Coord. Chem. Rev.*, **226**, **2002**, 81. (d) C. Rovira, *Chem. Rev.*, **104**, **2004**, 5289. (e) T. Hirao, *Macromolecules Containing Metal and Metal-Like Elements*, Metal-Coordination Polymers, **5**, **2005**, 209.
- [28] F. Le Derf, M. Mazari, N. Mercier, E. Levillain, G. Trippe, A. Riou, P. Richomme, J. Becher, J. Garin, J. Orduna, N. Gallego-Planas, A. Gorgues, M. Salle, *Marc. Chem. Eur. J.*, **7**, **2001**, 447.
- [29] K. S. Gavrilenko, Y. Le Gal, O. Cador, S. Golhen, L. Ouahab, *Chem. Commun.*, **2007**, 280.
- [30] J. L. Reddinger, J. R. Reynolds, *Macromolecules*, **30**, **1997**, 673.
- [31] I. Ratera, D. Ruiz-Molina, F. Renz, J. Ensling, K. Wurst, C. Rovira, P. Gütllich, J. Veciana, *J. Am. Chem. Soc.*, **125**, **2003**, 1462.
- [32] (a) D. Chang, T. Malinski, A. Ulman, K. M. Kadish, *Inorg. Chem.*, **23**, **1984**, 817. (b) J. Seth, V. Palaniappan, D. F. Bocian, *Inorg. Chem.*, **34**, **1995**, 2201.
- [33] A. Vlcek, *Comments Inorg. Chem.*, **16**, **1994**, 207.
- [34] (a) R. R. Rakhimov, P. M. Solozhenkin, N. N. Kopitaya, V. S. Pupkov, A. I. Prokofiev, *Dokl. Akad. Nauk. SSSR*, **300**, **1988**, 1177. (b) G. A. Abakumov, G. A. Razuvaev, V. I. Nevodchikov, V. K. Cherkasov, *J. Organomet. Chem.*, **341**, **1988**, 485. (c) C. W. Lange, M. Foldeaki, V. I. Nevodchikov, V. K. Cherkasov, G. A. Abakumov, C. G. Pierpont, *J. Am. Chem. Soc.*, **114**, **1992**, 4220.
- [35] (a) T. Mallah, S. Thiebaut, M. Verdaguer, P. Veillet, *Science*, **262**, **1993**, 1554. (b) J. S. Miller, *Adv. Mater.*, **6**, **1994**, 217. (c) W. R. Entley, G. S. Girolami, *Science*, **268**, **1995**, 397. (d) S. Ferlay, T. Mallah, R. Ouahes, P. Veillet, M. Verdaguer, *Nature*, **378**, **1995**, 701. (e) O. Sato, T. Iyoda, A. Fujishima, K. Hashimoto, *Science*, **271**, **1996**, 49.
- [36] (a) A. Bencini, A. Caneschi, A. Dei, D. Gatteschi, C. Sangregorio, D. Shultz, L. Sorace, M. G. F. Vaz, *C. R. Chimie*, **6**, **2003**, 663. (b) A. Dei, D. Gatteschi, *Inorg. Chim. Acta*, **198-200**, **1992**, 813.
- [37] E. R. Altwicker, *Chem. Rev.*, **67**, **1967**, 475.
- [38] P. Chaudhuri, K. Wieghardt, *Prog. Inorg. Chem.*, **50**, **2002**, 151.
- [39] A. K. Nairn, R. Bhalla, S. P. Foxon, X. Liu, L. J. Yellowlees, B. C. Gilbert, P. H. Walton, *J. Chem. Soc. Dalton. Trans.*, **2002**, 1253, and references cited therein.
- [40] K. S. Min, T. Weyhermüller, K. Wieghardt, *Dalton Trans.*, **2004**, 178, and references cited therein.
- [41] (a) J. B. Goodenough, *J. Phys. Rev.*, **79**, **1955**, 564. (b) J. B. Goodenough, *J. Phys. Chem. Solids*, **6**, **1958**, 287. (c) J. Kanamori, *J. Phys. Chem. Solids*, **10**, **1959**, 87.
- [42] (a) R. Schnepf, A. Sokolowski, J. Müller, V. Bachler, K. Wieghardt, P. Hildebrandt, *J. Am. Chem. Soc.*, **120**, **1998**, 2352. (b) P. Chaudhuri, C. N. Verani, E. Bill, E. Bothe, T. Weyhenmüller, K. Wieghardt, *J. Am. Chem. Soc.*, **123**, **2001**, 2213. (c) H. Chun, P. Chaudhuri, T. Weyhermüller, K. Wieghardt, *Inorg. Chem.*, **41**, **2002**, 790. (d) A. K. Nairn, R. Bhalla, S. P. Foxon, X. Liu, L. J. Yellowlees, B. C. Gilbert, P. H. Walton, *J. Chem. Soc. Dalton Trans.*, **2002**, 1253. (e) K. S. Min, T. Weyhermüller, K. Wieghardt, *Dalton Trans.*, **2003**, 1126. (f) S. Mukherjee, E. Rentschler, T. Weyhenmüller, K. Wieghardt, P. Chaudhuri, *Chem. Commun.*, **2003**, 1828. (g) K. S. Min, T. Weyhenmüller, E. Bothe, K. Wieghardt, *Inorg. Chem.*, **43**, **2004**, 2922. (h) S. Ye, B. Sarkar, F. Lissner, T. Sclleid, J. Van Slageren, J. Fiedler, W. Kaim, *Angew. Chem. Int. Ed.*, **44**, **2005**, 2.
- [43] (a) J. Rall, A. F. Stange, K. Hübler, W. Kaim, *Angew. Chem. Int. Ed.*, **37**, **1998**, 2681. (b) F. N. Penkert, T. Weyhermüller, E. Bill, P. Hildebrandt, S. Lecomte, K. Wieghardt, *J. Am. Chem. Soc.*, **122**, **2000**, 9663. (c) P. Ghosh, A. Begum, D. Herebian, E. Bothe, K. Hildebrandt, T. Weyhermüller, K. Wieghardt, *Angew. Chem. Int. Ed.*, **42**, **2003**, 563.

- [44] (a) P. Ghosh, E. Bill, T. Weyhermüller, K. Wieghardt, *J. Am. Chem. Soc.*, **125**, **2003**, 3967. (b) P. Ghosh, A. Begum, E. Bill, T. Weyhenmüller, K. Wieghardt, *Inorg. Chem.*, **42**, **2003**, 3208. (c) K. Ray, T. Weyhermüller, A. Goossens, M. W. J. Crajé, K. Wieghardt, *Inorg. Chem.*, **42**, **2003**, 4082.
- [45] (a) V. Bachler, G. Olbrich, F. Neese, K. Wieghardt, *Inorg. Chem.*, **41**, **2002**, 4179. (b) S. Patra, B. Sarkar, S. M. Mobin, W. Kaim, G. K. Lahiri, *Inorg. Chem.*, **42**, **2003**, 6469.
- [46] (a) O. Hayaishi, M. Nozaki, *Science*, **164**, **1969**, 389. (b) C. A. Tyson, A. E. Martell, *J. Am. Chem. Soc.*, **94**, **1972**, 939. (c) A. Y. Girgis, A. L. Balch, *Inorg. Chem.*, **14**, **1975**, 2724. (d) L. A. deLaire, R. C. Haltiwanger, C. G. Pierpont, *Inorg. Chem.*, **28**, **1989**, 644.
- [47] T. K. Paine, T. Weyhermüller, L. D. Slep, F. Neewe, E. Bill, E. Bothe, K. Wieghardt, P. Chaudhuri, *Inorg. Chem.*, **43**, **2004**, 7324.
- [48] (a) S. K. Larsen, C. G. Pierpont, *J. Am. Chem. Soc.*, **110**, **1988**, 1827. (b) C. L. Simpson, S. R. Boone, C. G. Pierpont, *Inorg. Chem.*, **28**, **1989**, 4379. (c) S. Bruni, A. Caneschi, F. Cariati, C. Delfs, A. Dei, D. Gatteschi, *J. Am. Chem. Soc.*, **116**, **1994**, 1388. (d) A. Caneschi, A. Cornia, A. Dei, *Inorg. Chem.*, **37**, **1998**, 3419.
- [49] P. Chaudhuri, M. Hess, T. Weihermüller, K. Wieghardt, *Angew. Chem. Int. Ed.*, **38**, **1999**, 1095.
- [50] This ligand may exhibit sometimes a more complicated behaviour: P. Chaudhuri, M. Hess, K. Hildebrand, E. Bill, T. Weyhermüller, K. Wieghardt, *Inorg. Chem.*, **38**, **1999**, 2781.
- [51] (a) D. N. Hendrickson, C. G. Pierpont, *Top. Curr. Chem.*, **234**, **2004**, 63. (b) O. Sato, J. Tao, Y. –Z. Zhang, *Angew. Chem. Int. Ed.*, **46**, **2007**, 2152. (c) D. A. Shultz, *Magnetism: Molecules to Materials*, Vol. II (Eds.) J. S. Miller, M. Drillon, Wiley-VCH, Weinheim, **2001**, 81.
- [52] (a) R. M. Buchanan, C. G. Pierpont, *J. Am. Chem. Soc.*, **102**, **1980**, 4951. (b) D. M. Adams, A. Dei, A. L. Rheingold, D. N. Hendrickson, *J. Am. Chem. Soc.*, **115**, **1993**, 8221
- [53] P. Güttlich, A. Dei, *Angew. Chem. Int. Ed.*, **36**, **1997**, 2734.
- [54] (a) D. M. Adams, B. Li, J. D. Simon, D. N. Hendrickson, *Angew. Chem. Int. Ed.*, **34**, **1995**, 1481. b) D. M. Adams, D. N. Hendrickson, *J. Am. Chem. Soc.*, **118**, **1996**, 11515.
- [55] (a) O. Sato, S. Hayami, Z. –Z. Gu, R. Saki, R. Nakajima, A. Fujishima, *Chem. Lett.*, **2001**, 874. (b) O. Sato, S. Hayami, Z. –Z. Gu, K. Takahashi, R. Nakajima, A. Fujishima, *Chem. Phys. Lett.*, **355**, **2002**, 169.
- [56] A. Cui, K. Takahashi, A. Fujishima, O. Sato, *J. Photochem. Photobiol. A: Chem.*, **167**, **2004**, 69.
- [57] (a) S. Decurtins, P. Güttlich, C. P. Khöler, H. Spiering, A. Hauser, *Chem. Phys. Lett.*, **105**, **1984**, 1. (b) O. Sato, S. Hayami, Z. –Z. Gu, K. Takahashi, R. Nakajima, K. Seki, A. Fujishima, *J. Photochem. Photobiol. A Chem.*, **149**, **2002**, 111. (c) O. Sato, S. Hayami, Y. Einaga, Z. –Z. Gu, *Bull. Chem. Soc. Jpn.*, **76**, **2003**, 443. (d) O. Sato, S. Hayami, Z. –Z. Gu, K. Takahashi, R. Nakajima, A. Fujishima, *Phase Transitions*, **75**, **2003**, 779.
- [58] J. Tao, H. Maruyama, O. Sato, *J. Am. Chem. Soc.*, **128**, **2006**, 1790.
- [59] F. V. R. Neuwahl, R. Righini, A. Dei, *Chem. Phys. Lett.*, **352**, **2002**, 408.
- [60] For the analogous spin crossover systems, studies using hydrostatic cells adapted to magnetic susceptibility, Mössbauer, optical absorption and reflectivity methods in conjunction with methods of detection, such as IR, EXAFS and X-ray diffraction techniques, have been successfully used in the last years: P. Güttlich, A. B. Gaspar, V. Ksenofontov, Y. Garcia, *J. Phys. Condens. Matter.*, **16**, **2004**, S1087.
- [61] C. Roux, D. M. Adams, J. P. Itié, A. Polian, D. N. Hendrickson, M. Verdaguer, *Inorg. Chem.*, **35**, **1996**, 2846.
- [62] A. Caneschi, A. Dei, F. F. De Biani, P. Güttlich, V. Ksenofontov, G. Levchenko, A. Hofer, F. Renz, *Chem. Eur. J.*, **7**, **2001**, 3926.
- [63] O. –S. Jung, C. G. Pierpont, *J. Am. Chem. Soc.*, **116**, **1994**, 2229.
- [64] (a) S. P. Solodovnikov, N. N. Bubnov, A. I. Prokofev, *Usp. Khim.*, **49**, **1980**, 1. (b) R. R. Rakhimov, S. P. Solodovnikov, V. S. Pupkov, A. I. Prokofev, *Isv. Akad. Nauk SSSR*, **1990**, 1385.
- [65] C. W. Lange, B. J. Conklin, C. G. Pierpont, *Inorg. Chem.*, **33**, **1994**, 1276.
- [66] A. Yamaguchi, K. Awaga, *J. Mater. Chem.*, **11**, **2001**, 2142.

Objectives

According to the introduction previously described, the **General Objectives** for this Thesis are:

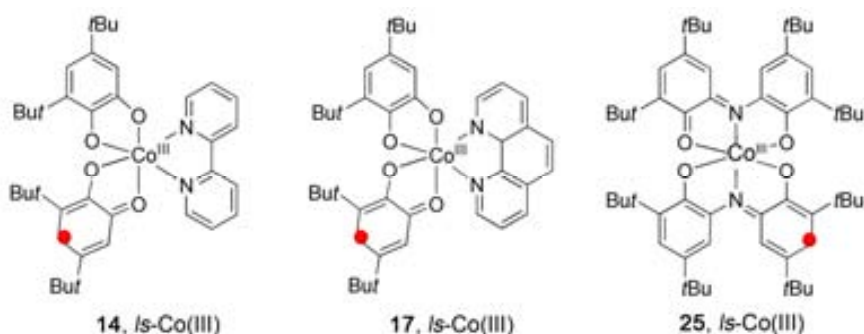
- I.- Gain more insight into the effect of the metal ion and network environment on the VT phenomena. These studies will complement those studies developed by other groups for understanding the different parameters (both intrinsic and extrinsic to the molecule) that influence VT phenomena and the possibility to tune it.
- II.- Asses the existence of more than one type of IET (ligand-to-ligand and ligand-to-metal) taking place simultaneously within the same complex.
- III.- Prepare and characterise new transition metal complexes with optically redox active-ligands on the quest for synergistic and multifunctional properties.

To achieve the objectives previously described, the following **Specific Objectives** were planned:

- I.1.- Study the influence of the metal ion into the VT processes on the series of complexes $[M(\text{Cat-N-SQ})(\text{Cat-N-BQ})]$ where $M = \text{Fe}$ (**24**), Co (**25**) and Ni (**26**).

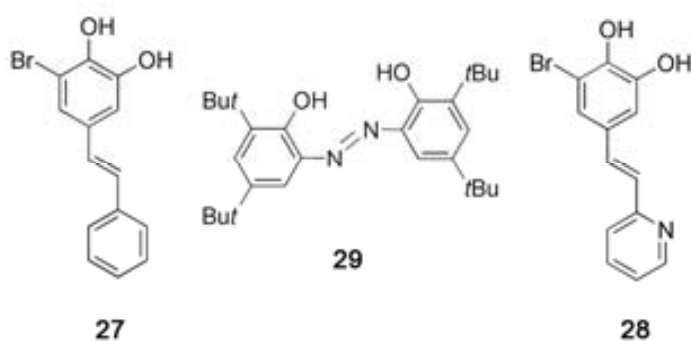


- I.2.- Study the VT behaviour of complexes $[\text{Co}(3,5\text{-DTBCat})(3,5\text{-DTBSQ})(\text{bpy})]$ (**14**), $[\text{Co}(3,5\text{-DTBSQ})_2(\text{phen})]$ (**17**) and $[\text{Co}(\text{Cat-N-SQ})(\text{Cat-N-BQ})]$ (**25**) in different matrices that range from a crystalline material, thin film or solution. The objective is to obtain information of the network environment on the IET process by comparison between them



II.1.- Study and assess the coexistence, for the first time, of two types of IET in a catechol or phenoxylate-base complex (ligand-to-ligand and ligand-to-metal (IET). For this, ligand-to-ligand IET will be studied and analysed in complexes **14**, **24** and **25**.

III.1.- Synthesis and characterisation of ligands **27**, **28** and **29**. Ligand **28** combines a pyridine with a catechol unit that ensures a large electronic delocalization, and therefore, the possibility to exhibit interesting fluorescence properties. Ligand **29** holds an azo group, which are well-known for their use as dyes, optical storage and devices. Both ligands have been designed to obtain VT-based multifunctional complexes.



III.2.- Study the capacity of the previous ligands to act as chromogenic pH sensors thanks to the presence of the pyridine (**28**), catechol (**27** and **28**) and phenoxylate (**29**) moieties, which exhibit a remarkable acid-base activity.

III.3.- Preparation of the corresponding cobalt complexes, and study the synergistic effects between IET and optical properties.

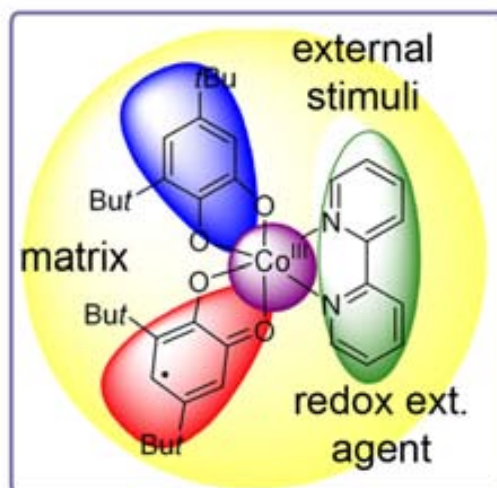
Results and Discussion

Chapter | 2

Valence Tautomerism: Metal Ion and Environmental Effects

Abstract

Valence tautomeric complexes combining electro-active ligands and transition metal ions are known for exhibiting two nearly degenerated electronic states (tautomers) with localised electronic structures. An IET between both redox active units activated by an external stimulus, such as photons, temperature and/or pressure, brings to a reversible interconversion between the degenerated electronic states. The equilibrium between these electronic states has been shown to have an important sensitivity to different parameters. These parameters can be inherent to the molecule or to the medium. These factors are the metal ion, the electro-active ligand, the counterligand, the partial oxidation or reduction of the complex and the nature of the matrix in which the molecule is surrounded. In this chapter, an overview of these factors is given in the Introduction: From them our experimental results are giving an special attention to the study of the metal ion and the effect of the network environment.



2.1 Introduction

Traditionally, the presence of valence tautomerism (VT) has been attributed to the good matching between two main actors: the redox-active ligand and the transition metal ion. For this reason, the potential candidates to exhibit VT were always seeking to fulfil the following requirements: first, the degree of covalency in the interaction between metal ion and electro-active ligand must be low. And second, the energy of their frontier orbitals must be similar. However, other factors, such as the nature of the counter ligand, the charge of the complex and/or the network environment, have been shown a marked influence on the IET process. A detailed review of all these factors can be consulted in Articles I and VII. Article I: *Valence Tautomerism: New Challenges for Electroactive Ligands*, Eur. J. Inorg. Chem., **2005**, 2957. Article VII: *Valence Tautomerism: More Actors than Just Electroactive Ligands and Metal Ions*, Comptes Rendues Chimie. **2008**, (Submitted).

2.1.1 Principal actors: metal ion and electro-active ligand

As already mentioned in Chapter 1, the number of electro-active ligands leading to the observation of VT is rather limited. Among them, catecholate and phenoxylate-based ligands are those most broadly used. A review of VT complexes obtained from the association of these ligands with different metal ions is presented in this chapter.

2.1.1.1 Catecholate complexes.

Because of the rich electrochemical behaviour of quinone or quinone-type ligands, most of the VT complexes thus far reported are based on this family of ligands with a series of transition metal ions.¹ As far as the metal ion is concerned, the pair Co(II)/Co(III) is one of the most effective in showing VT phenomena. Cobalt complexes bearing quinone-based ligands have exhibited not only localised structures but also a good matching between the energy of its frontier orbitals with those of the redox-active ligand. The simplest mononuclear cobalt-quinone complexes undergoing VT belong to the family of ionic complexes with the general formula [Co(cth)(Phendiox)]·Y (**18**·Y), where cth is a tetraazamacrocyclic ancillary ligand, Phendiox is 9,10-dioxophenanthrene and Y can be PF₆⁻, BPh₄⁻ or I⁻.² Other cobalt complexes that show VT phenomena are systems with a general formula [Co(DTBQ)₂(N-N)], where N-N is a ditopic nitrogen-based ligand and DTBQ is di-*tert*-butylquinone that can exist in two anionic forms: 3,5- (**10**²⁻, 3,5-DTBCat²⁻) or 3,6-di-*tert*-butylcatecholato (**30**²⁻, 3,6-DTBCat²⁻) and the corresponding semiquinone (**10**¹⁻, 3,5-DTBSQ⁻, **30**¹⁻, 3,6-DTBSQ⁻) forms.^{3,4,5} In addition to monomeric complexes, the synthesis of binuclear cobalt-dioxolene complexes has also been achieved. For example, the use of a modified (diimine)-bipyridine ligand as an electronic coupling of two cobalt centres led to the description of the first dinuclear VT complex [{Co(3,5-DTBCat)(3,5-DTBSQ)}₂(NN^Y)] (**31**). This complex, in which both cobalt units are bridged by the modified bis-bipyridine ligand, shows three possible tautomeric forms up to 500 K.⁶ Similar results were

observed for another cobalt bis(dioxolene) complex with formula $[(\text{Co}(3,5\text{-DTBCat})(3,5\text{-DTBSQ}))_2(4,6\text{-di-}2'\text{-pyridylpyrimidine})]$ (**32**) by near-IR absorption spectroscopy in a thin amorphous film.⁷ Also, Pierpont *et al.* studied modified bridging catecholate ligands to tune the critical temperature (T_C) in a related family of dinuclear complexes $[\text{Co}_2(\text{bpy})_4(\text{thM})](\text{PF}_6)_2$ (**33**), where bpy is 2,2'-bipyridine and thM is a derived 3,3',4,4'-tetrahydroxybenzaldazine ligand.⁸ T_C is defined as the temperature at which there are equal amounts of both electronic isomers. Simultaneously, Dei *et al.* reported the binuclear complex $[\{\text{Co}(\text{cth})\}_2(\text{DHBQ})](\text{PF}_6)_3$ (**34**), where cth is a voluminous aza type ligand and DHBQ is the deprotonated form of 2,5-dihydroxy-1,4-benzoquinone. This complex presents a gradual thermal tautomeric transition around 175 K as well as a quantitative VT photoconversion.⁹

In addition to mono- and binuclear systems, different polynuclear tautomeric complexes have also been reported. For example, Pierpont *et al.*⁴ reported a coordination polymer with formula $[\text{Co}(3,6\text{-DTBQ})_2(\text{pyz})]_n$ (**35**), where pyz is pyrazine, that exhibited a temperature-induced interconversion in the solid state. This VT transition is accompanied by variations in the bond lengths. Interestingly, hysteresis phenomena for a coordination polymer was recently reported by Schultz *et al.*¹⁰ This polymer with formula $[\text{Co}(\text{phen})\text{L}]0.5\text{CH}_2\text{Cl}_2$ (**36**), where L is 3,5-bis(3',4'-dihydroxy-5'-*tert*-butylphenyl)-1-*tert*-butylbenzene, exhibits cooperative properties that lead to thermal hysteresis in VT equilibrium, even though the transition could be classified as gradual. Finally, a new strategy based on coordination polymerization and precipitation in a poor solvent has been recently reported. The main objective of this strategy was the obtaining of a cross-linked VT metal-organic nanospheres formed by the polymer with general formula $[\text{Co}(3,5\text{-DTBSQ})(3,5\text{-DTBCat})(\text{bix})]_n$ (**37**), where bix is 1,4-bis(imidazol-1-ylmethyl)benzene.¹¹ A schematic representation of the nanospheres formation is shown in Figure 2.1.

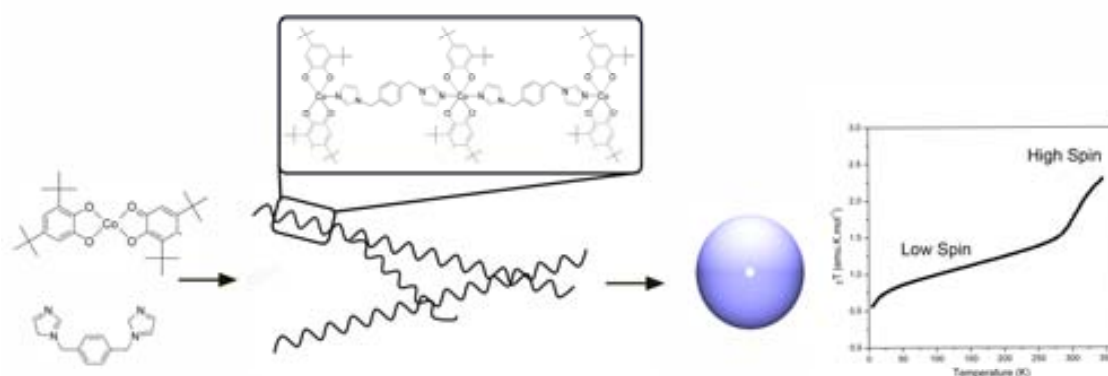
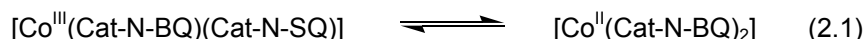


Figure 2.1: Coordination polymerization-precipitation technique used to obtain VT nanoscale metal-organic particles with general formula $[\text{Co}(3,5\text{-DTBSQ})(3,5\text{-DTBCat})(\text{N-N})]$, where N-N stands for the 1,4-bis(imidazol-1-ylmethyl)benzene ligand (**37**). Representation of the χT values as a function of T for the amorphous nanospheres, showing the transition between both electronic isomers.

2.1.1.2 Phenoxylate-like Complexes.

In spite of the large number of phenoxylate-based complexes so far reported, only a few of these examples have exhibited VT. One of these examples was reported by Wiegardt *et al.*,¹² who described an octahedral iron complex $\{\text{Fe-NO}\}^7$ with formula $[\text{L}^{\text{Pr}}\text{Fe}(\text{NO})\cdot 2.5\text{CH}_2\text{Cl}_2]$ (**38**, Figure 2.2a), where L^{Pr} is 1-isopropyl-4,7-(4-tert-butyl-2-mercaptobenzyl)-1,4,7-triazacyclononane). This complex showed the first temperature dependent $S=1/2$ to $S=3/2$ spin equilibrium in solid state. Other phenoxylate-type complexes exhibiting VT equilibria in solution were the N,S-coordinated *o*-aminothiophenolate cobalt (**39**), the S,S-coordinated *o*-dithiolate iron (**40**)¹³ complexes and the trinuclear nickel complex **41** (Figure 2.2 b-d).¹⁴ Among them, it is interesting to highlight the trinuclear nickel complex that exhibit a VT phenomena where only one of the three Ni(III) metal ions presents the conversion to Ni(II). Therefore two VT isomers can exist as is represented in Figure 2.2d. Finally, a poly(propylene imine) (PPI) dendrimer complexed with Cu(II) metal ion showed the appearance of a dimer structure formed by two dissimilar Cu(II) dendrimeric complexes ($[\text{Cu}(\text{H}_2\text{O})_6]^{2+}$ and $\text{Cu}^{\text{II}}\text{-PPI}$).¹⁵ EPR experiments confirm a VT behaviour below 30 K, allowing to the formation of the MV specie ($\text{Cu}^{\text{II}}\text{L-NO}_3^{\cdot-}\text{-Cu}^{\text{I}}\text{L}$) (**42**) with an activation energy of 0.35 meV (40 K) associated to a tunnel effect IET phenomena.

However, the most important phenoxylate ligand that has been used to synthesise VT complexes is the tridentate Schiff-base ligand¹⁶ Cat-N-BQ (**10¹**). Compared to the quinone-based ligands, this tridentate ligand shows a richer electrochemical behaviour, as we mentioned in Chapter 1 (Figure 1.8). Complex $[\text{Co}^{\text{III}}(\text{Cat-N-BQ})(\text{Cat-N-SQ})]$ (**25**)¹⁷ was described in 1988 by Pierpont *et al.*, though the first account of VT phenomenon for this complex (Eq. 2.1) in solution was observed ten years later by Prof. A. Dei around room temperature (300 K).¹⁸ In a subsequent work, the same authors showed that this complex also exhibits a tautomeric interconversion in the solid state at much higher temperature, with a transition that starts at approximately 400-410 K.¹⁹



In summary, the number of catecholate and phenoxylate based complexes exhibiting VT are considerable. Such a large number of examples embrace from monomeric to polymeric species as well as different behaviours both in solution and in solid state. It is also important to emphasise that although most of the examples so far described use the cobalt metal ion, other metal ions as the iron or nickel have also been successfully used. However, in spite of the large number of examples, a systematic study facing the effect of the nature of the metal ion in VT is missing.

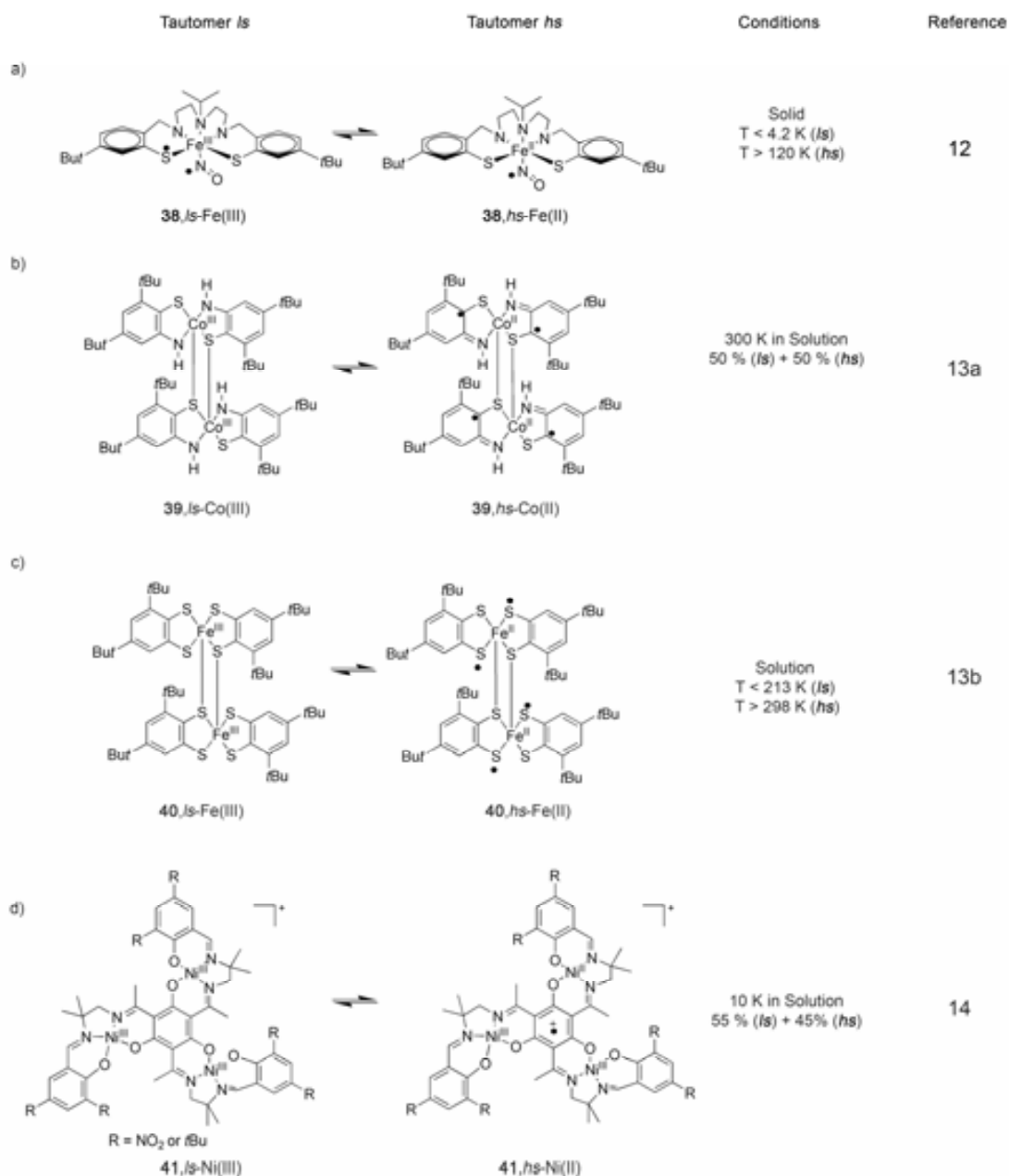


Figure 2.2. Examples of phenoxylate-type complexes that exhibit VT phenomena.

2.1.2 Secondary actors

In addition to the nature of the electro-active ligand and the metal ion, several other factors that can modulate the observation of VT have also been detected along all these years. Thus, the same complex may exhibit considerable shifts on the VT process depending on other structural and environmental parameters.



Figure 2.3. Schematic representation of the different factors that have been shown to modulate VT represented as casual ordered/disordered puzzles. Such representation is intended to emphasise the need for a good understanding of the effect of these parameters to fully understand and predict VT.

The external factors that can affect the VT equilibrium can be grouped into three main areas of influence: the counter-ligand, the charge-induced, and the environmental effects. It is the aim of the following section to revise more in detail such factors, which must be taken into consideration for a proper evaluation of potential VT candidates. A schematic representation of the different factors that have been shown to modulate VT is represented in Figure 2.3.

2.1.2.1 Counter-ligand effect

Most of the work devoted to elucidate the role played by the counter-ligand have been performed on the family of complexes with general formula $[\text{Co}^{\text{III}}(3,5\text{-DTBCat})(3,5\text{-DTBSQ})(\text{N-N})]$. Even though the ditopic N-N' nitrogen-based ligand is not directly involved in the electron transfer process, Hendrickson *et al.*,²⁰ Pierpont *et al.*,²¹ and Dei *et al.*²² have concluded that the donor-acceptor character of these auxiliary ligands can be used to systematically shift the T_C for the equilibrium shown in Eq 2.2.



For example, the systematic variation on the series of complexes with the general formula $[\text{Co}(\text{py}_2\text{X})(3,5\text{-DTBSQ})_2]$ ($\text{X} = \text{O}$ (**43**), Te (**44**), Se (**45**) and S (**46**)) has shown to clearly shift T_C from 110 K to 370 K respectively, inducing a large hysteresis effect even for **43**.^{21a} An identical effect was also reported by Sato *et al.*²³ By choosing an auxiliary ligand with a strong coordination field, these authors published complex $[\text{Co}^{\text{III}}(3,5\text{-DTBSQ})(3,5\text{-DTBCat})(\text{dpa})]$ (**47**), where dpa is N,N-bis(2-pyridylmethyl)amine, which shows one of the highest T_C values so far reported for a VT complex (around 380 K, Figure 2.4a).

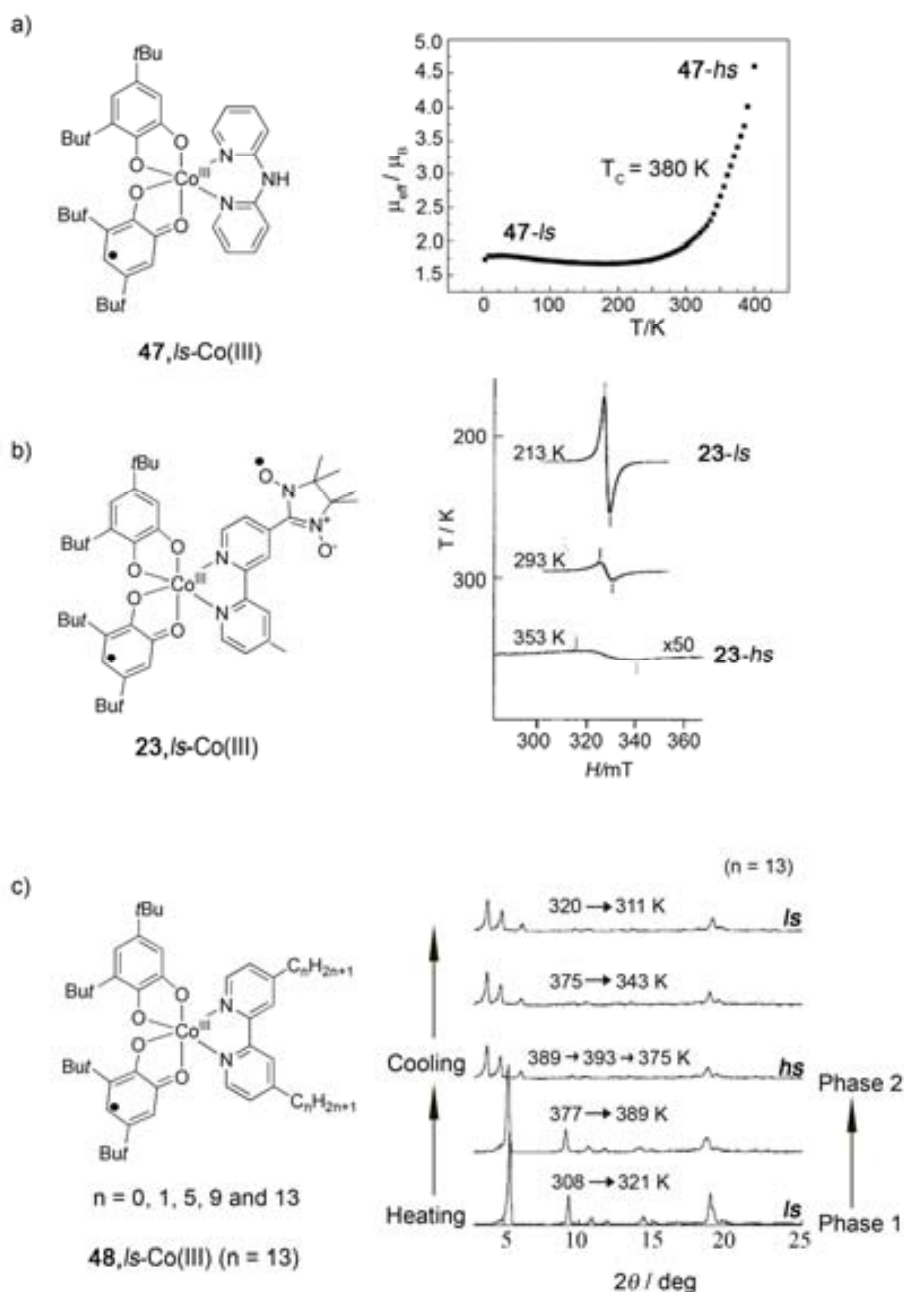


Figure 2.4. Representative examples of the counter-ligand effect on the VT for complexes with the general formula $[\text{Co}(3,5\text{-DTBCat})(3,5\text{-DTBSQ})(\text{N-N})]$. A variation of such counter-ligand may induce the obtaining of a high interconversion temperature (**47**, Figure 2a), a considerable T_c shift (**23**, Figure 2b) or even modifications of the fraction of both electronic isomers induced by a crystal phase transition (**48**, Figure 2c).

Another interesting example of the counterligand effect on the VT processes was described by Awaga *et al.*,²⁴ who reported VT in the spin-labelled complex $[\text{Co}^{\text{II}}(\text{nnbpy})(3,5\text{-DTBSQ})_2]$ (**23**), where nnbpy is a bipyridine substituted nitronyl nitroxide radical. Even though the magnetic measurements indicates a tautomeric interconversion above 250 K (Figure 2.4b), the ligand radical behaves as a Curie spin over the whole temperature region. Finally, an interesting counter-ligand effect was also observed for a series of complexes with formula

[Co(*C_nbpy*)(3,5-DTBQ)₂] (**48**, Figure 2.4c), where the bpy counter-ligand is modified with alkyl chains ranging from 0 to 13 carbon atoms. For this family of complexes, VT equilibrium is tuned by increasing the number of carbon atoms. Furthermore, the elongation of chain lengths induces crystal phase transition for the longest alkyl chains examples, observing cooperativity with the VT phenomena.²⁵ All these studies have shown that the charge distribution in metal-quinone complexes is sensitive to the balance of metal and quinone orbital energies, tuned by the appropriate choice of the counterligand. Of special relevance is the possibility to use such modulation for the development of VT complexes that show hysteresis if a future molecular switching device based on these complexes needs to be realised. Finally, it is worth to mention that these counter-ligand effects have been found with other transition metal ions. For example, the acceptor characteristics of the counterligand in a series of copper-quinone synthetic model with the general formula [(Qⁿ⁻)Cuⁿ⁺L] have been studied due to their relevance not only for VT purposes but also on other biological and commercial processes.^{26,27,28,29}

2.1.2.2 Charge-induced effects

Other factors that can affect VT equilibrium are charge-induced effects, including the nature of the counter-ion and redox processes. One of the few examples where the nature of the counter-ion has been shown to modify VT is that of the ionic (charged) cobalt-quinone complexes **18**·Y.² Dei *et al.* demonstrated that the volume and columbic interaction of the counterion Y⁻ varies the *T_C* of temperature and pressure-induced VT equilibrium. Another example of the counterion effect was reported by Cador *et al.*¹⁹ on the series of complexes [M(tpy)L]Y, where M is Ni (**49**) or Co (**50**), tpy is 2,2':6',2''-terpyridine, L is Cat-N-SQ or Cat-N-BQ and Y can be PF₆⁻ or BPh₄⁻. It is found that the *T_C* for the interconversion in the cobalt case is strongly affected by the counterion. Whereas no VT transition was detected for the tetraphenylborate **50**·BPh₄ compound, the related hexaphenylphosphate **50**·PPh₆ complex exhibits a VT interconversion in solid state around 200 K, as confirmed by magnetic measurements. Interestingly, the VT interconversion for this complex in solution takes place at lower temperatures, as shown by spectrophotometric measurements.

Another important characteristic that has been exploited over the last few years is the redox activity of the electro-active ligands. Indeed, the redox activity of the ligands not only allows for the existence of VT but also for additional switching capacities resulting from an electrochemical process. Such a strategy has been shown to be very useful for the systematic tuning of the *T_C* as well as for establishing arrays of four or six members depending on the redox possibilities of the metal ion. The first example of redox-tuned VT was based on the reduction of complex **14**.³⁰ Interestingly, the resulting reduced complex exhibited a temperature-dependent VT equilibrium. This fact allowed establishing an array of four states (Figure 2.5a), showing different optical and magnetic ground states controlled by two temperature-induced VT equilibria and two reversible redox processes. The possibility of entering the cycle at each state and advancing through the square array in a clockwise and counter-clockwise direction was

also established. Following an identical approach, Rovira *et al.*³¹ also established an array of four states (Figure 2.5b) based on the oxidation of the tautomeric complex [Co^{III}(Cat-N-BQ)(Cat-N-SQ)] (**25**). Later on, three different oxidation states, where the manganese metal ion can be in the most frequently forms [Mn(IV)-Mn(III)-Mn(II)], allowed to expand the array from four to six members with complex **51** (Figure 2.5c).³²

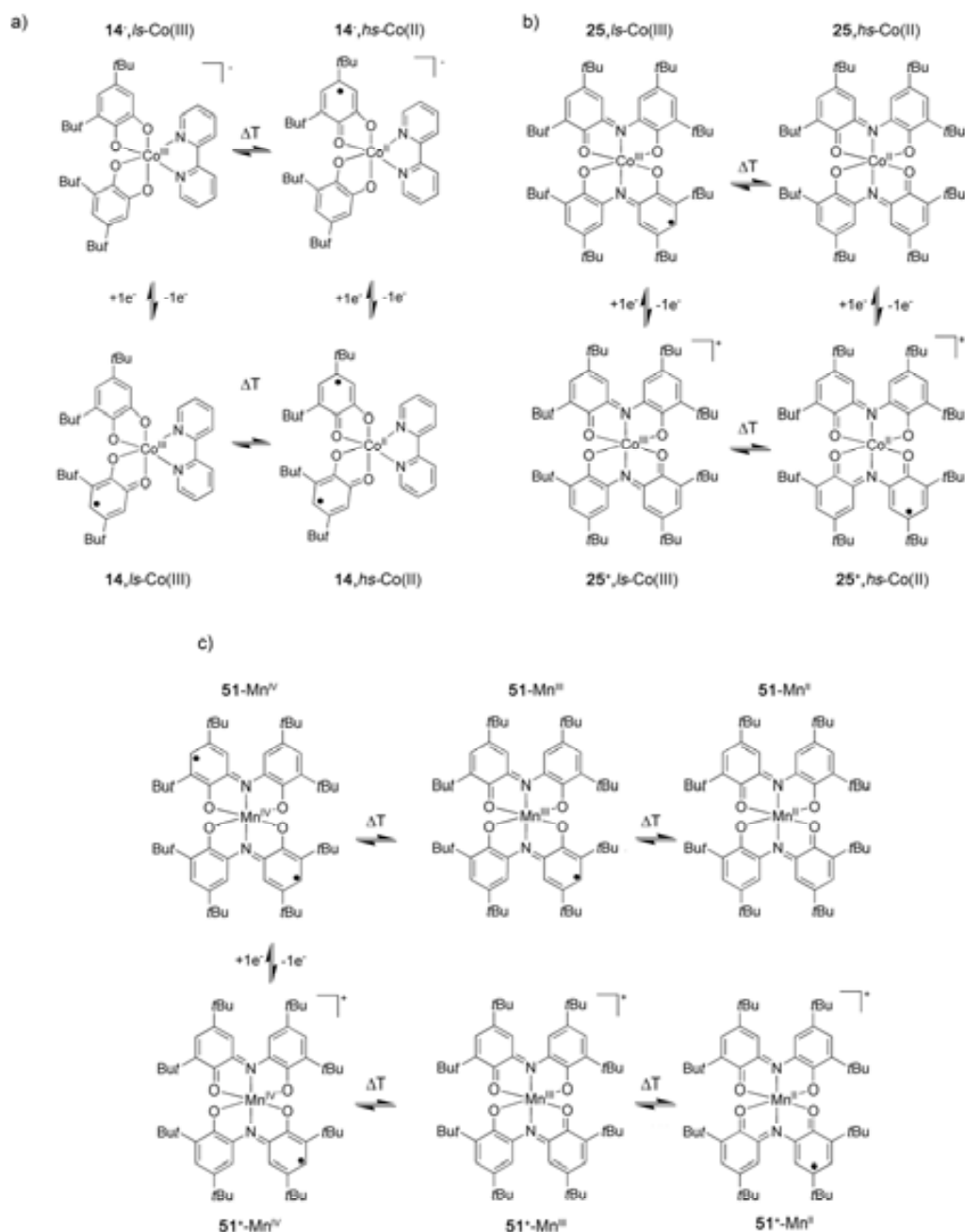


Figure 2.5. Array of four states showing different optical and magnetic properties controlled by two temperature-controlled VT equilibria and two reversible redox processes for complex [Co(3,5-DTBSQ)(3,5-DTBCat)(bpy)] (**14**,*ls*-Co(III)) (a) and complex [Co(Cat-N-SQ)(Cat-N-BQ)] (**25**,*ls*-Co(III)) (b). (c) Array of six states with different optical and magnetic properties controlled by two temperature and a reversible redox processes for complex [Mn(Cat-N-SQ)₂] (**51**-Mn(IV)).

2.1.2.3 Environmental Effects

Environmental effects, such as the solvent, the degree of crystallinity and the matrices, have been shown to clearly influence on the VT phenomena. For example, the effect of the nature of the solvent on the VT equilibrium has already been studied for the family of complexes $[\text{Co}^{\text{III}}(\text{Cat})(\text{SQ})(\text{N-N})]$.²⁰⁻²² Complexes with formula $[\text{Co}(3,5\text{-DTBCat})(3,5\text{-DTBSQ})(\text{N-N})]$, where N-N is 2,2'-bipyridine (bpy, complex **14**) or 1,10-phenanthroline (phen, complex **17**), exhibit VT transition.²⁰ These complexes can be interconverted by means of different external stimuli between a high-spin $hs\text{-}[\text{Co}^{\text{II}}(\text{SQ})_2(\text{N-N})]$ ($S_{\text{complex}} = 3/2 + 2 \cdot S_{\text{rad}} = 1/2$) form and a low-spin $ls\text{-}[\text{Co}^{\text{III}}(\text{Cat})(\text{SQ})(\text{N-N})]$ ($S_{\text{rad}} = 1/2$) form. This interconversion may take place both in solution and in the solid state with significant differences. Indeed, whereas in solution the interconversion takes place over a large temperature range, in a crystalline matrix they can interconvert cooperatively on a narrow temperature range of 40 K. For instance, it was shown that for complex **17**- $\text{C}_6\text{H}_5\text{CH}_3$,²⁰ the tautomeric interconversion between the **17**, $ls\text{-Co(III)}$ and **17**, $hs\text{-Co(II)}$ isomers can be reversible driven with temperature and monitored by large changes in the magnetic susceptibilities that occurs abruptly within a narrow temperature range of around 30 K. Similar differences between the VT of complex **25**, $hs\text{-Co(III)}$ have already been described.^{19,33} For this later example, the VT takes place in solid state with a difference of at least 150 K compared to the same interconversion in solution. Moreover, whereas no discrepancies between the results obtained in deuterated and non-deuterated solvents were found, appreciable differences were revealed between the lifetimes determined for $[\text{Co}^{\text{III}}(\text{Cat-N-BQ})(\text{Cat-N-SQ})]$ (**25**) in chloroform and those obtained in dichloromethane by time-resolved spectroscopic characterization.³⁴

The variations found for the behaviour of these complexes in solution and in solid state are not atypical. In fact, it is important to emphasise that while most of the VT complexes exhibit a temperature-dependent interconversion in solution, the number of examples exhibiting a VT interconversion in the solid state is rather limited.³⁵ Such variations between the behaviour in solution and solid state have been attributed by Dei *et al.*³⁶ to variations of the entropy factor, as deduced by comparison of the thermodynamic quantities obtained for the same VT process in a toluene solution and in solid state. And this is not surprising at all. The VT interconversion from the $ls\text{-Co(III)}$ to the $hs\text{-Co(II)}$ leads to a gain in electronic entropy (ΔS_{elec}) due to the higher spin state degeneracy of the $hs\text{-Co(II)}$ form and the longer metal-ligand bond lengths of the $hs\text{-Co(II)}$ tautomer, which results in lower energy vibrations and a higher density of vibrational states. The spin state degeneracy is not expected to vary with the different solvents under study. However, the variations on the metal-ligand bond lengths, i.e., the density of vibrational states, are expected to be strongly dependent on the surrounding matrix. For this reason, the presence of solvate molecules within the crystalline network and their effects on the phonon relaxation play a critical role.

2.1.3 Summary

To summarise the introduction, the effect of different factors on VT has been established. Some of these parameters, such as the counter-ligand, have been studied and analysed in detail. However, there are other important parameters that either have not been studied or simply (in spite of a large number of examples described) have not been rationalized. If a real knowledge of VT must be achieved, further studies that reveal a deeper knowledge on such parameters are highly required.

Among them, there are two parameters especially interesting. The first one is the role played by the metal ion, or in other words, how we can tune the VT by changing the nature of the metal ion. And the second one is the role played by the matrix (solution, crystalline or amorphous material and embedded into a polymeric matrix) in a given VT complex. Therefore, there is a question that remains an open issue: **how do solvate molecules and/or the nature of the network affect the vibronic relaxation of the molecules in solution and in solid state?** There are previous works that have partially faced this challenge. For example, the family of complexes reported by Dei *et al.*,² $[M(\text{cth})(\text{Phendiox})]\cdot Y\cdot\text{solv}$ ($M = \text{Co}$ (**18**)). The critical interconverting temperature was found to depend not only on the nature of the counterion Y but also on the nature of the solvent trapped in the lattice. Within this scenario, the differential “softness” that the solvent molecules are giving to the crystalline network is clearly affecting the vibrational relaxation of the molecules. In spite of all the previous precedents that reflect the considerable influence of the environment on the VT process, a systematic study that shed light on the origin of such variations is missing. Both challenges were faced on this work, and the results are summarized next.

2.2 Results

2.2.1 Metal ion influence: VT on the series of complexes $[M(\text{Cat-N-SQ})(\text{Cat-N-BQ})]$; $M = \text{Fe}$ (**24**), Co (**25**), Ni (**26**).

The temperature dependence of the series of complexes $[M(\text{Cat-N-SQ})(\text{Cat-N-BQ})]$; $M = \text{Fe}$ (**24**), Co (**25**), Ni (**26**) has been analysed and studied by different spectroscopic and magnetic techniques, both in solution and in solid state. All these results are presented in the Article VI: *Intramolecular Electron Transfer in the Series of Mixed-Valence Complexes $[M^{III}(\text{Cat-N-SQ})(\text{Cat-N-BQ})]$ ($M = \text{Fe}, \text{Co}, \text{Ni}$) bearing Non-Innocent Ligands: a Combined Experimental and Theoretical Study*. Chem. Eur. J., **2008**. (*In preparation*). This work has been done in collaboration with Prof. Andrea Dei from the University of Firenze (physical characterisation), Dr. Motohiro Nakano from Osaka University (physical interpretation), Marie Laure Bonet and Dr. Vincent Robert from l'École Normale Supérieure de Lyon (theoretical calculations), Dr. Jean-Pascal Sutter from the Laboratoire de Chimie de la Coordination (spectroscopic measurements) and Dr. Miquel Cabañas from the Universitat Autònoma de Barcelona (NMR spectroscopy).

2.2.1.1 Variable –temperature UV-visible spectroscopy

Variable-temperature UV-Vis spectra of a toluene solution of cobalt complex **25** was obtained in the 203-360 K temperature range. The choice of toluene is justified both on the basis of the high solubility of the complex in this solvent and its relative large working temperature range. A schematic representation for the VT equilibrium of complex **25** is shown in Figure 2.6.

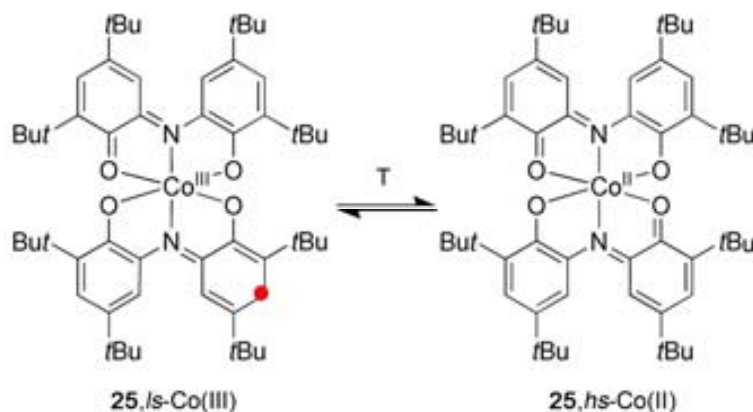


Figure 2.6. VT equilibrium of complex **25** induced by temperature.

At low temperatures, the UV-Vis spectra of complex **25** show bands at 391 nm, 439 nm and 533 nm characteristic of the **25,ls-Co(III)** ($S=1/2$) tautomer. An increase of the temperature promotes an IET from the ligand to the metal ion. Indeed, one of the ligands is oxidised by one electron from the radical Cat-N-SQ²⁻, which at the same time is reduced to the diamagnetic form Cat-N-BQ¹⁻ (Eq. 2.1). As a consequence, the intensity of such bands decreases and bands at 721 nm and 797 nm characteristic of the **25,hs-Co(II)** tautomer increase in intensity (Figure 2.7c). Furthermore, two isobestic points appear at 856 nm and 590 nm, indicating that at least two species are interconverting under the studied temperature range.

In a previous work, Girgis *et al.*³⁷ predicted that most of the bands observed in the electronic spectra of complexes with general formula ML₂, where L is Cat-N-BQ¹⁻ and/or Cat-N-SQ²⁻, are associated with electronic transitions within the ligands though modulated specially at higher wavelengths depending on the nature of the metal ion. Among them, of special interest is the band centred around 390 nm, which has been tentatively attributed to the radical character of the Cat-N-SQ²⁻ ligand. This characteristic band has also been observed in other organic radicals.³⁸ The intensity of this band decreases on the interconversion from the **25,ls-Co(III)** to the **25,hs-Co(II)** since no radicals are observed in the last tautomer. Therefore, the visualization of such a band can give direct information on the radical character of the ligand and on the electronic distribution of the complex at a given temperature.

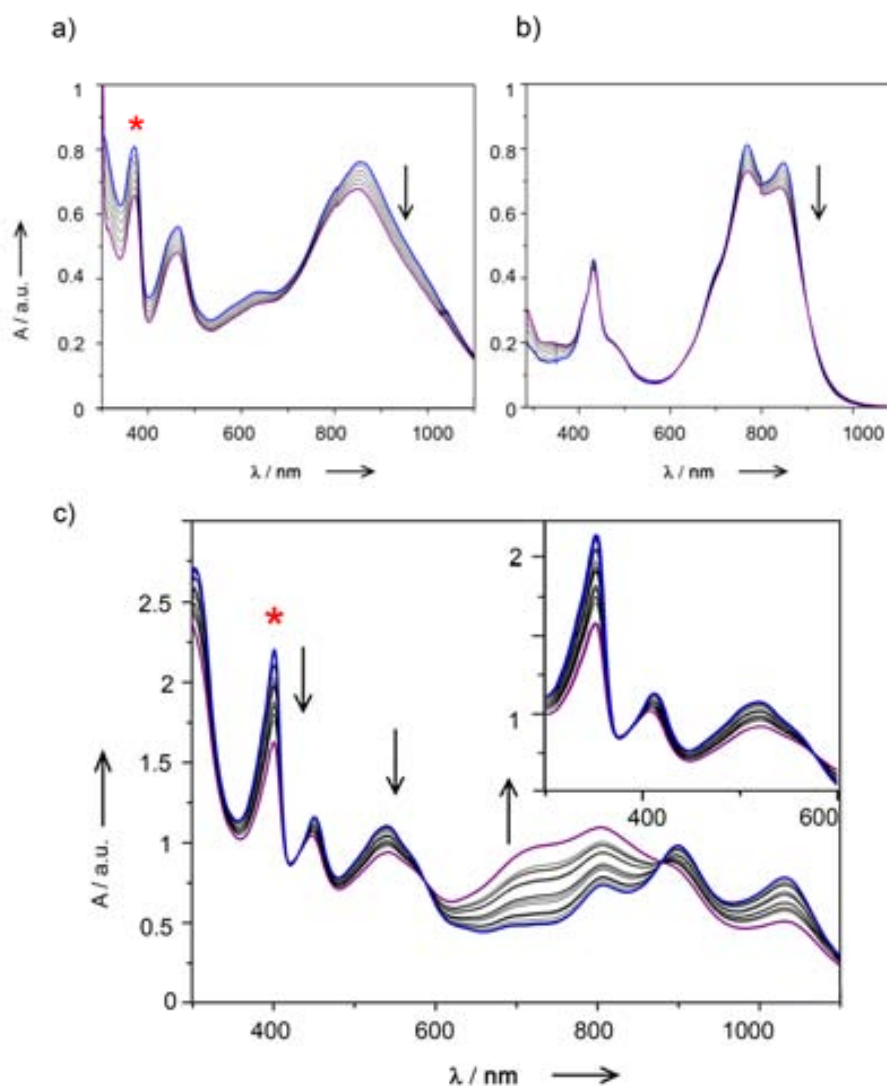


Figure 2.7. Variable-temperature UV-Vis spectra (temperature range: 203 K (blue line)-363 K (violet line)) for complexes **24** (a) **26** (b) and **25** (c). The characteristic band associated to the presence of the ligand in its radical form is marked with an asterisk.

To further support this assignment, the UV-Vis spectra of complexes [Ga(Cat-N-SQ)(Cat-N-BQ)] (**52**) and [Zn(Cat-N-BQ)₂] (**53**) were also recorded and studied for comparison purposes. Complex **52** has one radical Cat-N-SQ²⁻ ligand, and therefore, is expected to exhibit the band centred around 390 nm, whereas complex **53** is not. Confirming this hypothesis, the UV-Vis spectrum at 298 K of complex **53** shows two intense bands at 793 nm and 736 nm, which are similar to those observed for the cobalt complex **25**, *hs*-Co(II) tautomer. Importantly, no band around 350-400 nm was detected since both ligands are present in the non-radical form Cat-N-BQ¹⁻. On the contrary, the electronic spectra of complexes **25**, *ls*-Co(III) and **52**, *ls*-Ga(III) are dominated by an intense transition at 390 nm associated to the presence of the Cat-N-SQ²⁻ radical ligand.

Keeping this in mind, the variable-temperature UV-Vis spectra of a toluene solution of complex **24**,*l*-Fe(III) was also studied (Figure 2.7a). Bands at 357, 451 and 853 nm with shoulders around 560 nm, 620 nm, and 790 nm can be observed in the low-temperature regime. The observation of a band at 357 nm is an indication that the iron complex **25**,*l*-Fe(III) most likely bears a radical Cat-N-SQ²⁻, so it can be formulated as [Fe(Cat-N-SQ)(Cat-N-BQ)]. An increase of the temperature only induces a slight variation of the intensity of all bands, without the presence of any isobestic point. Such spectral variations may be associated to variations of the solution viscosity, among others, rather than to the existence of VT. Therefore, complex [Fe(Cat-N-SQ)(Cat-N-BQ)] remains in the **24**,*l*-Fe(III) tautomeric form at least along the considered temperature range. On the contrary, the variable-temperature UV-Vis spectrum of the nickel complex **26**,*h*s-Ni(II) (Figure 2.7b) exhibits bands at 432 nm, 766 nm and 846 nm with a shoulder around 690 nm. Moreover, once more, an increase of the temperature does not induce any considerable change on the electronic spectrum. Only a slight variation of the intensity bands is observed. The presence and intensity of the two bands at higher wavenumbers as well as the lack of the characteristic radical band are an indication that the nickel complex remains in the **26**,*h*s-Ni(II) tautomeric form [Ni(Cat-N-BQ)₂] over the whole temperature range studied. In fact, its spectrum is quite reminiscent to these observed for complex **53** which is not expected to exhibit VT.

2.2.1.2 Magnetic measurements in solution: Evans Method

The magnetic behaviour of complexes **24**, **25** and **26** in solution were studied by ¹H-NMR and the Evans Method.³⁹ This technique is applicable to the measurement of the magnetic susceptibility of paramagnetic species in solution, and it is based on the frequency shift occasioned in the NMR signal of a standard compound (for instance, tetramethylsilane (TMS)) by the additional magnetic field of the tested paramagnetic species. For more information on this technique, please refer to Annex II.

The NMR samples for susceptibility measurements using the Evans Method were prepared by dissolving a weighted amount of complex in a measured volume of solvent, as it is explained in the Annex II. All the experiments were performed in deuterated toluene (Tol-D⁸) solvent. The concentration of the paramagnetic solute was in the range of 1-2 mg·mL⁻¹. Critical Tables⁴⁰ were used to correct the temperature-dependent density changes of the solvent. A solution of the complex studied was transferred into a tube which contains a concentric capillary with a deuterated diamagnetic solvent and one drop of TMS. The different signal shifts found for the methyl groups of the TMS were used in order to determine the magnetic susceptibility in solution.

The effective susceptibility (μ_{eff}) vs. temperature plots for complexes **24**, **25** and **26** obtained by applying the Evans method are shown in Figure 2.8. The most relevant values from the study are listed in Tables II.1 and II.2 of the Annex II.

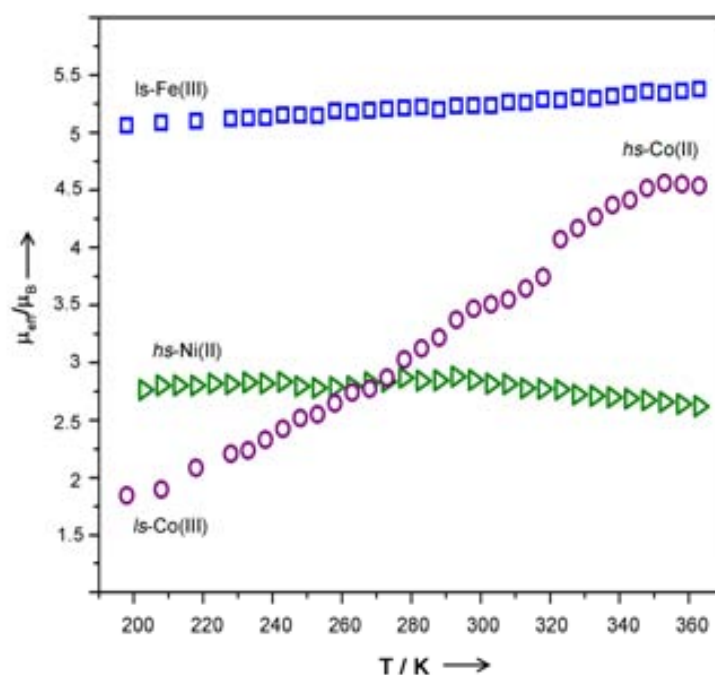


Figure 2.8. Representation of μ_{eff} vs T for complexes **24** (\square), **25** (\circ) and **26** (Δ) obtained through the Evans Method under the same range of temperatures than in the UV-Vis experiments (from 203 K to 363 K).

At low temperatures, the μ_{eff} vs. T plot of complex **25** exhibits a value of $1.82 \mu_{\text{B}}$, which is close to the theoretical value of $1.73 \mu_{\text{B}}$ expected for the single unpaired electron of the **25**,*ls*-Co(III) ($S=1/2$) tautomer. An increase of the temperature induces a gradual increase of μ_{eff} until a maximum value of $4.64 \mu_{\text{B}}$ is reached at 353 K. This value is close to the theoretical value expected for a Co(II) octahedral specie with a $S=3/2$. This fact is in agreement with the existence of the equilibrium between the tautomers **25**,*ls*-Co(III) ($S=1/2$) and **25**,*hs*-Co(II) ($S=3/2$), as previously observed by UV-Vis spectroscopy. Under these conditions, one may track the thermodynamic parameters associated with the rearrangement of the electronic configuration in writing $\chi_{\text{m}}T$ as follows,

$$\chi_{\text{m}}T = \chi_{\text{m}}T_{\text{ls-Co(III)}} + Y_{\text{hs-Co(II)}} (\chi_{\text{m}}T_{\text{hs-Co(II)}} - \chi_{\text{m}}T_{\text{ls-Co(III)}}) \quad (2.3)$$

considering

$$Y_{\text{hs-Co(II)}} = 1 / [\exp(\Delta H/RT - \Delta S/R) + 1] \quad (2.4)$$

where $\chi_{\text{m}}T_{\text{ls-Co(III)}}$ and $\chi_{\text{m}}T_{\text{hs-Co(II)}}$ are the $\chi_{\text{m}}T$ values for isolated **25**,*ls*-Co(III) ($S=1/2$) and **25**,*hs*-Co(II) ($S=3/2$), respectively, and $Y_{\text{hs-Co(II)}}$ is the molar fraction of **25**,*hs*-Co(II). When $\chi_{\text{m}}T_{\text{ls-Co(III)}}$ and $\chi_{\text{m}}T_{\text{hs-Co(II)}}$ are fixed to the theoretical values ($g = 2$) of $1.73 \mu_{\text{B}}$ [*ls*-Co(III)] and $4.9 \mu_{\text{B}}$ [*hs*-Co(II)], the least-square fitting of Eq. 2.4 to $\chi_{\text{m}}T$ gives the values of $\Delta H = 21.5 \text{ kJ.mol}^{-1}$ and $\Delta S =$

$67 \text{ J.K}^{-1}.\text{mol}^{-1}$ ($T_c = \Delta H / \Delta S = 313 \text{ K}$) (Figure 2.9). Interestingly, the observation of a T_c around room temperature opens the door for using these systems as possible candidates for bistable molecular switching materials and devices. The thermodynamic values slightly differ from those previously described.¹⁹

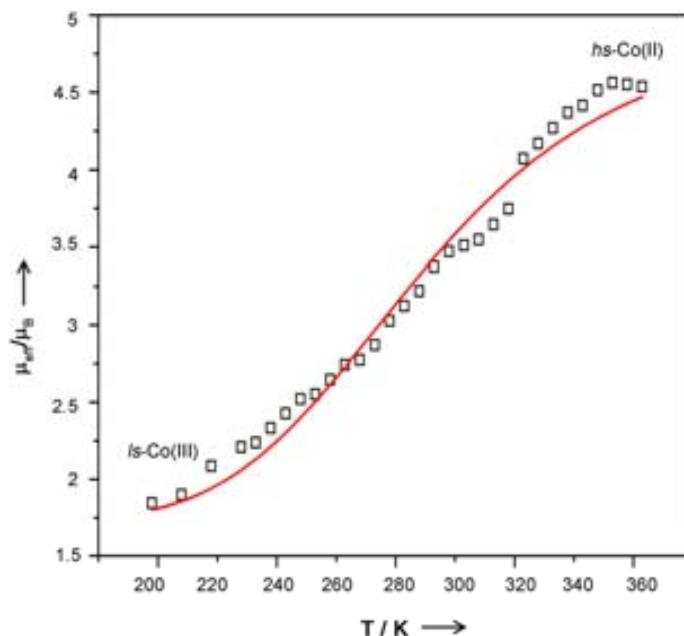


Figure 2.9. Fit of μ_{eff} vs. T following Eq. 2.4 for complex **25**. This result allow us to obtain the thermodynamic parameters of this equation.

The μ_{eff} vs. T plot of complexes **24**, *ls*-Fe(III) and **26**, *hs*-Ni(II) are also shown in Figure 2.8. The iron complex (**24**) exhibits a constant magnetic susceptibility value of around $5.20 \mu_B$ along the whole temperature range. This value can be explained if we consider that the main species in solution along the whole temperature range is the [Fe(Cat-N-BQ)(Cat-N-SQ)] **24**, *ls*-Fe(III) tautomer. These results are in agreement with our electronic spectra analysis that shows a characteristic band of the radical Cat-N-SQ²⁻ ligand around 350 nm. In this complex, a strong antiferromagnetic interaction between the radical ligand Cat-N-SQ²⁻ ($S=1/2$) and the *hs*-Fe(III) ion ($S=5/2$) leads to a $S=2$ magnetic ground state for which a theoretical value of $4.90 \mu_B$ is expected (the μ_{eff} value expected for a non-interacting Fe(III) and a organic radical would be $6.16 \mu_B$). Similar behaviour was observed for complex **26**, *hs*-Ni(II), which exhibits a constant magnetic susceptibility value close to $2.8 \mu_B$ along the whole temperature range. This is the expected value for the $S = 1$ ground state of the *hs*-Ni(II) form, which is also in agreement with the results obtained from spectroscopic characterization.

2.2.1.3 Solid state magnetic measurements

The magnetic properties of complex **25** have already been described in a previous work by Dei *et al.*¹⁹ These authors showed that complex **25** exhibits a tautomeric interconversion in solid state but at much higher temperatures than in solution. The transition starts at approximately 410 K, i.e., at least 100 K higher than in solution. Variable-temperature magnetic susceptibility data for crystalline samples of complexes **24** and **26** were measured over the temperature range of 5-400 K with an applied external field of 10 kG. At high temperatures, both complexes are characterized by a μ_{eff} value of 4.7 and 3.1 μ_{B} , respectively. These values remain constant down to approximately 30 K, whereupon they gradually decrease more likely due to the presence of small intermolecular antiferromagnetic exchange interactions. In the case of complex **26**, such a value is close to the theoretical value of 2.83 μ_{B} expected for the *hs*-Ni(II) (S=1) tautomer with both ligands in the diamagnetic form Cat-N-BQ¹⁻. This behaviour confirms that in solid state this complex also remains in its *hs*-Ni(II) form even down to very low temperatures. Similarly, the μ_{eff} value of iron complex can be explained if we consider that the main species in solid state along the whole temperature range is the **24**,*s*-Fe(III) tautomer bearing a radical Cat-N-SQ²⁻ ligand, in agreement with the solution measurements previously described.

2.2.1.4 Discussion

The experimental results indicate that the energy of the **24**,*s*-Fe(III) tautomer remains much lower than that of the **24**,*hs*-Fe(II) tautomer along the temperature range studied, both in solution and in solid state. Therefore, the IET between the imino ligand and the iron metal ion in complex **24**, i.e. VT phenomena, does not take place. In other words, as far as the ligand to metal IET is concerned, complex **24** can be considered as a Class I or a Class II system with very large activation energy, according to the classification of Robin and Day.⁴¹ Even if the molecule acquires sufficient activation energy to reach the intersection region, the probability of an electron exchange would be null or very small in the temperature range under study due to a rather weak interaction between the imino ligand and the iron ion. On the contrary, the energy gap between the **25**,*s*-Co(III) and **25**,*hs*-Co(II) tautomers gets smaller and lies within the same range of the energy applied in the temperature range studied. Therefore, even though **25**,*s*-Co(III) is energetically more stable, an increase of the temperature promotes an IET from the ligand Cat-N-SQ²⁻ to the Co(III) ion, i.e., the VT interconversion takes place. Complex **25** can be then formally considered as a Class II system, where the interaction between the redox centres is moderate. In this complex, the electron is vibrationally localised in one of the redox centres due to the presence of an activation energy barrier (ΔG), although such a barrier may be overcome by an external thermal stimulus to promote an IET process. Finally, in the case of complex **26**, the tautomeric form **26**,*hs*-Ni(II) remains lower in energy than the **26**,*s*-Ni(III) isomer, reason why only the *hs*-Ni(II) isomer is detected in the whole temperature range. The differential VT behaviour along the series of complexes **24**, **25**, and **26** can be tentatively

assigned to the different ionization potentials of the iron, cobalt and nickel complexes that induce a differential overlapping of the d metal orbitals with the π -orbitals of the iminoquinone ligands. The differential filling effects of the metal-centred d orbitals should also be considered. The influence of such factors into the VT equilibria of the three complexes is shown in Figure 2.10.

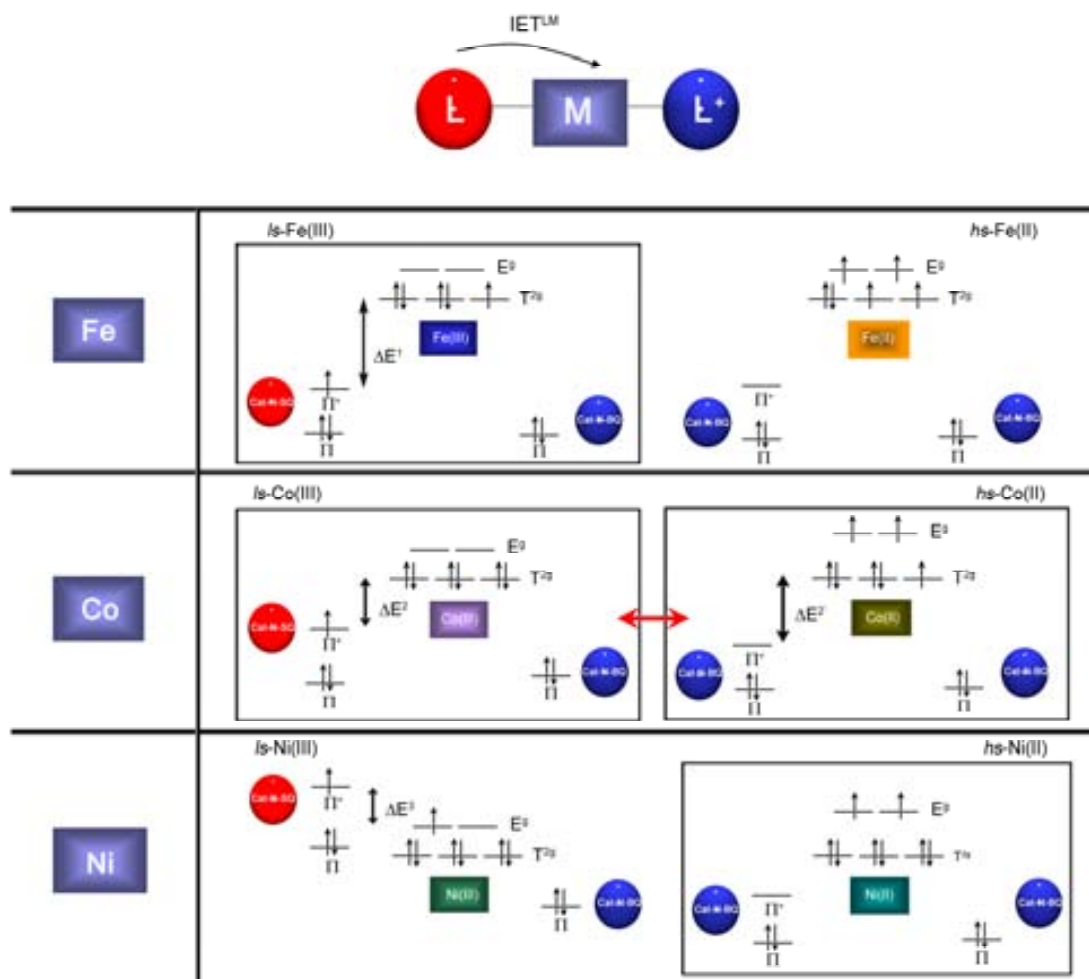


Figure 2.10. Schematic representation of the relative energies for complexes **24**, **25** and **26** justified according with the matching of the metal and ligand centred orbitals. Stable forms are labelled with a square.

It is important to remark that all these experimental results were fully supported by quantum chemical calculations. The quantum chemical calculations were developed by Marie Laure Bonet and Dr. Vincent Robert from the l'École Normale Supérieur de Lyon, (for calculation details see the Experimental Section). The resulting CASPT2 energies, which are referenced to the ground state (GS) energy, are summarized in Table 2.1. The energy difference (ΔE) corresponds to vertical transitions (so-called intervalence transition in mixed-valence compounds),⁴² which results as the sum of the reorganization energy and the energy difference between the tautomers. For the Ni compound **26**, the ground state is consistent with

a d^8 Ni(II) ion, holding two unpaired electrons in the $d_{x^2-y^2}$ and d_{z^2} atomic orbitals in a distorted octahedral environment. The energy difference (ΔE) is 20100 cm^{-1} , thus ruling out the possibility of the coexistence of Ni(II) and Ni(III). Similar strategy was used for the iron complex **24**. The ground state is consistent with a d^5 Fe(III) ion and an energy difference with its electronic isomer of 12400 cm^{-1} . Therefore, in agreement with the experimental data, the VT transition is unlikely to occur. Finally, the energy separation between the two electronic configurations for the cobalt case (**25**) is 3500 cm^{-1} , a reflection of the VT phenomena that take places in complex **25**.

Table 2.1. Resulting CASPT2 energies referenced to the ground state (GS) energy.

Complex	GS spin state	Tautomer spin state	ΔE
24	Fe(III) S=2 (<i>ls</i>)	Fe(II) S=1/2 (<i>ls</i>)	12400
25	Co(III) S=1/2 (<i>ls</i>)	Co(II) S=3/2 (<i>hs</i>)	3500
26	Ni(II) S=1 (<i>hs</i>)	Ni(III) S=1/2 (<i>ls</i>)	20100

2.2.2 Environmental effects on VT: A comparison between the interconversion in solution and solid state.

The VT of complexes **14**, **17** and **25** have been studied in different matrices (in solution, crystalline samples obtained from different solvents and embedded into a polymeric matrix). The results shown are also presented in the Article II: *Solvent Effects on VT: A comparison between the interconversion in solution and solid state*. Solid State Sciences, **2008**. (Accepted). DOI: 10.1016/j.solidstatesciences.2007.11.039. This work has been done in collaboration with Clara Rodríguez Blanco and Dr. Javier Campo from the Universidad de Zaragoza (magnetic measurements), Dr. Jean-Pascal Sutter and Dr. Yannick Coppel from Laboratoire de Chimie de la Coordination (LCC-Toulouse) (NMR spectroscopy) and Dr David N. Hendrickson from the University of California at San Diego.

2.2.2.1 VT in solution

In solution, VT can be induced by variations of temperature and monitored by UV-Vis spectroscopy. As an example, the temperature dependence of the UV-Vis spectrum of complex **14** in CH_2Cl_2 is shown in Figure 2.11.

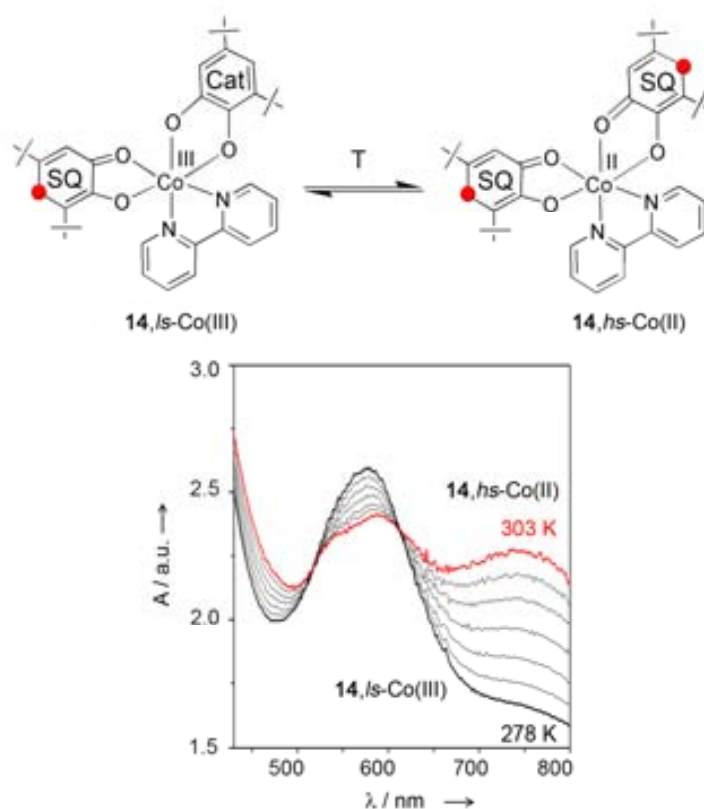


Figure 2.11. Temperature dependence of the electronic absorption spectrum of an CH_2Cl_2 solution of complex $[\text{Co}(3,5\text{-DTBCat})(\text{DTBSQ})(\text{bpy})]$ (**14**) in the temperature range from 278 to 303 K.

At room temperature, the UV-Vis spectrum of complex **14** shows a band at 600 nm with a shoulder close to 800 nm, which is characteristic of the *ls*-Co(III) isomer. The self-consistent field (SCF) nonlocal density functional molecular orbital calculations have shown that the intense visible transition at 600 nm is likely due to $\pi\text{-}\pi^*$ transitions, whereas the shoulder close to 800 nm is due mostly to an orbital forbidden ligand-to-metal charge transfer (LMCT).²⁰ As the temperature of the solution is increased from 278 K to 303 K, the intensity of the 600 nm band decreases, whereas a band around 770 nm increases in intensity. This band is characteristic of the *hs*-Co(II) isomer, and results from a MLCT transition from a t_{2g} metal orbital to the SQ and *bpy* π^* ligand orbitals. Such temperature dependence was also monitored in four additional solvents selected on the basis of their different dielectric constant (ϵ): toluene (2.4), methylene chloride (8.9), acetone (20.7), ethanol (24.3) and acetonitrile (36.2). The temperature-dependent VT is fully reproduced along all these solvents, but with a major significant change: the critical temperature (T_c) is shifted from one solvent to the other.⁴³ Or in other words, the ratio of the absorption bands associated with each valence tautomer at the same temperature considerably differs. More precisely, T_c was shifted following the order: acetonitrile (~ 345 K) > ethanol (~ 336 K) > methylene chloride (~ 313 K) > acetone (~ 300 K) and toluene (~ 273 K).

Significantly, T_c not only is modified from one solvent to the other but shifts by almost 70 K on changing from acetonitrile to toluene.

Substitution of the bipyridine by a phenantroline ligand in complex **17** induces a modification of its T_c value with respect to that of complex **14**. For instance, the spectrum of a toluene solution of complex **17** at 305 K is highly characteristic of a **17**,*hs*-Co(II) tautomer, as indicated by an intense broad band at 780 nm with a shoulder at 660 nm and a weaker band at 548 nm. At the same temperature, the electronic absorption spectrum of complex **14** exhibits a band at 600 nm with a shoulder at close to 800 nm, which is characteristic of the *ls*-Co(III) isomer. Therefore, even though the N-N'-nitrogen-based ligand is not directly involved in the electron transfer process, it is modulating the relative energy of the molecular orbitals directly involved, mostly from the quinone and the metal ion. However, such substitution has no influence on the solvent dependence of the thermally induced IET since both complexes exhibit the same T_c shift along the series of solvents. Most likely, this is due to the highly aromatic character of both ligands. It is also important to emphasise that neither complex **14** nor **17** exhibit a correlation between the T_c values obtained experimentally for each solvent and their corresponding ϵ values. This fact evidences that the displacement of the tautomeric equilibrium most probably is not only controlled by ϵ but also by other solute-solvent interactions as discussed later on.

Finally, the temperature dependence of the electronic absorption spectrum of complex **25** along the series of five different solvents was also studied. The variable-temperature absorption spectra of a toluene solution have been previously described in Figure 2.7. At high temperatures (353 K), the spectrum is dominated by two intense bands at 797 nm and 721 nm. As the temperature decreases, the intensity of such bands decreases, whereas that of the bands at 533 nm, 439 nm and 391 nm increases. As previously indicated, the spectrum of the complex is dominated by the internal transitions of the coordinated ligands. Therefore, whereas in the case of catecholate-complexes (**14** and **17**) there are two apparent absorption bands associated to each one of the isomers that favour an estimation of T_c , in the case of complex **25**, such an estimation results much more difficult since the changes on the absorption band arises mostly from variations on the internal transitions of the coordinated ligands. Accordingly, any estimation of T_c for complex **25** and its modifications along the series of solvents turned out unfeasible. In any case, and for comparison purposes, the temperature dependence of the electronic absorption spectrum of solutions of complex **25** in acetonitrile, ethanol, methylene chloride and acetone was also studied. The variation of its electronic absorption spectra in five different solvents at room temperature is shown in Figure 2.12. As can be seen there, there are significant changes between them, confirming the influence of the nature of the solvent on VT, as previously reported for complexes **14** and **17**.

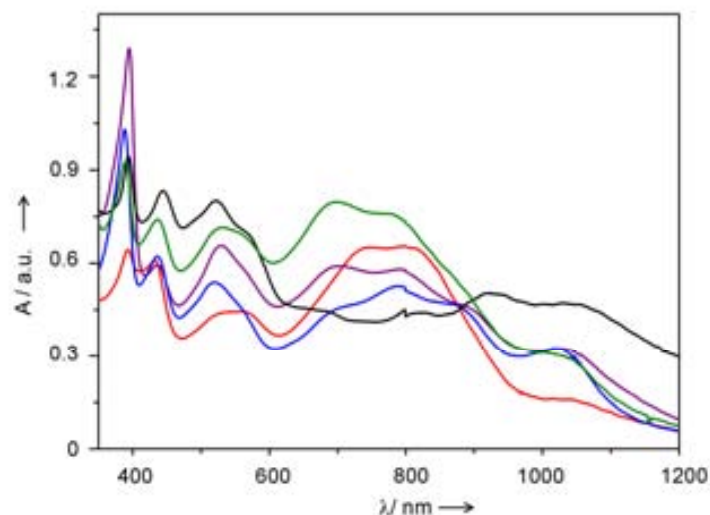


Figure 2.12. Electronic absorption spectra of complex **25** in toluene (violet line), acetonitrile (black line), methylene chloride (green line), acetone (blue line) and ethanol (red line) at room temperature.

Due to the experimental limitations to evaluate the solvent influence in complex **25**, alternatively the Evans Method has been used. The magnetic susceptibility plotted as a function of the temperature in five different solvents is shown in Figure 2.13. The behaviour of complex **25** in toluene has been previously described (Figure 2.7c), thought it is again reproduced for comparison purposes. At low temperatures, the μ_{eff} vs. T plot presents a value of $1.82 \mu_{\text{B}}$ associated to the **25**,*s*-Co(III) tautomer with a single unpaired electron from the Cat-N-SQ²⁻ ligand ($S=1/2$). An increase of the temperature induces the gradual increase of μ_{eff} until a maximum value of $4.64 \mu_{\text{B}}$ at 353 K, indicating the existence of the **25**,*hs*-Co(II) specie. Similar behaviour was observed for the methanol, acetone and chloroform solutions (Figure 2.13). In chloroform, the T_c is shifted towards a lower temperature although the interconversion was not completed since it usually takes place gradually over a large temperature range (≥ 353 -363 K). In fact, this temperature range is larger than the working temperature range of the solvent. On the contrary, the acetonitrile solution exhibits a constant value of $1.82 \mu_{\text{B}}$ in the whole temperature range. This value is in agreement with the expected value for the **25**,*s*-Co(III), indicating that no interconversion takes place at least up to 340 K.

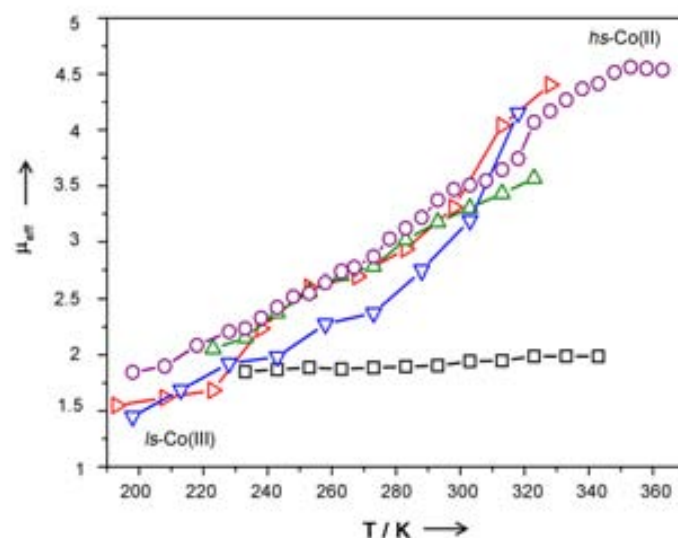


Figure 2.13. Temperature dependence of the effective magnetic moment of complex **25** in toluene (○), acetonitrile (□), chloroform (△), acetone (△) and methanol (△).

Finally, it is important to emphasise that these results are in agreement with those previously obtained with the UV-Vis spectroscopy. Indeed, according to the magnetic susceptibility data shown for this complex in acetonitrile, methanol, acetone and toluene, complex **25** is mostly in the **25**,*hs-Co(II)* at room temperature. The UV-Vis spectra of the same solutions at room temperature (Figure 2.12) exhibit a predominant band centred around 800 nm, which is associated to the isomer **25**,*hs-Co(II)*. On the contrary, the spectrum of an acetonitrile solution exhibits a band around 900 nm, which is characteristic of the isomer **25**,*ls-Co(III)*, in agreement with the magnetic moment found by the Evans method.

With these experiments, we have shown how the VT in solution can be modified simply by changing the nature of the solvent. By choosing a solvent and by controlling the temperature of the solution, the tautomeric equilibrium of complexes can be modulated, and one of the two isomers can be made to be the dominant species in solution. Moreover, the T_C shift is not only controlled by ϵ but also by several other solvent parameters, such as the endoergic term (Ω). For this puzzle to be solved, further experiments based on the *Linear Solvation Energy Relationship* methodology are being planned nowadays.⁴⁴

2.2.2.2 VT in solid state

Since complexes **14** and **17** exhibit a very similar solvent-dependence in solution, the solid state studies were only done for one of these complexes. Variable-temperature (150-320 K) magnetic susceptibility data were gathered for five different solvates of complex **17**, which were obtained by recrystallisation in acetonitrile, toluene, methylene chloride, ethanol and acetonitrile. The X-Ray powder diffraction (XRPD) data of the samples revealed that none of the

samples was amorphous, and that different crystallographic phases are obtained as a function of the solvate. For comparison purposes, the different XRPD obtained for the samples recrystallised from toluene, ethanol and acetonitrile are shown in Figure 2.14. Moreover, special attention was taken on the preparation of the samples for the magnetic measurements since the lost of solvent guest molecules may induce that a fraction of the sample becomes amorphous, and therefore, to fake results. For this reason, the crystals were always maintained within the mother liquor until the measurement was done, and manipulated very rapidly during the preparation of the capsule. Finally, an amorphous sample obtained by a fast precipitation process from a mixture of ethanol and water was also studied.

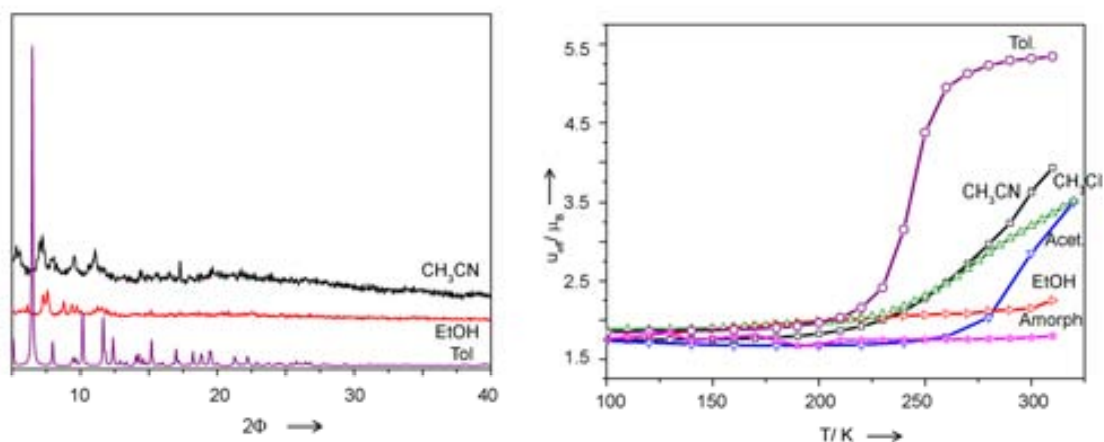


Figure 2.14: (Left) XRPD of complex **17** in three different solvents. (Right) Temperature dependence of the μ_{eff} product curves of complex **17** recrystallised in five different solvents, including an amorphous sample.

The magnetisation data of the six samples is shown in Figure 2.14. As can be observed there, the interconversion in solid state can occur abruptly even in a short temperature range of roughly 30 K. This is the case of the toluene solvate of complex **17** (**17**·C₇H₈).²⁰ From 150 to 225 K, there is little change in the χT vs. T plot with a constant μ_{eff} value of 1.7 μ_B , which is in agreement with that expected for the unpaired electron of the isomer **17**,*ls*-Co(III). Then, it abruptly converts from the *ls*-Co(III) to the *hs*-Co(II) complex in the 230-260 K range. However, when the sample is recrystallised in ethanol, the resulting crystalline sample exhibits a μ_{eff} value essentially independent of temperature, and close to the value of 1.7 μ_B . Such value confirms that this sample remains on the **17**,*ls*-Co(III) form along the whole temperature range. This fact indicates that either the VT interconversion is suppressed or most likely is considerably shifted to higher temperatures. Similar results were obtained for the amorphous sample. In between, the samples recrystallised in acetonitrile, acetone and methylene chloride exhibit incomplete transitions. Such variations have been attributed to a shift of T_C according with this order: toluene < acetonitrile < acetone < methylene chloride < ethanol, which is different from that obtained in solution. This fact is a clear evidence of the different contribution of the solvent molecules on the VT process both in solution and intercalated within a crystalline network.

Surprisingly, all the attempts to obtain different crystallographic phases of complex **25**,/s-Co(III) by recrystallisation from different solvents were unsuccessful. Independently of the solvent, the same crystallographic phase was obtained as confirmed by XRPD. This result prevented any study of the solvate guest influence on the VT equilibrium. The variable temperature magnetic susceptibility data of this phase has already been described in the previous section. From low temperatures up to 360-370 K, there is little change in the χT vs. T plot with a constant μ_{eff} value of $1.7 \mu_B$. This value is in agreement with that expected for the **25**,/s-Co(III). Above these temperatures, the μ_{eff} value increases monotonically beyond 500 K although the transition is not completed due to a thermal instability (decomposition) of the sample.

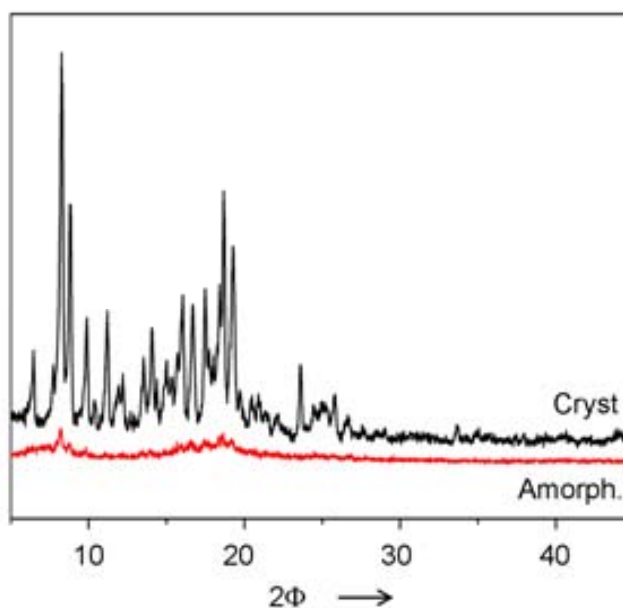


Figure 2.15. XRPD of a crystalline sample of **25** obtained by recrystallisation in toluene (slow evaporation) and an amorphous sample obtained by a fast precipitation process.

To shed more light onto the interaction of the molecular vibronic interactions with the network, an amorphous sample of complex **25** was obtained and studied as a paradigm of a system with defects or with reduced intermolecular interactions. XRPD of the amorphous sample is shown in Figure 2.15. The magnetisation vs. T plot of the sample exhibits a μ_{eff} value that increases monotonically with temperature up to 500 K, as previously described for the crystalline sample. Without any apparent reason, the disorder introduced within the network in complex **25** did not suppress or shift the VT to much higher temperatures, as previously observed for complex **17**.

2.2.2.3 VT in a polymeric matrix

The temperature dependence of the electronic absorption of complexes **14** and **17** doped into a polystyrene thin film was already reported prior to this work.²⁰ For the case of complex **17**, the polymeric matrix shows an appreciable amount of both tautomeric forms at 298 K, whereas, its toluene solution spectrum only indicates the presence of the **17**,*hs*-Co(II) tautomer at the same temperature. Similar divergence was detected for complex **14**. The absorption spectrum of its polystyrene film at 298 K displays the absorption characteristic of the **14**,*s*-Co(III) isomer, whereas the UV-Vis spectrum of this complex in toluene at room temperature shows the presence of the **14**,*hs*-Co(II) isomer.

We have also monitored the temperature dependence of the electronic absorption spectra of complex **25** doped into a polymeric matrix in the 295-350 K temperature range. The resulting spectra are shown in Figure 2.16. For comparison purposes, the temperature dependence of the same compound in a toluene solution is also shown. As can be seen there, the behaviour of complex **25** in both environments is similar, in contraposition with the results obtained for complexes **14** and **17**.

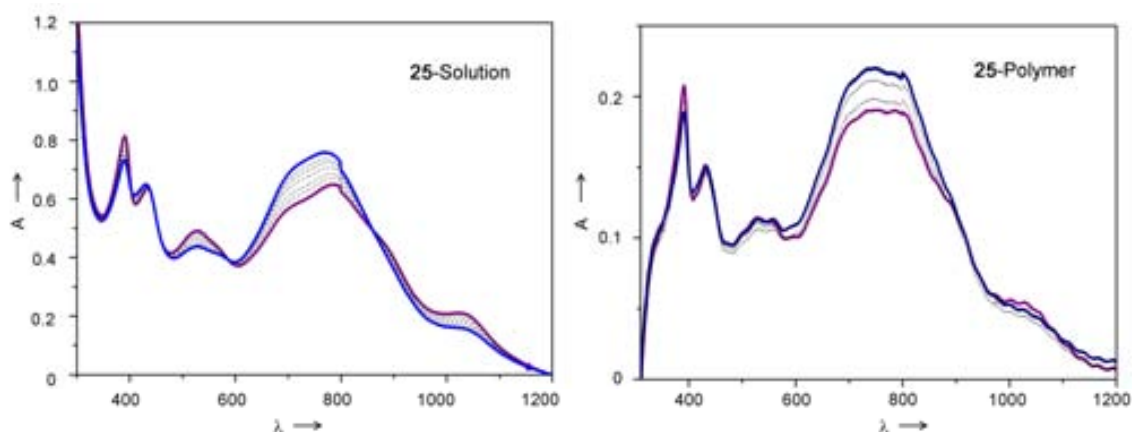


Figure 2.16. UV-vis spectra of complex **25** in toluene in the temperature range of 273-363 K (left) compared to the spectrum obtained from this complex embedded in a polymeric matrix in the temperature range of 273-433 K (4% height).

2.3. Conclusions

1.- The need of several complementary techniques to fully characterise VT processes has been evidenced. Such techniques embrace from variable-temperature UV-Vis spectroscopy and the Evans Method (NMR) in solution to X-ray diffraction and magnetisation measurements in solid state. All of them are supported by theoretical calculations.

2.- The combination of such techniques has allowed to unequivocally establish the influence of the metal ion on the VT for the series of complexes [M(Cat-N-SQ)(Cat-N-BQ)] (M = Fe (**24**), Co (**25**) and Ni (**26**)). The energy of the frontier orbitals is shifted from one metal to the other, and therefore, the matching of the orbitals of the electro-active ligands with the metal ions is significantly varied. The use of metal ions with higher ionization potentials will favour the displacement of the VT equilibrium towards the high-spin isomer, whereas the use of metal ions with lower ionization potentials will favour the low-spin isomer, although orbital filling considerations must be also taken into account.

3.- The use of different solvents has been clearly shown to influence the VT phenomena, i.e., to shift T_C , in solution. This influence can not only be attributed to ϵ but rather to a combination of solvatochromic parameters.

4.- Crystallization of the same compound from different solvents leads to the obtaining of different crystallographic phases, where differential vibronic coupling with VT complexes induces a modulation of the corresponding T_C . This modulation differs from that found in solution.

5.- Complexes **14**, **17** and **25** have different VT behaviour depending not only if they are found embedded into a polymeric matrix, but even in the solution, depending of the solvent used. However, a systematisation of the results that allow for a control of the system can not be done.

In summary, all these results are very important to address future investigations in the field since they reveal the need for a very systematic approach when identifying new VT candidates.

References

- [1] A. Vlcek, *Comments Inorg. Chem.*, **16**, **1994**, 207.
- [2] (a) A. Caneschi, A. Dei, F. F. De Biani, P. Gütllich, V. Ksenofontov, G. Levchenko, A. Hoefler, F. Renz, *Chem. Eur. J.*, **7**, **2001**, 3926. (b) A. Bencini, A. Caneschi, C. Carbonera, A. Dei, D.-Gatteschi, R. Righini, C. Sangregorio, J. VanSlageren, *J. Mol. Struct.*, **656**, **2003**, 141.
- [3] R. M. Buchanan, C. G. Pierpont, *J. Am. Chem. Soc.*, **102**, **1980**, 4951.
- [4] O. -S. Jung, C. G. Pierpont, *J. Am. Chem. Soc.*, **116**, **1994**, 2229.
- [5] (a) G. A. Abakumov, V. I. Nevodchikov, V. K. Cherkasov, *Dokl. Akad. Nauk SSSR*, **278**, **1984**, 641. (b) G. A. Abakumov, G. A. Razuvaev, V. I. Nevodchikov, V. K. Cherkasov, *J. Organomet. Chem.*, **341**, **1988**, 485.
- [6] S. Bin-Salamon, S. H. Brewer, E. C. Depperman, S. Franzen, J. W. Kampf, M. L. Kirk, R. K. Kumar, S. Lappi, K. Peariso, K. E. Preuss, D. A. Shultz, *Inorg. Chem.*, **45**, **2006**, 4461.
- [7] N. G. R. Hearn, J. L. Kořcok, M. M. Paquette, K. E. Preuss, *Inorg. Chem.*, **45**, **2006**, 8817.
- [8] Y. Suenaga, C. G. Pierpont, *Inorg. Chem.*, **44**, **2005**, 6183.
- [9] C. Carbonera, A. Dei, J. -F. Letard, C. Sangregorio, L. Sorace, *Angew. Chem. Int. Ed.*, **43**, **2004**, 3136.
- [10] S. H. Bodnar, A. Caneschi, D. A. Shultz, L. Sorace, *Chem. Commun.*, **2001**, 2150.
- [11] I. Imaz, D. Maspoch, C. Rodríguez-Blanco, J. M. Pérez-Falcón, J. Campo, D. Ruiz-Molina, *Angew. Chem. Int. Ed.*, **47**, **2008**, 1857.
- [12] M. Li, D. Bonnet, E. Bill, F. Neese, T. Weyhermüller, N. Blum, D. Sellmann, K. Wieghardt, *Inorg. Chem.*, **41**, **2002**, 3444.
- [13] (a) D. Herebian, P. Ghosh, H. Chun, E. Bothe, T. Weyhermüller, K. Wieghardt, *Eur. J. Inorg. Chem.*, **2002**, 1957. (b) K. Ray, E. Bill, T. Weyhermüller, K. Wieghardt, *J. Am. Chem. Soc.*, **127**, **2005**, 5641.
- [14] T. Glaser, M. Heidemeier, R. Fröhlich, P. Hildebrandt, E. Bothe, E. Bill, *Inorg. Chem.*, **44**, **2005**, 5467
- [15] N. Domracheva, A. Mirea, M. Schwoerer, L. Torre-Lorente, G. Lattermann, *Chem. Phys. Chem.*, **7**, **2006**, 2567.
- [16] (a) O. Hayaishi, M. Nozaki, *Science*, **164**, **1969**, 389. (b) C. A. Tyson, A. E. Martell, *J. Am. Chem. Soc.*, **94**, **1972**, 939. (c) A. Y. Girgis, A. L. Balch, *Inorg. Chem.*, **14**, **1975**, 2724. (d) L. A. deLaire, R. C. Haltiwanger, C. G. Pierpont, *Inorg. Chem.*, **28**, **1989**, 644.
- [17] S. K. Larsen, C. G. Pierpont, *J. Am. Chem. Soc.*, **110**, **1988**, 1827.
- [18] A. Caneschi, A. Cornia, A. Dei, *Inorg. Chem.*, **37**, **1998**, 3419.
- [19] O. Cador, F. Chabre, A. Dei, C. Sangregorio, J. Van Slageren, M. G. F. Vaz, *Inorg. Chem.*, **42**, **2003**, 6432.
- [20] (a) D. M. Adams, A. Dei, A. L. Rheingold, D. N. Hendrickson, *Angew. Chem. Int. Ed. Engl.*, **32**, **1993**, 880. (b) D. M. Adams, A. Dei, A. L. Rheingold, D. N. Hendrickson, *J. Am. Chem. Soc.*, **115**, **1993**, 8221. (c) D. M. Adams, L. Noodleman, D. N. Hendrickson, *Inorg. Chem.*, **36**, **1997**, 3966.
- [21] (a) O. -S. Jung, D. H. Jo, Y. A. Lee, B. J. Conklin, C. G. Pierpont, *Inorg. Chem.*, **36**, **1997**, 19. (b) O. -S. Jung, D. H. Lee, Y. S. Sohn, C. G. Pierpont, *Inorg. Chem.*, **37**, **1998**, 5875.
- [22] (a) C. Benelli, A. Dei, D. Gatteschi, L. Pardi, *Inorg. Chim. Acta*, **163**, **1989**, 99. (b) A. Caneschi, A. Dei, D. Gatteschi, V. Yangoulis, *Inorg. Chem.*, **41**, **2002**, 3508.
- [23] A. Cui, K. Takahashi, A. Fujishima, O. Sato, *J. Photochem. and Photobiol. A: Chem.*, **161**, **2004**, 243.
- [24] A. Yamaguchi, K. Awaga, *J. Mater. Chem.*, **11**, **2001**, 2142.
- [25] D. Kiriya, H. -C. Chang, A. Kamata, S. Kitagawa, *Dalton Trans.*, **2006**, 1377.
- [26] (a) J. Rall, W. Kaim, *J. Chem. Soc. Faraday Trans.*, **90**, **1994**, 2905. (b) G. Speier, S. Tisza, Z. Tyeklar, C. W. Lange, C. G. Pierpont, *Inorg. Chem.*, **33**, **1994**, 2041.
- [27] R. M. Buchanan, C. Wilson-Blumenberg, C. Trapp, S. K. Larsen, D. L. Green, C. G. Pierpont, *Inorg. Chem.*, **25**, **1986**, 3070.
- [28] W. Kaim, M. Wanner, A. Knödler, S. Zalis, *Inorg. Chim. Acta*, **337**, **2002**, 163.
- [29] S. Ye, B. Sarkar, M. Niemeyer, W. Kaim, *Eur. J. Inorg. Chem.*, **2005**, 4735.

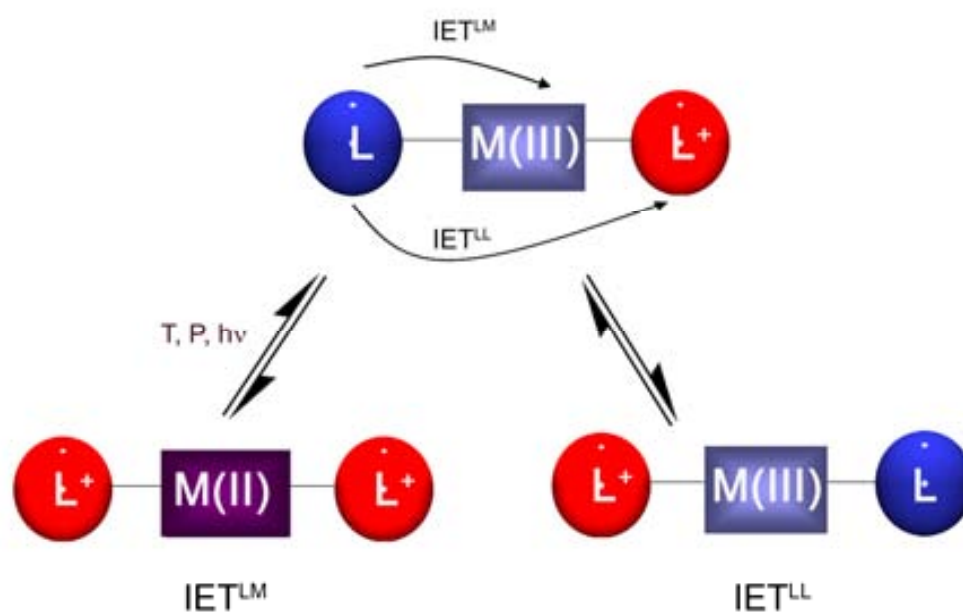
- [30] (a) D. Ruiz-Molina, J. Yoo, I. Guzei, A. L. Rheingold, D. N. Hendrickson, *Chem. Commun.*, **1998**, 2089. (b) D. Ruiz-Molina, L. N. Zakharov, A.L. Rheingold, D.N. Hendrickson, *J. Phys. Chem. Sol.*, **65**, **2004** 831.
- [31] D. Ruiz-Molina, J. Veciana, K. Wurst, D. N. Hendrickson, C. Rovira, *Inorg. Chem.*, **39**, **2000**, 617.
- [32] D. Ruiz-Molina, K. Wurst, D. Hendrickson, C. Rovira, J. Veciana, *Adv. Funct. Mater.*, **12**, **2002**, 347.
- [33] Similar behavior was observed in its related oxidised form: D. Ruiz-Molina, J. Veciana, K. Wurst, D. N. Hendrickson, C. Rovira, *Inorg. Chem.*, **39**, **2000**, 617.
- [34] P. L. Gentili, L. Bussotti, R. Righini, A. Beni, L. Bogani, A. Dei, *Chem. Phys.*, **314**, **2005**, 9.
- [35] For examples of other complexes exhibiting VT only in solution, please see: D. N. Hendrickson, C. G. Pierpont, *Top. Curr. Chem.*, **234**, **2004**, 63.
- [36] O. Cador, A. Dei, C. Sangregorio, *Chem. Commun.*, **2004**, 652.
- [37] A. Y. Girgis, A. L. Balch, *Inorg. Chem.*, **14**, **1975**, 2724.
- [38] M. Bauscher, W. Mäntele, *J. Phys. Chem.*, **96**, **1992**, 11101.
- [39] D. F. Evans, *J. Chem. Soc.*, **1959**, 2003.
- [40] Values obtained from the reviews of *J. Chem. Eng. Data*, **39**, **1994**, 876, (MeOH); **42**, **1997**, 2, (Acetone); **44**, **1999**, 411, (Toluene); **46**, **2001**, 2 (Chloroform) and **47**, **2002**, 1037 (Acetonitrile).
- [41] M. B. Robin, P. Day, *Adv. Inorg. Chem. Radiochem.*, **10**, **1967**, 247.
- [42] N. S. Hush, *Prog. Inorg. Chem.*, **8**, **1967**, 391.
- [43] The critical temperature at which there are equal amounts of both isomers is extracted from the spectrum where the 600 nm and 770 nm bands exhibit the same intensity. The operating temperature window for each solvent does not allow us to determine the absorption of the pure low and high-spin species, and therefore, to have an accurate estimation of T_c . However, such theoretical error is considerably smaller than the difference of observed for the different solvents, which can not be attributed to such implicit errors.
- [44] N. Ventosa, D. Ruiz-Molina, J. Sedo, X. Tomas, B. Andre, C. Rovira, J. Veciana, *Chem. Eur. J.*, **5**, **1999**, 12.

Chapter | 3

Ligand-to-Ligand Intramolecular Electron Transfer

Abstract

Transition metal complexes containing at least two redox-active catecholate or phenoxylate ligands with different oxidation states had shown a new type of intramolecular interaction. Indeed, in addition to the well-known ligand-to-metal intramolecular electron transfer (IET^{LM} or VT), the existence of a new IET between the different redox-active ligands has been demonstrated. This IET, termed as ligand-to-ligand intramolecular electron transfer (IET^{LL}) can be defined as the electronically coupling between the orbitals of the redox-active ligands through the orbitals of the metal unit. The coexistence of both IET is studied in two different families of complexes, one bearing a catecholate and the other a phenoxylate-based ligand. This coexistence opens exciting perspectives to design new mixed-valence (MV) systems, and new applications that could be derived out of them.



3.1 Introduction

3.1.1 Pure organic mixed-valence systems

The flexibility of organic chemistry may allow the synthesis of organic mixed-valence (MV) molecular wires with specified and sophisticated topologies. Moreover, the study of their properties should lead to the synthesis of systems where the electron transfer could be fine-tuned in a more precise way than had been done with redox-active transition metal ions.^{1,2}

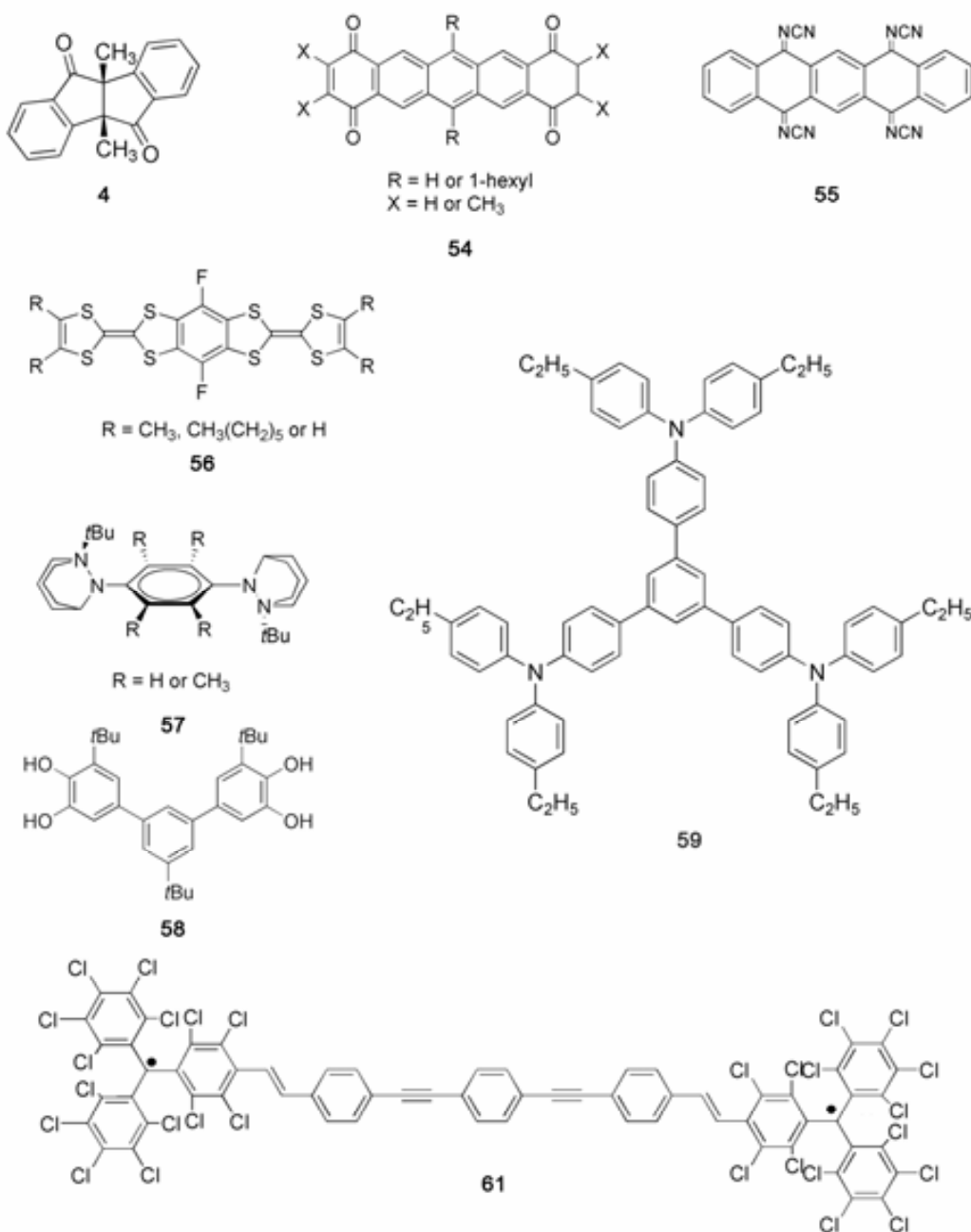


Figure 3.1. Examples of the most representative organic-based MV compounds reported in the literature.

As mentioned in Chapter 1, bis(indandone) (**4**) was the first pure organic MV compound studied.³ Since then, other examples of pure organic MV compounds showing IET phenomena have been described. Examples (Figure 3.1) are anion-radicals derived from conjugated diquinones (**54**) and diimides (**55**),⁴ cation-radicals derived from bis(tetrathiafulvalenes) (**56**),⁵ cation-radicals derived from bis(hydrazines) (**57**),⁶ quinoid groups (**58**)⁷ and ion-radicals derived from π -conjugated polyarylmethyl/polyarylamines (**59**)⁸ and systems based on the polychlorotriphenylmethyl radical (PTM, **60**) such as the biradical **61** shown in Figure 3.1.⁹ Representative examples of all these organic-based molecules are the systems based on PTM radicals reported by the group of Prof. J. Veciana.¹⁰ The central carbon atom of these radicals, where most of the spin density is localised, is sterically shielded by six chlorine atoms localised at the *ortho* positions of the three phenyl rings, which increase its thermal and chemical stability. Moreover, their cyclic voltammetry shows the formation of two different stable ionic species that corresponds to their oxidation (**60**⁺) and reduction (**60**⁻), as represented in Figure 3.2a. As a consequence, symmetrical molecules consisting of two or more of these radical units linked by different types of bridges can be converted by a partial reduction (or oxidation) to the corresponding anion-radicals (or cation-radicals) resulting mixed-valence species that display interesting long-distance electron transfer phenomena. Especially significant was the case of diradical **61**, for which a significantly large through-space radical-to-radical centre distance of 32 Å and an end-to-end distance up to 40 Å were found by molecular modelling.

The existence of intervalence transition band (IVT), which implies an IET process, has been confirmed by the generation of different species that can be derived by partial oxidation and/or reduction of a given compound. For instance, IET phenomena in the series of complexes derived from diradical **62**^{••} have been studied. This diradical and the corresponding dianionic species obtained by its double reduction can be regarded as full-valence species that not should exhibit an IVT band (Figure 3.2). In such system, the IVT only should be observed on the MV anion-radical **62**^{•-}. The appearance of this band was studied by using the combined spectro-electrochemical method. During the reduction of diradical **62**^{••}, the sharp band at 386 nm, which is characteristic of the radical centre, decreases and disappears completely. On the contrary, the band at 522 and 606 nm grow, indicating the continuous formation of **62**²⁻. In addition to the aforementioned bands, during the reduction process of diradical **62**^{••}, a weak and broad band centred at 1400 nm increases until the complete formation of the MV radical-anion species **62**^{•-}, from where its intensity decreases until it disappears completely when the dianion **62**²⁻ is formed. From the treatment of this system, the electronic coupling between the radical units was extracted.

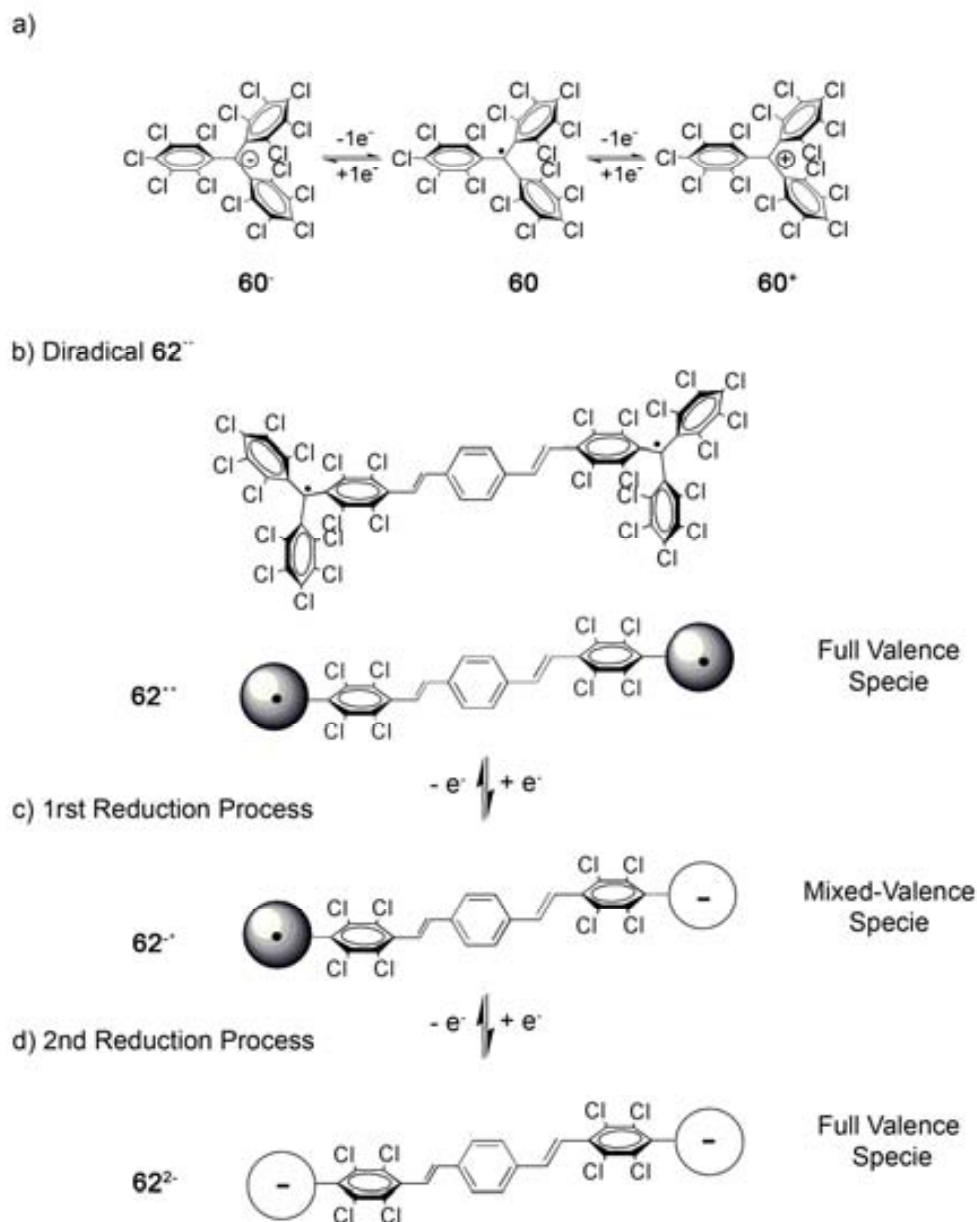


Figure 3.2. a) Representation of the PTM radical **60** unit showing the high steric shielding of the central carbon atom. b-d) Representation of the different species that can be derived from the reduction of the PTM diradical **62^{••}**.

3.1.2 IET between organic units mediated through a metal ion.

Whereas most of the examples previously described are based on pure organic systems where both electro-active units are linked through an organic bridge, the number of systems with the electro-active units linked through a metal ion are rather scarce.^{11,12} One of such rare examples is the family of ruthenium and rhenium polynuclear complexes bearing redox-active bipyridinium ligands reported by Abe *et al.*¹³ These authors showed that metal-cluster units often behave as redox mediators in spite of their large size and of the remote distance of the ligand-based redox centres. Even though a single Ru(II) metal centre does not effectively

mediate the redox interaction between two monodentate ligands, the authors observed an effective interaction when this Ru(II) metal ions were substituted by trinuclear Ru(III) clusters. Interestingly, such IET processes have been maintained even when these systems were attached on a surface. Indeed, as shown in Figure 3.3, linear pentamers of triruthenium complex units (**63**) bridged by redox-active 4,4'-bipyridine ligands¹⁴ deposited on a gold surface in the form of multilayer showed electron transfer applying a potential to induce redox reactions of these clusters.

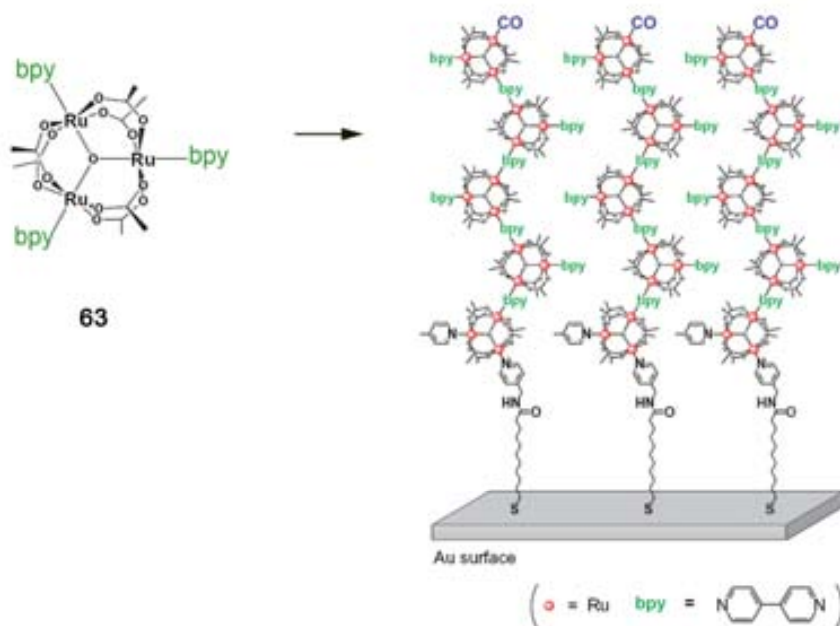


Figure 3.3. Oligomers of μ_3 -oxo-triruthenium units bridged by aromatic 4,4'-bipyridine ligands, which are used to construct linear pentamers on a gold electrode surface showing redox interactions.

Transition metal complexes containing at least two redox-active catecholate or phenoxylate ligands with different oxidation states may also belong to this family of MV systems. In addition to the well-known ligand-to-metal IET (IET^{LM} or VT),¹⁵ these complexes can also present ligand-to-ligand IET (IET^{LL}) through the transition metal centres.¹⁶ For example, the family of systems with the general formula [M(DTBCat)(DTBSQ)(N-N)] containing mixed-charge ligands may be a good example of such MV metal systems. In this sense, Prokofev *et al.*¹⁷ demonstrated the dynamic exchange of charge between ligands on the system [M(3,6-DBSQ)(3,6-DBCat)₂]²⁻, where M is Sn (**21**). Also, Pierpont *et al.*¹⁸ showed that the spin of the radical in [Ga(tmeda)(3,6-DBSQ)(3,6-DBCat)] (**22**) is equally distributed over both ligands by EPR spectroscopy. This fact has been assigned to an intramolecular charge transfer mechanism between both ligands, as confirmed by the absence of concentration dependence. Interestingly, no evidence of an IVT band was observed in this case.

The examples previously described pointed out to the existence of IET^{LL} in this family of complexes, although none of them has been shown to exhibit simultaneously VT (IET^{LM}). Therefore, an issue that remains open is the extent to which both electron transfer processes can coexist within the same complex. The interest for this to be demonstrated is twofold. First, the coexistence of two different IET mechanisms allows them to be a unique model system to provide insight into the basic factors affecting IET in molecular complexes. And second, since the two isomers involved in the VT process exhibit different optical, electric and magnetic properties,¹⁹ these complexes offer potential applications in bistable molecular switching materials and devices.

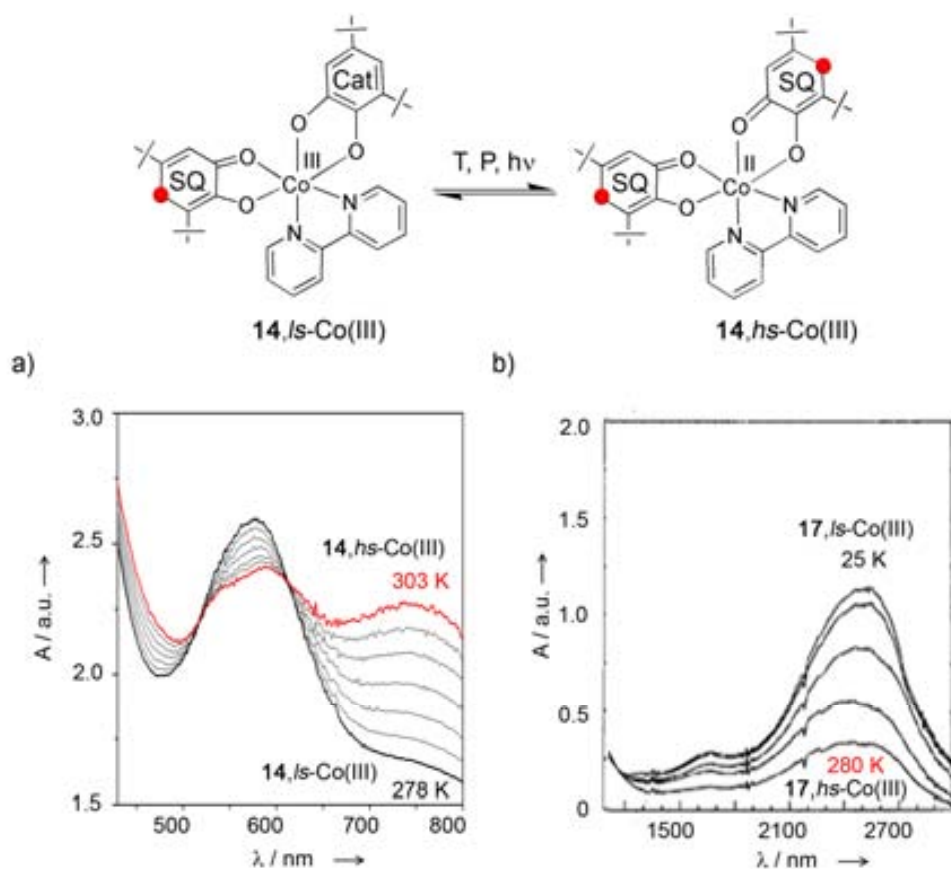


Figure 3.4. a) Temperature dependence of the electronic absorption spectra of a CH₂Cl₂ solution of complex **14**. b) Temperature dependence of the electronic absorption spectrum of a polystyrene film of complex **17** obtained at 280, 200, 150, 80, and 15 K.

Thus far, only some previous experiments in complexes of general formula [Co(3,5-DTBCat)(3,5-DTBSQ)(N-N)],²⁰ where N-N is a chelating ligand, such as 2,2'-bipyridine (**14**) or 1,10-phenanthroline (**17**), pointed towards this direction. In these systems, accompanying the characteristic IET^{LM} changes of the variable-temperature UV-Vis spectra, large changes in the near-infrared (near-IR) are also observed.^{20a,b,e} The temperature dependence from 285 to 25 K of the electronic absorption spectra in the visible and near-IR regions of complex **17** doped into a polystyrene polymer film is shown in Figure 3.4. At low temperatures, a low energy band at

2500 nm associated with the **17**,*l*-Co(III) isomer appears. The exact origin of this band transition has been the subject of some speculation. This band has been assigned as a transition from the highest occupied $\text{Cat}^{2-} 3b_1 \pi^*$ orbital to the lowest unoccupied cobalt e_g^* molecular orbital. i.e., as a LMCT transition from the Cat^{2-} ligand to the *l*-Co(III) ion.^{20c} An alternative hypothesis is that *l*-Co(III) complexes with a semiquinone and a catecholate ligand are analogous of classical mixed-valence complexes.¹⁵ As a consequence, the low-energy band transition arises from an IVT band from the Cat^{2-} to the SQ^- ligand.^{20a,b} This assignment was supported by self-consistent field (SCF) nonlocal density functional calculations for **17**,*l*-Co(III), which showed that the lowest energy transition involves an intervalence transfer of an electron from the predominantly $\text{Cat}^{2-} 3b_1 \pi^*$ HOMO to the $\text{SQ}^- 3b_1 \pi^*$ orbital. To best illustrate this attribution, a schematic representation of the different IET processes that can take place in complex **14** is shown in Figure 3.5.

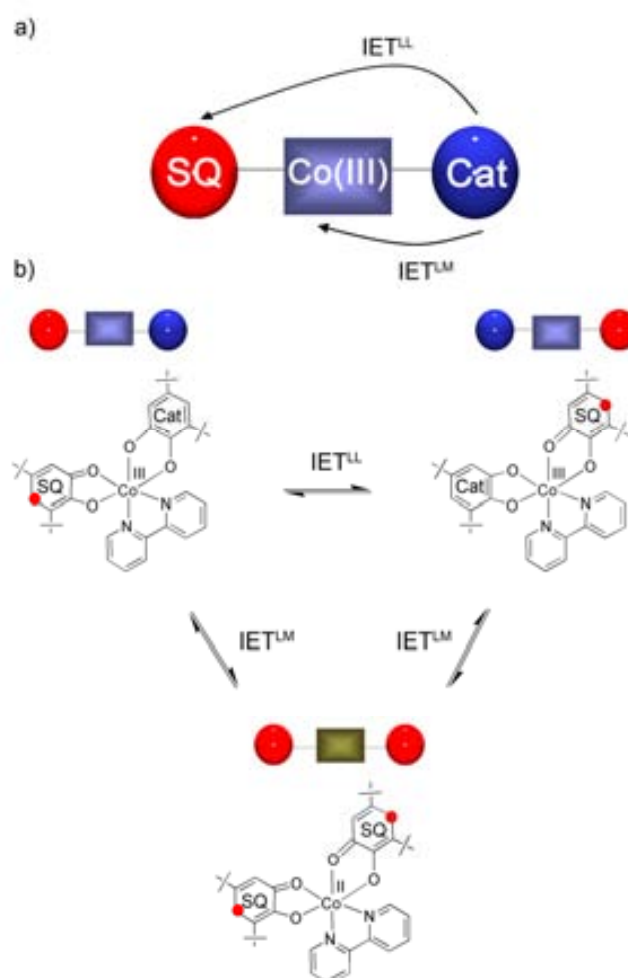


Figure 3.5. a) A MV compound is made up of three components: a donor unit (Cat^{2-}), an acceptor unit (SQ^{1-}) and a bridge, such as Co(III) ion. b) Schematic representation of the two different IET mechanisms that can take place in **14**,*l*-Co(III).

3.1.3 Summary

According to the introduction previously described, the objective for this part of the work was the confirmation that the low energy band transition that appears at 2500 nm for **14**,*l*-Co(III) can be assigned as an IVT, and therefore, to confirm the coexistence of VT (IET^{LM}) and IET^{LL} electron transfer processes in this complex. To achieve this goal, we have followed a similar approach to that used for studying IET in PTM radicals (Figure 3.2). This approach consists on the generation of different species that can be derived by partial oxidation and/or reduction of a given compound. Such a series represents an excellent scenario for the study of the IVT band since only the neutral complex **14**,*l*-Co(III) can be formally considered as a MV specie, whereas the corresponding oxidised and reduced species are not. Accordingly, the observation of an IVT band is expected only for the neutral form **14**,*l*-Co(III). Moreover, a systematic and detailed extension of this work was faced in the family of complexes derived from the tridentate Schiff-base ligand $(\text{Cat-N-BQ})^{1-}$ (**10**¹⁻). This ligand leads to stable coordination complexes involving several metal ions in a variety of oxidation states although it usually coordinates in the Cat-N-BQ^{1-} (**10**¹⁻) or the Cat-N-SQ^{2-} (**10**²⁻) radical forms, being therefore formally considered as MV species.¹⁵ Therefore, in this work, the series of complexes $[\text{M}(\text{Cat-N-SQ})(\text{Cat-N-BQ})]$, where M can be Fe (**24**) or Co (**25**), have been thoroughly revised. For this, electron transfer has been studied by means of NMR combined with *ab initio* wavefunction based CASPT2 calculations. The schematic representation of the two IET that can take place in complexes **24** and **25** is shown in Figure 3.6.

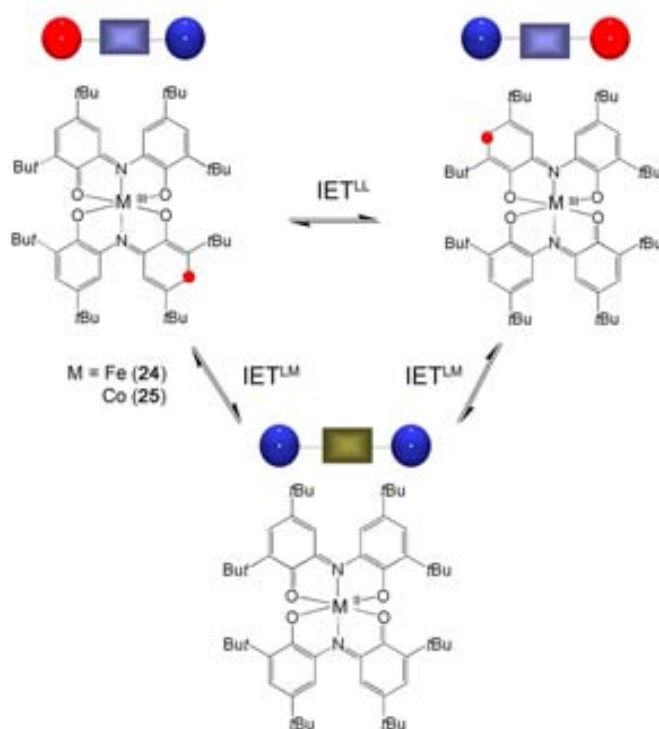


Figure 3.6. Schematic representation of the two different IET mechanisms that can take place in **25**,*l*-Co(III).

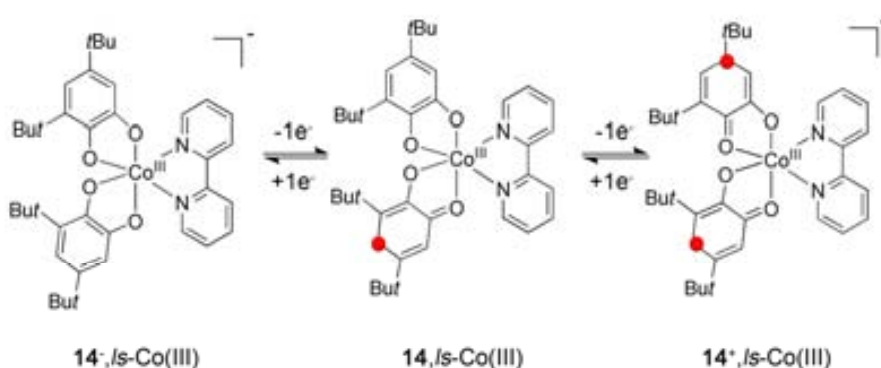
3.2 Results

3.2.1 Ligand-to-ligand IET in complex [Co(3,5-DTBCat)(3,5-DTBSQ)(bpy)] (14)

The results shown in this section are summarized in the Article III: *Intramolecular electron transfer in the mixed-valence [Co(3,5-DTBCat)(3,5-DTBSQ)(bpy)] complex. Beyond valence tautomerism*. Inorg. Chim. Acta, **2008**. (Accepted). DOI: 10.1016/j.ica.2008.02.069. This work has been done in collaboration with Prof. D. N. Hendrickson from the University of California at San Diego following the work started by Dr. Daniel Ruiz-Molina during his postdoctoral stay in Hendrickson's research group.

3.2.1.1 Electrochemistry

Electrochemical characterization of complex **14**, in dichloromethane with 0.1 M Bu₄NPF₆ (tetrabutylammonium hexafluorophosphate) as supporting electrolyte, was performed. In dichloromethane and at 273 K, complex **14** is mostly in the **14**,/s-Co(III) isomer as revealed the variable-temperature electronic spectra. Its cyclic voltammogram at 273 K shows two well-defined processes at $E_{1/2}$ of -0.34 and + 0.25 V vs. Ag wire (E_0 of ferrocene under the same experimental conditions is +0.36 V). Previous studies on different *o*-quinone transition metal complexes have shown that the electrochemical processes, by either chemical or electrochemical means, occur at the quinone ligands.²¹ Therefore, the redox couple observed at $E_{1/2}$ of -0.34 V can be associated to the reduction of the semiquinone ligand to the catecholate form, whereas the second redox process is characteristic of the oxidation of the catecholate ligand to the semiquinone form. The resulting reduced **14**·Co(Cp)₂ from now on named **14**⁻,/s-Co(III)) and oxidised (**14**⁺·Cl from now on named **14**⁺,/s-Co(III)) species formed along the electrochemical process are shown in Scheme 3.1.



Scheme 3.1

The study of the scan rate ($v^{1/2}$) dependence of the two redox processes showed a linear dependence of the peak current with respect $v^{1/2}$, suggesting that these electrochemical processes are reversible and diffusion-controlled. Potential-controlled electrolysis experiments

also confirmed the possibility to oxidise and reduce reversibly the low-spin **14**,/s-Co(III) isomer. This fact is an indication of no structural changes, such as ligand loss or decomposition, in the time scale of the experiment. So, the corresponding ionic (cationic and anionic) species were generated chemically and characterised by different means. The detailed synthetic procedure is given in the Experimental Section.

3.2.1.2 Magnetism.

Variable-temperature magnetic susceptibility data in the 2-300 K temperature range under an external magnetic field of 10 kG were obtained. The magnetisation data for an amorphous sample of **14**,/s-Co(III) exhibits a μ_{eff} value close to 1.76 μ_B , which is essentially independent of the temperature. This value is similar to that expected for a /s-Co(III) complex with one semiquinone ligands ($\mu_{eff} = 1.8 \mu_B$).²² These measurements also confirm the S=0 ground state for the reduced complex **14**,/s-Co(III), as expected for a diamagnetic complex with a /s-Co(III) metal ion and two catecholate ligands. The μ_{eff} of **14**⁺,/s-Co(III) (oxidised complex) at 300 K was 2.8 μ_B , which is close to that expected for a /s-Co(III) complex with two semiquinone ligands ($\mu_{eff} = 2.5\mu_B$). The magnetic moment dropped slightly to 2.6 μ_B at 50 K, whereupon a steeper drop down to 2.1 μ_B at 5.0 K can be observed. This is attributed to the presence of semiquinone-semiquinone intra- and/or intermolecular antiferromagnetic interactions.

EPR spectroscopy is also a useful tool to characterize transition metal o-quinone complexes since provides valuable information on the location of unpaired spin density within the complex. In our case, EPR spectroscopy has been used to show that the unpaired spin density in /s-Co(III) complexes with coordinated SQ⁻ ligands resides predominantly on the SQ⁻ ligand. However, some spin density is delocalised onto the cobalt ion since a signal centred at g=2 split into eight lines due to the hyperfine coupling to the ⁵⁹Co (I=7/2) nucleus. X-band EPR spectra were run for toluene/CH₂Cl₂ (1:1) solutions of complexes **14**,/s-Co(III) and **14**⁺,/s-Co(III) at 300 K. The reduced form **14**⁻,/s-Co(III) was not measured because it is not expected to exhibit EPR signals due to its diamagnetic character. The EPR spectrum of **14**,/s-Co(III) shows a signal centred at g=2.0 split into eight lines due to the hyperfine coupling to the ⁵⁹Co nucleus, with a hyperfine coupling constant of $a(^{59}\text{Co})=12.0$ G. Similar signals were observed for complex **14**⁺,/s-Co(III), which exhibits an hyperfine coupling constants $a(^{59}\text{Co})$ of 10.1 G. No hyperfine interactions arising from coupling of the proton in the *para* position of the oxygen were observed.

It has been clearly shown that the oxidation states of these complexes influence the spin density distribution along the semiquinone-derived complexes. The hyperfine couplings with the ⁵⁹Co nucleus, which are a reflection of the spin density on the cobalt nucleus, changed following the order: **14**,/s-Co(III) ($a(^{59}\text{Co})= 12.0$ G) > **14**⁺,/s-Co(III) ($a(^{59}\text{Co})= 10.1$ G). Similar tendency has been observed for the previously reported double-oxidised complex [Co^{III}(3,5-DTBSQ)(bpy)₂](BF₄)₂ (**14**²⁺,/s-Co(III)), which shows a ⁵⁹Co hyperfine coupling constant of 8.4

G.²³ This fact seems to evidence that an increase of the overall positive charge of the complex tends to localise the electron distribution on the quinone-derived ligand leaving less on the Co(III) ion.

3.2.1.3 Electronic and vibrational spectroscopy.

The electronic spectrum of complexes $\mathbf{14}^-/s\text{-Co(III)}$ and $\mathbf{14}^+/s\text{-Co(III)}$ were taken at low temperatures (200 K) to avoid band broadening effects and/or additional electron transfer processes. The spectrum of complex $\mathbf{14}^-/s\text{-Co(III)}$ exhibits an intense band at 405 nm and a second less intense transition at 610 nm, whereas the spectrum of complex $\mathbf{14}^+/s\text{-Co(III)}$ is dominated by intense bands below 400 nm and a characteristic band at 720 nm. Interestingly, during the reduction and oxidation reactions of complex $\mathbf{14}/s\text{-Co(III)}$ the intensity of the band centred at 2500 nm disappears completely. This result was confirmed by FT-IR emphasising its origin associated to an IVT band. The FT-IR spectra of complexes $\mathbf{14}/s\text{-Co(III)}$, $\mathbf{14}^-/s\text{-Co(III)}$ and $\mathbf{14}^+/s\text{-Co(III)}$ were registered on KBr pellets, and are shown in Figure 3.7.

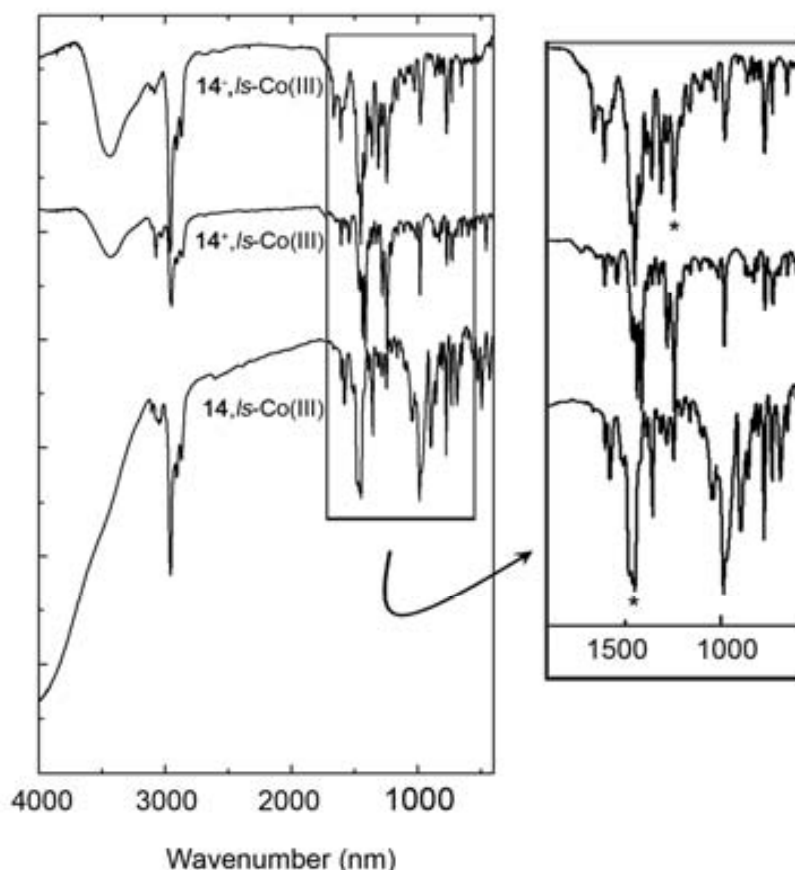


Figure 3.7. FT-IR spectra of complexes $\mathbf{14}/s\text{-Co(III)}$, $\mathbf{14}^-/s\text{-Co(III)}$ and $\mathbf{14}^+/s\text{-Co(III)}$ registered on KBr pellets. The characteristic peak associated to the oxidation state of the ligand (catecholate or semiquinone) is marked with an asterisk.

IR spectroscopy is also a useful tool to define the oxidation state of the quinone-derived ligands, since each oxidation state of the ligand display a characteristic pattern of peaks. Coordinated quinones, semiquinones and catecholates display C-O frequencies in the range of $1600\text{-}1675\text{ cm}^{-1}$, $1400\text{-}1500\text{ cm}^{-1}$ and $1250\text{-}1480\text{ cm}^{-1}$, respectively. The spectrum of **14**,/s-Co(III) is dominated by a strong absorption at $1450\text{-}1500\text{ cm}^{-1}$. The spectrum of **14**⁻,/s-Co(III) shows a C-O peak at $\sim 1250\text{ cm}^{-1}$, which is characteristic of a catecholate ligand although the FT-IR spectrum of **14**⁺,/s-Co(III) does not provide clear evidence of its oxidation state. An expansion of this region is also given in Figure 3.7 for a clearly view. Finally, a peak in the low energy region (low wavenumbers) of the spectra associated to the IVT band tailing into the IR region is observed only for **14**,/s-Co(III), whereas no peak is observed for **14**⁻,/s-Co(III) and **14**⁺,/s-Co(III). This broad peak can be associated to the IVT band²⁴ previously observed with the electronic spectroscopy since the 2500 nm band tails into the IR region. This is a further confirmation that no IVT band is observed for complexes **14**⁻,/s-Co(III) and **14**⁺,/s-Co(III), since it rules out any decomposition and/or shift of the band towards lower energies (Figure 3.8).

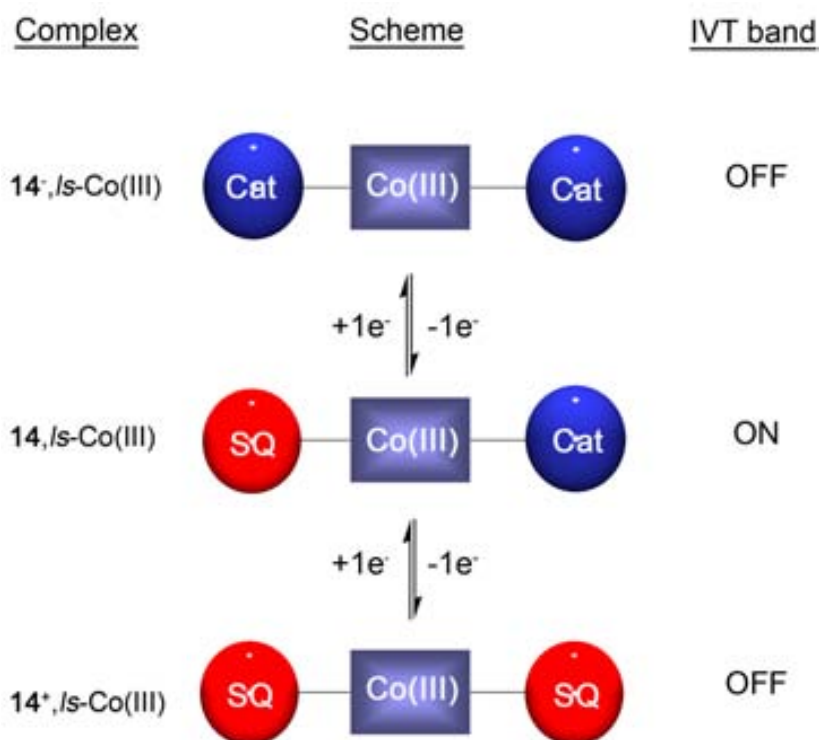


Figure 3.8. Evolution of the species formed during the course of the reversible oxidation and reduction of **14**,/s-Co(III). Intramolecular electron transfer (IVT band) phenomena can only be observed for **14**,/s-Co(III).

Following the classification of Robin and Day,²⁵ it is therefore possible to maintain this complex **14**,/s-Co(III) as a Class II system because both, IET^{LM} and the new studied IET^{LL} , have an energetically barrier and this barrier can be overcome by an external stimuli. Accordingly, the

more realistic picture for all the intramolecular electron transfer processes present in **14**,*s*-Co(III) is best described by the triple-well potential energy curve shown in Figure 3.9.

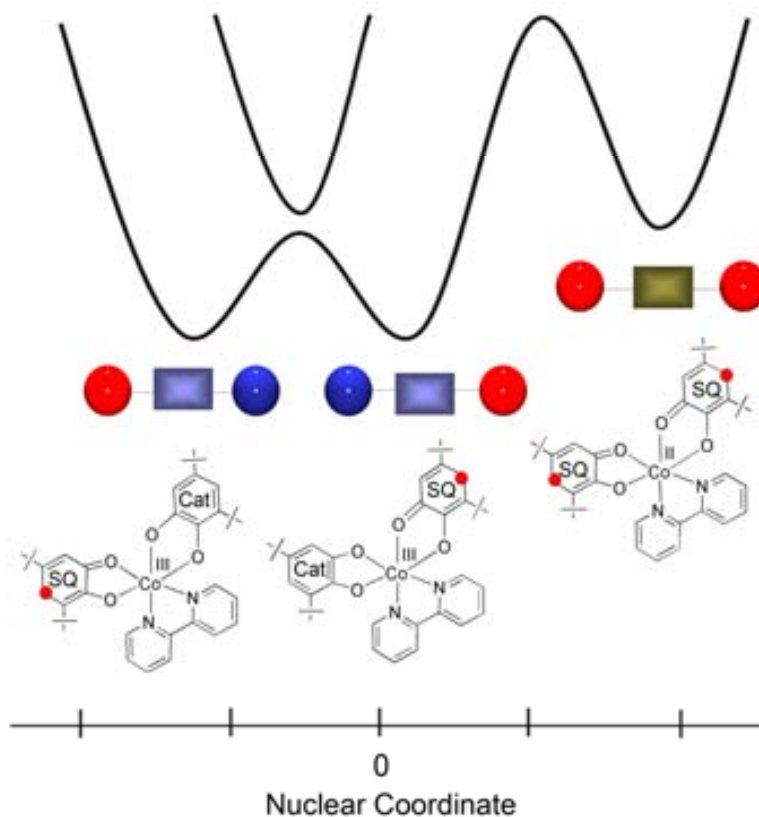


Figure 3.9. Resulting potential energy curve considering the two different electron transfer mechanisms present in complex **14**,*s*-Co(III).

Coupling between SQ^- and Cat^{2-} ligands in **14**,*s*-Co(III) is expected to take place through the π -type orbitals involving the metal ion though other mechanisms can not be discarded at this point.¹⁸ For instance, Pierpont *et al.* pointed out the possibility to have rapid electron transfer even for systems where electronic coupling between the ligands is very weak or negligible. This was the case of complex $[\text{Ga}(\text{tmeda})(3,6\text{-DBSQ})(3,6\text{-DBCat})]$ (**22**), where the IET was tentatively assigned to take place through a tunnelling mechanism and/or through the solvent shell since no significant π -bonding of the quinone ligands with the metal were observed.

3.2.2 Ligand-to-ligand IET in the series of complexes $\text{M}(\text{Cat-N-SQ})(\text{Cat-N-BQ})$ $\text{M} = \text{Fe}$ (**24**) and Co (**25**)

Once the presence of IET in complex **14**,*s*-Co(III) was shown, we focused our attention into the family of complexes $[\text{M}(\text{Cat-N-SQ})(\text{Cat-N-BQ})]$, where M can be Fe (**24**) or Co (**25**). The presence of two electro-active ligands with different oxidation states ensures the possibility to

have IET^{LL}. However, the approach used in this case is different from the selective oxidation or reduction of the complex since no IVT has been detected for these complexes. Indeed, as previously explained in Chapter 1, the UV-visible spectroscopy of complexes **24**,*s*-Fe(III) and **25**,*s*-Co(III) exhibit bands that tail slightly into the near-IR, which have been attributed in both cases to ligand internal transitions.²⁶ No further near-IR bands have been detected. For this reason, the IET studies on this family of complexes were faced by means of ¹H-NMR and theoretical calculations.

The results shown in this section are summarized in the Article VI: *Intramolecular Electron Transfer in the Series of Mixed-Valence Complexes [M^{III}(Cat-N-SQ)(Cat-N-BQ)] (M=Fe, Co, Ni) bearing Non-Innocent Ligands: a Combined Experimental and Theoretical Study*. Chem. Eur. J., **2008**. (*In preparation*). This work has been done in collaboration with Prof. Andrea Dei from the University of Firenze (physical interpretation), Dr. Motohiro Nakano from Osaka University (physical interpretation), Marie Laure Bonet and Dr. Vincent Robert from l'École Normale Supérieure de Lyon (theoretical calculations), Dr. Jean-Pascal Sutter from the Laboratoire de Chimie de la Coordination (spectroscopic measurements) and Dr. Miquel Cabañas from the Universitat Autònoma de Barcelona (NMR spectroscopy).

3.2.2.1 ¹H-NMR experiments

The ¹H-NMR spectra of complexes **24**, and **25** were recorded at different temperatures, and the signal of the *tert*-butyl groups monitored along the whole temperature range. The variable-temperature ¹H-NMR of a toluene solution of complex **25** (C₀ = 10 mg of compound / 0.75 mL Toluene-d⁸) in the 203-363 K temperature range is shown in Figure 3.10a. The spectrum obtained at high temperatures, where the dominant specie is the **25**,*hs*-Co(II) tautomer, exhibits two main signals each one embracing four *tert*-butyl groups. This fact is in agreement with the theoretical expectations. Indeed, since the **25**,*hs*-Co(II) tautomer is bearing two symmetrical monoanionic Cat-N-BQ¹⁻ ligands, the eight *tert*-butyl groups of the complex are expected to be equivalent 4:4, depending whether they are located at the *para* or *ortho* positions of the oxygen atom, and therefore, only two main broad signals are expected. When the temperature is decreased, a VT interconversion is induced from the **25**,*hs*-Co(II) to the **25**,*s*-Co(III) tautomer, which is followed by a remarkable shift of the *tert*-butyl signals with chemical shifts as large as $\Delta\delta = -7.2$ ppm and $\Delta\delta = 3.1$ ppm. The remarkable variations arise from the electronic rearrangement experienced by the complex along the VT interconversion. While in the **25**,*hs*-Co(II) tautomer the spin density is localised in the Co(II) ion, the spin density in **25**,*s*-Co(III) is localised directly into the ligand (Cat-N-SQ)²⁻, inducing a larger paramagnetic shift and broadening of the peaks. Even more remarkable is the fact that still only two main peaks are observed even at very low temperatures where the main predominant form is the **25**,*s*-Co(III) tautomer. This observation is rather unexpected since the **25**,*s*-Co(III) tautomer is bearing two ligands with different oxidation states, Cat-N-BQ¹⁻ and Cat-N-SQ²⁻. Accordingly, the *tert*-butyl groups should be not any longer equivalent 4:4 but 2:2:2:2 and therefore, at least four

different peaks should be observed at low temperatures. A feasible explanation for this observation would rely on a fast IET between the ligands Cat-N-BQ^{1-} and Cat-N-SQ^{2-} . If the extra electron is fully delocalised over both ligands on the time scale of the experiment, the *tert*-butyl groups could be equivalent 4:4 again. Similar results were found for the iron complex (**24**). This complex remains mainly in the **24**,*ls*-Fe(III) form in the whole temperature range, and once more *tert*-butyl signals are equivalents 4:4 instead 2:2:2:2 as theoretically expected.

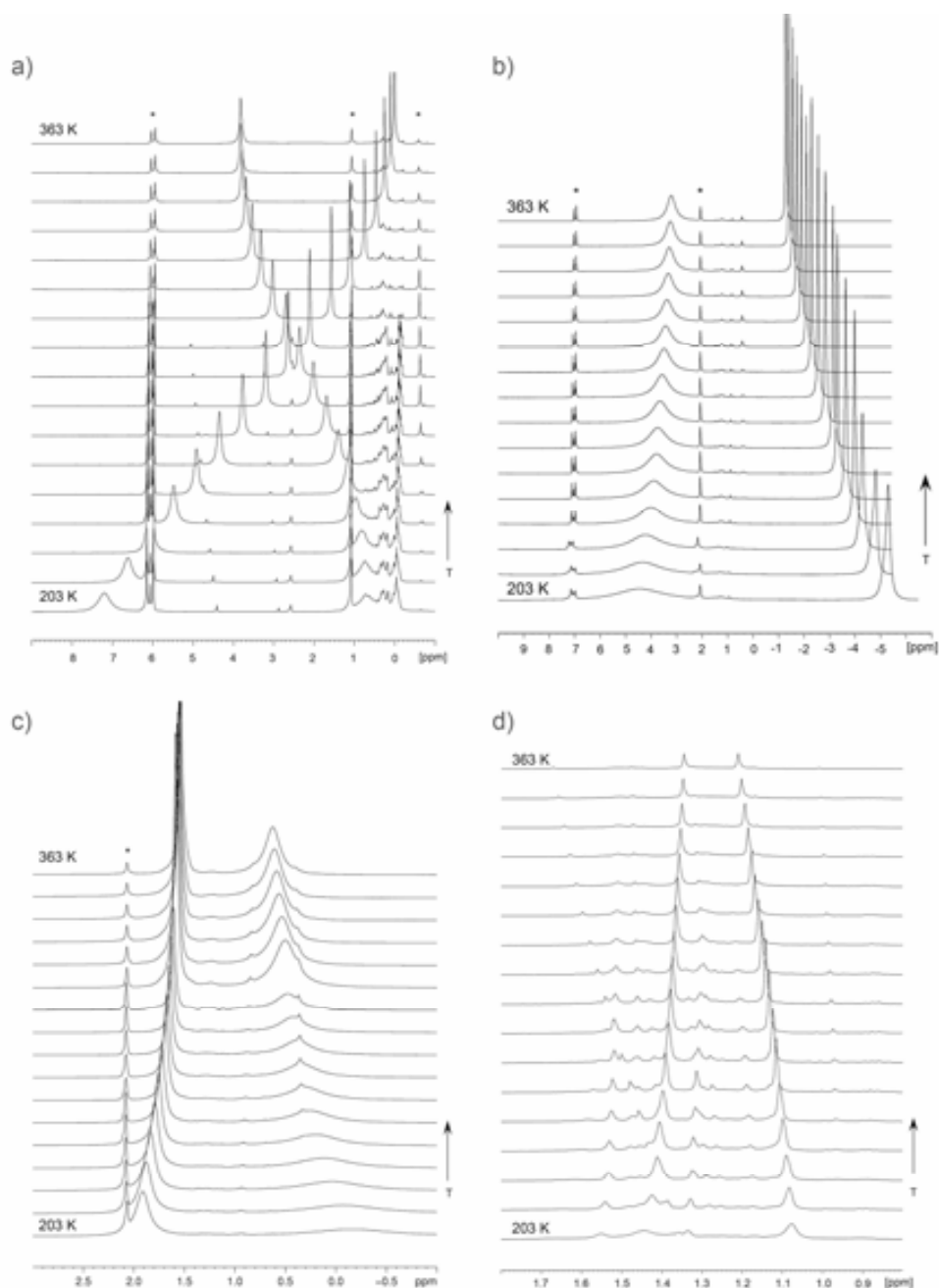


Figure 3.10. $^1\text{H-NMR}$ (400 MHz) shift peak of the *tert*-butyl groups in the iminoquinone ligand for complexes **25** (a), **24** (b) **26** (c) and **57** (d). The working temperature ranges from 203 K to 363 K. Each intermediate spectrum corresponds to an increment of 10 K. Solvent peaks are marked with an asterisk.

The variable-temperature $^1\text{H-NMR}$ of a toluene solution of complex **26**, *hs*-Ni(II)) was also studied for comparison purposes. The spectra obtained for this complex in the temperature range of 203 K - 363 K are shown in Figure 3.10c (**26**). As previously described for complex **25**, *ls*-Co(III), only two types of peaks associated to the *tert*-butyl groups are observed in all the temperature range. This observation indicates that once more such *tert*-butyl are equivalent 4:4. The observation of only two signals is in agreement with the theoretical expectations for complex **26**, which stays in its **26**, *hs*-Ni(II) tautomeric form bearing two symmetrical monoanionic Cat-N-BQ $^{1-}$ ligands. As can be observed in Figure 3.11, the chemical shift of the two *tert*-butyl signals for complex **25**, *ls*-Co(III) varies considerably among them, crossing between them at some point due to the VT interconversion. In the case of complexes **24**, *ls*-Fe(III) and **26**, *hs*-Ni(II), the changes in the paramagnetic shift for both *tert*-butyl signals are smaller, especially for complex **26**, *hs*-Ni(II). While complex **24** exhibits paramagnetic shifts of $\Delta\delta = -3$ ppm and 5 ppm, the related chemical shifts for complex **26**, *hs*-Ni(II) remain between $\Delta\delta = -0.5$ ppm and 1 ppm. As expected, the paramagnetic shift of the *tert*-butyl groups for complex **24**, *ls*-Fe(III) is larger than for complex **26**, *hs*-Ni(II) since the presence of the unpaired electron in the same ligand through its form Cat-N-SQ $^{2-}$ induces a larger paramagnetic shift. Moreover, there is no crossing between the chemical shifts of both *tert*-butyl signals as previously described for complex **25**, *ls*-Co(III) fact that has been attributed to the lack of VT for both complexes. Finally, we also analyzed complex $[\text{Zn}(\text{Cat-N-BQ})_2]$ (**57**) ($S=0$) as a totally diamagnetic model compound. In this case, a small chemical shift of the two *tert*-butyl signals (4:4) is observed (see Figure 3.10).

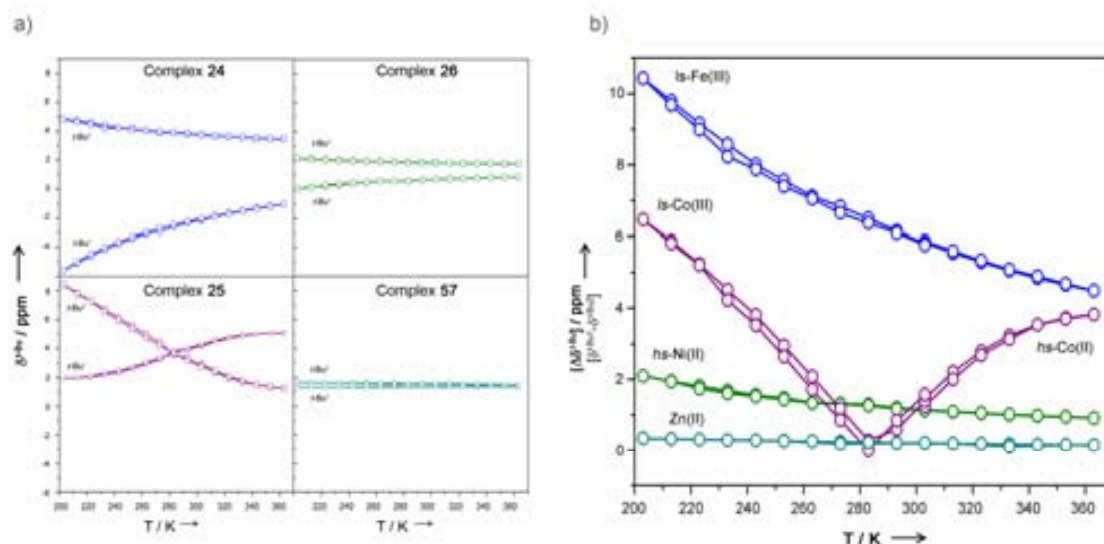


Figure 3.11. a) Representation of the *tert*-butyl shift peaks vs. temperature for complexes **24** (\circ), **25** (\circ), **26** (\circ) and **57** (\circ). b) Representation of $\Delta^{\text{tert-Bu}}$ vs. T obtained by the rest of the *tert*-butyl peaks in the same range of temperatures that in the UV-Vis experiments (203 K to 363 K).

In this sense, $^1\text{H-NMR}$ experiments indicate that extra electron can not be formally considered localised within one of the ligands Cat-N-SQ $^{2-}$, but rather fully delocalised between

both of them. It is important to remark that these experimental results were fully supported by quantum chemical calculations (for more details, please refer to the Experimental Section and Article VI). These calculations showed the existence of two competing states with the extra-electron localised in a different ligand in each case that lie close in energy, so they can be thermally populated. Therefore, according to the classification of Robin and Day,²⁵ the ligand-to-ligand IET can be considered as a Class III MV system, where the electronic interaction is so intense that the electron is completely delocalised all over the molecule. Then, the properties of each isolated unit are lost and the delocalisation gives into new properties. Further support for this hypothesis was obtained after revising the X-ray structures of complexes **24**,/s-Fe(III) and **25**,/s-Co(III).²⁷ The single-crystal X-ray crystallographic data reported in the literature support charge delocalisation over the entire molecule. Indeed, the structural features exhibit C-O and C-N bond lengths which average to 1.305 (7) Å and 1.362 (7) Å, respectively, and do not significantly differ between the two ligands. On the other hand, the IET^{LM} that succeed in the case of **25**,/s-Co(III) is classified as a Class II system following the results observed by UV-Vis shown in the previous Chapter. Accordingly, the more realistic picture for all the intramolecular electron transfer processes present in all them is best described by the triple-well potential energy curve shown in Figure 3.12. Further quantum chemical calculations were developed in order to support all the experimental data observed for the IET^{LL} phenomena of complexes **24** and **25**.

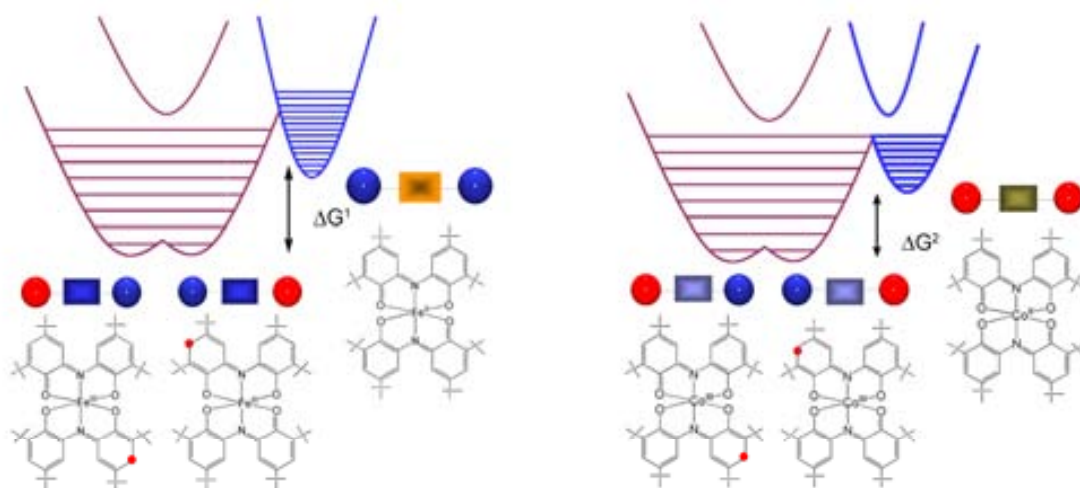


Figure 3.12. Resulting potential energy curve considering the two different electron transfer mechanisms present in complexes **24**,/s-Fe(III) and **25**,/s-Co(III).

3.3. Conclusions

1.- We have demonstrated the existence of ligand-to-ligand IET in complexes **14**,/s-Co(III), **24**,/s-Fe(III) and **25**,/s-Co(III). Complex **14**,/s-Co(III) can be associated to a Class II system according to the observation of an IVT band in the near-IR region. On the contrary, complexes **24**,/s-Fe(III) and **25**,/s-Co(III) exhibit a complete electronic delocalisation between both ligands, being assigned as a Class III system.

2.- Both family of complexes (catecholate and phenoxylate-based) are one of the few examples so far described in the literature where an electron transfer between two organic units is mediated through a metal ion instead of an organic bridge. Therefore, they can be considered as a reversal of the classical ligand-bridged MV metal complexes, opening a completely new phenomenological challenge within the field of IET.

3.- We have unequivocally demonstrated the coexistence of IET^{LM} and IET^{LL} in the catecholate (**14**) and phenoxylate (**25**) based complexes. These interesting results open new scientific challenges on the quest to control multielectron transfer systems and the corresponding new phenomenologies and synergies that can be extracted out of them. Further work has to be developed on the quest for possible synergies between both IET processes.

References

- [1] (a) M. D. Ward, *Chem. Ind.*, **1996**, 568. (b) R. Ziessel, M. Hissler, A. El-Ghayoury, A. Harriman, *Coord. Chem. Rev.* **178-180**, **1998**, 1251. (c) M. N. Paddon-Row, *Acc. Chem. Res.*, **27**, **1994**, 18. (d) M. R. Wasielewski, *Chem. Rev.*, **92**, **1992**, 435. (e) J. -P. Launay, *Chem. Soc. Rev.*, **30**, **2001**, 386.
- [2] (a) T. M. Figueira-Duarte, V. Lloveras, J. Vidal-Gancedo, A. Gégout, B. Delavaux-Nicot, R. Welter, J. Veciana, C. Rovira, J.-F. Nierengarten, *Chem. Commun.*, **2007**, 4345. (b) S. Barlow, D. O'Hare, *Chem. Rev.*, **97**, **1997**, 637, and references therein.
- [3] (a) S. Mazur, C. Sreekumar, A. H. Schroeder, *J. Am. Chem. Soc.*, **98**, **1976**, 6713. (b) A. H. Schroeder, S. Mazur, *J. Am. Chem. Soc.*, **100**, **1978**, 7339.
- [4] (a) S. F. Rak, L. L. J. Miller, *J. Am. Chem. Soc.*, **114**, **1992**, 1388. (b) L. L. Miller, C. A. Liberko, *Chem. Mater.*, **2**, **1990**, 339 and references cited therein.
- [5] (a) K. Lahlii, A. Moradpour, C. Bowlas, F. Menou, P. Cassoux, J. Bonvoisin, J. -P. Launay, G. Dive, D. Dehareng, *J. Am. Chem. Soc.*, **117**, **1995**, 9995.
- [6] (a) S. F. Nelsen, H. Q. Tran, M. A. Nagy, *J. Am. Chem. Soc.*, **120**, **1998**, 298. (b) S. F. Nelsen, R. F. Ismagilov, Y. Teki, *J. Am. Chem. Soc.*, **120**, **1998**, 2200.
- [7] A. Dei, D. Gatteschi, C. Sangregorio, L. Sorace, *Acc. Chem. Res.*, **37**, **2004**, 827.
- [8] (a) J. Bonvoisin, J. -P. Launay, M. Van der Auweraer, F. C. De Schryver, *J. Phys. Chem.*, **98**, **1994**, 5052. (b) C. Lambert, G. Nöll, *J. Am. Chem. Soc.*, **121**, **1999**, 8434. (c) S. Utamapanya, A. Rajca, *J. Am. Chem. Soc.*, **113**, **1991**, 9242.
- [9] (a) O. Elsner, D. Ruiz-Molina, J. Vidal-Gancedo, C. Rovira, J. Veciana, *J. Nano Lett.*, **1**, **2001**, 117. (b) J. Sedo, D. Ruiz, J. Vidal-Gancedo, C. Rovira, J. Bonvoisin, J. -P. Launay, J. Veciana, *Adv. Mater.*, **8**, **1997**, 748.
- [10] C. Rovira, D. Ruiz-Molina, O. Elsner, J. Vidal-Gancedo, J. Bonvoisin, J. -P. Launay, J. Veciana, *Chem. Eur. J.*, **7**, **2001**, 240.
- [11] (a) B. P. Sullivan, H. Abruña, H. O. Finklea, D. J. Salmon, J. K. Nagle, T. J. Meyer, H. Sprintsxhnik, *Chem. Phys. Lett.*, **58**, **1978**, 389. (b) C. -F. Shu, M. S. Wrighton, *Inorg. Chem.*, **27**, **1988**, 4326.
- [12] (a) A. B. P. Lever, *Inorg. Chem.*, **29**, **1990**, 1271, (b) A. B. P. Lever, *Inorg. Chem.*, **30**, **1991**, 1980.
- [13] Y. Sasaki, M. Abe, *Chem. Rec.*, **4**, **2004**, 279, and references cited herein.
- [14] S. Ye, W. Zhou, M. Abe, T. Nishida, L. Cui, K. Uosaki, M. Osawa, Y. Sasaki, *J. Am. Chem. Soc.*, **126**, **2004**, 7434.
- [15] In mixed-valence complexes electron transfer phenomena can be monitored easily by the study of intervalence transitions which usually appear in the near-IR region: C. Creutz, *Prog. Inorg. Chem.*, **30**, **1983**, 1.
- [16] (a) A. A. Vlcek, *Coord. Chem. Rev.*, **95**, **1982**, 39. (b) B. K. Ghosh, A. Chakravorty, *Coord. Chem. Rev.*, **95**, **1989**, 239. (c) A. Juris, V. Balzani, S. Campagna, P. Belser, A. V. Zelewesky, *Coord. Chem. Rev.*, **95**, **1989**, 239. (d) C. G. Pierpont, C. W. Lange, *Prog. Inorg. Chem.*, **41**, **1993**, 331.
- [17] (a) S. P. Solodovnikov, N. N. Bubnov, A. I. Prokofev, *Usp. Khim.*, **49**, **1980**, 1. (b) R. R. Rakhimov, S. P. Solodovnikov, V. S. Pupkov, A. I. Prokofev, *Isv. Akad. Nauk SSSR*, **1990**, 1385.
- [18] C. W. Lange, B. J. Conklin, C. G. Pierpont, *Inorg. Chem.*, **33**, **1994**, 1276.
- [19] (a) O. Sato, J. Tao, Y. -Z. Zhang, *Angew. Chem. Int. Ed.*, **46**, **2007**, 2152. (b) H. Tian, S. Yang, *Chem. Soc. Rev.*, **2004**, 85. (c) A. Beyeler, P. Belser, *Coord. Chem. Rev.*, **230**, **2002**, 28. (d) L. Fabbrizzi, L. Prodi, *Chem. Soc. Rev.*, **24**, **1995**, 197. (e) J.-P. Launay, *Chem. Soc. Rev.*, **2001**, 386.
- [20] [Co(3,5-DTBCat)(3,5-DTBSQ)(phen)]: (a) D. M. Adams, D. N. Hendrickson, *J. Am. Chem. Soc.*, **118**, **1996**, 11515. (b) D. M. Adams, J. Noodleman, D. N. Hendrickson, *Inorg. Chem.*, **36**, **1997**, 3966. [[Co(3,6-DTBSQ)₂(pyz)][∞]: (c) O. -S. Jung, C. G. Pierpont, *J. Am. Chem. Soc.*, **116**, **1994**, 2229. [Mn(3,6-DTBCat)(3,6-DTBSQ)(μ-pyz)][∞]: (d) A. S. Attia, C. G. Pierpont, *Inorg. Chem.*, **36**, **1997**, 6184. [Co(3,5-DTBCat)(3,5-DTBSQ)(bpy)], [Co(3,6-DTBSQ)₂(tmeda)], [Co(3,6-DTBCat)(3,6-DTBSQ)(phen)]: (e) O. -S. Jung, C. G. Pierpont, *Inorg. Chem.*, **33**, **1994**, 2227.
- [21] A. B. P. Leven, P. R. Auburn, E. S. Dodsworth, M. Haga, W. Liu, M. Melnik, W. A. Nervin, *J. Am. Chem. Soc.*, **110**, **1988**, 8076.
- [22] R. M. Buchanan, C. G. Pierpont, *J. Am. Chem. Soc.*, **102**, **1980**, 4951.

[23] D. Ruiz-Molina, L. N. Zakharov, A. L. Rheingold, D. N. Hendrickson *J. Phys. Chem. Sol.*, **65**, **2004**, 831.

[24] (a) T. -Y. Liu, Y. J. Chen, C. C. Tai, K. S. Kwan, *Inorg. Chem.*, **38**, **1999**, 674. (b) A. -C. Ribou; J. -P. Launay, K. Takahashi, T. Nihira, S. Tarutani, C. W. Spangler, *Inorg. Chem.*, **33**, **1994**, 1325. (c) N. S. Hush, *Coord. Chem. Rev.*, **64**, **1985**, 135.

[25] M. B. Robin, P. Day, *Adv. Inorg. Chem. Radiochem.*, **10**, **1967**, 247.

[26] a) O. Hayaishi, M. Nozaki, *Science*, **164**, **1969**, 389. b) C. A. Tyson, A. E. Martell, *J. Am. Chem. Soc.*, **94**, **1972**, 939. c) A. Y. Girgis, A. L. Balch, *Inorg. Chem.*, **14**, **1975**, 2724. d) L. A. deLaire, R. C. Haltiwanger, C. G. Pierpont, *Inorg. Chem.*, **28**, **1989**, 644.

[27] C. L. Simpson, S. R. Boone, C. G. Pierpont, *Inorg. Chem.*, **28**, **1989**, 4379.

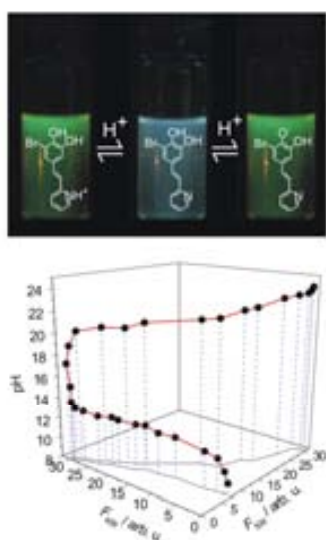
Chapter | 4

New Optically-Active Catecholate and Phenoxylate Based Ligands

Abstract

Three new optical ligands have been obtained and their coordination capabilities analysed. The first two ligands belong to a family of catecholates bearing aromatic groups where the electron localisation along both constituents leads to interesting emission properties. The third system is an azo unit bearing bis-phenolate ligand that shows interesting chromogenic properties. In addition to the multifunctional extra value that these ligands add into the field of VT phenomena, they also have potential applicability as organic chemosensors thanks to the presence of the diol ($-OH$) groups, which ensures a strong acid-base character.

a) Fluorescence Properties



b) Chromophoric Properties



4.1 Introduction

4.1.1 Multifunctional VT systems

The objective for this chapter was the design and synthesis of new optically active redox based ligands that can add an extra multifunctional value to the valence tautomerism phenomena. Previous examples of multifunctionality have already been reported. For example, Schultz *et al.*¹ generated a series of metal complexes with general formula $[\text{Tp}^{\text{Cum,Me}}\text{M}(\text{SQNN})]$ where M can be Zn (**64**), Cu (**65**) or Ni (**66**), $\text{Tp}^{\text{Cum,Me}}$ is hydro-tris(3-cumenyl-5-methylpyrazolyl)borate and SQNN is the donor-acceptor semiquinone-nitronyl nitroxide biradical ligand. Linking the nitronyl nitroxide (NN) moiety to a SQ ligand, the authors were able to stabilize the high spin triplet (S=1). Moreover, the spectroscopic techniques showed an interesting intraligand $\text{SQ}-\pi \rightarrow \text{NN}-\pi^*$ charge transfer transition unique into this type of chromophore molecules. In fact, this is one of the scarce examples where the same redox-active ligand has been properly functionalised. In other cases, such as those described by Awaga *et al.*² and Kitagawa *et al.*³ the functionalisation took place on the counter-ligand. In this order, Awaga *et al.*, reported the VT phenomena in the catechol-based complex **23**, where the bipyridine ligand is substituted with a nitronyl nitroxide radical ensuring additional switchable magnetic properties. In the second case, Kitagawa *et al.*, have prepared VT complexes where the bipyridine ligand is functionalised with long alkyl chains (**48** for n =13) that favour the presence of crystal phase transitions. A more detailed resume of all these examples is done in the introduction of Chapter 2 (Figure 2.4). However, as far as we know, the obtaining of optically-based VT multifunctional systems have not been described, in spite of their enormous interest. The combination of optical properties and IET could bring important implications in molecular scale electronic devices. For instance, any synergism where the optical property could be modulated in an “on-off” manner according to the presence or absence of an IET process could pave the definitive way for the development of VT-based molecular devices. A more detailed explanation about this concept is given in Figure 4.1.

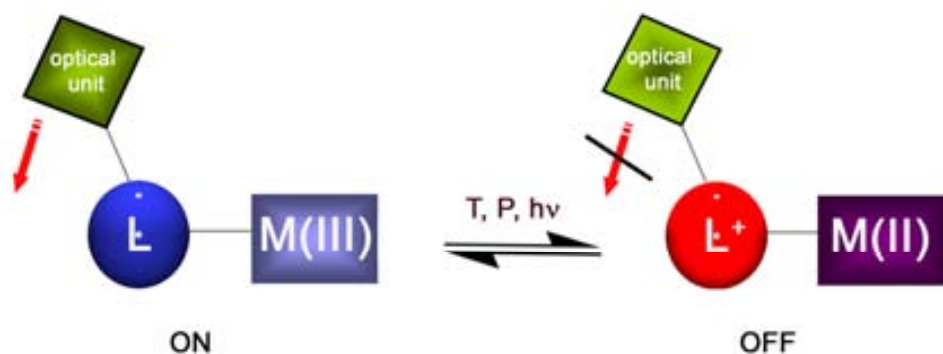
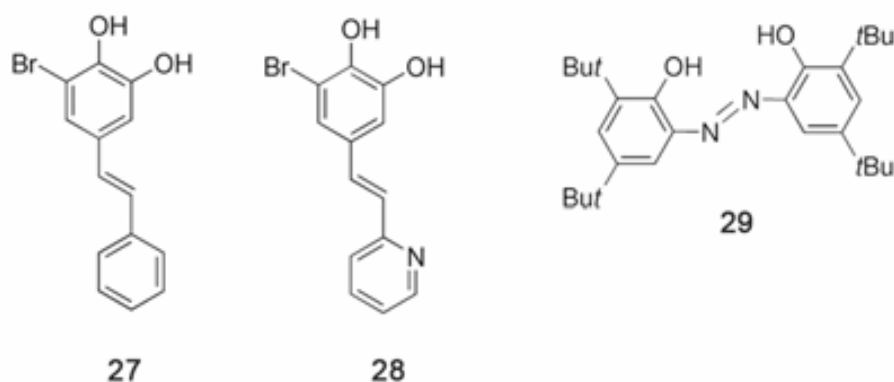


Figure 4.1. Schematic representation of a molecular system exhibiting a synergism between VT and an extra-optical property, such as fluorescence. The IET between the metal ion and the redox-active ligand influence (modulates) the optical properties of the pendant group.

On the quest to find suitable candidates that allow us to establish the observed multifunctional systems, ligands **27-29** were studied. The first two ligands belong to a family of catechol ligands bearing phenyl (**27**) and pyridine (**28**) moieties where the electron delocalisation along both constituent groups is expected to lead to fluorescence emission. The third system (**29**) is an azo ligand bearing bis-phenol units. The incorporation of the azo group ensures a multifunctional character thanks to their interesting optical properties.



Scheme 4.1.

In addition to the multifunctional extra value that these ligands can add into the VT field, they can also have potential as effective pH sensors. Indeed, in its free state, prior to any coordination process, the presence of -OH groups in the three aforementioned ligands ensures an acid-base response that is prompted to modulate their optical responses, both absorbance or fluorescence. A schematic representation of such modulation is given in Figure 4.2. This interesting pH-responsive behaviour may have important implications for the use of these systems as chemosensors. For this reason, in the next section, a revision of optical chemosensors is given.

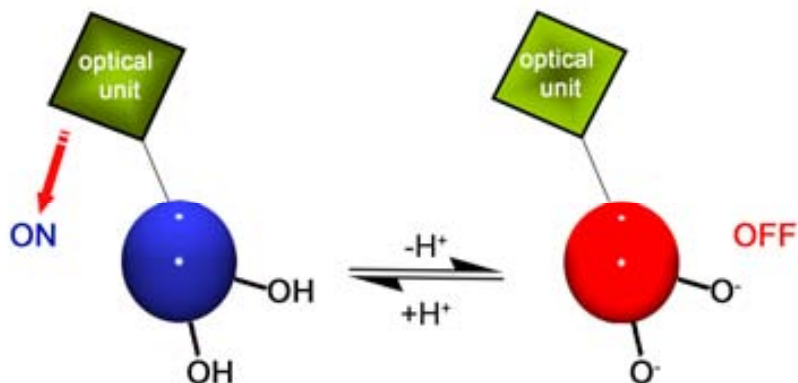


Figure 4.2. Representation of an aromatic pH-responsive chemosensor based on the presence of -OH groups.

4.1.2 Molecular optical chemosensors.

The design, characterization and device implementation of chemosensors has emerged as an active area of research due to their wide range applications in various fields of science and industry.⁴ In a general way, chromophore molecules show the ability to change their optical properties in response to the external environment that is acting in a physical or chemical manner into the molecule. Depending on the scientific field the architecture of the optical sensor should be adapted. For example, analytical and environmental chemist usually requires populations of sensor molecules which need to be bound to surfaces such as optical fibres.⁵ On the contrary, biochemists, clinical and medical scientists as well as cell biologists prefer to work with populations of freely mobile sensor molecules under a microscope,⁶ although fibre optic work is also possible.⁷ Nanotechnology scientist wish to deal with optical switches at the single molecule level with the help of scanning tunnelling microscopy⁸ and/or near-field scanning optical microscopy.⁹

Among the different sensing capabilities that can be explored, a great effort is being done in the sensing of cations (Hg^+ , Zn^{2+} or Cu^{2+})¹⁰ and anions, (ATP , PO_4^{3-} or ClO_4^-).¹¹ Nevertheless, chemosensors that report on acidity changes are becoming of increasingly interest due to the need for monitoring pH in many chemical and biological processes, clinical analysis and environmental protection.¹² In addition, pH-responsive molecular systems displaying optical activity have been proposed as logical operators to perform molecular computing.¹³ The optical pH sensors can be active to the absorbance (colorimetric detector) or the fluorescence¹⁴. The first one has lower sensitivity and selectivity than other types of detectors. For this reason, the use of strong chromophore groups, such as the azo group that is bearing ligand **29**, is highly recommended. More sensitive are the fluorescent based sensors.¹⁵ One of the simplest approaches consists on a fluorophore covalently linked to a polyamine.¹⁶ The mechanism that controls the emission properties in these types of systems is based on a photoinduced electron transfer (PET). The fluorescence intensity (I_f) decreases with an increase of the pH solution due to the deprotonation of the nitrogen atom and the subsequent electron transfer phenomena from the nitrogen atom to the photoexcited fluorophore that blocks the fluorescence.^{17,18} A representation of the PET mechanism is shown in Figure 4.3a. One of the groups most active on this field is that of Prof. A. P. de Silva and co-workers who have reported several of these examples as possible logic gates constituted by a receptor and a fluorophore separated by a spacer.¹⁹

An important issue of these fluorescent chemosensors, in comparison to glass electrodes, is that they allow for acidity detection in a narrow pH windows.^{12e-h} However their main disadvantage is that usually they are not suitable for measurements over wide pH ranges. In fact, the dynamic range of most common chemosensors, which present only a single pH-responsive group leading to one fluorescent and one non-fluorescent states upon pH variation (i.e. 'on-off' or 'off-on' probes), is limited to ~2 pH units.^{12f} Several strategies can be followed to broaden the sensing range of fluorescent pH chemosensors. On the one hand, this can be

achieved by mixing different systems responding to distinct pH values (Figure 4.3b).^{12f-h} More interestingly, pH detection over large intervals can also be attained with specific chemosensors, provided that they possess multiple pH-responsive groups giving rise to several protonation states with distinct optical properties.^{12e,20} Multistate molecular systems displaying pH-induced 'off-on-off'^{12e,21} or 'on-off-on'²² fluorescence profiles are particularly relevant examples of this latter case, that have attracted our attention.

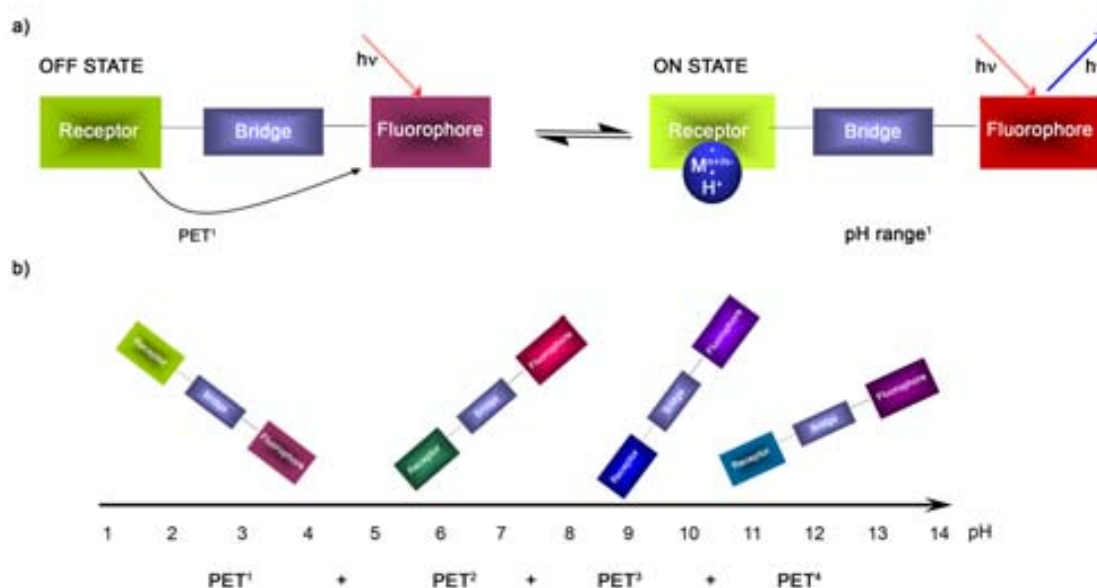


Figure 4.3. a) PET sensor design, where the signalling process depends on a molecular recognition event to PET between a covalently linked fluorophore and a receptor by the bridge. b) Approach designed by Prof. A. P. de Silva *et al.* consisting on parallel running PET sensor family with different receptors so that the sensing range of one members lies adjacent to that of another.

4.1.3 Summary

The vast majority of multistate fluorescent pH chemosensors so far reported are complex molecular systems composed by multiple fluorophore and electronically uncoupled pH-sensitive units capable of modulating its luminescent properties. The mechanisms for such modulation are various including PET and electronic energy transfer, among others.^{12e,20-22} Alternatively, the development of intrinsic fluorescent probes²³ for wide range pH detection, i.e. chemosensors where multiple pH-responsive groups are part of the π -system of the fluorophore, whose inherent emissive properties therefore vary with pH are attracting more attention in the last few years. These molecules allow for a relatively more simple synthesis of the chemosensors as well as an easier manipulation of the resulting structures. A nice example of this family of chemosensors is that of the well-known pH-responsive fluorescent probes such as fluorescein (67, Figure 4.4),^{13a,24} Specially considering that so far only a few examples have been reported. Compounds 27 and 28, prepared by covalently coupling a catechol unit with phenyl and pyridine moieties, respectively, are expected to fill such gap. π -Electron delocalisation along both

constituent groups is expected to lead to fluorescence emission in the visible region of the spectrum with a significant pH sensitivity thanks to the –OH groups of the catechol unit. More importantly, the additional acid-base activity of pyridine ($pK_a=5.2$ for pyridinium ion in water²⁵) should make compound **28** a suitable fluorescent probe for acidity detection over a broad pH interval.²⁶

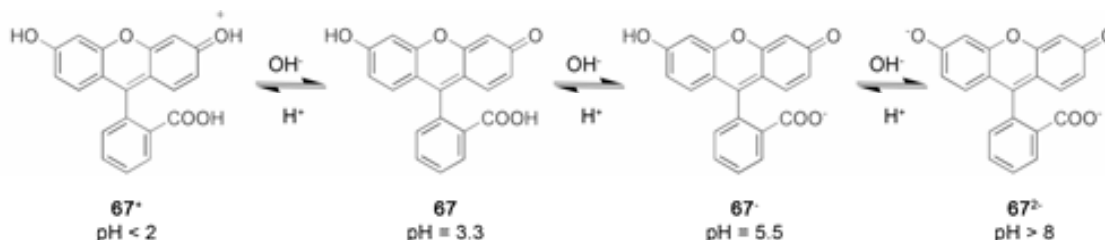


Figure 4.4. The four ionization states of fluorescein, each of which has a unique absorption spectrum.

On the other side, azo systems are synthetic organic dyes that have been used in the textile, cosmetic, paper, drug and food processing industries. Moreover, if combined with hydroxyl radicals were extensively used as primary oxidants in advanced oxidation processes for the degradation of organic pollutants²⁷ and textile dyes²⁸ from industrial wastes owing to their high reactivity. Finally, metal-azo complexes dyes were used also for the construction of DVD-R as a kind of efficient optical data storage,²⁹ thanks to their thermal stability at high temperatures and good solubility for a spin coating process onto a polycarbonate substrate. Metal-azo complexes present a high stability against light and provide an easier control of the wavelength according to the substituted groups. Then, the development of optically redox-active ligands, such as ligand **29**, is an ideal testing ground for the observation of sophisticated physical properties thanks to the synergistic effects. All these precedents make ligand **29** an excellent candidate to be also studied in this work.

In the first part of this chapter the fluorescent properties of ligands **28** and **29** will be detailed. In the second part, the chromogenic properties of compound **29** and its corresponding transition metal complexes will be described.

4.2 Results

4.2.1 Catechol derivatives as fluorescent chemosensors for wide range pH detection

The results are presented in Article V: *Catechol Derivatives as Fluorescent Chemosensors for Wide range pH Detection*. *Chem. Eur. J.*, 2008. (Submitted) The synthesis and characterization of these two ligands was developed by Gisela G. Bardají under the direction of Dr. Félix Busqué from the Universitat Autònoma de Barcelona. Experimental details of the different synthetic methodologies followed for the obtaining of ligands **27** and **28** were developed in Annex III. Quantum chemical calculations were developed by Dr. Jordi Hernando from Universitat Autònoma de Barcelona.

4.2.1.1 X-ray structure

All the attempts to obtain single crystals of **27** were unsuccessful in spite of the recurrent use of different crystallization techniques and solvents. More successful were the attempts to crystallize ligand **28**·HCl, for which single crystals were obtained after several different crystallisation trials. However, the crystals were too small to be solved by conventional CCD equipment, reason why they were solved at the BM16 Spanish-line of the synchrotron radiation facility (ESRF of Grenoble) with the help of Dr. Inhar Imaz from the Institut Català de Nanotecnologia (ICN).

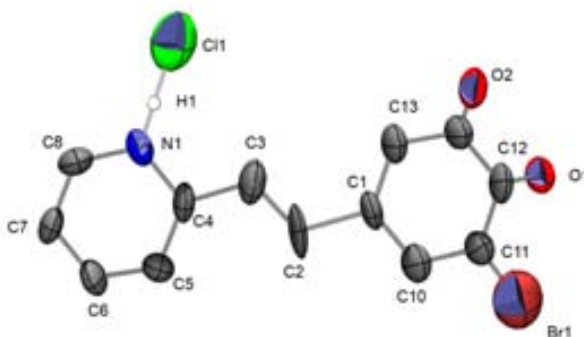


Figure 4.5. ORTEP view of the asymmetric unit of **28**·HCl at the 30 % probability level. Hydrogen atoms but those implicated in the H-bond with CL1 are omitted for clarity

The ORTEP view of ligand **28**·HCl which presents a planar structure with a C1-C2-C3-C4 dihedral angle of 173° as is shown in Figure 4.5. Hydrochloric acid is connected to the molecule through a very strong hydrogen bond (N···Cl⁻: 2.218 Å NHCl: 178.3°). Long intermolecular separation distances are observed (5.583 Å) result that lack of π - π interactions between the rows observed in the structure due to the voluminous halogenated atoms.

4.2.1.2 Acid-Base equilibrium of ligands **27** and **28**·HCl

The acid-base activity of the catechol and phenyl/pyridine moieties in compounds **27** and **28**·HCl was investigated by means of UV-Vis absorption spectroscopy. Figure 4.6b displays the changes measured in the absorption spectrum of an acetonitrile solution of **27** ($c_1=1 \times 10^{-5}$ M) upon base addition (tetrabutyl ammonium hydroxide, TBA). Clearly, a new band at $\lambda_{\text{abs}}=388$ nm appears with increasing pH, while the intensity of the initial peak at $\lambda_{\text{abs}}=319$ nm decreases. Similar results were obtained in other solvents different from acetonitrile (Table 4.1). The absorption red-shift encountered upon base addition is consistent with the deprotonation of a hydroxyl group in the neutral form **27** to yield an anionic species (**27**⁻), as previously reported for monohydroxystilbenes.^{30,31} Importantly, this process can be fully reverted back upon acid addition (hydrochloric acid), thus recovering the absorption spectrum of **27**.

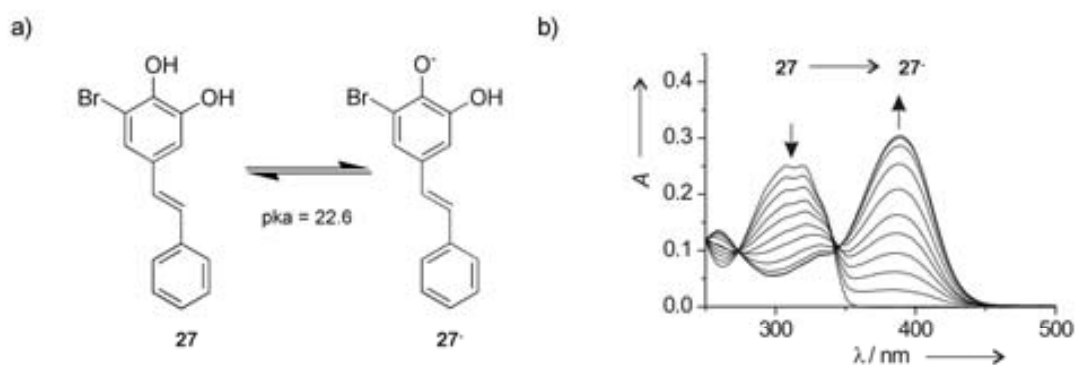


Figure 4.6. a) Molecular structures of the neutral (**27**) and anionic (**27**⁻) states of ligand **27**. The acidity constant determined spectrophotometrically for the reversible acid-base equilibrium between these states in acetonitrile is indicated. b) Variation of the absorption spectrum of **27** upon pH increase in acetonitrile ($c_1=1 \times 10^{-5}$ M). The spectra shown were measured at pH values of 17.0, 17.7, 19.0, 20.5, 21.9, 22.4, 22.6, 23.1, 23.2, 23.5, 24.0.

The acid-base equilibrium between **27** and **27**⁻ is also depicted in Figure 4.6b. As can be seen there, deprotonation to yield **27**⁻ has been tentatively assigned to take place on the –OH moiety at the *para* position of the catechol group according to inductive and conjugation considerations. This fact was confirmed by quantum chemical calculations (*vide infra*). From the variations of the absorption spectra with pH,³² an acidity constant value of $pK_a=22.6$ has been determined for this process in acetonitrile. Unfortunately, further basification of **27**⁻ to yield the double phenolate form of **27** ($\text{pH} > 25$ in acetonitrile), results in irreversible degradation of the compound. This fact has been attributed to both, (photoinduced) addition of water to the ethylenic double bond³³ or a polymerization process.

Interestingly, the presence of the pyridine unit in ligand **28**·HCl favours a more complex acid-base activity (see Figure 4.7a). The absorption spectrum of a 1×10^{-5} M solution of compound **28**·HCl in acetonitrile displays two different bands at $\lambda_{\text{abs}}= 327$ and 371 nm. The relative intensities of these bands vary with addition of HCl and TBA, the peaks at 327 and 371

nm becoming predominant at pH=14.1 and 8.5, respectively (Figure 4.7b). This indicates that even though ligand **28**·HCl was originally in its cationic form (**28**⁺), an equilibrium between the cationic form **28**⁺ ($\lambda_{\text{abs}}=371$) and its neutral state in which the pyridinium group is deprotonated (**28**, $\lambda_{\text{abs}}=327$) occurs on the acetonitrile solution. Interestingly this process can be controlled and reversibly displaced forward or backwards by acid-base titration, as already reported for related styrylpyridine compounds.^{34,35} Moreover, from the variations of the absorption spectra with pH, an acidity constant value of $\text{p}K_{\text{a}}=12.5$ has been determined for the deprotonation of the pyridinium group in acetonitrile.

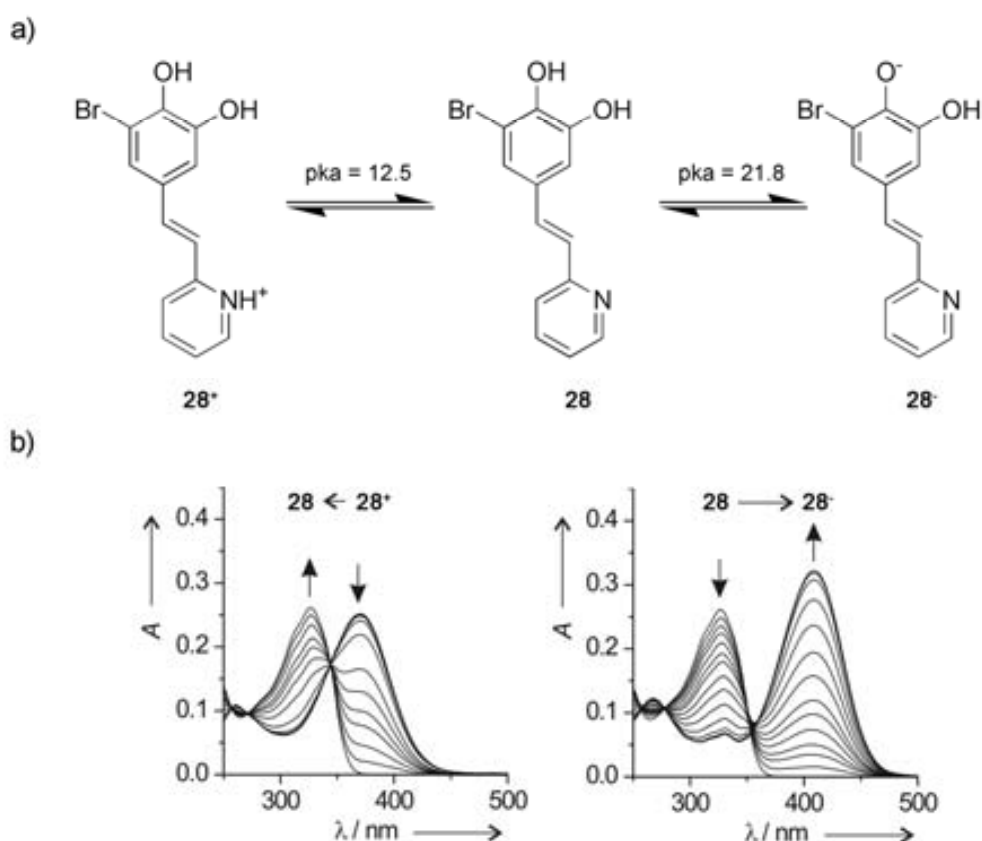


Figure 4.5. a) Cationic (**28**⁺), neutral (**28**) and anionic (**28**⁻) states of **28**·HCl. The acidity constants determined spectrophotometrically for the reversible acid-base equilibria between these states in acetonitrile are indicated. b) Variation of the absorption spectrum of **28**·HCl upon pH increase in acetonitrile ($c_2=1 \times 10^{-5}$ M). The left figure displays the changes arising from the acid-base equilibrium between **28**⁺ and **28**, which were measured at pH values of 8.5, 9.9, 10.7, 11.4, 11.8, 12.4, 12.5, 12.6, 12.9, 13.0, 13.7 and 14.1. The spectra shown in the right figure report on the acid-base equilibrium between **28** and **28**⁻, and they were registered at pH=14.1, 15.0, 16.9, 18.5, 19.8, 20.4, 20.9, 21.5, 22.2, 22.8, 23.1, 23.9, 24.2 and 24.8.

Table 4.1. Experimental and TD-DFT energies and intensities of the UV-vis absorption bands of the different protonation states of **27** and **28**·HCl.

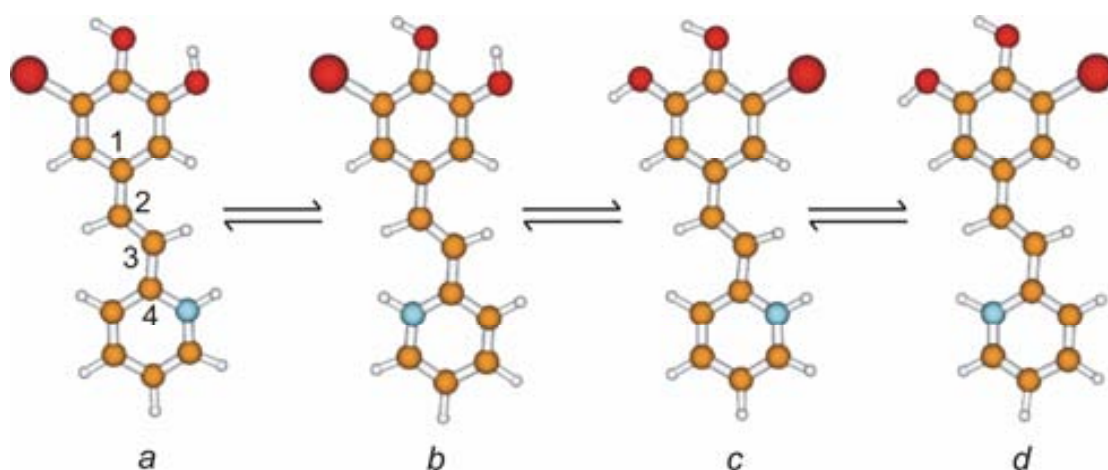
State	Solvent	Experimental ^[a]		TD-DFT ^[b]
		λ_{abs} [nm]	ϵ_{abs} [L mol ⁻¹ cm ⁻¹]	λ_{abs} [nm]
27	THF	325	21259	
	acetonitrile	319	25098	346
	DMSO	329	20711	
27⁻	THF	398	24621	
	acetonitrile	388	30385	406
	DMSO	399	21274	
28⁺	THF	379	22248	
	acetonitrile	371	24558	408
	DMSO	382	22164	
28	THF	334	25095	
	acetonitrile	327	26773	350
	DMSO	338	24178	
28⁻	THF	424	32169	
	acetonitrile	406	32362	422
	DMSO	421	28564	

[a] Measured at the absorption maxima. [b] B3LYP/6-311+G(d,p) level and accounting for acetonitrile solvent.

Subsequent deprotonation of neutral **28** to yield the anionic monophenolate state **28⁻** leads to additional variations in the absorption bands, as depicted in Figure 4.7b. Such variations are indeed in agreement with those previously found for compound **27**, i.e. red-shifted absorption upon base addition. This confirms deprotonation of the hydroxyl group at the *para* position of the catechol moiety of **28** at larger pH values ($pK_a=21.8$ in acetonitrile). Interestingly this second acid-base equilibrium is also fully reversible, i.e. the **28⁻** species can be reverted back to the **28** species, making feasible the three-state device shown in Figure 4.7a. However, as already described for compound **27**, further basification to deprotonate the second -OH group of **28⁻** leads to a degradation process (at pH >25 in acetonitrile), thereby preventing reversible conversion of **28⁻** into the double anionic diphenolate form. Similar results are

obtained in other solvents different from acetonitrile as summarized in Table 4.1, where the experimental energies and intensities of the UV-vis absorption bands of the different protonation states of **27** and **28**·HCl are shown.

. Density functional theory (DFT) calculations accounting for acetonitrile solvent were carried out to obtain the ground electronic state energies and optimal geometries of the different protonation states of **27** and **28**·HCl. In this case it is necessary to consider the different conformational forms,³⁶ of **27** and **28**·HCl that can be derived from the rotation of the catechol and pyridine rings around the C(1)-C(2) and C(3)-C(4) bonds, respectively. This fact is illustrated in Scheme 4.2, where the optimal geometries computed for the four possible rotamers of **27**⁺ are shown as a representative example. In all the cases, the calculations yield very similar ground electronic state energies for all possible rotamers of a given protonation state of **27** and **28**·HCl (less than 2.5 kcal mol⁻¹ of difference) suggesting the occurrence of an equilibrium mixture of different rotamers in acetonitrile solution confirming that an average behaviour is therefore measured in our spectroscopic experiments.



Scheme 4.2.

Finally, time-dependent functional theory (TD-DFT) calculations were carried out to compute the excitation energies and oscillator strengths of the absorption bands of the different protonation states of **27** and **28**·HCl. To account for conformational equilibria, TD-DFT calculations on the optimal geometries of all possible rotamers were performed. Minor differences of their spectroscopic parameters were observed for a given protonation state. Therefore, the final values of absorption energies and oscillator strengths were averaged over all possible rotamers taking into account the Boltzmann distribution of conformer populations at room temperature. The resulting values are compared to the experimental ones in Table 4.1. As can be seen there, clearly a good agreement between quantum chemical calculations and spectrophotometric measurements is observed. Thus, our computations reproduce into a good

extent the spectral shifts obtained experimentally upon pH variation since the deviations between the calculated excitation energies and the experimental absorption maxima (in energy units) fall below 10% in all cases. TD-DFT calculations also reveal that the absorption transitions measured occur between the HOMO and LUMO states of all investigated molecules. These frontier orbitals are delocalised over both the catechol and phenyl/pyridine rings, thereby explaining why the absorption spectrum changes upon protonation/deprotonation of substituents located in any of the two constituent units of compounds **27** and **28**·HCl.

4.2.1.3 pH modulated fluorescence

The emission properties of the different protonation states of compounds **27** and **28**·HCl have been evaluated. The fluorescence spectral maxima (λ_f) and quantum yields (Φ_f) measured on different solvents are shown in Table 4.2, whereas the corresponding fluorescence spectra in acetonitrile are given in Figure 4.8. Clearly, **27** and **27**⁻ as well as **28**⁺, **28** and **28**⁻ show distinct emissive behaviours confirming their potential use as fluorescent pH chemosensors.

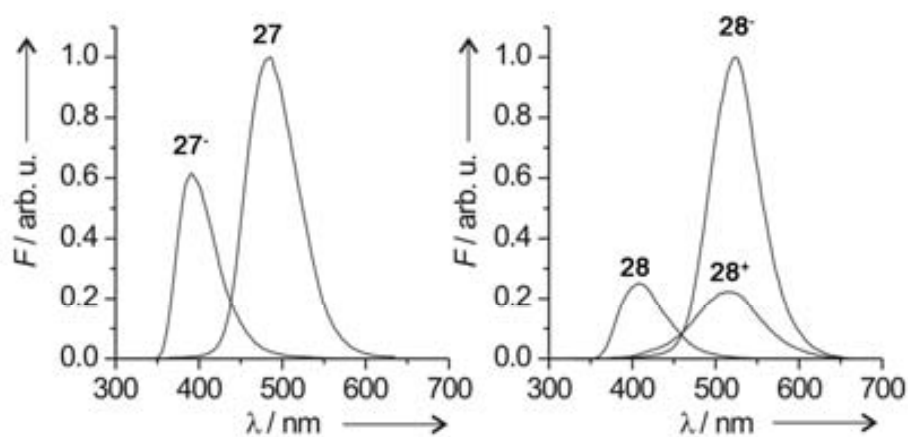


Figure 4.8. Fluorescence emission spectra of the different protonation states of compounds **27** ($\lambda_{\text{exc}}=280$ nm, $c_1=1\times 10^{-5}$ M) and **28**·HCl ($\lambda_{\text{exc}}=310$ nm, $c_2=1\times 10^{-5}$ M) in acetonitrile. Each spectrum is normalized with respect to the absorption at the excitation wavelength. Acid (HCl) or base (TBA) was added to adjust the pH of the solution to the values at which full conversion into the desired protonation state was achieved in each case: pH=17.0 (**27**) and 24.0 (**27**⁻) and pH=8.5 (**28**⁺), 14.5 (**28**) and 24.0 (**28**⁻).

Table 4.2. Fluorescence properties of the different protonation states of **27** and **28**·HCl.

State	Solvent ^[a]	λ_f [nm] ^[b]	Φ_f
27	THF	388	0.065
	acetonitrile	392	0.031
	DMSO	414	0.072
27⁻	THF	488	0.036
	acetonitrile	484	0.066
	DMSO	501	0.054
28⁺	THF	500	0.19
	acetonitrile	511	0.069
	DMSO	501	<0.01
28	THF	406	0.097
	acetonitrile	409	0.053
	DMSO	442	0.34
28⁻	THF	523	0.20
	acetonitrile	524	0.22
	DMSO	532	0.36

[a] Solvent dielectric constants are $\epsilon_{\text{THF}}=7.5$, $\epsilon_{\text{ACN}}=36.6$ and $\epsilon_{\text{DMSO}}=47.2$, whereas the Kamlet-Taft β factors accounting for their hydrogen bond acceptor capacity are $\beta_{\text{THF}}=0.55$, $\beta_{\text{ACN}}=0.31$ and $\beta_{\text{DMSO}}=0.76$;^[37] [b] Measured at the emission maxima.

The neutral forms **27** and **28** display a large red-shift in fluorescence spectra upon deprotonation (~100 nm), as previously observed for related monohydroxystilbenes^{30,31} or even for the absorption measurements. Similarly, protonation of **28** to yield **28⁺** not only leads to bathochromic absorption, but additionally results in red-shifted fluorescence. Solvatochromic effects on the fluorescence spectra of compounds **27** and **28**·HCl are also observed, which were ascribed to both changes in solvent polarity as well as in solvent hydrogen bond accepting capacity, as quantified by means of the Kamlet-Taft β factor.³⁷ Thus, similar fluorescence maxima are in general observed in THF and acetonitrile, since the higher hydrogen bond accepting capacity of the former ($\beta_{\text{THF}}=0.55$, $\beta_{\text{ACN}}=0.31$) is counterbalanced by the larger polarity

of the latter ($\epsilon_{\text{THF}}=7.5$, $\epsilon_{\text{ACN}}=36.6$). In the case of DMSO, its higher ϵ ($\epsilon_{\text{DMSO}}=47.2$) and β ($\beta_{\text{DMSO}}=0.76$) values lead to red-shifted emission for **27**, **27'**, **28** and **28'**. An opposite behaviour is found for **28⁺**, for which larger hydrogen bond interaction between the pyridinium group and THF or DMSO molecules results in hypsochromic displacement of the emission spectrum. Our experimental data shows that fluorescence quantum yields also vary for different solvents and protonation states of **27** and **28**·HCl (see Table 4.2). In case of compound **27**, both **27** and **27'** states present relatively low Φ_f values within the 0.03-0.07 range. However, while larger fluorescence quantum yields are obtained for **28** in solvents with high hydrogen bond accepting capacity (THF and DMSO), an opposite trend is observed for **28⁺**. Most importantly, larger Φ_f values are determined for all **28**·HCl states under selected conditions, a relevant feature for potential fluorescent sensing applications. This contrasts with previous studies on the effect of introducing a nitrogen atom in the styryl system, in which a decrease in fluorescence emission from stilbene to 2-styrylpyridine was observed.³⁸ Most probably, this difference arises from the effect of the hydroxyl and bromo substituents of the catechol ring. Indeed, a ten-fold increase in Φ_f has been reported for 3-hydroxystilbene with respect to stilbene in organic solvents,³⁰ thus demonstrating the critical effect of *meta*-substitution with –OH moieties on the photochemical properties of styryl systems. Consequently, the combined effect of the nitrogen atom and the hydroxyl substitution must account for the larger values of Φ_f typically obtained in this work for **28**·HCl with respect to **27** and stilbene ($\Phi_f=0.04$ in hexane³⁸).

4.2.1.4 Fluorescence pH-sensing

As we have shown in the previous sections the operation of the fluorescent compound **28**·HCl over a large pH interval has been attained thanks to the combination of two distinct acid-base groups displaying distinct pK_a values. Yet the capacity of this species to univocally respond to acidity changes must still be proved if a future pH sensor based on compound **28**·HCl is to be achieved. Therefore, to unambiguously prove that a single value of pH can be obtained under a given experimental condition a dual-wavelength detection process based on the determination of pair of F_{409} and F_{524} values at two different wavelengths (409 and 524 nm) has been established.

The three different protonation stable states of compound **28**·HCl exhibit different emissive properties in solution. The fluorescence spectrum of the neutral form **28** is ~100 nm blue-shifted with respect to **28⁺** and **28'**, whereas these two ionic species emit in the same spectral region but with different quantum yields (see Figure 4.9). As a consequence, if selective detection at the maximum of the emission spectrum of state **28** is performed (~400 nm), the fluorescence signal measured will be maximal at intermediate pH values and it will decrease for increasingly acid or basic media. This means that compound **28**·HCl behaves as an 'off-on-off' pH sensor under such detection conditions,^{12e,21} a situation depicted in Figure 4.9a (dark spheres). On the contrary, if the fluorescence detection window is centred on the

maximum of emission of $\mathbf{28}^+$ and $\mathbf{28}^-$ (~500 nm), the response of the system upon pH variation becomes of the 'on-off-on' type.²² Therefore, maximal fluorescence signal is detected at extreme values of pH in this case, as illustrated in Figure 4.9a (red squares). In the same Figure 4.7a the fluorescent 'off-on-off' and 'on-off-on' behaviours of $\mathbf{28}\cdot\text{HCl}$ in acetonitrile at different detection conditions are compared with simulations performed using the values of pK_a , absorption extinction coefficients and fluorescence quantum yields previously determined for this species. Clearly, a good agreement exists between the simulated and experimental data. Thus, the dependence of fluorescence intensity at $\lambda_{em}=409$ nm is rather symmetric around pH=17, as expected from the calculations. More importantly, an asymmetric curve describes the variation of the emission intensity with pH at $\lambda_{em}=524$ nm, which arises from the different Φ_f values of $\mathbf{28}^+$ and $\mathbf{28}^-$. This situation contrasts with the behaviour observed for previously reported fluorescence on-off-on systems.²²

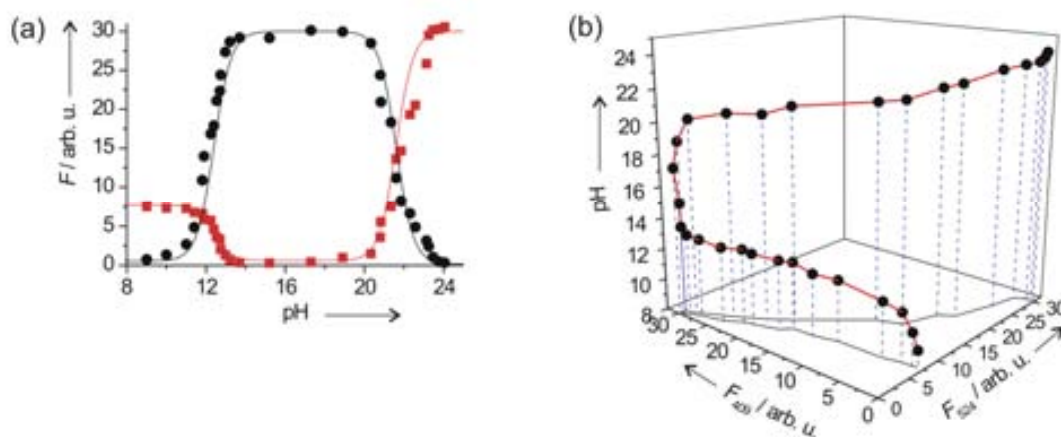


Figure 4.9.(a) pH dependence of the fluorescence intensity of $\mathbf{28}\cdot\text{HCl}$ in acetonitrile ($\lambda_{exc}=310$ nm, $c_2=1\times 10^{-5}$ M) at $\lambda_{em}=409$ nm (black) and $\lambda_{em}=524$ nm (red). Experimentally measured intensities are shown as symbols. Solid lines plot the simulated emission intensities computed using the pK_a constants, absorption extinction coefficients and fluorescence quantum yields determined for $\mathbf{28}\cdot\text{HCl}$ in acetonitrile. (b) 3D plot showing the correspondence between pH and the fluorescence intensities measured for $\mathbf{28}\cdot\text{HCl}$ in acetonitrile by means of dual-wavelength detection at $\lambda_{em}=409$ and 524 nm (F_{409} and F_{524}).

The coexistence of the fluorescent 'off-on-off' and 'on-off-on' behaviours of $\mathbf{28}\cdot\text{HCl}$ in acetonitrile at different detection conditions is an excellent scenario for the development of the sensing routine. Indeed, fluorescent molecular sensors exclusively displaying 'off-on-off' or 'on-off-on' profiles are mainly suited for detection of pH windows. Unfortunately, they can hardly provide any information on the pH values at which the system is *off*, thus preventing from sensing over larger pH intervals. This drawback can be overcome by the use of $\mathbf{28}\cdot\text{HCl}$ as fluorescent pH probe, since this compound shows both *off-on-off* and *on-off-on* responses upon pH variation when dual-wavelength detection is applied. Yet this condition is not sufficient for univocal pH sensing. To be capable of discerning low from high pH values at which the

fluorescence of the system simultaneously turns *off* (at $\lambda_{em} \sim 400$ nm) or *on* (at $\lambda_{em} \sim 500$ nm), the compound must display an asymmetric '*on-off-on*' profile, i.e. it must show different luminescent properties at those two pH ranges. As abovementioned, this is accomplished by **28**·HCl in some organic media due to the different fluorescence quantum yields of the **28**⁺ and **28**[•] states. Consequently, each value of pH will result in a univocal set of emission intensities at the two monitored wavelengths (e.g. F_{409} and F_{524} in acetonitrile).

This is demonstrated by the 3D plot in Figure 4.9b, which unambiguously proves that a single value of pH can be recovered from a given pair of F_{409} and F_{524} values measured by means of dual-wavelength detection. Therefore, we envisage compound **28**·HCl as a potential acidity sensor over large pH intervals in organic media. Moreover, since the '*on-off-on*' response can be altered by changing the solvent, compound **28**·HCl can behave as a multiply configurable pH chemosensor.^{12e} For instance, emission at $\lambda_{em} \sim 500$ nm of **28**·HCl in DMSO displays a simpler '*off-on*' profile with pH due to the very low fluorescence quantum yield of **28**⁺ in this medium. Therefore, since all the different protonation states of this species are fluorescent and show different luminescent properties, ratiometric methods can be used to retrieve pH values from the fluorescence response of **28**·HCl upon acidity variations, thus preventing from previous calibration of the sensing system.^{12d,f,20d}

4.2.1.5 Complexation ability of **28**·HCl

Unfortunately, all the attempts to obtain cobalt complexes with ligand **28**·HCl were unsuccessful in spite of the several different methodologies used. In most of the cases a mixture of diverse decomposition products and/or the starting materials were recovered after the reaction instead of the desired complexes. Compilations of five of the different synthetic experimental routes followed with this aim are explained in Experimental Section. The different reactivity of ligand **28**·HCl with respect to the classical 3,5-di-*tert*-butylcatechol (**11**) has been tentatively attributed to the bromine ion. Its high inductive effect, as well as its high volume, can make unstable the resulting complexes.

4.2.2 Synthesis, X-ray structure and reactivity of a sterically protected azo bisphenol ligand (**29**): on the quest for new multifunctional active ligands

In this section, the pH-modulated chromogenic properties of ligand **29** were studied. The objective was to modulate the intense absorption properties associated to the azo group and the electronic delocalisation through the deprotonation of this hydroxyl groups. The results are presented in Article IV: *Synthesis, X-Ray structure and Reactivity of a Sterically Protected Azo bisphenol Ligand: on the Quest for New Multifunctional Active Ligands*. Eur. J. Inorg. Chem., **2008**, 2278. The synthesis and characterisation of ligand **29** was developed by Javier Saiz under the direction of Dr. Félix Busqué at the Universitat Autònoma de Barcelona. The X-ray

single crystal structure of ligand **29** was solved by Dr. Klaus Wurst from Innsbruck University and analysed with the help of Daniel MasPOCH from the Institut Català de Nanotecnologia (ICN)

4.2.2.1 Synthesis and X-ray structure

Suitable crystals of **29** for X-ray diffraction experiments were obtained after slow evaporation of an ethanolic solution of the compound obtained by the synthetic procedure explained more in detail in the Experimental Section. Ligand **29** crystallizes in the $C2/c$ monoclinic space group with an inversion centre due to its symmetry, leading a *trans* geometry of the azo group with respect to both quinone moieties (Figure 4.10). This configuration seems to be favoured by two intramolecular hydrogen bonds between O1–H···N1 with distances of 1.695 Å and angles of 148.6°. More details about the synthesis and chemical characterization were developed in the Experimental Section.

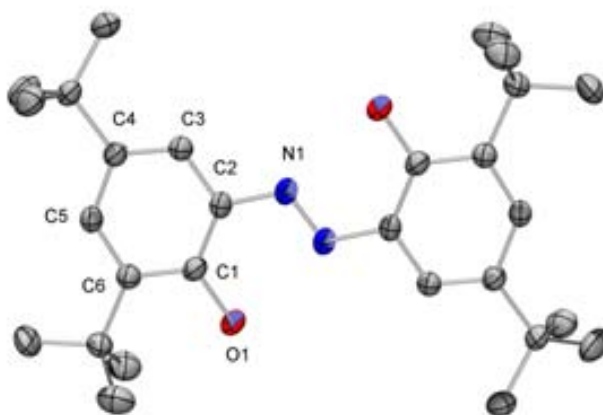


Figure 4.10. ORTEP drawing of the azo bisphenol **29** at the 30 % probability level. Hydrogen atoms have been omitted for the sake of simplicity.

4.2.2.2 Acid-base equilibrium of **29**

The acid–base activity of azo bisphenol **29** was investigated by means of UV–Vis absorption spectroscopy. An ethanolic solution of **29** displays two intense broad absorptions at 347 nm, most likely associated to the $n-\pi^*$ transition of the azo (N=N) group, and at 453 nm associated to the presence of the hydroxyl groups. Both bands are expected to be sensitive and experience variations upon acid/base addition, especially in the case of the second band.³⁹

Figure 4.11b displays the changes measured in the absorption spectrum of an ethanolic solution of **29** ($C_0 = 5.7 \times 10^{-5}$ M) upon base addition (80 μ l of tetrabutyl ammonium hydroxide (TBA, $C_0 = 4.3 \times 10^{-3}$ M)). As the pH increases, the band at 347 nm associated to the $n-\pi^*$ transition experiences a small variation with a decrease of its intensity. However, a new band at $\lambda_{\text{abs}} = 520$ nm appears, whereas the intensity of the initial peak at $\lambda_{\text{abs}} = 453$ nm, associated to

the presence of the hydroxyl groups decreases until it almost disappears. Deprotonation of the phenolic groups in the basic conditions causes a charge density shift and consequently a bathochromic shift of the new band that is accompanied by a colour change from yellow to violet.

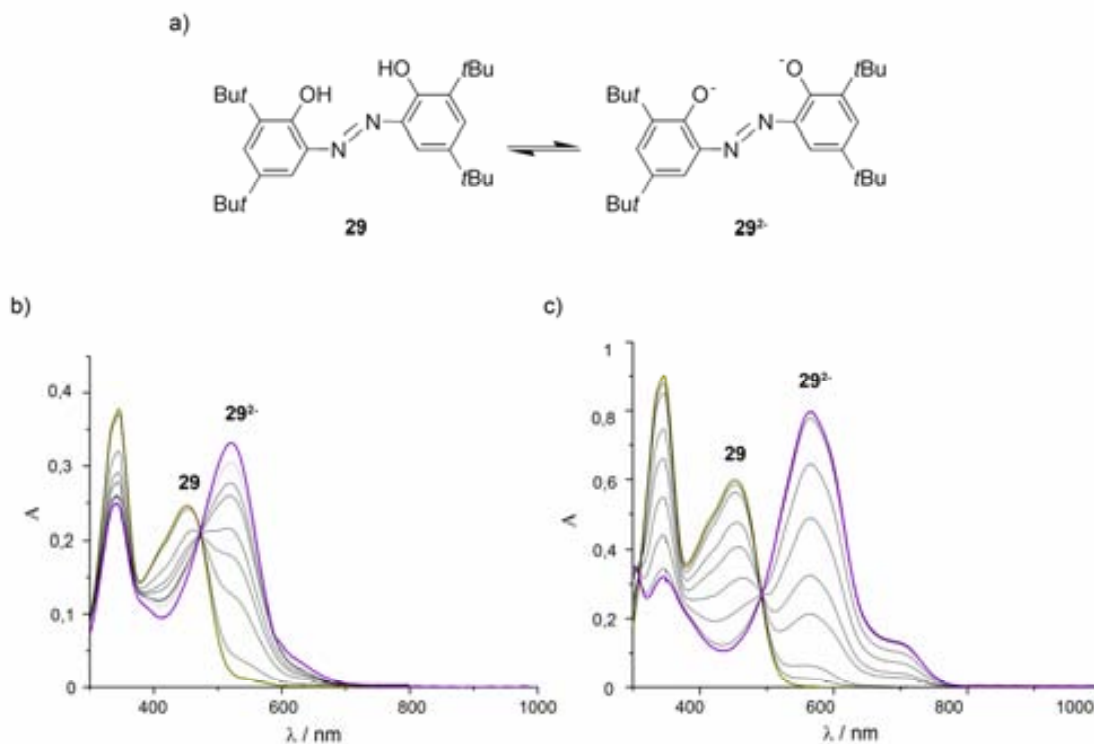


Figure 4.11. (a) Schematic representation of the acid–base equilibrium of **29**. (b) UV–Vis spectra of **29** (0.057 mM) upon pH increase in ethanol. (c) UV–Vis spectra of **29** (0.057 mM) upon pH increase in THF. In (b) and (c) each black line corresponds to the addition of 40 μL of TBA (0.4 mM) until the total deprotonation of **29**. The process is fully reversible upon addition of HCl.

The clean isosbestic point peaked at 493 nm also implies an equilibrium among the acid **29** and the basic **29²⁻** (Figure 4.11a), which most likely takes place through the formation of the monoanionic form. This basic form **29²⁻** will be named from now on as Cat-N=N-Cat²⁻, in the derived complexes by analogy with ligand Cat-N-SQ²⁻ (**10²⁻**). Finally, it is important to emphasise that this process can be fully reverted back upon acid addition (HCl), thus recovering the absorption spectrum of the neutral form **29** and the yellow colour of the solution. In any case, no protonation of the azo group was detected after addition of controlled amounts of acid.

The acid–base activity of **29** was also investigated in a THF solution (Figure 4.9c). In this solvent, the spectrum of **29** also displays the two intense broad absorptions at 347 nm and 453 nm, with no significant solvatochromic shift. Upon base addition, deprotonation of the phenolic groups takes place, inducing the appearance of the new band at $\lambda_{\text{abs}} = 565$ nm, whereas the intensity of the initial peak at $\lambda_{\text{abs}} = 453$ nm decreases. However, two main differences can be remarked. First, a solvatochromic effect was detected on the absorbance spectra for the **29²⁻**

species (the spectral parameters for the species **29** and **29²⁻** are summarized in Table 4.3), which could be tentatively ascribed to changes in solvent polarity as well as in solvent hydrogen bond accepting capacity.⁴⁰ And second, the intensity of the band at 347 nm decreases more considerably.

Table 4.3. UV/Vis spectroscopic data for ethanolic and THF solutions of the species **29** and **29²⁻**.

State	Solvent	λ / nm	$\epsilon / \text{M}^{-1} \text{cm}^{-1}$
29	EtOH	347, 453	13899, 9322
29²⁻		347, 520	7834, 11624
29	THF	347, 453	15789, 10488
29²⁻		347, 565	5623, 14348

4.2.2.3 Complexation ability of **29**

The complexation ability of **29** in front of transition metal ions such as Co(II) was initially studied in solution. In a first step, the deprotonated form **29²⁻** was obtained after basification of a 3 mL ethanolic solution of **29** ($C_0 = 1 \times 10^{-5}$ M) with 5 μL of TBA ($C_0 = 5 \times 10^{-2}$ M), as confirmed by UV–Vis spectroscopy. Afterwards, 25 μL of an aqueous solution of $\text{CoCl}_2 \cdot 6\text{H}_2\text{O}$ ($C_0 = 9 \times 10^{-4}$ M) was added. Immediately, the band at $\lambda_{\text{abs}} = 520$ nm characteristic of the **29²⁻** form starts to decrease, whereas a new band at $\lambda_{\text{abs}} = 560$ nm with two shoulders at $\lambda_{\text{abs}} = 520$ nm and at $\lambda_{\text{abs}} = 484$ nm, associated to the formation of the corresponding cobalt complex **29·Co**, increases. The appearance of the new band is accompanied by a colour change from violet to red–purple. The complexation ability of ligand **29** was also tested by direct reaction of **29** with an ethanolic solution of cobalt acetate, whose basic character is expected to deprotonate the azo bisphenol ligand. The UV–Vis spectra of an ethanolic solution of **29** upon constant additions of cobalt acetate are shown in Figure 4.10b. In this case, addition of 240 μL of a solution of $\text{Co}(\text{CH}_3\text{COO})_2 \cdot 4\text{H}_2\text{O}$ ($C_0 = 1 \times 10^{-3}$ M) into the ethanolic solution of the ligand **29** ($C_0 = 5.5 \times 10^{-5}$ M) also induces a shift of the band at $\lambda_{\text{abs}} = 453$ nm characteristic of **29** to $\lambda_{\text{abs}} = 560$ nm with both shoulders at $\lambda_{\text{abs}} = 520$ nm and $\lambda_{\text{abs}} = 484$ nm due to the formation of complex **29·Co**. As expected, the acetate counterion of the metal salt is sufficiently acid to deprotonate the azo ligand, leading to the formation of complex **29·Co**. Moreover, the process can be fully reverted back upon acid addition (HCl), thus recovering the absorption spectrum of the neutral form **29**, and consequently, the yellow colour of the solution.

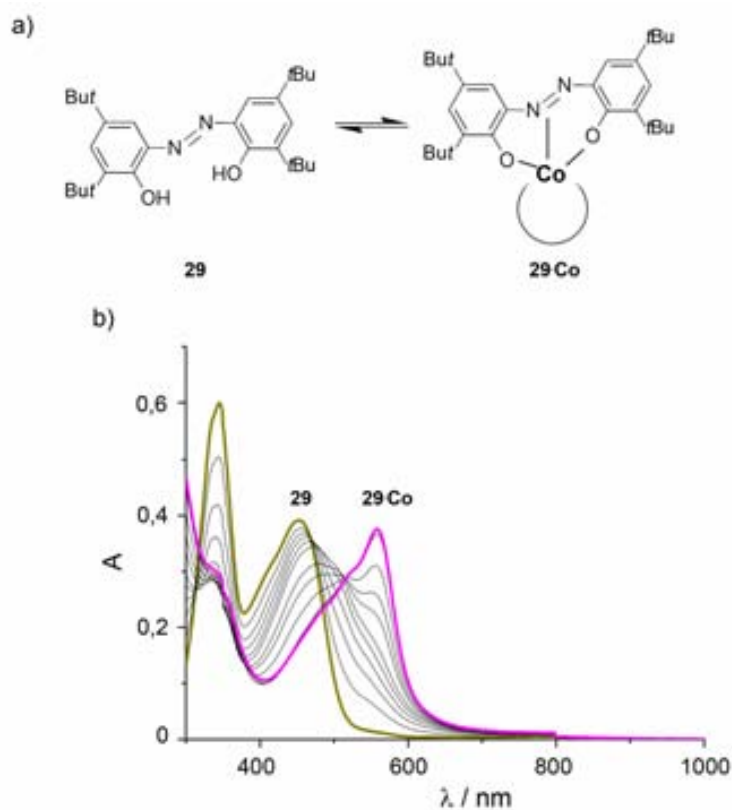


Figure 4.12. (a) Schematic representation of the complexation equilibrium of **29**. (b) UV-Vis spectra of **29** (0.057 mM) where $\text{Co}(\text{CH}_3\text{COO})_2 \cdot 4\text{H}_2\text{O}$ (1 mM) was added at constant volumes of 24 μL .

To shed more light into the reactivity of ligand **29** and the nature of the complex formed upon reaction with a cobalt salt, we also faced the straight chemical synthesis of a transition metal complex bearing ligand **29**. For this, we were inspired by the methodology described by Pierpont⁴¹ and Dei *et al.*,⁴² for the synthesis of transition metal complexes bearing Schiff-base iminoquinone ligand (**10**). These authors showed that 3d metal ions react with 3,5-di-*tert*-butylcatechol (**11**) and aqueous ammonia in the presence of air, yielding complexes of the Schiff-base biquinone ligand. Moreover, for the case of the copper metal ion, an excess of ammonia induces a redox cascade reaction coupled with air oxidation that is responsible for the formation of a related azophenolate complex (**68**).⁴³ Taking these precedents into account and only after several different reaction trials, reaction of **11** (6 eq.), ammonia (excess) in aerobic conditions and a mixture (50:50) EtOH:H₂O with $\text{CoCl}_2 \cdot 6\text{H}_2\text{O}$ (1 eq.) yielded complex $[\text{Co}(\text{Cat-N=N-Cat})(\text{H}_2\text{O})_3] \cdot 2.5\text{EtOH} \cdot \text{H}_2\text{O} \cdot \text{Cl}$ (**69**) as characterized by X-ray diffraction and chemical analysis. More details about the synthesis, X-ray diffraction and chemical characterisation are given in Experimental Section. Most likely, the reaction mechanism takes place through the formation of complex **25**. Indeed, upon addition of an excess of concentrated aqueous ammonia into a solution of 3,5-di-*tert*-butylcatechol and $\text{CoCl}_2 \cdot 6\text{H}_2\text{O}$, the solution turned to a dark violet colour characteristic of the formation of **25**. However, after 10 minutes under stirring the solution started to turn gradually to lighter violet and finally to the characteristic red-purple colour of

complex **25**. After 4 hours of stirring, the solution was filtered recovering a purple compound characterized by chemical analysis as complex $[\text{Co}(\text{Cat-N-SQ})(\text{Cat-N-BQ})]$, which partially confirms its formation as an intermediate species along the reaction. Afterwards, the solution was rested for two hours, and crystals of complex **69** suitable for X-ray diffraction analysis were collected.

Complex **69** crystallises in the $P\bar{1}$ triclinic space group. The asymmetric unit contains one molecule of **69**, one chlorine counter ion, two and a half ethanol molecules and one water molecule of crystallisation. As is depicted in Figure 4.13, the cobalt ion displays octahedral coordination geometry by binding to two oxygen and one nitrogen atoms of $\mathbf{29}^{2-}$ (Cat-N=N-Cat^{2-}) and three water molecules. In this case, **29** is acting as a tridentate ligand with the cobalt ion forming both typical five- and six-membered chelate rings with the cobalt atom. All bond lengths and angles are characteristic and similar to those previously reported for other azo bisphenolate-based complexes.⁴³ The most important cell parameters, bond lengths and angles are given in the Experimental Section.

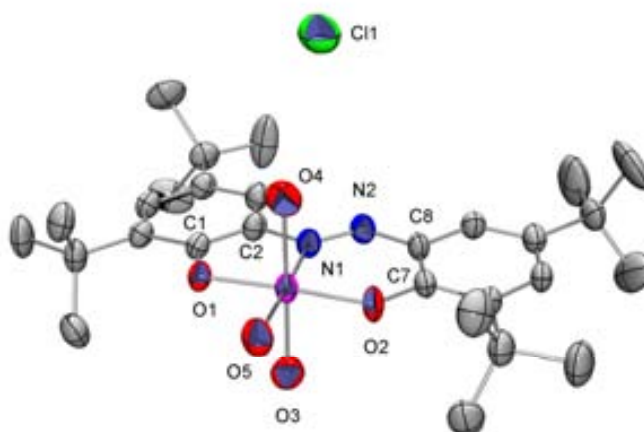


Figure 4.13. ORTEP drawing of azo bisphenol **69** at the 30 % probability level. Hydrogen atoms, chlorine counterion and solvent molecules are omitted for clarity.

Elemental analysis and electrospray-(+) in methanol of a polycrystalline sample of **69** are in agreement with the structure previously described. The FT-IR spectrum (KBr pellet) of **69** exhibits peaks at 1268 cm^{-1} and 1450 cm^{-1} , which are characteristic of the $\nu(\text{C-O})$ and $\nu(\text{N=N})$ modes.³⁹ The $\nu(\text{O-H})$ mode for the three coordinated water molecules appears as a broad band from 3300 to 3100 cm^{-1} . The electronic spectra in ethanol consists of an intense band with maxima at 553 nm ($1.2 \times 10^4\text{ M}^{-1}\text{ cm}^{-1}$) followed by two shoulders at 512 nm and 476 nm , respectively. Interestingly, these bands are similar to those observed for $\mathbf{29}\cdot\text{Co}$ in solution, which confirmed the series of experiments shown in Figure 4.12.

For comparison purposes the electronic spectrum of complex **69** was also monitored in two additional solvents. The most intense band shifts its maxima at 560 nm ($7.4 \times 10^3 \text{ M}^{-1} \text{ cm}^{-1}$) in THF and at 565 nm ($6.2 \times 10^3 \text{ M}^{-1} \text{ cm}^{-1}$) in toluene. The shoulders are shifted at 523 nm and 489 nm in THF, and 529 nm and 492 nm in toluene, confirming the existence of a solvatochromic effect as previously described for compound **29²⁻** (Cat-N=N-Cat²⁻). In addition, ¹H-NMR spectra of deuterated methanolic solutions of **29·Co** and **69** also suggest that both complexes are almost identical. Indeed, as described in the Experimental Section, the signals attributed to the four *tert*-butyls groups and the four aromatic protons are very similar, with small shift differences according to the expected different coordination environment of the Co(III) ion in **25·Co** and **69**.

The magnetisation temperature dependence in the temperature range of 5–300 K under an external applied magnetic field of 0.5 T exhibited a diamagnetic behaviour along the whole temperature range. These results are consistent with the formulation of the ligand in the form of a diamagnetic azo bisphenolate (**29²⁻**) and Co(III). The extra positive charge is compensated by the presence of the chloride anion. This charge assignment was also confirmed by cyclic voltammetry. The cyclic voltammetry of complex **69** shows two reversible one-electron waves at +1.093 V, assigned as an oxidation ligand-centred process, and –1.083 V, which has been as the reduction of Co(III) to Co(II) or in less extent to a ligand-centred process.

Finally, the redox activity of ligand **29** previously described suggested us to explore the possible existence of valence tautomerism for complex **69** by means of variable-temperature UV-Vis spectroscopy in the 280–370 K temperature range. An external stimuli such a temperature may induce a reversible IET between the redox active ligand and the metal ion. However, and in spite of the different solvents and solvent mixtures used, no valence tautomerism could be detected for **69**. In all the cases, a strong reduction of the intensity bands followed by the apparition of new bands at very short wavelengths is observed. This behaviour has been attributed to a decomposition of the complex under the used experimental conditions as confirmed by the irreversibility of the process.

4.2.2.4 Three-states switching array

The studies previously described did not exhibited VT phenomena but confirmed the suitability of **29** to create a chromophoric array of three states with significantly different colours that can interconvert reversibly between them by means of acid/base and complexation reactions. The UV-Vis spectra of the three species **29**, **29²⁻** and **29·Co** and a schematic representation of the different mechanisms that can be followed to interconvert between them are shown in Figure 4.14.

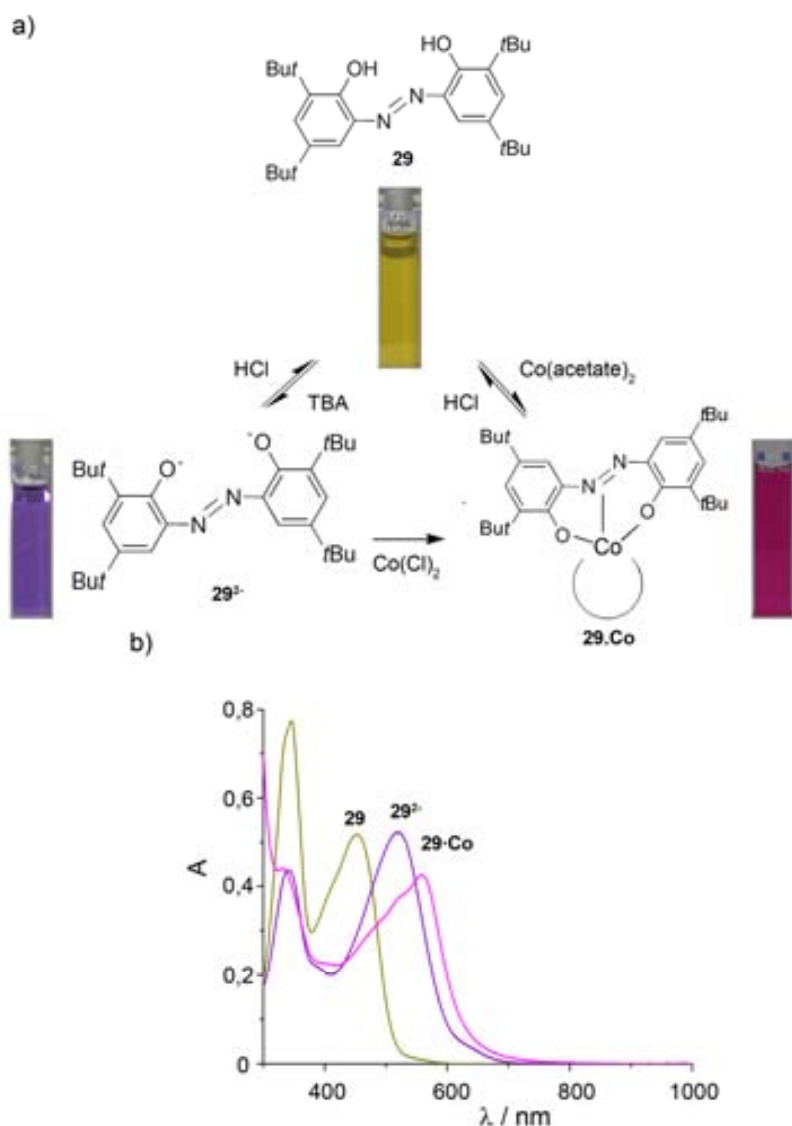


Figure 4.14. a) Schematic representation of the three–state switching array. b) UV–Vis spectra of an ethanolic solution of **29** (0.055 mM) with the initial addition of 20 μL TBA (0.8 M) to generate $\mathbf{29}^{2-}$ and subsequent addition of 240 μL of $\text{Co}(\text{Cl})_2 \cdot 6\text{H}_2\text{O}$ (1 mM) to generate $\mathbf{29} \cdot \text{Co}$.

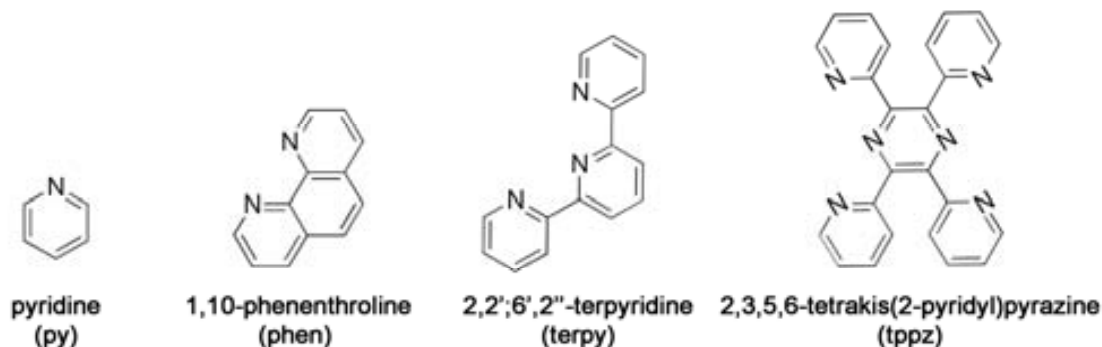
The yellow colour of **29** changes to violet and red–purple upon addition of a base such as TBA and $\text{Co}(\text{Cl})_2 \cdot 6\text{H}_2\text{O}$, respectively. In the first case, the dianionic compound $\mathbf{29}^{2-}$ (Cat=N=N–Cat²⁻) is formed, whereas the addition of the cobalt salt induces the formation of the $\mathbf{29} \cdot \text{Co}$ complex. In both cases, subsequent addition of HCl makes the process fully reversible. The colour changes can be nicely detected via the naked eyes, as shown in Figure 4.14a. This fact was also observed for complex **69**. Upon addition of HCl to an ethanolic solution of complex **69**, crystals of pure **29** (40 % yield) were obtained by recrystallisation from the solution, opening an alternative high–yield methodology for the obtaining of **29** to those described in a previous section. Finally, the reverse reaction, i.e., addition of further base to the acidic solution of **29** and free cobalt ion did not work. For this to be done, further addition of cobalt acetate is necessary

4.2.3 Cobalt complexes based on the azo bisphenol ligand 29

The spectroelectrochemical characterisation was realised in collaboration with Dr. Vega Lloveras and Dr. José Vidal from the Institut de Ciència de Materials de Barcelona. All the crystalline structures that will be shown next were solved by Dr. Klaus Wurst from Innsbruck University and analysed with the help of Daniel MasPOCH from the Institut Català de Nanotecnologia (ICN)

4.2.3.1 Synthesis, X-ray structures and molecular geometry

In a previous section we showed that the reaction of 3,5-di-*tert*-butylcatechol (**11**) with cobalt acetate in the presence of ammonia yielded complex **69** in a straightforward way, without the need of the previous ligand (**29**) synthesis. The feasibility of this synthetic procedure was used to prepare new complexes where the water molecules of complex **69** have been replaced by different nitrogen-based counterligands, such as pyridine or 1,10'-terpyridine. The list of the different nitrogen-based counterligands used in these experiments is shown in Scheme 4.3.



Scheme 4.3.

The addition of the nitrogen-based ligands is prompted to ensure the stability of these complexes by replacing the labile water ligands. On the other side, these ligands are also expected to favour the presence of IET processes, including VT phenomena by giving the appropriate electronic balance. The summary of the different synthetic routes followed is shown in Figure 4.15.

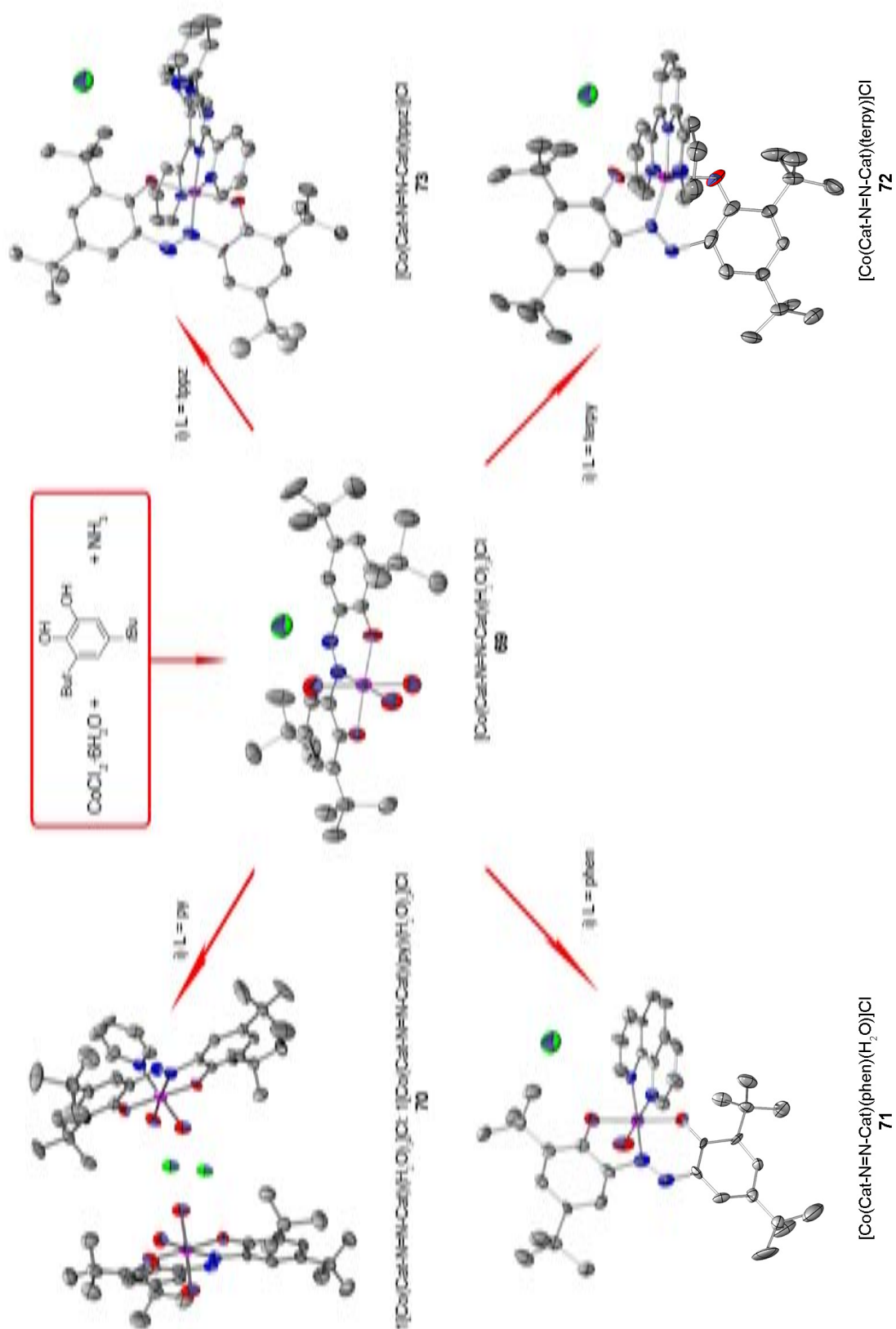


Figure 4.15. Schematic representation for the synthesis of complexes **70-73**. In all the cases the first step consists in the obtaining of complex **69**, by a direct reaction of 3,5-di-*tert*-butylcatechol with $\text{CoCl}_2 \cdot 6\text{H}_2\text{O}$ in ammonia medium. After this, complex **69** (1 mmol) was mixed with 1 mmol of a nitrogen-based ligand in a mixture solution ethanol: CH_2Cl_2 , yielding the desired complex. Slow diffusion of hexane into a CH_2Cl_2 solution of the complex yielded suitable crystals.

As can be seen there, initially complex **69** was synthesised by direct reaction of compound **11** with cobalt acetate in aqueous ammonia media. Later, complex **69** is reacted with the different counterligands in a mixture of ethanol:CH₂Cl₂ yielding a precipitate after 30 minutes of reaction. Finally, the slow diffusion of hexane in a CH₂Cl₂ concentrated solution of each complex allowed the obtaining of suitable crystals for X-ray diffraction. More details on the synthesis and crystallographic data are given in the Experimental Section.

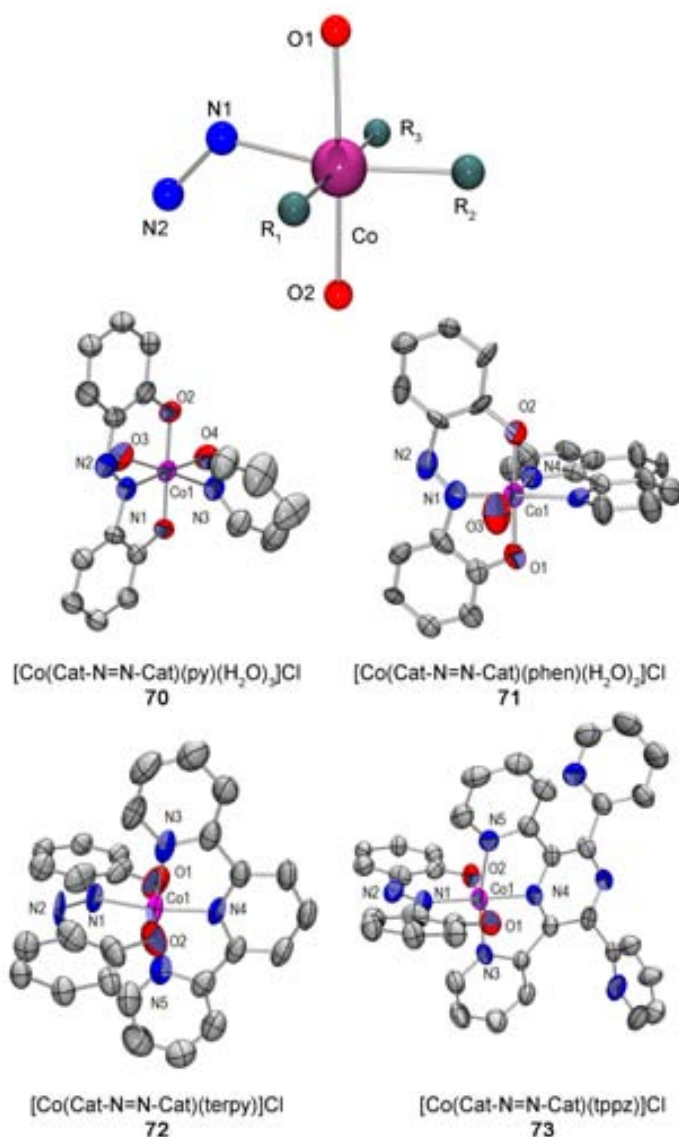


Figure 4.16. ORTEP plot at the 30% probability level for complexes **70-73**. *Tert*-butyl groups of the azo bisphenolate ligand (**29**²⁻) are omitted for clarity.

In all the cases the cobalt ion displays octahedral coordination geometry, as represented in Figure 4.16, with **29** as a tridentate ligand in the dianionic form **29**²⁻ (Cat-N=N-Cat²⁻). And the rest of the coordination sphere completed by the nitrogen-based counter-ligand and water molecules.⁴⁴ Indeed, the use of the tridentate ligands terpyridine (**72**) and pyrazine (**73**)

completed the octahedral coordination sphere. On the contrary, the use of a bidentate ligand such as phenanthroline leaves an empty coordination position which is occupied by a water molecule (**71**). As expected, in the case of the monodentate pyridine there are two water molecules filling the coordination sphere though it has to be emphasised that it co-crystallises with complex **69** with a 1:1 ratio. All the attempts to obtain the pure pyridine complex were unsuccessful. In addition to the crystallographic characterization, all the complexes were also chemically characterised by elemental analysis and electrospray experiments. Moreover the FT-IR spectrum (KBr pellet) of all complexes exhibit peaks around 1280 and 1480 cm^{-1} characteristic of the $\nu(\text{C-O})$ and $\nu(\text{N=N})$ modes.³⁹

4.2.3.2 Magnetic and spectroscopic characterization.

The molar paramagnetic susceptibility data of crystalline samples of complexes **70-73** were obtained with a SQUID susceptometer in the 2-400 K temperature range at a constant field of 0.1T. The diamagnetic contribution was corrected taken into account the Pascal constants and the measurement of an empty holder. The magnetisation temperature dependence of all the samples under such experimental conditions indicates a μ_{eff} close to zero along the whole temperature range, as expected for a diamagnetic species. This is in agreement with the presence of the cobalt ion in its diamagnetic Co(III) oxidation state, and the azo bisphenolate ligand also in its diamagnetic form (Cat-N=N-Cat^{2-}), being the extra positive charge compensated by the presence of a chlorine anion. Increase of the χT value at high temperatures was observed, fact that was attributed both to a temperature independent paramagnetism (TIP) effect associated to the cobalt ion and/or to a strong diamagnetic contribution, rather than to any VT process. As a representative example, the μ_{eff} vs. T of complex **72** is shown in Figure 4.16.

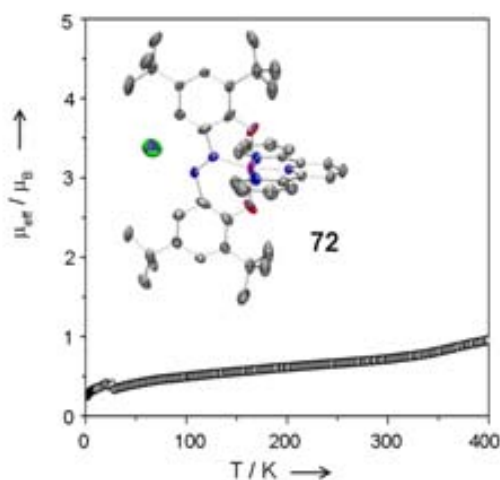


Figure 4.17. μ_{eff} vs. T plot for a microcrystalline sample of complex **72**.

These results were fully supported by the measurements of the magnetisation curves versus the external field at different temperatures in solid state as well as by EPR spectroscopy in solution, for which no signal was observed.

The electronic spectra of complexes **70-73** were very similar to that previously reported for **69**, consisting of an intense band centred around 565-590 nm followed by two shoulders at smaller wavelengths (Figure 4.18). A resume of the $\lambda_{\max}(\epsilon)$ found for each one of the complexes is presented in Table 4.4. The corresponding value for complex **70** has not been calculated since it contains not only the desired pyridine derivative but also another molecule of complex **69** within the asymmetric unit.

Table 4.4. Spectral characterisation of a CH_2Cl_2 solution of complexes **69**, **71-73**, showing the red-shift of the maxima band due to the different counterligand.

Complex	69	71	72	73
$\lambda_{\max} / \text{nm}$	565	579	581	583
$\epsilon / 10^4 \text{ M}^{-1}\text{cm}^{-1}$	2.0	1.3	1.2	1.7

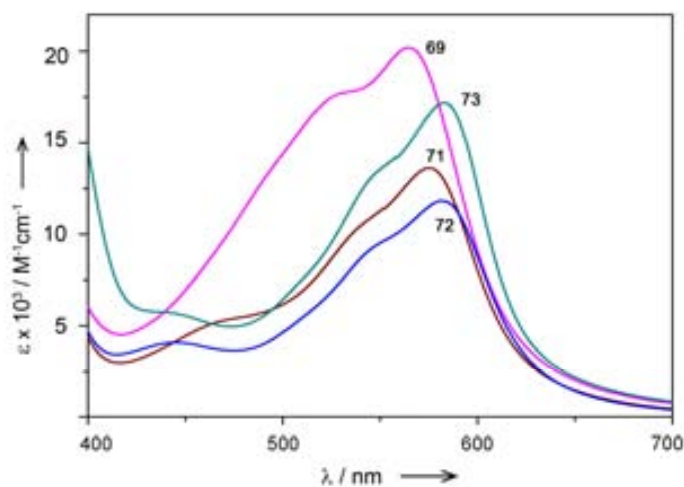


Figure 4.18. UV-Vis. spectra obtained for a CH_2Cl_2 solution of **69** and **71-73**, complexes ($1 \times 10^{-4} \text{M}$).

Finally, the variable temperature UV-Visible spectroscopy of all the complexes over the broad temperature range of 173-363 K was studied on the quest for the existence of VT within this family of complexes. The low temperature experiments ($< 273 \text{ K}$) were performed at the laboratory of Prof. J. -P. Sutter, at the Laboratoire de Chimie de la Coordination (LCC-CNRS). In none of the cases significant variations that could be attributed to the presence of an IET between the redox-active ligand and the metal ion were observed. As an example, the variable

temperature UV-Vis spectroscopy of a toluene solution (1×10^{-4} M) of complex **72** is shown in Figure 4.19. As can be seen there, a temperature decrease induces an increase of the intensity of the bands, fact that is most likely due to the variations of the solvent density, among others. No significant isosbestic points were also observed. The lack of VT for these complexes was also confirmed by EPR and $^1\text{H-NMR}$ in solution. Indeed, toluene solutions of these complexes are EPR silent over the same temperature range whereas the Evans Method reveal a similar magnetic behaviour to that observed in solid state, with no signal of interconversion at all. If present, VT phenomena would be observed by the different techniques previously described with significant variations.

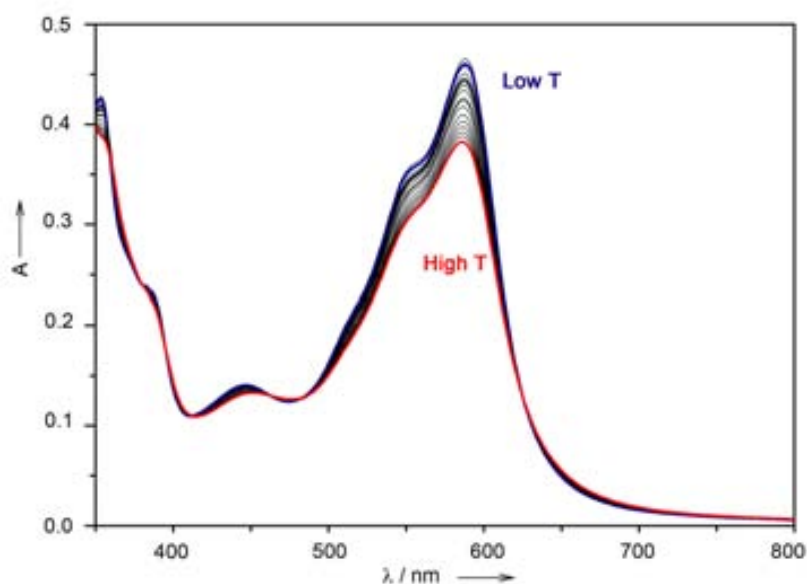


Figure 4.19. Temperature dependence of the electronic absorption spectrum of a toluene solution (1×10^{-4} M) of complex **72** obtained in the temperature range of 173 K to 363 K. Each intermediate spectrum corresponds to an increment of 10 K.

4.2.3.4 Spectroelectrochemistry.

The cyclic voltammetry of dichloromethane solutions of (2×10^{-3} M) of complexes **71-73** were obtained with Bu_4NPF_6 (tetrabutylammonium hexafluorophosphate) 0.1 M as supporting electrolyte. As an example, the cyclic voltammogram of complex **72** is shown in Figure 4.20.

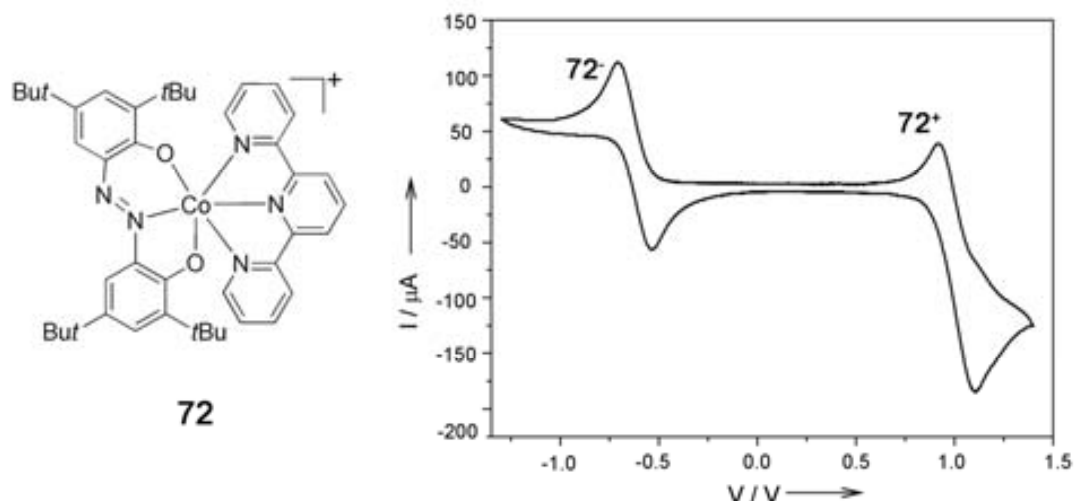


Figure 4.20. Cyclic voltammetry of a CH_2Cl_2 solution (2×10^{-3} M) of complex **72** containing 0.1 M Bu_4NPF_6 .

The cyclic voltammetry of complex **72** exhibits two reversible redox couples, a reversible oxidation process with a $E_{1/2} = 1.0$ V and a reversible reduction process at $E_{1/2} = -0.6$ V vs. the Ag/AgCl electrode. A close look to the oxidation process reveals the presence of a second oxidation process, which was assigned to the presence of an impurity. The oxidation process has been tentatively assigned to the oxidation of ligand **29**²⁻ whereas the reduction has been tentatively assigned⁴⁵ as an azo centred redox-process. The possible reduction of the Co(III) metal ion or the terpyridine ligand are expected to take place at higher voltages.⁴⁶ The reversibility of both processes was confirmed by combined coulombimetric and spectroscopic experiments.

Table 4.5. Electrochemical data for complexes **71-73** in V vs Ag/AgCl with Pt working electrode in a CH_2Cl_2 solution ($\sim 2 \times 10^{-3}$ M) containing 0.1 M Bu_4NPF_6 at 298 K and 100 mV/s. Potential values are given vs. Ag/AgCl. $\Delta E_{1/2} = E_{1/2}^2 - E_{1/2}^1$.

Complex	$E_{1/2}^1 / \text{V}$	$E_{1/2}^2 / \text{V}$	$\Delta E_{1/2} / \text{V}$
71	0.8	1.1	0.3
72	-0.6	1.0	1.6
73	-0.4	1.2	1.6

The reduction of a dichloromethane solution of the complex **72** at -1.1 V (2.4×10^{-3} M) was followed by UV-visible-NIR spectroscopy (Figure 4.21). The stepwise reduction leads to a decrease of the band centred around 600 nm characteristic of the azo group as the shoulder

localised at high energies (521 nm) increases. These experimental results confirm that the reduction process takes place selectively in the azo group. Moreover no IVT band attributed to the presence of an IET was observed in the whole frequency range. Finally it has to be emphasised that the reduced species is EPR silent

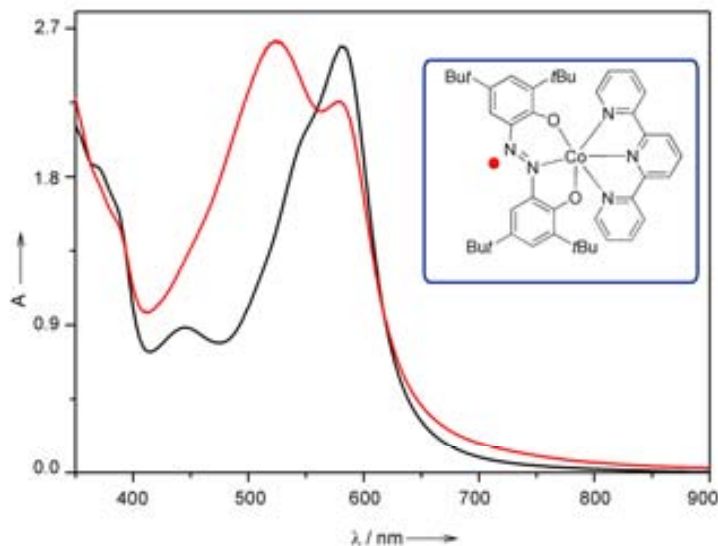


Figure 4.21. UV-Visible-near IR spectra for the spectroelectrochemistry of complex **72** at -1.1 V in a CH_2Cl_2 solution (2×10^{-3} M) containing 0.15 M of Bu_4NPF_6 at 298 K. In black is depicted form **72**, and in red the reduced form **72'**.

On the other side, the EPR spectrum of an electrochemically oxidised solution of complex **72** (Figure 4.22) shows the typical spectrum of a semiquinone radical coordinated to a cobalt ion.⁴⁷ It consist of an 8-lines pattern originated by the hyperfine coupling with the ^{59}Co nuclei with a nuclear spin $I=7/2$ (100% abundance). No hyperfine coupling with the aromatic protons was observed.

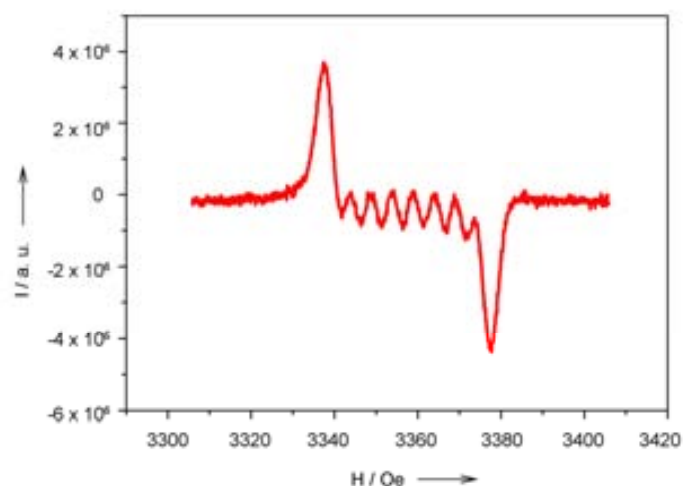


Figure 4.22. X-band EPR spectra of a CH_2Cl_2 solution of radical oxidised form **72'** at 298 K.

The oxidation of a dichloromethane solution of complex **72** (2×10^{-3} M) was also followed by UV-Vis NIR spectroscopy (Figure 4.23). The stepwise oxidation leads to a small decrease of the band centred around 600 nm as new small bands at 480 and 750 nm increases. More interesting is the observation of two new bands in the near-IR region where the maxima have been assigned at 1681 and 2167 nm by a deconvolution process as is shown in Figure 4.23.

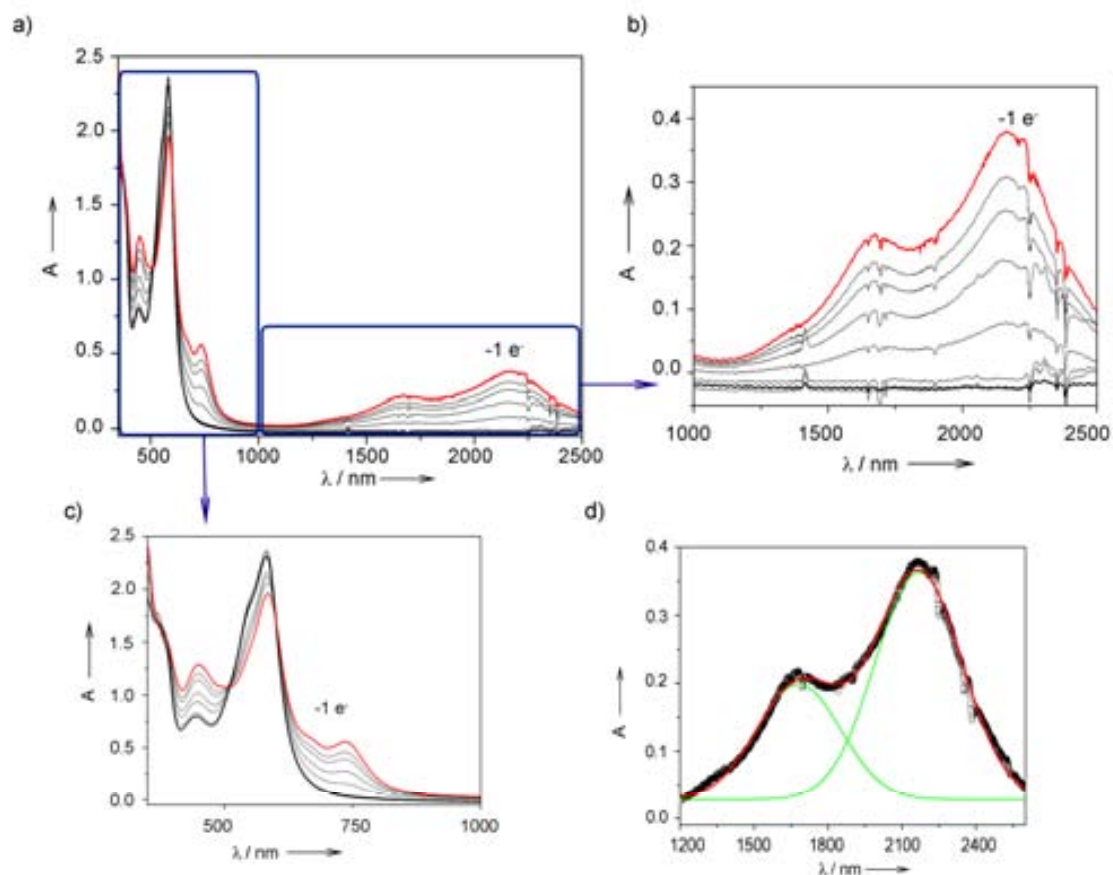


Figure 4.23. a) UV-Visible-Near IR spectra for complex **72** (black line) and the electrochemically generated oxidised form **72⁺** (red line) in a CH_2Cl_2 solution (2×10^{-3} M) containing 0.15 M of $\text{Bu}_4\text{NPF}_6^-$ at 298 K. Zoom of the spectrum at different wavelength ranges; b) near-IR 1000-2800 nm and c) 480-1000 nm, where each intermediate spectrum corresponds to the partial oxidation forms (0.2, 0.4, 0.6, 0.8, 0.9 $-e^-$). d) Deconvolution of the near-IR bands.

Finally, it is important to emphasise that the two IVT bands have been assigned to the presence of an IET as shown in Figure 4.24. Indeed, the oxidation of complex **72** leads to the existence of an electron hole that is localised in one of the aromatic rings, resulting in the formation of a ligand-centred MV system. Therefore, the two aromatic rings with different oxidation state, formally the electro-active organic units, are connected through an azo group that is acting as a bridge for the electron transfer process.^{1, 48}

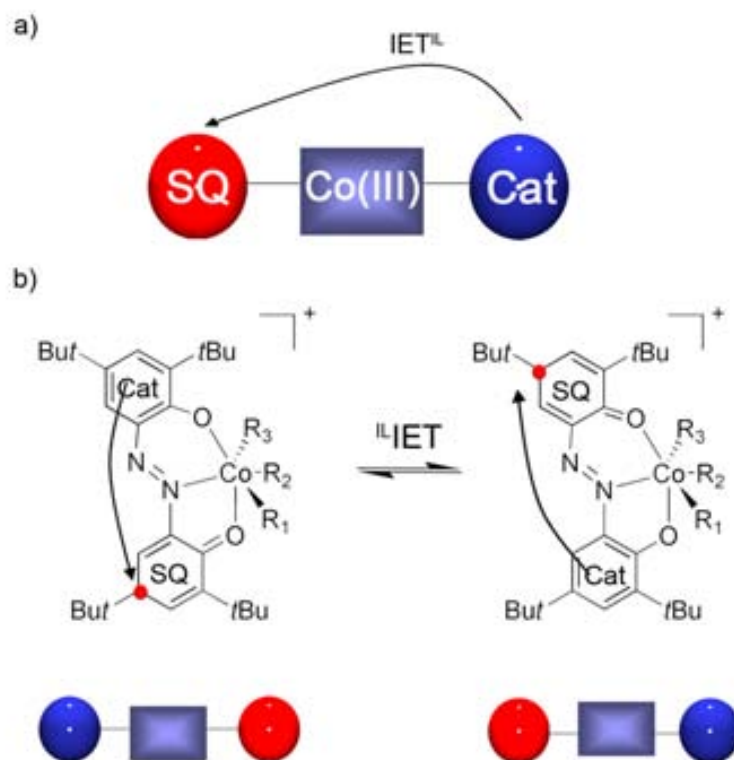


Figure 4.24. Schematic representation of the intraligand IET (IET_{IL}) process that occurs on the azo bisphenol complexes 70^+ - 73^+ .

Moreover, the possibility for the electron transfer to take place between the azo bisphenolate ligand and the terpyridine was ruled out after the study of complexes **71** and **73** under the same experimental conditions. As can be seen in Figure 4.25, both complexes bearing different nitrogen-based ligands also exhibit the same IVT bands after partial oxidation.

More difficult to understand and justify is the observation of two IVT bands, instead of one. To explain this situation, two main reasons can be argued. The first one is the presence of more than one IET, within the same molecule. And second, and most likely, is the possibility that the IET between the aromatic rings takes place through two different pathways, the azo bridge and/or the metal ion.⁴⁹ Further studies are currently being developed to assess this possibility.

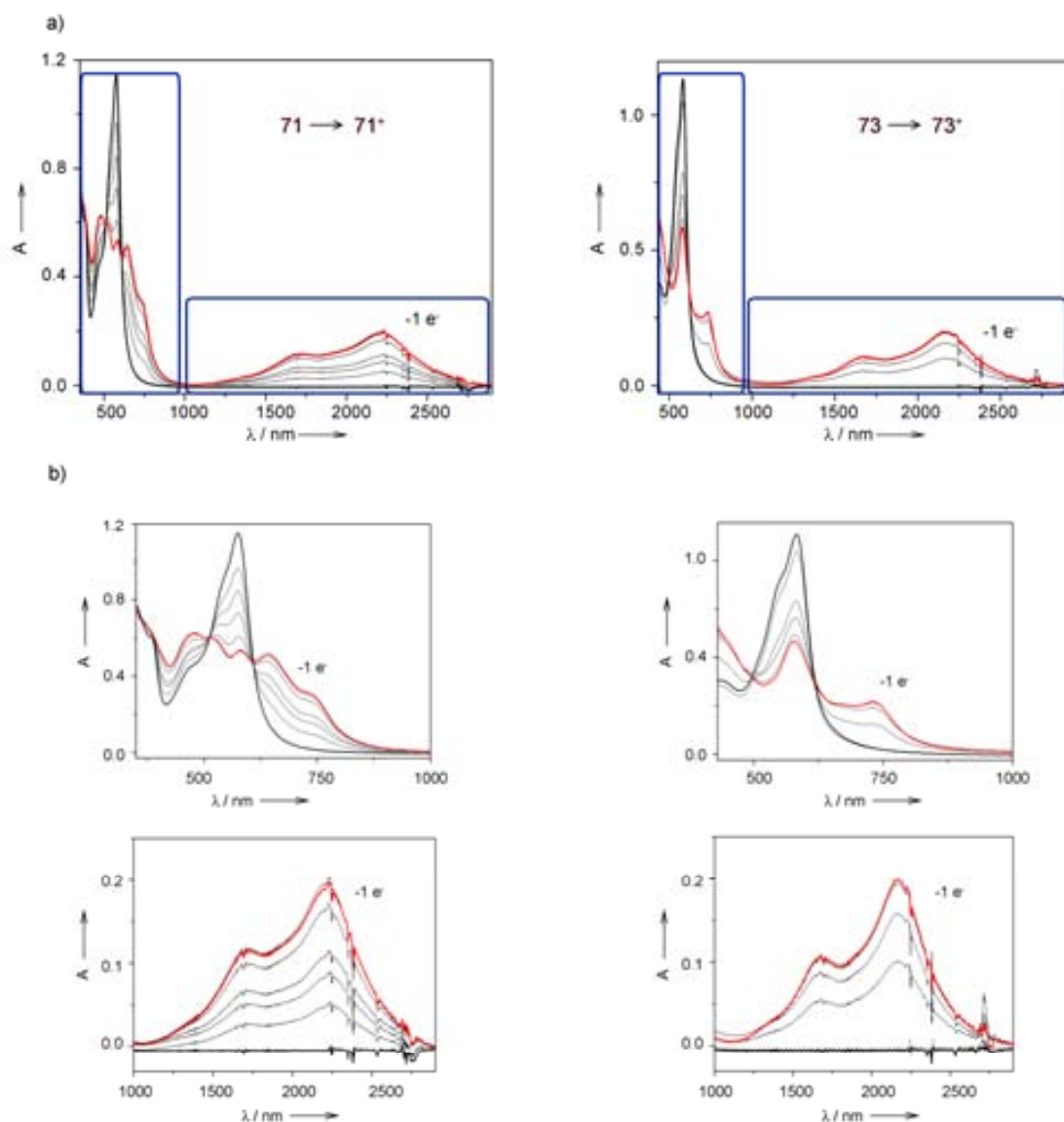


Figure 4.25. a) UV-Visible-Near IR spectra for complexes **71** and **73** (black lines) and the electrochemically generated oxidised form **71⁺** and **73⁺** (red lines) in a CH_2Cl_2 solution (9×10^{-4} M; 6×10^{-4} M) containing 0.15 M of Bu_4NPF_6 at 298 K. b) Zoom of the spectrum at different wavelength ranges; UV-Vis. 480 -1000 nm and near-IR 1000-2800 nm region. Each intermediate spectra corresponds to the partial oxidation forms (0.2, 0.4, 0.6, 0.8, 0.9 $-e^-$)

4.2.3.4 Synthesis, X-ray structure and physico-chemical characterisation of the neutral complex $[\text{Co}(\text{Cat-N=N-Cat})(\text{Cat-N=N-SQ})]$ (**74**)

The interesting IET previously described have been finally enforced by the synthesis and characterisation of complex **74**, where the combination of two azo bisphenolate ligands can be used to tune the IET, as will be explained next. Complex **74** was obtained after refluxing a toluene solution of complex **69** during 2 hours. After cooling the solution, a slow evaporation of the mother liqueur yielded red single crystals suitable for X-ray diffraction experiments. As previously described for the family of complexes **69-73**, the cobalt ion displays the typical octahedral coordination geometry. The two azo bisphenolate ligands are binded to the metal ion

in a tridentate manner, forming five- and six-membered chelate rings around the metal ion with an orthogonal disposition between them, similar to complex **25**. A schematic representation of this geometry is shown in Figure 4.26a.

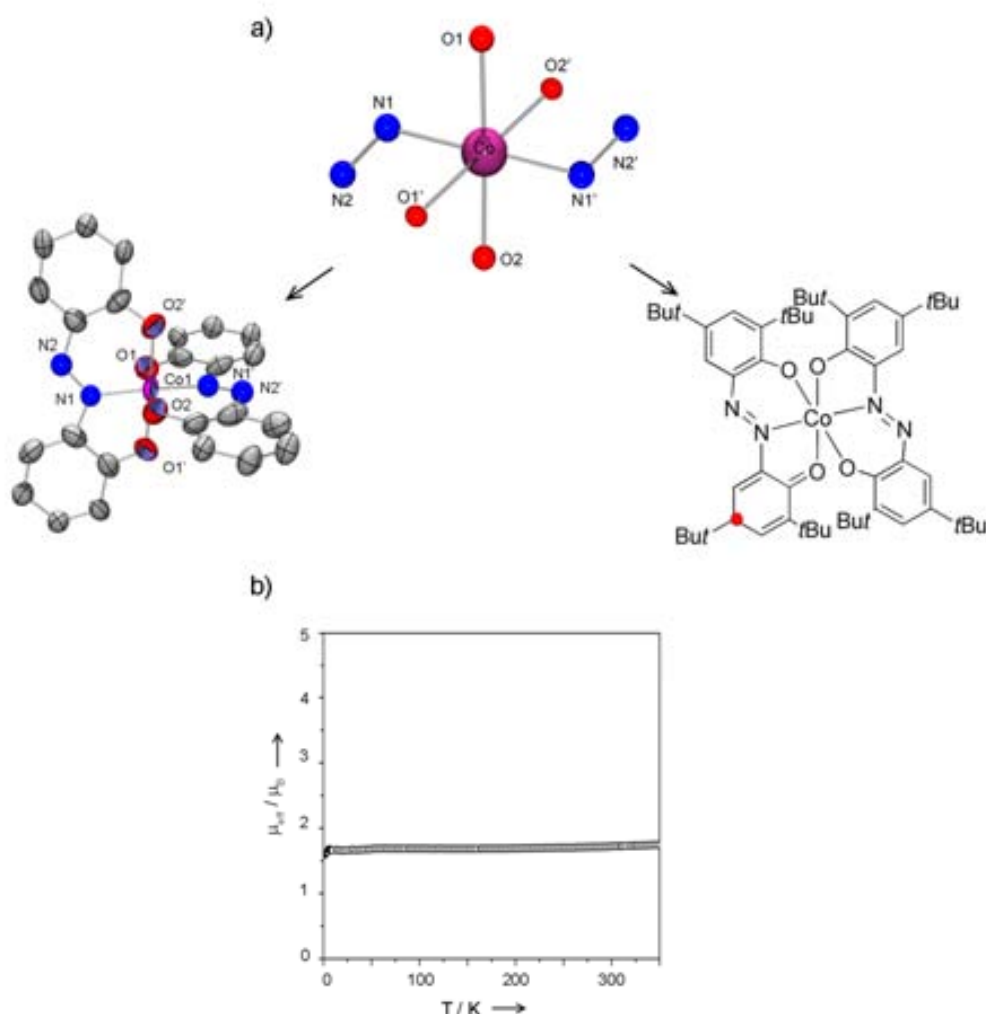


Figure 4.26. a) Schematic representation of octahedral geometry around the cobalt metal ion and the ORTEP plot at the 30% of probability level for complex **74**. b) μ_{eff} as a function of the temperature under an external field of 0.1 T for a microcrystalline sample of **74**.

The μ_{eff} for a polycrystalline sample of complex **74** shows a value of 1.70 μ_B along the whole temperature range studied (Figure 4.26b). This value is close to the theoretical value expected for a $S=1/2$ system with $g=2$ coming from the unpaired electron of one of the ligands Cat-N=N-SQ¹⁻ (**29**¹⁻). The other ligand remains in its diamagnetic form Cat-N=N-Cat²⁻ (**29**²⁻) whereas the metal ion remains as a diamagnetic Co(III).

The electronic spectra of complex **74** presents typical band for this family of complexes centred at 556 nm ($\epsilon = 1.3 \text{ M}^{-1} \text{ cm}^{-1}$) followed by a second band at 512 nm ($\epsilon = 1.2 \text{ M}^{-1} \text{ cm}^{-1}$) and a shoulder at around 456 nm. Interestingly, an IVT band with maxima at 1580 nm and a shoulder at 1324 nm appears in the near-IR, as shown in Figure 4.27. The absorbance

behaviour of this band shows a linear dependence with the concentration following the Lambert-Beer law, ruling out any intermolecular electron transfer based origin.

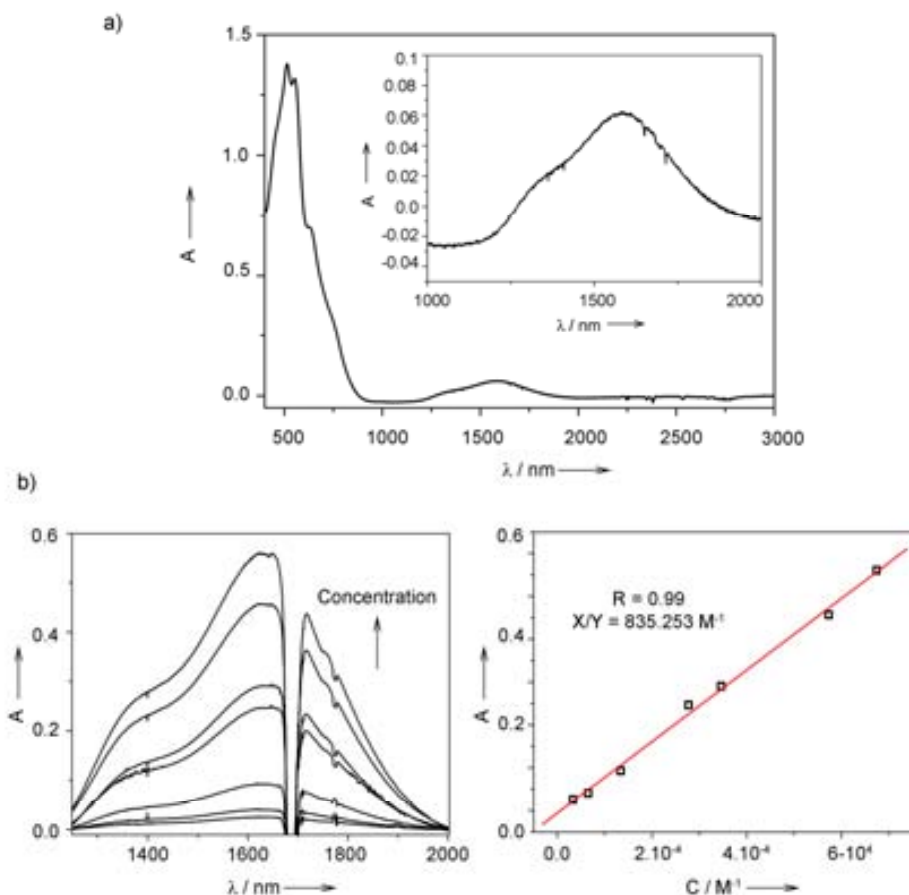


Figure 4.27. a) UV-Visible-Near IR spectra for complex **74** in a CH_2Cl_2 solution (1×10^{-3} M) and zoom of the spectrum at the near-IR 1000-2000 nm region. b) Study of the IVT double band at different concentrations ($0.33, 0.65, 1.34, 2.77, 3.46, 5.73$ and 6.74×10^{-4} M) of a toluene solution of complex **74** with the respective linear regression applied into absorbance values obtained at each concentration studied.

Moreover, this IVT band initially differs from those found for complexes **71-73**. Accordingly, the mechanism for the IET is expected to be different between such complexes. However, a closer look to the near-IR region reveals that the IVT band found for **74** at 1580 nm with a shoulder at 1324 nm is reminiscent to the IVT band found for complexes **71-73** at higher energies i.e., at smaller wavelengths. This could be an indication that the IET in complex **74** could follow similar mechanisms than for complexes **71-73**, though the process found at smaller energies is blocked for an unidentified reason. An explanation for the modulation of the energy barrier at which the electron transfer can take place comes from the presence of additional IET processes.

The presence of VT phenomena as the origin for the additional IET was ruled out by studying the variable-temperature UV-Visible spectroscopy over the 173 K-363 K temperature

range evidence the lack of VT, fact that was confirmed by $^1\text{H-NMR}$ experiments in solution. Indeed, the Evans Method of a toluene solution of complex **74** exhibited a constant value of $1.82 \mu_{\text{B}}$ in the same temperature range. This result is in agreement with the magnetic measurements in solid state.

Another possibility is that complex **74** could be considered as well as a reversal of a classical MV system where two electro-active units (ligands **29**) are connected through a metal ion that is acting as a bridge (Figure 4.28).

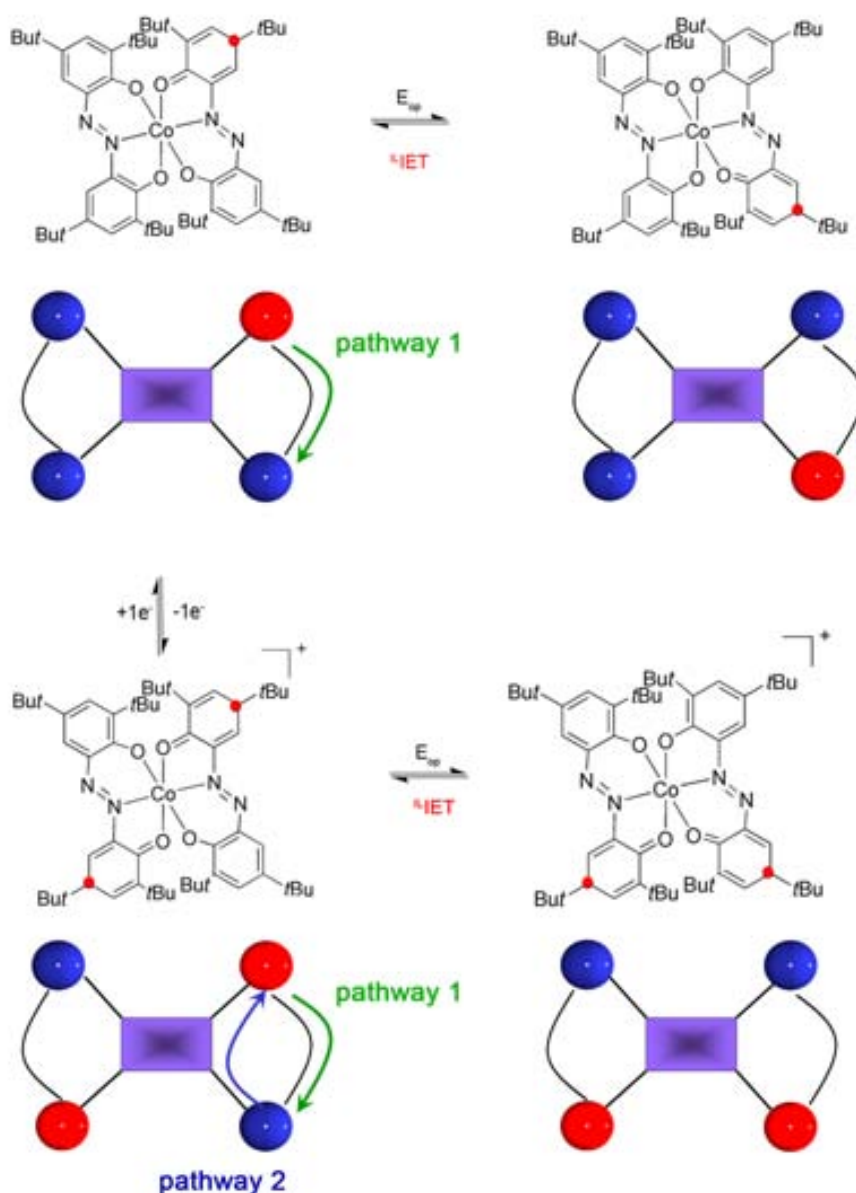


Figure 4.28. The optical stimuli applied into complex **74⁺**, allows for a ligand-to-ligand IET. Contrary, when this complex is oxidised, the external stimuli allows for a two types of IET. In fact the ligand-to-ligand and the intra-ligand IET occurs at the same time.

Should this be the case, a fast IET between ligands $\mathbf{29}^{2-}$ (Cat-N=N-Cat $^{2-}$) and $\mathbf{29}^{1-}$ (Cat-N=N-SQ $^{1-}$) (ligand-to-ligand IET or IET LL) could take place converting it into a Class III system as previously described for the imino-catechol derivative **25**. In this way, the presence of this additional electron transfer (IET LL) is modifying the intra-ligand IET (IET L) for complex **74**. As a schematic representation, both pathways for the intra-ligand IET were depicted in Figure 4.28.

To support this theory, the oxidation of **74** was done in solution and the evolution of the IVT followed by UV-Vis near-IR spectroscopy. Oxidation of complex $\mathbf{29}^{2-}$ into $\mathbf{29}^{1-}$ will convert this complex into a full valence species, where the two ligands were on the same oxidation state ($\mathbf{29}^{1-}$). Therefore complex $\mathbf{74}^+$ is not anymore MV specie and the ligand-to-ligand IET is eliminated. Accordingly, as can be seen in Figure 4.29, after oxidation of the complex **74** the characteristic pattern of IVT bands for complexes **71-73** is recovered, confirming the synergism between the two processes. To finally asses this explanation further theoretical calculations together with the synthesis of new complexes bearing different transition metal ions is being developed nowadays.

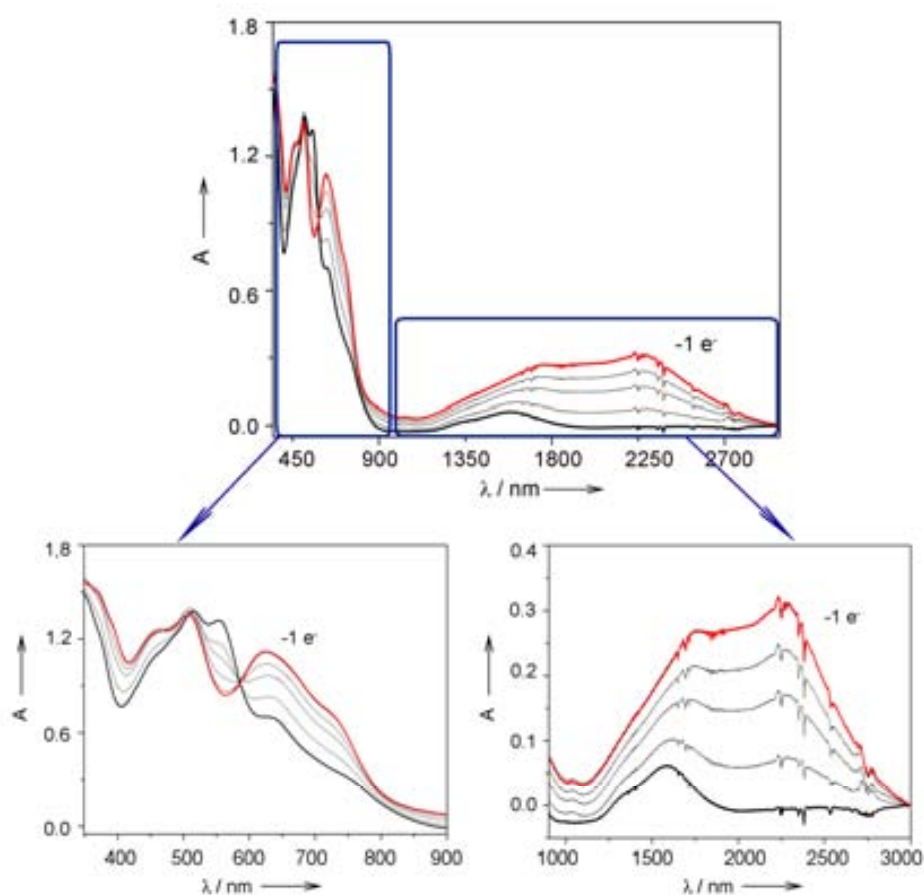


Figure 4.29. a) UV-Visible-Near IR spectra for complex **74** and the electrochemically generated oxidised form ($\mathbf{74}^+$) (red lines) in a CH_2Cl_2 solution (1×10^{-3} M) containing 0.15 M of Bu_4NPF_6 at 298 K. Zoom of the spectrum at different wavelength ranges; UV-Vis. 480 -1000 nm and near-IR 1000-2800 nm region. Each intermediate spectra corresponds to the partial oxidation forms electrochemically generated forms (0.2, 0.4, 0.6, 0.8, 0.9 $-e^-$).

4.3 Conclusions

1.- Two new families of catecholate and phenoxylate-based ligands **27-29** with interesting optical properties (fluorescence and chromophoric properties) have been described and the synthetic methodologies optimized.

2.- The catechol-derivative **28**·HCl has been shown to behave as a fluorescent chemosensor for wide pH range detection. For this, an innovative dual-wavelength detection technique, combining both “off-on-off” and “on-off-on” emission profiles upon pH variation by detection at two different wavelengths has been established.

3.- The azo bisphenolate ligand **29** has been used to create a chromophoric array of three states with significantly different colours. The three states can interconvert reversibly between them by means of acid/base and complexation reactions.

4.- A series of azo complexes bearing ligand **29** together with different nitrogen-based counter-ligands (py, phen, terpy, and tppz) have been reported. Partial oxidation of ligand **29** in these complexes results in the formation of a ligand-centred MV system exhibiting IET^{LL}.

5.- Finally, and more interesting, the same ligand-centred IET^{LL} in complex **74** can be modulated by the presence of an additional IET^{LL} between the two ligands. These results open the door to the development of molecular systems where IET can be controlled (gated) at will, and the important technological implications that could be derived from there.

References

- [1] M. L. Kirk, D. A. Shultz, E. C. Depperman, C. L. Brannen, *J. Am. Chem. Soc.*, **129**, **2007**, 1937.
- [2] A. Yamaguchi, K. Awaga, *J. Mater. Chem.*, **11**, **2001**, 2142.
- [3] D. Kiriya, H. -C. Chang, A. Kamata, S. Kitagawa, *Dalton Trans.*, **2006**, 1377
- [4] B. R. Eggins, *Chemical Sensors and Biosensors* (Analytical Techniques in the Sciences), Wiley-VCH, Weinheim, **2002**.
- [5] (a) O. S. Wolfbeis, *Fibre optic Chemical Sensors and Biosensors*, Ed.: CRC Press: Boca Raton, **1991**: Vols. 1 and 2. (b) D. L. Wise, L. B. Wingard, *Biosensors, Fiberoptics*, Ed.: Humana Press, Clifton, **1991**.
- [6] (a) R. Y. Tsien, *Chem. Eng. News*, **18**, **1994**, 34. (b) A. J. Dixon, G. S. Benham, *Int. Lab.*, **4**, **1988**, 38.
- [7] (a) W. Tan, Z. Y. Shi, R. Kopelman, *Anal. Chem.*, **64**, **1992**, 2985. (b) W. Tan, Z. Y. Shi, S. Smith, D. Birnbaum, R. Kopelman, *Science*, **258**, **1992**, 778.
- [8] S. L. Sharp, R. J. Warmack, J. P. Goudonnet, I. Lee, T. L. Ferrell, *Acc. Chem. Res.*, **26**, **1993**, 377.
- [9] A. Lewis, K. Lieberman, *Anal. Chem.*, **63**, **1991**, 625.
- [10] S. Alvés, F. Pina, M. T. Albelda, E. García-España, C. Soriano, S. V. Luis, *Eur. J. Inorg. Chem.*, **2001**, 405.
- [11] C. Bazzicalupi, A. Bencina, E. Berni, A. Bianchi, S. Ciattini, C. Giogi, S. Maoggi, P. Paoletti, B. Valtancoli, *J. Org. Chem.*, **67**, **2002**, 9107.
- [12] (a) A. P. de Silva, R. A. D. D. Rupasinghe, *J. Chem. Soc. Chem. Commun.*, **1985**, 1669. (b) S. G. Schulman, S. Chen, F. Bai, M. J. P. Leiner, L. Weiss, O. S. Wolfbeis, *Anal. Chim. Acta*, **304**, **1995**, 165. (c) L. M. Daffy, A. P. de Silva, H. Q. N. Gunaratne, C. Huber, P. L. M. Lynch, T. Werner, O. S. Wolfbeis, *Chem. Eur. J.* **4**, **1998**, 1810. (d) S. Charier, O. Ruel, J.-B. Baudin, D. Alcor, J.-F. Allemand, A. Meglio, L. Jullien, *Angew. Chem. Int. Ed.*, **43**, **2004**, 4785. (e) G. Nishimura, Y. Shiraishi, T. Hirai, *Chem. Commun.*, **2005**, 5313. (f) A. S. Vasylevska, A. A. Karasyov, S. M. Borisov, C. Krause, *Anal. Bional. Chem.*, **387**, **2007**, 2131. (g) B. Tang, X. Liu, K. Xu, H. Huang, G. Yang, L. An, *Chem. Commun.*, **2007**, 3726-2728. (h) A. P. de Silva, S. Sisira K. de Silva, N. C. W. Goodnesekera, H. Q. N. Gunaratne, P. L. M. Lynch, K. R. Nesbitt, S. T. Patuwathavithana, N. L. D. Ramyalal, *J. Am. Chem. Soc.*, **129**, **2007**, 3050.
- [13] (a) D. Margulies, G. Melman, A. Shanzer, *Nat. Mater.*, **4**, **2005**, 768. (b) A. P. de Silva, S. Uchiyama, *Nat. Nanotechnol.*, **2**, **2007**, 399.
- [14] P. C. Malins, H. G. Glever, T. E. Keyes, J. G. Vos, W. J. Dressick, B. D. MacCraith, *Sens. Actuat. B Chem.*, **67**, **2000**, 89.
- [15] (a) S. G. Schulman, S. Chen, F. Bai, M. J. P. Leiner, L. Weiss, O. S. Wolfbeis, *Anal. Chim. Acta*, **304**, **1995**, 165. (b) G. Liebsch, I. Klimant, C. Krause, O. S. Wolfbeis, *Anal. Chem.*, **73**, **2001**, 4354. (c) H. R. Kermis, Y. Kostov, P. Harms, G. Rao, *Biotechnol. Prog.*, **18**, **2002**, 1047. d) K. M. -C. Wong, W. -S. Tang, X. -X. Lu, V. W. -W. Yam, *Inorg. Chem.*, **44**, **2005**, 1492. (e) T. Gunnlaugsson, C. P. McCoy, F. Stomeo, *Tetrahedron Lett.*, **45**, **2004**, 8403.
- [16] (a) E. U. Akkaya, M. E. Huston, A. W. Czarnik, *J. Am. Chem. Soc.*, **112**, **1990**, 3590. b) S. Alves, F. Pina, M. T. Albelda, E. García-España, C. Soriano, S. V. Luis, *Eur. J. Inorg. Chem.*, **2001**, 405.
- [17] G. Grenier, I. Maier, *J. Chem. Soc., Perkin Trans.*, **2**, **2002**, 1005.
- [18] (a) M. I. Burguete, F. Galindo, M. A. Izquierdo, S. V. Luis, L. Vígara, *Tetrahedron*, **63**, **2007**, 9493. (b) Y. Shiraishi, H. Maehara, K. Ishizumi, T. Hirai, *Org. Lett.*, **9**, **2007**, 3125. c) X. Zhang, Y. Shiraishi, T. Hirai, *Tetrahedron Lett.*, **48**, **2007**, 5455.
- [19] (a) A. P. de Silva, I. M. Dixon, H. Q. N. Gunaratne, T. Gunnlaugsson, Pamela R. S. Maxwell, T. E. Rice, *J. Am. Chem. Soc.*, **121**, **1999**, 1393. (b) A. P. de Silva, N. D. McClenaghan, *J. Am. Chem. Soc.*, **122**, **2000**, 3965. (c) A. P. de Silva, D. B. Fox, T. S. Moody, S. M. Weir, *Trends in Biotech.*, **19**, **2001**, 29.
- [20] (a) T. Gunnlaugsson, D. Parker, *Chem. Commun.* **1998**, 511. (b) M. Su, H. Ma, Q. Ma, Z. Wang, J. Yang, M. Wang, *Chem. Commun.* **2001**, 960. (c) F. Pina, J. C. Lima, C. Lodeiro, J. S. de Melo, P. Díaz, M. T. Albelda, E. García-España, *J. Phys. Chem. A*, **106**, **2002**, 8207. (d) V. F. Valuk, G. Duportail, V. G. Pivovarenko, *J. Photochem. Photobiol. A: Chem.* **175**, **2005**, 226. (e) Y. Shiraishi, Y. Tokitoh, G. Nishimura, T. Hirai, *J. Phys. Chem. B*, **111**, **2007**, 5090.
- [21] (a) A. P. de Silva, H. Q. N. Gunaratne, C. P. McCoy, *Chem. Commun.*, **1996**, 2399. (b) T. Gunnlaugsson, J. P. Leonard, K. Sénéchal, A. J. Harte, *J. Am. Chem. Soc.*, **125**, **2003**, 12062. (c) S. A. de Silva, K. C. Loo, B. Amorelli, S. L. Pathirana, M. Nyakirangani, M. Dharmasena, S. Demarais, B. Dorcley, P. Pullay, Y. A. Salih, *J. Mater. Chem.*, **15**, **2005**, 2791. (d) Y. Diaz-Fernandez, F. Fori, C.

- Mangano, P. Pallavicini, S. Patroni, A. Perez-Gramatges, S. Rodriguez-Calvo, *Chem. Eur. J.*, **12**, **2006**, 921.
- [22] (a) P. Pallavicini, V. Amendola, C. Massera, E. Mundum, A. Taglietti, *Chem. Commun.* **2002**, 2452. (b) V. Amendola, L. Fabrizzi, C. Mangano, H. Miller, P. Pallavicini, A. Parotti, A. Taglietti, *Angew. Chem., Int. Ed.*, **41**, **2002**, 2553. (c) Z. Wang, G. Zheng, P. Lu, *Org. Lett.*, **7**, **2005**, 3669. (d) G. Zheng, Z. Wang, L. Tang, P. Lu, W. P. Weber, *Sens. Actuators B*, **122**, **2007**, 389.
- [23] L. Basabe-Desmonts, D. N. Reinhoudt, M. Crego-Calama, *Chem. Soc. Rev.*, **36**, **2007**, 993.
- [24] R. Sjöback, J. Nygren, M. Kubista, *Spectrochimica Acta Part A*, **51**, **1995**, L7.
- [25] S. Espinosa, E. Bosch, M. Rosés, *J. Chromatogr. A*, **964**, **2002**, 55.
- [26] As a proof-of-concept, the implementation of **28**-HCl in a nanostructured pH sensor and the performance of the resulting device has also already been reported in a previous communication: A. Martinez-Otero, E. Evangelio, R. Alibes, J. L. Bourdelande, D. Ruiz-Molina, F. Busque, J. Hernando, *Langmuir*, **24**, **2008**, 2963.
- [27] (a) K. Vinodgopal, P. V. Kamat, *Environmental Applications of Ionizing Radiation*, Ed.: W. J. Cooper, R. Curry, K. O'Shea. Wiley-Interscience, New York, **1998**, 587. (b) N. H. Ince, D. T. Gonenc, *Environ. Sci. Technol.*, **18**, **1997**, 179.
- [28] (a) Y. -S. Li, *Arch. Environ. Contam. Toxicol.*, **31**, **1996**, 557. (b) R. Bauer, H. Fallmann, *Res. Chem. Intermed.*, **23**, **1997**, 341.
- [29] (a) E. Hamada. *Jpn. Patent*, 10-181211, **1998**. (b) E. Hamada, T. Fujii, Y. Tomizawa, S. Iimura, *Jpn. J. Appl. Phys.*, **36**, **1997**, 593. (c) Y. Suzuki, Y. Okamoto, Y. Kurose, S. Maeda, *Jpn. J. Appl. Phys.*, **38**, **1999**, 1669. (d) H. Nakazumi, E. Hamada, T. Ishiguro, H. Shiozaki, T. Kitao, *J. Soc. Dyes Colour.*, **26**, **1989**, 105.
- [30] F.D. Lewis, E. M. Crompton, *J. Am. Chem. Soc.*, **125**, **2003**, 4044.
- [31] E. M. Crompton, F.D. Lewis, *Photochem. Photobiol. Sci.*, **3**, **2004**, 660.
- [32] H. Ilhmels, A. Meiswinkel, C. J. Mohrschladt, D. Otto, M. Waidelich, M. Towler, R. White, M. Albrecht, A. Schnurpfeil. *J. Org. Chem.*, **70**, **2005**, 3929.
- [33] T. Murohoshi, K. Kaneda, M. Ikegami, T. Arai, *Photochem. Photobiol. Sci.*, **2**, **2003**, 1247.
- [34] G. Favaro, U. Mazzucato, F. Masetti, *J. Phys. Chem.*, **77**, **1973**, 601.
- [35] G. Ginocchietti, U. Mazzucato, A. Spalletti, *Int. J. Photoenergy*, **6**, **2004**, 241.
- [36] U. Mazzucato, F. Momicchioli, *Chem. Rev.*, **91**, **1991**, 1679.
- [37] M.J. Kamlet, J.L.M. Abboud, M.H. Abraham and R.W. Taft, *J. Org. Chem.*, **48**, **1983**, 2982.
- [38] G. Marconi, G. Bartocci, U. Mazzucato, A. Spalletti, F. Abbate, L. Angeloni, E. Castellucci, *Chem. Phys.*, **196**, **1995**, 383.
- [39] P. Pattanayak, J. L. Pratihari, D. Patra, A. Burrows, M. Mohan, S. Chattopdhyay, *Eur. J. Inorg. Chem.*, **27**, **2007**, 4263, and references listed in the article.
- [40] N. Ventosa, D. Ruiz-Molina, J. Sedó, C. Rovira, X. Tomas, J. -J. André, A. Bieber, J. Veciana, *Chem. Eur. J.*, **5**, **1999**, 3533.
- [41] S. K. Larsen, C. G. Pierpont, *J. Am. Chem. Soc.*, **110**, **1988**, 1827.
- [42] A. Caneschi, A. Cornia, A. Dei, *Inorg. Chem.*, **37**, **1998**, 3419.
- [43] G. Speier, J. Csihony, A. M. Whalen, C. G. Pierpont, *Inorg. Chem.*, **35**, **1996**, 3519.
- [44] E. Evangelio, J. Saiz, D. MasPOCH, K. Wurst, F. Busque, D. Ruiz-Molina, *Eur. J. Inorg. Chem.*, **2008**, 2278.
- [45] Y. Suenaga, C. Pierpont, *Inorg. Chem.*, **44**, **2005**, 6183. This ligand, which bears an azo group acting as a bridge, presented an electrochemical behaviour similar to our case. Unfortunately, the one-step chemical oxidation was not stable, so the azo form was not able to be studied. Importantly, the VT phenomenon was associated to an electron transfer from the catecholate regions of the bridge.
- [46] T. -Y. Dong, M. -C. Lin, M. -Y. Chiang *Inorg. Chem. Commun.*, **7**, **2004**, 687.
- [47] D. Ruiz-Molina, J. Yoo, I. A. Guzei, A. Rheingold, D. N. Hendrickson, *Chem. Commun.*, **1998**, 2089.
- [48] A. Dei, D. Gatteschi, C. Sangregorio, L. Sorace, *Acc. Chem. Res.*, **11**, **2004**, 827.
- [49] C. Lambert, G. Nöll, J. Schelter, *Nature Mater.*, **1**, **2002**, 69, and references therein. These studies were based on the presence of a double band in the near-IR region. Focused on the investigation of

electron-transfer pathways, these authors attributed the double band to the presence of both, hopping and super-exchange mechanisms, in the same molecular system.

Chapter | 5

Experimental Section

5.1 Instruments

5.1.1 Physical Measurements

➤ *Electronic absorption spectra* were recorded on a Varian Cary05e spectrophotometer at the Institut de Ciència de Materials de Barcelona (ICMAB-CSIC) and in a Perkin Elmer Lambda 35 spectrophotometer in the Laboratoire de Chimie de la Coordination (LCC-CNRS) of Toulouse. Both of them were equipped with a thermostatic cell holder that can operate between 280K and 370 K and 180 K and 370 K respectively. Temperature stability was better than ± 5 K. Spectra were collected after the sample had been allowed to thermally equilibrate at each temperature for 10 min. In some specific experiments, T_C , the temperature at which the isomer ratio is 1:1, was deduced from the temperature at which the peaks of the low-spin and the high-spin exhibit similar intensities.

➤ *Fluorescence spectra* were recorded at room temperature in a Perkin Elmer LS 45 fluorescence spectrophotometer. The fluorescence quantum yields of all the investigated solutions were determined with respect to N,N'-bis(1-hexylheptyl)perylene-3,4,9,10 in acetonitrile ($\Phi_f=1$).¹

➤ *pH measurements* upon acid-base addition on acetonitrile solutions were performed at room temperature by using a Crison 52-01 pH electrode with a Crison BASIC 20 potentiometer. pH values are given relative to the acetonitrile solvent (^spH scale).² To calibrate the electrode system we used reference buffers in acetonitrile (pyridine-pyridinium bromide and phenol-sodium phenolate), whose ^spH can be derived from the Henderson-Hasselbach equation using the pKa values in acetonitrile reported for these systems.³

➤ *Direct current (dc) magnetic susceptibility* measurements were carried out on a Quantum Design MPMS SQUID susceptometer at the Institut de Ciència de Materials de Barcelona (ICMAB-CSIC) and at the Instituto de Ciencia de Materiales de Aragón (CSIC) with a 55KG magnet and operating in the temperature range of 1.7-320K. All measurements were collected with a field of 10kG. Background correction data were collected from magnetic susceptibility measurements of the holder capsules. Diamagnetic corrections estimated from the Pascal contents were applied to all data for determination of the molar paramagnetic susceptibilities of the compounds.

➤ *NMR spectra* were recorded on a DPX250 (250 MHz), a Bruker DPX360 (360 MHz) and an ARX400 (400 MHz) at the Servei de Ressonància Magnètica Nuclear of the Universitat Autònoma de Barcelona and on a Bruker AV400 spectrometer of the Laboratoire de Chimie de la Coordination (LCC-CNRS) of Toulouse. It was Equipped with a 5 mm triple resonance inverse probe with dedicated ^{31}P channel operating at 500.33 MHz for ^1H equipped with a BVT3000 variable temperature unit. TMS was used as an internal reference. Proton chemical shifts are reported in ppm (δ) (CDCl_3 , δ 7.26, DMSO-d_6 , δ 2.50 or Tol-d_8 , δ 2.03). ^{13}C -NMR spectra were recorded on Bruker DPX250 (62.5 MHz) and Bruker DPX360 (90 MHz) spectrometers with complete proton decoupling. Carbon chemical

shifts are reported in ppm δ) (CDCl_3 , δ 77.2 or DMSO-d_6 , δ 39.5). NMR signals were assigned with the help of COSY, HSQC, HMBC, and NOESY experiments.

➤ *Infrared spectra* were recorded on a Sapphire-ATR Spectrophotometer at the Universitat Autònoma de Barcelona and on a Perkin Elmer spectrum one FT-IR Fourier transform spectrometer at the Institut de Ciència de Materials de Barcelona (ICMAB-CSIC). Peaks are reported in cm^{-1} .

➤ *High resolution mass spectra* (HRMS) were recorded on a Micromass-AutoSpec using (ESI+ or ESI-) at the Universitat Autònoma de Barcelona.

➤ *Elemental analyses* were obtained from the Servei d'Anàlisi of the Universitat Autònoma de Barcelona.

➤ *Electrochemical experiments* (Cyclic Voltammetry and Chronoamperometry) were performed with a potentiostat Galvanostat 263 A of EG&PAR, using a platinum wire as working electrode and a Ag/AgCl electrode as the reference electrode. Anhydrous solvents were freshly distilled over P_2O_5 under nitrogen. Commercial tetrabutylammonium hexafluorophosphate (Fluka, electrochemical grade) was used as the supporting electrolyte.

➤ *EPR spectra* were recorded on a Bruker ESP-300E spectrometer operating in the X-band (9,3 GHz) at the Institut de Ciència de Materials de Barcelona (ICMAB-CSIC). Signal-to-noise ratio was increased by accumulation of scans using the F/F lock accessory to guarantee high-field reproducibility. Precautions to avoid undesirable spectral line broadening, such as that arising from microwave power saturations and magnetic field over-modulation, were taken. To avoid dipolar broadening, the solutions were carefully degassed three times using vacuum cycles with pure Argon. The g values were determined against the DPPH standard ($g=2.0030$). The program used to simulate the spectra is WIN-EPR from Bruker Analytische Messtechnik Rheinstetten (Germany) and Sinfonia v.1.0 from Bruker Instruments Billerica, MA (USA).

➤ Computational details for complexes **24**, **25** and **26** were performed by Marie Laure Bonet, under the direction of Dr. Vincent Robert from the l'École Normale Supérieure de Lyon. Both density functional theory (DFT) based and wavefunction based *ab initio* quantum chemical approaches. All CASPT2 calculations were performed with an imaginary shift of 0.3 Hartree to avoid the presence of intruder states. All electrons were correlated except those in the core parts. Both CASSCF and CASPT2 procedures are available in the Molcas 6.2 package used throughout the theoretical analysis.

➤ Quantum chemical calculations in compounds **27** and **28**·HCl were performed by Dr. Jordi Hernando at the Chemistry Department of the Universitat Autònoma de Barcelona. Quantum chemical calculations were performed employing the Gaussian 03 package of programs⁴ on a 32-bit multiprocessor computer. Density functional theory (DFT) geometrical optimization of ground electronic states of all investigated molecules was carried out at the B3LYP hybrid functional level with the 6-311+G(d,p) basis set. To account

for solvent polarity effects, calculations were performed in acetonitrile solvent by means of the polarizable continuum model (PCM, $\epsilon=36.64$). The resulting geometries and molecular orbitals were plotted using Molden. The excitation energies and oscillator strengths (f) of the UV-visible absorption transition bands were then computed by means of time-dependent density functional theory at the B3LYP/6-311G+(d,p) level on the B3LYP/6-311+G(d,p) ground state geometries and accounting for acetonitrile solvent (PCM). For each protonation state of **27** and **28**·HCl, the spectroscopic properties of all possible rotamers were calculated, and the final average values were obtained by using Boltzmann coefficients at room temperature ($\exp(-E_{\text{rotamer}} / k_B T) / \sum \exp(-E_{\text{rotamer}} / k_B T)$) as weighting factors. Time-dependent functional theory (TD-DFT) calculations at the B3LYP/6-311+G(d,p) level and accounting for acetonitrile solvent were carried out to compute the excitation energies and oscillator strengths of the absorption bands of the different protonation states of **27** and **28**·HCl.

➤ X-Ray powder diffraction data have been recorded on an INEL diffractometer (Debye-Scherrer geometry and CPS120 curved detector) at the Institut de Ciència dels Materials de Barcelona (ICMAB-CSIC) which collects 120 ° of the diffraction circle using the $K\alpha$ radiation of copper. The sample was introduced in the diffractometer in capillars of 0.3 mm.

➤ *Crystals of compounds 29 and 69-74* were measured by Dr. Klaus Wurst on a Nonius Kappa CCD located at the Institute of General, Inorganic and Theoretical Chemistry, Innsbruck University equipped with graphite-monochromatized Mo- $K\alpha$ -radiation ($\lambda=0.71073$ Å) and a nominal crystal to area detector distance of 36 mm. Intensities were integrated using DENZO and scaled with SCALEPACK. Several scans in ϕ and ω direction were made to increase the number of redundant reflections, which were averaged in the refinement cycles. This procedure replaces in a good approximation an empirical absorption correction. The structures were solved with direct methods SHELXS86 and refined against F2 SHELX97.

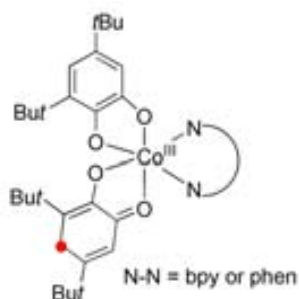
➤ *Diffraction data* for ligand **28**·HCl were collected under synchrotron radiation ($\lambda=0.977$ Å) at 150 K with a CCD detector in the BM16 Spanish beamline at the ESRF (Grenoble). The crystal was coated in paratone®. The structure was solved by direct methods and refined by full-matrix least-squares techniques on F2 with SHELX-97.⁵ Crystal adsorption was corrected by Scalepack.⁶ Non-hydrogen atoms were refined anisotropically.

5.2 Synthesis and Characterization

5.2.1 General Procedures

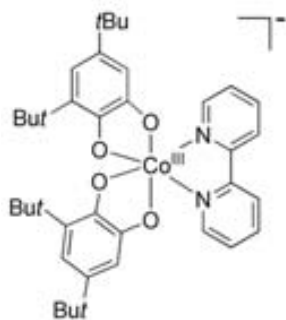
Commercially available reagents were used as received. All reagents, organic and inorganic, were of high purity grade and obtained from E. Merck, Fluka, Chemie and Aldrich Co. The solvents were dried by distillation over the appropriate drying agents. Some of the reactions were performed avoiding moisture by standard procedures and under nitrogen atmosphere. Reactions were monitored by analytical thin-layer chromatography (TLC) using silica gel 60 F₂₅₄ pre-coated aluminum plates (0.25 mm thickness). Flash column chromatography was performed using silica gel 60 Å (particle size 35-70 μm).

5.2.1.1 Synthesis of [Co(3,5-DTBCat)(3,5-DTBSQ) N-N] where N-N = bipyridine (14) or phenanthroline (17)



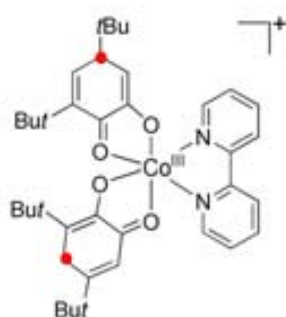
Complex **14** and **17** were synthesised as previously described.⁷ All the reactions were carried out using degassed solvents and manipulated under argon atmosphere.

5.2.1.2 Synthesis of [Co(Cp)₂][Co(3,5-DTBCat)₂(bpy)]; (**14**-Co(Cp)₂)



Cobaltocene (58 mg., 0.31 mmol) was added to a solution of complex [Co(3,5-DTBCat)(3,5-DTBSQ)(bpy)] (**14**, *is*-Co(III)) (200 mg., 0.31 mmol) in CH₂Cl₂ (15 mL) in an oxygen-free environment. The resulting dark green solution was stirred for 3 h at 273 K. The solution was concentrated approximately to one half by slow evaporation of the solvent, appearing a dark-green microcrystalline material that was filtered in an oxygen-free atmosphere. The microcrystalline product was dried under vacuum (70% yield). Anal. Calc. for C₄₈H₅₈N₂O₄Co₂: C, 68.20; H, 6.94; N, 3.33. Found: C, 68.07; H, 7.04; N, 3.63.

5.2.1.3 Synthesis of [Co(3,5-DTBSQ)₂(bpy)].Cl; (**14**-Cl)



Complex [Co(3,5-DTBCat)(3,5-DTBSQ)(bpy)] (**14**, *is*-Co(III)) (300 mg., 0.46 mmol) was dissolved in degassed 95% EtOH (20 mL). This mixture was stirred under argon for 3 h, during which time the solution turned an intense olive-green color. The solution was concentrated approximately to one half by slow evaporation of the solvent, to give an olive-green microcrystalline material that

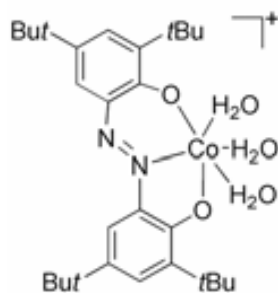
was dried under vacuum (30 % yield). Anal. Calc. for $C_{38}H_{48}N_2O_4Co_2Cl$: C, 65.70; H, 7.00; N, 4.04. Found: C, 65.24; H, 7.18; N, 4.28.

5.2.1.4 Synthesis of $[M(\text{Cat-N-SQ})(\text{Cat-N-BQ})]$ $M=\text{Fe}$ (**24**) or Co (**25**) and $[M(\text{Cat-N-BQ})_2]$ $M=\text{Ni}$ (**26**)



Complexes **24-26** were synthesised as previously described.⁸ Amorphous samples were prepared both, by a fast precipitation method (avoiding correct crystallization) or by removal of the solvent guest molecules under vacuum. Polymeric samples were prepared by dissolving a given sample into a CH_2Cl_2 solution of polycarbonate (4% of the VT compound) and deposited by spin-coating.

5.2.1.5 Synthesis of $[\text{Co}(\text{Cat-N=N-Cat})(\text{H}_2\text{O})_3]\text{Cl}$; (**69**)

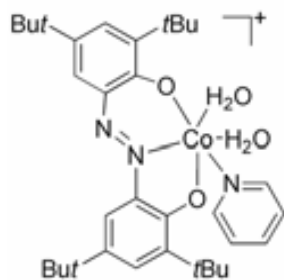


Method 1: an ethanolic solution (25 mL) of 3,5-di-*tert*-butylcatechol (5 g, 23 mmol) was added to an aqueous solution (25 mL) of $\text{CoCl}_2 \cdot 6\text{H}_2\text{O}$ (6.2 g, 26 mmol) under stirring. Immediately, an aqueous solution (25 mL) of ammonia was added. The colour of the mixture turned to dark violet, which changed to lighter violet after 10 min under stirring. Then the mixture was stirred for four additional h, and after filtration, crystals of **69** were collected from the solution.

FT-IR (KBr, cm^{-1}): 3109 (ν (H_2O)), 2955, 2905, 2866 (ν (C-H)), 1612, 1480, 1438, 1360, 1278, 1254, 1162. Anal. Calcd. for $C_{28}H_{52}O_5N_6\text{CoCl}$ (646.69): C, 51.4; H, 8.5; N, 12.8. Found: C, 50.3; H, 7.9; N, 12.6. ES-(+) (MeOH, m/z): 512 (M^+ , $C_{28}H_{41}CoN_2O_3$). $^1\text{H-NMR}$ (400 MHz, MeOH-d^4): δ = 1.347 (s, 9H, CH_3), 1.353 (s, 9H, CH_3), 1.44 (s, 9H, CH_3), 1.48 (s, 9H, CH_3), 7.29 (s, 1H, aromatic H), 7.34 (s, 1H, aromatic H), 7.70 (s, 1H, aromatic H), 8.15 (s, 1H, aromatic H).

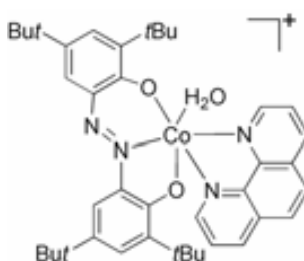
Method 2: an ethanolic solution (20 μL) of $\text{Co}(\text{CH}_3\text{COO})_2 \cdot 4\text{H}_2\text{O}$ (28 mg, 0.11 mmol) was added to an ethanolic solution (0.75 mL) of 2,2'-dihydroxy-4,3,4',3'-tetratert-butylazobenzene (**29**) (1.3 mg, 0.003 mmol) in the NMR tube under stirring. The colour of the mixture turned to lighter violet, and the obtaining of the product was followed by $^1\text{H-NMR}$ spectroscopy. $^1\text{H-NMR}$ (400 MHz, MeOH-d^4): δ = 1.41 (s, 18H, CH_3), 1.62 (s, 9H, CH_3), 1.66 (s, 9H, CH_3), 7.35 (s, 1H, aromatic H), 7.49 (s, 1H, aromatic H), 7.77 (s, 1H, aromatic H), 8.10 (s, 1H, aromatic H).

5.2.1.6 Synthesis $[\text{Co}(\text{Cat-N=N-Cat})(\text{py})(\text{H}_2\text{O})_2]\cdot\text{Cl}$ and $[\text{Co}(\text{Cat-N=N-Cat})(\text{H}_2\text{O})_3]\cdot\text{Cl}$; (70)



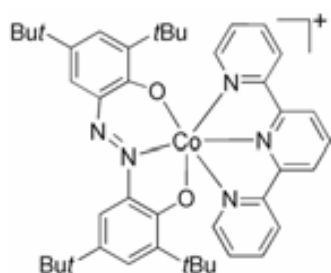
An ethanolic solution of complex **69** (200 mg; 1 mmol) was added to a hexane solution of pyridine (27 μl ; 1 mmol). The insoluble complex formed was recrystallised by slow diffusion of hexane into a CH_2Cl_2 solution of the formed complex. Suitable crystals for X-Ray diffraction were obtained in the mother liqueur. Furthermore in the unit cell, two different complexes were presented (69 and 70). FT-IR (KBr, cm^{-1}): 3101 (ν (H_2O)), 2955, 2905, 2866 (ν (C-H)), 1610, 1481, 1277, 1255, 1161. Anal. Calcd. for $\text{C}_{30.5}\text{H}_{47.5}\text{O}_{2.5}\text{N}_{2.5}\text{CoCl}\cdot\text{CH}_2\text{Cl}_2$ (667.30): C, 58.8; H, 8.4; N, 11.3. Found: C, 54.9; H, 7.1; N, 5.2. ES-(+) (MeOH, m/z): 574 (M^+ , $\text{C}_{33}\text{H}_{45}\text{CoN}_3\text{O}_2$), 512 (M^+ , $\text{C}_{28}\text{H}_{41}\text{CoN}_2\text{O}_3$).

5.2.1.7 Synthesis of $[\text{Co}(\text{Cat-N=N-Cat})(\text{phen})(\text{H}_2\text{O})]\cdot\text{Cl}$; (71)



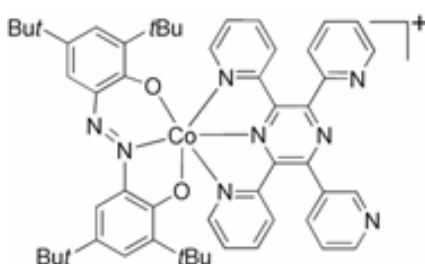
An ethanolic solution of complex **69** (200 mg; 1 mmol) was added to an hexane solution of 1,10-phenanthroline (61.8 mg; 1 mmol). The insoluble complex formed was recrystallised by slow diffusion of hexane into a CH_2Cl_2 solution of the formed complex. Suitable crystals for X-ray diffraction were obtained in the mother liqueur. FT-IR (KBr, cm^{-1}): 3318 (ν (N-H)), 2955, 2915, 2846 (ν (C-H)), 1629, 1451, 1267. Anal. Calcd. for $\text{C}_{40}\text{H}_{50}\text{O}_3\text{N}_4\text{CoCl}\cdot 4\text{H}_2\text{O}$ (801.28): C, 59.9; H, 6.2; N, 5.2. Found: C, 59.5; H, 6.0; N, 5.0. ES-(+) (MeOH, m/z): 675 (M^+ , $\text{C}_{40}\text{H}_{48}\text{CoN}_4\text{O}_2$).

5.2.1.8 Synthesis of $[\text{Co}(\text{Cat-N=N-Cat})(\text{terpy})]\cdot\text{Cl}$; (72)



An ethanolic solution of complex **69** (200 mg; 1 mmol) was added to an hexane solution of 2,2':6',2''-terpyridine (79.8 mg; 1 mmol). The insoluble complex formed was recrystallised by slow diffusion of hexane into a CH_2Cl_2 solution of the formed complex. Suitable crystals for X-ray diffraction were obtained in the mother liqueur. FT-IR (KBr, cm^{-1}): 3392 (ν (N-H)), 2953, 2866 (ν (C-H)), 1606, 1478, 1452, 1254, 1159. Anal. Calcd. for $\text{C}_{43}\text{H}_{51}\text{O}_2\text{N}_5\text{CoCl}\cdot\text{CH}_2\text{Cl}_2$ (849.19): C, 60.8; H, 6.0; N, 8.2. Found: C, 61.4; H, 6.9; N, 8.1. ES-(+) (MeOH, m/z): 728 (M^+ , $\text{C}_{43}\text{H}_{51}\text{CoN}_5\text{O}_2$).

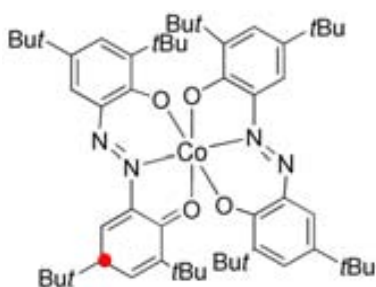
5.2.1.9 Synthesis of $[\text{Co}(\text{Cat-N=N-Cat})(\text{tppz})]\cdot\text{Cl}$; (73)



An ethanolic solution of complex **69** (200 mg; 1 mmol) was added to an hexane solution of 2,3,5,6-tetrakis(2-pyridyl)pyrazine (120 mg; 1 mmol). The insoluble complex formed is recrystallised by slow

diffusion of hexane into a CH_2Cl_2 solution of the formed complex. Suitable crystals for X-ray diffraction were obtained in the mother liqueur. FT-IR (KBr, cm^{-1}): 3380 (ν (N-H)), 2958, 2870, 2643 (ν (C-H)), 1612, 1463, 1190, 1102. Anal. Calcd. for $\text{C}_{52}\text{H}_{62}\text{O}_2\text{N}_8\text{CoCl}\cdot 1.4\text{CH}_2\text{Cl}_2\cdot 1.6\text{H}_2\text{O}$ (1067.15): C, 60.0; H, 6.4; N, 10.5. Found: C, 59.8; H, 6.0; N, 10.1. ES $^{-}$ (-) (MeOH, m/z): 889 (M^+ , $\text{C}_{52}\text{H}_{62}\text{CoN}_8\text{O}_2$).

5.2.1.10 Synthesis of [Co(Cat-N=N-Cat)(Cat-N=N-SQ)]; (74)



A toluene solution of complex **69** (200 mg) was heated and stirred at refluxing conditions during two h. The insoluble complex formed was recrystallised by slow diffusion of hexane into a CH_2Cl_2 solution of the formed complex. Suitable crystals for X-ray diffraction were obtained by slow evaporation of the toluene solution. FT-IR (KBr, cm^{-1}): 2953, 2905, 2866 (ν (C-H)), 1578, 1461, 1361, 1254, 1163. Anal. Calcd. for $\text{C}_{56}\text{H}_{80}\text{O}_4\text{N}_4\text{Co}$ (932.17): C, 70.8; H, 8.6; N, 5.9. Found: C, 70.7; H, 8.8; N, 5.8. ES $^{-}$ (-) (MeOH, m/z): 931 (M^+ , $\text{C}_{56}\text{H}_{80}\text{CoN}_4\text{O}_4$).

5.2.1.11 Synthetic approaches for the obtaining of cobalt complexes derived of ligand 28·HCl

All synthetic approaches to obtain catechol complexes with ligand **28**·HCl were unsuccessful. A resume of the synthetic approaches done is revised next.

Attempt 1.- A solution of ligand **28**·HCl in EtOH (60 mL) was added to a 10 mL of ammonia yielding a red precipitate. The precipitate was washed in EtOH solvent, and redissolved onto heated DMSO (20 mL). A solution of 1 mmol of $\text{CoCl}_2\cdot 6\text{H}_2\text{O}$ in 50 mL of EtOH was then layered onto the DMSO solution of **28**·HCl (2mmol). Slow diffusion over 10 days yielded a red precipitate, which is characterized as the unreacted ligand **28**·HCl.

Attempt 2.- A DMSO solution (10 mL) of ligand **28**·HCl (4 mmol) and $\text{CoCl}_2\cdot 6\text{H}_2\text{O}$ (2 mmol) was added to an ethanolic solution (50 mL) of ammonia (10 mL). Slow diffusion over 18 day yielded 18 % of red pyramidal crystals of $\text{CoCl}_2\cdot 6\text{H}_2\text{O}$.

Attempt 3.- A DMSO solution (10 mL) of ligand **28**·HCl (5 mmol) and $\text{CoCl}_2\cdot 6\text{H}_2\text{O}$ (2 mmol) was added to an ethanolic solution (50 mL) of ammonia (10 mL). Slow diffusion over 18 day yielded 64 % of red pyramidal crystals of $\text{CoCl}_2\cdot 6\text{H}_2\text{O}$.

Attempt 4.- A DMSO solution (10 mL) of ligand **28**·HCl (1 mmol) and $\text{CoCl}_2\cdot 6\text{H}_2\text{O}$ (4 mmol) was added to an ethanolic solution (50 mL) of ammonia (10 mL). Slow diffusion over 18 day yielded 9 % of red pyramidal crystals of $\text{CoCl}_2\cdot 6\text{H}_2\text{O}$.

Attempt 5.- A DMSO solution (10 mL) of **28**·HCl (4 mmol) and $\text{CoCl}_2\cdot 6\text{H}_2\text{O}$ (1 mmol) was allowed to stand at saturated atmosphere of NH_3 during all the night. 2 days after the characterization of the products reveal decomposition products.

5.3 Crystallographic Data

The cif files of all crystal structures presented below are compiled in the CD of the Thesis.

5.3.1 (E)-2-[(3-bromo-4,5-dihydroxyphenyl)-1-ethenyl]pyridinium chloride; (**28**·HCl)

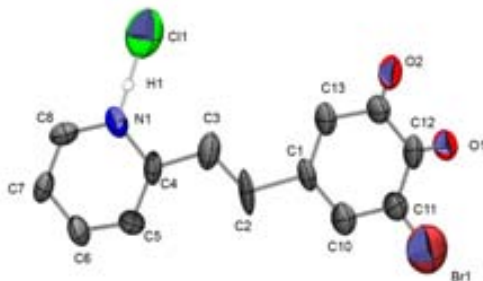


Figure 5.1. Ortep plot of **28**·HCl at the 30% probability level. Hydrogen atoms excepting the hydrogen implicated in the H-bond with Cl1 are omitted for clarity.

Table 5.1. Crystallographic data for **28**·HCl.

Empirical formula	C ₁₃ H ₁₁ BrClO ₂
Formula weight (g·mol ⁻¹)	441.84
Temperature (K)	150(2)
Radiation	Synchrotron radiation
Wavelength (Å)	0.977
Crystal system	monoclinic
Space group	P2 ₁ /c (no. 14)
a (Å)	9.97 (2)
b (Å)	20.79 (3)
c (Å)	16.67(7)
α (°)	90
β (°)	93.46(2)
χ (°)	90
Volume (Å ³)	3578(5)
Z	8
Density (g·cm ⁻³)	1.078
Absorption coefficient (mm ⁻¹)	0.642
F(000)	926
Crystal size (mm ³)	0.3 x 0.2 x 0.03
θ range (°)	2.83 – 28.88
h	-14 / 14
k	-28 / 28
l	-25 / 25
Reflections collected	17129
Independent reflections	13560 [R(int) = 0.0235]
Reflections [I > 2σ(I)]	9653
Data / restraints / parameters	2287 / 0 / 682
Goodness-of-fit on F ²	1.044
R _{obs} (F) (all data)	0.0936
wR ₂ _{obs} (all data)	0.1821

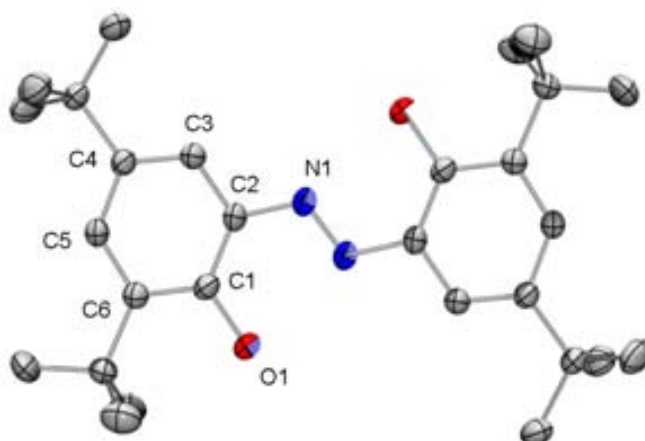
5.3.2 2,2'-dihydroxy-4,3,4',3'-tetra*tert*-butylazobenzene; (**29**)

Figure 5.2. Ortep plot of **29** at the 30% probability level. Hydrogen atoms are omitted for clarity.

Table 5.2. Crystallographic data for **29**.

Empirical formula	C ₂₈ H ₄₂ N ₂ O ₂
Formula weight (g.mol⁻¹)	438.64
Temperature (K)	233(2)
Radiation	MoK α
Wavelength (Å)	0.71073
Crystal system	Monoclinic
Space group	C2/c (no.15)
a (Å)	19.4693(2)
b (Å)	6.2499(3)
c (Å)	21.6187(7)
α (°)	90
β (°)	91.94(2)
χ (°)	90
Volume (Å³)	2629.8(15)
Z	4
Density (g.cm⁻³)	1.108
Absorption coefficient (mm⁻¹)	0.069
F(000)	960
Crystal size (mm³)	0.4 x 0.25 x 0.1
θ range (°)	2.77 - 25.00
h	0 / 22
k	-7 / 7
l	-25 / 25
Reflections collected	6873
Independent reflections	2287 [R(int) = 0.0190]
Reflections [$I > 2\sigma(I)$]	1977
Data / restraints / parameters	2287 / 0 / 150
Goodness-of-fit on F²	1.044
R_{obs}(F) (all data)	0.0460
wR₂_{obs} (all data)	0.1060

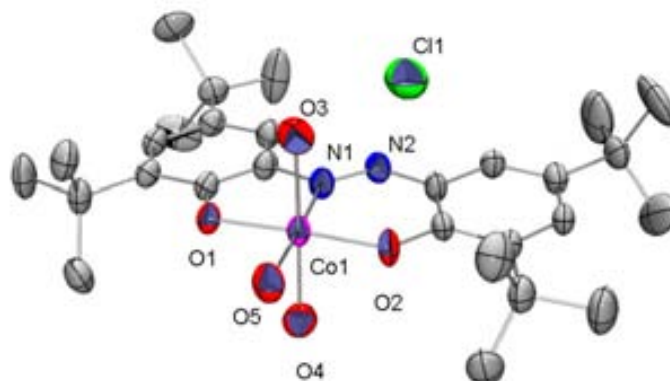
5.3.3 [Co(Cat-N=N-Cat)(H₂O)₃]-Cl; (69)

Figure 5.3. Ortep plot of **69** at the 30% probability level. Hydrogen atoms are omitted for clarity.

Table 5.3. Crystallographic data for **69**.

Empirical formula	C ₂₈ H ₄₆ ClCoN ₂ O ₅ ·H ₂ O·2.5EtOH
Formula weight (g·mol⁻¹)	718.23
Temperature (K)	233(2)
Radiation	MoK α
Wavelength (Å)	0.71073
Crystal system	Triclinic
Space group	P-1 (no.2)
a (Å)	10.916(4)
b (Å)	14.204(5)
c (Å)	14.874(6)
α (°)	101.34(2)
β (°)	103.32(2)
χ (°)	99.69(2)
Volume (Å³)	2144.3(2)
Z	2
Density (g·cm⁻³)	1.112
Absorption coefficient (mm⁻¹)	0.506
F(000)	774
Crystal size (mm³)	0.3 x 0.2 x 0.02
θ range (°)	1.81 - 22.47
h	0 / 11
k	-15 / 15
l	-15 / 15
Reflections collected	10710
Independent reflections	5557 [R(int) = 0.0411]
Reflections [$I > 2\sigma(I)$]	3905
Data / restraints / parameters	5557 / 2 / 346
Goodness-of-fit on F²	1.052
R_{obs}(F) (all data)	0.1041
wR₂_{obs} (all data)	0.2024

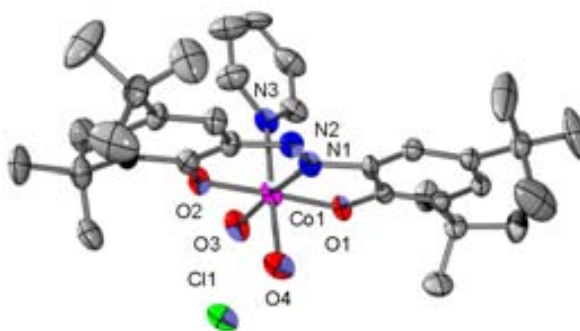
5.3.4 [Co(Cat-N=N-Cat)(py)(H₂O)₂]-Cl and [Co(Cat-N=N-Cat)(H₂O)₃]-Cl; (70)

Figure 5.4. Ortep plot of **70** at the 30% probability level. Hydrogen atoms are omitted for clarity.

Table 5.4. Crystallographic data for **70**.

Empirical formula	C ₆₁ H ₉₅ Cl ₂ Co ₂ N ₅ O ₉ ·2CH ₂ Cl ₂ ·C ₆ H ₁₄
Formula weight (g·mol⁻¹)	1487.20
Temperature (K)	233(2)
Radiation	Mo K α
Wavelength (Å)	0.71073
Crystal system	Triclinic
Space group	P-1(no.2)
a (Å)	14.815(5)
b (Å)	17.737(5)
c (Å)	18.378(7)
α (°)	105.11(2)
β (°)	111.67(2)
χ (°)	94.75(2)
Volume (Å³)	4245.9(2)
Z	2
Density (g·cm⁻³)	1.163
Absorption coefficient (mm⁻¹)	0.628
F(000)	1580
Crystal size (mm³)	0.4 x 0.15 x 0.12
θ range (°)	1.45 - 23.00
h	0 / 16
k	-19 / 19
l	-11 / 11
Reflections collected	20771
Independent reflections	11775 [R _{int} = 0.0232]
Reflections [I > 2σ(I)]	9221
Data / restraints / parameters	11775 / 10 / 868
Goodness-of-fit on F²	1.049
R_{obs}(F) (all data)	0.0938
wR_{2,obs} (all data)	0.1971

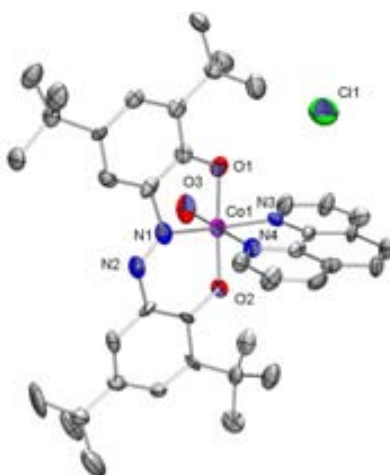
5.3.5 [Co(Cat-N=N-Cat)(phen)(H₂O)]·Cl; (71).

Figure 5.5. Ortep plot of **71** at the 30% probability level. Hydrogen atoms are omitted for clarity.

Table 5.5. Crystallographic data for **71**.

Empirical formula	C ₄₀ H ₅₀ ClCoN ₄ O ₃ ·4H ₂ O
Formula weight (g·mol⁻¹)	801.28
Temperature (K)	233(2)
Radiation	MoK α
Wavelength (Å)	0.71073
Crystal system	Monoclinic
Space group	P2 ₁ /c (no.14)
a (Å)	10.916(3)
b (Å)	19.795(6)
c (Å)	20.606(6)
α (°)	90
β (°)	103.93
χ (°)	90
Volume (Å³)	4322(2)
Z	4
Density (g·cm⁻³)	1.232
Absorption coefficient (mm⁻¹)	0.508
F(000)	1704
Crystal size (mm³)	0.3 x 0.1 x 0.03
θ range (°)	1.92 - 19.00
h	0 / 9
k	-17 / 17
l	-18 / 17
Reflections collected	7305
Independent reflections	3016 [R(int) = 0.0945]
Reflections [$I > 2\sigma(I)$]	2061
Data / restraints / parameters	3016 / 0 / 478
Goodness-of-fit on F²	1.096
R_{obs}(F) (all data)	0.1538
wR2_{obs} (all data)	0.2197

5.3.6 [Co(Cat-N=N-Cat)(terpy)]·Cl; (72)

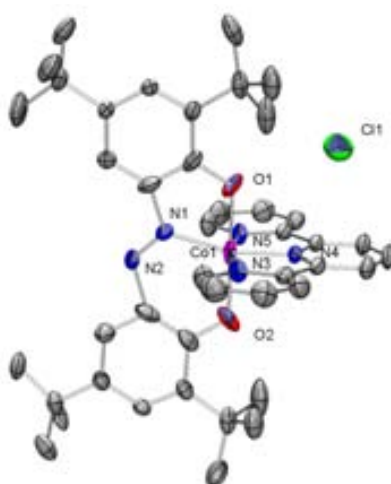


Figure 5.6. Ortep plot of **72** at the 30% probability level. Hydrogen atoms are omitted for clarity.

Table 5.6. Crystallographic data for **72**.

Empirical formula	C ₄₃ H ₅₁ ClCoN ₅ O ₂ ·CH ₂ Cl ₂
Formula weight (g·mol⁻¹)	849.19
Temperature (K)	233(2)
Radiation	MoK α
Wavelength (Å)	0.71073
Crystal system	Orthorhombic
Space group	Fdd2 (no.43)
a (Å)	39.5227(5)
b (Å)	41.6167(5)
c (Å)	10.9710(2)
α (°)	90
β (°)	90
γ (°)	90
Volume (Å³)	18045.1(5)
Z	16
Density (g·cm⁻³)	1.250
Absorption coefficient (mm⁻¹)	0.598
F(000)	7136
Crystal size (mm³)	0.3 x 0.2 x 0.15
θ range (°)	1.99 - 24.00
h	-45 / 39
k	-47 / 47
l	-12 / 12
Reflections collected	22735
Independent reflections	7067 [R(int) = 0.0372]
Reflections [$I > 2\sigma(I)$]	6214
Data / restraints / parameters	7067 / 1 / 571
Goodness-of-fit on F²	1.076
R_{obs}(F) (all data)	0.0629
wR_{2,obs}(all data)	0.1467

5.3.7 [Co(Cat-N=N-Cat)(tppz)]·Cl; (73)

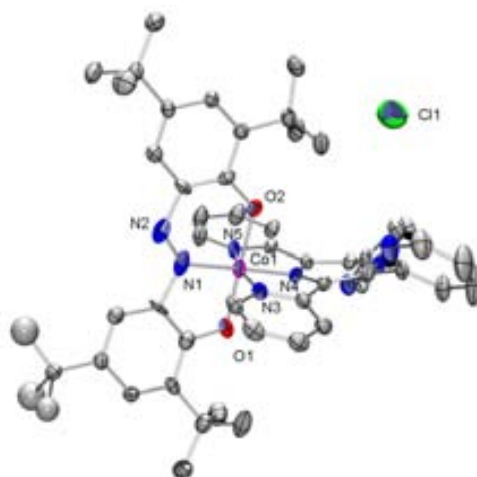


Figure 5.7. Ortep plot of **73** at the 30% probability level. Hydrogen atoms are omitted for clarity.

Table 5.7. Crystallographic data for **73**.

Empirical formula	$C_{52}H_{62}ClCoN_8O_2 \cdot 1.6H_2O \cdot 1.1$
	CH_2Cl_2
Formula weight (g·mol⁻¹)	1067.15
Temperature (K)	233(2)
Radiation	MoK α
Wavelength (Å)	0.71073
Crystal system	Tetragonal
Space group	I4 ₁ /a (no.88)
a (Å)	44.949(1)
b (Å)	44.949(2)
c (Å)	10.720(1)
α (°)	90
β (°)	90
γ (°)	90
Volume (Å³)	21659(2)
Z	16
Density (g·cm⁻³)	1.309
Absorption coefficient (mm⁻¹)	0.555
F(000)	8941
Crystal size (mm³)	0.25 x 0.15 x 0.1
θ range (°)	1.95 - 21.50
h	-46 / 42
k	-46 / 46
l	-11 / 11
Reflections collected	26869
Independent reflections	6117 [R(int) = 0.0965]
Reflections [$I > 2\sigma(I)$]	4273
Data / restraints / parameters	6117 / 2 / 591
Goodness-of-fit on F²	1.063
R_{obs}(F) (all data)	0.1209
wR₂_{obs} (all data)	0.1949

5.3.8 [Co(Cat-N=N-Cat)(Cat-N=N-SQ)]; (74)

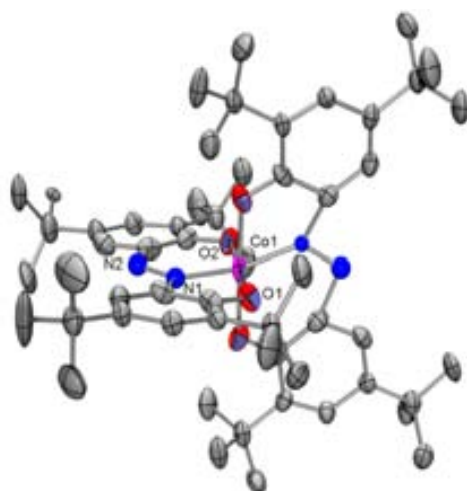


Figure 5.8. Ortep plot of **74** at the 30% of probability level. Hydrogen atoms are omitted for clarity.

Table 5.8. Crystallographic data for **74**.

Empirical formula	C ₅₆ H ₈₀ CoN ₄ O ₄
Formula weight (g·mol⁻¹)	932.17
Temperature (K)	233(2)
Radiation	MoK α
Wavelength (Å)	0.71073
Crystal system	Triclinic
Space group	P-1 (no.2)
a (Å)	10.769(1)
b (Å)	10.903(1)
c (Å)	25.243(2)
α (°)	95.49(6)
β (°)	100.81(4)
χ (°)	107.94(4)
Volume (Å³)	2732(4)
Z	2
Density (g·cm⁻³)	1.133
Absorption coefficient (mm⁻¹)	0.360
F(000)	1006
Crystal size (mm³)	0.2 x 0.1 x 0.03
θ range (°)	1.67 - 20.50
h	0 / 10
k	-10 / 10
l	-24 / 24
Reflections collected	10293
Independent reflections	5472 [R(int) = 0.0587]
Reflections [$I > 2\sigma(I)$]	3691
Data / restraints / parameters	5472 / 0 / 609
Goodness-of-fit on F²	1.019
R_{obs}(F) (all data)	0.1048
wR₂_{obs} (all data)	0.1449

53.9 Selected bond lengths and angles for 29 and 69-74.**Table 5.1.** Selected Bond lengths and angles for ligand **29** and complexes **69-74**. Distances are expressed in Å and angles in °.

Azo bisphenolate compound	C1-O1	C7-O2	N1-N2	O1-Co-O2
29	1.357 (1)	1.357 (1)	1.280 (2)	—
69	1.334 (8)	1.326 (8)	1.266 (8)	177.0 (2)
70	1.328 (5)	1.307 (5)	1.254 (5)	177.70 (15)
71	1.316 (16)	1.319 (14)	1.230 (14)	176.7 (4)
72	1.319 (6)	1.324 (5)	1.296 (14)	179.00 (18)
73	1.350 (9)	1.319 (8)	1.199 (8)	177.9 (2)
74	1.282 (6)	1.297 (5)	1.317 (9)	178.23 (17)
	1.313 (6)	1.317 (6)	1.326 (6)	179.65 (17)

References

- [1] T. Kircher, H.-G. Löhmansröben, *Phys. Chem. Chem. Phys.*, **1**, **1999**, 3987.
- [2] S. Espinosa, E. Bosch, M. Rosés, *Anal. Chem.*, **72**, **2000**, 72, 5193.
- [3] S. Espinosa, E. Bosch, M. Rosés, *J. Chromatogr. A*, **964**, **2002**, 55.
- [4] Gaussian 03 (Revision B.04), M. J. Frisch, G. W. Trucks, H. B. Schlegel, G. E. Scuseria, M. A. Robb, J. R. Cheeseman, J. A. Montgomery, Jr., T. Vreven, K. N. Kudin, J. C. Burant, J. M. Millam, S. S. Iyengar, J. Tomasi, V. Barone, B. Mennucci, M. Cossi, G. Scalmani, N. Rega, G. A. Petersson, H. Nakatsuji, M. Hada, M. Ehara, K. Toyota, R. Fukuda, J. Hasegawa, M. Ishida, T. Nakajima, Y. Honda, O. Kitao, H. Nakai, M. Klene, X. Li, J. E. Knox, H. P. Hratchian, J. B. Cross, V. Bakken, C. Adamo, J. Jaramillo, R. Gomperts, R. E. Stratmann, O. Yazyev, A. J. Austin, R. Cammi, C. Pomelli, J. W. Ochterski, P. Y. Ayala, K. Morokuma, G. A. Voth, P. Salvador, J. J. Dannenberg, V. G. Zakrzewski, S. Dapprich, A. D. Daniels, M. C. Strain, O. Farkas, D. K. Malick, A. D. Rabuck, K. Raghavachari, J. B. Foresman, J. V. Ortiz, Q. Cui, A. G. Baboul, S. Clifford, J. Cioslowski, B. B. Stefanov, G. Liu, A. Liashenko, P. Piskorz, I. Komaromi, R. L. Martin, D. J. Fox, T. Keith, M. A. Al-Laham, C. Y. Peng, A. Nanayakkara, M. Challacombe, P. M. W. Gill, B. Johnson, W. Chen, M. W. Wong, C. Gonzalez, J. A. Pople, Gaussian, Inc., Wallingford CT, **2004**.
- [5] G. M. Sheldrick, Program for the Refinement of Crystal Structures; University of Göttingen, Germany, **1997**.
- [6] Otwinowski, Z.; Minor, W., *Methods Enzymol.*, **276**, **1997**, 307-326
- [7] R. M. Buchanan, C. G. Pierpont, *J. Am. Chem. Soc.*, **102**, **1980**, 4951.
- [8] S. K. Larsen, C. G. Pierpont, *J. Am. Chem. Soc.*, **110**, **1988**, 1827.

Annex | I

Self Exchange Intramolecular Electron Transfer

I.1 Mechanisms for the intramolecular electron transfer (IET)

The interest for molecular wires arises from the potential use of such systems on integrated molecular-sized devices^{1,2} and, from a theoretical point of view, to study the role of various parameters governing the intramolecular electron transfer (IET) rates.³ Mixed-valence compounds⁴ are excellent candidates for such studies since IET phenomena can be easily determined from the position, intensity and width of the so-called intervalence transition (IVT) band that usually appears in the near-infrared (near-IR) region.⁵ To better understand the origin of this band, it is necessary to have a look to potential energy curves that define a Class II MV system. In fact we can present these molecules as donor-bridge-acceptor (D-bridge-A) dyads where the IET phenomena may take place through two different mechanisms:

- 1.- Optically self-exchange IET
- 2.- Thermally self-exchange IET

The difference between the optical and thermal electron-transfer processes in Class II MV systems is shown in Figure I.1.

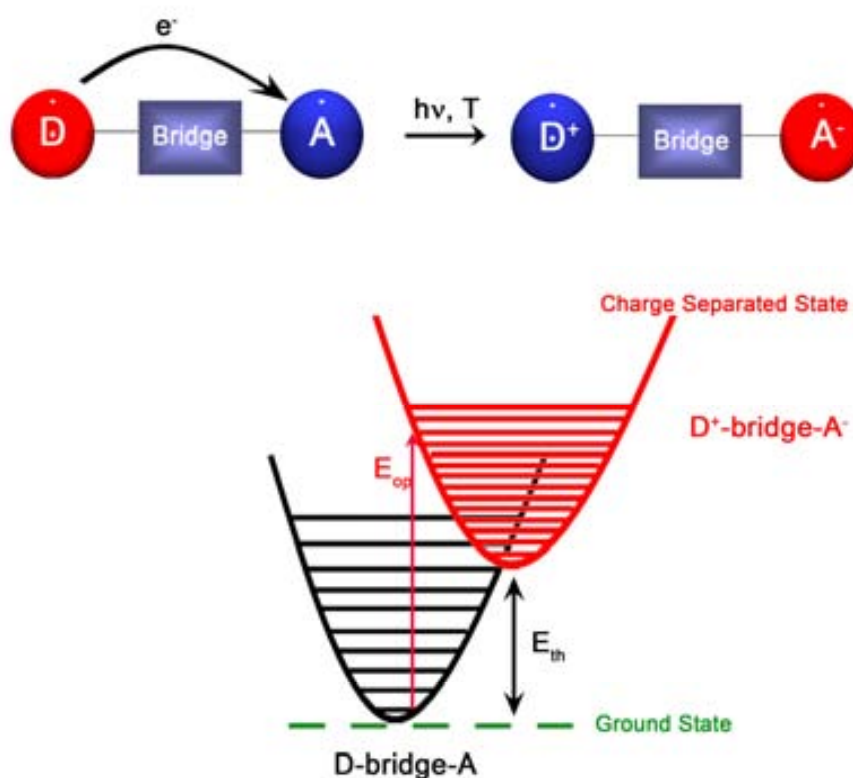


Figure I.1. Schematic representation of the free energy surfaces and definition of the two mechanisms for the IET in D-bridge-A systems.

I.1.1 Self-exchange intramolecular electron transfer (IET).

This phenomenon in fact can be optical or thermal. The charge transfer requires the reorganization of the inner and the outer sphere, and the energy from this reorganisation is related to the IET activation barrier, which can be overcome by a thermal or optical stimuli. A more descriptive image of both mechanisms is given in Figure I.2. In this figure, the vibrational levels have been omitted for the sake of simplicity.

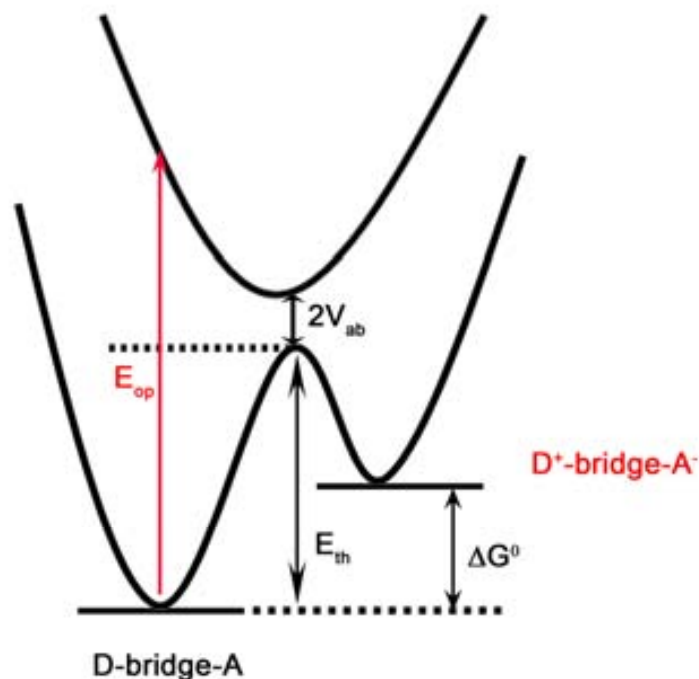


Figure I.2. Potential energy curves of a Class II system where the optically (E_{op}) and thermally (E_{th}) induced IET processes are compared.

The equilibrium geometry of the electron when it is localised on the left side centre (D-bridge-A) is represented on the left side of the curve, whereas the minimum on the right side corresponds to the equilibrium geometry of the electron localised on the other centre (A^+ -bridge-D $^-$). Obviously, the character of donor and acceptor of each centre depends on where the electron is localised. To have a thermally induced IET, the electron must move from the left to the right along the nuclear coordinate, without changing the electronic state, overcoming an energy barrier, E_{th} , which arises from the nuclear reorganization required before the IET takes place. This means, that the IET occurs through an intermediate state ((U-bridge-U, Figure I.3) where bond lengths around D and A are now equivalent and in between the values of both equilibrium state. When the energy applied is the necessary, the reaction is adiabatic and the system crosses from one energy well to another with the maximum probability ($K_{ei}=1$). When the interaction becomes small the reaction becomes significantly non-adiabatic.

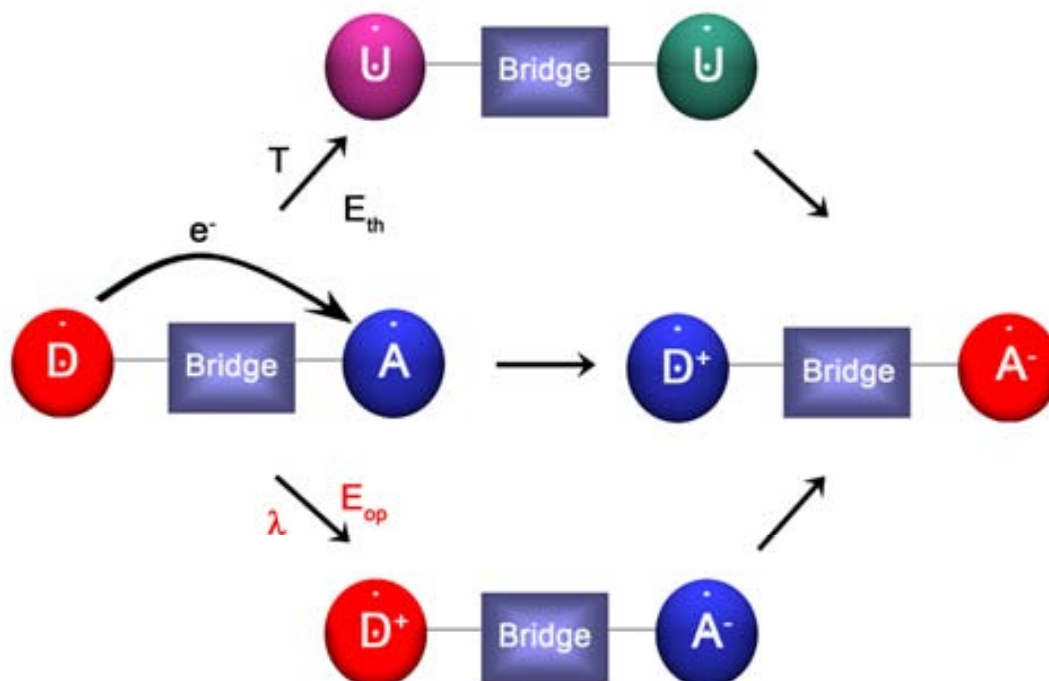


Figure I.3. Representation of the intermediate states of a thermally and an optically induced self-exchange IET

For the contrary, when the IET becomes optically induced, and according with the Frank-Condon principle,⁶ the reaction takes place through an excited state (D⁺-bridge-A⁻, Figure I.3)* where neither the solvent nor the internal geometry are allowed to relax. Then, the new oxidised centre D⁺, retains the bond distances and the solvation sphere of the neutral centre (D), whereas the new A⁻ centre retains the bond distances and the solvation sphere of the oxidised centre (A). As a consequence IVT corresponding to the vertical excitation are observed in the optical absorption spectra. From the position, intensity, and width of the IVT transition, which occurs generally in the near infrared region,⁷ the IET can be easily characterized.

Then the E_{th} can be estimated considering two basic parameters: The vertical reorganization energy λ, and the electronic interaction matrix element V_{AB}.⁸ The vertical reorganization energy λ is the vertical gap between the minimum on the energy surface of the precursor and the energy surface of the excited state. Such energy can be expressed as the sum of two independent contributions corresponding to the reorganisation contributions of the inner (λ_i) and the outer (λ_o) nuclear modes.⁹

$$\lambda = \lambda_i + \lambda_o \quad (I.1)$$

The outer reorganisation energy, λ_o, use to be the predominant term for IET processes in polar solvents and is originated by the reorientation of the solvent molecule layer around both

redox centres, which differs before and after the IET takes place.¹⁰ λ_0 can be estimated from Eq I.2:

$$\lambda_0 = e^2 (1/2a_1 + 1/2a_2 - 1/r) * (1/\epsilon_{op} - 1/\epsilon_S) \quad (I.2)$$

where e is the electronic charge, ϵ_{op} and ϵ_S are the optical and static dielectric constants of the solvent, a_1 and a_2 are the radii of the reactants and r is the interreactant centre-to-centre distance. According to Marcus-Hush theory,¹¹ these parameters of the optical and thermal IET processes are closely interrelated by the relevant Eq I.3 and I.4:

$$E_{th} = (\lambda + \Delta G^0)^2 / 4\lambda \quad (I.3)$$

$$E_{op} = \lambda + \Delta G^0 \quad (I.4)$$

E_{op} is the energy required for the optical transition, E_{th} is the activation barrier for thermal IET, V_{ab} is the electronic coupling matrix between the potential energy surfaces of reactants and products, and ΔG^0 is the free energy difference between products and reactants. Finally, to determine the effective electronic coupling V_{ab} (in cm^{-1}) between both active nuclei, next Eq I.5 developed by Hush, can be used.

$$V_{ab} = (2.05 \times 10^{-2}) [\epsilon_{max} \Delta v_{1/2} / v_{max}]^{1/2} v_{max} / r \quad (I.5)$$

where r is the effective separation of the two redox sites (in Å), ϵ_{max} is the maximum extinction coefficient (in $\text{M}^{-1} \text{cm}^{-1}$), v_{max} is the transition energy, and $\Delta v_{1/2}$ is the full width at half height (both in cm^{-1}) of the IVT band.¹²

References

- [1] N. Dulic, S. J. van der Molen, T. Judernac, H. T. Jonkman, J. J. D. de Jongm T. N. Bowden, J. van Esch, B. L. Feringa, B. J. Wees, *Phys. Rev. Lett.*, **91**, **2003**, 207402.
- [2] J. He, F. Chem, P. A. Liddell, J. Andreasson, S. D. Straight, D. Gust, T. A. Moore, A. L. Moore, J. Li, O. F. Sankey, S. M. Lindsay, *Nanotechnology*, **16**, **2005**, 695, and references cited herein.
- [3] (a) C. Creutz, *Prog. Inorg. Chem.*, **30**, **1983**, 1. (b) R. J. Crutchley, *Adv. Inorg. Chem.*, **41**, **1994**, 273.
- [4] J. J. P. Fackler, *Encyclopedia of Inorganic compounds*, **15**, **2006**, 2270.
- [5] (a) O. Elsner, D. Ruiz-Molina, J. Vidal-Gancedo, C. Rovira, J. Veciana, *J. Nano Lett.*, **1**, **2001**, 117. (b) J. Sedo, D. Ruiz, J. Vidal-Gancedo, C. Rovira, J. Bonvoisin, J. -P. Launay, J. Veciana, *Adv. Mater.*, **8**, **1997**, 748.
- [6] S. Thompson, J. Staley, *Foundations of Spectroscopy*, <http://www.smallscalechemistry.colostate.edu/PowerfulPictures/FoundationsOfSpectroscopy.pdf>
- [7] R. J. Crutchley, *Adv. Inorg. Chem.*, **41**, **1994**, 273.
- [8] S. E. Nelsen, J. J. Ramm, D. R. Powell, *J. Am. Chem. Soc.*, **119**, **1997**, 6863.
- [9] (a) R. A. Marcus, *Angew. Chem. Int. Ed.*, **31**, **1993**, 111, and references cited herein. (b) J. P: Sauvage, J. -P. Collin, J. -C. Chambron, S. Guillerez, C. Courdet, *Chem. Rev.*, **94**, **1994**, 993.
- [10] (a) N. S. Hush, *Prog. Inorg. Chem.*, **8**, **1967**, 391. (b) R. A. Marcus, N. Sutin, *Inorg. Chem.*, **14**, **1975**, 213. (c) N. J. Sutin, *Photochem*, **10**, **1979**, 19. (d) R. A. Marcus, P. Siders, *J. Phys. Chem.*, **86**, **1982**, 622. (e) R. A. Marcus, N. Sutin, *Biochim. Biophys. Acta*, **811**, **1985**, 265. f) N. S. Hush, *Coord. Chem. Rev.*, **64**, **1985**, 135.
- [11] (a) R. A. Marcus, *J. Chem. Phys.*, **24**, **1956**, 966. b) R. A. Marcus, *J. Chem. Phys.*, **24**, **1956**, 979. (c) R. A. Marcus, *J. Chem. Phys.*, **26**, **1957**, 867. (d) R. A. Marcus, *J. Chem. Phys.*, **26**, **1957**, 872. (e) R. A. Marcus, *Disc. Faraday. Soc.*, **29**, **1960**, 21. (f) R. A. Marcus, *J. Phys. Chem.*, **67**, **1963**, 853. (g) R. A. Marcus, *Annu. Rev. Phys. Chem.*, **15**, **1964**, 155. (h) R. A. Marcus, *J. Chem. Phys.*, **811**, **1965**, 679. (h)D. E. Richardson, H. Taube, *Coord. Chem. Rev.*, **60**, **1984**, 107.
- [12] (a) K. Y. Wong, P. N. Schatz, *Prog. Inorg. Chem.*, p.369. Wiley, New York. **1983**. (b) N. S. Hush, *Prog. Inorg. Chem.*, p. 391. Wiley, New York. **1983**.

Annex | II

¹H-NMR Spectroscopy

II.1 Evans Method

II.1.1 Equations Development

This methodology, suitable for the calculation of the number of unpaired electrons in solution samples, is based on the frequency shift of the NMR signal of a reference sample by the magnetic field of a co-dissolved paramagnetic species.¹ The relative frequency shift $\Delta\nu/\nu_0$ with $\Delta\nu = \nu^{\text{TMS}}(\text{Outer tube}) - \nu^{\text{TMS}}(\text{Inner tube})$, produced by the presence of the paramagnetic species is used to calculate the magnetic moment according to Eq. II.1,²

$$\chi_g = \chi_0 + [(3 \cdot \Delta\nu) / (2 \cdot \pi \cdot \nu_0 \cdot c)] + [(\chi_0 \cdot (\rho_0 - \rho_s)) / c] \quad (\text{II.1})$$

where χ_g is the mass magnetic susceptibility of the solute (cm^3/g); χ_0 is the magnetic susceptibility of the solvent (cm^3/g); $\Delta\nu$ is the separation in paramagnetic chemical shift (Hz); ν_0 is the spectrometer radiofrequency; c is the concentration of the solution (mol/mL); ρ_0 is the density of the pure solvent and ρ_s is the density of the solution

The last term in Eq. (II.1) can often be neglected without appreciable error and the expression simplifies to:

$$\chi_g = \chi_0 + [(3 \cdot \Delta\nu) / (2 \cdot \pi \cdot \nu_0 \cdot c)] \quad (\text{II.2})$$

Because of the fact that these equations have been derived for an iron-core magnet in which the magnetic field is perpendicular to the cylindrical sample-tube axis, the accuracy of this technique depends on two terms. First, on the accurate knowledge of the concentration (c), and secondly also depends on the accurate determination of the paramagnetic shift ($\Delta\nu$). To obtain a larger shift, is possible to increase the concentration, but, this also causes the line broadening of the reference signal due to a shorter T_1 , thereby limiting the accuracy in the determination of the chemical shift. The measurements by high-field NMR leads to a fast sensitive and convenient method for obtaining paramagnetic susceptibility. The calculations are carried out by an equation appropriately modified to consider parallel sample geometry.

For a long cylindrical tube oriented parallel to B , the paramagnetic shift ($\Delta\nu$) can be written as Eq. II.3. Also, molar magnetic susceptibility can be expressed as Eq. II.4.

$$\Delta\nu/\nu_0 = (4 \cdot \pi \cdot \chi_g) / 3 \quad (\text{II.3})$$

$$\chi_m = \chi_g \cdot M' \quad (\text{II.4})$$

where χ_m is molar magnetic susceptibility and M' is the molecular weight (g/mol).

By the substitution of both equations into Eq. II.2, the new Eq. II.5 is obtained.

$$\chi_g = \chi_0 + [(3 \cdot \Delta\nu) / (4 \cdot \pi \cdot \nu_0 \cdot c \cdot M')] \quad (c = \text{mol/mL}) \quad (\text{II.5})$$

or Eq. II.6 expressed as molar susceptibility

$$\chi_m = \chi_0 \cdot M' + [(3 \cdot \Delta\nu) / (4 \cdot \pi \cdot \nu_0 \cdot c)] \quad (\text{II.6})$$

where, c is now the concentration (mol/mL), M' is the molecular weight (g/mol) and χ_m is the molar magnetic susceptibility of the Solute (cm^3/g).

Also, the introduction of the chemical shift defined as the difference between the resonance frequency of the nucleus and a standard, relative to the standard was done. This chemical shift is reported in ppm and written with the delta, δ , symbol." Eq. II.7 and Eq. II.8.

$$\delta = (v - v_{\text{REF}}) \cdot 10^6 / v_{\text{REF}} \quad (\text{II.7})$$

$$\Delta v / v_0 = \Delta \delta \cdot 10^{-6} \quad (\text{II.8})$$

This converts Eq. II.6 in Eq. II.9:

$$\chi_m = \chi_0 \cdot M' + [(3 \cdot \Delta \delta \cdot 10^{-6}) / (4 \cdot \pi \cdot c)] \quad (\text{II.9})$$

where $\Delta \delta$ is the separation in paramagnetic chemical shift (ppm). Subsequently, by taking into account the diamagnetic contribution, which can be estimated as the sum of constants (called Pascal's constants; Eq. II.10) for each diamagnetic species in the sample, is obtained Eq. II.11.

$$\chi_m^{\text{corr}} = \chi_m - \sum \chi_\alpha \quad (\text{II.10})$$

$$\chi_m^{\text{corr}} = \chi_0 \cdot M' + [(3 \cdot \Delta \delta \cdot 10^{-6}) / (4 \cdot \pi \cdot c)] - \sum \chi_\alpha \quad (\text{II.11})$$

Finally the $\chi_{\text{mol}}^{\text{corr}}$ obtained from Eq. II.11 is used to calculate the effective magnetic moment.

$$\mu_{\text{eff}} = \sqrt{[(3 \cdot K \cdot T \cdot \chi_m^{\text{corr}}) / N \beta^2] = 2,828 \sqrt{(\chi_m^{\text{corr}} \cdot T)} \quad (\text{II.12})$$

where K is the Boltzmann constant ($1.38 \times 10^{-23} \text{ J K}^{-1}$); T is the absolute temperature (K); N is the Avogadro's number ($6.022 \times 10^{23} \text{ mol}^{-1}$); β is the Bohr magneton ($9.274 \times 10^{-24} \text{ J T}^{-1}$).

II.1.1.1 Variation of the equation by using the molar mass

Returning to Eq. II.3, which represents the paramagnetic shift as a function of the mass magnetic susceptibility for a cylindrical sample oriented parallel to B :³

$$\Delta v/v_0 = (4 \cdot \pi \cdot \chi) / 3 \quad (\text{II.3})$$

The mass magnetic susceptibility can also be expressed in function of the volume susceptibility, as in Eq. II.13

$$\chi_g = \kappa / \rho \quad (\text{II.13})$$

where κ is the volume susceptibility (dimensionless) and ρ is the density, that introduced in Eq. II.3 gives the paramagnetic shift as a function of the volume susceptibility (Eq. II.14), previously substitution of Eq. II.8, as explained before:

$$\Delta \delta \cdot 10^{-6} = (4 \cdot \pi / 3) \cdot (\kappa^{\text{solvent}} - \kappa^{\text{solution}}) \quad (\text{II.14})$$

Next table, is done in order to can follow the equation development for Eq. II.14, in order to obtain the factor $[\kappa^{\text{solvent}} - \kappa^{\text{solution}}]$; To the solvent is assigned the 0, while for the complex is the 1.

	Mass	Amount of substance	Molar mass
Solvent (0)	m_0	n_0	M_0
Complex (1)	m_1	n_1	M_1

- 1) $\chi_g^{(\text{solution})} = [m_1 / (m_1 + m_0)] \cdot \chi_{g(1)} + [m_0 / (m_1 + m_0)] \cdot \chi_{g(0)}$; $[\chi_{g(1)} = \chi_{m(1)} / M_1]$
- 2) $\chi_g^{(\text{solution})} = [1 / (m_1 + m_0)] \cdot [\chi_{m(1)} \cdot (m_1 / M_1) + \chi_{g(0)} \cdot m_0]$ $[m_1 / M_1 = n_1]$
- 3) $\chi_g^{(\text{solution})} = [1 / (m_1 + m_0)] \cdot [\chi_{m(1)} \cdot (n_1) + (\chi_{g(0)} \cdot m_0)]$
- 4) $\kappa^{\text{solution}} = \chi_g^{(\text{solution})} \cdot \rho^{(\text{solution})} = [1 / (m_1 + m_0)] \cdot [\chi_{m(1)} \cdot n_1 + \chi_{g(0)} \cdot m_0] \cdot \rho_{\text{solution}} = (1 / V_{\text{solution}}) \cdot [\chi_{m(1)} \cdot n_1 + \chi_{g(0)} \cdot m_0] = [\chi_{m(1)} \cdot C_1 + \chi_{g(0)} \cdot (m_0 / V_{\text{solution}})] = \chi_{m(1)} \cdot C_1 + \chi_{g(0)} \cdot \rho_0 \cdot V_0 / V_{\text{solution}} = \chi_{m(1)} \cdot C_1 + \chi_{g(0)} \cdot \rho_0 \cdot (1 + \{(V_0 - V_{\text{solution}}) / V_{\text{solution}}\})$
- 5) $\kappa^{\text{solvent}} = \chi_{g(0)} \cdot \rho_0$

Obtaining the equation II.12 for the factor $[\kappa^{\text{solvent}} - \kappa^{\text{solution}}]$;

$$\kappa^{\text{solvent}} - \kappa^{\text{solution}} = \chi_{m(1)} \cdot C_1 - \chi_{g(0)} \cdot \rho_0 \cdot \{(V_{\text{solution}} - V_0) / V_{\text{solution}}\} \quad (\text{II.15})$$

from where doing the analogy: $m_1 \approx 2$ mg and $m_0 \approx 500$ mg and $m \approx V$, $[V_{\text{solution}} - V_0 / V_{\text{solution}} = 0.004]$, finally, introducing this final Eq. II.16 into the Eq. II.12, is obtained Eq. II.17,

$$\chi_m^{\text{corr}} = [(3 \cdot \Delta\delta \cdot 10^{-6}) / (4 \cdot \pi) + \chi_{g(0)} \cdot \rho_0 \cdot \{(V_{\text{solution}} - V_0) / V_{\text{solution}}\}] / C_1 - \Sigma \chi_{\alpha} =$$

$$[(3 \cdot \Delta\delta \cdot 10^{-6}) / (4 \cdot \pi) + \chi_{g(0)} \cdot \rho_0 \cdot 0,004] / C_1 - \Sigma \chi_{\alpha} \quad (\text{II.16})$$

which will be used for calculate the effective magnetic moment, according to the Eq. II.12.

II.1.2 Sample preparation

The NMR samples for susceptibility measurements using the Evans Method were prepared by dissolving a weighted amount (from 1 mg to 2 mg) of complex in a measured volume of solvent (0.65 mL). The complex solution was transferred into a 5 mm tube containing a 1 mm capillary with the deuterated diamagnetic solvent and one drop of tetramethylsilane (TMS) as a reference (near to 0.1 mL). The $^1\text{H-NMR}$ of a sample prepared in this way, present a peak for the TMS protons $[\delta\text{TMS}^{(\text{OuterTube})}]$, and a variation of this peak depending on the temperature for the inner tube $[\delta\text{TMS}^{(\text{InnerTube})}]$, due to the magnetic field generated by the paramagnetic sample in the outer tube. The different signal shifts, $\Delta\delta^{\text{TMS}}$, found for the methyl groups of the TMS was used to determine the susceptibility in solution at each temperature. All the experiments are done in non-deuterated solvents. For the case of toluene, the experiment was performed in both cases, not observing important differences in the results. The temperature-dependent density changes of the solvent were corrected using equations and

data from the International Critical Tables.⁴ All this results were done in collaboration with Dr. Miquel Cabañas, from the Servei de Resonància Magnètica Nuclear at the Universitat Autònoma de Barcelona and Dr. Motohiro Nakano from Osaka University.

II.1.3 Experiment realised with complex **25**.

To explain the methodology used for the treatment of the ¹H-NMR experimental data with the Evans Method, complex **25** has been selected as a representative example. As can be observed in Figure II.1, the *tert*-butyl peaks due to the complex appear in a low fraction compared with the solvent peaks, which were marked with an asterisk (Figure II.1b). Therefore, an enlargement of the TMS region marked with red the asterisk (around 0 ppm) shows the variation of the TMS peak for the inner tube (in lower intensity) with respect to the TMS peak of the outer tube. Such variation depends on the temperature, increasing as the temperature increases (from 203 K to 636 K). This difference, $\Delta\delta^{\text{TMS}}$, was calculated and introduced in the formula II.16, in order to obtain the molar magnetic susceptibility, represented in Figure II.1d. Finally the application of the Eq. II.12 allows obtaining the values of the effective moment in all the temperature range (Figure II.1d). As can be observed the μ_{eff} vs. T presents non-Curie Weiss Law behaviour, which can be ascribed to the equilibrium process between *ls*-Co(III) and *hs*-Co(II).

Relevant values for complex **25**, were also expressed in tables II.1 (203 K) and II.2 (363 K), where can be observed that at low temperature the effective moment (1.82 μ_{eff}) is near to that expected for the single unpaired electron. Although at high temperature, the effective moment (4.64 μ_{eff}) is close to the theoretical value expected for a Co(II) octahedral specie with a S=3/2. In these tables were also compiled the values obtained for complexes **24** and **26**.

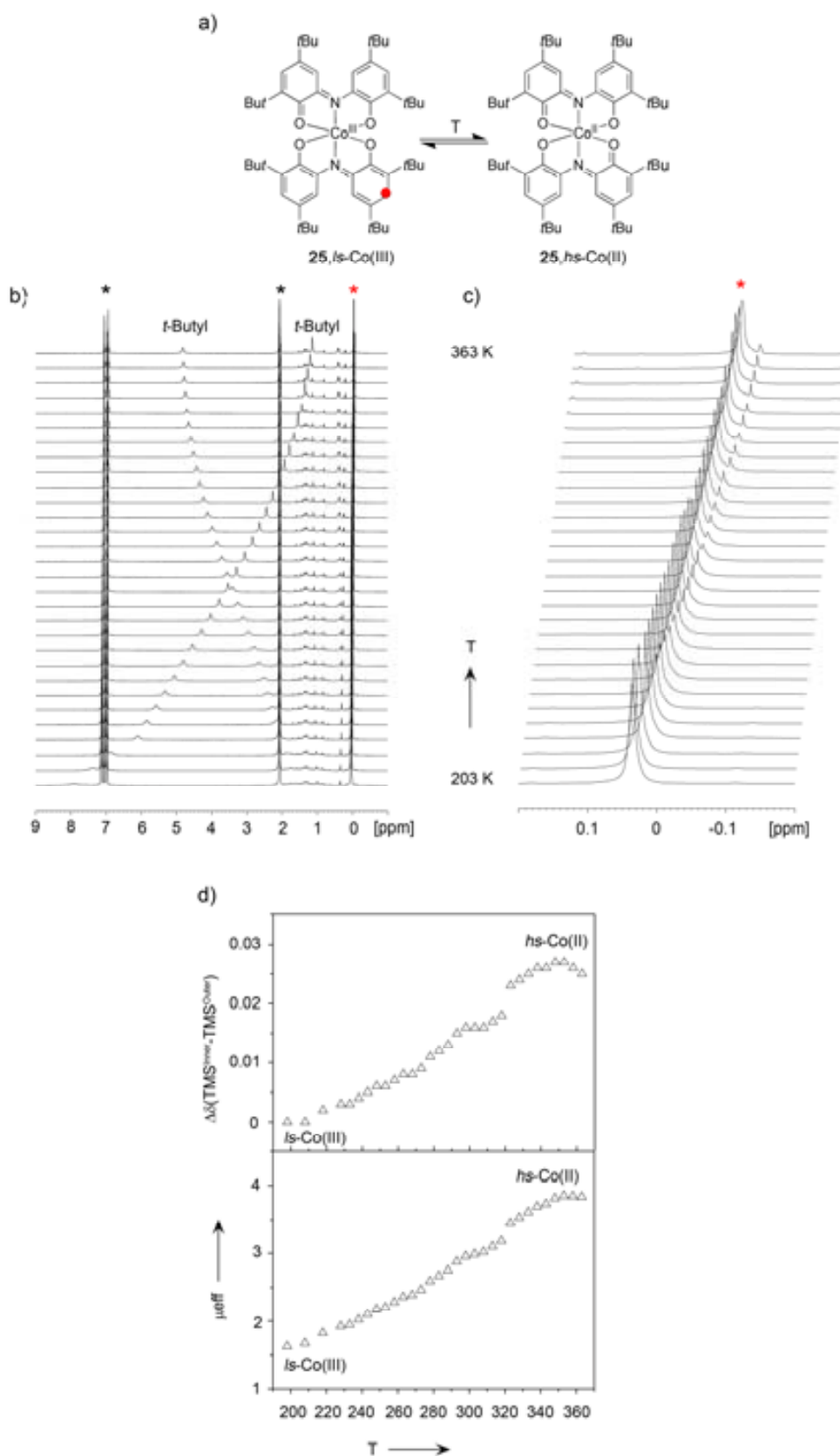


Figure II.1. a) Equilibrium of VT phenomena for complex **25**. b) $^1\text{H-NMR}$ (400 MHz) for complex **25** under the Evans Method conditions at variable temperature. Temperature range from 203 K to 363 K. c) shift peak of the TMS-proton groups in the inner tube vs. the outer tube at the same temperature range. d) Representation of the $\Delta\delta(\text{TMS}^{\text{Inner-Outer}}$) vs. T (top) and applying this values to Eq. II.13 (bottom).

Table II.1.- Table of μ_{eff} values derived from Evans Method at 203 K applied to complexes **24**, **25** and **26**.

203 K			
Compound	$\delta\text{TMS}^{(\text{Inner Tube})}$	$\delta\text{TMS}^{(\text{Outer Tube})}$	μ_{eff}
24	0.130	0	5.38
25	0	0	1.82
26	0.052	0	2.86

Table II.2.- Table of μ_{eff} values derived from Evans Method at 363 K applied to complexes **24**, **25** and **26**.

363 K			
Compound	$\delta\text{TMS}^{(\text{Inner Tube})}$	$\delta\text{TMS}^{(\text{Outer Tube})}$	μ_{eff}
24	0.058	0	5.09
25	0.025	0	4.64
26	0.012	0	2.72

References

[1] Evans, D. F., J. Chem. Soc., **1959**, 2003.

[2] Sur, S. K., J. Mag. Res., **82**, **1989**, 169.

[3] R. March, W. Clegg, R. A. Coxall, P. González-Duerte, Inorg. Chim. Acta, **346**, **2003**, 87.

[4] Valours obtained from the reviews of J. Chem. Eng. Data, MeOH: **39**, **1994**, 876; acetone: **42**, **1997**, 2; toluene: **44**, **1999**, 411; chloroform: **46**, **2001**, 2 and acetonitrile: **47**, **2002**, 1037.

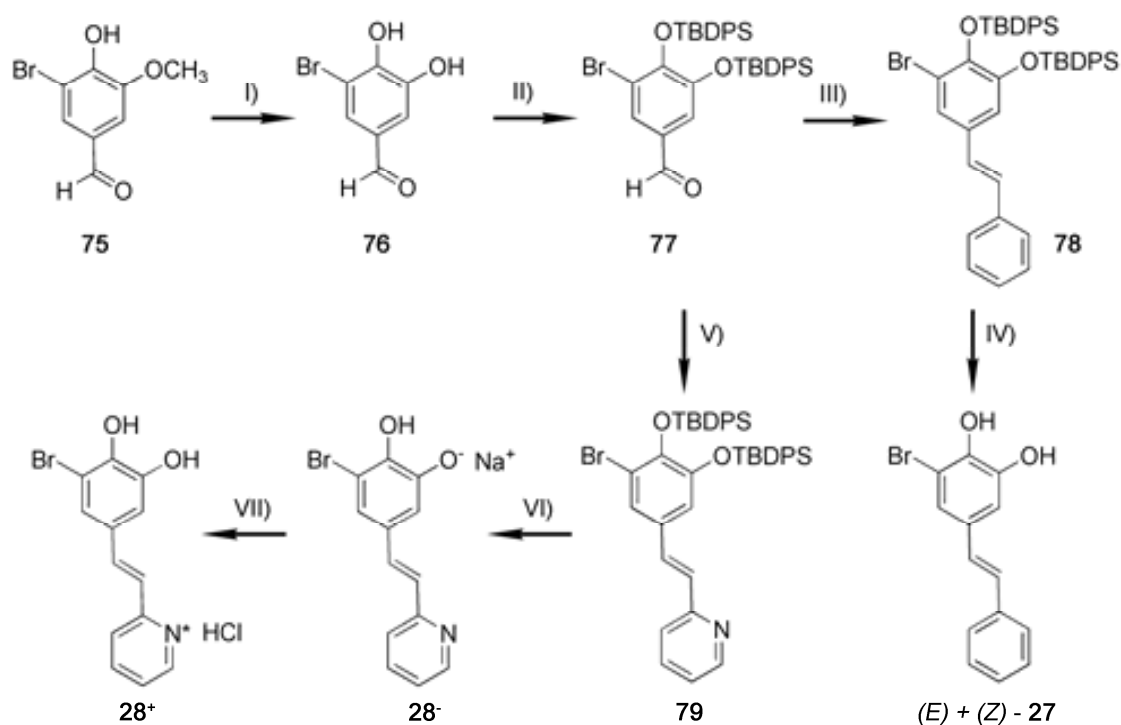
Annex | III

Organic Synthesis

III.1 Organic synthesis

The complete synthesis and characterization of ligands **27-29** was developed by Gisela G. Bardají and Javier Saiz under the direction of Dr. Félix Busqué at the Universitat Autònoma de Barcelona. A brief resume of the synthetic steps and the characterisation of the compounds are given for information purposes.

III.1.1 Synthesis of catecholate-based ligands



I) AlCl_3 , pyridine, CH_2Cl_2 , 24 h reflux, 77%. II) TBDPDCI, DBU, THF-DMF, rt, 3h, 58%. III) $(\text{Ph})_3\text{P}^+\text{CH}_2\text{-Ph Cl}^-$, *t*-BuOK, THF, rt, 2h, 75%. IV) TEA-3THF, THF, rt, 2h, 78%. V) $(\text{Ph})_3\text{P}^+\text{CH}_2\text{-py-HCl Cl}^-$, *t*-BuOK, THF, rt, 2h, 83%. VI) (i) TEA-3THF, THF, rt, 2h (ii) HCl 35%, 65%. VII) NaOH 1M, CH_2Cl_2 , 94%.

Scheme III.1.

As a general summary here is included the sequence of reactions leading to target compounds **27** and **28**·HCl. Synthesis began with commercially available 5-bromovanillin (**75**). Thus, cleavage of methyl ether of 5-bromovanillin (**75**) using anhydrous AlCl_3 in the presence of pyridine furnished catechol **76**¹ in 77% yield. Next, protection of the hydroxyl groups of **75** as their TBDPS derivatives was accomplished using TBDPSCI and DBU in a mixture of THF and DMF, affording compound **77** in 58% yield along with monoprotected product in 7% yield. This reaction failed when other bases different from anhydrous DBU were used. Wittig reaction of aldehyde **77** with benzyl-triphenyl-phosphonium chloride using *t*-BuOK as base yielded an inseparable 1:2 mixture of the (*E*)- and (*Z*)- isomers of olefine **78** in 75% yield. This mixture was

treated with triethylamine trihydrofluoride, affording a 1:2 mixture of the neutral form of the (*E*)- and (*Z*)- isomers of **27** in 78% yield (**27** neutral state). These isomers were separated by means of successive chromatographies. The isolated (*E*)-isomer proved to be stable enough to be used for further experiments. On the contrary, the (*Z*)-isomer isomerized back in a few days to the original (*Z*)- and (*E*)-**27** neutral state mixture even upon storage in the dark and at 4°C.

Wittig reaction of intermediate **77** and triphenyl-(2-pyridylmethyl)-phosphonium chloride hydrochloride using *t*-BuOK as base yielded (*E*)-olefine **79** in 83% yield. Final removal of protecting silyl groups of **79** was achieved using triethylamine trihydrofluoride, affording, after HCl 35% addition, the hydrochloride salt of **28**-HCl in 65% yield (**28**⁺ cationic state). This yield decreased when TBAF was used as fluoride source for this reaction

III.1.1.1 Synthesis of 3-Bromo-4,5-dihydroxybenzaldehyde; (76)¹

Anhydrous aluminum chloride (3.2 g, 23.8 mmol) was suspended in a solution of 5-bromovanillin (5.0 g, 21.6 mmol) in 50 ml of CH₂Cl₂. While cooling to maintain the temperature at 30-35 °C, 7.7 ml (95.2 mmol) of pyridine was added slowly. The resulting clear solution was heated to reflux for 24 hours, allowed to come to room temperature, quenched by slowly addition of 10% HCl solution (60 ml) and further diluted with CH₂Cl₂ (30 ml). The resulting suspension was filtered to afford 3.60 g (16.6 mmol, 77%) of catechol **76** as a white solid. Mp 225-227 °C.

III.1.1.2 Synthesis of 3-Bromo-4,5-bis(tert-butylidiphenylsilyloxy)benzaldehyde; (77)

DBU (6.5 ml, 43.8 mmol) was added dropwise over 20 min to a stirred solution of **76** (3.8 g, 17.5 mmol) and TBDPSCI (10.5 ml, 40.3 mmol) in a mixture of dry THF (100 ml) and anhydrous DMF (20 mL) at 0 °C. After stirring at room temperature for 3 hours, ethyl ether (100 ml) was added and the resulting suspension filtered. The filtrate was concentrated under vacuum and the resulting yellowish wax was purified by flash chromatography on silica gel (gradient, hexanes: CH₂Cl₂ 4:1 to 1:1) to afford the following fractions: I) 7.10 g (10.2 mmol, 58%) of 3-bromo-4,5-bis(*tert*-butylidiphenylsilyloxy)benzaldehyde, **77**, as a solid; and II) 0.56 g (1.20 mmol, 7%) of 3-bromo -5-(*tert*-butylidiphenylsilyloxy)-4-hydroxybenzaldehyde, as a solid. **77**: mp: 151-153°C (ethyl ether); ¹H-NMR (250 MHz, CDCl₃) δ 9.29 (s, 1H), 7.83-7.72 (m, 4H), 7.61 (d, *J* = 1.9 Hz), 7.53-7.20 (m, 16H), 6.86 (d, *J* = 1.9 Hz), 1.13 (s, 9H), 0.76 (s, 9H); ¹³C-NMR (62.5 MHz, CDCl₃) δ 189.4, 149.3, 147.6, 135.5, 135.3, 133.0, 132.0, 130.1, 130.0, 129.9, 127.9, 127.8, 127.3, 122.2, 117.0, 27.1, 26.4, 20.7, 19.3; IR (ATR, cm⁻¹) 3267, 2930, 2856, 1669, 1428, 1314, 1300, 1100, 885, 701; HRMS (ESI-) *m/z* [M+2+Na]⁺ calcd for C₃₉H₄₁BrNaO₃Si₂ 717.1657, found 717.1640. **77**: mp:126-127°C (ethyl ether); ¹H-NMR (250 MHz, CDCl₃) δ 9.42 (s, 1H), 7.75-7.64 (m, 4H), 7.60 (d, *J* = 1.7 Hz, 1H), 7.53-7.34 (m, 6H), 6.84 (d, *J* = 1.7 Hz, 1H), 6.57 (s, 1H), 1.15 (s, 9H); ¹³C-NMR (62.5 MHz, CDCl₃) δ 189.3, 150.3, 143.5, 135.5, 130.9, 129.8, 128.5, 128.4, 117.9, 109.2, 26.8, 19.7; IR (ATR, cm⁻¹) 2960, 2856, 1696, 1424, 1310, 1107, 917, 870, 697; HRMS (ESI+) *m/z* [M+2+Na]⁺ calcd for C₂₃H₂₃BrNaO₃Si 479.0475, found 479.0464.

III.1.1.3 Synthesis of (*E*)-3-bromo-5-(2-phenyl-1-ethenyl)-1,2-di(*tert*-butyldiphenylsilyloxy)benzene; (**78**)

*t*BuOK (0.419 g, 3.75 mmol) was added portionwise at 0 °C to a solution of benzyltriphenyl-phosphonium chloride (1.23 g, 3.17 mmol) in dry THF (25 ml). After stirring for 30 min at room temperature, a solution of **77** (2.0 g, 2.88 mmol) in dry THF (5ml) was added. The mixture was stirred for 2 hours at rt, quenched with brine (0.3 ml), diluted with ethyl ether (20 ml) and filtered. The filtrate was concentrated under vacuum and the resulting crude material was purified by flash chromatography on silica gel (gradient, hexanes: CH₂Cl₂ 5:1 to 3:1) to afford 1.65 g (2.15 mmol, 75%) of a 1:2 mixture of (*E*)- and (*Z*)- isomers of 3-bromo-5-(2-phenyl-1-ethenyl)-1,2-di(*tert*-butyldiphenylsilyloxy)benzene, **78** as a wax. ¹H-NMR (360 MHz, CDCl₃) δ 7.88-7.70 (m, 4H), 7.50-6.90 (m) + 6.84 (d, *J* = 1.8 Hz, *Z*) (22H), 6.56 (d, *J* = 1.8 Hz, *E*) + 6.26 (d, *J* = 1.8 Hz, *Z*) (1H), 6.49 (d, *J* = 16.2 Hz, *E*) + 6.22 (d, *J* = 12.2 Hz, *Z*) (1H), 6.05 (d, *J* = 16.2 Hz, *E*) + 5.89 (d, *J* = 12.2 Hz, *Z*) (1H), 1.09 (s, *E*) + 1.07 (s, *Z*) (9H), 0.76 (s, *E*) + 0.73 (s, *Z*) (9H); ¹³C-NMR (90 MHz, CDCl₃) δ 147.2, 147.1, 143.4, 143.0, 137.3, 136.7, 135.6, 135.5, 135.4, 133.7, 133.01, 132.8, 130.9, 130.8, 130.0, 129.9, 129.8, 129.7, 129.7, 128.9, 128.7, 128.4, 128.2, 128.1, 127.9, 127.8, 127.7, 127.6, 127.2, 126.8, 126.4, 125.9, 124.8, 121.7, 118.3, 116.0, 115.7; HRMS (ESI+) *m/z* [M+Na]⁺ calcd for C₄₆H₄₇BrNaO₂Si₂ 791.2180, found 791.2168.

III.1.1.4 Synthesis of (*E*)-3-bromo-5-(2-phenyl-1-ethenyl)-1,2-benzenediol; (**27**)

Triethylamine trihydrofluoride (0.63 ml, 3.92 mmol) was added dropwise at 0 °C to a solution of **78** (1.50 g, 1.96 mmol) in dry THF (20 ml). The mixture was stirred for 2 hours at room temperature, quenched with brine (0.3 ml), diluted with ethyl ether (20 ml) and filtered. The filtrate was concentrated under vacuum and the resulting crude material was purified by flash chromatography on silica gel (gradient, hexanes: CH₂Cl₂ 5:1 to 3:1) to afford 0.443 g (1.52 mmol, 78%) of a 1:2 mixture of (*E*)- and (*Z*)- isomers of 3-bromo-5-(2-phenyl-1-ethenyl)-1,2-benzenediol, **27** as a solid. Repeated column chromatographies allowed isolation of pure (*E*)-isomer and a (*Z*)-enriched mixture (4:1) of isomers. (*E*)-**27**: mp: 95-96°C (ethyl ether); ¹H-NMR (250 MHz, CDCl₃) δ 7.50-7.39 (m, 2H), 7.39-7.28 (m, 2H), 7.28-7.18 (m, 1H), 7.14 (d, *J* = 2.7 Hz, 1H), 7.03 (d, *J* = 2.7 Hz, 1H), 6.93 (d, *J* = 16.3 Hz, 1H), 6.86 (d, *J* = 16.3 Hz, 1H), 5.52 (br s, 2H); ¹³C-NMR (62.5 MHz, CDCl₃) δ 144.7, 139.9, 137.2, 132.2, 128.9, 128.6, 127.9, 127.0, 126.6, 121.9, 112.8, 109.9; IR (ATR, cm⁻¹) 3422, 3356, 1590, 1521, 1427, 1291, 959, 858, 830, 750, 692; HRMS (ESI-) *m/z* [M-H]⁺ calcd for C₁₄H₁₀BrO₂ 288.9859, found 288.9861. Mixture (4:1) of (*Z*)- and (*E*)- **33** isomers: ¹H-NMR (360 MHz, CDCl₃) δ 7.50-7.43 (m, *E*) + 7.39-7.31 (m, *E*) + 7.30-7.15 (m) (5H), 7.17 (d, *J* = 1.8 Hz, *E*) + 7.06 (d, *J* = 1.8 Hz, *E*) + 6.75 (d, *J* = 1.6 Hz, *Z*), + 6.92 (d, *J* = 1.6 Hz, *Z*) (2H), 6.96 (d, *J* = 16.2 Hz, *E*) + 6.90 (d, *J* = 16.2 Hz, *E*) + 6.55 (d, *J* = 12.0 Hz, *Z*) + 6.40 (d, *J* = 12.0 Hz, *Z*) (2H), 5.52 (br s, *E*) + 5.48 (br s, *Z*) + 5.39 (br s, *Z*) + 5.29 (br s, *E*) (2H); ¹³C-NMR (90 MHz, CDCl₃) δ 144.7, 144.1, 139.9, 139.5, 137.2, 137.0, 132.2, 131.6, 130.6, 129.0, 128.9, 128.6, 128.5, 128.5, 127.9, 127.5, 127.0, 126.6, 124.1, 121.9, 115.5, 112.8, 109.9, 109.3.

III.1.1.5 Synthesis of (*E*)-2-[3-bromo-4,5-di(*tert*-butyldiphenylsilyloxy)phenyl]-1-ethenyl]pyridine; (**79**)

*t*BuOK (1.11 g, 9.94 mmol) was added portionwise at 0 °C to a solution of triphenyl-(2-pyridylmethyl)-phosphonium chloride hydrochloride (1.84 g, 4.32 mmol) in dry THF (40 ml). After stirring for 30 min at room temperature, a solution of **77** (3.0 g, 4.32 mmol) in dry THF (10 ml) was added. The mixture was stirred for 2 hours at room temperature, quenched with brine (0.5 ml), diluted with ethyl ether (30 ml) and filtered. The filtrate was concentrated under vacuum and the resulting crude material was purified by flash chromatography on silica gel (gradient, hexanes: EtOAc 6:1 to 4:1) to afford 2.76 g (3.58 mmol, 83%) of (*E*)-2-[3-bromo-4,5-di(*tert*-butyldiphenylsilyloxy)phenyl]-1-ethenyl]pyridine, **79** as a solid. Mp: 182-185°C (ethyl ether); ¹H-NMR (360 MHz, CDCl₃) δ 8.52-8.47 (m, 1H), 7.81-7.75 (m, 4H), 7.56 (dt, *J* = 7.9 Hz, *J* = 1.8 Hz, 1H), 7.45-7.20 (m, 16H), 7.22 (d, *J* = 2.2 Hz, 1H), 7.07 (d, *J* = 15.8 Hz, 1H), 7.09-7.02 (m, 1H), 7.02 (d, *J* = 7.9 Hz, 1H), 6.60 (d, *J* = 2.2 Hz, 1H), 6.21 (d, *J* = 15.8 Hz, 1H), 1.10 (s, 9H), 0.75 (s, 9H); ¹³C-NMR (90 MHz, CDCl₃) δ 155.4, 149.7, 147.2, 144.0, 136.6, 135.5, 135.4, 133.6, 132.8, 130.9, 130.3, 129.9, 129.7, 127.9, 127.7, 127.1, 125.1, 122.6, 122.0, 119.2, 116.1, 27.1, 26.5, 20.7, 19.3; IR (ATR, cm⁻¹) 2932, 2858, 1584, 1563, 1547, 1477, 1333, 1307, 1265, 1107, 929, 701; HRMS (ESI+) *m/z* [M+H]⁺ calcd for C₄₅H₄₇BrNO₂Si₂ 770.2313, found 770.2289.

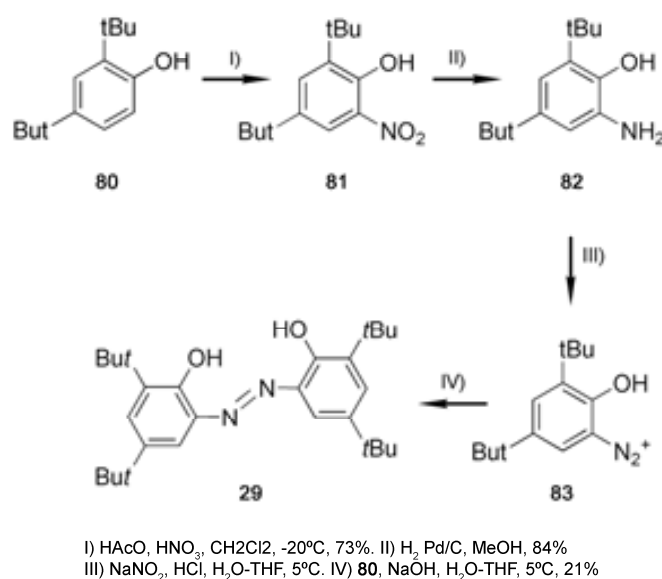
III.1.1.6 Synthesis of (*E*)-2-[(3-bromo-4,5-dihydroxyphenyl)-1-ethenyl]pyridinium chloride; (**28·HCl**)

Triethylamine trihydrofluoride (0.38 ml, 2.34 mmol) was added dropwise at 0 °C to a solution of **79** (0.60 g, 0.78 mmol) in dry THF (10 ml). After stirring for 2 hours at room temperature, HCl 35% was added (0.5 ml) and the resulting suspension was stirred for 10 min at room temperature, and filtered. The solid was washed with ethyl ether (2x5 ml) and dried under vacuum to afford 0.166 g (0.51 mmol, 65%) of (*E*)-2-[(3-bromo-4,5-dihydroxyphenyl)-1-ethenyl]pyridinium chloride, **28·HCl** as a yellow solid. Mp: 210-212°C (acetone); ¹H-NMR (360 MHz, DMSO-*d*₆) δ 10.44 (br s, 1H), 9.93 (br s, 1H), 8.70 (d, *J* = 5.0 Hz, 1H), 8.43 (t, *J* = 7.7 Hz, 1H), 8.26 (d, *J* = 8.3 Hz, 1H), 7.96 (d, *J* = 16.6 Hz, 1H), 7.75 (t, *J* = 6.8 Hz, 1H), 7.31 (d, *J* = 2.0 Hz, 1H), 7.19 (d, *J* = 2.0 Hz, 1H); ¹³C-NMR (90 MHz, DMSO-*d*₆) δ 150.5, 146.6, 145.6, 144.8, 141.4, 139.2, 127.2, 124.0, 123.7, 123.5, 116.9, 113.2, 110.0; IR (ATR, cm⁻¹) 3049, 2811, 1637, 1614, 1593, 1429, 1296, 1163, 964, 830, 760; HRMS (ESI-) *m/z* [M-HCl-H⁺] calcd for C₁₃H₉BrNO₂ 289.9822, found 289.9817.

III.1.2 Synthesis of phenoxylate-based ligands

As in the case of the catechol-based ligands, here is presented a brief summary for the synthesis of azo bisphenol **29**. Four different synthetic approaches were initially envisaged following the synthetic routes before described for the obtaining of azo derived ligands.^{2,3,4,5} Three of them failed in the synthesis of it,²⁻⁴ fortunately, the last synthetic route,⁵ which in fact is the most extended strategy for the synthesis of this kind of compounds, was most successful.

Initially, nitrophenol **81** was obtained in a 73% yield by nitration of phenol **80** following a modified experimental route previously described.⁶ The modification consisted in performing the reaction around $-20\text{ }^{\circ}\text{C}$ to avoid byside di-nitration reaction. This compound was then reduced using Pd/C in methanol⁷ to afford aniline **82** in a 84% yield. Finally, the coupling reaction of the diazonium salt **83**, derived from aniline **83**, with fenol **80**, afforded diazo derivative **29** in 21% yield. This last reaction was performed at a slightly basic or neutral media to avoid conversion of the diazonium salt to the corresponding diazohydroxide compound.



Scheme III.2.

III.2.1.1 Synthesis of 2,2'-dihydroxy-4,6,4',6'-tetratert-butylazobenzene; (29)

A solution of sodium nitrite (0.027 g, 0.40 mmol) in a mixture of water (0.2 mL) and 35 % HCl acid (0.1 mL, 0.90 mmol) was first cooled to $5\text{ }^{\circ}\text{C}$. Then, a THF solution (0.6 mL) of aniline **82** (0.080 g, 0.36 mmol) was added, and the resulting mixture was stirred at $5\text{ }^{\circ}\text{C}$ for 20 min. Afterwards, this solution was added dropwise to another solution of compound **80** (0.075 g, 0.36 mmol) and NaOH (0.036 g, 0.90 mmol) in a mixture of THF (0.5 mL) and water (0.5 mL). The whole mixture was stirred at $10\text{ }^{\circ}\text{C}$ for 30 min, adjusted to pH 6–7 and extracted with ethyl acetate (3x10 mL). The whole organic extracts were dried with magnesium sulfate, filtered and concentrated under reduced pressure to yield an oil that was chromatographed through silica gel using a mixture of ethyl acetate–ethyl ether (15:1) to afford 0.033 g (0.08 mmol, 21% yield) of azobisphenol **29**. FT-IR (KBr, cm^{-1}): 3428 (ν (O–H)), 2963, 2905, 2862 (ν (C–H)), 1613, 1479, 1461, (ν (N=N)) 1428, 1393, 1360, 1266 (ν (C–O)), 1249, 1220, 1197, 1169. Anal. Calcd. For $\text{C}_{28}\text{H}_{42}\text{O}_2\text{N}_2$ (438.31): C, 76.0; H, 9.5; N, 6.4. Found: C, 75.9; H, 9.5; N, 6.3. ES-(+) (MeOH, m/z): 439 (M^+ , $\text{C}_{28}\text{H}_{43}\text{O}_2\text{N}_2$). $^1\text{H-NMR}$ (400 MHz, ToI-d^8): δ = 1.46 (s, 18H, CH_3), 1.81 (s, 18H, CH_3), 7.67–7.72 (m, 4H, aromatic H), 13.70 (s, 2H, OH).

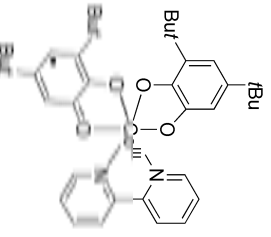
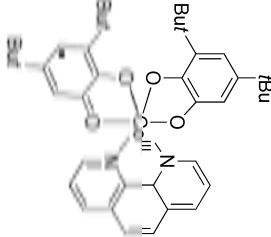
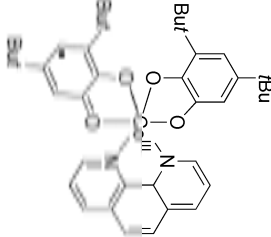
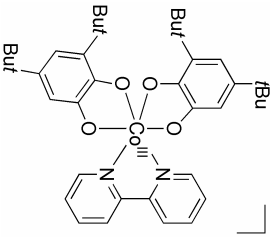
References

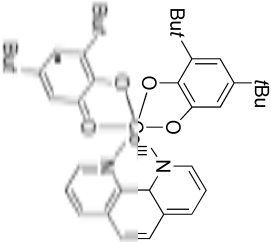
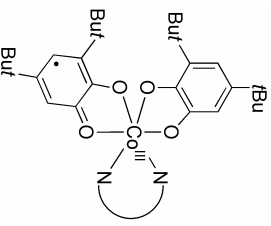
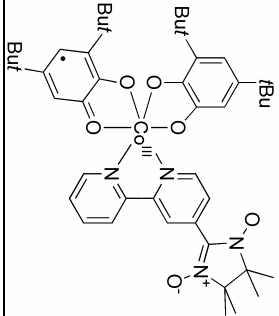
- [1] R. G. Lange, *J. Org. Chem.*, **27**, **1962**, 2037.
- [2] K. Haghbeen, W. Tan, *J. Org. Chem.*, **63**, **1988**, 4503–4505.
- [3] a) C. Ruslim, K. J. Ichimura, *J. Mat. Chem.*, **9**, **1999**, 673–681. b) K. Srinivasa, K. Abiraj, D. C. Gowda, *Tetrahedron Lett.*, **45**, **2003**, 5835–5837.
- [4] S. Patel, B. K. Mishra, *Tetrahedron Lett.*, **45**, **2004**, 1371–1372.
- [5] Q. Wang, Y. Yang, Y. Li, W. Yu, Z. T. Hou, *Tetrahedron Lett.*, **62**, **2006**, 6107–6112.
- [6] J. Vinsova, K. Cermakova, A. Tomeckova, M. Ceckova, J. Jampilek, P. Cermak, J. Kunes, M. Dolezal, F. Staud, *Bioorg. Med. Chem.*, **14**, **2006**, 5850–5865.
- [7] S. Yoshida, S. Shiokawa, K. Kawano, T. Ito, H. Murakami, H. Suzuki, Y. J. Sato, *Med. Chem.*, **48**, **2005**, 7575–7079.

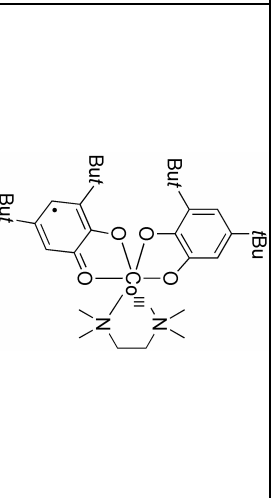
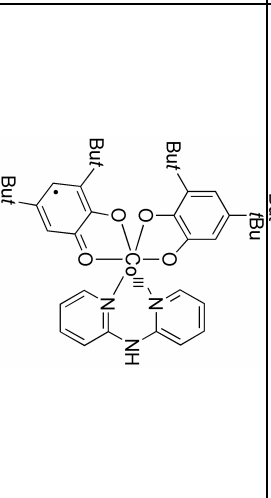
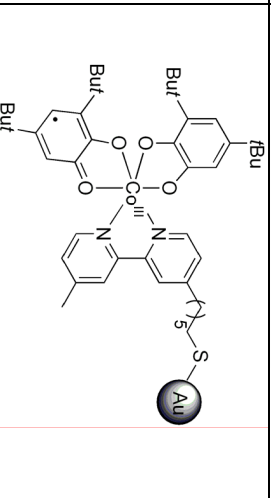
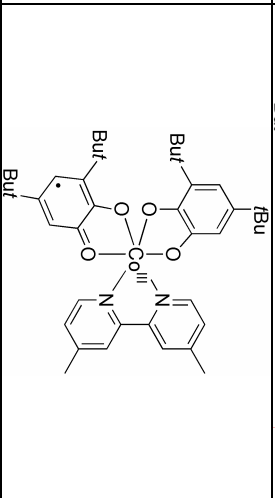
Annex | IV

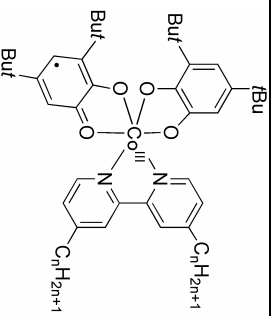
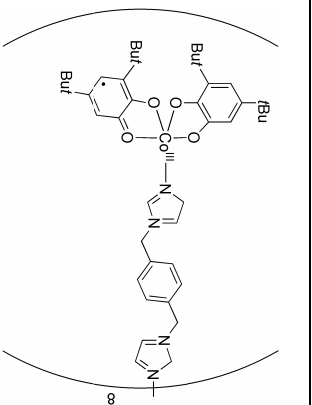
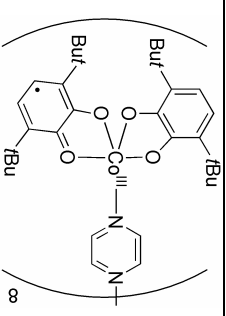
Complexes with Valence Tautomerism Phenomena

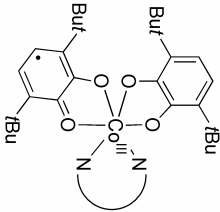
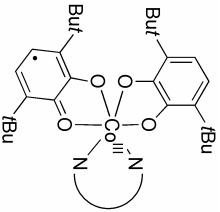
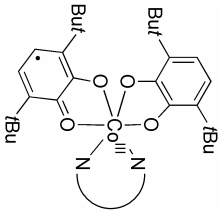
IV.1 Table of complexes presenting VT phenomena induced by temperature

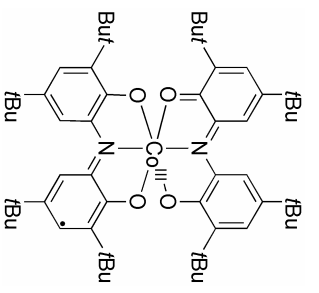
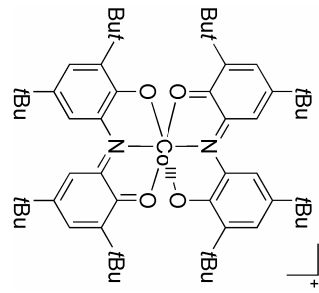
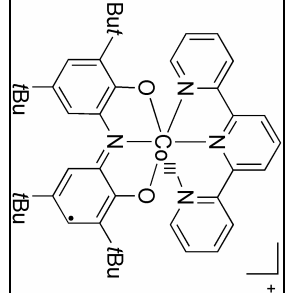
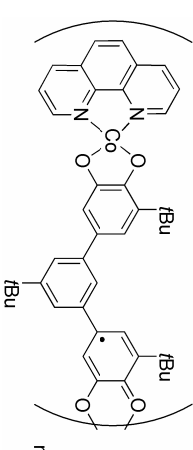
Representative Compounds		State	T _c / Temperature Range	Reference	
[Co(3,5-DTBBSQ)(3,5-DTBCat)(bpy)]		Solid	Abrupt 310 K	J. Am. Chem. Soc., 102, 1980 , 4951	
		Solution	Gradual 273 K	J. Am. Chem. Soc., 102, 1980 , 4951 J. Am. Chem. Soc., 115, 1993 , 8221.	
[Co(3,5-DTBBSQ)(3,5-DTBCat)(Phen)]		Solid	Gradual 215 K	Inorg. Chem., 35, 1996 , 2846	
		Solution	Abrupt 240K/	Angew. Chem., 105, 1993 , 954	
[Co(3,5-DTBBSQ)(3,5-DTBCat)(Phen)]		Solid	without solvent	No Transition	Inorg. Chem., 35, 1996 , 2846
			Solvent: C ₆ H ₅ Cl	Gradual 215 K	Inorg. Chem., 35, 1996 , 2846
[Co(3,5-DTBBSQ)(3,5-DTBCat)(bpy)] [CoCp ₂]		Solution	> 320 K <i>hs</i> -(CoII)	Chem Commun., 1998 , 2089.	
			< 200 K <i>ls</i> -(CoIII)		

Representative Compounds		State	T _c / Temperature Range	Reference
[Co(3,5-DTBSQ)(3,5-DTBCat)(Phen)]		Solid	Abrupt 320 K 4.24 μs 3 K 3.07 μs	Chem. Commun., 1998 , 2089
[Co(3,5-DTBSQ)(3,5-DTBCat)(N=N)]		Solution	Gradual (N=N) -(dpppy): 348 K -(dmppy): 298 K -(bpz) : < 190 K -(bppm) : ~190 K	J. Am. Chem. Soc., 115, 1993 , 8221.
[Co(3,5-DTBSQ)(3,5-DTBCat)(mbpy)]		Solid	Abrupt 250 K	J. Mater. Chem., 11, 2001 , 2142

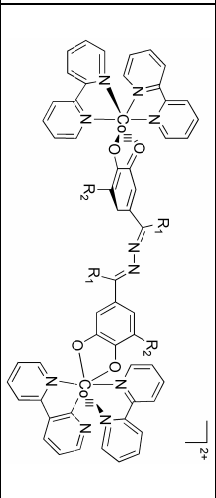
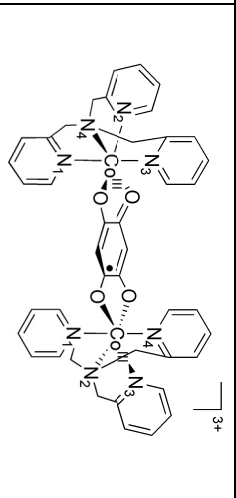
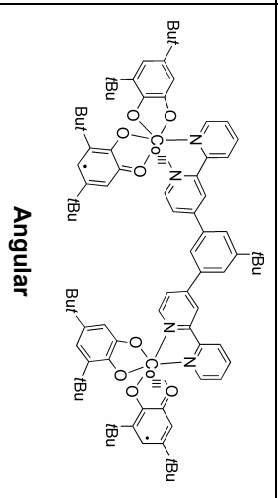
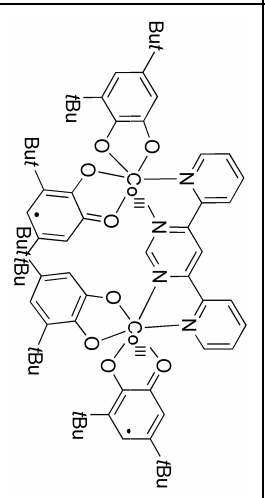
Representative Compounds		State	T _c / Temperature Range	Reference
<p>[Co(3,5-DTBSQ)(3,5-DTBcat)(tmeda)]·0.5C₆H₅CH₃</p>		Solution	195 K	Chem. Phys. Lett., 355, 2002, 169.
<p>[Co(3,5-TBSQ)(3,5-DTBcat)(dpa)]</p>		Solid	Abrupt 380 K	J. Photochem. Photobiol., 161, 2004, 243
<p>Auⁿnanoparticle-S-(CH₂)_n-4'-(CH₃)-bpy-[Co(3,5-DTBSQ)(3,5-DTBcat)]</p>		Solid	389 K	J. Am. Chem. Soc., 127, 2005, 5328.
<p>[Co(3,5-DTBSQ)(3,5-DTBcat)-4,4'-(CH₃)₂-bpy]</p>		Solid	318 K	

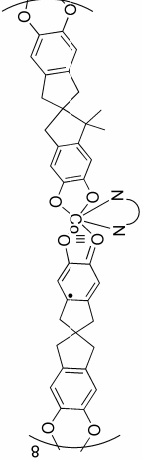
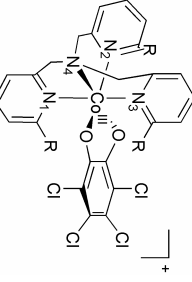
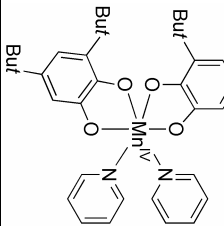
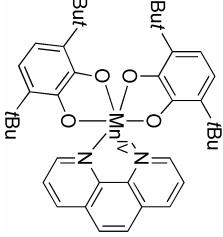
Representative Compounds		State	T _c / Temperature Range	Reference
[Co (3,5TBBSQ)(3,5-DTBBCat)(C _n bpv)]		Solid	n=1 : 298 K n=5 : 357 K n=9 : 417 K + Phase Transition n=13 : 384 K + Phase Transition	Dalton Trans., 2006, 1377.
[Co(3,5-DTBBSQ)(3,5-DTBBCat)(bix)] _n		Solid	Abrupt Crystalline : ~ 340 K Amorphous : ~ 275 K	Angew. Chem. 47, 2008, 1.
[Co(3,6DTBSQ)(3,6-DTBBCat)(N-N) _n]		Solid	Abrupt (N-N) - (pyz): 350 K 5,86 μs 5 K 1,71 μs	J. Am. Chem. Soc., 116, 1994, 2229

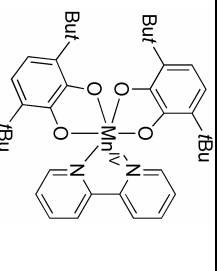
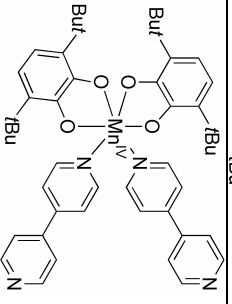
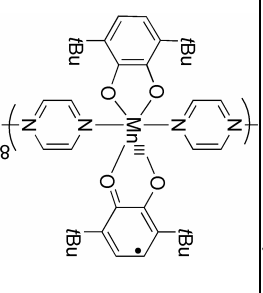
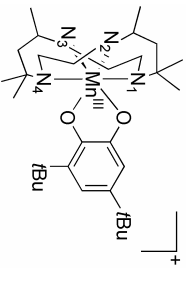
Representative Compounds		State	T _c / Temperature Range	Reference
[Co(3,6-DTBSQ)(3,6-DTBCat)(N-N)]		Solid	(N-N): -bpy : 310 K	Inorg. Chem., 33, 1994 , 2227.
[Co(3,6-DTBSQ)(3,6-DTBCat)(N-N)]		Solid	(N-N) -(py ₂ S) : 370 K -(py ₂ Se) : 290 K -(py ₂ Te) : 210 K -(py ₂ O) : Tc↑ 330 K Tc↓ 100 K	Inorg. Chem., 36, 1997 , 19
[Co(3,6DTBSQ)(3,6-DTBCat)(N-N)]		Solid Solution	(N-N) -tmmda : > 350 K -timda : > 350 K -tmpda : 178 K (N-N) -tmmda : 280 K -timda : 310 K -tmpda : > 300 K	Angew. Chem., 35, 1996 , 1694. Inorg. Chem., 37, 1998 , 5875

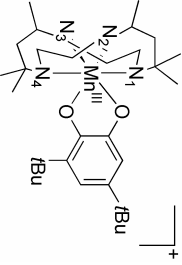
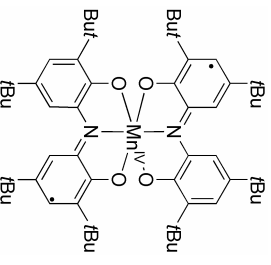
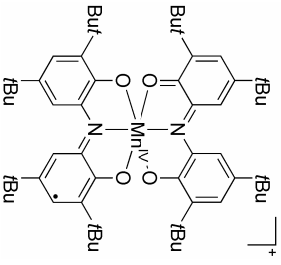
Representative Compounds		State	T _c / Temperature Range	Reference
[Co(Cat-N-SQ)(Cat-N-BQ)]		Solid	597 K	Inorg. Chem., 42, 2003 , 6432
[Co(Cat-N-BQ) ₂]:ClO ₄		Solid	No tested	Inorg. Chem., 39, 2000 , 617.
		Solution	328 K	
[Co(Cat-N-SQ)(ppy)]BPh ₄		Solid	588 K	Inorg. Chem., 42, 2003 , 6432.
[Co(<i>m</i> -Ph(Cat-SQ) ₂ (phen)) _n ·0.5CH ₂ Cl ₂		Solid	Gradual T _c ↑ 310 K T _c ↓ 300 K	Chem Commun 2001 , 2150

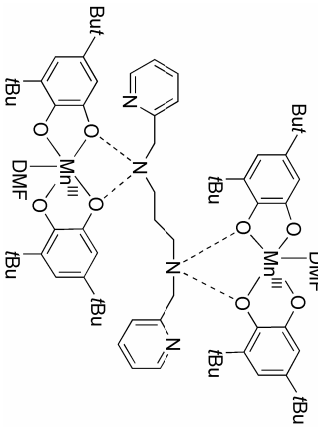
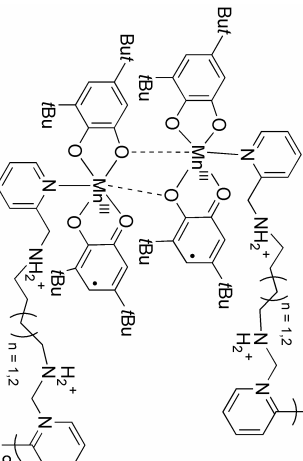
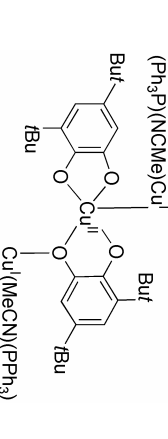
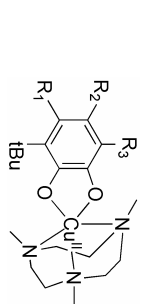
Representative Compounds		State	T _c / Temperature Range	Reference
[Co (phenCat)(ctn)](Y) ⁺ solv		Solid	(Y) ⁺ solv -PF ₆ ⁻ : H ₂ O : 267 K Abrupt -PF ₆ ⁻ : 1,5CH ₂ Cl ₂ : 273 K more gradual -I ⁻ : 303 K Abrupt -BPh ₄ ⁻ : No tested	J. Molec. Struct., 565, 2003 , 141. Chem Commun., 2004 , 6245.
[Co(L _s ^{IP})(L _s ^{ISQ})]		Solution	Gradual 267 K (CH ₂ Cl ₂) 270 K (methylcyclohexane)	Eur. J. Inorg. Chem., 2002 , 1957
[Co (3,5-DTBcat)(Me ₄ cyclam)]Y ⁺		Solid	No transition (Y) ⁺ -PF ₆ ⁻ 300 - 2 K 3,6 emuKmol ⁻¹ Indicates <i>hs</i> -Co(II)	Inorg. Chem., 41, 2002 , 3508
[Co(ctn)] ₂ (dhbq)](PF ₆) ₃		Solid	Abrupt ~ 175 K	Angew. Chem., 43, 2004 , 3136

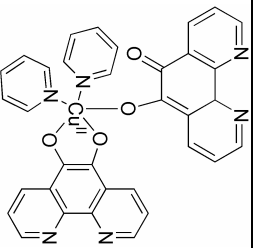
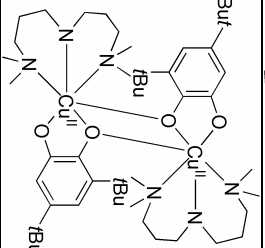
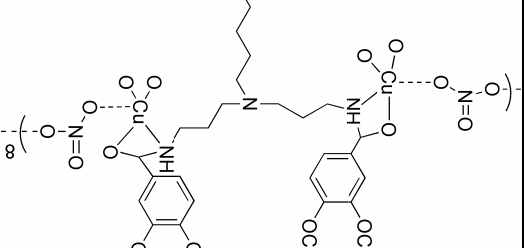
Representative Compounds		State	T _c / Temperature Range	Reference
[Co ₂ (bpy) ₄ (thM)](PF ₆) ₂		Solution	Poor changes in ACN from 283 K to 300 K	Inorg. Chem., 44, 2005, 6183
[Co(dhbx)(tpa) ₂](PF ₆) ₃		Solid	Abrupt T _c ↑ 310 K T _c ↓ 297 K	J. Am. Chem. Soc., 128, 2006, 1790
[Co(Cat-Cat) ₂ (NN ^Y)]		Solid	General < 10 K [Co(III)-Co(III)] > 10 K [Co(III)-Co(II)] < 400 K > 400 K [Co(II)-Co(II)] Transition to Co(III)-Co(II) - Linear: 347 K - Angular: 335 K	Inorg. Chem., 45, 2006, 4461
[Co(diox) ₂](4,6-di-2'-py ^Y m)]		Solid	Two steps Co(III)-Co(II): 125-225 K Co(II)-Co(II): up to 225 K	Inorg. Chem., 45, 2006, 8817

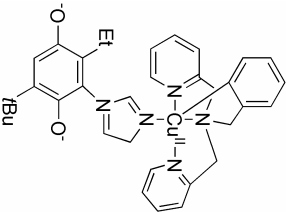
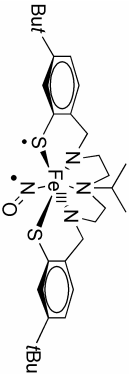
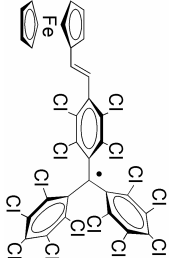
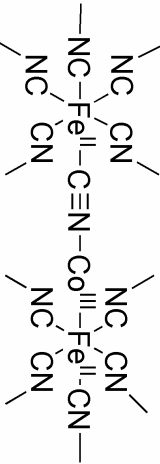
Representative Compounds		State	T _c / Temperature Range	Reference
[Co(Cat-SQ)(ppy)] _n ·3H ₂ O		Solid	Gradual < 210 K [Co(III)-Co(III)] > 210 K [Co(II)-Co(II)] < 210 K < 210 K [Co(III)-Co(III)] > 210 K [Co(II)-Co(II)] < 210 K Field-induced transition to triplet spin state	Dalton Trans., 2007, 5253
[Co(Cat-SQ)(phen)] _n ·3H ₂ O		Solid	Abrupt n = 2, solv: C ₆ H ₅ OH 370 K	Chem. Eur. J., 14, 2008, 1804.
[Co(Me ₄ tpa)(TCCat)]·PF ₆ ·sol n = 0, 1, 2, 3.		Solid	Abrupt to Mn(py) ₂ (3,5-DTBSSQ) ₂ 250 K	J. Am. Chem. Soc., 106, 1984, 2041
[Mn(3,5-DTBCat) ₂ (py) ₂]		Solid	Gradual to Mn(phen) ₂ (3,6-DTBSSQ)(3,6-DTBCat) T ₀ ~ 350 K (temp of the magnetic measurements)	Inorg. Chem., 34, 1995, 1172
[Mn(3,6-DTBSSQ) ₂ (phen)]		Solid		

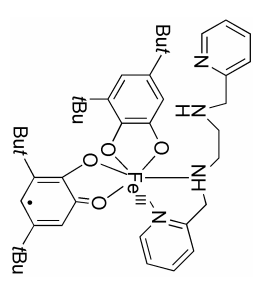
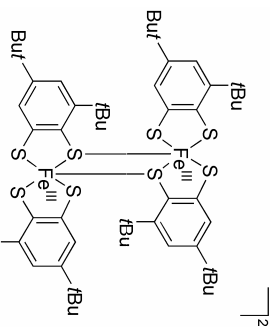
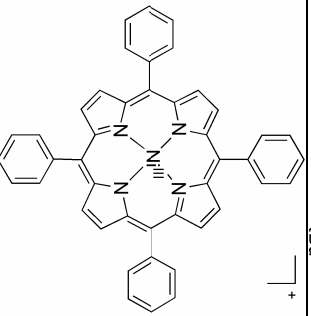
Representative Compounds		State	T _c / Temperature Range	Reference
[Mn(3,6-DTBSQ) ₂ (2,2'-bpy)]		Solid	Gradual to Mn(2,2'bpy) ₂ (3,6-DTBSQ)(3,6-DTBCat) T ₀ ~ 350 K	Inorg. Chem., 34, 1995 , 1172
[Mn(3,6-DTBSQ)(3,6-DTBCat)(4,4'-bpy) ₂] _n		Solid	Gradual to Mn(4,4'bpy) ₂ (3,6-DTBSQ) ₂ T ₀ ~ 350 K	
[Mn(3,6DTBSQ)(3,6-DTBCat)(L-pyz) ₂] _n		Solid	Abrupt 350 K 4.3 μs 5 K 3.4 μs	Inorg. Chem., 36, 1997 , 6184
[Mn(3,5-DTBCat) ₂ (ch)] ₁ ·BPh ₄		Solid	300 K 3.1 emuKmol ⁻¹ 4.2 K 2.4 emuKmol ⁻¹ 70 K starts to decrease	Angew. Chem., 37, 1998 , 3005
		Solution	365 K complete <i>hs</i> -Co(II)	

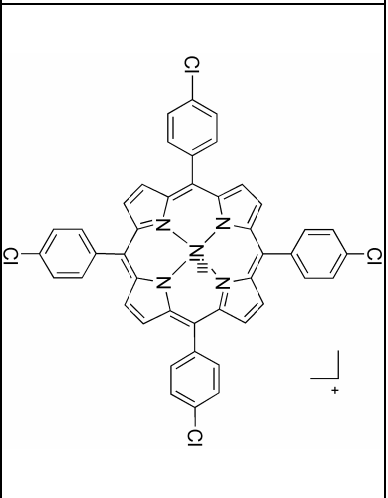
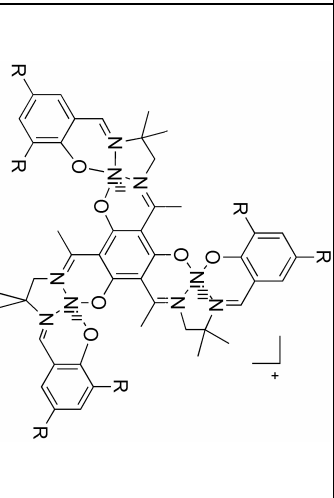
Representative Compounds		State	T _c / Temperature Range	Reference
[Mn(3,5-DTBCat) ₂ (ctn)]·ClO ₄		Solid	Y = ClO ₄ 300 K 3.5 emuKmol ⁻¹ 4.2 K 2.4 emuKmol ⁻¹ 90 K decrease monotonically	Angew. Chem., 37, 1998, 3005
[Mn(Cat-N-SQ) ₂]		Solid	No transition 300-30 K 1.9 μ _B (Mn(IV) ⁺)	J. Am. Chem. Soc., 110, 1988, 1827
		Solution	Gradual Mn(IV) < 5 K > 5 K Mn(III) < 270 K Mn(II) > 360 K	
[Mn(Cat-N-SQ)(Cat-N-BQ)]·BF ₄		Solid	No Transition 300-5 K 5.1 μ _B (Mn(III) ⁺)	Adv. Func. Mater., 12, 2002, 347
		Solution	Gradual > 5 K Mn(IV) < 120K > 120 Mn(III) < 360 K Mn(II) > 360 K	

Representative Compounds		State	T _c / Temperature Range	Reference
[Mn ₂ (Cl ₄ Cat) ₄ (DMF) ₂](H ₂ bispictrn)		Solid	High T Mn(II) Low T Mn(III)	Inorg. Chem., 43, 2004, 5908
[Mn ₂ (Cl ₄ Cat) ₄ (DMF) ₂](H ₂ bispictrn)] _n [Mn ₂ (Cl ₄ Cat)(Cl ₄ SO)(bispictrn)] _n		Solution	DMF High T Mn(II) Low T Mn(III)	Inorg. Chem., 44, 2005, 9714
[Cu(NCCH ₃)(PPh) ₃] ₂ [Cu(3,5-DTBCat) ₂]		Solution	Abrupt < 300 K	J. Am. Chem. Soc., 33, 1994, 2041.
[Cu(Cat)(Me ₃ TACN)]		Solution	Gradual (Cat) -3-BSQ-(5-CH ₃): 370 K -3,6-DTBSQ: 320 K -3,5-DTBSQ: 380 K -3-BSQ-(5-OMe): 340 K -3,6-BSQ-(5-OMe): 330 K -3,6-BSQ-(4,5-OMe): 330 K	Chem. Eur. J., 5, 1999, 2802

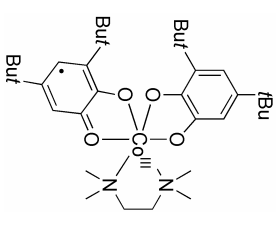
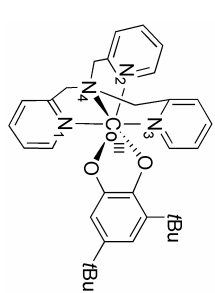
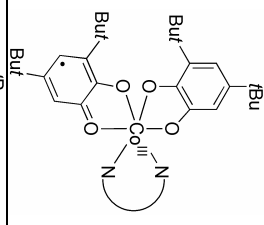
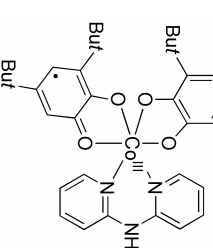
Representative Compounds		State	T _c / Temperature Range	Reference
[Cu (PhenCat)(PhenBQ)(L)]		Solution (Pyr)	Solvent dependence (L) (Pyr) ₂ and (tmeda): 233 K Cu(II) 373 K Cu(I)	Inorg. Chem., 40, 2001, 5653
[Cu(DTBcat)(idpa)] ₂		Solution	~ 390 K	J. Inorg. Biochem., 91, 2002, 190.
[Cu ^{II} (PP1)-NO ₃ -Cu ^{II} (PP1)]		Solid	< 30 K Cu(II)-NO ₃ -Cu(II) > 30 K Cu(II)-NO ₃ -Cu(I)	Chem. Phys. Chem., 7, 2006, 2567

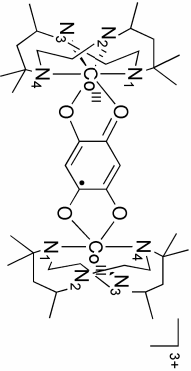
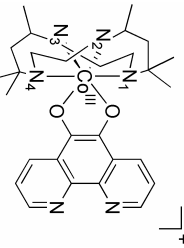
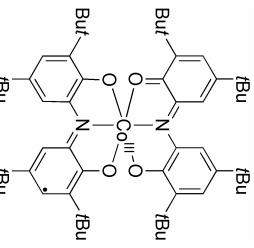
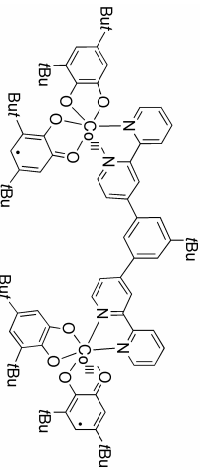
Representative Compounds		State	T _c / Temperature Range	Reference
$[\text{Cu}(\text{Im-hq}^{*2})(\text{tpa})](\text{OTf})_2$		Solution	—	J. Am. Chem. Soc., 129, 2007, 5800.
$[\text{Fe}(\text{L}^{\text{Pr}})(\text{NO})\{\text{Fe}(\text{NO})_7\}]$		Solid	~ 390 K	Inorg. Chem., 41, 2002, 3444.
$[\text{Fe}(\text{Fe}^{\text{II}})(\text{CH}=\text{CH})\text{-PTM}]$		Solid	300 K Fe(II)-PTM. 15 K Fe(III)-PTM.	J. Am. Chem. Soc., 125, 2003, 1462.
$[\text{Fe}^{\text{II,LS}}\text{-CN-CO}^{\text{III,LS}}]$ Structure "Prussian Blue" type		Solid	Abrupt Fe ^{III,LS} -CN-CO ^{III,HS} Tc↑ 230 K Tc↓ 197 K	Phys. Rev. Lett., 90, 2003, 167403-1

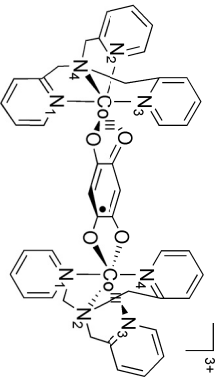
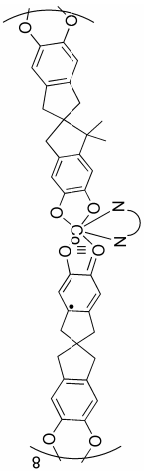

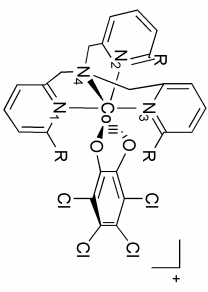
Representative Compounds		State	T _c / Temperature Range	Reference
[Fe(C ₁₄ Cat)(C ₁₄ SO)(bispicen)]		Solid	High T <i>hs</i> -Fe(II) Low T <i>ls</i> -Fe(III)	Inorg. Chem., 43, 2004 , 5908
[Fe ₂ (3,5-DTBDT) ₄][N(n-Bu) ₄] ₂		Solution	CH ₂ Cl ₂ ~ 250 K	J. Am. Chem. Soc., 127, 2005 , 5641.
[Ni(TPP)]·ClO ₄		Solution	Gradual 77 K	J. Am. Chem. Soc., 97, 1975 , 5288.

Representative Compounds	State	T _c / Temperature Range	Reference
<p>[Ni(<i>p</i>-Cl)TPP)]⁺</p> 	Solution	Gradual 150 K	J. Am. Chem. Soc., 23, 1984, 817.
<p>[Ni₃(alen^X)]⁺ electrochemically generated</p> 	Solution Solution	Gradual X <i>t</i> -Bu ₂ ~ 10 K 54% <i>Is</i> -Ni(III) NO ₂ ~ 10 K 57% <i>Is</i> -Ni(III)	Inorg. Chem., 44, 2005, 5467.

IV.2 Table of complexes presenting VT phenomena induced by irradiation

Representative Compounds		State	T _c or hν	Reference
[Co (3,5-DTBBSQ)(3,5-DTBSCat)(tmeda)]·0.5C ₆ H ₆ CH ₃		¹ (hν) Solution 532 nm	5 K life time of [Co (3,5-DTBBSQ) ₂ (tmeda)]·0.5C ₆ H ₆ CH ₃ (<i>hs</i> -Co(II))-175 min	Chem. Phys. Lett., 355, 2002, 169
		² (hν) Solution 830 nm		
[Co (DBCat)(Me ₄ cyclam)]PF ₆		Solution 400 nm	Co(Me ₄ cyclam)(DBCat) ⁺ in two steps: (1) ~ 150 femtoseconds (from d _π (M) to T ⁺ (L)) (2) ~ 7 picoseconds: species with triplet ground state	Chem. Phys. Lett., 352, 2002, 408
[Co (3,5-DTBBSQ)(3,5-DTBSCat)(N-N)]		Solid 532 nm 830 nm reverse	LIEST Phen: 70% converted after illumination tmda: 50% converted after illumination tmpda: 10% converted after illumination	Bull. Chem. Soc. Jpn., 76, 2003, 443.
[Co (3,5DTBBSQ)(3,5-DTBSCat)(dpa)]		Solid 532 nm 830 nm reverse	Photoreversible VT and LIEST	J. Photochem. Photobiol., 161, 2004, 243

Representative Compounds		State	T _c or hv	Reference
[Co(cth) ₂ (dhbq)](PF ₆) ₃]		Solid 647 nm	% Converted after illumination 43%	Angew Chem., 43, 2004 , 3136.
[Co (phenCat)(cth)]·PF ₆ ·H ₂ O		Solid 980 nm	Abrupt 253 K	Chem. Phys. Lett., 396, 2004 , 198.
[Co(Cat-N-SQ)(Cat-N-BQ)]		Solution 480nm	Two steps Solvent lifetime 1- hs-Co(II) CHCl ₃ 180 fs CH ₂ Cl ₂ 160 fs 2-'Is-Co(II)' CHCl ₃ 410 ps CH ₂ Cl ₂ 490 ps	Chem. Phys. Lett., 374, 2005 , 9.
[Co(<i>m</i> -Ph(Cat-SQ) ₂)(phen)] _n ·0.5CH ₂ Cl ₂		Solid (658 nm)	% Interconversion 10% [Co(phen)(<i>m</i> -Ph(SQ-SQ) ₂)] _n E _a = 125 cm ⁻¹ ; τ ₀ = 175 s	Chem. Phys. Lett., 428, 2006 , 400.

Representative Compounds		State	T _c or hv	Reference
[Co(tpa) ₂ (DHBQ)]·(PF ₆) ₃		Solution 532 nm	Abrupt Transition to [Co ^{III} is-DHBQ ²⁻ -Co ^I hs ⁺]	J. Am. Chem. Soc., 128, 2006 , 1790
[Co(Cat-SQ)(bpy) ₂] _n ·3H ₂ O		Solid 658 nm	Relaxation time: 2.5 x 10 ⁵ s with charge redistribution in the decay	Dalton Trans., 2007 , 5253.
[Co(phen) ₂ (Cat-SQ)] _n ·3H ₂ O		Solid 658 nm	Relaxation time: 2.5 x 10 ⁵ s with charge redistribution in the decay	
[Co(TCCat)(Me _n tpa)]PF ₆ n = 0, 1, 2, 3.		Solid	Relaxation time n = 0: 1000s n=1: 1.9 x 10 ⁶ n=2: 4.5 x 10 ⁶	Chem. Eur. J., 14, 2008 , 1804.
		Solution	n = 1: 8 x 10 ⁵ s.	

IV.3 Table of complexes presenting VT phenomena induced by pressure

Representative Compounds	State	P _c		Reference
[Co(3,5-DTBSQ)(3,5-DTBCat)(Phen)]	Solid	No solvent	1.1 GPa	Inorg. Chem., 35, 1996 , 2846
		surrounded by C ₆ H ₅ CH ₃	0.37GPa	
[Co(phenCat)(ctn)]PF ₆ ·H ₂ O	Solid	-PF ₆ ·H ₂ O 7.4 Kbar /s-Co(III)		Chem. Eur. J., 7, 2001 , 3926.

Chapter | 6

Articles

Articles Revised by the Doctoral Commission

Article I

Title: Valence Tautomerism: New Challenges for Electroactive Ligands.

Authors: E. Evangelio, D. Ruiz-Molina

Publication: Eur. J. Inorg. Chem., 2005, 2957.

Valence Tautomerism: New Challenges for Electroactive Ligands

Emilia Evangelio^[a] and Daniel Ruiz-Molina^{*[a]}

Keywords: Valence tautomerism / Electroactive / Intramolecular electron transfer / Bistability / Switch

Valence tautomeric complexes combine redox-active ligands and transition metal ions with two or more accessible oxidation states, exhibiting two nearly degenerated electronic states with localized electronic structures. Charge distribution in such electronic isomers has an appreciable sensitivity to the environment so an external perturbation, like photons, temperature and/or pressure, may lead to an intramolecular electron transfer between both redox active units and therefore to a reversible interconversion between the two degenerated electronic states. Moreover, since each electronic isomer exhibits different optical, electronic and/or magnetic properties, these complexes are being proposed as candi-

dates for future use in molecular electronic devices and switches. Most of the valence tautomeric complexes reported thus far are based on quinone or quinone-type ligands with a series of transition metal ions such as Co, Cu, Ni and Mn. Nevertheless, in the last few years, the number of electroactive ligands identified to be active in valence tautomeric complexes is being expanded by including new radical ligands such as polychlorotriphenylmethyl, phenoxy or tetraphenylporphyrin radicals.

(© Wiley-VCH Verlag GmbH & Co. KGaA, 69451 Weinheim, Germany, 2005)

Introduction

Development of molecular-scale systems that exhibit intramolecular electron-transfer phenomena induced by external stimuli has attracted considerable attention.^[1] The

interest is twofold. First, the possibility of inducing a reversible change in the electronic distribution of a molecular system opens the door to their potential use in information storage and integrated molecular-sized devices. And second, from a theoretical point of view, to study the role of various parameters governing the intramolecular electron transfer (IET) rates. Mixed-valence systems are excellent candidates for such studies since they contain at least two redox sites with different oxidation states linked by a bridge that medi-

[a] Institut de Ciència dels Materials de Barcelona (CSIC), Esfera UAB, 08193, Cerdanyola, Catalonia, Spain
Fax: +34-935801853
E-mail: dani@icmab.es



Emilia Evangelio was born in Barcelona, Spain, in 1977. She studied Chemistry at the University of Barcelona where she received her laureate degree in 2002 and Masters degree in 2004 with the work "Organometallic Compounds of Platinum(II) and Platinum(IV) Derivatives from Phenanthrene and Anthracene". She is currently busy with a PhD at the Institut de Ciència de Materials de Barcelona. Her research is devoted to structural, magnetic and optical properties of catechol compounds and derivatives.



Daniel Ruiz-Molina obtained his PhD in 1996 at the Institut of Materials Science of Barcelona (ICMAB) working with Prof. J. Veciana. His work focused on the controlled synthesis of dendrimers and magnetic organic materials. In 1997, he joined Hendrickson's Group at UCSD as a postdoctoral research fellow for three years. His project involved the synthesis and characterization of new molecular switches and single-molecule magnets. Since July 2001, he holds a permanent position at the ICMAB. His main interests are the preparation and characterization of multifunctional molecular materials and switches (optical, magnetic and electric properties) and the preparation of molecular ordered arrays on surfaces (2D) for molecular electronics.

MICROREVIEWS: This feature introduces the readers to the authors' research through a concise overview of the selected topic. Reference to important work from others in the field is included.

ates the transfer of electrons from one site to the other.^[2] Depending on the strength of the interaction between the redox centers, Robin and Day^[3] classified the mixed-valence systems into three main groups. The potential energy curves for the three types of mixed-valence compounds, which represent the systems for any geometry along the nuclear coordinate, are shown in Figure 1.

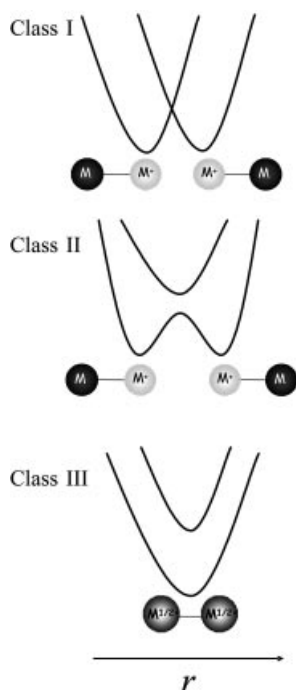


Figure 1. Potential energy curves for mixed-valence systems. The curves are arranged into three main groups according to the Robin and Day classification. In Class I the interaction between the redox centers is negligible; in Class II the interaction between the redox centers is weak or moderate and in Class III the electronic interaction is so intense that the electron is completely delocalized over the molecule.

In the Class I mixed-valence systems the interaction between the redox centers is zero or extremely weak and, therefore, the system only exhibits the properties of the isolated redox units. Even if the molecule acquires sufficient activation energy to reach the intersection region, the probability of electron exchange would be negligible. On the contrary, in Class III mixed-valence systems the electronic interaction is so intense that the electron is completely delocalized over the entire molecule. Then, the properties of each isolated unit are no longer observed and new properties associated with the delocalized species appear. Finally, for Class II systems the interaction between the redox centers is moderate. The electronic interaction has almost no effect on the potential energy curves in the vicinity of the equilibrium geometries but causes mixing in the vicinity of the crossing point. In other words, the electron is vibrationally localized in one of the redox centers due to the presence of an activation energy barrier (ΔG), although such a barrier may be overcome by an external optical or thermal stimulus, to promote an IET process.

The study of molecular mixed-valence class II systems was initiated by Taube's seminal work on compounds such as $[(\text{NH}_3)_5\text{Ru-bridge-Ru}(\text{NH}_3)_5]^{5+}$. Since then, most of the mixed-valence complexes that have been shown to exhibit intramolecular electron-transfer phenomena are homo- and heteronuclear metallic complexes where the two metal atoms with different oxidation states are connected through an organic bridging ligand.^[4] From them, ruthenium complexes and ferrocene moieties have been widely used thanks to their great stability, ease of oxidation and their kinetic inertness.^[5] Mixed-valence molecular systems where the electro-active units are pure organic groups have so far received less attention, probably due to their high instability,^[6] although for these systems electron transfer could be fine-tuned in a far more precise manner thanks to the flexibility of organic synthesis. The different types of electroactive organic units used thus far are: i) anion radicals derived from conjugated diquinones and diimides,^[7] ii) cation radicals derived from bis(tetrathiafulvalenes),^[8] iii) cation radicals derived from bis(hydrazines),^[9] iv) quinoid groups^[10] and v) ion radicals derived from π -conjugated polyaryl-methyl/polyarylamines^[11] and polychlorotriphenylmethyl radicals.^[12] In most of these cases the intramolecular electron transfer is mediated through an organic bridge and only in a few cases does it take place through a bridging metal ion.^[13]

Finally, a third type of class II mixed-valence systems is the heterogeneous complexes combining both redox-active ligands and transition metal ions. Some complexes with non-innocent electro-active ligands exhibit a reversible intramolecular electron transfer between the metal ion and the ligand, leading to an internal charge redistribution and therefore to the existence of two different electronic isomers. This family of complexes, termed Valence Tautomeric (VT), is of considerable interest. First, they are unique model systems, which provide insight into the basic factors affecting intramolecular electron transfer in coordination complexes. And second, from an applied perspective, the large changes in the optical, structural, and magnetic properties that often accompany the valence tautomeric interconversion have potential applications in bistable molecular switching materials and devices. In this review, we will first give a brief introduction to the concepts of valence tautomerism, its origin, physical properties and interconversion mechanisms. In a subsequent section, we will make a compendium of the different redox-active ligands used thus far in valence tautomeric complexes, and we will finally mention some new ideas based on the combination of valence tautomeric equilibrium with additional redox reactions involved with the redox-active ligand.

Valence Tautomerism

Valence tautomeric metal complexes with at least two redox-active centers, the metal ion and an electro-active ligand, are characterized by the existence of two electronic isomers (valence tautomers) with different charge distribu-

tions, and consequently, different optical, electric and magnetic properties. The interconversion between the different electronic isomers is accomplished by a reversible intramolecular electron transfer involving the metal ion and the redox active ligand, analogous with that observed for Prussian blue analogs.^[14] A schematic representation of valence tautomerism together with the corresponding potential energy curve plotted as a function of the nuclear coordinate, is shown in Figure 2.

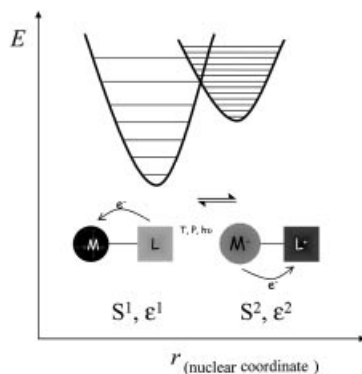
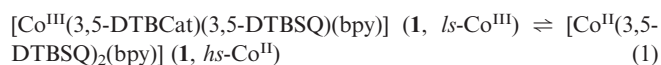


Figure 2. Potential energy curves for a valence tautomeric complex with a schematic representation emphasizing the intramolecular electron transfer between the metal ion and the ligand.

One of the first descriptions of valence tautomerism and an excellent example of the above mentioned charge distribution sensitivity is exhibited by the cobalt bis(quinone) complex $[\text{Co}^{\text{III}}(3,5\text{-DTBCat})(3,5\text{-DTBSQ})(\text{bpy})]$ (**1**), where 3,5-DTBCat²⁻ and 3,5-DTBSQ⁻ refer, respectively, to the catecholate (Cat²⁻) and semiquinonate (SQ⁻) forms of 3,5-di-*tert*-butyl-*o*-quinone, and bpy is 2,2'-bipyridine.^[15] In solution, the equilibrium in Equation (1) can be induced by variations of temperature and monitored by magnetic measurements and spectroscopic techniques such as UV/Vis, NMR and/or EPR spectroscopy.^[16]



For instance, a solution of complex **1** in toluene at low temperatures shows a band at 600 nm characteristic of the **1**, *l*-Co^{III} tautomer. An increase of temperature promotes an intramolecular electron transfer so the **1**, *l*-Co^{III} converts into the **1**, *h*s-Co^{II} tautomer as one of the ligands is oxidized by one electron from a Cat²⁻ to an SQ⁻ ligand. As a consequence, the intensity of the 600 nm band decreases and a band at 770 nm characteristic of the **1**, *h*s-Co^{II} tautomer increases in intensity (see Figure 3). Accompanying the optical changes, variations in the magnetic response are also observed. The **1**, *l*-Co^{III} isomer has an *S* = 1/2 ground state whereas the **1**, *h*s-Co^{II} isomer has an *S* = 2 ground state.

This interconversion is an entropy-driven process, analogous with the extensively studied low-spin to high-spin crossover phenomena. The large entropy gain arises from: 1) a gain in electronic entropy due to the higher spin state degeneracy of the *h*s-Co^{II} form and 2) the higher density of vibrational states of the *h*s-Co^{II} form due its longer metal-

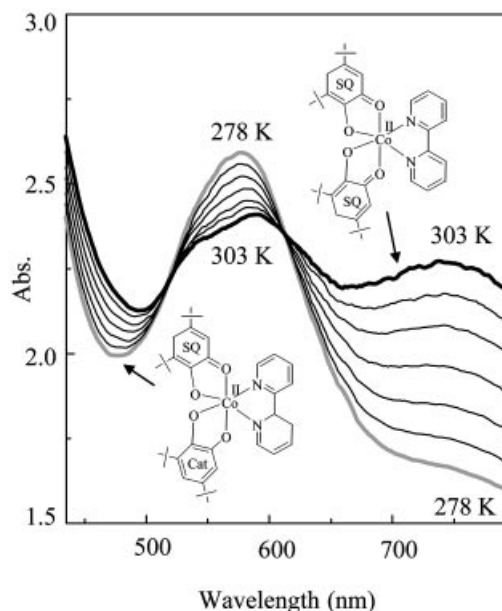


Figure 3. Temperature dependence of the electronic absorption spectrum of a CH₂Cl₂ solution of complex **1**.

ligand bond lengths. Thus thermal population of tautomeric states is dictated by the Gibbs free energy expression shown in Equation (2). At low temperatures, *TΔS* is negligible compared to ΔH , and consequently if $\Delta H > kT$ only the *l*s-Co^{III} state is populated. An increase in the temperature will increase the *TΔS* contribution, making it non-negligible and favoring the population of the *h*s-Co^{II} state, up to a critical temperature *T_c* where $\Delta G = 0$ and $\Delta H = T\Delta S$. A further increase in the temperature will change the sign of ΔG .

$$\Delta G = \Delta G_{h\text{s-Co}^{\text{II}}} - \Delta G_{l\text{s-Co}^{\text{III}}} = \Delta H - T\Delta S \quad (2)$$

It is important to emphasize that whereas most of the valence tautomeric complexes reported thus far exhibit a temperature-dependent interconversion in solution, the number of examples exhibiting a valence-tautomeric interconversion in the solid state is rather limited. For this, the presence of solvate molecules within the crystalline network and their effects on the phonon relaxation, play a critical role. For instance, a plot of the magnetic susceptibility vs. temperature for a sample of complex **2** recrystallized from four different solvents is shown in Figure 4. In this figure it is shown that for complex $[\text{Co}^{\text{III}}(3,5\text{-DTBSQ})(3,5\text{-DTBCAT})(\text{phen})]\cdot\text{C}_6\text{H}_5\text{CH}_3$ (**2**), the tautomeric interconversion between the **2**, *l*s-Co^{III} and **2**, *h*s-Co^{II} isomers can be reversibly driven with temperature and monitored by large changes in the magnetic susceptibilities, with an interconversion that occurs abruptly within a narrow temperature range of ca. 30 °C. On the contrary, a polycrystalline sample recrystallized from ethanol has a μ_{eff} value essentially independent of the temperature and close to the value of 1.7 μ_{B} expected for the low-spin isomer. For samples recrystallized from acetonitrile and dichloromethane, incomplete transitions were observed (see Figure 4).^[17]

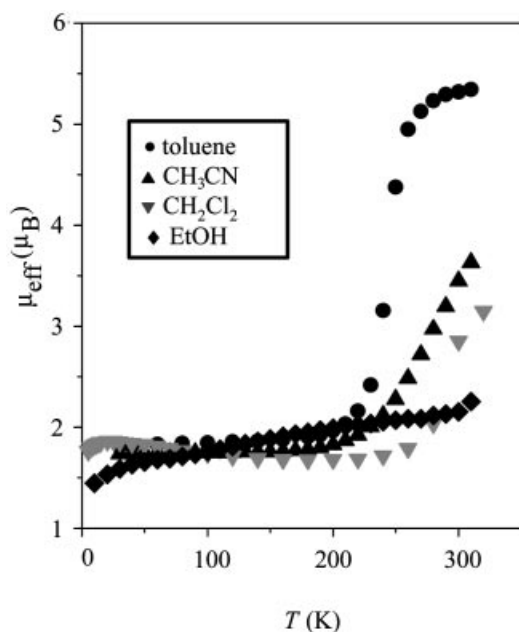


Figure 4. Plots of the effective magnetic moment (μ_{eff}) vs. temperature for complex **2** in different solvents: toluene, acetonitrile, dichloromethane, and ethanol.

Moreover, since valence tautomeric complexes are electronically labile, they exhibit significant vibronic interactions and therefore an appreciable sensitivity to the environment. As a consequence, intramolecular electron transfer can be induced not only by temperature variations but also by irradiation or pressure.

Light-Induced Tautomerism

Adams et al. reported results of the first picosecond time-resolved optical experiments on valence tautomeric complexes in solution.^[18] In such work, pulsed laser photolysis, both on the picosecond (90 ps pulse) and the nanosecond (24 ns pulse) time-scales, were carried out for a series of complexes with the general formula $[\text{Co}(3,5\text{-DTBSQ})_2(\text{N-N})]$. The authors showed that when the complex is in the *ls*- Co^{III} form, a laser pulse could excite it to a LMCT excited state. Such excited states experience a rapid intersystem crossing to the *hs*- Co^{II} state with a subsequent electron recombination to finally yield the *ls*- Co^{III} isomer. At room temperature, the rate of *hs*- Co^{II} to *ls*- Co^{III} conversion (k_{bvt}) ranges from 6.1×10^7 to $6.7 \times 10^8 \text{ s}^{-1}$ and its temperature dependence follows an Arrhenius-like behavior in the 140–300 K range. However, below 140 K, deviations from linearity are seen, most likely due to the involvement of quantum mechanical tunneling. Valence tautomerism for this family of complexes was also shown to take place in the solid state after illumination at low temperatures.^[19] For instance, variations on the μ_{eff} vs. T plot of $[\text{Co}^{\text{III}}(3,5\text{-DTBSQ})(3,5\text{-DTBCAT})(\text{phen})] \cdot \text{C}_6\text{H}_5\text{Cl}$ (**2**) before and after illumination are shown in Figure 5.^[20] Similar interconversion in the solid state has been reported by Dei et al. for the new dinuclear complex $[\{\text{Co}(\text{cth})\}_2(\text{dqbq})](\text{PF}_6)_3$ (**3**), both by irradi-

ation with a laser connected to the SQUID magnetometer and by reflectivity spectra.^[21] Their results showed that the light-induced phenomenon is perfectly reversible although the photoinduced population rate corresponds to only 43% of the sample, most likely due to opacity phenomena.

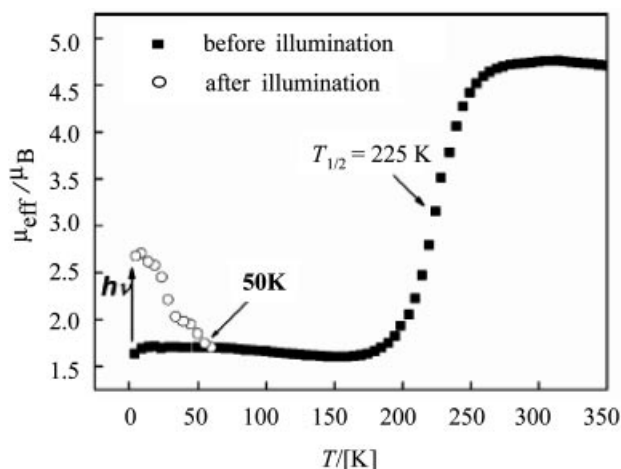


Figure 5. Plot of the χT product as a function of temperature T for complex **3** measured before and after irradiation at 647 nm. The bump at 45 K on the irradiation curve is a result of a small amount of oxygen.

Finally, additional femtosecond spectroscopic experiments by Neuwahl et al. in a simple cobalt-dioxolene derivative in solution demonstrated the involvement of not two but at least three states in a two-step process for a valence tautomeric interconversion in solution.^[22] Besides the Co^{III} -Cat and Co^{II} -Sq pairs involved in the tautomerism, the third species may originate from several possible electronic isomers, such as a Co^{III} -Cat species with divergent electronic configurations or a low-spin Co^{II} -Sq isomer, which is expected to be characterized by a triplet electronic ground state.

Pressure-Induced Tautomerism

The X-ray structure analysis of complex **2** at three different temperatures (137, 238 and 295 K) revealed an average metal-ligand bond length increase of 0.18 Å on passing from the **2**, *ls*- Co^{III} to the **2**, *hs*- Co^{II} tautomer. As shown in Figure 6, such a change is due to a drastic change in the population of the antibonding e_g^* orbitals.

Such increase of the molecular size when passing from the low-spin to the high-spin isomer has also been used to modulate valence tautomerism by pressure effects.^[23] Verdaguer et al.^[24] studied the nonsolvated complex **2** and its related solvated form $[\text{Co}^{\text{II}}(3,5\text{DTBSQ})_2(\text{phen})] \cdot \text{C}_6\text{H}_5\text{CH}_3$ by EXAFS and XANES. EXAFS data indicated that the **2**, *hs*- Co^{II} tautomer has bond lengths of $\text{Co}-\text{O} = 2.08 \text{ \AA}$ and $\text{Co}-\text{N} = 2.13 \text{ \AA}$ whereas the **2**, *ls*- Co^{III} tautomeric complex is smaller with $\text{Co}-\text{O} = 1.91 \text{ \AA}$ and $\text{Co}-\text{N} = 1.93 \text{ \AA}$. Both complexes could be reversibly driven from the larger **2**, *hs*- Co^{II} tautomer to the smaller **2**, *ls*- Co^{III} tautomeric form upon application of pressure, within the 0.075–0.700 GPa

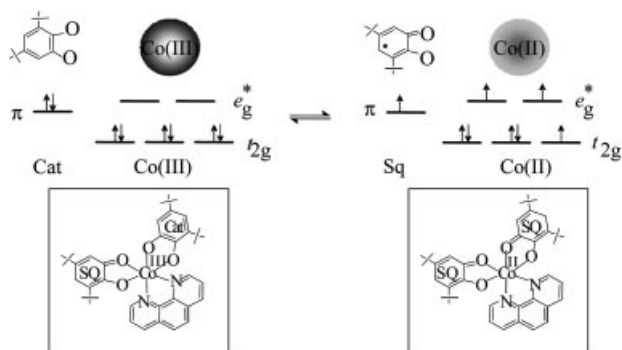


Figure 6. Representation of the orbital occupancy, both metal and ligand based, on the two different tautomeric forms for complex 2.

range for the solvated form and 0.10–2.5 GPa for the non-solvated form. In addition to EXAFS and XANES, pressure-induced valence tautomerism has also been recently monitored by changes in the magnetic response.^[25]

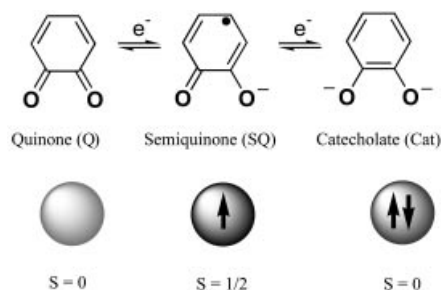
Redox-Active Ligands

So far, many different types of redox-active ligands have been described in the literature. Among them are π -conjugated molecules with coordinating capabilities such as quinone-types,^[26] crown-ethers,^[27] ferrocene,^[28] tetrathiafulvalenes derivatives,^[29] and polymers/oligomers,^[30] such as polyanilines and polythiophenes.^[31] However, we must emphasize that even though the number of metal complexes based on redox-active ligands is considerable, those exhibiting valence tautomerism are rather limited since they must simultaneously satisfy two conditions: 1) the degree of covalency in the interaction between metal ion and electroactive ligand must be low, and 2) the energy of their frontier orbitals must be similar.^[32] In other words, it is necessary that these complexes exhibit localized electronic structures, low orbital mixing, and a small energy difference between the two electronic tautomers. Most of the valence tautomeric complexes reported thus far are based on quinone or quinone-type ligands with a series of transition metal ions. Nevertheless, in the last few years the number of electroactive ligands inducing valence tautomerism is being expanded by including new electroactive ligands such as schiff-base, phenoxyl, tetraphenylporphyrin and polychlorotriphenylmethyl radicals. Examples of each case are revised below.

Quinone Ligands

Metal dioxolene complexes have been the subject of a vigorously growing and fascinating research field for a long time due to their rich structural, physical and chemical properties.^[33] In addition to exhibiting valence tautomerism, the subject of the present review, several other interesting features such as the design of paramagnetic molecules with predetermined spin topologies^[34] and activation of small molecules like O_2 and N_2 have also been described.^[35]

Most of these interesting features are related to their rich redox activity, since they are “noninnocent” electroactive ligands that may exist as neutral quinones (Q), radical semiquinones (SQ^-) or dianionic catecholates (Cat^{2-}) (Scheme 1), although in valence tautomeric complexes they are only found in the SQ^- and Cat^{2-} forms due to the limiting binding ability of the quinone ligand.^[36] Charge localization within the metal-quinone chelate ring has been observed for different transition metal complexes (cobalt, manganese, nickel and copper among them),^[37] allowing the observation in some cases of valence tautomerism. However, in other cases such as for ruthenium complexes, charge distribution is less clear and a delocalized electronic structure may be an appropriate description.^[16]



Scheme 1.

Cobalt Complexes

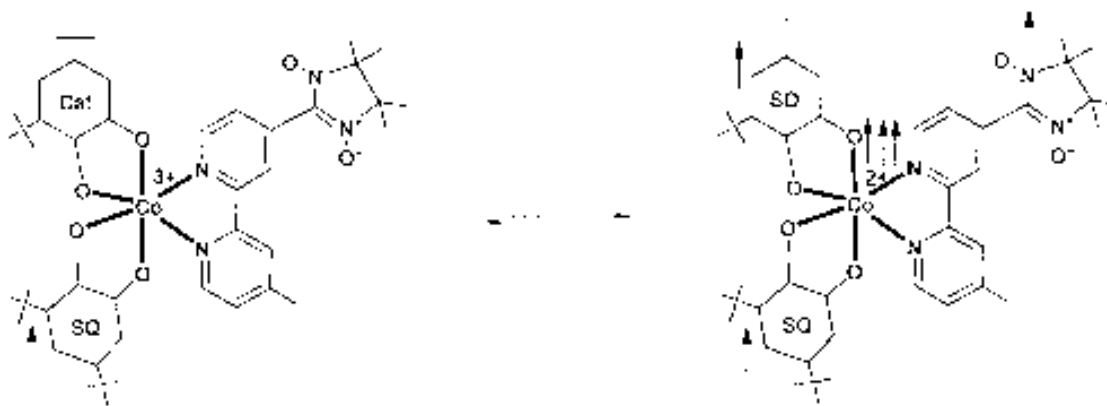
The best investigated family of quinone-based valence tautomeric complexes is that of cobalt-dioxolene molecules, where the valence tautomeric interconversion involves an intramolecular electron transfer between a six-coordinate cobalt ion and a coordinated dioxolene ligand. The simplest cobalt-quinone complexes undergoing valence tautomerism belong to the family of ionic complexes with the general formula $[ML(diox)]Y$, where L = tetraazamacrocyclic ancillary ligand, diox = 9,10-dioxophenanthrene and Y = PF_6^- , BPh_4^- , I^- .^[25] Such complexes undergo a temperature- and pressure-induced intramolecular electron-transfer equilibrium with a transition temperature that varies with the volume and coulombic interaction of the counterion Y. Moreover, substitution of CH_2Cl_2 solvent molecules with their deuterated analogs drastically modifies its magnetic properties giving rise to a thermal hysteresis, an important issue if future technological applications are envisaged for these molecular systems.^[38]

Before the previous monodioxolene complexes were reported, most cobalt complexes shown to exhibit valence tautomerism were of the general formula $[Co(N-N)(Q)_2]$, where N-N is a diazine ligand, Q = 3,5- and 3,6-di-*tert*-butylcatecholato or semiquinone form. Several interesting features have been observed for this family of complexes, among them a marked effect of the nature of the quinone and ancillary ligands on the tautomerism. For instance, whereas in complex $[Co(bpy)(3,6-DBSQ)(3,6-DBCat)]$ bipyridine ligands of adjacent molecules stack to form a one-dimensional lattice resulting in a remarkable photomechanical effect upon irradiation, replacement by the 3,5-di-*tert*-

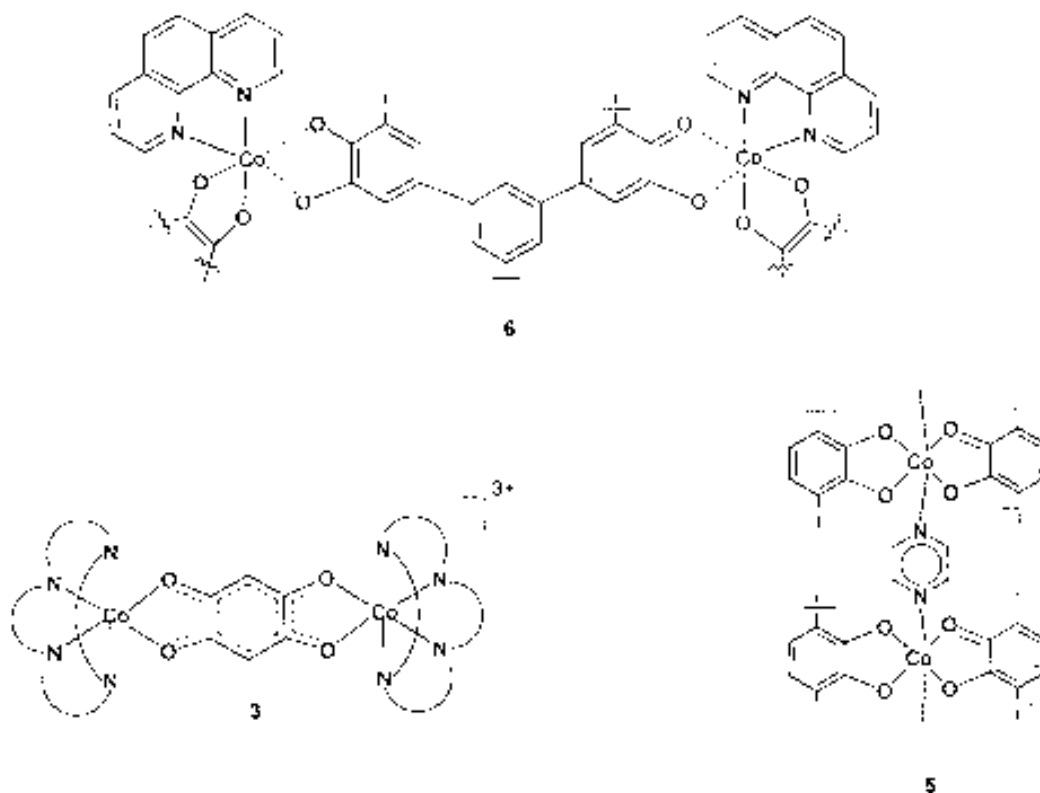
butylcatecholato induces a dimerization. As far as the ancillary ligand is concerned, Hendrickson et al.^[39] and Pierpont et al.^[40] have also concluded that it is possible to systematically control valence tautomerism by changing the counterligand chelate ring flexibility and their donor abilities. Another interesting example has been described by Awaga et al., who reported valence tautomerism in the spin-labeled complex $[\text{Co}(\text{nnbpy})(3,5\text{-DTBSQ})_2]$ (**4**), where nnbpy is a bipyridine substituted nitronyl nitroxide radical. Even though the temperature dependence of the magnetic susceptibility indicates a tautomeric interconversion above 250 K, the radical ligand behaves as a Curie spin over the whole temperature region.^[41] A schematic representation of

the valence tautomerism observed for complex **4** is shown in Scheme 2.

In addition to variations in the number and nature of the electroactive and counter ligands, different polynuclear tautomeric complexes have also been reported (see Scheme 3). For instance, Dei et al. reported the dinuclear complex $[\{\text{Co}(\text{cth})\}_2(\text{dnhq})](\text{PF}_6)_3$ (**3**) that undergoes a gradual thermal tautomeric transition at around 175 K and quantitative photoconversion.^[21] Pierpont et al. followed this approach to establish the photomechanical polymer $[\text{Co}(\text{pyz})(3,6\text{-DBQ})_2]_n$ (**5**). This coordination polymer exhibited a temperature-induced tautomeric interconversion in the solid state that is derived from a mechanical process



Scheme 2.



Scheme 3.

due to variations on the bond lengths although no hysteresis effects were observed.^[42] On the contrary, such hysteresis was observed more recently by Schultz et al., who used a bis-bidentate ligand to obtain the coordination polymer $[\text{Co}(\text{phen})\text{L}] \cdot 0.5\text{CH}_2\text{Cl}_2$ (**6**). This cobalt-dioxolene polymer exhibits the necessary cooperative properties that lead to thermal hysteresis in a valence tautomeric equilibrium, even though the transition could be classified as gradual.^[43]

Copper Complexes

Some copper complexes containing dioxolene ligands may yield, under the right conditions, the valence tautomeric interconversion shown in Equation (3) and Figure 7.^[44]

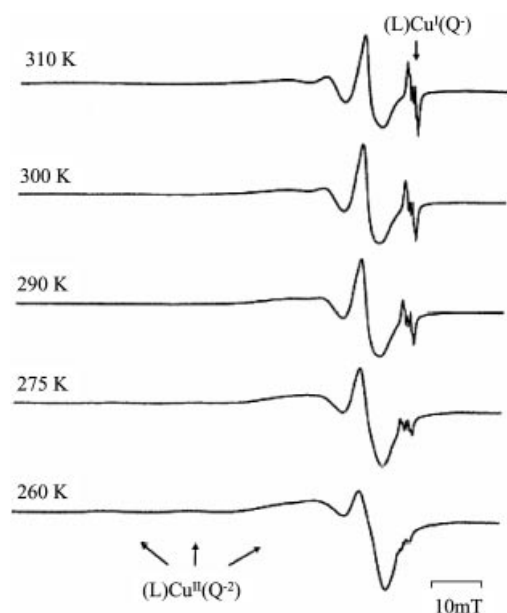


Figure 7. EPR spectra illustrating the temperature-dependent redox isomerism (3), with $\text{L} = \text{mtb}$ and $\text{Q} = 3,5\text{-di-tert-butyl-}o\text{-quinone}$, in THF solution.

One of the first examples of valence tautomerism involving the $\text{Cu}^{\text{II}}/\text{Cu}^{\text{I}}$ pair was reported in a copper containing amine oxidase enzyme that catalyzes the oxidation of amines to aldehydes,^[45] an important process involved in relevant biological functions such as growth regulation and tissue maturation. Indeed, the oxidation of primary amines to aldehydes takes place through a two-electron reduction of O_2 to H_2O_2 catalyzed by the active copper center of the homodimeric enzyme. For this to be achieved and to circumvent spin conservation problems an interconversion from its initial Cu^{II} -catechol form to the Cu^{I} -semiquinone form, mediated by an intramolecular electron transfer between both units, takes place. Dooley et al. presented evidence for the generation of such a Cu^{I} -semiquinone natural form on several amine oxidases under anaerobic conditions by taking advantage of the very different EPR characteristics (g factor and hyperfine-coupling constants) between the pairs Cu^{II} /diamagnetic ligand and Cu^{I} /radical ligand.^[45]

These studies suggested that the Cu^{I} -semiquinone and the Cu^{II} -catechol forms are in equilibrium; the Cu^{II} -catechol form being more stable at low temperatures and the Cu^{I} -semiquinone form at high temperatures.

These exciting results and other biological and commercial processes have motivated the synthesis and characterization of different copper-quinone synthetic models. These studies have shown that the electronic distribution in a series of complexes with the general formula $[(\text{Q}^{\text{n-}})\text{Cu}^{\text{m+}}\text{L}]$ depends on the donor or acceptor characteristics of the ligand L . With strong π -acceptor ligands, such as $\text{L} = \text{CO}$, CNR , PR_3 or AsR_3 , the Cu^{I} -semiquinone form is favored, whereas the use of non π -acceptor ligands, such as amine ligands, favors the Cu^{II} -semiquinone form.^[46] For instance, Kaim et al. have reported the use of a thioether ligand that favors the Cu^{I} -semiquinone form to induce sensitive valence tautomerism in paramagnetic copper complexes related to amine oxidase enzymes.^[47] Similar studies have also been done by Speier et al., who described the existence of valence tautomerism for the species $[\text{Cu}(\text{py})_2(\text{PhenQ})_2]$ (**7**).^[48] The temperature dependence of the isotropic ESR spectrum of complex **7** in a pyridine solution indicates that at 373 K the complex is in the form $[\text{Cu}^{\text{I}}(\text{PhenSQ})]$ whereas at 233 K the $[\text{Cu}^{\text{II}}(\text{PhenCat})]$ tautomer is present, exclusively.

Manganese Complexes

A few years after the first report on cobalt tautomerism, similar temperature-dependent shifts in electronic spectra were observed for a related complex of manganese.^[49] The main difference is that valence tautomerism in this case involves three different tautomeric forms associated with three different oxidation states where the manganese ions can be found. Complex $[\text{Mn}(\text{py})_2(3,5\text{-DBCat})_2]$ (**8**) experienced a reversible change in color from the intense purple of the Mn^{IV} form to the pale green-brown characteristic color of the Mn^{II} form. The interconversion takes place through a Mn^{III} form, which usually exhibits similar colors to that of the Mn^{IV} form, as confirmed later in the solid state^[50] and in solution.^[51] More recently, valence tautomerism in an adduct of a tetrazamacrocycle complex of manganese with a single o -benzoquinone ligand has also been reported.^[52] The tautomeric interconversion involves two species with nearly degenerate electronic states and a strong sensitivity to variations of the counterion.

Iron and Nickel Complexes

Very recently, two new examples of nickel and iron-quinone complexes have been reported to exhibit valence tautomerism. Tanaka et al. reported complexes $[\text{Ni}(\text{PyBz}_2)(\text{tBu}_2\text{SQ})]\text{PF}_6$ (**9**) and $[\text{Ni}(\text{MePyBz}_2)(\text{tBu}_2\text{Cat})]\text{PF}_6$ (**10**) as the first examples for the successful control of valence tautomerism between the Ni^{II} -SQ and Ni^{III} -Cat frameworks.^[53] Moreover, drastic differences in the electronic states of both complexes are observed due to the steric effects induced by the o -methyl group in the MePyBz_2 ligand, which weakens the coordination of the pyridine moiety to the nickel ion compared with the unsubstituted PyBz_2 ligand. On the other hand, Banerjee et al. reported a semiquinone-cate-

cholate based mixed valence complex $[\text{Fe}(\text{bispicen})(\text{Cl}_4\text{Cat})(\text{Cl}_4\text{SQ})]\cdot\text{DMF}$ (**11**), for which valence tautomerism has been followed by electronic absorption spectroscopy. The tautomer $\text{Fe}^{\text{III}}(\text{Cl}_4\text{Cat})(\text{Cl}_4\text{SQ})$ is favored at low temperatures, while at an elevated temperature, the $\text{Fe}^{\text{II}}(\text{Cl}_4\text{SQ})_2$ tautomeric form dominates. This is the first example where a mixed valence semiquinone/catechol iron(III) complex undergoes intramolecular electron transfer.^[54]

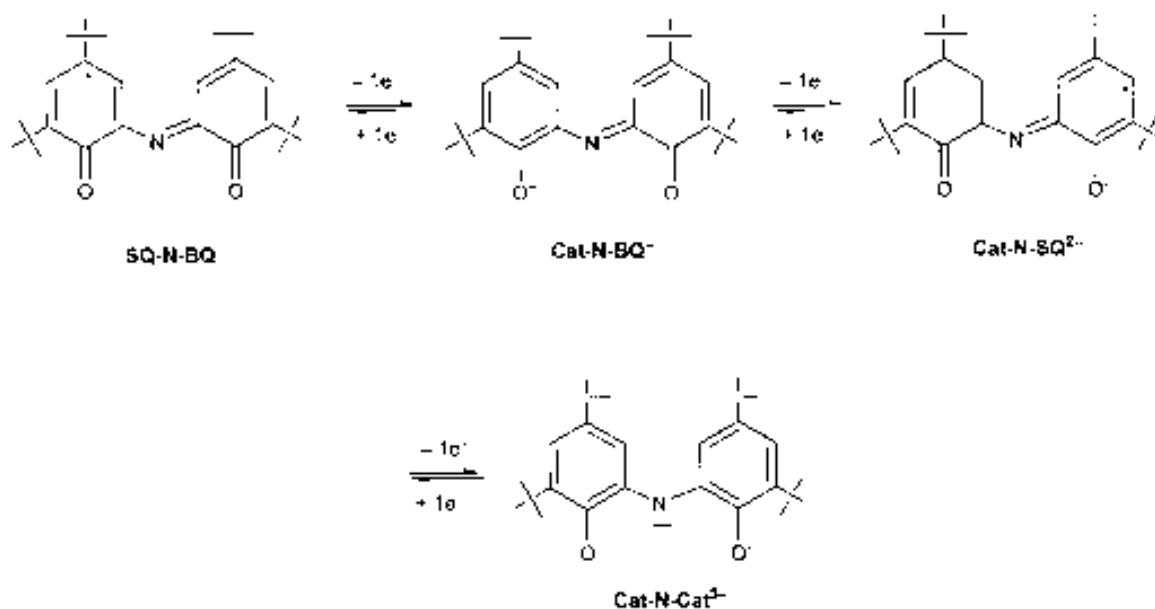
Phenoxy Ligands

Transition metal complexes in which one or more of the ligands is present as a phenoxy radical have attracted much interest due to their broad occurrence in technical processes^[55] and enzymatic metalloproteins such as galactose oxidase (GAO)^[56] or glyoxal oxidase (GLO).^[57] Phenoxy radicals are monovalent oxygen radical species that exhibit delocalization of the unpaired electron over the aromatic ring and in most cases *ortho* and *para* substituents that give steric protection.^[58] For instance, it has been shown that *tert*-butyl substituents at the *ortho* and *para* positions of the phenolates facilitate one-electron oxidation to the corresponding phenoxy radicals, because these substituents decrease the oxidation potential of the phenolates and provide enough steric bulk to suppress bimolecular decay reactions of the generated phenoxy radicals.^[59] Several groups have prepared metal-phenoxy complexes giving new insights into the chemical factors that govern the generation and stability of this type of radicals,^[60] among those worth mentioning are the ones produced by Wieghardt et al. They have established that bidentate *O,N*-coordinated *o*-aminophenolato ligands can be found in one of the following different protonation and oxidation levels: *o*-imidophenolate(2⁻) anions, *o*-iminobenzosemiquinonate(1⁻) radical monoanions or even *o*-iminobenzoquinone. All these forms can exist in coordination compounds as confirmed by low-

temperature X-ray crystallography.^[61] In addition, *o*-iminobenzosemiquinonate(1⁻) anions are paramagnetic ($S = 1/2$) ligands that couple either ferro- or antiferromagnetically when coordinated to a paramagnetic transition metal ion, depending on the symmetry of the magnetic *d* orbital of the metal ion.

A further step has been the study and characterization of *O,N*-coordinated type ligands containing two phenolate donor groups. These ligands, in addition to producing phenoxy radicals in the presence of air, exhibit better chelating capabilities and good π -donor atoms that stabilize higher oxidation states,^[62] which has allowed the observation of valence tautomerism in some of their complexes. The advantages of valence tautomeric Schiff-base complexes over transition metal complexes with *o*-quinone ligands are considerable. First, valence tautomeric Schiff-base complexes display higher stabilities relative to atmospheric oxygen in solution and in the solid state. Second, the differences between the optical properties of isomers involved in the valence tautomerism of the cobalt Schiff-base complex are enhanced when compared to those observed for cobalt complexes with *o*-quinone ligands. Third, the Schiff-base ligand exhibits a richer electrochemical behavior since it can exist in different oxidation forms, ranging from +1 to -3, which may lead to stable coordination complexes with several metal ions in a variety of oxidation states. For instance, the tridentate ligand [(2-hydroxy-3,5-di-*tert*-butyl-1-phenyl)imino]-3,5-di-*tert*-butyl-1,2-benzoquinone ligand (Cat-N-BQ), may in principle exist in different oxidation states although it usually coordinates in the mononegative Cat-N-BQ or dinegative Cat-N-SQ radical forms (see Scheme 4).^[63]

Using such a ligand, in 1988 Pierpont et al. reported the new complex $[\text{Co}^{\text{III}}(\text{Cat-N-BQ})(\text{Cat-N-SQ})]$ (**12**), although at that time no evidence for tautomeric interconversion was shown to take place.^[64] A few years later, the temperature



Scheme 4.

dependence of the spectral and magnetic properties of solutions of this compound in nonpolar solvents suggested the existence of the valence tautomeric equilibrium shown in Equation (4). The temperature dependence of the ^1H NMR spectrum of a $[\text{D}_8]$ toluene solution of complex $[\text{Co}^{\text{III}}(\text{Cat-N-BQ})(\text{Cat-N-SQ})]$ is shown in Figure 8.^[65]

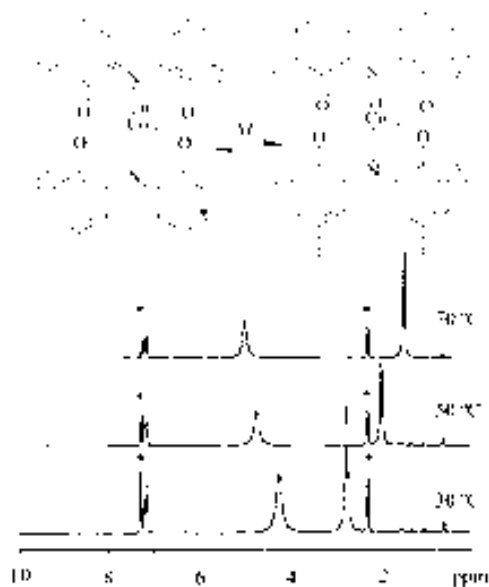
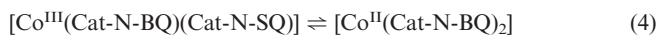


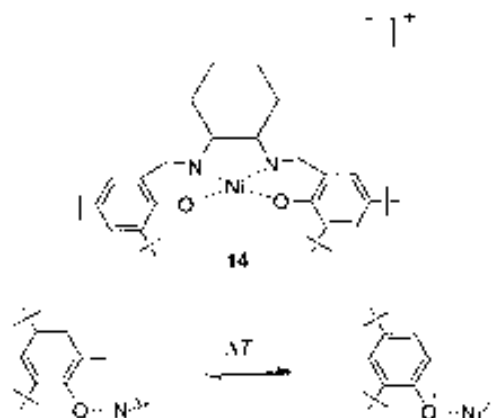
Figure 8. Temperature dependence of the ^1H NMR spectrum of a $[\text{D}_8]$ toluene solution of $[\text{Co}(\text{Cat-N-BQ})(\text{Cat-N-SQ})]$. The observed signals are due to the *tert*-butyl groups of the ligand. Resonances associated with ring protons are not shown.

The interconversion temperature (T_c) was determined to be close to 300 K by the ratio between the enthalpy and the entropy changes in solution but no tautomerism was observed in the solid state, as evidenced by the lack of changes in the variable-temperature magnetic susceptibility data. This fact was initially attributed to the lack of solvate molecules within the crystalline network, which are assumed to impart a “softness” to the lattice that makes it possible to appreciate the dimensional change in the complex. However, in subsequent work, the same authors showed that complex **12** exhibits a tautomeric interconversion in the solid state but at much higher temperatures than in solution.^[66] The large difference between the interconversion T_c in the solid state and in solution is suggested to come from the entropy changes associated with the modifications of vibronic interactions.

Valence tautomerism has also been reported for the related manganese complex $[\text{Mn}^{\text{IV}}(\text{Cat-N-SQ})_2]$ (**13**). In this case, valence tautomerism involves three different tautomeric isomers associated with the three different oxidation states in which the manganese ion can be found: Mn^{IV} , Mn^{III} and Mn^{II} .^[67] Variable-temperature magnetic susceptibility data for a crystalline sample of complex **13** is characterized by a constant μ_{eff} value of $1.9 \mu_{\text{B}}$ consistent with the formulation $[\text{Mn}^{\text{IV}}(\text{Cat-N-SQ})_2]$ (**13**, Mn^{IV}). This fact

evidenced the lack of valence tautomerism for complex **13** in the solid state, at least in the temperature range studied. For this reason, variable-temperature magnetic susceptibility data for a $[\text{D}_8]$ toluene solution of complex **13** were recorded. From 5 to 270 K complex **13** exhibits a constant μ_{eff} value of $1.8\text{--}1.9 \mu_{\text{B}}$ in solution, characteristic of the **13**, Mn^{IV} tautomer. Then, from 270 to 360 K the value of μ_{eff} increases gradually to a value of $4.8 \mu_{\text{B}}$, which is over the spin-only value of $3.9 \mu_{\text{B}}$ ($g = 2$) expected for the **13**, Mn^{III} isomer but below that expected for the **13**, Mn^{II} tautomer ($5.9 \mu_{\text{B}}$). Since the tautomeric interconversion in solution usually occurs gradually over a large temperature range ($>80\text{--}100 \text{ }^\circ\text{C}$) it was impossible to completely shift the tautomeric equilibrium to the $[\text{Mn}^{\text{II}}(\text{Cat-N-Q})_2]$ isomer. Further support of the existence of the valence tautomerism shown in Scheme 4 was provided by variable temperature electronic absorption spectra for a toluene solution of complex **13** in the 293–353 K temperature range.

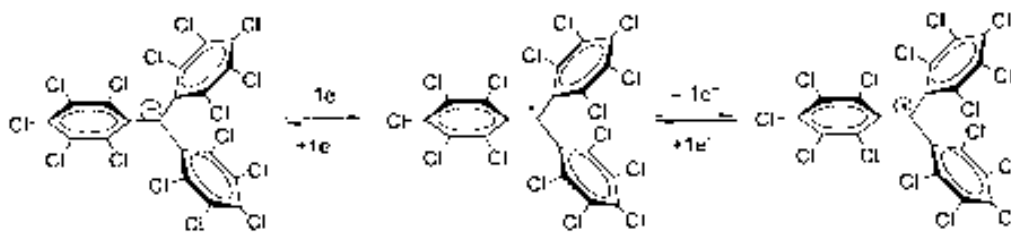
In addition to the Schiff-base ligands previously described and in the course of studies on metal-phenoxyl radical complexes, Shimazaki et al. have recently reported that the one-electron oxidized form of a new mononuclear nickel(II)-bis(salicylidene)diamine complex exhibits valence tautomerism. Indeed, the one-electron oxidation of **14** has been found to be temperature dependent in CH_2Cl_2 yielding the corresponding Ni^{III} -phenolate complex at $T < -120 \text{ }^\circ\text{C}$ and the Ni^{II} -phenoxyl radical species at $T > -100 \text{ }^\circ\text{C}$, which is regarded as a tautomerism of the oxidation states governed by temperature.^[68] A schematic representation for the tautomeric equilibrium of this species in solution is shown in Scheme 5.



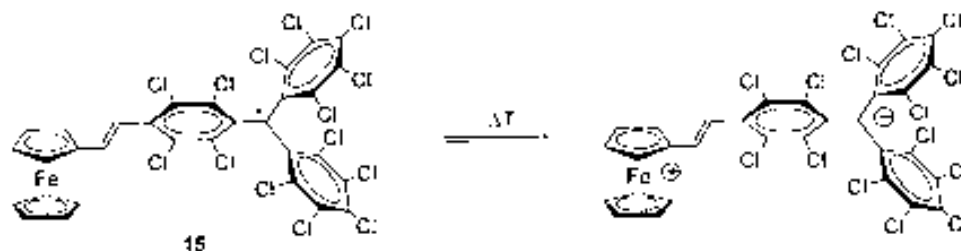
Scheme 5.

Polychlorotriphenylmethyl Radicals

Perchlorotriphenylmethyl radicals (PTM) have their central carbon atom, where most of the spin density is localized, sterically shielded by an encapsulation with six bulky chlorine atoms that increases its life expectancy and thermal and chemical stability.^[69] Moreover, the cyclic voltammetry of perchlorotriphenylmethyl radicals shows the formation of two different stable ionic species that correspond



Scheme 6.



Scheme 7.

to the oxidation and reduction of this radical (see Scheme 6). This allows the corresponding anions and cations to be obtained, either chemically or electrochemically, both in solution and in solid state, which also show considerable stabilities in accordance with the steric shielding of their central carbon atoms. Such persistence as well as the particular structural and conformational characteristics of radicals of this family, has enabled them to be functionalized in order to build pure organic open-shell dendrimers with high-spin ground states^[70] and pure-organic mixed-valence molecular wires exhibiting intramolecular electron-transfer phenomena.^[71]

More recently, Veciana et al. have described the use of perchlorotriphenylmethyl radicals, properly functionalized with carboxylic groups, to obtain complexes combining paramagnetic metal ions and pure organic radicals as ligating sites. Even though this approach has been successfully used to obtain novel mononuclear^[72] and extended transition metal complexes exhibiting nonconventional structural motifs, such as nanoporous frameworks with exotic magnetic behavior,^[73] no valence tautomerism has been reported on such complexes so far. Nevertheless, the same authors did report valence tautomerism on a new family of molecular systems comprising PTM radicals and ferrocene

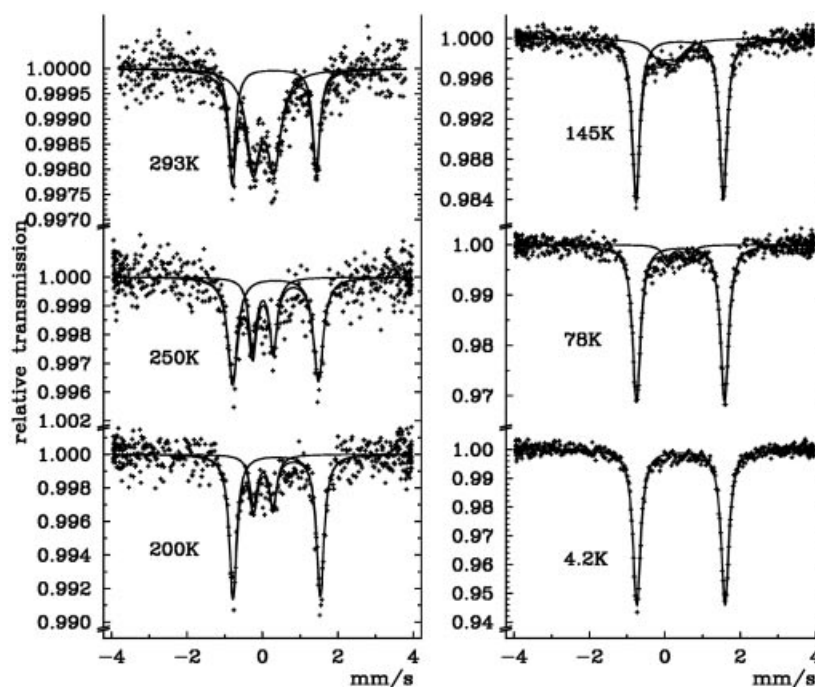


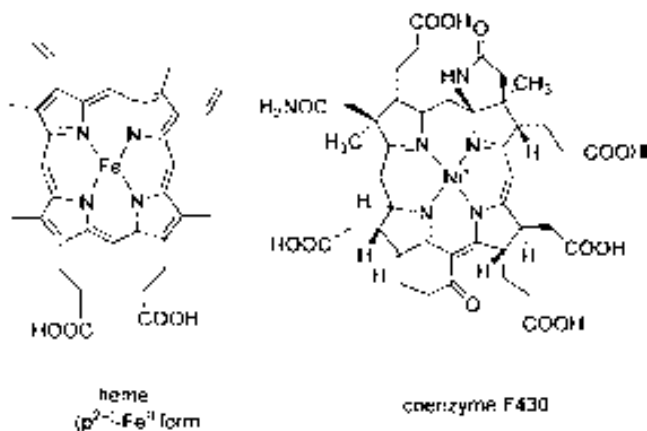
Figure 9. ⁵⁷Fe Mössbauer spectra of radical **15** as a function of temperature, showing the interconversion between the Fe^{III} and Fe^{II} redox states.

units (see Scheme 7).^[74] Ferrocene chromophores are interesting not only because of their electron donor capacities and rich electrochemistry but also because they are electroactive species whose oxidation state can be controlled by means of a chemical or electrochemical stimulus, with their oxidized states being of open-shell character.

As far as we know, this is the only example described, so far, where valence tautomerism was followed by variable-temperature Mössbauer experiments. The ⁵⁷Fe Mössbauer spectra of radical **15** as a function of temperature are shown in Figure 9. As can be seen in this figure, the Mössbauer spectrum of **15** exhibited a temperature-dependent behavior, in solid state, that is in agreement with the observation of a temperature-dependent intramolecular electron transfer from the ferrocene center to the radical as shown from left to right in Scheme 7. The conversion appears to be gradual up to room temperature and fully reversible as confirmed by repetitive temperature-variable Mössbauer experiments.

Metalloporphyrins

The cation radicals of metalloporphyrins have been extensively studied because they serve as model systems for biological-redox intermediates. In these systems, the formation of a ring vs. a metal centered cation is determined by factors such as the intrinsic redox potentials of the porphyrin ring and metal center, the number and type of ligands on the metal ion and the nature of the solvent. Thanks to such electronic lability, some metalloporphyrins are susceptible to exhibiting valence tautomerism. A well-recognized case is the heme system, in which the porphyrinoid macrocyclic ligand can participate directly in the electron-transfer process, or nickel complexes of porphyrinoid ligands related to the function of factor F430 in the methane-releasing coenzyme M reductase.^[75] A drawing of the heme and coenzyme F430 are shown in Scheme 8.



Scheme 8.

In addition to the occurrence in natural systems, in 1975 Dolphin et al. showed the existence of a reversible intramolecular electron transfer in an oxidized nickel tetraphenylporphyrin (TPP).^[76] The reversible temperature-depend-

ent transformation can be described as shown in Equation (5).



At room temperature, oxidation of complex Ni(TPP) (where TPP = tetraphenylporphyrin) yields a green solution associated with the electronic form $[\text{Ni}^{\text{II}}(\text{TPP})^{\cdot+}]$ with a π -cation radical. Upon freezing at 77 K, the green solution becomes orange. These spectral changes are consistent with conversion to a low-spin $[\text{Ni}^{\text{III}}(\text{TPP})]^+$ ($S = 1/2$) in which the unpaired electron resides in a metal ion orbital, as confirmed by temperature-dependent ESR spectroscopy. Kadish et al. also studied electron-transfer mechanisms of five different nickel(II) porphyrins by replacing the phenyl groups with alkyl groups, all of them exhibiting a temperature-dependent valence tautomerism.^[77] In addition to variations on the porphyrin ring, it has been proposed that axial ligation also plays a significant role in mediating the tautomerism. For instance, Bocian et al.^[78] have shown based on spectroscopic data that relatively stable $[\text{Ni}^{\text{III}}(\text{TPP})]^+$ can be obtained, even at ambient temperatures, when coordinating ligands such as THF, py and CH_3CN , are present. The spectroscopic data indicate that the conversion to Ni^{III} species is facilitated by mixing of the metal ion and porphyrin ring orbitals, the latter of which contains the hole in the π -cation form.

Redox-Tuned Valence Tautomerism

The redox activity of the ligands not only allows for the existence of valence tautomerism but also for additional switching capacities resulting from an electrochemical process. Such a strategy has been shown to be very useful for the systematic tuning of the critical temperature (T_c), at which there are equal amounts of both tautomers, as well as of the net magnetic moments and optical properties of the tautomeric isomers. Different examples of redox-tuned valence tautomerism are revised below.

Quinone Ligands

A study of the influence of the temperature on the cyclic voltammetric behavior of complex $[\text{Co}^{\text{III}}(3,5\text{-DTBCat})(3,5\text{-DTBSQ})(\text{bpy})]$ (**1**, *ls*- Co^{III}) revealed interesting features. This was the first time that changes in the redox properties of both isomers were followed.^[79] As shown in Figure 10, at 273 K the **1**, *ls*- Co^{III} tautomer shows two well-defined processes at $E_{1/2}$ of -0.34 and $+0.25$ V vs. Ag wire. The redox couple observed at $E_{1/2} = -0.34$ V is associated with the reduction of the semiquinone ligand to the catecholate form, whereas the second redox process is characteristic of the oxidation of the catecholate ligand to the semiquinone form. As the temperature is increased, slight shifts of the redox processes into the direction of more positive potentials and the apparition of new redox processes at approximately $E_{1/2} = -0.75$ and $+0.40$ V, are observed. Since the tautomeric interconversion in solution occurs gradually

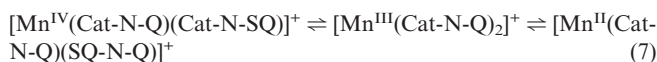
yield in both cases $[\text{Co}^{\text{III}}(3,5\text{-DTBSQ})(\text{bpy})_2]\cdot\text{X}_2$, where $\text{X} = \text{BF}_4$ or ClO_4 , respectively.^[81]

Phenol Ligands

To avoid the low donor capabilities of quinone ligands, Rovira et al. established an array of four states based on the oxidation of the tautomeric complex $[\text{Co}^{\text{III}}(\text{Cat-N-BQ})(\text{Cat-N-SQ})]$ (**12**).^[82] The advantage of this complex lies in the rich electrochemical behavior of the Schiff-base ligand, which can exist in up to five different oxidation forms, ranging from +1 to -3. Its cyclic voltammogram shows a one-electron oxidation process at $E_{1/2} = +0.18$ V and a reversible one-electron reduction at $E_{1/2} = -0.38$ V, both being associated with electrochemical processes occurring at ligand-based orbitals. Potential controlled electrolysis experiments demonstrated the reversibility of both redox processes, indicating no structural changes such as ligand loss or decomposition on the time-scale of the experiment. Therefore, the charged species formed from partial oxidation of complex **12** was generated chemically. Interestingly, the variable-temperature absorption spectra of a toluene solution of complex $[\text{Co}^{\text{III}}(\text{Cat-N-BQ})_2]^+$ (**12**⁺) shows the existence of an equilibrium consistent with the existence of a temperature-induced valence tautomerism [Equation (6)].



This allowed the establishment of an array of four states showing different optical and magnetic ground states by using a reversible oxidation process as an additional stimulus. In a further step, to expand the number of states within the array, Ruiz-Molina et al. converted the valence tautomeric equilibrium of complex $[\text{Mn}^{\text{IV}}(\text{Cat-N-SQ})_2]$ (**13**, Mn^{IV}) by an additional reversible oxidation process to an array of six states. The cyclic voltammogram of complex **13** shows two oxidation processes at $E_{1/2} = +0.68$ V and $E_{1/2} = +0.15$ V and a reversible reduction at $E_{1/2} = -0.46$ V (vs. Ag wire), which have been identified as electrochemical processes involving ligand-based orbitals. Therefore, the charged species **13**⁺ formed from partial oxidation of complex **13** was generated chemically. Moreover, the variable-temperature magnetic susceptibility data and electronic spectroscopy for a $[\text{D}_8]$ toluene solution of a toluene solution was consistent with the valence tautomerism shown in Equation (7).



Polychlorotriphenylmethyl Radicals

The polychlorotriphenylmethyl radical **17**, derived from the valence tautomeric complex **15**, by replacing the ferrocene unit by a permethylated ferrocene, has been converted into an array of three redox states that exhibit distinct physical properties by reduction into their diamagnetic anionic form **17**⁻ and/or oxidation into the ferrocenium radical de-

rivative **17**⁺.^[83] Interest in these molecular systems is considerable since they not only exhibit variations in color and magnetic properties but also show nonlinear optical responses due to their octupolar nature and their donor-acceptor dyad topology. Indeed, the color of the $[\text{K}([\text{18-crown-6}])^+ \text{17}^-]$ salt is deep purple, radical **17** is brown, the **17**⁺ BF_4^- salt is yellow, and the hydrocarbon **17**-H is pale pink. In accordance with their distinct colors, the optical absorption spectra of the three species **17**, **17**⁺, **17**⁻ show striking differences. Among them, is a remarkable broad intervalence charge-transfer (IVCT) absorption band in the NIR region observed for radical **17**, centered at 1520 nm which is associated with an intramolecular electron transfer from the ferrocene donor unit to the radical acceptor unit (the PTM unit). On the other hand the IVCT band is absent, in agreement with the lack of electron-donor character of the organometallic unit when it is oxidized or reduced. The dynamic hyperpolarizabilities of these three species were measured by hyper-Rayleigh scattering (HRS) experiments. In accordance with the presence of an intense IVCT band, radical **17** gives a large nonlinear optical response with a dynamic hyperpolarizability value $\beta = 545(\pm 30) \times 10^{-30}$ esu. This value is reduced almost ninefold to $66(\pm 7) \times 10^{-30}$ esu for **17**⁺, and even more for the carbanion **17**⁻ which has a $\beta = 30(\pm 3) \times 10^{-30}$ esu. The magnetic properties of the three species that have been studied are also different. Thus, while $[\text{K}([\text{18-crown-6}])^+ \text{17}^-]$ is diamagnetic, the paramagnetic susceptibility of compounds **17** and **17**⁺ BF_4^- in the solid state between 4–300 K showed quasi-ideal paramagnetic behavior with effective magnetic moments of 1.72 for **17** and $2.50 \mu_B$ for **17**⁺ BF_4^- at 300 K; as expected for systems with $S = 1/2$ and $S = 2 \times 1/2$ units.

To demonstrate the complete reversibility of the redox reactions of radical **17**, several oxidation and reduction cycles were performed. As shown in Figure 11, the optical

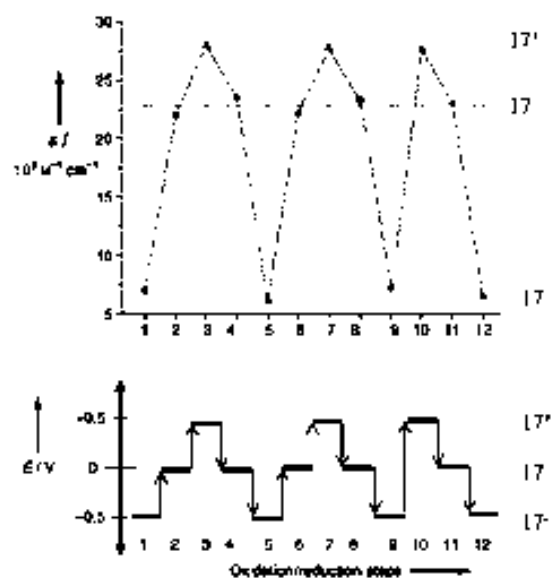


Figure 11. Cyclic stepwise oxidations and reductions carried out in THF with a chronoamperometric technique monitoring the changes in the visible spectrum for **17**-H, $[\text{K}([\text{18-crown-6}])^+ \text{17}^-]$, **17**, and **17**⁺ BF_4^- .

spectrum was recorded, after each step, and could be fully recovered after each cycle. Analogous switching behavior was also detected with EPR spectroscopy by studying the magnetic response in solution of the redox-switchable molecular array. Such chemical transformations along with the conversions by electrical stimuli led us to expect a plethora of signal transduction mechanisms should this molecular switchable array be used as a molecular logic gate. Therefore, radical **17** appeared as an ideal candidate for developing a multiproperty three-state switching molecular device governed by electrical and/or thermal inputs.

Acknowledgments

Authors are grateful to the Spanish Ministry of Education for financial support from the DGI (Spain), project MAT2003-04699 and COST Chemistry D14 Action "Functional Materials". D. R. M. would also like to thank Prof. A. Dei and Prof. D. N. Hendrickson for fruitful discussions and sharing their knowledge.

- [1] a) P. Gütllich, Y. Garcia, T. Woike, *Coord. Chem. Rev.* **2001**, 219–221, 839–879; b) O. Kahn, J. P. Launay, *Chemtronics* **1988**, 3, 140–151; c) A. Hauser, *Coord. Chem. Rev.* **1991**, 111, 275–290.
- [2] N. Sutin, *Acc. Chem. Res.* **1982**, 15, 275–282.
- [3] M. B. Robin, P. Day, *Adv. Inorg. Chem. Radiochem.* **1967**, 10, 247–422.
- [4] a) M. D. Ward, *Chem. Ind.* **1996**, 568–573; b) R. Ziessel, M. Hissler, A. El-Ghayoury, A. Harriman, *Coord. Chem. Rev.* **1998**, 178–180, 1251–1298; c) M. N. Paddon-Row, *Acc. Chem. Res.* **1994**, 27, 18–25; d) M. R. Wasielewski, *Chem. Rev.* **1992**, 92, 435–461.
- [5] J. P. Launay, *Chem. Soc., Rev.* **2001**, 30, 386–397.
- [6] For a general review on pure organic mixed-valence systems, see: D. Ruiz-Molina, J. Sedó, C. Rovira, J. Veciana, in: *Handbook of Advanced Electronic Materials and Devices* (Ed.: H. S. Nalwa) **2001**, 303–327 and references cited therein.
- [7] a) S. F. Rak, L. L. J. Miller, *J. Am. Chem. Soc.* **1992**, 114, 1388–1394; b) L. L. Miller, C. A. Liberko, *Chem. Mater.* **1990**, 2, 339–340 and references cited therein.
- [8] a) K. Lahlil, A. Moradpour, C. Bowlas, F. Menou, P. Cassoux, J. Bonvoisin, J. P. Launay, G. Dive, D. Dehareng, *J. Am. Chem. Soc.* **1995**, 117, 9995–10002.
- [9] a) S. F. Nelsen, H. Q. Tran, M. A. Nagy, *J. Am. Chem. Soc.* **1998**, 120, 298–304; b) S. F. Nelsen, R. F. Ismagilov, Y. Teki, *J. Am. Chem. Soc.* **1998**, 120, 2200–2201.
- [10] A. Dei, D. Gatteschi, C. Sangregorio, L. Sorace, *Acc. Chem. Res.* **2004**, 37, 827–835.
- [11] a) J. Bonvoisin, J. P. Launay, M. Van der Auweraer, F. C. De Schryver, *J. Phys. Chem.* **1994**, 98, 5052–5057; b) C. Lambert, G. Nöll, *J. Am. Chem. Soc.* **1999**, 121, 8434–8442; c) S. Utamapanya, A. Rajca, *J. Am. Chem. Soc.* **1991**, 113, 9242–9251.
- [12] a) J. Bonvoisin, J. P. Launay, C. Rovira, J. Veciana, *Angew. Chem. Int. Ed.* **1994**, 33, 2106–2109; b) J. Sedo, D. Ruiz, J. Vidal-Gancedo, C. Rovira, J. Bonvoisin, J. P. Launay, J. Veciana, *Adv. Mater.* **1997**, 8, 748–752.
- [13] D. M. Adams, M. Noodleman, D. N. Hendrickson, *Inorg. Chem.* **1997**, 36, 3966–3984.
- [14] a) J. S. Miller, *Adv. Mater.* **1994**, 6, 217–221; b) W. R. Entley, G. S. Girolami, *Science* **1995**, 268, 397–400; c) S. Ferlay, T. Mallah, R. Ouahes, P. Veillet, M. Verdager, *Nature* **1995**, 378, 701–702; d) T. Mallah, S. Thiebaut, M. Verdager, P. Veillet, *Science* **1993**, 262, 1554–1557; e) O. Sato, T. Iyoda, A. Fujishima, K. Hashimoto, *Science* **1996**, 271, 49–51.
- [15] R. M. Buchanan, C. G. Pierpont, *J. Am. Chem. Soc.* **1980**, 102, 4951–4957.
- [16] C. G. Pierpont, *Coord. Chem. Rev.* **2001**, 217, 99–125.
- [17] Similar differential behavior has been observed for a series of Co(CTH)(Phendiox)Y-solvent complexes: A. Bencini, A. Caneschi, C. Carbonera, A. Dei, D. Gatteschi, R. Righini, C. Sangregorio, J. Van Slageren, *J. Mol. Struct.* **2003**, 656, 141–154.
- [18] a) D. M. Adams, B. Li, J. D. Simon, D. N. Hendrickson, *Angew. Chem. Int. Ed. Engl.* **1995**, 34, 1481–1483; b) D. M. Adams, D. N. Hendrickson, *J. Am. Chem. Soc.* **1996**, 118, 11515–11528.
- [19] a) O. Sato, S. Hayami, Z.-Z. Gu, K. Takahashi, R. Nakajima, A. Fujishima, *Chem. Phys. Lett.* **2002**, 355, 169–174; b) O. Sato, S. Hayami, Z.-Z. Gu, R. Saki, R. Nakajima, A. Fujishima, *Chem. Lett.* **2001**, 874–875.
- [20] A. Cui, K. Takahashi, A. Fujishima, O. Sato, *J. Photochem. Photobiol. A: Chem.* **2004**, 167, 69–73.
- [21] C. Carbonara, A. Dei, J.-F. Letard, C. Sangregorio, L. Sorace, *Angew. Chem. Int. Ed.* **2004**, 43, 3136–3138.
- [22] F. V. R. Neuwahl, R. Righini, A. Dei, *Chemical Physics Letters* **2002**, 352, 408–414.
- [23] For the analogous spin crossover systems, studies using hydrostatic cells adapted to magnetic susceptibility, Mössbauer, optical absorption and reflectivity methods in conjunction with methods of detection such as IR, EXAFS and X-ray diffraction techniques, have been successfully used in the last years: P. Gütllich, A. B. Gaspar, V. Ksenofontov, Y. Garcia, *J. Phys.: Condens. Matter* **2004**, 16, S1087–S1108.
- [24] C. Roux, D. M. Adams, J. P. Itie', A. Polian, D. N. Hendrickson, M. Verdager, *Inorg. Chem.* **1996**, 35, 2846–2852.
- [25] A. Caneschi, A. Dei, F. F. De Biani, P. Gütllich, V. Ksenofontov, G. Levchenko, A. Hofer, F. Renz, *Chem. Eur. J.* **2001**, 7, 3926–3930.
- [26] C. G. Pierpont, C. W. Lange, *Prog. Inorg. Chem.* **1994**, 41, 331.
- [27] A. M. Costero, C. Andreu, R. Martínez-Mañez, J. Soto, L. E. Ochando, J. M. Amigó, *Tetrahedron* **1998**, 54, 8159–8170.
- [28] W. R. Cullen, J. D. Woollins, *Coord. Chem. Rev.* **1981**, 39, 1–30.
- [29] C. Rovira, *Chem. Rev.* **2004**, 104, 5289–5318.
- [30] T. Hirao, *Coord. Chem. Rev.* **2002**, 226, 81–91.
- [31] J. L. Reddinger, J. R. Reynolds, *Macromolecules* **1997**, 30, 673–675.
- [32] P. Gütllich, A. Dei, *Angew. Chem. Int. Ed. Engl.* **1997**, 36, 2734–2736.
- [33] A. Vlcek, *Comments, Inorg. Chem.* **1994**, 16, 207–228.
- [34] a) A. Bencini, A. Caneschi, A. Dei, D. Gatteschi, C. Sangregorio, D. Shultz, L. Sorace, M. G. F. Vaz, *C. R. Chimie* **2003**, 6, 663–676; b) A. Dei, D. Gatteschi, *Inorg. Chim. Acta* **1992**, 198–200, 813–822.
- [35] C. G. Pierpont, C. W. Lange, *Prog. Inorg. Chem.* **1994**, 41, 331–443.
- [36] a) C. G. Pierpont, R. M. Buchanan, *Coord. Chem. Rev.* **1981**, 38, 45–87.
- [37] The solution behavior of some nickel, rhodium and iridium complexes can also be correctly explained by valence tautomeric equilibria: a) R. R. Rakhimov, P. M. Solozhenkin, N. N. Kopitaya, V. S. Pupkov, A. I. Prokofiev, *Dokl. Akad. Nauk. SSSR* **1988**, 300, 1177; b) G. A. Abakumov, G. A. Razuvaev, V. I. Nevodchikov, V. K. Cherkasov, *J. Organomet. Chem.* **1988**, 341, 485–494; c) C. W. Lange, M. Foldeaki, V. I. Nevodchikov, V. K. Cherkasov, G. A. Abakumov, C. G. Pierpont, *J. Am. Chem. Soc.* **1992**, 114, 4220–4222.
- [38] O. Cador, A. Dei, C. Sangregorio, *Chem. Commun.* **2004**, 652–653.
- [39] a) D. M. Adams, A. Dei, A. L. Rheingold, D. N. Hendrickson, *Angew. Chem. Int. Ed. Engl.* **1993**, 32, 880–882; b) D. M. Adams, A. Dei, A. L. Rheingold, D. N. Hendrickson, *J. Am. Chem. Soc.* **1993**, 115, 8221–8229.

- [40] a) O.-S. Jung, D. H. Lee, Y. S. Sohn, C. G. Pierpont, *Inorg. Chem.* **1998**, *37*, 5875–5880; b) O.-S. Jung, D. H. Jo, Y. A. Lee, B. J. Conklin, C. G. Pierpont, *Inorg. Chem.* **1997**, *36*, 19–24; c) O.-S. Jung, C. G. Pierpont, *J. Am. Chem. Soc.* **1994**, *116*, 2229–2230.
- [41] A. Yamaguchi, K. Awaga, *J. Mater. Chem.* **2001**, *11*, 2142–2145.
- [42] O.-S. Jung, C. G. Pierpont, *J. Am. Chem. Soc.* **1994**, *116*, 2229–2230.
- [43] S. H. Bodnar, A. Caneschi, A. Dei, D. A. Shultz, L. Sorace, *Chem. Commun.* **2001**, 2150–2151.
- [44] W. Kaim, *Dalton Trans.* **2003**, 761–768.
- [45] M. S. Dooley, M. A. McGuirl, D. E. Brown, P. N. Turowski, W. S. McIntire, P. F. Knowles, *Nature* **1991**, *349*, 262–264.
- [46] a) J. Rall, W. Kaim, *J. Chem. Soc., Faraday Trans.* **1994**, *90*, 2905–2908; b) G. Speier, S. Tisza, Z. Tyeklar, C. W. Lange, C. G. Pierpont, *Inorg. Chem.* **1994**, *33*, 2041–2045.
- [47] a) W. Kaim, M. Wanner, A. Knödler, S. Zalis, *Inorg. Chim. Acta* **2002**, *337*, 163–172; b) J. Rall, M. Wanner, M. Albrecht, F. M. Hornung, W. Kaim, *Chem. Eur. J.* **1999**, *5*, 2802–2809.
- [48] G. Speier, Z. Tyeklar, P. Toth, E. Speier, S. Tisza, A. Rothenbauer, A. M. Whalen, N. Alkire, C. G. Pierpont, *Inorg. Chem.* **2001**, *40*, 5653–5659.
- [49] M. W. Lynch, D. N. Hendrickson, B. J. Fitzgerald, C. G. Pierpont, *J. Am. Chem. Soc.* **1981**, *103*, 3961–3963.
- [50] A. S. Attia, O.-S. Jung, C. G. Pierpont, *Inorg. Chim. Acta* **1994**, *226*, 91–98.
- [51] a) A. S. Attia, C. G. Pierpont, *Inorg. Chem.* **1998**, *37*, 3051–3056; b) A. S. Attia, C. G. Pierpont, *Inorg. Chem.* **1997**, *36*, 6184–6187.
- [52] A. Caneschi, A. Dei, *Angew. Chem. Int. Ed.* **1998**, *37*, 3005–3007.
- [53] H. Ohtsu, K. Tanaka, *Angew. Chem. Int. Ed.* **2004**, *43*, 6301–6303.
- [54] N. Shaikh, S. Goswami, A. Panja, X.-Y. Wang, S. Gao, R. J. Butchler, P. Banerjee, *Inorg. Chem.* **2004**, *43*, 5908–5918.
- [55] B. A. Jazdzewski, W. B. Tolman, *Coord. Chem. Rev.* **2000**, *200*–202, 633–685.
- [56] J. W. Whittaker, *Chem. Rev.* **2003**, *103*, 2347–2363.
- [57] M. M. Whittaker, P. J. Kersten, D. Cullen, J. W. Whittaker, *J. Biol. Chem.* **1999**, *274*, 36226–36232.
- [58] E. R. Altwick, *Chem. Rev.* **1967**, *67*, 475–531.
- [59] P. Chaudhuri, K. Wieghardt, *Prog. Inorg. Chem.* **2002**, *50*, 151.
- [60] A. K. Nairn, R. Bhalla, S. P. Foxon, X. Liu, L. J. Yellowlees, B. C. Gilbert, P. H. Walton, *J. Chem. Soc., Dalton Trans.* **2002**, 1253–1255 and references cited therein.
- [61] K. S. Min, T. Weyhermüller, K. Wieghardt, *Dalton Trans.* **2004**, 178–186 and references cited therein.
- [62] T. K. Paine, T. Weyhermüller, L. D. Slep, F. Neewe, E. Bill, E. Bothe, K. Wieghardt, P. Chaudhuri, *Inorg. Chem.* **2004**, *43*, 7324–7338.
- [63] This ligand may sometimes exhibit a more complicated behavior: P. Chaudhuri, M. Hess, K. Hildebrand, E. Bill, T. Weyhermüller, K. Wieghardt, *Inorg. Chem.* **1999**, *38*, 2781.
- [64] S. K. Larsen, C. G. Pierpont, *J. Am. Chem. Soc.* **1988**, *110*, 1827.
- [65] A. Caneschi, A. Cornia, A. Dei, *Inorg. Chem.* **1998**, *37*, 3419–3452.
- [66] O. Cador, F. Chabre, A. Dei, C. Sangregorio, J. Van Slageren, M. G. F. Vaz, *Inorg. Chem.* **2003**, *42*, 6432–6440.
- [67] D. Ruiz-Molina, K. Wurst, D. Hendrickson, C. Rovira, J. Veciana, *Adv. Funct. Mater.* **2002**, *12*, 347–351.
- [68] Y. Shimazaki, F. Tani, K. Fukui, Y. Naruta, O. Yamauchi, *J. Am. Chem. Soc.* **2003**, *125*, 10512–10513.
- [69] M. Ballester, *Acc. Chem. Res.* **1985**, *18*, 380–387.
- [70] D. Ruiz-Molina, J. Veciana, F. Palacio, C. Rovira, *J. Org. Chem.* **1997**, *62*, 9009–9017.
- [71] a) C. Rovira, D. Ruiz-Molina, O. Elsner, J. Vidal-Gancedo, J. Bonvoisin, J.-P. Launay, J. Veciana, *Chem. Eur. J.* **2001**, *7*, 240–250; b) O. Elsner, D. Ruiz-Molina, J. Vidal-Gancedo, C. Rovira, J. Veciana, *Nano Letters* **2001**, *1*, 117–120.
- [72] a) D. Maspoch, D. Ruiz-Molina, K. Wurst, C. Rovira, J. Veciana, *Chem. Commun.* **2002**, 2958–2959; b) D. Maspoch, D. Ruiz-Molina, K. Wurst, J. Vidal-Gancedo, C. Rovira, J. Veciana, *Dalton Transactions* **2004**, 1073.
- [73] D. Maspoch, D. Ruiz-Molina, K. Wurst, N. Domingo, J. Tejada, C. Rovira, J. Veciana, *Nature Materials* **2003**, *3*, 190–195.
- [74] I. Ratera, D. Ruiz-Molina, F. Renz, J. Enslin, K. Wurst, C. Rovira, P. Gütllich, J. Veciana, *J. Am. Chem. Soc.* **2003**, *125*, 1462–1463.
- [75] W. Kaim, B. Schwederski, *Pure Appl. Chem.* **2004**, *76*, 351–364 and references cited therein.
- [76] D. Dolphin, T. Niem, R. H. Felton, I. Fujita, *J. Am. Chem. Soc.* **1975**, *97*, 5288–5290.
- [77] D. Chang, T. Malinski, A. Ulman, K. M. Kadish, *Inorg. Chem.* **1984**, *23*, 817–824.
- [78] J. Seth, V. Palaniappan, D. F. Bocian, *Inorg. Chem.* **1995**, *34*, 2201–2206.
- [79] D. Ruiz-Molina, D. N. Hendrickson, *Submitted for Publication*.
- [80] D. Ruiz, J. Yoo, I. Guzei, A. L. Rheingold, D. N. Hendrickson, *Chem. Commun.* **1998**, 2089–2090.
- [81] D. Ruiz-Molina, L. N. Zakharov, A. L. Rheingold, D. N. Hendrickson, *J. Phys. Chem. Sol* **2004**, *65*, 831–837.
- [82] D. Ruiz-Molina, J. Veciana, K. Wurst, D. N. Hendrickson, C. Rovira, *Inorg. Chem.* **2000**, *39*, 617–619.
- [83] C. Sporer, I. Ratera, D. Ruiz-Molina, Y. Zhao, J. Vidal-Gancedo, K. Wurst, P. Jaitner, K. Clays, A. Persoons, C. Rovira, J. Veciana, *Angew. Chem. Int. Ed.* **2004**, *43*, 5266–5268.

Received: April 19, 2005

Published Online: June 28, 2005

Article II

Title: Solvent effects on valence tautomerism: A comparison between the interconversion in solution and solid state.

Authors: E. Evangelio, C. Rodriguez-Blanco, Y. Coppel, D. N. Hendrickson, J. –P. Sutter, J. Campo, and D. Ruiz-Molina,

Publication: Solid State Sciences, Accepted. DOI: 10.1016/j.solidstatesciences.2007.11.039.



Solvent effects on valence tautomerism: A comparison between the interconversion in solution and solid state

Emi Evangelio^a, Clara Rodriguez-Blanco^b, Yannick Coppel^d, David N. Hendrickson^c, Jean Pascal Sutter^d, Javier Campo^b, Daniel Ruiz-Molina^{a,e,*}

^a Institut de Ciència de Materials de Barcelona (CSIC), Esfera UAB, Campus UAB, 08193 Cerdanyola del Vallés, Catalonia, Spain

^b Instituto de Ciencia de Materiales de Aragón (CSIC), Universidad de Zaragoza, 50009 Zaragoza, Spain

^c Department of Chemistry-0358, University of California at San Diego, La Jolla, CA 92093-0358, USA

^d Laboratoire de Chimie de Coordination du CNRS, Université Paul Sabatier, 205 route de Narbonne, 31077 Toulouse, France

^e Centro de Investigación en Nanociencia y Nanotecnología, Edifici CM7, Campus UAB, 08193 Cerdanyola del Vallés, Catalonia, Spain

Received 5 June 2007; received in revised form 9 November 2007; accepted 30 November 2007

Abstract

A detailed comparative study of the valence tautomeric interconversion of complexes **1–3** in three different environments is reported. The three environments are solid state (both crystalline and amorphous materials), solution and embedded into a polymeric matrix. The VT behavior of the three complexes strongly differs from one to the other, though no systematization can be established. In solution, different solvational parameters seem to affect the equilibrium. However, such solvate effect cannot be translated either into the solid state or polymeric matrix, where the equilibrium is controlled by the vibrational relaxation of the network.

© 2007 Elsevier Masson SAS. All rights reserved.

Keywords: Valence tautomerism; Interconversion; Bistability; Solvent effects; Solid state; Polymeric matrix

1. Introduction

There is currently active interest in the development of molecular electronic devices that can be used as optical and/or magnetic data storage media [1]. Compounds of specific interest are bistable molecular materials having two nearly degenerated states with different optical and/or magnetic properties. These complexes have an appreciable sensitivity to the environment so an external perturbation, such as temperature or irradiation, may lead to an interconversion between the two degenerated electronic states. Examples of electronic labile complexes are valence tautomeric (VT) complexes [2].

Valence tautomeric metal complexes combine a transition metal ion, which can exist at least in two different oxidation states, and an electro-active ligand, both with well-defined charge localization [3]. External stimuli may induce a reversible intramolecular electron transfer between the metal ion and the redox active ligand, leading to the existence of two electronic isomers (valence tautomers) with different charge distributions, and consequently, different optical, electric and magnetic properties. An excellent example of the above mentioned charge distribution sensitivity is exhibited by cobalt bis(quinone) complexes. Complexes of the composition $[\text{Co}(3,5\text{-DTBCat})(3,5\text{-DTBSQ})(\text{N}^{\wedge}\text{N})]$, where 3,5-DTBCat²⁻ and 3,5-DTBSQ⁻ refer, respectively, to the catecholate (Cat²⁻) and semiquinonate (SQ⁻) forms of 3,5-di-*tert*-butyl-*o*-quinone, and N[^]N is a chelating diiminium ligand such as 2,2'-bipyridine (bpy, complex **1**) or 1,10-phenanthroline (phen, complex **2**), exhibit valence tautomerism [4]. These complexes can be interconverted by means of different external stimuli such as temperature [4], pressure [5] or irradiation

* Corresponding author. Centro de Investigación en Nanociencia y Nanotecnología, Edifici CM7, Campus UAB, 08193 Cerdanyola del Vallés, Catalonia, Spain. Tel.: +34 935814777; fax: +34 935813717.

E-mail address: dani@icmab.es (D. Ruiz-Molina).

[6] between a high-spin $hs\text{-}[\text{Co}^{\text{II}}(\text{SQ})_2(\text{N}^{\wedge}\text{N})]$ ($S_{\text{Co}} = 3/2 + 2 \times S_{\text{rad}} = 1/2$) or a low-spin $ls\text{-}[\text{Co}^{\text{III}}(\text{Cat})(\text{SQ})(\text{N}^{\wedge}\text{N})]$ ($S_{\text{rad}} = 1/2$) form. The nature of a valence tautomeric interconversion can be best illustrated by Scheme 1. Intramolecular electron transfer converts the $hs\text{-}[\text{Co}^{\text{II}}(\text{SQ})_2(\text{N}^{\wedge}\text{N})]$ into the $ls\text{-}[\text{Co}^{\text{III}}(\text{Cat})(\text{SQ})(\text{N}^{\wedge}\text{N})]$ form as one of the ligands is reduced by one electron from an $\text{SQ}^{\cdot-}$ to a Cat^{2-} ligand. Such an interconversion may take place both in solution and in the solid state, though with significant differences. Indeed, whereas in solution the interconversion takes place over a large temperature range, in a crystalline matrix they can interconvert cooperatively on a narrow temperature range of 40° .

In addition to the series of complexes $[\text{Co}(\text{Q})_2(\text{N}^{\wedge}\text{N})]$, valence tautomerism has also been found in transition metal ions bearing redox active Schiff base diquinone ligand such as $[\text{Co}^{\text{III}}(\text{Cat-N-BQ})(\text{Cat-N-SQ})]$ (**3**), where Cat-N-BQ stands for the tridentate ligand ((2-hydroxy-3,5-di-*tert*-butyl-1-phenyl)imino)-3,5-di-*tert*-butyl-1,2-benzoquinone ligand and the corresponding dinegative Cat-N-SQ $^{\cdot-}$ radical form. Although previously synthesized [7], the first account of VT for complex **3** was reported in 1998 [8]. The UV–vis temperature dependence of a toluene solution of complex **3** in solution suggested the existence of a valence tautomeric equilibrium between the low-spin $[\text{Co}^{\text{III}}(\text{Cat-N-BQ})(\text{Cat-N-SQ})]$ and the high-spin $[\text{Co}^{\text{II}}(\text{Cat-N-BQ})_2]$ forms close to 300 K, as deduced by the ratio between the enthalpy and the entropy changes in solution. Moreover, whereas no discrepancies between the results obtained in deuterated and non-deuterated solvents were found, appreciable differences were instead revealed between the lifetimes determined for $[\text{Co}^{\text{III}}(\text{Cat-N-BQ})(\text{Cat-N-SQ})]$ in chloroform and those obtained in dichloromethane by time-resolved spectroscopic characterization [9]. However, no tautomerism was observed in the solid state, as evidenced by the lack of changes in the variable-temperature magnetic susceptibility data up to 300 K. This fact was initially attributed to the lack of solvate molecules within the crystalline network, which are assumed to impart softness to the lattice. However, in a subsequent work [10], the same authors showed that indeed complex **3** exhibits a tautomeric interconversion in the solid state but at higher temperatures, with a transition that starts at approximately 370–380 K, i.e., at least 150 K higher than in solution [11].

The variations found for the behavior of complexes **1–3** in solution and in solid state are not atypical. In fact, it is important

to emphasize that whereas most of the valence tautomeric complexes thus far reported exhibit a temperature-dependent interconversion in solution, the number of examples exhibiting a valence tautomeric interconversion in the solid state is rather limited [12]. For this, the presence of solvate molecules within the crystalline network and their effects on the phonon relaxation play a critical role.

The question remains an open issue: how do solvate molecules and/or the nature of the environment affect the vibronic relaxation of the molecules in solution and in solid state? There are previous works that have partially faced this challenge. For instance, Dei et al. have already reported a family of complexes of general formula $[\text{Co}(\text{CTH})(\text{Phendiox})]\text{Y} \cdot \text{solv}$, where CTH stands for tetraazamacrocyclic and Phendiox for the catecholato or semiquinonato form of 9,10-dioxophenanthrene [13]. The critical interconversion temperature was found to depend not only on the nature of the counterion Y but also on the nature of the solvent trapped in the lattice. Moreover, significant hysteresis effects were detected by substituting the solvent guest molecules found within the lattice by their deuterated analogues. Hendrickson et al. reported the magnetic susceptibility data for a polycrystalline sample of complex **2**, results that were compared with the temperature dependence of a toluene solution [14] and a polystyrene film [15]. Finally, some of us have also reported the selective oxidation or reduction of one of the two tautomeric isomers shifting T_c at convenience, simply by controlling the nature of the solvent [16].

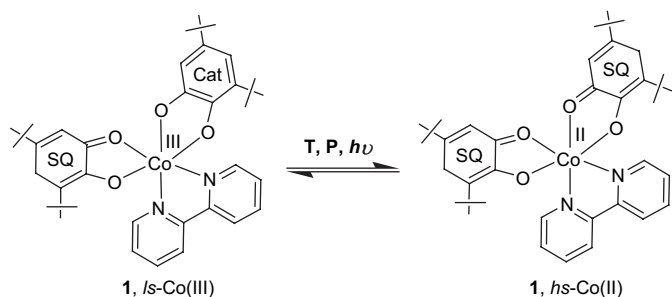
In spite of all the previous precedents that reflect the considerable influence of the environment on the VT process, a systematic study that shed light on the origin of such variations was missing. Herein we present the methodical investigation of the VT of complexes **1–3** in three different environments, which are: (I) solution, (II) solid state, for both crystalline and amorphous samples, and (III) embedded into a polymeric matrix. The results have been used to compare and rationalize the effects of the environment and nature of the matrix on the VT processes.

2. Experimental section

All the reagents used were purchased from Aldrich and Fluka and used as received unless otherwise specified. Complexes **1–3** were synthesized as previously described. Solvents were distilled prior to use to eliminate all the impurities and traces of water, which can clearly modify the VT behavior. Amorphous samples were prepared both by a fast precipitation method (avoiding any correct crystallization) and by removal of the solvent guest molecules under vacuum. Polymeric samples were prepared by dissolving a given sample into a CH_2Cl_2 solution of polycarbonate (4% of the VT compound) and deposited by spin-coating.

2.1. Physical measurements

Electronic absorption spectra were recorded with a Varian Cary05e spectrophotometer equipped with a thermostated



Scheme 1.

cell holder that can operate between 280 and 370 K. Temperature stability was better than ± 5 K. Spectra were collected after the sample had been allowed to thermally equilibrate at each temperature for 10 min. T_c , the temperature at which the isomer ratio is 1:1, was deduced from the temperature at which the peaks of the low-spin and the high-spin species exhibit similar intensities. The operating temperature window for each solvent does not allow to collect the absorption of the pure low- and high-spin species, and therefore, to have an accurate estimation of T_c . Direct current (dc) magnetic susceptibility measurements were carried out on a Quantum Design MPMS SQUID susceptometer with a 55 kG magnet and operating in the range of 1.7–320 K. All measurements were collected in a field of 10 kG. Background correction data were collected from magnetic susceptibility measurements on the holder capsules. Diamagnetic corrections estimated from the Pascal contents were applied to all data for determination of the molar paramagnetic susceptibilities of the compounds. X-ray powder diffraction data have been recorded on an INEL diffractometer (Debye–Scherrer geometry and CPS120 curved detector) which collects 120° of the diffraction circle using the $K\alpha$ radiation of copper. The sample is introduced in the diffractometer in capillars of 0.3 mm. NMR spectra were recorded on a Bruker AV500 spectrometer equipped with a 5 mm triple resonance inverse probe with dedicated 31P channel operating at 500.33 MHz for 1H equipped with a BVT3000 variable-temperature unit. TMS was used as internal reference.

2.2. Evans method

This methodology, suitable for the calculation of the number of unpaired electrons in solution samples, is based on the frequency shift of the NMR signal of a reference sample by the magnetic field of a co-dissolved paramagnetic species [17]. The relative frequency shift $\Delta\nu/\nu$ with $\Delta\nu = \nu^{\text{TMS}}(\text{Outer tube}) - \nu^{\text{TMS}}(\text{Inner tube})$, produced by the presence of the paramagnetic species is used to calculate the magnetic moment according to Eq. (1) [18],

$$\chi_g = \chi_0 + \left[\frac{(3 \times \Delta\nu)}{(2 \times \pi \times \nu_0 \times c)} \right] + \left[\frac{(\chi_0 \times (\rho_0 - \rho_s))}{c} \right] \quad (1)$$

where χ_g = mass magnetic susceptibility of the solute (cm^3/g); χ_0 = magnetic susceptibility of the solvent (cm^3/g); $\Delta\nu$ = separation in paramagnetic chemical shift (Hz); ν_0 = spectrometer radiofrequency; c = concentration (mol/mL); ρ_0 = density of the pure solvent and ρ_s = density of the solution.

Eq. (1) can be transformed then to

$$\chi_m = \chi_0 \times M' + \left[\frac{(3 \times \Delta\delta \times 10^{-6})}{(4 \times \pi \times c)} \right] \quad (2)$$

and subsequently into Eq. (3) by taking into account the diamagnetic contribution, which can be estimated as the sum of constants (called Pascal's constants) for each diamagnetic species in the sample.

$$\chi_m^{\text{corr}} = \chi_m - \sum \chi_\alpha$$

$$\chi_m^{\text{corr}} = \chi_0 \times M' + \left[\frac{(3 \times \Delta\delta \times 10^{-6})}{(4 \times \pi \times c)} \right] - \sum \chi_\alpha \quad (3)$$

Finally, χ_m^{corr} obtained from Eq. (3) is used to calculate the effective magnetic moment as shown in Eq. (4).

$$\mu_{\text{eff}} = 2828 \sqrt{(\chi_m^{\text{corr}} \times T)} \quad (4)$$

The NMR samples for susceptibility measurements using the Evans method were prepared by dissolving a weighted amount of complex **3** in a measured volume of solvent. All the experiments are done in non-deuterated solvents. For the case of toluene, the experiment was performed in both cases, not observing important differences in the results. The concentration of the paramagnetic solute was in the range of 1–2 mg mL^{-1} . The temperature-dependent density changes of the solvent were corrected using equations and data from the International Critical Tables [19]. The complex solution was transferred into a 5 mm tube containing a 1 mm capillary with the deuterated diamagnetic solvent and one drop of tetramethylsilane (TMS) as a reference. The different signal shifts found for the methyl groups of the TMS were used to determine the susceptibility in solution.

3. Results

3.1. Valence tautomerism in solution

In solution, the equilibrium shown in Scheme 1 can be induced by variations of temperature and monitored by UV–vis spectroscopy. As an example, the temperature dependence of the UV–vis spectrum for complex **1** in acetone is shown in Fig. 1.

At room temperature there is a band at 600 nm with a shoulder at ~ 800 nm characteristic of the *ls*-Co(III) isomer. SCF calculations have shown that the intense visible transition at 600 nm is likely due to $\pi-\pi^*$ transitions whereas the shoulder at ~ 800 nm is due mostly to an orbital forbidden LMCT. As the temperature of the solution is increased from 278 to 303 K, the intensity of the 600 nm band decreases while a band at ~ 770 nm increases in intensity. This band is characteristic of the *hs*-Co(II) isomer of the complex and results from an MLCT transition from a t_{2g} orbital to the SQ and by π^* orbitals. Such temperature dependence was also monitored in four additional solvents selected on the basis of their differing dielectric constants (ϵ): toluene (2.4), methylene chloride (8.9), acetone (20.7), ethanol (24.3) and acetonitrile (36.2). The temperature-dependent VT shown in Fig. 1 is fully reproduced along the series of solvents though with a major significant change: the critical temperature (T_c) is shifted from one solvent to the other [20]. Or in other words, the ratio of the absorption bands associated with each valence tautomer at the same temperature considerably differs. More precisely, T_c was shifted following the order: acetonitrile (~ 345 K) > ethanol

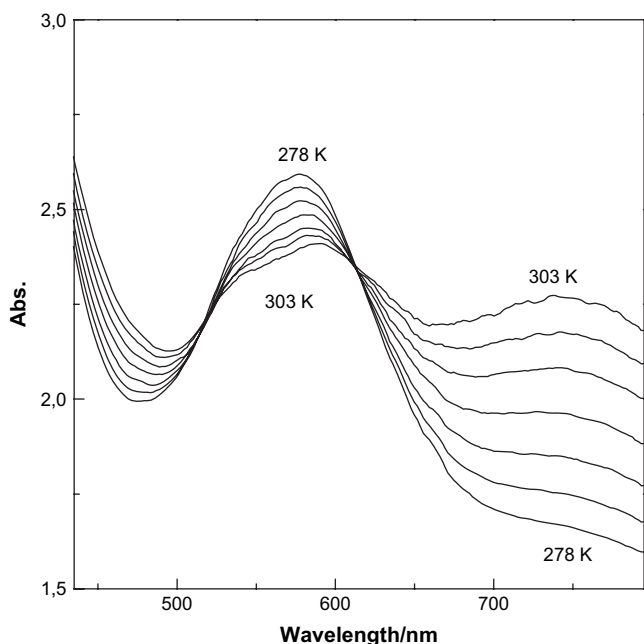


Fig. 1. Temperature dependence of the electronic absorption spectrum of an acetone solution of complex **1** in the temperature range of 278–303 K.

(~ 336 K) > methylene chloride (~ 313 K) > acetone (~ 300 K) and toluene (~ 273 K). Significantly, T_c not only is modified from one solvent to the other but shifts by almost 70 K on changing from acetonitrile to toluene.

Substitution of the bipyridine by a phenanthroline ligand in complex **2** induces a modification of its T_c value with respect to that of complex **1**. For instance, the spectrum of a toluene solution of complex **2** at 305 K is highly characteristic of a *hs*-Co(II) tautomer, as indicated by an intense broad band at 780 nm with a shoulder at 660 nm and a weaker band at 548 nm. At the same temperature, the electronic absorption spectrum of complex **1** exhibits a band at 600 nm with a shoulder at ~ 800 nm characteristic of the *ls*-Co(III) isomer. Therefore, even though the diiminum ligand is not directly involved in the electron transfer process it is modulating the relative energy of the molecular orbitals directly involved, mostly from the quinone and the metal ion. However, such substitution has no influence on the solvent dependence on the thermally induced electron transfer since both complexes exhibit the same T_c shift along the series of solvents, most likely due to the highly aromatic character of both the ligands. It is also important to emphasize that neither complex **1** nor **2** exhibits a correlation between the T_c values obtained experimentally for each solvent and their corresponding dielectric constant values. This fact evidences that the displacement of the tautomeric equilibrium most probably is not only controlled by ϵ but also by other solute–solvent interactions as discussed later on.

Finally, the temperature dependence of the electronic absorption spectrum of complex **3** along the series of five different solvents was also studied. In the case of toluene, the variable-temperature absorption spectra have been previously described by Dei et al. [9]. At high temperatures (340 K), the spectrum is dominated by two intense bands at 797 and

721 nm. As the temperature is decreased, the intensity of such bands decreases whereas that of the bands at 533, 439 and 391 nm increases. By comparison with the electronic absorption of the related model compounds $M(\text{Cat-N-SQ})_2$ ($M = \text{Zn, Al, Ge and Sn}$), the authors indicated that the spectrum of the complex is dominated by the internal transitions of the coordinated ligands. Therefore, whereas in the case of complexes **1** and **2** there are two apparent absorption bands associated to each one of the isomers that favors an estimation of T_c , in the case of complex **3** such an estimation is much more difficult since the changes on the absorption band arise mostly from variations on the internal transitions of the coordinated ligands. Accordingly, any estimation of T_c for complex **3** and its modification along the series of solvents turned out unfeasible. In any case, and for comparison purposes, the temperature dependence of the electronic absorption spectrum of solutions of complex **3** in acetonitrile, ethanol, methylene chloride and acetone was also studied. The variation of electronic absorption spectra of a solution of complex **3** in five different solvents at room temperature is shown in Fig. 2. As can be seen there, there are significant changes between them, qualitatively confirming the influence of the nature of the solvent on VT, as previously reported for complexes **1** and **2**.

The studies previously described for complex **3** involve the measurement of the intensity of the π – π and charge-transfer bands as a function of the polarity of the solvent. The concentration of the two species is however unknown as the extinction coefficients are not determined in the different solvents studied, hiding any correlation between the absorbance and the ratio of both isomers present in the solution. Moreover, the extinction coefficient may be as well disturbed by the polarity of the solvent. For this reason, as a quantitative

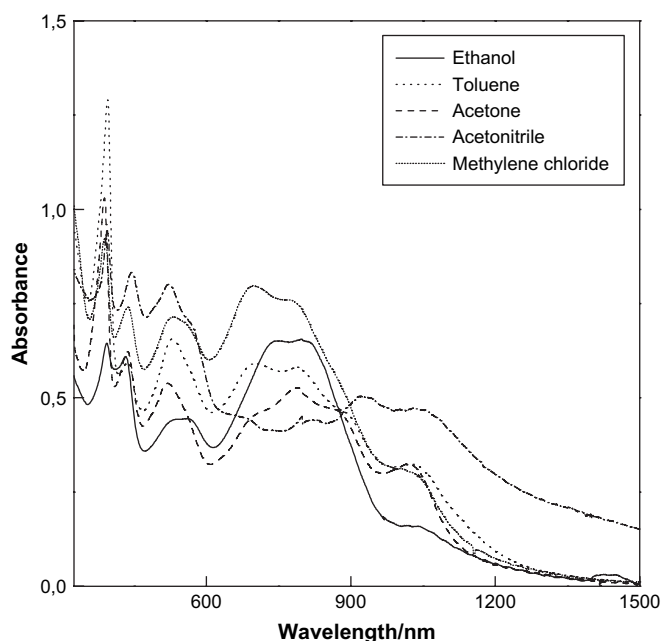
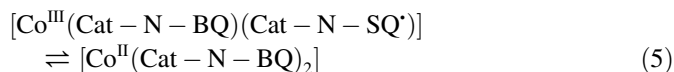


Fig. 2. Temperature dependence of the electronic absorption spectrum of complex **3** in toluene, acetonitrile, methylene chloride, acetone and ethanol at room temperature.

measurement of the solvent dependence of the valence tautomerism of complex **3** we have used the Evans method. The Evans technique is applicable to the measurement of the magnetic susceptibility in solution based on the frequency shift occasioned in an NMR signal of a standard compound, for instance TMS, by the additional magnetic field of the tested paramagnetic species. Fig. 3 shows the solution magnetic susceptibility obtained with the Evans method plotted as a function of temperature in five different solvents for complex **3**.

Even though the valence tautomeric interconversion of complex **3** in a toluene solution was already reported by Dei et al., here it was re-measured for comparison purposes. As can be seen in Fig. 3, at low temperatures the effective magnetic moment exhibits a constant value of approximately $1.6 \mu_B$, close to the theoretical value of $1.7 \mu_B$ expected for the single unpaired electron ($g = 2$) found in the low-spin $[\text{Co}^{\text{III}}(\text{Cat-N-BQ})(\text{Cat-N-SQ})]$ isomer. This value remains constant up to 220 K whereupon μ_{eff} increases up to a value of $3.7 \mu_B$ at 360 K, which is close to the theoretical value of $3.9 \mu_B$ ($g = 2$) expected for the high-spin isomer $[\text{Co}^{\text{II}}(\text{Cat-N-BQ})_2]$. Such an increase is consistent with the following valence tautomerism,



Similar behavior was observed for the methanol, acetone and chloroform solutions. In the latter case T_c is shifted towards a lower temperature although the interconversion was not completed since it usually takes place gradually over a large temperature range ($\geq 80\text{--}100^\circ\text{C}$), larger than the working temperature range of the solvent. On the contrary,

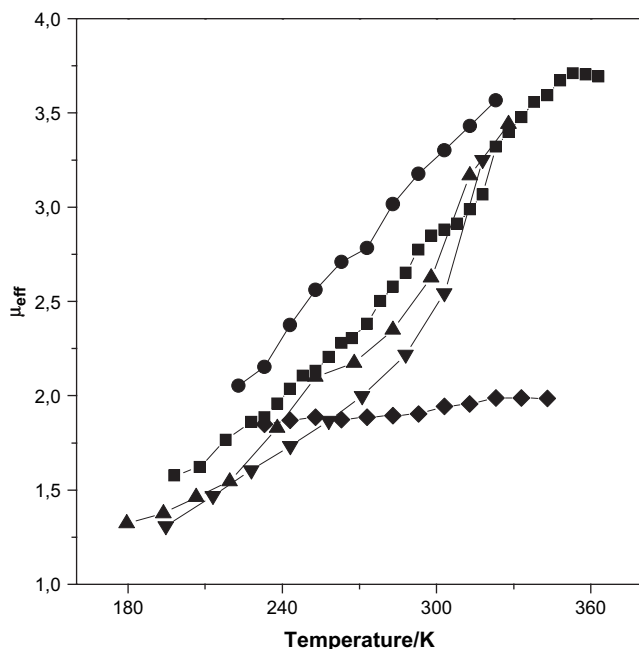


Fig. 3. Plots of the effective magnetic moment (μ_{eff}) versus temperature for complex **3** obtained by the Evans method in different solvents: chloroform (●) toluene (■), acetonitrile (◆), acetone (▼) and methanol (▲).

the acetonitrile solution exhibits a constant value of $1.8 \mu_B$ in the whole temperature range studied. This value is in agreement with the expected value for the low-spin isomer $[\text{Co}^{\text{III}}(\text{Cat-N-BQ})(\text{Cat-N-SQ})]$, indicating that no interconversion takes place at least up to 340 K.

Finally, it is important to emphasize that these results are in agreement with those previously obtained with UV–vis spectroscopy. Indeed, according to the magnetic susceptibility data shown in Fig. 3 the acetonitrile, methanol, acetone and toluene solutions of complex **3** at room temperature are mostly in the high-spin isomer $[\text{Co}^{\text{II}}(\text{Cat-N-BQ})_2]$. The UV–vis spectra of the same solutions at room temperature shown in Fig. 2 exhibit a predominant band centred around 800 nm associated to the high-spin isomer $[\text{Co}^{\text{II}}(\text{Cat-N-BQ})_2]$. On the contrary, the spectrum of an acetonitrile solution exhibits a band around 900 nm characteristic of the low-spin isomer $[\text{Co}^{\text{III}}(\text{Cat-N-BQ})(\text{Cat-N-SQ})]$, in agreement with the magnetic moment found by the Evans method. These results confirm, as previously observed for complexes **1** and **2**, the lack of a correlation between the T_c values obtained experimentally for each solvent and their corresponding dielectric constant values.

3.1.1. Valence tautomerism in solid state

Since complexes **1** and **2** exhibited a very similar solvent dependence in solution, the solid state studies were done for only one of the complexes, for simplification purposes. Variable-temperature (150–320 K) magnetic susceptibility data were gathered for five different solvates of complex **2** obtained by recrystallization in acetonitrile, toluene, methylene chloride, ethanol and acetonitrile. The X-ray powder diffraction data of the samples revealed that none of the samples was amorphous and that different crystallographic phases are obtained as a function of the solvate. For comparison purposes, the X-ray diffraction data obtained for the samples recrystallized from toluene, ethanol and acetonitrile are shown in Fig. 4. Moreover, special care was taken on the preparation of the samples for the magnetic measurements since the loss of solvent guest molecules may induce that a fraction of the sample becomes amorphous, and therefore, to fake results. For this, the crystals were always maintained within the mother liquor until the measurement is done and manipulated very rapidly along the preparation of the capsule. Finally, an amorphous sample obtained by a fast precipitation process from a mixture of ethanol and water was also studied.

The χT vs. T plot of the six samples is shown in Fig. 5. As can be observed there, the interconversion in solid state can occur abruptly even in a short temperature range of roughly 30 K. This is the case of the toluene solvate of complex **2** ($2 \cdot \text{C}_7\text{H}_8$) [4b]. From 150 to 225 K there is little change in the χT vs. T plot with a constant μ_{eff} value of $1.7 \mu_B$, which is in agreement with that expected for the unpaired electron of the *ls*- $[\text{Co}^{\text{III}}(\text{Cat})(\text{SQ})(\text{N}^{\wedge}\text{N})]$ isomer. Then, it abruptly converts from the *ls*-Co(III) to the *hs*- $[\text{Co}^{\text{II}}(\text{SQ})_2(\text{N}^{\wedge}\text{N})]$ complex in the 230–260 K range. However, when the sample is recrystallized from ethanol, the resulting crystalline sample exhibits a μ_{eff} value essentially independent of temperature and close

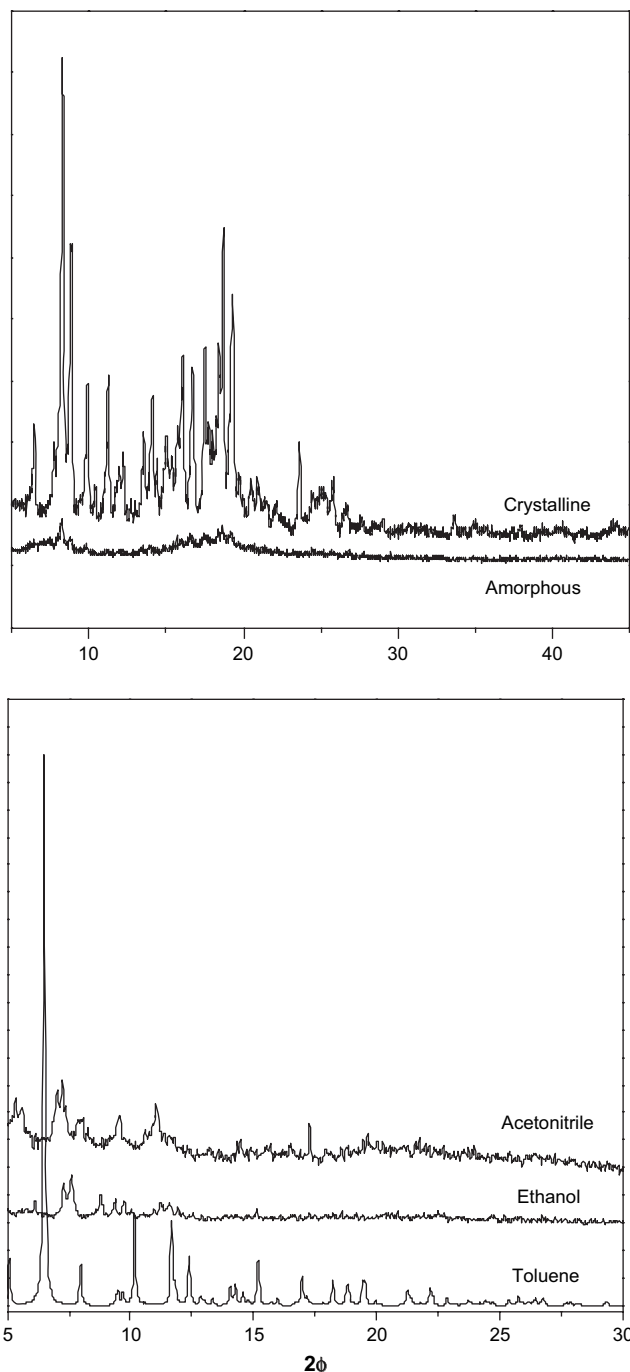


Fig. 4. Bottom: X-ray powder diffractograms of crystalline samples of complex **2** recrystallized from toluene, ethanol and acetonitrile. Top: X-ray powder diffractograms of a crystalline sample and an amorphous sample of complex **3**.

to the value of $1.7 \mu_B$. Such value confirms that this sample remains on the Is -[Co^{III}(Cat)(SQ)(N[^]N)] form along the whole temperature range. This fact indicates that either the VT interconversion is suppressed or most likely is considerably shifted to higher temperatures. Similar results were obtained for the amorphous sample. In between, the samples recrystallized from acetonitrile, acetone and methylene chloride exhibit incomplete transitions. Such variations have been attributed to a shift of T_c according to the order: toluene

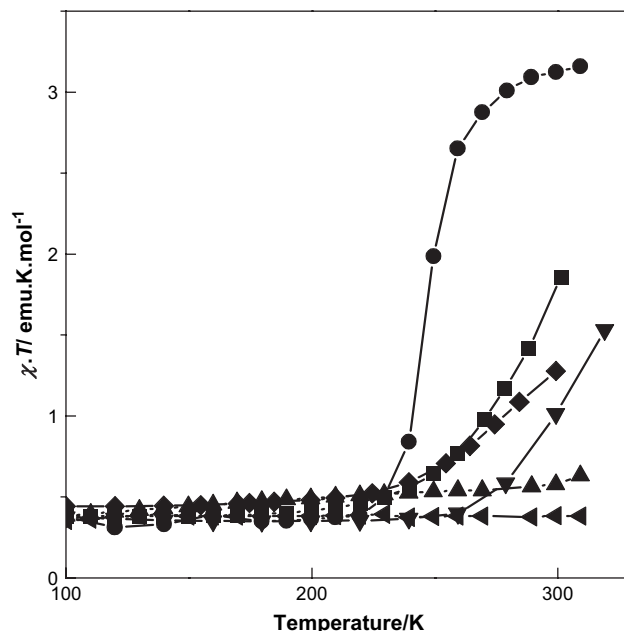


Fig. 5. Plots of the effective magnetic moment (μ_{eff}) versus temperature for complex **2** in different solvents: toluene (●) acetonitrile (■), methylene chloride (◆), acetone (▼), ethanol (▲) and an amorphous sample (◄).

< acetonitrile < acetone < methylene chloride < ethanol, which is different from that obtained in solution. This fact is a clear evidence of the different contribution of the solvent molecules on the VT process both in solution and intercalated within a crystalline network.

Surprisingly, all the attempts to obtain different crystallographic phases of complex **3** by recrystallization from different solvents were unsuccessful. Independently of the solvent, the same crystallographic phase was obtained as confirmed by X-ray powder diffraction data, preventing any study of the solvate guest influence on the VT equilibrium. The variable-temperature magnetic susceptibility data of this phase was already described by Dei et al. [9]. From low temperatures up to 360–370 K, there is little change in the χT vs. T plot with a constant μ_{eff} value of $1.7 \mu_B$, in agreement with that expected for the low-spin isomer [Co^{III}(Cat-N-BQ)(Cat-N-SQ)]. Above these temperatures, the μ_{eff} value increases monotonically beyond 500 K although the transition is not completed due to a thermal instability (decomposition) of the sample. To shed more light on to the interaction of the molecular vibronic interactions with the network, an amorphous sample was obtained and studied as a paradigm of a system with defects or with reduced intermolecular interactions. For comparison purposes, the X-ray diffraction data obtained for the crystalline and amorphous samples are shown in Fig. 4 (up). The χT vs. T plot of the amorphous sample exhibits a μ_{eff} value that increases monotonically with temperature up to 500 K, as previously described for the crystalline sample. Without any apparent reason, the disorder introduced within the network in this case did not suppress or shift the VT to much higher temperatures, as previously observed for complex **2**.

3.1.2. Valence tautomerism in a polymeric matrix

We have already reported the temperature dependence of the electronic absorption spectrum of complexes **1** and **2** doped into a polystyrene polymer [14]. The absorption spectrum of complex **2** doped into the polystyrene matrix shows that an appreciable amount of both tautomeric forms are present at 298 K while at the same temperature, its toluene solution spectrum shows only the characteristics of the *hs*-Co(II) tautomer. Similar divergence was detected for complex **1**. The absorption spectrum of its polystyrene film at 298 K displays the absorption characteristic of the **1**,*ls*-Co(III) isomer whereas in the toluene solution at room temperature the complex shows the characteristics of the *hs*-Co(II) isomer.

For comparison purposes, we have also monitored the temperature dependence of the electronic absorption spectrum of complex **3** doped into a polymeric matrix in the 295–350 K temperature range. The resulting spectra are shown in Fig. 6, where the temperature dependence of the same compound in a toluene solution is also shown for comparison purposes. As can be seen there, in this case the temperature dependence is in full agreement in both cases, in contraposition with the results obtained for complexes **1** and **2**.

4. Discussion

Valence tautomerism is an entropy driven process where the thermal population of the tautomeric states is dictated by the Gibbs free energy difference,

$$\Delta G = \Delta G_{hs-Co(II)} - \Delta G_{ls-Co(III)} = \Delta H - T\Delta S \quad (6)$$

The *hs*-Co(II) tautomer zero-point energy must lie at higher enthalpic energy than that for the *ls*-Co(III) form. At low temperatures, $T\Delta S$ is negligible compared to ΔH , and consequently if $\Delta H > kT$ only the *ls*-Co(III) state is populated. However, $T\Delta S$ is not negligible at higher temperatures, and ΔG will change sign at a critical temperature T_c where $\Delta G = 0$ and $\Delta H = T\Delta S$.

The variations of T_c observed for complexes **1–3** in the three different matrixes may come from both modulation of the zero-point energy differences between tautomeric isomers and variations of the entropy factor. Recently, Dei et al. indicated that the T_c difference between solution and solid state most likely arises from variations of the entropy factor, as deduced by comparison of the thermodynamic quantities obtained for the same VT process in a toluene solution and in solid state [8]. And this is not surprising at all. The valence tautomeric interconversion from the *ls*-Co(III) to the *hs*-Co(II) leads to a gain in electronic entropy (ΔS_{elec}) due to the higher spin state degeneracy of the *hs*-Co(II) form and the longer metal–ligand bond lengths of the *hs*-Co(II) tautomer, which result in lower energy vibrations and a higher density of vibrational states. The spin state degeneracy is not expected to vary on the different solvents under study. However, the variations on the metal–ligand bond lengths, i.e. the density of vibrational states, are expected to be strongly dependent on the surrounding matrix.

This fact can be in agreement with the results obtained in solution. Neither complex **1** nor **2** exhibits a correlation between

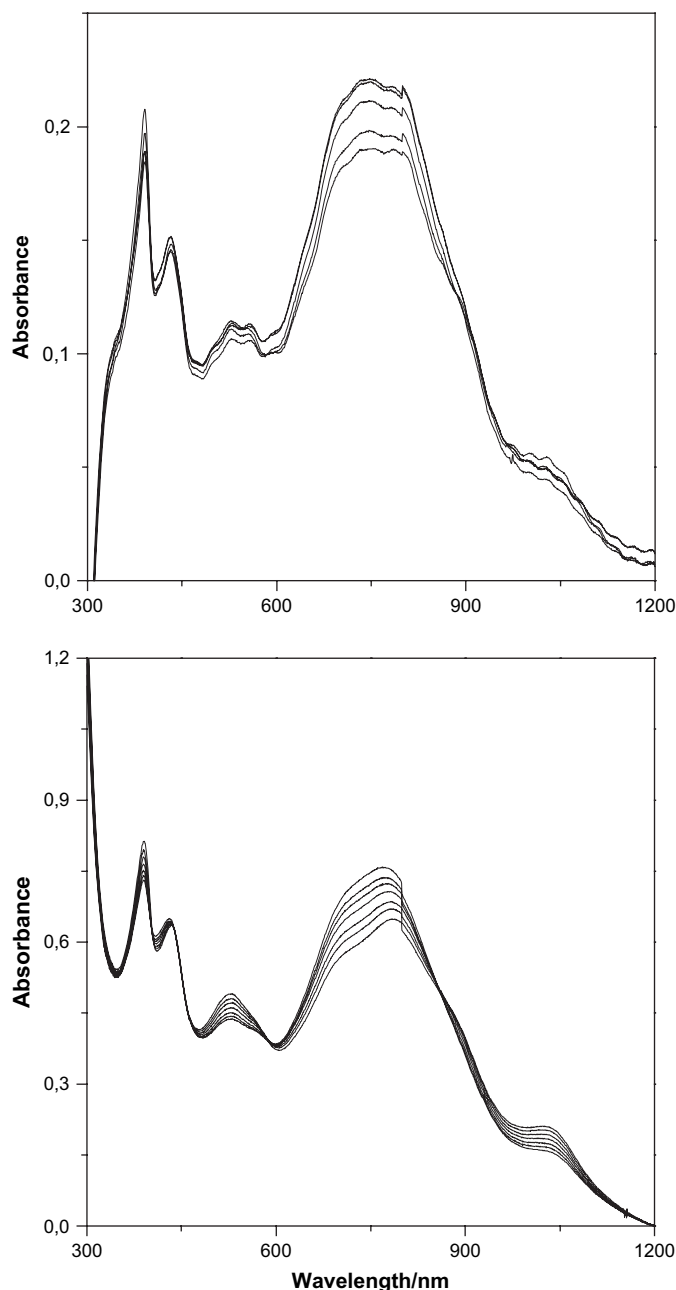


Fig. 6. Temperature dependence of the electronic absorption spectrum of complex **3** in toluene (bottom) and embedded in a polymeric matrix (top) in the 295–350 K range.

the T_c values obtained experimentally for each solvent and their corresponding dielectric constant values. This fact evidences that the displacement of the tautomeric equilibrium most probably is not only controlled by ϵ but also by other solute–solvent interactions. Since the tautomeric interconversion brings changes in the Co–L bond lengths, the endoergic term (Ω), characteristic of each solvent, probably has a reasonable influence. This term measures the required work for separating the solvent molecules to provide a suitably sized and shaped enclosure in which the solvate molecule can be accommodated.

Whereas in solution the target molecules are mostly surrounded by solvent molecules, in the crystalline network

they are surrounded by other neighbor molecules. Within such a scenario, the model of the solvational parameters previously described is not eligible any more. Accordingly, the correlation of T_c found in the different solvate crystallographic forms differs from that observed in solution. Due to the lack of their single crystal X-ray structure our structural information on the interaction between the molecules of complex **2** and the guest solvate molecules is rather poor. However, the differential “softness” that the molecules are giving to the crystalline network is clearly affecting the vibrational relaxation of the molecules. The two paradigms or extremes are the toluene solvate and the amorphous material. Whereas in the first of the cases the solvate molecules are favoring a strong cooperative effect that induces an abrupt transition over a short range of temperatures, the amorphous material is either suppressing or shifting the interconversion to much higher temperatures. Surprisingly, this was not the case for complex **3**, avoiding accordingly any a priori expectative.

Finally, significant divergences have been found between the behavior of complexes **1–2** and complex **3** embedded within a polymeric matrix. Whereas the T_c of the first two complexes is strongly modified when compared for instance with that found in a corresponding toluene solution, in the case of complex **3** no significant changes were detected. This fact can be attributed to the different interaction between the molecules and the polymeric matrix in both cases or to the inhomogeneity of the material. For instance, a phase segregation of the embedded molecules may induce their aggregation or crystallization faking all the results.

5. Conclusions

We have shown how the VT in solution can be modified simply by changing the nature of the solvent. In short, by choosing a solvent and by controlling the temperature of the solution, the tautomeric equilibrium of complexes **1–3** can be modulated and one of the two isomers can be made to be the dominant species in solution. Moreover, the T_c shift is not only controlled by ϵ but also by several other solvent parameters such as the endoergic term (Ω). For this puzzle to be solved, further experiments based on the *Linear Solvation Energy Relationship* methodology are being planned nowadays [21]. Solvent effects have also been identified in solid state although obtaining a systematic correlation between T_c and the nature of the solvent remains elusive due to the lack of the required structural information. These results are very important for future investigations in the field. Among others, they reveal the necessity to use a very systematic approach when identifying new VT candidates since the use of an inappropriate solvent may mask the VT interconversion.

Acknowledgements

We acknowledge the financial support of the Ministerio de Educación y Ciencia under grant (MAT2006-13765-C02) and the network of Excellence Magmanet. E.E. thanks the

Ministerio de Educación y Ciencia for a predoctoral grant. This work was supported by the Communauté de Travail des Pyrénées program for cooperation, research and technological development.

References

- [1] (a) P. Gütllich, Y. Garcia, T. Woike, *Coord. Chem. Rev.* 219–221 (2001) 839–879;
(b) O. Kahn, J.P. Launay, *Chemtronics* 3 (1988) 140;
(c) A. Hauser, *Coord. Chem. Rev.* 111 (1991) 275.
- [2] For a review of VT, please see: E. Evangelio, D. Ruiz-Molina *Eur. J. Inorg. Chem.* (2005) 2957.
- [3] P. Gütllich, A. Dei, *Angew. Chem., Int. Ed. Engl.* 36 (1997) 2734.
- [4] (a) D.M. Adams, A. Dei, A.L. Rheingold, D.N. Hendrickson, *Angew. Chem., Int. Ed. Engl.* 32 (1993) 880;
(b) D.M. Adams, A. Dei, A.L. Rheingold, D.N. Hendrickson, *J. Am. Chem. Soc.* 115 (1993) 8221;
(c) O.-S. Jung, D.H. Lee, Y.S. Sohn, C.G. Pierpont, *Inorg. Chem.* 37 (1998) 5875;
(d) O.-S. Jung, D.H. Jo, Y.A. Lee, B.J. Conklin, C.G. Pierpont, *Inorg. Chem.* 36 (1997) 19;
(e) O.-S. Jung, C.G. Pierpont, *J. Am. Chem. Soc.* 116 (1994) 2229.
- [5] (a) C. Roux, D.M. Adams, J.P. Itie, A. Polian, D.N. Hendrickson, M. Verdaguer, *Inorg. Chem.* 35 (1996) 2846;
(b) A. Caneschi, A. Dei, F.F. De Biani, P. Gütllich, V. Ksenofontov, G. Levchenko, A. Hofer, F. Renz, *Chem.—Eur. J.* 7 (2001) 3926.
- [6] D.M. Adams, B. Li, J.D. Simon, D.N. Hendrickson, *Angew. Chem., Int. Ed. Engl.* 34 (1995) 1481.
- [7] S.K. Larsen, C.G. Pierpont, *J. Am. Chem. Soc.* 110 (1988) 1827.
- [8] A. Caneschi, A. Cornia, A. Dei, *Inorg. Chem.* 37 (1998) 3419.
- [9] P.L. Gentili, L. Bussotti, R. Righini, A. Beni, L. Bogani, A. Dei, *Chem. Phys.* 314 (2005) 9.
- [10] O. Cador, F. Chabre, A. Dei, C. Sangregorio, J. Van Slageren, M.G.F. Vaz, *Inorg. Chem.* 42 (2003) 6432.
- [11] Similar behavior was observed in its related oxidized form: D. Ruiz-Molina, J. Veciana, K. Wurst, D.N. Hendrickson, C. Rovira *Inorg. Chem.* 39 (2000) 617.
- [12] For examples of other complexes exhibiting VT only in solution, please see: D.N. Hendrickson, C.G. Pierpont *Top. Curr. Chem.* 234 (2004) 63–95.
- [13] A. Bencini, A. Caneschi, Ch. Carbonera, A. Dei, D. Gatteschi, R. Righini, C. Sangregorio, J. Van Slageren, *J. Mol. Struct.* 656 (2003) 141.
- [14] D.M. Adams, L. Noodleman, D.N. Hendrickson, *Inorg. Chem.* 36 (1997) 3966.
- [15] D.M. Adams, D.N. Hendrickson, *J. Am. Chem. Soc.* 118 (1996) 11515.
- [16] (a) D. Ruiz, J. Yoo, I. Guzei, A.L. Rheingold, D.N. Hendrickson, *Chem. Commun.* (1998) 2089;
(b) D. Ruiz-Molina, L.N. Zakharov, A.L. Rheingold, D.N. Hendrickson, *J. Phys. Chem. Solids* 65 (2004) 831.
- [17] D.F. Evans, *J. Chem. Soc.* (1959) 2003.
- [18] S.K. Sur, *J. Magn. Reson.* 82 (1989) 169.
- [19] Values obtained from the reviews of MeOH: *J. Chem. Eng. Data* 39 (1994) 876;
Acetone: *J. Chem. Eng. Data* 42 (1997) 2;
Toluene: *J. Chem. Eng. Data* 44 (1999) 411;
Chloroform: *J. Chem. Eng. Data* 46 (2001) 2;
Acetonitrile: *J. Chem. Eng. Data* 47 (2002) 1037.
- [20] The critical temperature at which there are equal amounts of both isomers is extracted from the spectrum where the 600 and 770 nm bands exhibit the same intensity. The operating temperature window for each solvent does not allow us to determine the absorption of the pure low- and high-spin species, and therefore, to have an accurate estimation of T_c . In any case, any implicit error is expected to be much smaller than the observed difference between the T_c for the different solvents.
- [21] N. Ventosa, D. Ruiz-Molina, J. Sedo, X. Tomas, B. Andre, C. Rovira, J. Veciana, *Chem.—Eur. J.* 5 (1999) 12.

Article III

Title: Intramolecular electron transfer in the mixed-valence [Co(3,5-DTBCat)(3,5-DTBSQ)(bpy)] complex: Beyond Valence tautomerism,

Authors: E. Evangelio, D. N. Hendrickson and D. Ruiz-Molina

Publication: Inorg. Chim. Acta, 2008, Accepted. DOI: 10.1016/j.ica.2008.02.069



Contents lists available at ScienceDirect

Inorganica Chimica Acta

journal homepage: www.elsevier.com/locate/ica



Intramolecular electron transfer in the mixed-valence [Co(3,5-DTBCat)(3,5-DTBSQ)(bpy)] complex: Beyond valence tautomerism

Emi Evangelio^a, David N. Hendrickson^b, Daniel Ruiz-Molina^{a,c,*}

^a Institut de Ciència dels Materials de Barcelona (CSIC), Esfera UAB, Campus UAB, 08193, Cerdanyola del Vallès, Catalonia, Spain

^b Department of Chemistry-0358, University of California at San Diego, La Jolla, CA 92093-0358, USA

^c Centro de Investigación en Nanociencia y Nanotecnología, Esfera UAB, Campus UAB, Edifici CM7, 08193, Cerdanyola del Vallès, Catalonia, Spain

ARTICLE INFO

Article history:

Received 12 February 2008

Received in revised form 20 February 2008

Accepted 22 February 2008

Available online xxxxx

This paper is dedicated to Professor Dante Gatteschi.

Keywords:

Electron transfer
Redox active ligand
Mixed-valence
Radicals

ABSTRACT

The series of complexes [Co(Q)₂(bpy)]ⁿ ($n = -1, 0, +1$) that can be derived by partial reduction or oxidation of complex **1**, *ls*-Co(III) has been synthesized and studied. The results support the theoretical calculations which pointed to an intervalence transfer (IT) from the Cat²⁻ to the SQ⁻ ligand rather than a LMCT transition as the origin for the low-energy band transition centered at 2500 nm observed for **1**, *ls*-Co(III).

© 2008 Elsevier B.V. All rights reserved.

1. Introduction

Development of molecular-scale systems that exhibit intramolecular electron transfer phenomena induced by external stimuli has attracted considerable attention [1]. The interest is twofold. First, the possibility of inducing a reversible change in the electronic distribution of a molecular system opens the door to their potential use on information storage and integrated molecular-sized devices. And second, to study the role of various parameters governing the intramolecular electron transfer (IET) rates. Mixed-valence systems are excellent candidates for such studies since they contain at least two redox sites with different oxidation states linked by a bridge that mediates the transfer of electrons from one site to the other [2].

The study of molecular mixed-valence systems was initiated by Taube's seminal work on compounds such as [(NH₃)₅Ru-bridge-Ru(NH₃)₅]⁵⁺. Since then, most of the mixed-valence complexes shown to exhibit intramolecular electron transfer phenomena are homo and heteronuclear metallic complexes [3] or metallocene [4] units where the two metal atoms with different oxidation states are connected through an organic bridging ligand. Mixed-valence

molecular systems where the electro-active units are pure organic groups have so far received less attention, probably due to their high instability, [5] although for these systems electron transfer could be fine-tuned in a far more precise way thanks to the flexibility of organic synthesis. The different types of electroactive organic units so far used are: (i) anion-radicals derived from conjugated diquinones and diimides [6], (ii) cation-radicals derived from bis(tetrathiafulvalenes) [7], (iii) cation-radicals derived from bis(hydrazines) [8], (iv) quinoid groups [9] and (v) ion-radicals derived from π -conjugated polyarylmethyl/polyarylamines [10] and polychlorotriphenylmethyl radicals [11]. Finally, a third type of mixed-valence systems are heterogeneous complexes combining both, redox-active ligands and transition metal ions. These complexes exhibit a reversible intramolecular electron transfer between the metal ion and the ligand, leading to an internal charge redistribution and therefore to the existence of two different electronic isomers. This family of complexes has been termed with the generic term of valence-tautomerism (VT).

Valence-tautomeric complexes exhibit localized electronic structures with well-defined charges for the metal and the ligands where the charge distribution is dictated by the nature of the counterligand and the metal center [12]. An excellent example of the above mentioned charge distribution sensitivity is exhibited by cobalt bis(quinone) complexes. Complexes of the composition [Co(3,5-DTBCat)(3,5-DTBSQ)(NⁿN)], where 3,5-DTBCat²⁻ and 3,5-DTBSQ⁻

* Corresponding author. Address: Institut de Ciència dels Materials de Barcelona (CSIC), Esfera UAB, Campus UAB, 08193, Cerdanyola del Vallès, Catalonia, Spain.
E-mail address: dani@icmab.es (D. Ruiz-Molina).

refer, respectively, to the catecholate (Cat^{2-}) and semiquinonate (SQ^-) forms of 3,5-di-*tert*-butyl-*o*-quinone, and N^{N} is a chelating diiminium ligand such as 2,2'-bipyridine (bpy, complex **1**) or 1,10-phenanthroline (phen, complex **2**), exhibit valence tautomerism. These complexes can be interconverted in solution or in the solid state by means of different external stimuli such as temperature [13], pressure [14] or irradiation [15] between a high-spin $[\text{Co}^{\text{II}}(\text{SQ})_2(\text{N}^{\text{N}})]$ (*hs*- Co^{II}) or a low-spin $[\text{Co}^{\text{III}}(\text{Cat})(\text{SQ})(\text{N}^{\text{N}})]$ (*ls*- Co^{III}) form. Intramolecular electron transfer converts the *hs*- Co^{II} into a *ls*- Co^{III} complex as one of the ligands is reduced by one electron from a SQ^- to a Cat^{2-} ligand. The nature of a valence-tautomeric interconversion can be best illustrated by Fig. 1 [16].

The valence-tautomeric interconversion can be induced by temperature changes and monitored by different spectroscopic and magnetization techniques. As an example, the temperature dependence of the electronic spectrum for complex **1** in CH_2Cl_2 is shown in Fig. 2. At room temperature there is a band at 600 nm with a shoulder at ~ 800 nm which is characteristic of the **1**, *ls*- Co^{III} isomer. SCF calculations have shown that the intense visible transition at 600 nm is likely due to $\pi-\pi^*$ transitions whereas the shoulder at ~ 800 nm is due mostly to an orbital forbidden LMCT [17]. As the temperature of the solution is increased from 278 to 303 K, the intensity of the 600 nm band decreases while a band at ~ 770 nm increases in intensity. This band is characteristic of the *hs*- Co^{II} isomer of the complex and is originated by a MLCT transition from a t_{2g} orbital to the SQ^- and bpy π^* orbitals.

Interestingly, accompanying the changes of the variable-temperature UV-Vis spectra of this family of complexes, large changes in the near-infrared (near-IR) are also observed. For instance, the temperature dependence of the electronic absorption spectra of complex **2** doped into a polystyrene polymer film in the visible and near-IR regions over the temperature range of 280–25 K, is shown in Fig. 2. At low temperatures, a band at 2500 nm associated with the **2**, *ls*- Co^{III} isomer appears. By comparison to the solution spectra, an approximate molar extinction coefficient (ϵ) at the maximum absorption of this low-energy band of $2000 \text{ cm}^{-1} \text{ M}^{-1}$ was given (see Fig. 2b).

The exact origin of this low-energy band transition has been the subject of some speculation. This band has been assigned as a transition from the highest occupied $\text{Cat}^{2-} 3b_1 \pi^*$ orbital to the lowest unoccupied cobalt e_g^* molecular orbital, i.e., as a LMCT transition from the Cat^{2-} ligand to the *ls*- Co^{III} ion [18]. An alternative assignment is that *ls*- Co^{III} complexes with a semiquinonate and a catecholate ligand are analogous of classical mixed-valence complexes [19] and as a consequence, the low-energy band transition arises from an intervalence transfer (IT) from the Cat^{2-} to the SQ^- ligand [17]. These compounds may be considered as a reversal of the ligand-bridged mixed-valence complexes where the extent to which metal ions are electronically coupled depends upon orbital interactions with the bridge. This assignment was supported by self-consistent field (SCF) nonlocal density functional

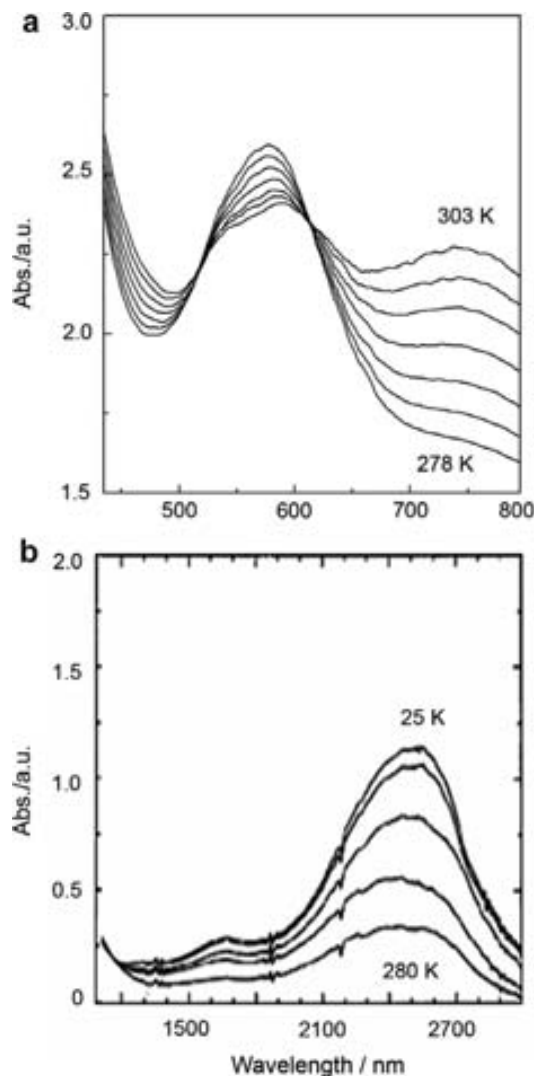


Fig. 2. (a) Temperature dependence of the electronic absorption spectrum of a CH_2Cl_2 solution of complex **1**. (b) Temperature dependence of the electronic absorption spectrum of a polystyrene film of complex **2** obtained at 280, 200, 150, 80, and 25 K.

calculations for **2**, *ls*- Co^{III} , which showed that the lowest energy transition involves an intervalence transfer of an electron from the predominantly $\text{Cat}^{2-} 3b_1 \pi^*$ HOMO to the $\text{SQ}^- 3b_1 \pi^*$ orbital. To best illustrate this attribution, a schematic representation of the different IET processes that can take place in complex **1** are shown in Fig. 3.

The generation of different species that can be derived by partial oxidation and/or reduction of a given compound have been used to follow and demonstrate the existence of IT bands in pure organic mixed-valence systems. For instance, Veciana et al. have studied the intramolecular electron transfer (IET) phenomena in the series of complexes derived from a nanoscopic diradical composed of two PTM radical units and different phenylene units [20]. Such diradical and the corresponding dianionic species obtained by its double reduction can be regarded in principle as full-valence species that do not exhibit IT bands. On the contrary, the radical-anion obtained by partial reduction should be regarded as a mixed-valence species exhibiting an IT band centered at 1400 nm. In this paper we have followed such strategy to discuss the exact origin of the low-energy band transition that appears at 2500 nm for **1**, *ls*- Co^{III} . Detailed information of the synthesis and characterization of the series of complexes $[\text{Co}(\text{Q})_2(\text{bpy})]^n$

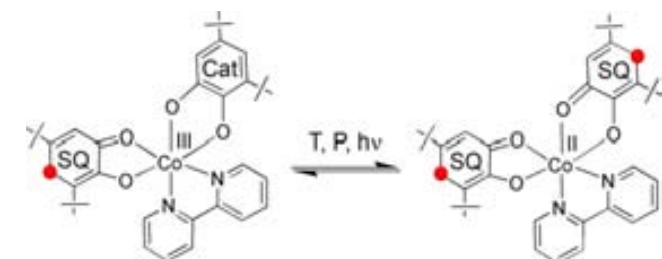


Fig. 1. Valence-tautomeric transformation of complex **1** under the influence of temperature (T), pressure (P) and light ($h\nu$).

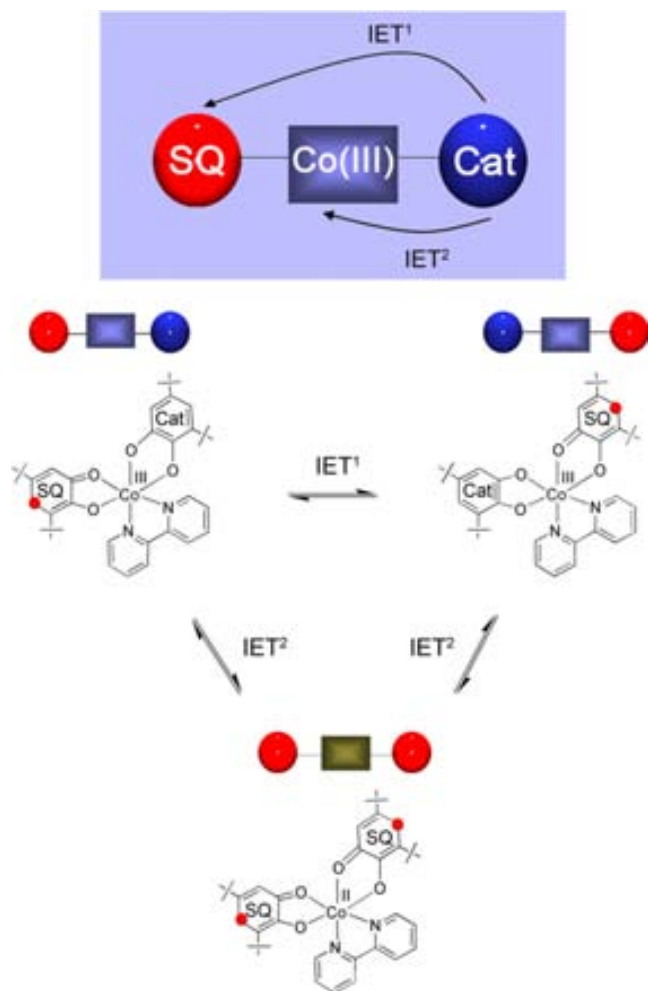


Fig. 3. (Top) A mixed-valence compound is made up of three components: a donor unit, an acceptor unit and a bridge that allows the electron transfer between both electrophores. (Bottom) Schematic representation of the two different electron transfer mechanisms that can take place in **1**, *ls*-Co(III).

($n = -1, 0, +1$) that can be derived by partial reduction or oxidation of complex **1** is reported [21]. Such a series represents an excellent scenario for the study of the IT band since only the neutral species **1**, *ls*-Co(III) can be formally considered as a mixed-valence whereas the corresponding oxidized and reduced species are not. Accordingly, the observation of an IT band is expected only for the neutral form **1**, *ls*-Co(III).

2. Experimental

2.1. Compound preparation

All the reagents used were purchased from Aldrich and Fluka and used as received unless otherwise specified. Samples of complex **1** were synthesized as previously described [22]. All the reactions were carried out using degassed solvents and manipulated under argon atmosphere.

2.2. $[Co(Cp)_2][Co^{III}(3,5-DTBCat)_2(bpy)]$ (**3**)

Cobaltocene (58 mg, 0.31 mmol) was added to a solution of complex $[Co^{III}(3,5-DTBCat)(3,5-DTBSQ)(bpy)]$ (**1**, *ls*-Co(III)) (200 mg, 0.31 mmol) in CH_2Cl_2 (15 mL) in an oxygen-free environment. The

resulting dark green solution was stirred for 3 h at 273 K. The solution was concentrated approximately to one half by slow evaporation of the solvent, appearing a dark-green microcrystalline material that was filtered in an oxygen-free atmosphere. The microcrystalline product was dried under vacuum (70% yield). *Anal. Calc.* for $C_{48}H_{58}N_2O_4Co_2$: C, 68.20; H, 6.94; N, 3.33. *Found:* C, 68.07; H, 7.04; N, 3.63%.

2.3. $[Co^{III}(3,5-DTBSQ)_2(bpy)] \cdot Cl$ (**4**)

Complex $[Co^{III}(3,5-DTBCat)(3,5-DTBSQ)(bpy)]$ (**1**, *ls*-Co(III)) (300 mg, 0.46 mmol) was dissolved in degassed 95% EtOH (20 mL) with an oxidant mixture of HCl/H₂O₂. This mixture was stirred under argon for 3 h, during which time the solution turned an intense olive-green color. The solution was concentrated approximately to one half by slow evaporation of the solvent, to give an olive-green microcrystalline material that was dried under vacuum (30%). *Anal. Calc.* for $C_{38}H_{48}N_2O_4Co_2Cl$: C, 65.70; H, 7.00; N, 4.04. *Found:* C, 65.24; H, 7.18; N, 4.28%.

2.4. Physical measurements

Electronic absorption spectra were recorded with a Hewlett-Packard 8452 A diode array spectrophotometer. Measurements above room temperature were obtained using a Hewlett-Packard 89054 A thermostated cell holder connected to a Fisher Model 800 Isotherm circulating temperature bath. Temperature stability was better than ± 5 K, being spectra collected after the sample had been allowed to thermally equilibrate at each temperature for 10 min. For electronic spectra run at temperatures below room temperature, the sample cell was placed in a Janis Model 8DT-SVT-OPT dewar equipped with optical windows. Temperature control was achieved with a Lake-Shore Model DST-80D temperature controller and a Model DT-470-SD-13 silicon diode. This factory diode is located below the sample region, a second diode (Lake-Shore, DT-500-DRC) has also been installed at a position approximately equidistant above the sample region. The average of the reading on the two diodes was taken as the temperature of the sample. Near-IR spectra were recorded with a Varian Cary05e spectrophotometer. Direct current (dc) magnetic susceptibility measurements were carried out on a Quantum Design MPMS SQUID susceptometer with a 55KG magnet and operating in the range of 1.7–320 K. All measurements were collected in a field of 10 kG. Background correction data were collected from magnetic susceptibility measurements on the holder capsules. Diamagnetic corrections estimated from the Pascal contents were applied to all data for determination of the molar paramagnetic susceptibilities of the compounds. EPR spectra were recorded on a Bruker ESP-300E spectrometer operating in the X-band (9.3 GHz). Signal-to-noise ratio was increased by accumulation of scans using the *F/F* lock accessory to guarantee a high-field reproducibility. Precautions to avoid undesirable spectral line broadening such as that arising from microwave power saturations and magnetic field over-modulation were taken. To avoid dipolar broadening, the solutions were carefully degassed three times using vacuum cycles with pure Ar. The *g* values were determined against the DPPH standard ($g = 2.003$). Infrared spectra were collected on a Nicolet Magna-IR spectrometer 556 with samples prepared as a KBr pellets. Electrochemical experiments were carried out on a BAS CV-50W using a Ag/Ag⁺ electrode as a reference electrode and a platinum spiral wire as the working electrode and a platinum thread as the counter electrode. Anhydrous CH_2Cl_2 was freshly distilled over P₂O₅ under nitrogen. Commercial tetrabutylammonium hexafluorophosphate (Fluka, electrochemical grade) was used as the supporting electrolyte.

3. Results

3.1. Electrochemistry

Electrochemical characterization of complex **1** in CH_2Cl_2 with 0.1 M $^n\text{Bu}_4\text{PF}_6$ as supporting electrolyte was done. In CH_2Cl_2 at 273 K complex **1** is mostly in the **1**, *ls*-Co(III) isomer as revealed from its variable-temperature electronic spectra. Its cyclic voltammogram at 273 K shows two well-defined processes at $E_{1/2}$ of -0.34 and $+0.25$ V versus Ag wire (E_0 of ferrocene under the same experimental conditions is $+0.36$ V). Previous electrochemical studies on different *o*-quinone transition metal complexes have shown that the electrochemical processes, by either chemical or electrochemical means, occur at the quinone ligands [23]. Therefore, the redox couple observed at $E_{1/2}$ of -0.34 V can be associated to the reduction of the semiquinone ligand to the catecholate form, whereas the second redox process is characteristic of the oxidation of the catecholate ligand to the semiquinone form. The study of the scan rate (ν) dependence of the two redox processes showed a linear dependence of the peak current with respect $\nu^{1/2}$ suggesting that these electrochemical processes are reversible and diffusion-controlled. Potential-controlled electrolysis experiments also confirmed the possibility to oxidize and reduce reversibly the low-spin **1**, *ls*-Co(III) isomer. This fact is an indication of no structural changes such as ligand loss or decomposition in the time scale of the experiment and that the corresponding ionic species are capable of being generated chemically.

The voltammetric response of complex **1** at different temperatures was also studied (see Fig. 4). A study of the influence of the temperature on the cyclic voltammetric behavior of these complexes is interesting in that the valence-tautomeric interconversion can be followed by changes in the redox properties of both isomers. As the temperature is increased, slight shifts of the redox processes into the direction of more positive potentials and the apparition of new redox processes at approximately -0.75 and $+0.40$ V, most likely assigned to the *hs*-Co(II), are observed. To assign unequivocally the shift in the potentials to the equilibria *ls*-Co(III)/*hs*-Co(II) and not to change of the potential of the reference electrode with the temperature, an internal standardization of the peak potentials was used. In the case that the shift arises from a change in the potential of the reference electrode, the differences between the peak potentials ($\Delta E_{\text{anodic}} = E_{\text{a}}^2 - E_{\text{a}}^1$ and $\Delta E_{\text{cathodic}} = E_{\text{c}}^2 - E_{\text{c}}^1$) of the first and second redox processes do not depend the temperature and/or the liquid junction potential. The

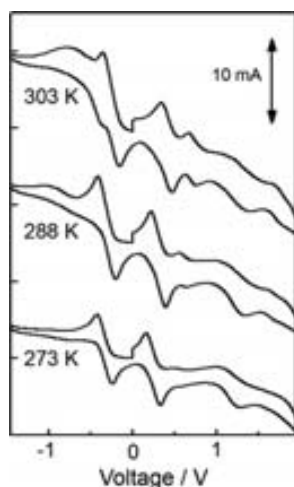


Fig. 4. Variable-temperature cyclic voltammetry of complex **1** in CH_2Cl_2 at 273, 288 and 303 K with 0.1 M $^n\text{Bu}_4\text{PF}_6$ as supporting electrolyte.

set of redox processes at $E_{1/2}$ of -0.34 and $+0.25$ V move in different manner ($\delta\Delta E_{\text{a}}/\delta T \neq \delta\Delta E_{\text{c}}/\delta T \neq 0$) concluding that the shift in the potentials is related with the tautomeric equilibria, and not to a change in the potential of the reference electrode. However, since the tautomeric interconversion in solution occurs gradually over a large temperature range, it was impossible to shift completely the tautomeric equilibrium to the **1**, *hs*-Co(II) isomer.

3.2. Synthesis

In CH_2Cl_2 at 273 K complex **1** is mostly in the **1**, *ls*-Co(III) form as shown by its variable-temperature electronic spectra. Therefore, treatment of $[\text{Co}^{\text{III}}(3,5\text{-DTBCat})(3,5\text{-DTBSQ})(\text{bpy})]$ (**1**, *ls*-Co(III)) in CH_2Cl_2 at 273 K with 1 equiv of CoCp_2 yielded $[\text{Co}^{\text{III}}(3,5\text{-DTBCat})_2(\text{bpy})][\text{CoCp}_2]$ (**3**) as a dark-green microcrystalline material. Complex **3** is highly air-sensitive, reason why all the manipulations were carried out under a strict oxygen-free environment. The corresponding oxidation reaction was carried out in methanol instead of CH_2Cl_2 for solubility reasons. Complex **1** in methanol at 273 K, which is also mostly in the **1**, *ls*-Co(III) form [24], was oxidized by a $\text{H}_2\text{O}_2/\text{HCl}$ mixture, following a procedure previously described by Wicklund et al. for the oxidation of catecholate ligands [25]. This reaction yielded an olive-green microcrystalline material characterized as $[\text{Co}^{\text{III}}(3,5\text{-DTBSQ})_2(\text{bpy})] \cdot \text{Cl}$ (**4**). All attempts to obtain single crystals of complexes **3** and **4** suitable for X-ray diffraction were unsuccessful. Both complexes were fully characterized both by chemical (see Section 2) and physical means as explained next.

3.3. Magnetism

Variable-temperature magnetic susceptibility data in the 2–300 K temperature range under an external magnetic field of 10 kG were obtained. Such measurements confirmed the $S=0$ ground state of complex $[\text{Co}^{\text{III}}(3,5\text{-DTBCat})_2(\text{bpy})][\text{CoCp}_2]$ (**3**), as expected for a diamagnetic complex with a *ls*-Co(III) metal ion and two catecholate ligands. The μ_{eff} of **4** at 300 K was $2.8 \mu_{\text{B}}$, close to that expected for a *ls*-Co(III) complex with two semiquinone ligands ($\mu_{\text{eff}} = 2.5 \mu_{\text{B}}$). Then, the magnetic moment dropped slightly to $2.6 \mu_{\text{B}}$ at 50 K, whereupon a steeper drop down to $2.1 \mu_{\text{B}}$ at 5.0 K can be observed most likely due to the presence of semiquinone–semiquinone intra- and/or intermolecular antiferromagnetic interactions. The magnetization data for **1**, *ls*-Co(III) is similar to that previously reported [22]. The sample exhibits a μ_{eff} value essentially independent of the temperature and close to the value of $1.7 \mu_{\text{B}}$, close to that expected for a *ls*-Co(III) complex with one semiquinone ligands ($\mu_{\text{eff}} = 1.8 \mu_{\text{B}}$).

EPR spectroscopy is also a useful tool to characterize transition metal *o*-quinone complexes since provides valuable information on the location of unpaired spin density within the complex. In the case of cobalt valence-tautomeric complexes, the main information available from EPR spectra is the cobalt hyperfine interaction. EPR spectroscopy has been used to show that the unpaired spin density in *ls*-Co(III) complexes with coordinated SQ^- ligands resides predominantly on the SQ^- ligand. However, some spin density is delocalized onto the cobalt ion since a signal centered at $g=2$ split into eight hyperfine lines due to the hyperfine coupling to the ^{59}Co ($I=7/2$) nucleus. In the present work X-band EPR spectra were run for toluene/ CH_2Cl_2 (1:1) solutions of complexes **1**, *ls*-Co(III) and **4** at 300 K. The EPR spectrum of **1**, *ls*-Co(III) shows a signal centered at $g=2.0$ split into eight lines due to the hyperfine coupling to the ^{59}Co nucleus, with a hyperfine coupling constant of $a(^{59}\text{Co}) = 12.0$ G. The EPR spectrum obtained for a 10^{-4} M toluene/ CH_2Cl_2 solution of **4** at 300 K is shown in Fig. 5. Similar signals were observed for complex **4**, which exhibits in this case an hyperfine coupling constants $a(^{59}\text{Co})$ of 10.1 G. No hyperfine interactions

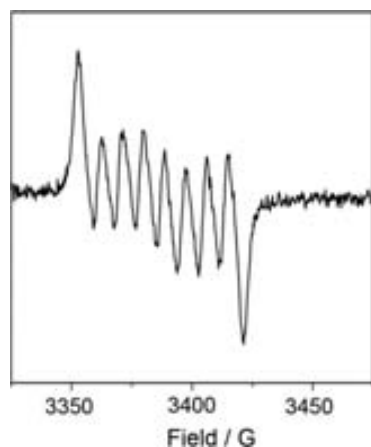


Fig. 5. EPR spectrum obtained for a 10^{-4} M toluene/ CH_2Cl_2 solution of **4** at 300 K.

arising from coupling of the proton in the *para* position of the oxygen was observed.

It has been clearly shown that the oxidation states of these complexes clearly influence the spin density distribution along the semiquinone-derived complexes. The hyperfine couplings with the ^{59}Co nucleus, which are a reflection of the spin density on the cobalt nucleus, changed following the order: **1**, *ls*-Co(III) ($a(^{59}\text{Co}) = 12.0$ G) > **4** ($a(^{59}\text{Co}) = 10.1$ G). Similar tendency has been observed for the previously reported double-oxidized complex $[\text{Co}^{\text{III}}(\text{3,5-DTBSQ})(\text{bpy})_2](\text{BF}_4)_2$, which shows a ^{59}Co hyperfine coupling constant of 8.4 G [26]. This fact seems to evidence that an increase of the overall positive charge of the complex tends to localize more the electron distribution on the quinone-derived ligand leaving less on the Co^{3+} ion.

3.4. Electronic and vibrational spectroscopy

The electronic spectrum of complexes **3** and **4** were taken at low temperatures (200 K) to avoid band broadening effects and/or additional electron transfer processes. The spectrum of complex **3** exhibits an intense band at 405 nm and a second less intense transition at 610 nm whereas the spectrum of complex **4** is dominated by intense bands below 400 nm and a characteristic band at 720 nm. Interestingly, during the reduction and oxidation reactions of complex **1**, *ls*-Co(III) the intensity of the band centered at 2500 nm disappears completely, behavior characteristic of an IT band.

FT-IR spectra of complexes **1**, *ls*-Co(III), **3** and **4** were registered on KBr pellets. IR spectroscopy is also a useful tool to define the oxidation state of the quinone-derived ligands, since each oxidation state of the ligand display a characteristic pattern of peaks. Coordinated quinones, semiquinones and catecholates display C–O frequencies in the range $1600\text{--}1675\text{ cm}^{-1}$, $1400\text{--}1500\text{ cm}^{-1}$ and $1250\text{--}1480\text{ cm}^{-1}$, respectively. As shown in Fig. 6, the spectrum of **1**, *ls*-Co(III) is dominated by two strong absorptions at $1450\text{--}1500$ and 1000 cm^{-1} . The spectrum of **3** shows a C–O peak at $\sim 1250\text{ cm}^{-1}$ characteristic of a catecholate ligand although the FT-IR spectrum of **4** does not provide clear evidence of its oxidation state. Finally, a peak in the high energy region of the spectra associated to the IT band tailing into the IR region, is observed only for **1**, *ls*-Co(III), whereas for **3** and **4** no peak is observed. This broad peak can be associated to the IT band previously observed with the electronic spectroscopy since the 2500 nm band tails into the IR region. This is a further confirmation that no IT band is observed for complexes **3** and **4** since it rules out any decomposition and/or shift of the band towards lower energies.

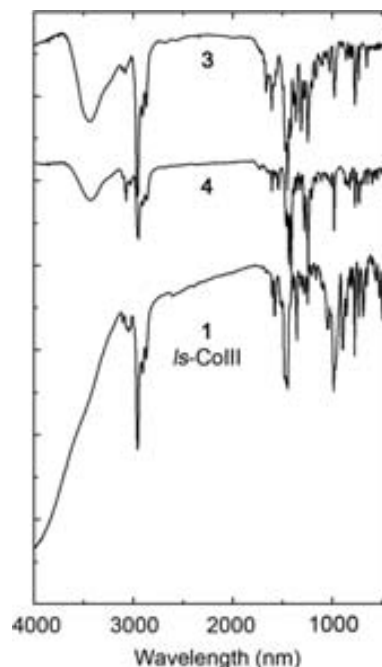


Fig. 6. FT-IR spectra of complexes **1**, *ls*-Co(III), **3** and **4** registered on KBr pellets.

4. Discussion

An important question that has been raised within the family of complexes with the general formula $[\text{M}(\text{DTBCat})(\text{DTBSQ})(\text{N}^{\text{N}})]$ containing mixed-charge ligands concerns the extent to which interligand (intramolecular) electron transfer occurs. These compounds may be considered as a reversal of the ligand-bridged mixed-valence metal complexes where redox-active quinone ligands are electronically coupled to an extent that depends upon orbital interactions with the bridge. In this sense, Prokofev et al. have demonstrated the dynamic exchange of charge between ligands on the complexes $[\text{P}(\text{3,5-DBSQ})(\text{3,5-DBCat})_2]$ and for the $[\text{M}(\text{3,6-DBSQ})(\text{3,6-DBCat})_2]^{2-}$ ($\text{M} = \text{Si}, \text{Sn}$) anions [27]. Among transition metal compounds, Pierpont et al. showed by EPR that the radical spin in $[\text{Ga}(\text{tmeda})(\text{3,6-DBSQ})(\text{3,6-DBCat})]$ is equally distributed over both ligands [28]. This fact has been assigned to an intramolecular rather than to an intermolecular mechanism for charge transfer between the two ligands as confirmed by the absence of a concentration dependence. Interestingly, no evidence of an IT band was observed in this case. More controversy arises for the series of complexes Co(III) and Mn(III) which show transitions at low energy, in the $2000\text{--}3000$ nm region. Whereas Pierpont et al. assigned this band as a LMCT transition from the Cat^{2-} ligand to the *ls*-Co(III) ion, some of us assigned such a low-energy band to an intervalence transfer (IT) from the Cat^{2-} to the SQ^- ligand.

Although X-band EPR spectroscopy could be a useful tool to discard any of the two previous assignments since it provides valuable information on the location of unpaired spin density in the complex, this was not the case for the cobalt complex. The spectrum of **1**, *ls*-Co(III) at 300 K shows an isotropic signal consisting of a pattern of eight signals due to the interaction of the cobalt-59 nucleus ($I = 7/2$) with the unpaired electron spin of the semiquinone ligand with a $a(^{59}\text{Co}) = 12.0$ G. A frozen glass solution of the same complex displays a broader eight line apparently isotropic signal with a ^{59}Co coupling that almost double that found at higher temperatures. This could be a signature of spin delocalization over the two equivalent quinone ligands, which usually decreases the

magnitude of the hyperfine coupling by half. However the broadening of the spectrum at different temperatures is similar to that found by our group in single quinone cobalt complexes [26], which initially discards this possibility. Coupling to the ring protons of one or both quinone ligands could also provide information on charge localization on the EPR time scale although unfortunately no hyperfine interactions arising from coupling of the proton are resolved.

In this paper, the generation of the different species that can be derived by partial oxidation or reduction of complex **1**, *ls*-Co(III) has been used to confirm the origin of such band. **1**, *ls*-Co(III) should be regarded as a mixed-valence species in view of the simultaneous existence of a catecholate and semiquinone, the donor and acceptor units respectively, whereas the bridge that allows the transfer of electrons from one site to the other is the Co(III) metal ion. On the contrary, complexes **3** (with two catecholates) and **4** (with two semiquinones) can be regarded in principle as full-valence species (see Fig. 7) for which no IT band is expected. Accordingly, the experimental results evidenced that the band centered at 2500 nm vanishes along the course of the reversible oxidation and reduction of **1**, *ls*-Co(III), being a signature of its origin as an inter-valence transition [29]. Should a LMCT transition from the $\text{Cat}^{2-} 3b_1 \pi^*$ to the lowest unoccupied cobalt e_g^* molecular orbital be the origin for the 2500 nm band, a similar band should be also observed for **3**, which is not the case.

Therefore, following the classification of Robin and Day [30], it is possible to classify this system as a class II not only as the intramolecular electron transfer from the ligand to the metal (valence tautomerism) is concerned, but also from one ligand to the other. Accordingly, the more realistic picture for all the intramolecular electron transfer processes present in **1**, *ls*-Co(III) is best described by the triple-well potential energy curve shown in Fig. 8.

Coupling between SQ^- and Cat^{2-} ligands in $[\text{Co}(3,5\text{-DTB-Cat})(3,5\text{-DTBSQ})(\text{bpy})]$ is expected to take place through the π type orbitals involving the metal ion though other mechanisms can not be discarded at this point [28]. For instance, Pierpont et al. pointed out the possibility to have rapid electron transfer even for systems where electronic coupling between the ligands is very weak

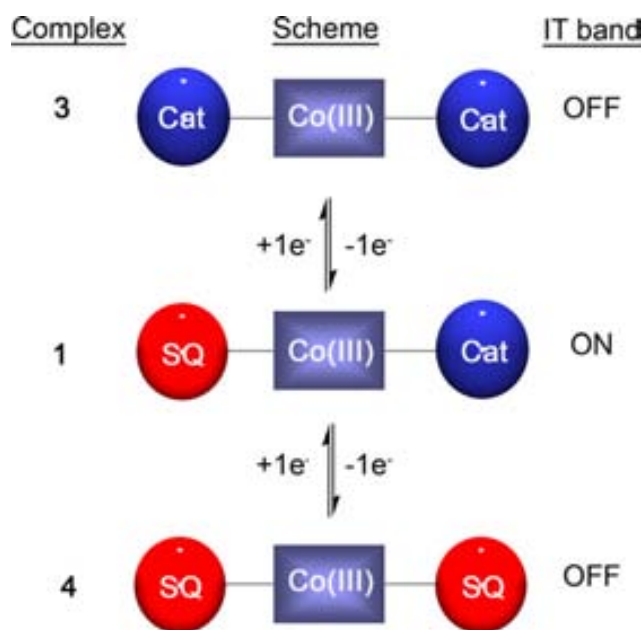


Fig. 7. Evolution of the species formed during the course of the reversible oxidation and reduction of **1**, *ls*-Co(III). Only for **1**, *ls*-Co(III) intramolecular electron transfer (IT) phenomena can be observed.

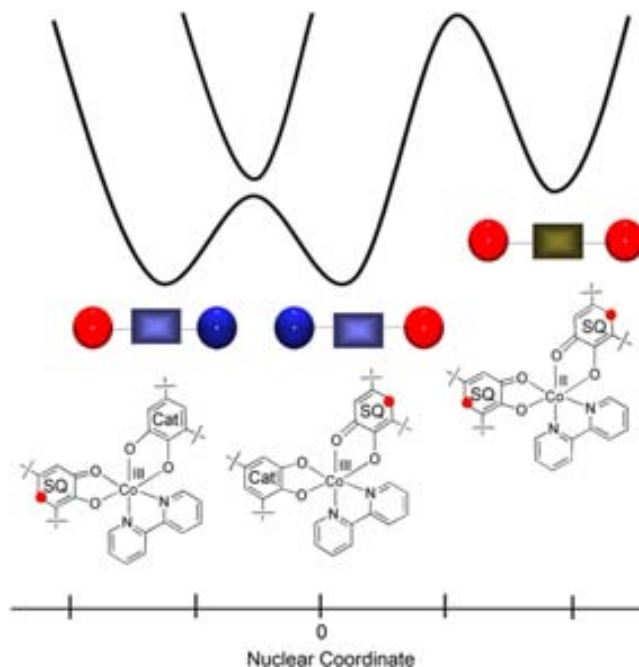


Fig. 8. Resulting potential energy curve considering the two different electron transfer mechanisms present in complex **1**.

or negligible. This was the case of complex $[\text{Ga}(\text{tmeda})(3,6\text{-DBSQ})(3,6\text{-DBCat})]$ where the intramolecular electron transfer was tentatively assigned to take place through a tunneling mechanism and/or through the solvent shell since no significant π -bonding of the quinone ligands with the metal was observed. Further studies to understand the mechanism by which the IET takes place are currently underway.

Acknowledgments

This work was supported by projects MAT2006-13765-C02 and the european network of excellence MAGMANet. E.E. thanks the Ministerio de Ciencia y Tecnología for a predoctoral grant. The authors also thank Professor Veciana for fruitful discussions and the use of its group facilities.

References

- [1] (a) P. Gütllich, Y. Garcia, T. Woike, *Coordin. Chem. Rev.* 219–221 (2001) 839; (b) O. Kahn, J.P. Launay, *Chemtronic* 3 (1988) 140; (c) A. Hauser, *Coordin. Chem. Rev.* 111 (1991) 275.
- [2] N. Sutin, *Acc. Chem. Res.* 15 (1982) 275.
- [3] (a) M.D. Ward, *Chem. Ind.* (1996) 568; (b) R. Ziessel, M. Hissler, A. El-Ghayoury, A. Harriman, *Coordin. Chem. Rev.* 178–180 (1998) 1251; (c) M.N. Paddon-Row, *Acc. Chem. Res.* 27 (1994) 18; (d) M.R. Wasielewski, *Chem. Rev.* 92 (1992) 435; (e) J.P. Launay, *Chem. Soc. Rev.* 30 (2001) 386.
- [4] (a) T.M. Figueira-Duarte, V. Lloveras, J. Vidal-Gancedo, A. Gégout, B. Delavaux-Nicot, R. Welter, J. Veciana, C. Rovira, J.-F. Nierengarten, *Chem. Commun.* 42 (2007) 4345; (b) S. Barlow, D. O'Hare, *Chem. Rev.* 97 (1997) 637. and references cited therein.
- [5] For a general review on pure organic mixed-valence systems, see: D. Ruiz-Molina, J. Sedó, C. Rovira, J. Veciana, in: *Handbook of Advanced Electronic Materials and Devices*, H.S. Nalwa (Ed.), 2001, p. 303, and references cited therein.
- [6] (a) S.F. Rak, L.L.J. Miller, *J. Am. Chem. Soc.* 114 (1992) 1388; (b) L.L. Miller, C.A. Liberko, *Chem. Mater.* 2 (1990) 339. and references cited therein.
- [7] (a) K. Lahlii, A. Moradpour, C. Bowlas, F. Menou, P. Cassoux, J. Bonvoisin, J.P. Launay, G. Dive, D. Dehareng, *J. Am. Chem. Soc.* 117 (1995) 9995.
- [8] (a) S.F. Nelsen, H.Q. Tran, M.A. Nagy, *J. Am. Chem. Soc.* 120 (1998) 298; (b) S.F. Nelsen, R.F. Ismagilov, Y. Teki, *J. Am. Chem. Soc.* 120 (1998) 2200.

- [9] A. Dei, D. Gatteschi, C. Sangregorio, L. Sorace, *Acc. Chem. Res.* 37 (2004) 827.
- [10] (a) J. Bonvoisin, J.P. Launay, M. Van der Auweraer, F.C. De Schryver, *J. Phys. Chem.* 98 (1994) 5052;
(b) C. Lambert, G. Nöll, *J. Am. Chem. Soc.* 121 (1999) 8434;
(c) S. Utamapanya, A. Rajca, *J. Am. Chem. Soc.* 113 (1991) 9242.
- [11] (a) O. Elsner, D. Ruiz-Molina, J. Vidal-Gancedo, C. Rovira, J. Veciana, *Nano Lett.* 1 (2001) 117;
(b) J. Sedo, D. Ruiz, J. Vidal-Gancedo, C. Rovira, J. Bonvoisin, J.P. Launay, J. Veciana, *Adv. Mater.* 8 (1997) 748.
- [12] E. Evangelio, D. Ruiz-Molina, *Eur. J. Inorg. Chem.* (2005) 2957.
- [13] (a) D.M. Adams, A. Dei, A.L. Rheingold, D.N. Hendrickson, *Angew. Chem., Int. Ed. Engl.* 32 (1993) 880;
(b) D.M. Adams, A. Dei, A.L. Rheingold, D.N. Hendrickson, *J. Am. Chem. Soc.* 115 (1993) 8221.
- [14] C. Roux, D.M. Adams, J. Itie, A. Polian, D.N. Hendrickson, M. Verdagner, *Inorg. Chem.* 35 (1996) 2846.
- [15] (a) D.M. Adams, B. Li, J.D. Simon, D.N. Hendrickson, *Angew. Chem., Int. Ed. Engl.* 34 (1995) 1881;
(b) D.M. Adams, D.N. Hendrickson, *J. Am. Chem. Soc.* 118 (1996) 11515.
- [16] (a) D.N. Hendrickson, C.G. Pierpont, *Top. Curr. Chem.* 234 (2004) 63;
(b) P. Gütllich, A. Dei, *Angew. Chem., Int. Ed. Engl.* 36 (1997) 2734;
(c) D.A. Shultz, in: J.S. Miller, M. Drillon (Eds.), *Magnetism: Molecules to Materials*, vol. II, Wiley-VCH, Weinheim, 2001, pp. 81–306;
(d) P. Gütllich, Y. Garcia, H.A. Goodwin, *Chem. Soc. Rev.* 29 (2000) 419.
- [17] D.M. Adams, L. Noodleman, D.N. Hendrickson, *Inorg. Chem.* 36 (1997) 3966.
- [18] O.S. Jung, C.G. Pierpont, *Inorg. Chem.* 33 (1994) 2227.
- [19] In mixed-valence complexes electron transfer phenomena can be monitored easily by the study of intervalence transitions which usually appear in the near-IR region: C. Creutz, *Prog. Inorg. Chem.* 30 (1983) 1.
- [20] C. Rovira, D. Ruiz-Molina, O. Elsner, J. Vidal-Gancedo, J. Bonvoisin, J.P. Launay, J. Veciana, *Chem. Eur. J.* 7 (2001) 240.
- [21] A partial communication of this work has already been reported D. Ruiz, J. Yoo, I. Guzei, A.L. Rheingold, D.N. Hendrickson, *Chem. Commun.* (1998) 2089.
- [22] R.M. Buchanan, C.G. Pierpont, *J. Am. Chem. Soc.* 102 (1980) 4951.
- [23] A.B.P. Leven, P.R. Auburn, E.S. Dodsworth, M. Haga, W. Liu, M. Melnik, W.A. Nerven, *J. Am. Chem. Soc.* 110 (1988) 8076.
- [24] The solvent dependence of the VT for complex **1** has already been reported. E. Evangelio, C. Rodriguez-Blanco, Y. Coppel, D.N. Hendrickson, J.P. Sutter, J. Campo, D. Ruiz-Molina, doi:10.1016/j.solidstatesciences.2007.11.039.
- [25] P.A. Wicklund, L.S. Beckman, D.G. Brown, *Inorg. Chem.* 15 (1976) 1996.
- [26] D. Ruiz-Molina, L.N. Zakharov, A.L. Rheingold, D.N. Hendrickson, *J. Phys. Chem. Solids* 65 (2004) 831.
- [27] (a) S.P. Solodovnikov, N.N. Bubnov, A.I. Prokofev, *Usp. Khim.* 49 (1980) 1;
(b) R.R. Rakhimov, S.P. Solodovnikov, V.S. Pupkov, A.I. Prokofev, *Isv. Akad. Nauk SSSR* (1990) 1385.
- [28] C.W. Lange, B.J. Conklin, C.G. Pierpont, *Inorg. Chem.* 33 (1994) 1276.
- [29] (a) T.-Y. Liu, Y.J. Chen, C.C. Tai, K.S. Kwan, *Inorg. Chem.* 38 (1999) 674;
(b) A.-C. Ribou, J.-P. Launay, K. Takahashi, T. Nihira, S. Tarutani, C.W. Spangler, *Inorg. Chem.* 33 (1994) 1325;
(c) N.S. Hush, *Coordin. Chem. Rev.* 64 (1985) 135.
- [30] M.B. Robin, P. Day, *Adv. Inorg. Chem. Radiochem.* 10 (1967) 247.

Article IV

Title: Synthesis, X-Ray Structure and Reactivity of Sterically Protected Azobisphenol Ligand: On the Quest for New Multifunctional Active Ligands

Authors: E. Evangelio, J. Saiz, D. Maspoch, K. Wurst, F. Busque and D. Ruiz-Molina

Publication: Eur. J. Inorg. Chem., 2008, 2278.

Synthesis, X-ray Structure and Reactivity of a Sterically Protected Azobisphenol Ligand: On the Quest for New Multifunctional Active Ligands

Emi Evangelio,^[a] Javier Saiz-Poseu,^[b] Daniel Maspocho,^[b] Klaus Wurst,^[c] Felix Busque,^{*,[d]} and Daniel Ruiz-Molina^{*,[a,e]}

Keywords: Azobisphenol ligand / Acid–base behaviour / Multifunctional ligands / Valence tautomerism / Chromophores

Different synthetic routes have been explored for the synthesis of the sterically protected 2,2'-dihydroxy-4,3,4,3'-tetra-*tert*-butylazobenzene ligand (**2**), which is an excellent candidate for the development of valence tautomeric complexes. As expected, such a ligand exhibits good reactivity with transition-metal ions, as shown by the synthesis and characterization of the new cobalt complex $[\text{Co}(\mathbf{2}^{2-})(\text{H}_2\text{O})_3]\text{Cl}\cdot$

2.5EtOH·H₂O (**8**). This fact together with the reversible deprotonation/protonation of the phenol groups has been used to create a chromophoric array of three states with significantly different colours, which can interconvert reversibly between them.

(© Wiley-VCH Verlag GmbH & Co. KGaA, 69451 Weinheim, Germany, 2008)

Introduction

There is currently active interest in the development of molecular electronic devices that can be used as optical and/or magnetic data storage media.^[1] Compounds of specific interest are bistable molecular materials having two nearly degenerated states with different optical and/or magnetic properties.^[2] These complexes have an appreciable sensitivity to the environment so an external perturbation, like photons or temperature, may lead to an interconversion between the two degenerated electronic states. Examples of electronic labile complexes are valence tautomeric complexes.^[3] Valence tautomeric metal complexes with at least two redox-active centres, the metal ion and an electroactive ligand, are characterized by the existence of two electronic isomers (valence tautomers).^[4] The interconversion between the two electronic isomers is accomplished by a reversible intramolecular electron transfer involving the metal ion and the redox-active ligand. Interestingly, each isomer exhibits different charge distributions, and consequently, different optical, electric and magnetic properties.^[5]

Ligands that display different oxidation states when coordinated to metallic centres have been broadly studied by both theoretical^[6] and experimental means.^[7] However, we

must emphasize that even though the number of redox-active ligands is considerable, those exhibiting valence tautomerism are rather limited since they must simultaneously satisfy two conditions: (i) the degree of covalency in the interaction between the metal ion and electroactive ligand must be low, and (ii) the energy of their frontier orbitals must be similar.^[8]

Most of the complexes that so far have shown to exhibit valence tautomerism are transition-metal complexes of quinone or quinone-based ligands.^[9] Nevertheless, the number of electroactive ligands inducing valence tautomerism is expanding with the inclusion of new electroactive ligands such as tetraphenylporphyrin,^[10] polychlorotriphenylmethyl^[11] and phenoxy radicals.^[12] Among them, phenoxy radicals are monovalent oxygen radical species that exhibit delocalization of the unpaired electron over the aromatic ring with *ortho* and *para* substituents that give steric protection.^[13] Several groups have prepared metal–phenoxylate complexes, which give new insights into the chemical factors that govern the generation and stability of this type of radical.^[14] It is worth mentioning the work developed by Wieghardt et al; they established that bidentate *O,N*-coordinated *o*-aminophenolato ligands can be found in different protonation and oxidation levels: *o*-imidophenolate(2⁻) anions, *o*-iminobenzosemiquinonate(1⁻) radical monoanions or even *o*-iminobenzoquinone. All these forms can exist in coordination compounds, as confirmed by low-temperature X-ray crystallography.^[15] A further step has been the study and characterization of *O,N,O*-coordinated ligands containing two phenolate donor groups, such as 2-[(3,5-bis(1,1-dimethylethyl)-6-hydroxyl-2,4-cyclohexadien-1-ylidene)amino]-4,6-bis(1,1-dimethylethyl)phenol (**1**).^[16] These ligands, in addition to producing phenoxy radicals in the presence of air, exhibit better chelating capabilities and good π -donor

[a] Institut de Ciència dels Materials de Barcelona (CSIC), Esfera UAB, 08193 Bellaterra, Catalonia, Spain

[b] Institut Català de Nanotecnologia, Campus UAB, 08193 Bellaterra, Catalonia, Spain

[c] Institut für Allgemeine Anorganische und Theoretische Chemie, Universität Innsbruck, Innrain 52a, Innsbruck, Austria

[d] Chemistry Department, Universitat Autònoma de Barcelona, Campus UAB, 08193 Bellaterra, Catalonia, Spain

[e] Centre de Nanociència i Nanotecnologia, Campus UAB, 08193 Bellaterra, Catalonia, Spain
Fax: +34-935814777
E-mail: dani@icmab.es

atoms that stabilize higher oxidation states, a fact that has allowed the observation of valence tautomerism in some of their complexes.^[17]

The advantages of the valence tautomeric complexes obtained from the Schiff base ligand **1** over transition-metal complexes with *o*-quinone ligands are considerable. First, valence tautomeric Schiff base complexes display higher stabilities in atmospheric oxygen in solution and in the solid state.^[18] Second, the differences between the optical properties of the isomers involved in the valence tautomerism of the cobalt Schiff base complex are enhanced relative to those observed for cobalt complexes with *o*-quinone ligands. Third, the Schiff base ligand exhibits a richer electrochemical behaviour since it can exist in different oxidation forms, ranging from +1 to -3, which may lead to stable coordination complexes with several metal ions in a variety of oxidation states.^[19]

Because of the interest in this family of ligands, we focused our attention on obtaining new bisphenol ligands similar to **1**, particularly bearing additional functional groups that can add a multifunctional character to the valence tautomeric behaviour. For this, 2,2'-dihydroxy-4,3,4,3'-tetra-*tert*-butylazobenzene (**2**) would be an excellent candidate. While keeping the same coordination capability and steric protection of the radicals through the presence of *tert*-butyl groups, the incorporation of the azo group ensures a multifunctional character thanks to their wide spread application as dyes, acid–base indicators and histological stain applications, among others.^[20] Moreover, the possibility to use azo compounds as electron–acceptor or radical ligands in transition-metal species has already been reported.^[21] However, in spite of its interest, reports on **2** have so far been scarce – there is a report on a Cu^{II} complex obtained as a side product^[22] and on a cumbersome and harsh low-yield synthesis.^[23]

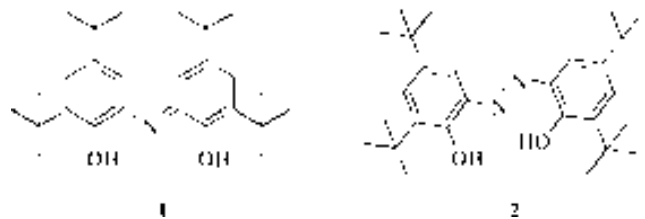
Herein we report on the exploration of several new synthetic routes for the synthesis of azobisphenol **2**, and include the one-pot synthesis of a related Co^{III} complex. In addition, both its acid–base character based on the presence of the phenol groups and its reactivity with transition-metal ions has been used to develop a chromophoric sensor. This fact adds value to the synthesis of **2** since the colour change of chromogenic sensors provides an informative and important signal for its use in analyte-sensing, environmental and biomedical applications.^[24]

Results and Discussion

Synthesis of **2**

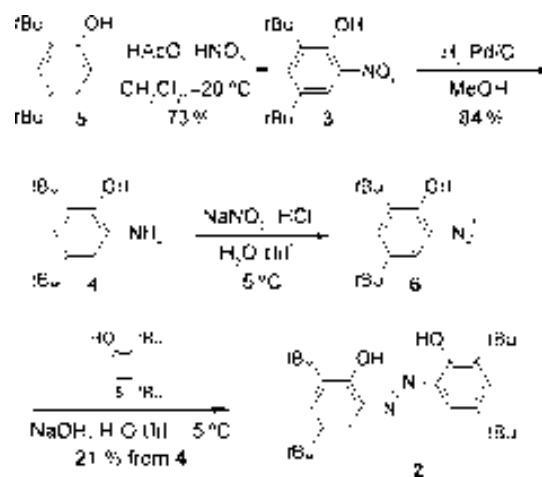
In the present work, four different synthetic approaches for the synthesis of azobisphenol **2** were initially envisaged.^[25–28] Our first synthetic trials toward the synthesis of **2** (Scheme 1) were done following three different routes,^[26–28] without any success. When nitro derivative **3** was exposed to reductive coupling conditions, either with LiAlH₄^[26a] or with the Pb⁰/HCOONH₄ system,^[26b] no desired diazo product **2** was obtained, and only the starting

material and aniline **4** were recovered. Similarly, oxidative coupling of aniline **4** with cetyltrimethylammonium dichromate^[27] failed, and degradation products were obtained. The *tert*-butylation reaction^[28] of 2,2'-dihydroxy-azobenzene was also tested, though no traces of the desired product were obtained.



Scheme 1. Molecular structures of **1** and **2**.

Fortunately, an alternative synthetic route, which in fact is the most extended synthetic strategy for the synthesis of this type of compounds,^[25] was most successful (see Scheme 2). Initially, nitrophenol **3** was obtained in a 73% yield by nitration of phenol **5** following a modified experimental route previously described.^[29] The reaction was performed at about -20 °C to avoid the side dinitration reaction. Compound **3** was then reduced by using Pd/C in methanol^[30] to afford aniline **4** in an 84% yield. Finally, the coupling reaction^[25] of the diazonium salt **6**, derived from aniline **4** with phenol **5**, afforded the diazo derivative **2** in 21% yield. This last reaction was performed under slightly basic or neutral conditions to avoid conversion of the diazonium salt to the corresponding diazohydroxide compound.



Scheme 2. Route for the synthesis of **2**.

Crystal Structure of **2**

The molecular and crystal structure of **2** was investigated by X-ray single crystal analysis. The crystallographic data and experimental parameters are summarized in Table 4. Selected bond lengths and angles are also given in Table 1. Molecule **2** crystallizes in the *C2/c* monoclinic space group, and the cell parameters are reported in Table 4. An ORTEP

view of **2** is shown in Figure 1. The high molecular symmetry is reflected by the presence of an inversion centre, which leads to a *trans* geometry of the hydrazone group with respect to both quinone moieties. This configuration seems to be favoured by two intramolecular hydrogen bonds between O1–H...N1 with distances of 1.695 Å and angles of 148.6°.

Table 1. Selected bond lengths [Å] and angles [°] for **2**.

Bond lengths			
N1–N1'	1.280(2)	O1–C1	1.357(1)
N1–C2	1.406(2)		
C1–C2	1.406(2)	C4–C5	1.406(2)
C2–C3	1.401(2)	C5–C6	1.390(2)
C3–C4	1.373(2)	C6–C1	1.498(2)
Angles			
C2–N1–N1'	117.1(1)		
O1–C1–C2	120.7(1)		
C1–C2–N1	125.1(1)		

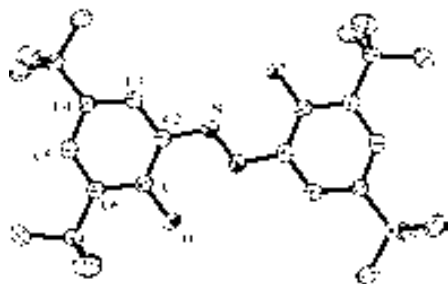


Figure 1. ORTEP drawing of the azobisphenol **2** at the 30% probability level. Hydrogen atoms have been omitted for clarity.

Acid–Base Equilibria of **2**

The acid–base activity of azobisphenol **2** was investigated by means of UV/Vis absorption spectroscopy. An ethanol solution of **2** displays two intense broad absorption bands at 347 nm, most likely assigned to the $n\text{--}\pi^*$ transition of the azo (N=N) group, and at 453 nm associated with the presence of the hydroxyl groups. Both bands are expected to be sensitive and to change upon acid/base addition, especially in the case of the second band.^[31]

Figure 2 displays the changes measured in the absorption spectrum of an ethanol solution of **2** ($C_0 = 5.7 \times 10^{-5}$ M) upon addition of base [80 μL of tetrabutylammonium hydroxide (tba) $C_0 = 4.3 \times 10^{-3}$ M]. As the pH increases, the intensity of the band at 347 nm associated with the $n\text{--}\pi^*$ transition decreases. However, a new band at 520 nm appears, and the intensity of the initial peak at 453 nm, associated with the hydroxyl groups, decreases until the band almost disappears. Deprotonation of the phenol groups under basic conditions leads to a charge density shift and consequently a bathochromic shift of the new band, which is accompanied by a colour change from yellow to violet. The clean isosbestic point at 493 nm also indicates an equilibrium between the acid (**2**) and the basic (**2**²⁻) form of this

molecule (Figure 2a), which most likely takes place through the formation of the monoanionic form. Finally, it is important to emphasize that this process is fully reversible upon addition of acid (HCl), and therefore the absorption spectrum of the neutral form **2** and the yellow colour of the solution can be recovered. In any case, protonation of the azo group was not detected after addition of controlled amounts of acid.

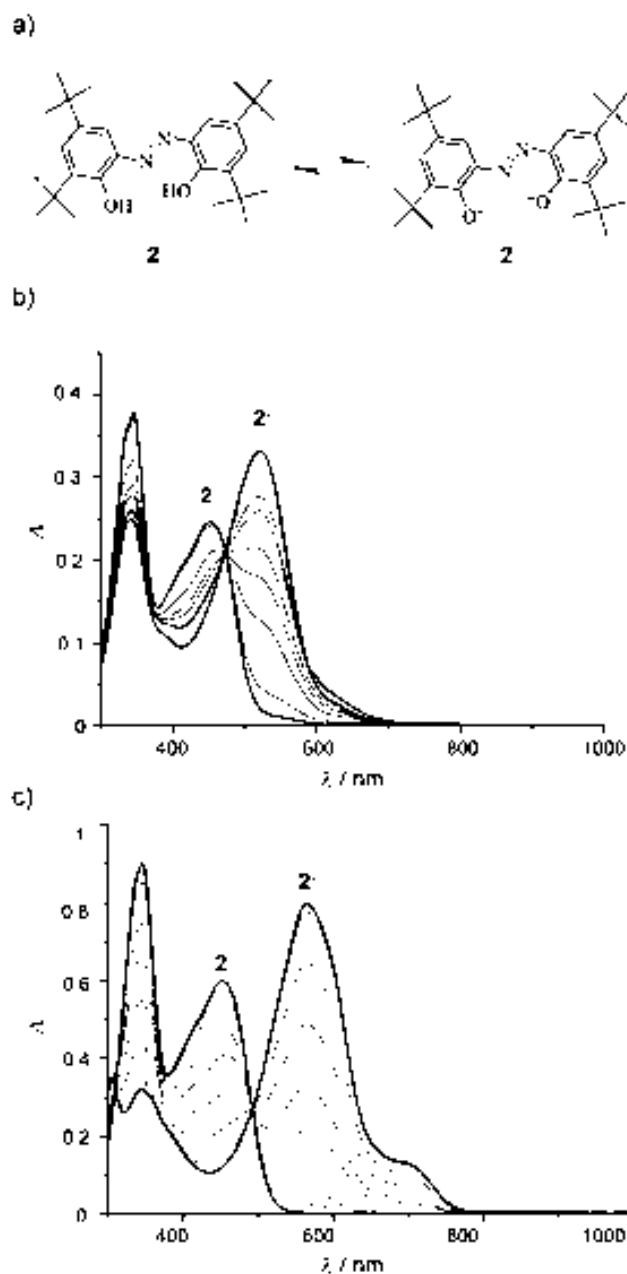


Figure 2. (a) Schematic representation of the acid–base equilibrium of **2**. (b) UV/Vis spectra of **2** (0.057 mM) in ethanol as the pH increases. (c) UV/Vis spectra of **2** (0.057 mM) in thf as the pH increases. In (b) and (c) each line corresponds to the addition of 40 μL of tba (0.4 mM) until total deprotonation of **2** occurs. The process is fully reversible upon addition of HCl.

The acid–base activity of **2** was also investigated in thf solution (Figure 2c). In this solvent, the spectrum of **2** also displays the two intense broad absorption bands at 347 nm and 453 nm, with no significant solvatochromic shift. Upon addition of base, deprotonation of the phenol groups takes place, as described previously for the ethanol solution, which leads to the appearance of a new band at 565 nm, and the intensity of the initial peak at 453 nm decreases. However, two main differences can be noted: (i) a solvatochromic effect is detected in the absorbance spectra for the 2^{2-} species (the spectral parameters for the species **2** and 2^{2-} are summarized in Table 2), which could be tentatively ascribed to changes in solvent polarity as well as in the solvent hydrogen-bond-accepting capacity,^[32] and (ii) the intensity of the band at 347 nm decreases more considerably.

Table 2. UV/Vis spectroscopic data for the species **2** and 2^{2-} in ethanol and thf solutions.

State	Solvent	λ [nm]	ϵ [$M^{-1} \text{cm}^{-1}$]
2	EtOH	347, 453	13899, 9322
2^{2-}		347, 520	7834, 11624
2	thf	347, 453	15789, 10488
2^{2-}		347, 565	5623, 14348

Complexation Ability of **2**

The complexation ability of **2** with transition-metal ions such as Co^{II} was initially studied in solution (Figure 3a). First, the deprotonated form 2^{2-} was obtained after an ethanol solution of **2** (3 mL, $C_0 = 1 \times 10^{-5} \text{ M}$) was made basic with tba (5 μL , $C_0 = 5 \times 10^{-2} \text{ M}$), as confirmed by UV/Vis spectroscopy. An aqueous solution of $\text{CoCl}_2 \cdot 6\text{H}_2\text{O}$ (25 μL , $C_0 = 9 \times 10^{-4} \text{ M}$) was then added. Immediately, the intensity of the band at 520 nm, characteristic of the 2^{2-} form, started to decrease and that of the new band at 560 nm with two shoulders at 520 and 484 nm, associated with the formation of the corresponding cobalt complex **2-Co**, increases. The appearance of the new band is accompanied by a colour change from violet to red–purple. The complexation ability of ligand **2** was also tested by direct reaction of **2** with an ethanol solution of cobalt acetate, whose basic character is expected to deprotonate the azobisphenol ligand. The UV/Vis spectra of an ethanol solution of **2** upon addition of cobalt acetate are shown in Figure 3b. Addition of a solution of $\text{Co}(\text{CH}_3\text{COO})_2 \cdot 4\text{H}_2\text{O}$ (240 μL , $C_0 = 1 \times 10^{-3} \text{ M}$) to the ethanol solution of **2** ($C_0 = 5.5 \times 10^{-5} \text{ M}$) also induces a shift in the band at 453 nm, which is characteristic of **2**, to 560 nm. The shoulders at 520 and 484 nm arise as a result of the formation of the complex **2-Co**. As expected, the acetate counterion of the metal salt is sufficiently acidic to deprotonate the azo ligand, which leads to the formation of complex **2-Co**. Moreover, the process is fully reversible on addition of acid (HCl) and the absorption spectrum of the neutral form **2** is thus recovered, and consequently, the yellow colour of the solution.

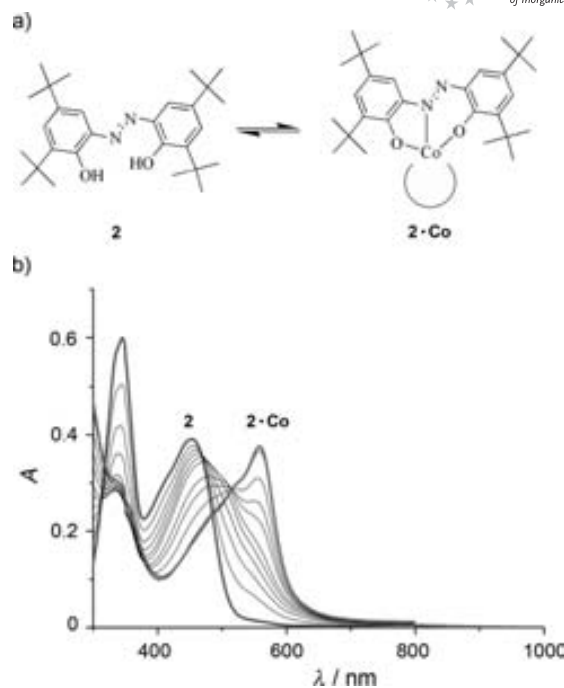


Figure 3. (a) Schematic representation of the complexation equilibrium of **2**. (b) UV/Vis spectra of **2** (0.057 mm) in the presence of $\text{Co}(\text{CH}_3\text{COO})_2 \cdot 4\text{H}_2\text{O}$ (1 mM), added at regular intervals of 24 μL .

To shed more light into the reactivity of ligand **2** and the nature of the complex formed upon reaction with a cobalt salt, we considered the straight chemical synthesis of a transition-metal complex bearing ligand **2**. For this, we were inspired by the methodology described by Pierpont^[17a] and Dei et al.^[17b] for the synthesis of transition-metal complexes bearing ligand **1**. These authors showed that 3d metal ions react with 3,5-di-*tert*-butylcatechol (3,5-DTBCatOH) and aqueous ammonia in the presence of air to yield complexes of the Schiff base bisquinone ligand. Moreover, for the case of the copper metal ion, excess ammonia induces a redox cascade reaction coupled with air oxidation, which is responsible for the formation of a related azophenolate complex.^[22] By taking these precedents into account, and only after several different reaction trials did the reaction of 3,5-DTBCatOH (6 equiv.), ammonia (excess) under aerobic conditions and a mixture EtOH/ H_2O (50:50) and $\text{CoCl}_2 \cdot 6\text{H}_2\text{O}$ (1 equiv.) yield complex $[\text{Co}(2^{2-})(\text{H}_2\text{O})_3]\text{Cl} \cdot 2.5\text{EtOH} \cdot \text{H}_2\text{O}$ (**8**), as characterized by X-ray diffraction and chemical analysis (vide infra). Most likely, the reaction mechanism takes place through the formation of complex $[\text{Co}(\text{Cat-N-SQ})(\text{Cat-N-BQ})]$, where $(\text{Cat-N-BQ})^-$ and $(\text{Cat-N-SQ})^{2-}$ refer to the monoanionic and dianionic forms of ligand **1**, respectively. Indeed, upon addition of excess concentrated aqueous ammonia to a solution of 3,5-DTBCatOH and $\text{CoCl}_2 \cdot 6\text{H}_2\text{O}$, the solution turned dark violet, characteristic of the formation of $[\text{Co}(\text{Cat-N-SQ})(\text{Cat-N-BQ})]$. However, after 10 min whilst stirring, the solution gradually became a lighter violet colour and finally the characteristic red–purple colour of complex **8**. After 4 h of stirring, the solution was filtered and a purple compound was obtained,

which was characterized by chemical analysis as complex [Co(Cat-NSQ)(Cat-N-BQ)]. This result partially confirms the formation of this species as an intermediate along the reaction. The solution was then kept for 2 h, and crystals of complex **8** suitable for X-ray analysis were collected.

Crystallographic data and experimental parameters used for the resolution of the X-ray structure of **8** are summarized in Table 4. Selected bond lengths and angles are given in Table 3. Complex **8** crystallizes in the $P\bar{1}$ triclinic space group with the cell parameters as reported in Table 4. An ORTEP drawing is shown in Figure 4. The asymmetric unit contains one molecule of **8**, one chloride counterion, two and a half ethanol molecules and one water molecule of crystallization. The cobalt ion displays an octahedral coordination geometry by binding to two oxygen and one nitrogen atoms of 2^{2-} and three water molecules. The Co1–O1, Co1–O2, Co1–N1 distances are 1.868(4), 1.856(4) and 1.849(6) Å, respectively, so 2^{2-} is a tridentately coordinated to the cobalt ion. In this coordination mode, the azobisphenolate ligand forms both typical five- and six-membered chelate rings with the cobalt atom. All bond lengths and angles are characteristic of and similar to those previously reported for other azobisphenolate-based complexes.^[22]

Table 3. Selected bond lengths and angles for **8**.

Bond lengths			
Co1–O1	1.868(4)	Co1–O2	1.856(4)
Co1–N1	1.849(6)	N1–N2	1.266(8)
N1–C2	1.422(8)	N2–C8	1.386(9)
O1–C1	1.334(8)	O2–C7	1.326(8)
C1–C2	1.391(10)	C7–C8	1.417(10)
Angles			
O1–Co1–O2	177.0(2)	O1–Co1–N1	86.6(2)
O2–Co1–N1	96.1(2)	N1–Co1–O3	88.9(3)
C2–N1–N2	118.4(6)	C8–N2–N1	119.9(6)
N1–Co1–O5	177.6(2)		

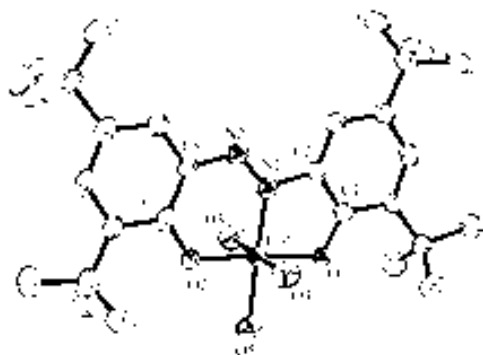


Figure 4. ORTEP drawing of the azobisphenol–Co complex **8** at the 30% probability level. Hydrogen atoms, the chloride counterion and the solvent molecules are omitted for clarity.

Elemental analysis and electropray-(+) measurements in methanol of a polycrystalline sample of **8** are in agreement with the structure previously described (see Experimental Section). The FTIR spectrum (KBr pellet) of **8** exhibits peaks at 1268 and 1450 cm^{-1} , which are characteristic of the $\nu(\text{C}=\text{O})$ and $\nu(\text{N}=\text{N})$ modes.^[31]

The $\nu(\text{O}=\text{H})$ mode for the three coordinated water molecules appears as a broad band from 3300–3100 cm^{-1} . The electronic spectra in ethanol consists of an intense band with a maximum at 553 nm ($1.2 \times 10^4 \text{ M}^{-1} \text{ cm}^{-1}$) and two shoulders at 512 and 476 nm. Interestingly, these bands are similar to those observed for $2 \cdot \text{Co}$ in solution, which confirms the series of experiments as described in Figure 3. For comparison purposes, the electronic spectrum of complex **8** was also monitored in two additional solvents. The most intense band shifts its maxima to 560 nm ($7.4 \times 10^3 \text{ M}^{-1} \text{ cm}^{-1}$) in thf and to 565 nm ($6.2 \times 10^3 \text{ M}^{-1} \text{ cm}^{-1}$) in toluene. The shoulders shift to 523 and 489 nm in thf and 529 and 492 nm in toluene, respectively, which confirms the existence of a solvatochromic effect as described previously for compound 2^{2-} . In addition, the ^1H NMR spectra of deuterated methanol solutions of $2 \cdot \text{Co}$ and **8** also suggest that both complexes are almost identical. Indeed, as described in the Experimental Section, the signals attributed to the four *tert*-butyls groups and the four aromatic protons are very similar, with small shift differences that are expected according to the different coordination environments of the Co^{III} ion in $2 \cdot \text{Co}$ and **8**.

The magnetization temperature dependence data in the temperature range 5–300 K under an external applied magnetic field of 0.5 T exhibits diamagnetic behaviour along the whole temperature range. These results are consistent with the formulation of the ligand in the form of diamagnetic azophenolate (2^{2-}) and Co^{III} ions. The extra positive charge is compensated for by the presence of the chloride anion. This charge assignment was also confirmed by cyclic voltammetry. Cyclic voltammetry of complex **8** shows two reversible one-electron waves at +1.093 V, which is assigned as an oxidation ligand-centred process, and at –1.083 V, which is assigned to the reduction of Co^{III} to Co^{II} or, to a lesser extent, of a ligand-centred process.

Finally, the redox activity of ligand **2** described previously inspired us to explore the possible existence of valence tautomerism for complex **8** by means of variable-temperature UV/Vis spectroscopy in the 280–370 K temperature range. An external stimuli such a temperature may induce a reversible intramolecular electron transfer between the redox-active ligand and the metal ion. However, in spite of the different solvents and solvent mixtures used, no valence tautomerism could be detected for **8**. In all cases, a large reduction in the intensity of the bands, followed by the appearance of new bands at very short wavelengths, is observed. This behaviour has been attributed to the decomposition of the complex under the experimental conditions, as confirmed by the irreversibility of the process.

Three-State Switching Array

The studies described previously confirmed the suitability of **2** to create a chromophoric array of three states with significantly different colours, thanks to the presence of the azo group, which can interconvert reversibly between them by means of acid/base and complexation reactions. The UV/Vis spectra of the three species **2**, 2^{2-} and $2 \cdot \text{Co}$ and a

schematic representation of the different mechanisms that can be followed to interconvert between them are shown in Figure 5. The yellow colour of **2** changes to violet and red-purple upon addition of a base such as tba and $\text{Co}(\text{Cl})_2 \cdot 6\text{H}_2\text{O}$, respectively. In the first case, the dianionic compound 2^{2-} is formed, whereas addition of the cobalt salt induces the formation of the $2 \cdot \text{Co}$ complex. In both cases, subsequent addition of HCl leads to **2**, which shows that the process is fully reversible. The colour changes can nicely be detected by the naked eye, as shown in Figure 5a. This fact was also observed for complex **8**. Upon addition of HCl to an ethanol solution of complex **8**, crystals of pure **2** (40% yield) were obtained by recrystallization from the solution, which opens an alternative high-yield methodology for obtaining **2** to those described in the previous section. Finally, the reverse reaction, i.e. addition of further base to the acidic solution of **2** and the free cobalt ion did not proceed. For this process to work, further addition of $\text{Co}(\text{CH}_3\text{COO})_2 \cdot 4\text{H}_2\text{O}$ is necessary.

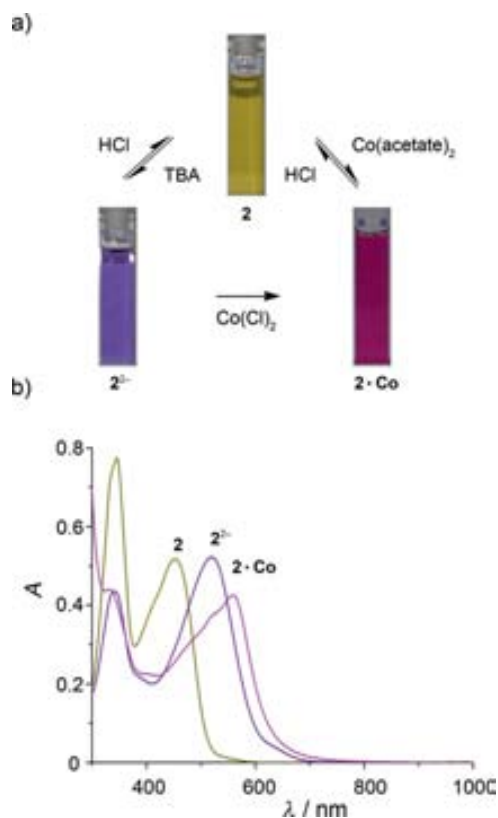


Figure 5. (a) Schematic representation of the three-state switching array. (b) UV/Vis spectra of an ethanol solution of **2** (0.055 mM) with the initial addition of 20 μL tba (0.8 M) to generate 2^{2-} and subsequent addition of 240 μL of $\text{Co}(\text{Cl})_2 \cdot 6\text{H}_2\text{O}$ (1 mM) to generate $2 \cdot \text{Co}$.

Conclusions

A new synthetic route for the synthesis of the sterically protected azobisphenol **2** has been described. The reversible deprotonation/protonation of the phenol groups has been

shown to take place under basic and acidic conditions, respectively. Moreover, ligand **2** exhibits good reactivity with transition-metal ions such as cobalt, as shown UV/Vis spectroscopy in solution. Both the acid–base character and the complexation ability of **2** have been used to create a chromophoric array of three states (**2**, 2^{2-} and $2 \cdot \text{Co}$) with significantly different colours (enhanced by the presence of the azo group), which can interconvert reversibly between them. The reactivity of ligand **2** has also been used to prepare complex **8**, although no evidence of valence tautomerism was detected. Further work is currently underway to prepare a new series of complexes bearing this ligand with different N, N' counter ligands, which will allow us to study valence tautomerism.

Experimental Section

All reagents were purchased from Aldrich Chemical Co. and used as received. The solvents were dried by distillation over the appropriate drying agents. All reactions were performed avoiding moisture by standard procedures and under an atmosphere of nitrogen and monitored by analytical thin-layer chromatography (TLC) by using silica gel 60 F_{254} pre-coated aluminium plates (0.25 mm thickness). Flash column chromatography was performed using silica gel 60 \AA , with particle sizes 35–70 μm .

Synthesis of 2,2'-Dihydroxy-4,3,4',3'-tetra-*tert*-butylazobenzene: A solution of sodium nitrite (0.027 g, 0.40 mmol) in a mixture of water (0.2 mL) and 35% HCl acid (0.1 mL, 0.90 mmol) was first cooled to 5 °C. A thf solution (0.6 mL) of aniline **4** (0.080 g, 0.36 mmol) was then added, and the resulting mixture was stirred at 5 °C for 20 min. This solution was then added dropwise to another solution of compound **5** (0.075 g, 0.36 mmol) and NaOH (0.036 g, 0.90 mmol) in a mixture of thf (0.5 mL) and water (0.5 mL). The whole mixture was stirred at 10 °C for 30 min, adjusted to a pH of 6–7 and extracted with ethyl acetate (3×10 mL). The entire organic extracts were dried with magnesium sulfate, filtered and concentrated under reduced pressure to yield an oil that was chromatographed through silica gel by using a mixture of ethyl acetate/ethyl ether (15:1) to afford 0.033 g of azobisphenol **2** (0.08 mmol, 21% yield). FTIR (KBr): $\tilde{\nu} = 3428$ [$\nu(\text{O-H})$], 2963, 2905, 2862 [$\nu(\text{C-H})$], 1613, 1479, 1461, 1428 [$\nu(\text{N=N})$], 1393, 1360, 1266 [$\nu(\text{C-O})$], 1249, 1220, 1197, 1169 cm^{-1} . $\text{C}_{28}\text{H}_{42}\text{N}_2\text{O}_2$ (438.31): calcd. C 76.0, H 9.5, N 6.4; found C 75.9, H 9.5, N 6.3. ES-(+) (MeOH): $m/z = 439$ [M^+ , $\text{C}_{28}\text{H}_{43}\text{O}_2\text{N}_2$]. ^1H NMR (400 MHz, $[\text{D}_8]$ toluene): $\delta = 1.46$ (s, 18 H, CH_3), 1.81 (s, 18 H, CH_3), 7.67–7.72 (m, 4 H, aromatic H), 13.70 (s, 2 H, OH) ppm.

Synthesis of Complex $2 \cdot \text{Co}$: An ethanol solution (20 μL) of $\text{Co}(\text{CH}_3\text{COO})_2 \cdot 4\text{H}_2\text{O}$ (28 mg, 0.11 mmol) was added to an ethanol solution (0.75 mL) of 2,2'-dihydroxy-4,3,4',3'-tetra-*tert*-butylazobenzene (**2**) (1.3 mg, 0.003 mmol) in the NMR tube, whilst stirring. The colour of the mixture turned to a lighter violet colour, and the obtention of the product was followed by ^1H NMR spectroscopy. ^1H NMR (400 MHz, $[\text{D}_4]$ MeOH): $\delta = 1.41$ (s, 18 H, CH_3), 1.62 (s, 9 H, CH_3), 1.66 (s, 9 H, CH_3), 7.35 (s, 1 H, aromatic H), 7.49 (s, 1 H, aromatic H), 7.77 (s, 1 H, aromatic H), 8.10 (s, 1 H, aromatic H) ppm.

Synthesis of Complex **8:** An ethanol solution (25 mL) of 3,5-di-*tert*-butylcatechol (5 g, 23 mmol) was added to an aqueous solution

(25 mL) of $\text{CoCl}_2 \cdot 6\text{H}_2\text{O}$ (6.2 g, 26 mmol) whilst stirring. Immediately, an aqueous solution (25 mL) of ammonia was added. The colour of the mixture turned to dark violet, which changed to a lighter violet colour after 10 min whilst stirring. The mixture was then stirred for a further 4 h, and after filtration, crystals of **8** were collected from the solution. FTIR (KBr): $\tilde{\nu} = 3109$ [$\nu(\text{H}_2\text{O})$], 2955, 2905, 2866 [$\nu(\text{C-H})$], 1612, 1480, 1438, 1360, 1278, 1254, 1162 cm^{-1} . $\text{C}_{28}\text{H}_{52}\text{ClCoN}_6\text{O}_5$ (646.69): calcd. C 51.4, H 8.5, N 12.8; found C 50.3, H 7.9, N 12.6. ES-(+) (MeOH): $m/z = 512$ [M^+ , $\text{C}_{28}\text{H}_{41}\text{CoN}_5\text{O}_3$]. ^1H NMR (400 MHz, $[\text{D}_4]\text{MeOH}$): $\delta = 1.347$ (s, 9 H, CH_3), 1.353 (s, 9 H, CH_3), 1.44 (s, 9 H, CH_3), 1.48 (s, 9 H, CH_3), 7.29 (s, 1 H, aromatic H), 7.34 (s, 1 H, aromatic H), 7.70 (s, 1 H, aromatic H), 8.15 (s, 1 H, aromatic H) ppm.

Physical Measurements: Microanalyses were performed by the Servei d'Anàlisi of the Universitat Autònoma de Barcelona. Electronic absorption spectra were recorded with a Varian Cary05e spectrophotometer equipped with a thermostatted cell holder that can operate between 280 K and 370 K. The stability of the temperature was better than ± 5 K. Spectra were collected on samples that were previously thermally equilibrated at each temperature for 10 min. Magnetic susceptibilities of both samples were measured in the temperature range 1.8–350 K with a Quantum Design MPMS®XL superconducting SQUID magnetometer operating at a magnetic field strength of 0.1 T. The paramagnetic susceptibility was corrected for the holder capsules and the tabulated Pascal constants. Cyclic voltammograms were recorded with a Perkin–Elmer instrument at 20 °C in CH_3CN solution containing 0.10 M commercial tetrabutylammonium hexafluorophosphate as supporting electrolyte, with a glassy carbon working electrode and an Ag/AgCl reference electrode. Ferrocene was used as an internal standard, and potentials are referenced versus the ferrocinium/ferrocene couple (Fc/Fc^+). NMR experiments were performed at the Servei de Resonància Magnètica Nuclear of the Universitat Autònoma de Barcelona. ^1H NMR spectra were recorded on Bruker DPX250 (250 MHz) and Bruker ARX400 (400 MHz) spectrometers. Proton chemical shifts are reported in ppm (CDCl_3 , $\delta = 7.26$ or $[\text{D}_6]\text{-DMSO}$, $\delta = 2.50$ ppm). Infrared spectra were recorded on a Sapphire-ATR Spectrophotometer; peaks are reported in cm^{-1} . High resolution mass spectra (HRMS) were recorded at Micro-mass-AutoSpec using (ESI+ or ESI-).

Table 4. Crystallographic data for azobisphenol (**2**) and $[\text{Co}(\text{2}^-)(\text{H}_2\text{O})_3]\text{Cl} \cdot 2.5\text{EtOH} \cdot \text{H}_2\text{O}$ (**8**).

	2	8
Formula	$\text{C}_{28}\text{H}_{42}\text{N}_2\text{O}_2$	$\text{C}_{33}\text{H}_{63}\text{N}_2\text{O}_{8.50}\text{CoCl}$
M_w	438.64	718.23
Color	yellow plates	red plates
Crystal system	monoclinic	triclinic
Space group	$C2/c$	$P\bar{1}$
a [Å]	19.4693(2)	10.9158(4)
b [Å]	6.2499(3)	14.2039(5)
c [Å]	21.6187(7)	14.8742(6)
α [°]		101.344(2)
β [°]	91.939(2)	103.320(2)
γ [°]		99.697(2)
V [Å ³]	2629.08(15)	2144.38(14)
Z	4	2
T [°C]	-40(2)	-40(2)
λ [Å]	0.71073 (Mo)	0.71073 (Mo)
D_{calcd} [mgm^{-3}]	1.108	1.112
μ [mm^{-1}]	0.069	0.506
R, R_w [a]	0.0393, 0.1021	0.0694, 0.1802

[a] $R = \Sigma||F_o| - |F_c||/\Sigma|F_o|$. $R_w = [\Sigma w(|F_o| - |F_c|)^2/\Sigma w(F_o)^2]^{1/2}$.

X-ray Data and Structure Determination of **2 and **8**:** Data collection was performed on a Nonius Kappa CCD equipped with graphite-monochromatized $\text{Mo-K}\alpha$ radiation ($\lambda = 0.71073$ Å) and a nominal crystal-to-area-detector distance of 36 mm. Intensities were integrated by using DENZO and scaled with SCALEPACK. Several scans in ϕ and ω direction were made to increase the number of redundant reflections, which were averaged in the refinement cycles. This procedure replaces, in a good approximation, an empirical absorption correction. The structures were solved with direct methods SHELXS86 and refined against F^2 SHELXL97. The crystallographic data for compounds **2** and **8** are listed in Table 4. CCDC-682913 and -682914 contain the supplementary crystallographic data for this paper. These data can be obtained free of charge from The Cambridge Crystallographic Data Centre via www.ccdc.cam.ac.uk/data_request/cif.

Acknowledgments

This work was supported by the European Network of Excellence MAGMANet through the project MAT2006-13765-C02. F. B. and D. M. thank the Ministerio de Ciencia y Tecnología and the European Regional Development Fund for a RyC contract. E. E. thanks the Ministerio de Ciencia y Tecnología for a pre-doctoral grant. The authors also thank J. M. Pérez for the magnetic measurements and A. Bernabe for the spectroscopic measurements.

- a) A. C. Benniston, P. R. Mackie, in *Handbook of Nanostructured Materials and Nanotechnology: Concise Edition* (Ed.: H. S. Nalwa), John Wiley & Sons, San Diego, California, **2001**, p. 693–747; b) P. F. Barbara, *Acc. Chem. Res.* **2001**, *34*, 409, and reviews within.
- a) O. Sato, J. Tao, Y.-Z. Zhang, *Angew. Chem. Int. Ed.* **2007**, *46*, 2152–2187; b) H. Tian, S. Yang, *Chem. Soc. Rev.* **2004**, *33*, 85–97; c) A. Beyeler, P. Belsler, *Coord. Chem. Rev.* **2002**, *230*, 28–38; d) L. Fabbri, L. Prodi, *Chem. Soc. Rev.* **1995**, *24*, 197–202; e) J.-P. Launay, *Chem. Soc. Rev.* **2001**, *30*, 386–397.
- E. Evangelio, D. Ruiz-Molina, *Eur. J. Inorg. Chem.* **2005**, *15*, 2957–2971.
- D. A. Shultz, “Valence Tautomerism in Dioxolene Complexes of Cobalt” in *Magnetism: Molecules to Materials II. Molecule-Based Materials* (Eds.: J. S. Miller, M. Drillon), Wiley-VCH, New York, **2001**, 281–306.
- a) D. M. Adams, A. Dei, A. L. Rheingold, D. N. Hendrickson, *Angew. Chem. Int. Ed. Engl.* **1993**, *32*, 880–882; b) D. M. Adams, A. Dei, A. L. Rheingold, D. N. Hendrickson, *J. Am. Chem. Soc.* **1993**, *115*, 8221–8229; c) O.-S. Jung, D. H. Jo, Y. A. Lee, B. J. Conklin, C. G. Pierpont, *Inorg. Chem.* **1997**, *36*, 19–24; d) O.-S. Jung, C. G. Pierpont, *J. Am. Chem. Soc.* **1994**, *116*, 2229–2230; e) O.-S. Jung, D. H. Lee, Y. S. Sohn, C. G. Pierpont, *Inorg. Chem.* **1998**, *37*, 5875–5880; f) S. Bin-Salamon, S. H. Brewer, E. C. Depperman, S. Franzen, J. W. Kampf, M. L. Kirk, R. K. Kumar, S. Lappi, K. Peariso, K. E. Preuss, D. A. Shultz, *Inorg. Chem.* **2006**, *45*, 4461–4467.
- S. Messaoudi, V. Robert, N. Guihéry, D. Maynau, *Inorg. Chem.* **2006**, *45*, 3212–3216 and references cited therein.
- a) W. R. Cullen, J. D. Woollins, *Coord. Chem. Rev.* **1981**, *39*, 1–30; b) C. G. Pierpont, C. W. Lange, *Prog. Inorg. Chem.* **1994**, *41*, 331; c) J. L. Reddinger, J. R. Reynolds, *Macromolecules* **1997**, *30*, 673–675; d) A. M. Costero, C. Andreu, R. Martínez-Mañez, J. Soto, L. E. Ochando, J. M. Amigó, *Tetrahedron* **1998**, *54*, 8159–8170; e) T. Hirao, *Coord. Chem. Rev.* **2002**, *226*, 81–91; f) C. Rovira, *Chem. Rev.* **2004**, *104*, 5289–5318.
- a) P. Gütllich, A. Dei, *Angew. Chem. Int. Ed. Engl.* **1997**, *36*, 2734–2736; b) A. Vlcek, *Comments, Inorg. Chem.* **1994**, *16*, 207–228; c) C. G. Pierpont, *Coord. Chem. Rev.* **2001**, *216*, 99–125.

- [9] a) D. N. Hendrickson, C. G. Pierpont, *Top. Curr. Chem.* **2004**, 234, 63–95; b) O. Sato, J. Tao, Y.-Z. Zhang, *Angew. Chem. Int. Ed.* **2007**, 46, 2152–2187.
- [10] a) D. Chang, T. Malinski, A. Ulman, K. M. Kadish, *Inorg. Chem.* **1984**, 23, 817–824; b) J. Seth, V. Palaniappan, D. F. Bocian, *Inorg. Chem.* **1995**, 34, 2201–2206.
- [11] I. Ratera, D. Ruiz-Molina, F. Renz, J. Ensling, K. Wurst, C. Rovira, P. Gütllich, J. Veciana, *J. Am. Chem. Soc.* **2003**, 125, 1462–1463.
- [12] a) M. Li, D. Bonnet, E. Bill, F. Neese, T. Weyhenmüller, N. Blum, D. Sellmann, K. Wieghardt, *Inorg. Chem.* **2002**, 41, 3444–3456; b) D. Herebian, P. Ghosh, H. Chun, E. Bothe, T. Weyhenmüller, K. Wieghardt, *Eur. J. Inorg. Chem.* **2002**, 8, 1957–1967; c) K. Ray, E. Bill, T. Weyhenmüller, K. Wieghardt, *J. Am. Chem. Soc.* **2005**, 127, 5641–5654; d) Y. Shimazaki, T. Yajima, F. Tani, S. Karasawa, K. Fukui, Y. Naruta, O. Yamuchi, *J. Am. Chem. Soc.* **2007**, 129, 2559–2568.
- [13] E. R. Altwickler, *Chem. Rev.* **1967**, 67, 475–531.
- [14] A. K. Nairn, R. Bhalla, S. P. Foxon, X. Liu, L. J. Yellowlees, B. C. Gilbert, P. H. Walton, *J. Chem. Soc., Dalton Trans.* **2002**, 1253–1255 and references cited therein.
- [15] K. S. Min, T. Weyhermüller, K. Wieghardt, *Dalton Trans.* **2004**, 178–186 and references cited therein.
- [16] a) O. Hayaishi, M. Nozaki, *Science* **1969**, 164, 389–396; b) C. A. Tyson, A. E. Martell, *J. Am. Chem. Soc.* **1972**, 94, 939–945; c) A. Y. Girgis, A. L. Balch, *Inorg. Chem.* **1975**, 14, 2724–2727; d) L. A. deLaire, R. C. Haltiwanger, C. G. Pierpont, *Inorg. Chem.* **1989**, 28, 644–650.
- [17] a) S. K. Larsen, C. G. Pierpont, *J. Am. Chem. Soc.* **1988**, 110, 1827–1832; b) A. Caneschi, A. Cornia, A. Dei, *Inorg. Chem.* **1998**, 37, 3419–3421; c) O. Cador, F. Chabre, A. Dei, C. Sangregorio, J. Van Slageren, M. G. F. Vaz, *Inorg. Chem.* **2003**, 42, 6432–6440.
- [18] T. K. Paine, T. Weyhermüller, L. D. Slep, F. Neewe, E. Bill, E. Bothe, K. Wieghardt, P. Chaudhuri, *Inorg. Chem.* **2004**, 43, 7324–7338.
- [19] The redox activity of these ligands not only allows for the existence of valence tautomerism but also for additional switching capacities resulting from an electrochemical process. Such a strategy has been shown to be very useful for the systematic tuning of the critical temperature (T_c), at which there are equal amounts of both tautomers, as well as of the net magnetic moments and optical properties of the tautomeric isomers; a) D. Ruiz-Molina, L. N. Zakharov, A. L. Rheingold, D. N. Hendrickson, *J. Phys. Chem. Sol.* **2004**, 65, 831–837; b) D. Ruiz-Molina, K. Wurst, D. Hendrickson, C. Rovira, J. Veciana, *Adv. Funct. Mater.* **2002**, 12, 347–351; c) D. Ruiz-Molina, J. Veciana, K. Wurst, D. N. Hendrickson, C. Rovira, *Inorg. Chem.* **2000**, 39, 617–619; d) D. Ruiz, J. Yoo, I. Guzei, A. L. Rheingold, D. N. Hendrickson, *Chem. Commun.* **1998**, 2089–2090.
- [20] a) M. Kurihara, H. Nishihara, *Coord. Chem. Rev.* **2002**, 226, 125–135; b) Y. Men, S. R. Korupolu, M. Kurihara, J. Mizutani, H. Nishihara, *Chem. Eur. J.* **2005**, 11, 7322–7327; c) J. Yoshino, M. Kano, T. Kawashima, *Chem. Commun.* **2007**, 559–561; d) J. Příkryl, M. Černý, H. Bělohlová, V. Macháček, A. Lyčka, *Dyes. Pigm.* **2007**, 72, 392–402.
- [21] W. Kaim, N. Doslik, S. Frantz, T. Sixt, M. Wanner, F. Baumann, G. Denniger, H.-J. Kümmerer, C. Duboc-Toia, J. Fiedler, S. Zalis, *J. Mol. Struct.* **2003**, 656, 183–194.
- [22] G. Speier, J. Csihony, A. M. Whalen, C. G. Pierpont, *Inorg. Chem.* **1996**, 35, 3519–3524.
- [23] a) F. Stunnenberg, H. Cerfontain, R. B. Rexwinkel, *Recl. Trav. Chim. Pays-Bas* **1992**, 111, 438–447; b) G. Bauer, K. Scheffler, H. B. Stegmann, *Chem. Ber.* **1976**, 109, 2231–2242.
- [24] V. K. Bhardwaj, N. Singh, M. S. Hundal, G. Hundal, *Tetrahedron* **2006**, 62, 7878–7886.
- [25] K. Haghbeen, W. Tan, *J. Org. Chem.* **1988**, 63, 4503–4505.
- [26] a) C. Ruslim, K. J. Ichimura, *J. Mat. Chem.* **1999**, 9, 673–681; b) K. Srinivasa, K. Abiraj, D. C. Gowda, *Tetrahedron Lett.* **2003**, 45, 5835–5837.
- [27] S. Patel, B. K. Mishra, *Tetrahedron Lett.* **2004**, 45, 1371–1372.
- [28] Q. Wang, Y. Yang, Y. Li, W. Yu, Z. T. Hou, *Tetrahedron Lett.* **2006**, 62, 6107–6112.
- [29] J. Vinsova, K. Cermakova, A. Tomeckova, M. Ceckova, J. Jampilek, P. Cermak, J. Kunes, M. Dolezal, F. Staud, *Bioorg. Med. Chem.* **2006**, 14, 5850–5865.
- [30] S. Yoshida, S. Shiokawa, K. Kawano, T. Ito, H. Murakami, H. Suzuki, Y. J. Sato, *Med. Chem.* **2005**, 48, 7075–7079.
- [31] P. Pattanayak, J. L. Pratihari, D. Patra, A. Burrows, M. Mohan, S. Chattopdhyay, *Eur. J. Inorg. Chem.* **2007**, 27, 4263–4271, and references therein.
- [32] N. Ventosa, D. Ruiz-Molina, J. Sedó, C. Rovira, X. Tomas, J.-J. André, A. Bieber, J. Veciana, *Chem. Eur. J.* **1999**, 5, 3533.

Received: December 13, 2007
Published Online: April 4, 2008

Articles After the Doctoral Commission

Article V

Title: Catechol Derivatives as Fluorescent Chemosensors for Wide range pH Detection

Authors: E. Evangelio, J. Hernando, I. Imaz, G. G. Bardají, R. Alibés, F. Busqué and D. Ruiz-Molina

Publication: Chem. Eur. J. 2008, Submitted

Catechol Derivatives as Fluorescent Chemosensors for Wide range pH Detection

Emilia Evangelio,^[a] Jordi Hernando,^[b] Inhar Imaz,^[c] Gisela G. Bardají,^[b] Ramon Alibés,^[b] Félix Busqué^{*[b]} and Daniel Ruiz-Molina^{*[d]}

Abstract: In this work we present the synthesis and characterization of a new family of catechol derivatives designed to behave as fluorescent chemosensors for wide range pH detection. These compounds were prepared by covalently coupling a catechol unit with other aromatic rings, thus obtaining π -delocalized systems with both pH-

responsive groups and fluorescent behavior. In the case of a pyridine-catechol derivative, this leads to present up to three different protonation states with distinct optical properties in organic media, as corroborated by density functional theory calculations. By applying dual-wavelength detection techniques, this compound shows

complementary ‘*off-on-off*’ and ‘*on-off-on*’ emission profiles upon pH variation, a behavior that can be exploited to perform acidity detection over a broad pH range.

Keywords: fluorescent pH probe chemosensor – catechol multiswitching *on-off-on* state

Introduction

In the last years the design, characterization and device implementation of chemosensors has emerged as an active area of research due to their wide-ranging applications in various fields of science and industry.^[1] Because of its high sensitivity and selectivity as well as its non-invasive character, fluorescence is very often selected as the transduction signal for chemical sensing events.^[2] Thus, great effort has been devoted to developing new materials for the luminescent detection of chemically and biologically relevant ions^[3] and molecules.^[4] Among them, fluorescent chemosensors that report on acidity changes are becoming of increasingly interest due to the need for monitoring pH in many chemical and biological

processes, clinical analysis and environmental protection.^[5] In addition, pH-responsive molecular systems displaying optical activity have been proposed as logical operators to perform molecular computing.^[6]

An important issue of fluorescent chemosensors comparing with glass electrodes is that they allow for acidity detection in a narrow pH windows.^[5e-g] However their main disadvantage is that usually they are not suitable for measurements over wide pH ranges. In fact, the dynamic range of most common chemosensors, which present only a single pH-responsive group leading to one fluorescent and one non-fluorescent states upon pH variation (i.e. ‘*on-off*’ or ‘*off-on*’ probes), is limited to ~ 2 pH units.^[5f] Several strategies can be followed to broaden the sensing range of fluorescent pH chemosensors. On the one hand, this can be achieved by mixing different systems responding to distinct pH values.^[5f,g] More interestingly, pH detection over large intervals can also be attained with specific chemosensors, provided that they possess multiple pH-responsive groups giving rise to several protonation states with distinct optical properties.^[5e, 7] Multistate molecular systems displaying pH-induced ‘*off-on-off*’^[7e,8] or ‘*on-off-on*’^[9] fluorescence profiles are particularly relevant examples of this latter case.

The vast majority of multistate fluorescent pH chemosensors so far reported are complex molecular systems composed of a fluorophore and electronically uncoupled pH-sensitive units capable of modulating its luminescent properties. The mechanisms for such modulation are various including photoinduced electron transfer and electronic energy transfer, among others.^[5e,7-9] Alternatively, another approach has been the development of *intrinsic fluorescent probes*,^[2d] for wide range pH detection, i.e. chemosensors where multiple pH-responsive groups are part of the π -system of the fluorophore, whose inherent emissive properties therefore vary with pH. This allows for a relatively more simple synthesis of the chemosensors as well as an easier manipulation of the resulting

[a] E. Evangelio
Institut de Ciència de Materials de Barcelona (CSIC), Esfera UAB
08193, Cerdanyola del Vallès, Spain

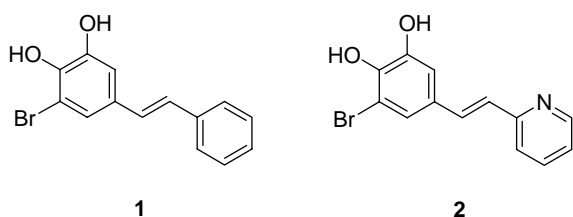
[b] Dr. J. Hernando, G.G. Bardají, Dr. R. Alibés, Dr. F. Busqué
Departament de Química
Universitat Autònoma de Barcelona
08193 Cerdanyola del Vallès, Spain
Fax: (+34) 93 581 1265
E-mail: felix.busque@uab.es

[c] Dr. Inhar Imaz
Institut Català de Nanotecnologia
Edifici CM7 08193, Cerdanyola del Vallès, Spain

[d] Dr. D. Ruiz-Molina
Centro de Investigación en Nanociencia y Nanotecnología
Edifici CM7, Campus UAB 08193, Cerdanyola del Vallès, Spain
Fax: (+34) 93 5801853
E-mail: druiz@cin2.es

structures.

Inspired by the behavior of well-known pH-responsive fluorescent probes such as fluorescein,^[6a, 10] our approach has consisted of the synthesis of new fluorophores containing several groups with acid-base activity. Specifically, we have focused our attention on catechol derivatives because of its intrinsic acid-base properties ($pK_a=9.2$ and 13.0 for pure catechol in water)^[11] and their interesting features. For instance, catechol derivatives have been successfully used on the design of molecular switches^[12] or have significant implications in relevant biological processes such as the activation of small molecules like O_2 and N_2 .¹³ In this contribution we describe the synthesis and the experimental and theoretical investigation of the optical properties of the catechol-derived compounds **1** and **2**. Compounds **1** and **2** have been prepared by covalently coupling a catechol unit with phenyl and pyridine moieties, respectively (see Scheme 1). π -Electron delocalization along both constituent groups is expected to lead to fluorescence emission in the visible region of the spectrum with a significant pH sensitivity thanks to the $-OH$ groups of the catechol unit. More importantly, the additional acid-base activity of pyridine ($pK_a=5.2$ for pyridinium ion in water^[14]) should make compound **2** a suitable fluorescent probe for acidity detection over a broad pH interval, as recently assessed.^[15]



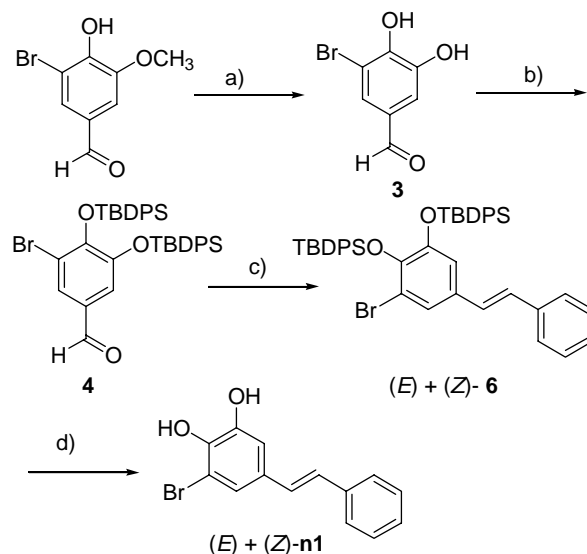
Scheme 1. Chemical structures of compounds **1** and **2**.

Results and Discussion

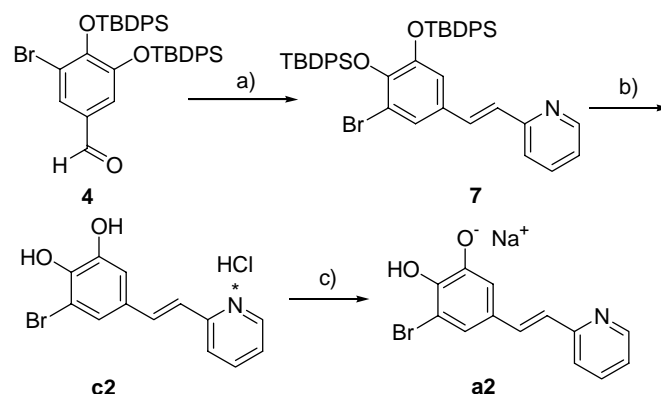
Synthesis. The sequence of reactions leading to target compounds began with commercially available 5-bromovanillin. Thus, cleavage of methyl ether of 5-bromovanillin using anhydrous $AlCl_3$ in the presence of pyridine furnished catechol **3**^[16] in 77% yield. Next, protection of the hydroxyl groups of **3** as their TBDPS derivatives was accomplished using TBDPSCl and anhydrous DBU in a mixture of THF and DMF, affording compound **4** in 58% yield along with monoprotected product **5** (**producto 5 no sale en los esquemas**) in 7% yield. This reaction failed when other bases different from anhydrous DBU were used. Wittig reaction of aldehyde **4** with benzyl-triphenylphosphonium chloride using *t*-BuOK as base yielded an inseparable 1:2 mixture of the (*E*)- and (*Z*)- isomers of olefine **6** in 75% yield. This mixture was treated with triethylamine trihydrofluoride, affording a 1:2 mixture of the neutral form of the (*E*)- and (*Z*)- isomers of **1** in 78% yield (**n1**, Scheme 2). These isomers were separated by means of successive column chromatographies. The isolated (*E*)-isomer proved to be stable enough to be used for further experiments. On the contrary, the (*Z*)-isomer isomerized back in a few days to the original (*Z*)- and (*E*)-**1** mixture even upon storage in the dark and at $4^\circ C$.

Wittig reaction of intermediate **4** and triphenyl-(2-pyridylmethyl)-phosphonium chloride hydrochloride using *t*-BuOK as base afforded (*E*)-olefine **7** in 83% yield. Final removal of protecting silyl groups of **7** was achieved using triethylamine

trihydrofluoride, affording, after HCl 35% addition, the hydrochloride salt of **2** in 65% yield (**c2**, Scheme 3). This yield decreased when TBAF was used as fluoride source for this reaction.



Scheme 2. Synthesis of compound **n1**: (a) $AlCl_3$, pyridine, CH_2Cl_2 , 24 h, reflux, 77%; (b) TBDPSCl, DBU, THF-DMF, rt, 3 h, 58%; (c) $(Ph)_3P^+CH_2-Ph Cl^-$, *t*-BuOK, THF, rt, 2 h, 75%; (d) TEA-3HF, THF, rt, 2 h 78%.



Scheme 3. Synthesis of compounds **c2** and **a2**: (a) $(Ph)_3P^+CH_2-Py-HCl Cl^-$, *t*-BuOK, THF, rt, 2 h, 83%; (b) (i) TEA-3HF, THF, rt, 2 h (ii) HCl 35%, 65%; (c) NaOH 1M, CH_2Cl_2 , 94%.

X-Ray structure. All the attempts to obtain single crystals of **1** were unsuccessful in spite of the recurrent use of different crystallization techniques and solvents. More successful were the attempts to crystallize compound **2**. Yellow needles suitable for X-ray diffraction experiments were obtained by slow evaporation of a solution of **2** in dichloromethane. Compound **2** crystallizes as the hydrochloride salt with one molecule in the asymmetric unit. Figure 1 shows the atom labelling and the anisotropic displacement ellipsoids of **2**. The resolved structure is planar ($C5-C6-C7-C8$ dihedral angle 173°), and the intramolecular bond lengths and angles agree with those expected. Hydrochloric acid is connected to the molecule through a very strong hydrogen bond ($N \cdots Cl^-$: 2.218 Å $NHCl$: 178.3°). Although the molecular packing shows that the different molecules are organized in parallel rows, no π - π interactions are expected between them due to the long

intermolecular separation distance observed (5.583 Å). We ascribe this result to the presence of the voluminous halogenated atoms.

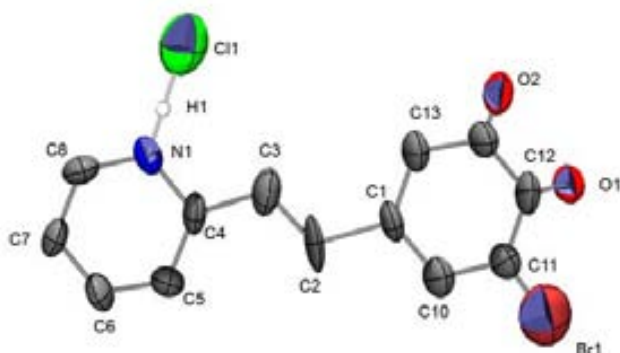


Figure 1. Ortep view of the asymmetric unit of **2**. Hydrogen atoms excepting the hydrogen implicated in the H-bond with Cl1 are omitted for clarity

Acid-base equilibria. The acid-base activity of the catechol and phenyl/pyridine moieties in compounds **1** and **2** was investigated by UV-vis absorption spectroscopy. Figure 2 displays the changes measured in the absorption spectrum of an acetonitrile solution of **n1** ($c_1=1 \times 10^{-5}$ M) upon base addition (tetrabutyl ammonium hydroxide, TBAH). Clearly, a new band at $\lambda_{\text{abs}}=388$ nm appears with increasing pH, while the intensity of the initial peak at $\lambda_{\text{abs}}=319$ nm decreases. Similar results are obtained in other solvents different from acetonitrile (Table 1). The absorption red-shift encountered upon base addition is consistent with the deprotonation of a hydroxyl group in the neutral form **n1** to yield an anionic species (**a1**), as previously reported for monohydroxystilbenes.^{[17][18]} Importantly, this process can be fully reverted back upon acid addition (hydrochloric acid), thus recovering the absorption spectrum of **n1**.

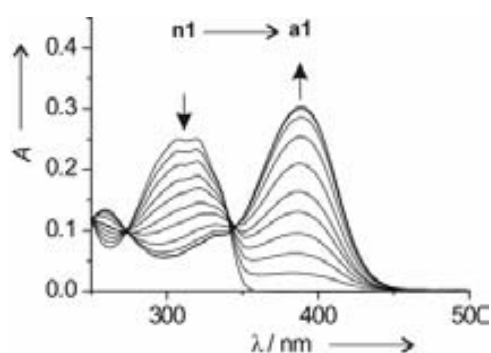


Figure 2. Variation of the absorption spectrum of **1** upon pH increase in acetonitrile ($c_1=1 \times 10^{-5}$ M). The spectra shown were measured at pH values of 17.0, 17.7, 19.0, 20.5, 21.9, 22.4, 22.6, 23.1, 23.2, 23.5, 24.0.

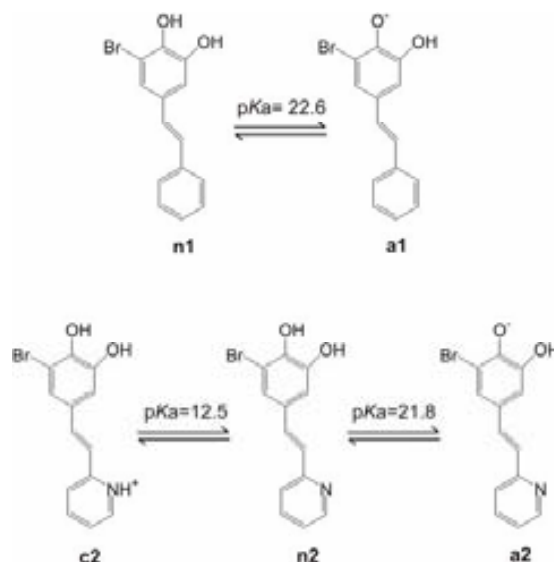
The acid-base equilibrium between **n1** and **a1** is depicted in Scheme 4. Deprotonation to yield **a1** has been tentatively assigned to take place on the -OH moiety at the *para* position of the catechol group according to inductive and conjugation considerations. This fact was confirmed by quantum chemical calculations (vide infra).

From the variations of the absorption spectra with pH,^[19] an acidity constant value of $pK_a=22.6$ has been determined for this process in acetonitrile. Unfortunately, further basification of **1** to yield the double phenolate form of **1** ($pH > 25$ in acetonitrile) results in irreversible degradation of the compound, which we ascribe to either (photoinduced) addition of water to the ethylenic double bond^[20] or a polymerization process.

Table 1. Experimental and TD-DFT energies and intensities of the UV-vis absorption bands of the different protonation states of **1** and **2**.

State	Solvent	Experimental ^[a]		TD-DFT ^{[b],[c]}
		λ_{abs} [nm]	ϵ_{abs} [L mol ⁻¹ cm ⁻¹]	λ_{abs} [nm]
n1	THF	325	21259	346
	acetonitrile	319	25098	
	DMSO	329	20711	
a1	THF	398	24621	406
	acetonitrile	388	30385	
	DMSO	399	21274	
c2	THF	379	22248	408
	acetonitrile	371	24558	
	DMSO	382	22164	
n2	THF	334	25095	350
	acetonitrile	327	26773	
	DMSO	338	24178	
a2	THF	424	32169	422
	acetonitrile	406	32362	
	DMSO	421	28564	

[a] Measured at the absorption maxima. [b] B3LYP/6-311+G(d,p) level and accounting for acetonitrile solvent. [c] The ratios of the computed oscillator strengths (f) are: $f_{a1}/f_{n1}=1.0$, $f_{c2}/f_{n2}=0.8$ and $f_{a2}/f_{n2}=1.0$.



Scheme 4. Molecular structures of the neutral (**n1**) and anionic (**a1**) states of **1** as well as of the cationic (**c2**), neutral (**n2**) and anionic (**a2**) states of **2**. The acidity constants determined spectrophotometrically for the reversible acid-base equilibria between these states in acetonitrile are indicated.

A more complex acid-base activity was encountered for compound **2** (see Scheme 4). The absorption spectrum of a 1×10^{-5} M solution of **c2** in acetonitrile displays two different bands at $\lambda_{\text{abs}}=327$ and 371 nm. The relative intensities of these bands vary with addition of HCl and TBA, the peaks at 327 and 371 nm becoming predominant at $pH=14.1$ and 8.5, respectively (Figure 3).

This indicates that even though complex **2** was originally in its cationic form, an equilibrium between the cationic form **c2** ($\lambda_{\text{abs}}=371$) and its neutral state in which the pyridinium group is deprotonated (**n2**, $\lambda_{\text{abs}}=327$) occurs on the acetonitrile solution. Interestingly, this process can be controlled and reversibly displaced forward or backwards by acid-base titration, as already reported for related styrylpyridine compounds.^[21-22] Moreover, from the variations of the absorption spectra with pH, an acidity constant value of $\text{p}K_{\text{a}}=12.5$ has been determined for the deprotonation of the pyridinium group in acetonitrile. Subsequent deprotonation of **n2** to yield the anionic monophenolate state **a2** leads to additional variations in the absorption bands, as depicted in Figure 3. Such variations are indeed in agreement with those previously found for compound **1**, i.e. red-shifted absorption upon base addition. This confirms deprotonation of the hydroxyl group at the *para* position of the catechol moiety of **2** at larger pH values ($\text{p}K_{\text{a}}=21.8$ in acetonitrile). Remarkably this second acid-base equilibrium is also fully reversible, i.e. the **a2** species can be reverted back to the **n2** species, making feasible the three-state device shown in Scheme 4. However, as already described for compound **1**, further basification to deprotonate the second -OH group of **2** leads to a degradation process (at $\text{pH} > 25$ in acetonitrile), thereby preventing reversible conversion of **a2** into the double anionic diphenolate form of this compound. Similar results are obtained in other solvents different from acetonitrile as summarized in Table 1, where the experimental energies and intensities of the UV-vis absorption bands of the different protonation states of **2** are shown.

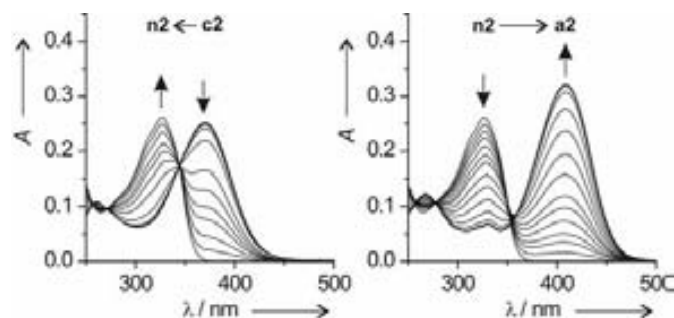
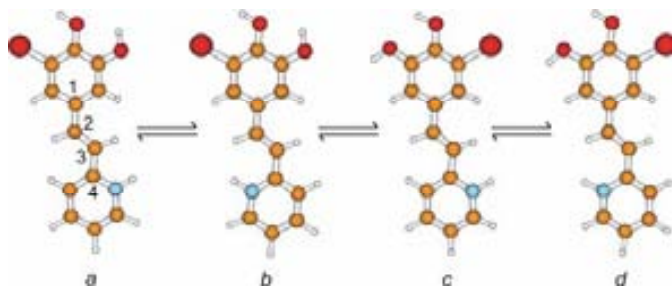


Figure 3. Variation of the absorption spectrum of **2** upon pH increase in acetonitrile ($c_2=1 \times 10^{-5}$ M). The left figure displays the changes arising from the acid-base equilibrium between **c2** and **n2**, which were measured at pH values of 8.5, 9.9, 10.7, 11.4, 11.8, 12.4, 12.5, 12.6, 12.9, 13.0, 13.7 and 14.1. The spectra shown in the right figure report on the acid-base equilibrium between **n2** and **a2**, and they were registered at $\text{pH}=14.1, 15.0, 16.9, 18.5, 19.8, 20.4, 20.9, 21.5, 22.2, 22.8, 23.1, 23.9, 24.2$ and 24.8 .

Quantum chemical calculations. Theoretical calculations were performed to further investigate the correspondence between the different absorption bands found in our spectrophotometric acid-base titration experiments and the distinct states of compounds **1** and **2**. Density functional theory (DFT) calculations employing the B3LYP hybrid functional and the 6-311+G(d,p) basis set and accounting for acetonitrile solvent were carried out to obtain the ground electronic state energies and optimal geometries of the different protonation states of **1** and **2**. Initially, computations of the monophenolate forms **a1** and **a2** where the deprotonated hydroxyl group was systematically modified to lay at either the *para* or *meta* position of the catechol moiety were done. Noticeably, the ground electronic state energy of the former molecules (phenolate at the *para* position) was found to be ~ 10 kcal mol⁻¹ lower in energy than that of the *meta* position. These results confirm the assignment of **a1** and **a2** to the structures shown in Scheme 4, thus demonstrating the

larger acidity of the -OH substituent at the *para* position of the catechol ring, as was tentatively done according to inductive and conjugation considerations.

As well-known for stilbene derivatives,^[23] each one of the protonation states of **1** and **2** can present several different conformations associated to the rotation of the catechol and pyridine rings around the C(1)-C(2) and C(3)-C(4) bonds, respectively. This fact is illustrated in Scheme 5, where the optimal geometries computed for the four possible rotamers of **c2** are shown (*a*, *b*, *c* and *d*) as a representative example.



Scheme 5. Optimal geometries computed for the different rotamers of **c2** at the B3LYP/6-311+G(d,p) level and accounting for acetonitrile solvent. The ground electronic state energies of these conformers relative to that of *a* are 0 (*a*), 1.3 (*b*), -1.4 (*c*) and -0.1 (*d*) kcal mol⁻¹.

Similar planar structures were calculated for **n2** and **a2**. For **n1** and **a1** only two different conformers are possible, which also present planar geometries. In all cases, our calculations yield very similar ground electronic state energies for all possible rotamers of a given protonation state of **1** and **2** (less than 2.5 kcal mol⁻¹ of difference). This result suggests the occurrence of an equilibrium mixture of different rotamers in acetonitrile solution, as previously observed for other stilbene derivatives.^[23] This has been confirmed by means of NMR measurements. ROESY experiments of **c2** in deuterated DMSO show nOe (Nuclear Overhauser) effect between both ethylenic protons and all the hydrogen atoms at the *ortho* positions of the pyridine and catechol rings. Together with the presence of only one series of proton signals in the ¹H-NMR spectrum, this indicates the occurrence of a dynamic equilibrium between different rotational conformers in solution at room temperature. An *average* behavior is therefore measured in our spectroscopic experiments.

Finally, time-dependent functional theory (TD-DFT) calculations at the B3LYP/6-311+G(d,p) level and accounting for acetonitrile solvent were carried out to compute the excitation energies and oscillator strengths of the absorption bands of the different protonation states of **1** and **2**. To account for conformational equilibria, TD-DFT calculations on the ground electronic state optimal geometries of all possible rotamers were performed. In general, minor differences of their spectroscopic parameters were observed for a given protonation state. In spite of this, the final values of absorption energies and oscillator strengths were averaged over all possible rotamers taking into account the Boltzmann distribution of conformer populations at room temperature. The resulting values are compared to the experimental ones in Table 1. As can be seen there, clearly a good agreement between quantum chemical calculations and spectrophotometric measurements is observed. Thus, our computations reproduce into a good extent the spectral shifts obtained experimentally upon pH variation since the deviations between the calculated excitation

energies and the experimental absorption maxima (in energy units) fall below 10% in all cases. TD-DFT calculations also reveal that the absorption transitions measured occur between the HOMO and LUMO states of all investigated molecules. These frontier orbitals are delocalized over both the catechol and phenyl/pyridine rings, thereby explaining why the absorption spectrum changes upon protonation/deprotonation of substituents located in any of the two constituent units of compounds **1** and **2**.

pH-modulated fluorescence. The emission properties of the different protonation states of compounds **1** and **2** have been evaluated. According to their stilbene character, the different ionic forms derived from them exhibit fluorescence. The fluorescence spectral maxima (λ_f) and quantum yields (Φ_f) measured on different solvents are shown in Table 2, whereas the corresponding fluorescence spectra in acetonitrile are given in Figure 4. Clearly, **n1** and **a1** as well as **c2**, **n2** and **a2** show distinct emissive behaviors confirming their potential use as fluorescent pH chemosensors.

Table 2. Fluorescence properties of the different protonation states of **1** and **2**.

State	Solvent ^[a]	λ_f [nm] ^[b]	Φ_f
n1	THF	388	0.065
	acetonitrile	392	0.031
	DMSO	414	0.072
a1	THF	488	0.036
	acetonitrile	484	0.066
	DMSO	501	0.054
c2	THF	500	0.19
	acetonitrile	511	0.069
	DMSO	501	<0.01
n2	THF	406	0.097
	acetonitrile	409	0.053
	DMSO	442	0.34
a2	THF	523	0.20
	acetonitrile	524	0.22
	DMSO	532	0.36

[a] Solvent dielectric constants are $\epsilon_{\text{THF}}=7.5$, $\epsilon_{\text{ACN}}=36.6$ and $\epsilon_{\text{DMSO}}=47.2$, whereas the Kamlet-Taft β factors accounting for their hydrogen bond acceptor capacity are $\beta_{\text{THF}}=0.55$, $\beta_{\text{ACN}}=0.31$ and $\beta_{\text{DMSO}}=0.76$.^[24] [b] Measured at the emission maxima.

Both the neutral forms of **1** and **2** display a large red-shift in fluorescence spectra upon deprotonation (~100 nm), as previously observed for related monohydroxystilbenes^[17,18] or even for the absorption measurements. Similarly, protonation of **n2** to yield **c2** not only leads to bathochromic absorption, but additionally results in red-shifted fluorescence, in agreement with previous reports on the luminescence of related styrylpyridine compounds.^[21,22] Solvatochromic effects on the fluorescence spectra of compounds **1** and **2** are also observed, which we ascribe to both changes in solvent polarity as well as in solvent hydrogen bond accepting capacity, as quantified by means of the Kamlet-Taft β factor.^[24] Thus, similar fluorescence maxima are in general observed in THF and acetonitrile, since the higher hydrogen bond accepting capacity of the former ($\beta_{\text{THF}}=0.55$, $\beta_{\text{ACN}}=0.31$) is counterbalanced by the larger polarity of the latter ($\epsilon_{\text{THF}}=7.5$, $\epsilon_{\text{ACN}}=36.6$). In case of DMSO

solvent, its higher ϵ ($\epsilon_{\text{DMSO}}=47.2$) and β ($\beta_{\text{DMSO}}=0.76$) values lead to red-shifted emission for **n1**, **a1**, **n2** and **a2**. An opposite behavior is found for **c2**, for which larger hydrogen bond interaction between the pyridinium group and THF or DMSO molecules results in hypsochromic displacement of the emission spectrum. Our experimental data shows that fluorescence quantum yields also vary for different solvents and protonation states of **1** and **2** (see Table 2).

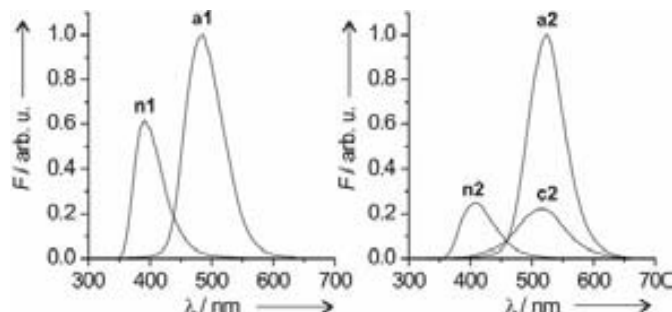


Figure 4. Fluorescence emission spectra of the different protonation states of compounds **1** ($\lambda_{\text{exc}}=280$ nm, $c_1=1 \times 10^{-5}$ M) and **2** ($\lambda_{\text{exc}}=310$ nm, $c_2=1 \times 10^{-5}$ M) in acetonitrile. Each spectrum is normalized with respect to the absorption at the excitation wavelength. Acid (HCl) or base (TBA) was added to adjust the pH of the solution to the values at which full conversion into the desired protonation state was achieved in each case: pH=17.0 (**n1**) and 24.0 (**a1**) and pH=8.5 (**c2**), 14.5 (**n2**) and 24.0 (**a2**).

In case of compound **1**, both **n1** and **a1** states present relatively low Φ_f values within the 0.03-0.07 range. However, while larger fluorescence quantum yields are obtained for **n1** in solvents with high hydrogen bond accepting capacity (THF and DMSO), an opposite trend is observed for **a1**. Most importantly, larger Φ_f values are determined for **2** under selected conditions, a relevant feature for potential fluorescent sensing applications. This contrasts with previous studies on the effect of introducing a nitrogen atom in the styryl system, in which a decrease in fluorescence emission from stilbene to 2-styrylpyridine was observed.^[25] Most probably, this difference arises from the effect of the hydroxyl and bromo substituents of the catechol ring. Indeed, a ten-fold increase in Φ_f has been reported for 3-hydroxystilbene with respect to stilbene in organic solvents,^[17] thus demonstrating the critical effect of *meta*-substitution with -OH moieties on the photochemical properties of styryl systems. Consequently, the combined effect of the nitrogen atom and the hydroxyl substitution must account for the larger values of Φ_f typically obtained in this work for **2** with respect to **1** and stilbene ($\Phi_f=0.04$ in hexane^[25]).

All protonation states of compound **2** display significant solvent effects on their fluorescence quantum yields. In case of **c2**, a Φ_f value as high as 0.19 is determined in THF. Nevertheless, increasing solvent polarity results in a dramatic decrease in fluorescence quantum yield, which leads to nearly complete suppression of emission for polar solvents such as DMSO (see Table 2) and DMF, ethanol and water (data not shown). A different behavior is encountered for the neutral state **n2**, whose fluorescence quantum yield rises with increasing hydrogen bond accepting capacity of the solvent, as also observed for **n1**. Unfortunately, such large emission efficiencies of **n2** in organic media are lost in aqueous solutions, as previously reported for other hydroxystilbenes.^[17] For the anionic form **a2**, solvent effects on fluorescence quantum yield seem less important, because large and similar Φ_f values are measured in THF, acetonitrile and DMSO. In this case, however, major effects are encountered when **a2** is dissolved in solvents with hydrogen bond donor capacity that can interact with the deprotonated hydroxyl

group of the phenolate. This results in very low Φ_f values (data not shown). Thus, for instance, aqueous solutions of **a2** in water are nearly no fluorescent, as also observed for **c2** and **n2**. In spite of this, the large emission efficiencies and different spectral properties observed for these species in several other solvents allows us envisaging compound **2** as a potential fluorescent pH chemosensor in organic media.

Fluorescence pH-sensing. In the previous sections the operation of the fluorescent compound **2** over a large pH interval has been attained thanks to the combination of two distinct acid-base groups displaying distinct pK_a values. Yet the capacity of this species to univocally respond to acidity changes must still be proved if a future pH sensor based on compound **2** is to be achieved. Therefore, to unambiguously prove that a single value of pH can be obtained under a given experimental condition a dual-wavelength detection process based on the determination of pair of F_{409} and F_{524} values at two different wavelengths (409 and 524 nm) has been established.

The three different protonation stable states of compound **2** exhibit different emissive properties in solution. The fluorescence spectrum of the neutral form **n2** is ~ 100 nm blue-shifted with respect to **c2** and **a2**, whereas these two ionic species emit in the same spectral region but with different quantum yields (see Figure 4). As a consequence, if selective detection at the maximum of the emission spectrum of **n2** is performed (~ 400 nm), the fluorescence signal measured will be maximal at intermediate pH values and will decrease for increasingly acid or basic media. This means that compound **2** behaves as an ‘off-on-off’ pH sensor under such detection conditions,^[7e,8] a situation depicted in Figure 5a (dark spheres). On the contrary, if the fluorescence detection window is centered on the maximum of emission of **c2** and **a2** (~ 500 nm), the response of the system upon pH variation becomes of the ‘on-off-on’ type.^[9] Therefore, maximal fluorescence signal is detected at extreme values of pH in this case, as illustrated in Figure 5a (red squares). In the same Figure 5a the fluorescent ‘off-on-off’ and ‘on-off-on’ behaviors of **2** in acetonitrile at different detection conditions are compared with simulations performed using the values of pK_a , absorption extinction coefficients and fluorescence quantum yields previously determined for this species. Clearly, a good agreement exists between the simulated and experimental data. Thus, the dependence of fluorescence intensity at $\lambda_{em}=409$ nm is rather symmetric around $pH=17$, as expected from the calculations. More importantly, an asymmetric curve describes the variation of the emission intensity with pH at $\lambda_{em}=524$ nm, which arises from the different Φ_f values of **c2** and **a2**. This situation contrasts with the behavior observed for previously reported fluorescence on-off-on systems.^[9]

The coexistence of the fluorescent ‘off-on-off’ and ‘on-off-on’ behaviors of **2** in acetonitrile at different detection conditions is an excellent scenario for the development of the sensing routine. Indeed, fluorescent molecular sensors exclusively displaying ‘off-on-off’ or ‘on-off-on’ profiles are mainly suited for detection of pH windows. Unfortunately, they can hardly provide any information on the pH values at which the system is off, thus preventing from sensing over larger pH intervals. This drawback can be overcome by the use of **2** as fluorescent pH probe, since this compound shows both off-on-off and on-off-on responses upon pH variation when dual-wavelength detection is applied. Yet this condition is not sufficient for univocal pH sensing. To be capable of discerning low from high pH values at which the fluorescence of the system simultaneously turns off (at $\lambda_{em}\sim 400$ nm) or on (at $\lambda_{em}\sim 500$ nm), the compound must display an asymmetric ‘on-off-on’ profile, i.e. it

must show different luminescent properties at those two pH ranges. As abovementioned, this is accomplished by **2** in some organic media due to the different fluorescence quantum yields of the **c2** and **a2** states. Consequently, each value of pH will result in a univocal set of emission intensities at the two monitored wavelengths (e.g. F_{409} and F_{524} in acetonitrile). This is demonstrated by the 3D plot in Figure 5b, which unambiguously proves that a single value of pH can be recovered from a given pair of F_{409} and F_{524} values measured by means of dual-wavelength detection. Therefore, we envisage compound **2** as a potential acidity sensor over large pH intervals in organic media. Moreover, since the ‘on-off-on’ response can be altered by changing the solvent, compound **2** can behave as a multiply configurable pH chemosensor.^[7e] For instance, emission at $\lambda_{em}\sim 500$ nm of **2** in DMSO displays a simpler ‘off-on’ profile with pH due to the very low fluorescence quantum yield of **c2** in this medium. Therefore, since all the different protonation states of this species are fluorescent and show different luminescent properties, ratiometric methods can be used to retrieve pH values from the fluorescence response of **2** upon acidity variations, thus preventing from previous calibration of the sensing system.^[5d,5f,7d]

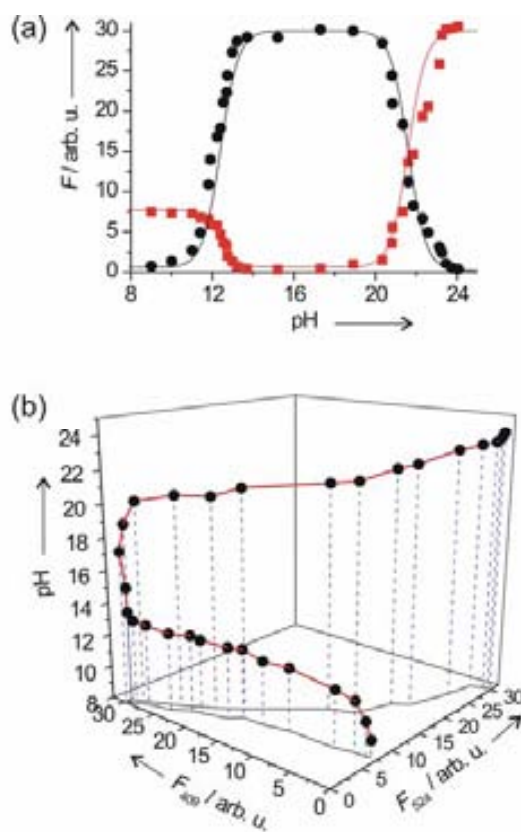


Figure 5. (a) pH dependence of the fluorescence intensity of **2** in acetonitrile ($\lambda_{exc}=310$ nm, $c_2=1\times 10^{-5}$ M) at $\lambda_{em}=409$ nm (black) and $\lambda_{em}=524$ nm (red). Experimentally measured intensities are shown as symbols. Solid lines plot the simulated emission intensities computed using the pK_a constants, absorption extinction coefficients and fluorescence quantum yields determined for **2** in acetonitrile. (b) 3D plot showing the correspondence between pH and the fluorescence intensities measured for **2** in acetonitrile by means of dual-wavelength detection at $\lambda_{em}=409$ and 524 nm (F_{409} and F_{524}).

Conclusion

This contribution describes the synthesis and characterization of a new chemosensor for wide range pH detection based on a fluorescent system decorated with several pH-responsive groups.

With this aim two catechol derivatives were prepared by covalently coupling a catechol unit to phenyl (**1**) and pyridine (**2**) rings. This led to π -delocalized systems displaying pH-sensitive fluorescence emission in the visible region. Whereas **1** presents two stable protonation states with distinct optical properties, both experimental measurements and density functional theory calculations reveal that compound **2** shows up to three different luminescent protonation states in organic media due to the combined acid-base activity of its constituent catechol and pyridine units. Importantly, the optical behavior of these states is such that compound **2** displays complementary ‘off-on-off’ and ‘on-off-on’ emission profiles upon pH variation by applying dual-wavelength detection techniques. This not only allows for application of ratiometric methods, but, more importantly, it can be exploited to perform acidity detection over a broad pH range in organic solvents.

Experimental Section

General Procedures. Commercially available reagents were used as received. The solvents were dried by distillation over the appropriate drying agents. All reactions were performed avoiding moisture by standard procedures and under nitrogen atmosphere and monitored by analytical thin-layer chromatography (TLC) using silica gel 60 F₂₅₄ pre-coated aluminum plates (0.25 mm thickness). Flash column chromatography was performed using silica gel 60 Å, particle size 35–70 μ m. NMR experiments were performed at the *Servei de Ressonància Magnètica Nuclear* of the *Universitat Autònoma de Barcelona*. ¹H-NMR spectra were recorded on Bruker DPX250 (250 MHz) and Bruker DPX360 (360 MHz), spectrometers. Proton chemical shifts are reported in ppm (δ) (CDCl₃, δ 7.26 or DMSO-*d*₆, δ 2.50). ¹³C-NMR spectra were recorded on Bruker DPX250 (62.5 MHz) and Bruker DPX360 (90 MHz) spectrometers with complete proton decoupling. Carbon chemical shifts are reported in ppm (δ) (CDCl₃, δ 77.2 or DMSO-*d*₆, δ 39.5). NMR signals were assigned with the help of COSY, HSQC, HMBC, and NOESY experiments. Infrared spectra were recorded on a Sapphire-ATR Spectrophotometer; peaks are reported in cm⁻¹. High resolution mass spectra (HRMS) were recorded at Micromass-AutoSpec using (ESI+ or ESI-).

3-Bromo-4,5-dihydroxybenzaldehyde, 3.^[16] Anhydrous aluminum chloride (3.2 g, 23.8 mmol) was suspended in a solution of 5-bromovanillin (5.0 g, 21.6 mmol) in 50 ml of CH₂Cl₂. While cooling to maintain the temperature at 30–35 °C, 7.7 ml (95.2 mmol) of pyridine was added slowly. The resulting clear solution was heated to reflux for 24 h, allowed to come to rt, quenched by slowly addition of 10% HCl solution (60 ml) and further diluted with CH₂Cl₂ (30 ml). The resulting suspension was filtered to afford 3.60 g (16.6 mmol, 77%) of catechol **3** as a white solid. Mp 225–227 °C.

3-Bromo-4,5-bis(tert-butylphenylsilyloxy)benzaldehyde, 4. DBU (6.5 ml, 43.8 mmol) was added dropwise over 20 min to a stirred solution of **3** (3.8 g, 17.5 mmol) and TBDPSCI (10.5 ml, 40.3 mmol) in a mixture of dry THF (100 ml) and anhydrous DMF (20 mL) at 0 °C. After stirring at rt for 3 h, ethyl ether (100 ml) was added and the resulting suspension filtered. The filtrate was concentrated under vacuum and the resulting yellowish wax was purified by column chromatography on silica gel (gradient, hexanes: CH₂Cl₂ 4:1 to 1:1) to afford the following fractions: (i) 7.10 g (10.2 mmol, 58%) of 3-bromo-4,5-bis(tert-butylphenylsilyloxy)benzaldehyde, **4**, as a solid; and ii) 0.56 g (1.20 mmol, 7%) of 3-bromo-5-(tert-butylphenylsilyloxy)-4-hydroxybenzaldehyde, **5** as a solid. 4: mp: 151–153 °C (ethyl ether); ¹H-NMR (250 MHz, CDCl₃) δ 9.29 (s, 1H), 7.83–7.72 (m, 4H), 7.61 (d, *J* = 1.9 Hz), 7.53–7.20 (m, 16H), 6.86 (d, *J* = 1.9 Hz), 1.13 (s, 9H), 0.76 (s, 9H); ¹³C-NMR (62.5 MHz, CDCl₃) δ 189.4, 149.3, 147.6, 135.5, 135.3, 133.0, 132.0, 130.1, 130.0, 129.9, 127.9, 127.8, 127.3, 122.2, 117.0, 27.1, 26.4, 20.7, 19.3; IR (ATR, cm⁻¹) 3267, 2930, 2856, 1669, 1428, 1314, 1300, 1100, 885, 701; HRMS (ESI-) *m/z* [M+2+Na]⁺ calcd for C₃₉H₄₁BrNaO₅Si₂ 717.1657, found 717.1640. **5**: mp: 126–127 °C (ethyl ether); ¹H-NMR (250 MHz, CDCl₃) δ 9.42 (s, 1H), 7.75–7.64 (m, 4H), 7.60 (d, *J* = 1.7 Hz, 1H), 7.53–7.34 (m, 6H), 6.84 (d, *J* = 1.7 Hz, 1H), 6.57 (s, 1H), 1.15 (s, 9H); ¹³C-NMR (62.5 MHz, CDCl₃) δ 189.3, 150.3, 143.5, 135.5, 130.9, 129.8, 128.5, 128.4, 117.9, 109.2, 26.8, 19.7; IR (ATR, cm⁻¹) 2960, 2856, 1696, 1424, 1310, 1107, 917, 870, 697; HRMS (ESI+) *m/z* [M+2+Na]⁺ calcd for C₂₃H₂₃BrNaO₅Si 479.0475, found 479.0464.

(E)-3-bromo-5-(2-phenyl-1-ethenyl)-1,2-di(tert-butylphenylsilyloxy)benzene, 6. *t*BuOK (0.419 g, 3.75 mmol) was added portionwise at 0 °C to a solution of benzyl-triphenyl-phosphonium chloride (1.23 g, 3.17 mmol) in dry THF (25 ml). After stirring for 30 min at rt, a solution of **4** (2.0 g, 2.88 mmol) in dry THF (5 ml) was added. The mixture was stirred for 2 h at rt, quenched with brine (0.3 ml), diluted with ethyl ether (20 ml) and filtered. The filtrate was concentrated under vacuum and the resulting crude material was purified by column chromatography on silica gel (gradient, hexanes: CH₂Cl₂ 5:1 to 3:1) to afford 1.65 g (2.15 mmol, 75%) of a 1:2 mixture of (*E*- and (*Z*-) isomers of 3-bromo-5-(2-phenyl-1-ethenyl)-1,2-di(tert-butylphenylsilyloxy)benzene, **6** as a wax. ¹H-NMR (360 MHz, CDCl₃) δ 7.88–7.70 (m, 4H), 7.50–6.90 (m) + 6.84 (d, *J* = 1.8 Hz, *Z*) (22H), 6.56 (d, *J* = 1.8 Hz, *E*) + 6.26 (d, *J* = 1.8 Hz, *Z*) (1H), 6.49 (d, *J* = 16.2 Hz, *E*) + 6.22 (d, *J* = 12.2 Hz, *Z*) (1H), 6.05 (d, *J* = 16.2 Hz, *E*) + 5.89 (d, *J* = 12.2 Hz, *Z*) (1H), 1.09 (s, *E*) + 1.07 (s, *Z*) (9H), 0.76 (s, *E*) + 0.73 (s, *Z*) (9H); ¹³C-NMR (90 MHz, CDCl₃) δ 147.2, 147.1, 143.4, 143.0, 137.3, 136.7, 135.6, 135.5, 135.4, 133.7, 133.01, 132.8, 130.9,

130.8, 130.0, 129.9, 129.8, 129.7, 129.7, 128.9, 128.7, 128.4, 128.2, 128.1, 127.9, 127.8, 127.7, 127.6, 127.2, 126.8, 126.4, 125.9, 124.8, 121.7, 118.3, 116.0, 115.7; HRMS (ESI+) *m/z* [M+Na]⁺ calcd for C₄₆H₄₇BrNaO₅Si₂ 791.2180, found 791.2168. **(E)-3-bromo-5-(2-phenyl-1-ethenyl)-1,2-benzenediol, n1.** Triethylamine trihydrofluoride (0.63 ml, 3.92 mmol) was added dropwise at 0 °C to a solution of **6** (1.50 g, 1.96 mmol) in dry THF (20 ml). The mixture was stirred for 2 h at rt, quenched with brine (0.3 ml), diluted with ethyl ether (20 ml) and filtered. The filtrate was concentrated under vacuum and the resulting crude material was purified by chromatography on silica gel (gradient, hexanes: CH₂Cl₂ 5:1 to 3:1) to afford 0.443 g (1.52 mmol, 78%) of a 1:2 mixture of (*E*- and (*Z*-) isomers of 3-bromo-5-(2-phenyl-1-ethenyl)-1,2-benzenediol, **7** as a solid. Repeated column chromatographies allowed isolation of pure (*E*-) isomer and a (*Z*-) enriched mixture (4:1) of isomers. (*E*-**8**): mp: 95–96 °C (ethyl ether); ¹H-NMR (250 MHz, CDCl₃) δ 7.50–7.39 (m, 2H), 7.39–7.28 (m, 2H), 7.28–7.18 (m, 1H), 7.14 (d, *J* = 2.7 Hz, 1H), 7.03 (d, *J* = 2.7 Hz, 1H), 6.93 (d, *J* = 16.3 Hz, 1H), 6.86 (d, *J* = 16.3 Hz, 1H), 5.52 (br s, 2H); ¹³C-NMR (62.5 MHz, CDCl₃) δ 144.7, 139.9, 137.2, 132.2, 128.9, 128.6, 127.9, 127.0, 126.6, 121.9, 112.8, 109.9; IR (ATR, cm⁻¹) 3422, 3356, 1590, 1521, 1427, 1291, 959, 858, 830, 750, 692; HRMS (ESI-) *m/z* [M-H]⁻ calcd for C₁₄H₁₀BrO₂ 288.9859, found 288.9861. Mixture (4:1) of (*Z*-) and (*E*-) 7 isomers: ¹H-NMR (360 MHz, CDCl₃) δ 7.50–7.43 (m, *E*) + 7.39–7.31 (m, *E*) + 7.30–7.15 (m) (5H), 7.17 (d, *J* = 1.8 Hz, *E*) + 7.06 (d, *J* = 1.8 Hz, *E*) + 6.75 (d, *J* = 1.6 Hz, *Z*), + 6.92 (d, *J* = 1.6 Hz, *Z*) (2H), 6.96 (d, *J* = 16.2 Hz, *E*) + 6.90 (d, *J* = 16.2 Hz, *E*) + 6.55 (d, *J* = 12.0 Hz, *Z*) + 6.40 (d, *J* = 12.0 Hz, *Z*) (2H), 5.52 (br s, *E*) + 5.48 (br s, *Z*) + 5.39 (br s, *Z*) + 5.29 (br s, *E*) (2H); ¹³C-NMR (90 MHz, CDCl₃) δ 144.7, 144.1, 139.9, 139.5, 137.2, 137.0, 132.2, 131.6, 130.6, 129.0, 128.9, 128.6, 128.5, 128.5, 127.9, 127.5, 127.0, 126.6, 124.1, 121.9, 115.5, 112.8, 109.9, 109.3.

(E)-2-[3-bromo-4,5-di(tert-butylphenylsilyloxy)phenyl]-1-ethenylpyridine, 7. *t*BuOK (1.11 g, 9.94 mmol) was added portionwise at 0 °C to a solution of triphenyl-(2-pyridylmethyl)-phosphonium chloride hydrochloride (1.84 g, 4.32 mmol) in dry THF (40 ml). After stirring for 30 min at room temperature, a solution of **4** (3.0 g, 4.32 mmol) in dry THF (10 ml) was added. The mixture was stirred for 2 h at rt, quenched with brine (0.5 ml), diluted with ethyl ether (30 ml) and filtered. The filtrate was concentrated under vacuum and the resulting crude material was purified by flash chromatography on silica gel (gradient, hexanes: EtOAc 6:1 to 4:1) to afford 2.76 g (3.58 mmol, 83%) of (*E*-)2-[3-bromo-4,5-di(tert-butylphenylsilyloxy)phenyl]-1-ethenylpyridine, **7** as a solid. Mp: 182–185 °C (ethyl ether); ¹H-NMR (360 MHz, CDCl₃) δ 8.52–8.47 (m, 1H), 7.81–7.75 (m, 4H), 7.56 (dt, *J* = 7.9 Hz, *J* = 1.8 Hz, 1H), 7.45–7.20 (m, 16H), 7.22 (d, *J* = 2.2 Hz, 1H), 7.07 (d, *J* = 15.8 Hz, 1H), 7.09–7.02 (m, 1H), 7.02 (d, *J* = 7.9 Hz, 1H), 6.60 (d, *J* = 2.2 Hz, 1H), 6.21 (d, *J* = 15.8 Hz, 1H), 1.10 (s, 9H), 0.75 (s, 9H); ¹³C-NMR (90 MHz, CDCl₃) δ 155.4, 149.7, 147.2, 144.0, 136.6, 135.5, 135.4, 133.6, 132.8, 130.9, 130.3, 129.9, 129.7, 127.9, 127.7, 127.1, 125.1, 122.6, 122.0, 119.2, 116.1, 27.1, 26.5, 20.7, 19.3; IR (ATR, cm⁻¹) 2932, 2858, 1584, 1563, 1547, 1477, 1333, 1307, 1265, 1107, 929, 701; HRMS (ESI+) *m/z* [M+H]⁺ calcd for C₄₅H₄₇BrNO₅Si₂ 770.2313, found 770.2289.

(E)-2-[(3-bromo-4,5-dihydroxyphenyl)-1-ethenyl]pyridinium chloride, c2. Triethylamine trihydrofluoride (0.38 ml, 2.34 mmol) was added dropwise at 0 °C to a solution of **7** (0.60 g, 0.78 mmol) in dry THF (10 ml). After stirring for 2 h at rt, HCl 35% was added (0.5 ml) and the resulting suspension was stirred for 10 min at rt, and filtered. The solid was washed with ethyl ether (2x5 ml) and dried under vacuum to afford 0.166 g (0.51 mmol, 65%) of (*E*-)2-[(3-bromo-4,5-dihydroxyphenyl)-1-ethenyl]pyridinium chloride, **c2** as a yellow solid. Mp: 210–212 °C (acetone); ¹H-NMR (360 MHz, DMSO-*d*₆) δ 10.44 (br s, 1H), 9.93 (br s, 1H), 8.70 (d, *J* = 5.0 Hz, 1H), 8.43 (t, *J* = 7.7 Hz, 1H), 8.26 (d, *J* = 8.3 Hz, 1H), 7.96 (d, *J* = 16.6 Hz, 1H), 7.75 (t, *J* = 6.8 Hz, 1H), 7.31 (d, *J* = 2.0 Hz, 1H), 7.19 (d, *J* = 2.0 Hz, 1H); ¹³C-NMR (90 MHz, DMSO-*d*₆) δ 150.5, 146.6, 145.6, 144.8, 141.4, 139.2, 127.2, 124.0, 123.7, 123.5, 116.9, 113.2, 110.0; IR (ATR, cm⁻¹) 3049, 2811, 1637, 1614, 1593, 1429, 1296, 1163, 964, 830, 760; HRMS (ESI-) *m/z* [M-HCl-H]⁻ calcd for C₁₃H₉BrNO₂ 289.9822, found 289.9817.

Crystal data: Due to the low diffraction intensity of the crystals, the diffraction data were collected under synchrotron radiation ($\lambda=0.977\text{\AA}$) at 150 K with a CCD detector in the BM16 Spanish beamline at the ESRF (Grenoble). The crystal was coated in paratone®. The structure was solved by direct methods and refined by full-matrix least-squares techniques on F² with SHELX-97.[30] Crystal adsorption was corrected by Scalepack.[31] Non-hydrogen atoms were refined anisotropically. Crystallographic details for **2**: Mr = 441.84, crystal size 0.3 × 0.2 × 0.03, monoclinic phase, space group P21/c, a = 9.975 Å (2), b = 20.793 Å (3), c = 16.760 Å (2) Å, V = 3578(5) Å³, Z = 8, pcalcd. = 1.078 g cm⁻³, F(000) = 23926, μ (Mo-K α) = 0.642 mm⁻¹. A total of 17129 reflections were measured in the range 5.66° ≤ 2 θ ≤ 56.78°, of which 13560 were unique (Rint = 0.0235). Final R indices: R1 = 0.0746 [I/2 σ (I)], wR2 = 0.1821 (all data) for 682 parameters; max./min. residual electron density 0.733/−1.130 e⁻Å⁻³.

Steady-state absorption and fluorescence spectroscopy: UV-Vis spectra were recorded at room temperature using a Varian Cary05e spectrophotometer. Fluorescence spectra were recorded at room temperature in a Perkin Elmer LS 45 fluorescence spectrophotometer. The fluorescence quantum yields of all solutions investigated were determined relative to *N,N'*-bis(1-hexylheptyl)perylene-3,4,9,10 in acetonitrile ($\Phi_F=1$).^[26]

pH measurements: pH measurements upon acid-base addition on acetonitrile solutions of **1** and **2** were performed at room temperature with a Crison 52-01 pH electrode in a Crison BASIC 20 potentiometer. pH values are given relative to the acetonitrile solvent (ϕ pH scale).^[27] To calibrate the electrode system we used reference buffers in acetonitrile (pyridine-pyridinium bromide and phenol-sodium phenolate), whose ϕ pH can be derived from the Henderson-Hasselbach equation using the pK_a values in acetonitrile reported for these systems.^[14]

Quantum chemical calculations: Quantum chemical calculations were performed employing the Gaussian 03 package of programs^[28] on a 32-bit multiprocessor computer. Density functional theory (DFT) geometrical optimization of ground electronic states of all investigated molecules was carried out at the B3LYP hybrid

functional level with the 6-311+G(d,p) basis set. To account for solvent polarity effects, calculations were performed in acetonitrile solvent by means of the polarizable continuum model (PCM, $\epsilon=36.64$). The resulting geometries and molecular orbitals were plotted using Molden. The excitation energies and oscillator strengths (f) of the UV-visible absorption transition bands were then computed by means of time-dependent density functional theory at the B3LYP/6-311G+(d,p) level on the B3LYP/6-311+G(d,p) ground state geometries and accounting for acetonitrile solvent (PCM). For each protonation state of **1** and **2** the spectroscopic properties of all possible rotamers were calculated and the final average values were obtained by using Boltzmann coefficients at room temperature ($\exp(-E_{\text{rotamer}}/k_B T)/\sum \exp(-E_{\text{rotamer}}/k_B T)$) as weighting factors.

Acknowledgements

We acknowledge the financial support of the Ministerio de Educación y Ciencia (MEC) through projects MAT2006-13765-C02-01, CTQ2004-02539 and CTQ2006-01040. F.B. and J.H. thank MCyT-ERDF for their "Ramon y Cajal" contracts, E.E. thanks the MEC for a predoctoral grant and G.G.B. thanks DURSI and FSE for a predoctoral grant.

Received: ((will be filled in by the editorial staff))

Revised: ((will be filled in by the editorial staff))

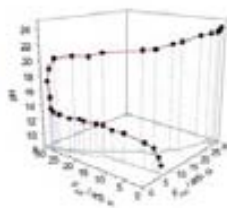
Published online: ((will be filled in by the editorial staff))

- [1] B. R. Eggins, *Chemical Sensors and Biosensors (Analytical Techniques in the Sciences)*, Wiley-VCH, Weinheim, **2002**.
- [2] a) *Fluorescent Chemosensors for Ion and Molecule Recognition* (Ed.: A. W. Czarnik), ACS Books, Washington, **1993**; b) A. P. de Silva, H. Q. N. Gunaratne, T. Gunnlaugsson, A. J. M. Huxley, C. P. McCoy, J. T. Rademacher, T. E. Rice, *Chem. Rev.* **1997**, *97*, 1515-1566; c) O. S. Wolfbeis, *J. Mat. Chem.* **2005**, *15*, 2657-2669; d) L. Basabe-Desmonts, D. N. Reinhoudt, M. Crego-Calama, *Chem. Soc. Rev.* **2007**, *36*, 993-1017.
- [3] a) B. Valeur, I. Leray, *Coord. Chem. Rev.* **2000**, *205*, 3-40; b) P. D. Beer, P. A. Gale, *Angew. Chem. Int. Ed.* **2001**, *40*, 487-516; c) R. Martínez-Máñez, F. Sancenón, *Chem. Rev.* **2003**, *103*, 4419-4476; d) L. Fabbrizzi, M. Licchelli, A. Taglietti, *Dalton Trans.* **2003**, 3471-3479; e) G. W. Gokel, W. M. Leevy, M. E. Weber, *Chem. Rev.* **2004**, *104*, 2723-2750.
- [4] a) J. W. Bell, N. M. Hext, *Chem. Soc. Rev.* **2004**, *33*, 589-598; b) R. Jelinek, S. Kolusheva, *Chem. Rev.* **2004**, *104*, 5987-6016.
- [5] a) A. P. de Silva, R. A. D. D. Rupasinghe, *J. Chem. Soc. Chem. Commun.* **1985**, 1669-1670; b) S. G. Schulman, S. Chen, F. Bai, M. J. P. Leiner, L. Weis, O. S. Wolfbeis, *Anal. Chim. Acta* **1995**, *304*, 165-170; c) L. M. Daffy, A. P. de Silva, H. Q. N. Gunaratne, C. Huber, P. L. M. Lynch, T. Werner, O. S. Wolfbeis, *Chem. Eur. J.* **1998**, *4*, 1810-1815; d) S. Charier, O. Ruel, J.-B. Baudin, D. Alcor, J.-F. Allemand, A. Meglio, L. Jullien, *Angew. Chem. Int. Ed.* **2004**, *43*, 4785-4788; e) G. Nishimura, Y. Shiraishi, T. Hirai, *Chem. Commun.* **2005**, 5313-5315; f) A. S. Vasylevska, A. A. Karasyov, S. M. Borisov, C. Krause, *Anal. Bional. Chem.* **2007**, *387*, 2131-2141; g) A. P. de Silva, S. S. K. de Silva, N. C. W. Goonesekera, H. Q. N. Gunaratne, P. L. Lynch, R. K. Nesbitt, S. T. Patuwathavithana, N. L. D. Ramyalai, *J. Am. Chem. Soc.* **2007**, *129*, 3050-3051; h) B. Tang, X. Liu, K. Xu, H. Huang, G. Yang, L. An, *Chem. Commun.* **2007**, 3726-2728.
- [6] a) D. Margulies, G. Melman, A. Shanzer, *Nat. Mater.* **2005**, *4*, 768-771; b) A. P. de Silva, S. Uchiyama, *Nat. Nanotechnol.* **2007**, *2*, 399-410.
- [7] a) T. Gunnlaugsson, D. Parker, *Chem. Commun.* **1998**, 511-512; b) M. Su, H. Ma, Q. Ma, Z. Wang, J. Yang, M. Wang, *Chem. Commun.* **2001**, 960-961; c) F. Pina, J. C. Lima, C. Lodeiro, J. S. de Melo, P. Diaz, M. T. Albelda, E. Garcia-España, *J. Phys. Chem. A* **2002**, *106*, 8207-8212; d) V. F. Valuk, G. Duportail, V. G. Pivovarenko, *J. Photochem. Photobiol. A: Chem.* **2005**, *175*, 226-231; e) Y. Shiraishi, Y. Tokitoh, G. Nishimura, T. Hirai, *J. Phys. Chem. B* **2007**, *111*, 5090-5100.
- [8] a) A. P. de Silva, H. Q. N. Gunaratne, C. P. McCoy, *Chem. Commun.* **1996**, 2399-2400; b) T. Gunnlaugsson, J. P. Leonard, K. Sénéchal, A. J. Harte, *J. Am. Chem. Soc.* **2003**, *125*, 12062-12063; c) S. A. de Silva, K. C. Loo, B. Amorelli, S. L. Pathirana, M. Nyakirangani, M. Dharmasena, S. Demarais, B. Dorcley, P. Pullay, Y. A. Salih, *J. Mater. Chem.* **2005**, *15*, 2791-2795; d) Y. Diaz-Fernandez, F. Fori, C. Mangano, P. Pallavicini, S. Patroni, A. Perez-Gramatges, S. Rodriguez-Calvo, *Chem. Eur. J.* **2006**, *12*, 921-930.
- [9] a) P. Pallavicini, V. Amendola, C. Massera, E. Mundum, A. Taglietti, *Chem. Commun.* **2002**, 2452-2453; V. Amendola, L. Fabbrizzi, C. Mangano, H. Miller, P. Pallavicini, A. Parotti, A. Taglietti, *Angew. Chem., Int. Ed.* **2002**, *41*, 2553-2556; c) Z. Wang, G. Zheng, P. Lu, *Org. Lett.* **2005**, *7*, 3669-3672; d) G. Zheng, Z. Wang, L. Tang, P. Lu, W. P. Weber, *Sens. Actuators B* **2007**, *122*, 389-394.
- [10] R. Sjöback, J. Nygren, M. Kubista, *Spectrochimia Acta Part A* **1995**, *51*, L7-L21.
- [11] R. J. Motekaitis, A. E. Martell, *Inorg. Chem.* **1984**, *23*, 18-23.
- [12] E. Evangelio, D. Ruiz-Molina, *Eur. J. Inorg. Chem.*, **2005**, *15*, 2957-2971.
- [13] C. G. Pierpont, C. W. Lange, *Prog. Inorg. Chem.* **1994**, *41*, 331-443.
- [14] S. Espinosa, E. Bosch, M. Rosés, *J. Chromatogr. A* **2002**, *964*, 55-66.
- [15] As a proof-of-concept, the implementation of **2** in a nanostructured pH sensor and the performance of the resulting device has also already been reported in a previous communication: A. Martínez-Otero, E. Evangelio, R. Alibes, J. L. Bourdelande, D. Ruiz-Molina, F. Busque, J. Hernando, *Langmuir* **2008**, *24*, 2963-2966.
- [16] R. G. Lange, *J. Org. Chem.* **1962**, *27*, 2037-2039.
- [17] F.D. Lewis, E.M. Crompton, *J. Am. Chem. Soc.* **2003**, *125*, 4044-4045.
- [18] E.M. Crompton, F.D. Lewis, *Photochem. Photobiol. Sci.* **2004**, *3*, 660-668.
- [19] H. Ilhmel, A. Meiswinkel, C. J. Mohrschladt, D. Otto, M. Waidelich, M. Towler, R. White, M. Albrecht, A. Schnurpfeil, *J. Org. Chem.* **2005**, *70*, 3929-3938.
- [20] T. Murohoshi, K. Kaneda, M. Ikegami, T. Arai, *Photochem. Photobiol. Sci.* **2003**, *2*, 1247-1249.
- [21] G. Favaro, U. Mazzucato, F. Masetti, *J. Phys. Chem.* **1973**, *77*, 601-604.
- [22] G. Ginocchietti, U. Mazzucato, A. Spalletti, *Int. J. Photoenergy* **2004**, *6*, 241-250.
- [23] U. Mazzucato, F. Momicchioli, *Chem. Rev.* **1991**, *91*, 1679-1719.
- [24] M.J. Kamlet, J.L.M. Abboud, M.H. Abraham and R.W. Taft, *J. Org. Chem.* **1983**, *48*, 2982-2996.
- [25] G. Marconi, G. Bartocci, U. Mazzucato, A. Spalletti, F. Abbate, L. Angeloni, E. Castellucci, *Chem. Phys.* **1995**, *196*, 383-393.
- [26] T. Kircher, H.-G. Löhmansröben, *Phys. Chem. Chem. Phys.* **1999**, *1*, 3987-3992.
- [27] S. Espinosa, E. Bosch, M. Rosés, *Anal. Chem.* **2000**, *72*, 5193-5200.
- [28] Gaussian 03 (Revision B.04), M. J. Frisch, G. W. Trucks, H. B. Schlegel, G. E. Scuseria, M. A. Robb, J. R. Cheeseman, J. A. Montgomery, Jr., T. Vreven, K. N. Kudin, J. C. Burant, J. M. Millam, S. S. Iyengar, J. Tomasi, V. Barone, B. Mennucci, M. Cossi, G. Scalmani, N. Rega, G. A. Petersson, H. Nakatsuji, M. Hada, M. Ehara, K. Toyota, R. Fukuda, J. Hasegawa, M. Ishida, T. Nakajima, Y. Honda, O. Kitao, H. Nakai, M. Klene, X. Li, J. E. Knox, H. P. Hratchian, J. B. Cross, V. Bakken, C. Adamo, J. Jaramillo, R. Gomperts, R. E. Stratmann, O. Yazyev, A. J. Austin, R. Cammi, C. Pomelli, J. W. Ochterski, P. Y. Ayala, K. Morokuma, G. A. Voth, P. Salvador, J. J. Dannenberg, V. G. Zakrzewski, S. Dapprich, A. D. Daniels, M. C. Strain, O. Farkas, D. K. Malick, A. D. Rabuck, K. Raghavachari, J. B. Foresman, J. V. Ortiz, Q. Cui, A. G. Baboul, S. Clifford, J. Cioslowski, B. B. Stefanov, G. Liu, A. Liashenko, P. Piskorz, I. Komaromi, R. L. Martin, D. J. Fox, T. Keith, M. A. Al-Laham, C. Y. Peng, A. Nanayakkara, M. Challacombe, P. M. W. Gill, B. Johnson, W. Chen, M. W. Wong, C. Gonzalez, J. A. Pople, Gaussian, Inc., Wallingford CT, **2004**.
- [30] G. M. Sheldrick, Program for the Refinement of Crystal Structures; University of Göttingen, Germany, **1997**.
- [31] Otwinowski, Z.; Minor, W. *Methods Enzymol.* **1997**, *276*, 307-326.

((Catch Phrase))

*Emilia Evangelio, Jordi Hernando,
Inhar Imaz, Gisela G. Bardají, Ramon
Alibés, Félix Busqué and Daniel Ruiz-
Molina*

**Catechol Derivatives as Fluorescent
Chemosensors for Wide range pH
Detection**



A new catechol-based derivative showing complementary 'off-on-off' and 'on-off-on' emission profiles upon pH variation has been described to exhibit excellent acidity detection over a broad pH range by applying dual-wavelength detection methodology

Article VI

Title: Intramolecular Electron Transfer in the Series of Mixed-Valence Complexes [M^{III}(Cat-N-SQ)(Cat-N-BQ)] (M=Fe, Co, Ni) bearing Non-Innocent Ligands: a Combined Experimental and Theoretical Study

Authors: E. Evangelio, M. –L. Bonnet, M. Cabañas, M. Nakano, J. - P. Sutter, L. Sorace, A. Dei, V. Robert and D. Ruiz-Molina

Publication: Chem. Eur. J. 2008, in preparation.

Intramolecular Electron Transfer in the Series of Mixed-Valence Complexes $[M^{III}(\text{Cat-N-SQ})(\text{Cat-N-BQ})]$ (M=Fe, Co, Ni) bearing Non-Innocent Ligands: a Combined Experimental and Theoretical Study

Emilia Evangelio,^[a] Marie-Laure Bonnet,^[b] Miquel Cabañas,^[c] Motohiro Nakano,^[d] J. -P. Sutter,^[e] Lorenzo Sorace,^[f] Andrea Dei,^[f] Vincent Robert^[b] and Daniel Ruiz-Molina^{*,[g]}

Abstract: ((Abstract text, max. 600-2000 characters))

Keywords: ((electron transfer · valence tautomerism · organic radical · redox active ligand))

Introduction

Development of molecular-scale systems that exhibit intramolecular electron transfer phenomena induced by external stimuli has attracted considerable attention.^[1] The interest is twofold. First, from a fundamental point of view, these complexes represent an excellent scenario to study the role of various parameters governing the intramolecular electron transfer (IET) phenomena in molecular systems. And second, the possibility of inducing a reversible change in the electronic distribution of a molecular system opens the door to their potential use on information storage and integrated molecular-sized devices. Mixed-valence systems are excellent candidates for such studies since they contain at least two redox sites with different oxidation states linked by a bridge that mediates the transfer of electrons from one site to the other.^[2] The study of molecular mixed-valence systems was initiated by Taube's seminal work on compounds such as $[(\text{NH}_3)_5\text{Ru-bridge-Ru}(\text{NH}_3)_5]^{5+}$.^[3] Since then, most of the mixed valence complexes shown to exhibit

intramolecular electron transfer phenomena are homo and heteronuclear metallic complexes^[4] or metallocene^[5] units where the two metal atoms with different oxidation states are connected through an organic bridging ligand.

Mixed-valence molecular systems where the electro-active units are pure organic groups have so far received less attention, probably due to their high instability.^[6] Nevertheless, the flexibility of organic synthesis may allow the obtaining of pure organic mixed-valence molecular wires with specific and sophisticated topologies required in the demanding and ever-increasing world of nanotechnology. Moreover, the study of their properties should lead to the synthesis of systems where the electron transfer could be fine-tuned in a far more precise way than had been done with coordination compounds. The different types of electroactive organic units so far used are: i) anion-radicals derived from conjugated diquinones and diimides,^[7] ii) cation-radicals derived from bis(tetrathiafulvalenes),^[8] iii) cation-radicals derived from bis(hydrazines),^[9] iv) quinoid groups^[10] and v) ion-radicals derived from π -conjugated polyarylmethyl/polyarylamines^[11] and polychlorotriphenylmethyl radicals.^[12] In all the previous examples, the different pure organic electroactive ligands with different oxidation states are linked by a bridge that mediates the transfer of electrons between them. However, in some cases the redox-active ligand is combined with a transition metal ion on a heterogeneous mixed-valence complex. These complexes exhibit a reversible intramolecular electron transfer between the metal ion and the ligand, leading to an internal charge redistribution and therefore to the existence of two different electronic isomers with different charge distributions, and consequently significantly different optical, electric and magnetic properties. This family of complexes has been termed with the generic term of Valence Tautomerism (VT).^[13]

An important issue of VT complexes that has attracted considerable interest in the last few years is the possibility to be unique systems that exhibit more than one type of intramolecular electron transfer process simultaneously.^[14] Indeed, these compounds containing at least two redox-active ligands with different oxidation state may be considered as a reversal of the

- [a] E. Evangelio
Institut de Ciència de Materials de Barcelona (CSIC)
Esfera UAB, Campus UAB 08193, Cerdanyola del Vallès, Catalonia, Spain
- [b] M.-L. Bonnet, Dr. V. Robert
Laboratoire de Chimie, UMR 5182, Ecole normale supérieure de Lyon,
69364 Lyon cedex 07
- [c] Dr. M. Cabañas
Servei de Ressonància Magnètica Nuclear, UAB, Campus de la UAB,
08193, Cerdanyola del Vallès, Catalonia, Spain.
- [d] Dr. M. Nakano
Department of Applied Chemistry, Graduate School of Engineering, Osaka
University, Yamada-oka, Suita, Osaka 565-0871, Japan
- [e] Dr. J. -P. Sutter
Materiaux Moléculaires, Supramoléculaires et Biomimétiques, Laboratoire
de Chimie de Coordination (LCC-CNRS), 205, Route de Narbonne,
31077, Toulouse Cedex 04, Toulouse, France.
- [f] Dr. L. Sorace, Prof. A. Dei
Laboratory of Molecular Magnetism, Dept. Of Chemistry, Polo Scientifico,
Via della Lastrucia, Italy.
- [g] Dr. D. Ruiz-Molina

ligand-bridged mixed-valence metal complexes^[15] where redox-active organic ligands are electronically coupled to an extent that depends upon orbital interactions with the bridge.^[16] Therefore, both ligand-to-metal (LM) and intramolecular ligand-to-ligand (LL) electron transfer processes may take place. A schematic representation of both electron transfer processes is shown in Figure 1.

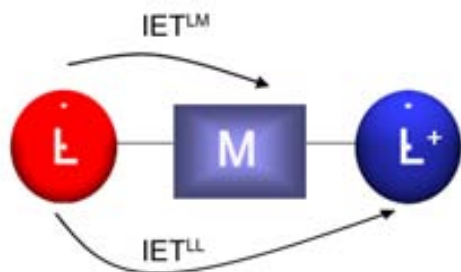
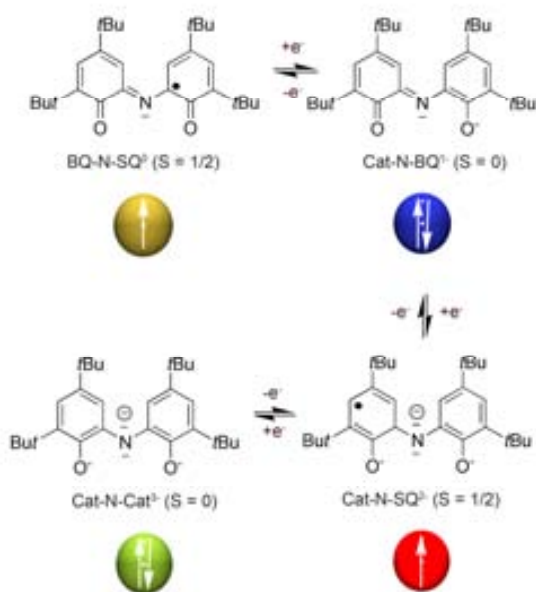


Figure 1. Graphical representation of different IET possible processes that may take place in a metal-based complex formed by an electroactive ligand and a first transition metal ion

The extent to which LM and LL electron transfer processes can coexist within the same complex remains an open-issue in spite of its enormous interest. First, the coexistence of two different electron transfer mechanisms allow them to be unique model systems to provide insight into the basic factors affecting intramolecular electron transfer in molecular complexes. And second, since the two isomers involved in the VT process exhibit different optical, electric and magnetic properties,^[17] these complexes offer potential applications in bistable molecular switching materials and devices. For this reason, we have initiated a systematic strategy to study the different electron transfer processes that can take place in VT complexes. Recently we confirmed for the first time the coexistence of both LM and LL electron transfer in complex [Co(3,5-DTBCat)(3,5-DTBSQ)(bpy)] (**1**),^[18] where 3,5-DTBCat²⁻ and 3,5-DTBSQ⁻ refer, respectively, to the catecholate (Cat²⁻) and semiquinonate (SQ⁻) forms of 3,5-di-tert-butyl-o-quinone.



Scheme 1. Different oxidation levels for Schiff-base iminoquinone ligand.

However a systematic and detailed extension of this work to shed more light into the electron transfer mechanisms within this

family of complexes is highly required. An excellent model for such studies is the family of complexes derived from the tridentate Schiff-base ligand 3,5-di-tert-butyl-1,2-quinone-1-(2-hydroxy-3,5-di-tert-butylphenyl)imine anion (Cat-N-BQ), which can exist in different oxidation forms as is shown in scheme 1, ranging from 0 to -3.^[19]

Such a range leads to stable coordination complexes involving several metal ions in a variety of oxidation states although it usually coordinates in the mononegative Cat-N-BQ⁻ or dinegative Cat-N-SQ²⁻ radical forms.^[20]

In this work the series of complexes [M(Cat-N-BQ)(Cat-N-SQ)], where M=Co (**2**),^[21] Fe (**3**) and Ni (**4**)^[22] has been thoroughly revised and the temperature-dependence of the two possible electron transfer mechanisms studied. Previously synthesized, they offer an excellent scenario to study the coexistence of both LM and LL electron transfer as well as an excellent model to study the systematic influence of the nature on the metal ion in such processes, only preliminary studies on the VT behaviour of complex **2** had been so far reported.^[23] For this, electron transfer have been studied by means of complementary spectroscopic techniques mainly UV-Vis and NMR. Such experimental studies have been combined with ab initio wavefunction based methods CASPT2 calculations to clarify the underlying electron distributions in the ground and speculated excited states. Depending on the metal ion, rather different behaviors are evidenced and theoretically rationalized.

Results

UV-Vis spectroscopy. Variable-temperature UV-Vis spectra of a toluene solution of complex **2** was obtained in the 200-360 K temperature range. The choice of toluene is justified both on the basis of the high solubility of the complex and its relative large working temperature range. The intramolecular electron transfer between the ligand and the metal ion can be induced by variations of the temperature and monitored by UV-Vis (see Figure 1b). For instance, bands at 391, 439 and 533 nm characteristic of the 2,*l*s-Co(III) (S=1/2) tautomer can be observed in the low-temperature regime. An increase of temperature promotes an intramolecular electron transfer from the ligand to the metal as one of the ligands then gets oxidized by one electron and evolves for a Cat-N-SQ²⁻ radical to a Cat-N-BQ¹⁻ ligand (see Equation 1).



Thus, the 2,*l*s-Co(III) (S=1/2) tautomer converts into the 2,*h*s-Co(II) (S=3/2) tautomer. As a consequence, the intensity of such bands decreases whereas bands at 721 and 797 nm characteristic of the 2,*h*s-Co(II) tautomer increase in intensity (see Figure 2b). Two isobestic points appear at 856 and 590 nm, indicating that at least two species are interconverting under the studied temperature range.

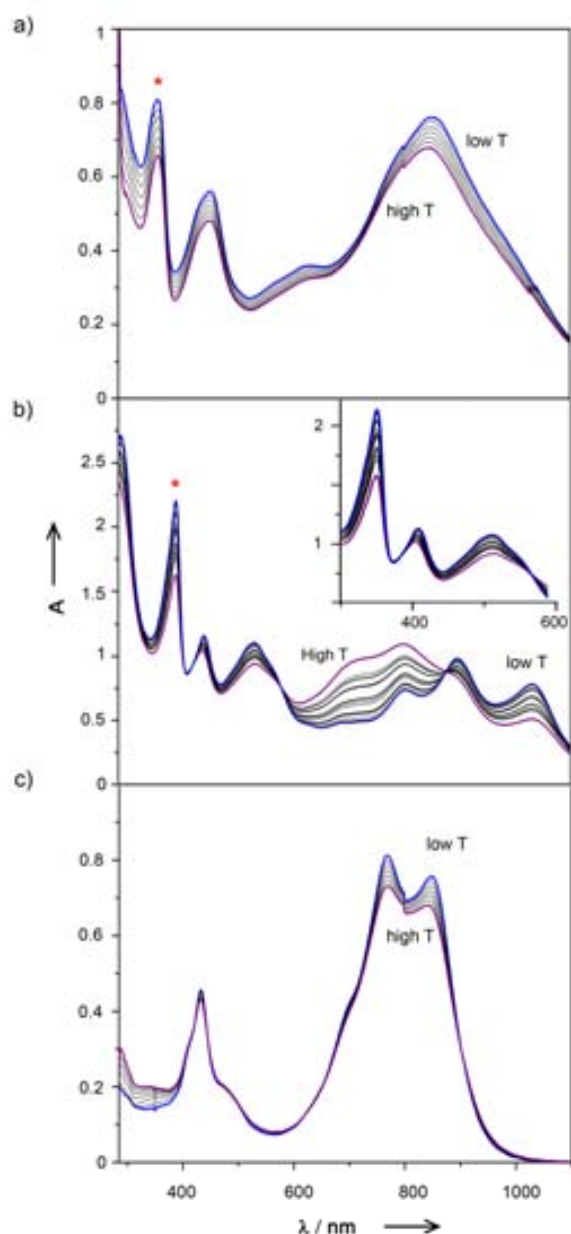


Figure 2. UV-Visible spectra at variable temperature (Temperature range from 203 K (low T) to 363 K (high T)), for complexes a) [Fe(cat-N-SQ)(Cat-N-BQ)], b) [Co(Cat-N-SQ)(Cat-N-BQ)] and c) [Ni(Cat-N-BQ₂)]. In the spectra is marked the band that corresponds to the radical with an asterisk.

In a previous work, Girgis et al.^[19c] predicted that most of the bands observed in the electronic spectra of complexes with general formula ML_2 ($L = \text{Cat-N-BQ}^{1-}$ and or Cat-N-SQ^{2-}), as the one shown in Figure 1, are associated with electronic transitions within the ligands though modulated specially at higher wavelengths depending on the nature of the metal ion. Among them, of special interest is the band centred around 390 nm, which can be tentatively attributed to the radical character of the Cat-N-SQ^{2-} ligand since most aromatic organic radicals usually display bands in this region of the spectra. The visualization of such a band can give direct information on the radical character of the ligand and therefore on the electronic distribution of the complex at a given temperature. In fact, the intensity of such band decreases on the interconversion from the *2-ls* to the *2-hs*, since no radicals are observed in the last tautomer. To further support this assignation, the UV-Vis spectra of complexes [Ga(Cat-N-SQ)(Cat-N-BQ)] (**5**) and [Zn(Cat-N-BQ₂)] (**6**) were also recorded and studied for comparison purposes (Figure 3).

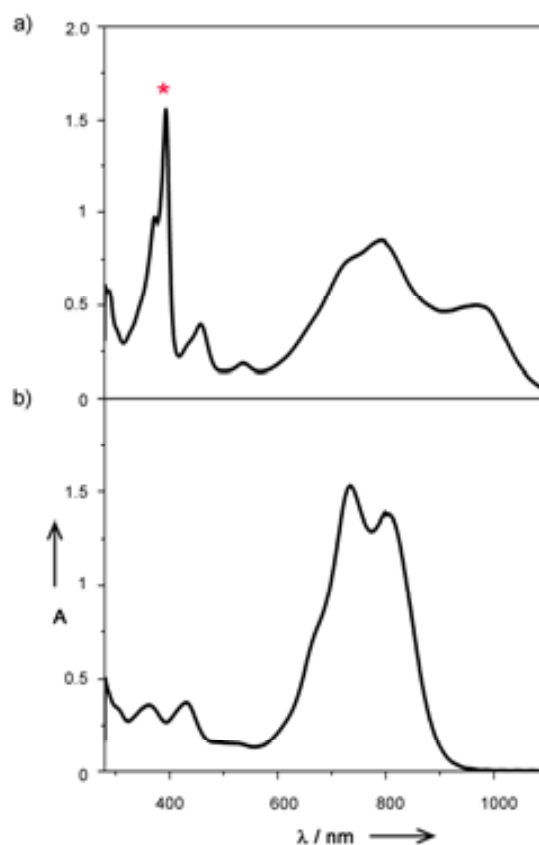


Figure 3. UV-Visible spectra at variable temperature (Temperature range from 203 K (low T) to 363 K (high T)), for complexes a) [Ga(Cat-N-SQ)(Cat-N-BQ)] and b) [Zn(Cat-N-BQ₂)]. In the spectra is marked the band that corresponds to the radical with an asterisk.

The former complex has one radical Cat-N-SQ^{2-} ligand, and therefore is expected to exhibit such a band, whereas the electronic spectra of [Zn(Cat-N-BQ₂)] does not. As expected, complex **6** shows two intense bands at 793 and 736 nm (figure 3b), similar to those observed for the *2,hs*-Co(II) tautomer lacking any band around 350-400 nm since both ligands are present in the non-radical form Cat-N-BQ^{1-} . On the contrary, the electronic spectrum of complexes **2,ls**-Co(III) and **5** (figure 3a) are dominated by an intense transition at 390 nm associated to the presence of the Cat-N-SQ^{2-} radical ligand.

Keeping this in mind, the variable-temperature UV-Vis spectra of a toluene solution of complex **3** was also studied (Figure 2a). Bands at 357, 451 and 853 nm with shoulders around 560, 620, and 790 nm can be observed in the low-temperature regime. The observation of a band at 357 nm is an indication that the iron complex **3** most likely bears a radical Cat-N-SQ^{2-} so it can be formulated as [Fe(Cat-N-SQ)(Cat-N-BQ)]. An increase of the temperature only induces a slight variation of the intensity of all bands, without the presence of any isobestic point. Such spectral variations may be associated to variations of the solution viscosity, among others, rather than to the existence of VT as previously described for complex **2**. Therefore, complex **3** remains in the *3,ls*-Fe(III) tautomeric form at least in the considered temperature range. On the contrary, the UV-Vis spectrum of the nickel complex **4**, as can be seen in figure 2c, exhibit bands at 432, 766 and 846 nm with a shoulder around 690 nm. Moreover, as previously described for complex **4**, an increase of the temperature does not induce any considerable change on the electronic spectrum, only a slight

variation of the bands intensity is observed. The presence and intensity of the two bands at higher wavenumbers as well as the characteristic radical band are an indication that the nickel complex remains in the $4,hs$ -Ni(II) tautomeric form over the whole temperature range studied. In fact its spectrum is quite reminiscent to these observed for complex **6** which is not expected to exhibit VT.

Finally, it has to be mentioned that beyond the bands previously described that tail into the 1000-1200 nm region, no bands in the near-infrared region were observed for all the complexes studied.

Magnetization measurements. The magnetic behaviour of complexes **2-4** in solution was studied by NMR and the Evans method.^[24] This technique is applicable to the measurement of the magnetic susceptibility in solution of a paramagnetic species based on the frequency shift occasioned in an NMR signal of a standard compound, for instance TMS, by the additional magnetic field of the tested paramagnetic species. The μ_{eff} vs. temperature plot for a toluene solution of complexes **2-4** obtained by applying the Evans method is shown in Figure 4.

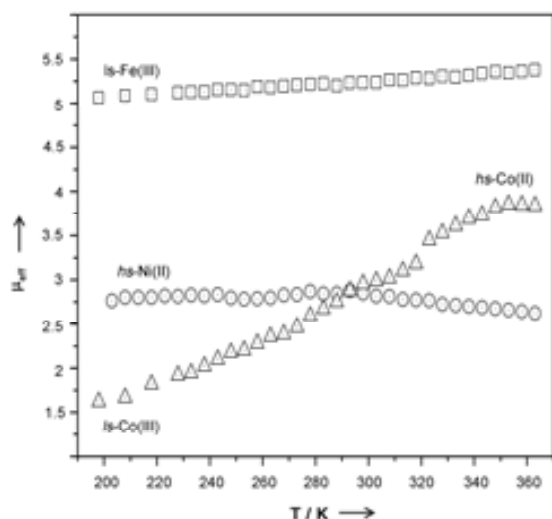


Figure 4. Representation of μ_{eff} vs T obtained by the application of Evans Method in complexes **2-4** in the same range of temperatures that in the UV-Visible experiments (203 K to 363 K), **2**: [Co(Cat-N-SQ)(Cat-N-BQ)] Δ ; **3**: [Fe(cat-N-SQ)(Cat-N-BQ)] \square and **4**: [Ni(cat-N-BQ)] \circ .

At low temperatures, the μ_{eff} vs. T plot of complex **2** exhibits a value of $1.62 \mu_B$ close to the theoretical value of $1.73 \mu_B$ expected for the single unpaired electron of the $2,ls$ -Co(III) ($S=1/2$) tautomer. An increase of the temperature induces a gradual increase of μ_{eff} till a maximum value of $3.84 \mu_B$ is reached at 353 K, close to the theoretical value of $3.87 \mu_B$ expected for a $S=3/2$ species. This fact is in agreement with the existence of the equilibrium between the tautomers $2,ls$ -Co(III) ($S=1/2$) and $2,hs$ -Co(II) ($S=3/2$) shown in Eq. 1 as previously observed by UV-Visible. Under these conditions, one may track the thermodynamic parameters associated with the rearrangement of the electronic configuration in writing $\chi_m T$ as

$$\chi_m T = \chi_m T_{ls-Co(III)} + \gamma_{hs-Co(II)} (\chi_m T_{hs-Co(II)} - \chi_m T_{ls-Co(III)}) \quad (2)$$

with

$$\gamma_{hs-Co(II)} = 1 / ((\exp(\Delta H/RT) - \Delta S/R) + 1) \quad (3)$$

where $\chi_m T_{ls-Co(III)}$ and $\chi_m T_{hs-Co(II)}$ are the $\chi_m T$ values for isolated $2,ls$ -Co(III) ($S=1/2$) and $2,hs$ -Co(II) ($S=3/2$), respectively, and $\gamma_{hs-Co(II)}$ is the molar fraction of $2,hs$ -Co(II). When $\chi_m T_{ls-Co(III)}$ and χ_m

$T_{hs-Co(II)}$ are fixed to the values of 1.62 and $3.84 \mu_B$, the least-square fitting of $\chi_m T$ to Eq. 3 gives the values of $\Delta H = 28.2 \text{ kJ.mol}^{-1}$ and $\Delta S = 95.2 \text{ J.K}^{-1}.\text{mol}^{-1}$ ($T_c = \Delta H / \Delta S = 296 \text{ K}$). The observation of a T_c around room temperature opens the door to them as possible candidates for bistable molecular switching materials and devices.

The μ_{eff} vs. T plot of complexes **3** and **4** is also shown in Figure 3 for comparison purposes. Complex **3** exhibits a constant magnetic susceptibility value along the whole temperature range of $\sim 5.20 \mu_B$. This value can be explained if we consider that the main species in solution along the whole temperature range is the [Fe (Cat-N-BQ)(Cat-N-SQ)] (**3**, ls -Fe(III)) tautomer. These results are in agreement with our electronic spectra analysis previously described that shows a characteristic band of the radical Cat-N-SQ $^{2-}$ around 350 nm. In this species then a strong antiferromagnetic interaction between the radical ligand Cat-N-SQ $^{2-}$ ($s=1/2$) and the hs -Fe(III) ion ($s = 5/2$) leads to a $S=2$ magnetic ground state for which a theoretical value of $4.90 \mu_B$ is expected (the μ_{eff} value expected for a non-interacting Fe(III) and a organic radical would be $6.16 \mu_B$). Similar behaviour was observed for complex **4**, which exhibits a constant magnetic susceptibility value along the whole temperature range of $\sim 2.8 \mu_B$. This is the value expected for a $S = 1$ magnetic ground state from the hs -Ni(II). All these values are synthesized in tables 1, 2, and 3 in supporting information.

Solid State Measurements. The magnetic properties of complex **2** have already been described in a previous work by Dei et al.^[23a] These authors showed that complex **2** exhibits a tautomeric interconversion in the solid state but at much higher temperatures than in solution, with a transition that starts at approximately 370-380 K, i.e., at least 150 K higher than in solution. Variable-temperature magnetic susceptibility data for crystalline samples of complexes **3-4** were measured here over the temperature range of 5-400 K with an applied external field of 10kG. Complexes **3** and **4** are characterized by a μ_{eff} value of 4.7 and $3.1 \mu_B$, respectively, at high temperatures that remains constant down to approximately 30 K, whereupon it gradually decreases more likely due to the presence of small intermolecular antiferromagnetic exchange interactions. In the case of complex **4** such a value is close to the theoretical value of $2.83 \mu_B$ expected for the $4,hs$ -Ni(II) ($S=1$) tautomer with both ligands in the diamagnetic form Cat-N-BQ, confirming that in solid state complex **4** also remains in its $4,hs$ -Ni(II) form even down to very low temperatures. The μ_{eff} value of complex **3** can be explained if we consider that the main species in solid state along the whole temperature range is the [Fe(Cat-N-BQ)(Cat-N-SQ)] (**3**, ls -Fe(III)) tautomer bearing a radical Cat-N-SQ $^{2-}$ ligand, in agreement with the solution measurements previously described.

$^1\text{H-NMR}$ experiments. The $^1\text{H-NMR}$ spectra of complexes **2-4** were recorded at different temperatures and the signal of the *t*-butyl groups monitored along the whole temperature range. The variable-temperature $^1\text{H-NMR}$ of a toluene solution of complex **2** in the 203-363 K temperature range is shown in Figure 5.

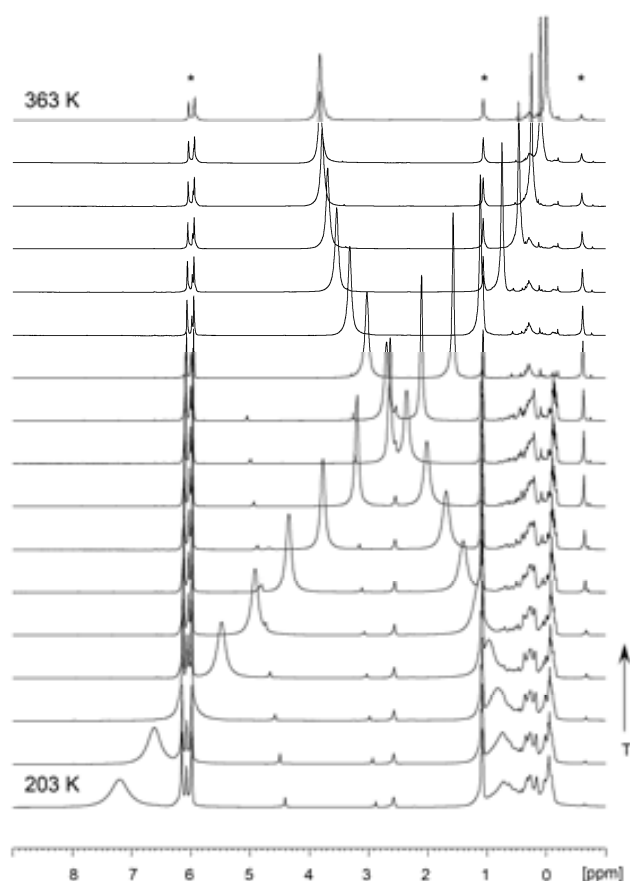


Figure 5. $^1\text{H-NMR}$ (400 MHz) shift peak of the *t*-butyl groups in the iminoquinone ligand for complex **2** at variable temperature in toluene- d_8 . The range of temperature is from 203 K to 363 K. Each intermediate spectra corresponds to increments of 10 K of temperature. In asterisk is indicated the peaks corresponding to the solvent.

The spectrum obtained at high temperatures, where the species dominant is the **2**,*hs*-Co(II) tautomer as previously confirmed, exhibits two main signals each one embracing four *t*-butyl groups. This fact is in agreement with the theoretical expectations. Indeed, since the **2**,*hs*-Co(II) tautomer is bearing two symmetrical monoanionic Cat-N-BQ ligands, the eight $^1\text{butyl}$ groups of the complex are expected to be equivalent 4 : 4 depending whether they are located at the *para*- or *ortho*- positions of the oxygen atom, and therefore only two main broad signals are expected to be observed. A temperature decrease induces an interconversion from the **2**,*hs*-Co(II) to the **2**,*ls*-Co(III) tautomer that is followed by a remarkable shift of the $^1\text{butyl}$ signals with chemical shifts as larger as $\Delta\delta = -7.2$ and $\Delta\delta = 3.1$ ppm (Tables 1, 2 and 3). Such remarkable variations arise from the electronic rearrangement experienced by the complex along the valence tautomeric interconversion. For instance, whereas in the **2**,*hs*-Co(II) tautomer the spin density is localized in the Co(II) ion, the spin density in the **2**,*ls*-Co(III) is localized directly in the ligand (Cat-N-SQ) $^{2-}$ inducing a larger paramagnetic shift and broadening of the peaks. Even more remarkable is the fact that still only two main peaks are observed even at very low temperatures where the main predominant form is the **2**,*ls*-Co(III) tautomer. This observation is rather unexpected since the **2**,*ls*-Co(III) tautomer is bearing two ligands with different oxidation state, Cat-N-BQ $^{1-}$ and Cat-N-SQ $^{2-}$, and accordingly the $^1\text{butyl}$ groups not any longer should be equivalent 4 : 4 but 2 : 2. Therefore, at least four different peaks should be observed at low temperatures. A feasible explanation for this observation would rely on a fast intramolecular electron transfer between the ligands Cat-N-BQ $^{1-}$ and Cat-N-SQ $^{2-}$. If the extra

electron is fully delocalized over both ligands on the time scale of the experiment, the *t*-butyl groups could be equivalent 4 : 4 again.

The variable-temperature $^1\text{H-NMR}$ of toluene solutions of complexes **3** and **4** in the 203-363 K temperature range was also studied as can be seen in figure 5 (values related in supplementary material). As previously described for complex **2** only two types of peaks associated to the *t*-butyl groups are observed in both cases, indicating that once more such *t*-butyl are equivalent 4 : 4. From this observation together with its variable-temperature behaviour, different conclusions can be extracted. First, the observation of only two signals is in agreement with the theoretical expectations for complex **4**, which stays in its **4**,*Ni*-Co(II) tautomeric form bearing two symmetrical monoanionic Cat-N-BQ $^{1-}$ ligands. However, once more is in disagreement with the expectations for complex **3**, which stays mostly in its **3**,*ls*-Fe(III) form. This can be attributed, as previously described for **2**,*ls*-Co(III) to a fast intramolecular electron transfer between the ligands Cat-N-BQ $^{1-}$ and Cat-N-SQ $^{2-}$. The second main observation lies in the remarkable differential shifts experienced by the *t*-butyl signals of complexes **3** and **4** and those of complex **2**. Such differential behaviour is better illustrated in Figure 6, where the same behaviour for complex **6** has also been included for comparison purposes.

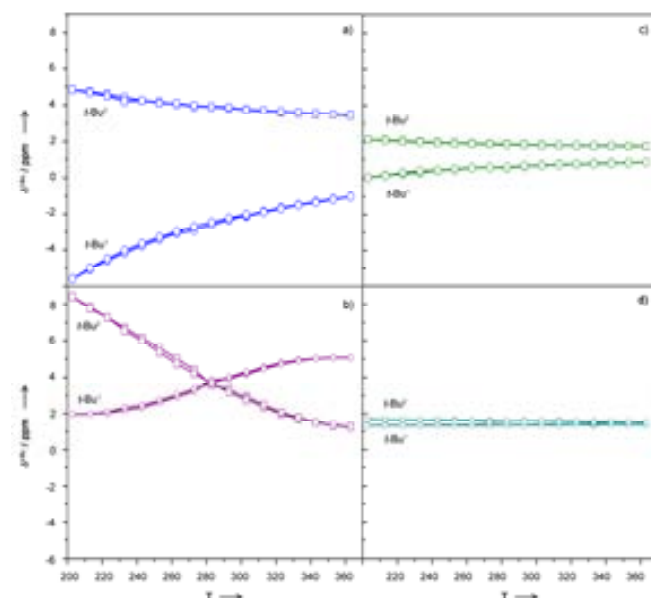


Figure 6. Representation of the *t*-butyl shift peaks vs temperature for Fe (a), Co (b), Ni (c) and Zn (d) complexes.

As can be observed in Figure 6, the chemical shift of the two *t*-butyl signals for complex **2** varies considerable, crossing between them at some point due to the VT interconversion. In the case of complexes **3** and **4** the changes in the chemical shift for both *t*-butyl signals are smaller, especially for complex **4**. Whereas complex **3** exhibits chemical shifts of $\Delta\delta = -3$ ppm and 5 ppm, the related chemical shifts for complex **4** remain between $\Delta\delta = -0.5$ and 1 ppm (for more detailed numbers look into tables 1, 2 and 3). As expected, the paramagnetic shift of the *t*-butyl groups for complex **3** is larger than for complex **4** since the presence of the unpaired electron in the same ligand through its form Cat-N-SQ $^{2-}$ induces a larger paramagnetic shift. Moreover, there is no crossing between the chemical shifts of both *t*-butyl signals as previously described for complex **2** fact that has been attributed to the lack of VT for both complexes. Finally, we also analyzed complex **6** as a model compound. This complex is a totally diamagnetic compound, [Zn(Cat-N-BQ) $_2$] ($S=0$). In this case, a small chemical shift of the

two *t*-butyl signals, which as expected means that the *t*-butyl groups are equivalent 4 : 4, is observed (see Figure 4).

Quantum chemical calculations. No geometry optimization was required for the calculations of complexes **2-4** since their X-ray optimized geometry was used as an initial file. Moreover, in order to account for the possible charge transfer between the ligand and the metal ions, specific spin states were considered for the three systems. Such strategy allows one to solicit selectively the speculated orbitals and to access the ground states and excited spin as well as charge transfer states. The resulting CASPT2 energies for complexes **2-4**, referenced to the ground state (GS) energy, are summarized in Table 1. The energy difference (ΔE) correspond to vertical transitions based on the ground state structures of each complex (so-called intervalence transition in mixed-valence compounds). Following the theory developed by Hush, ΔE is the sum of the reorganization energy and the energy difference between the tautomers (see Figure 6).

Figure 6. ((Figure Caption.))

Since the reorganization energy (mainly electrostatic) is expected to be very similar in all complexes, the larger ΔE , the less effective the intramolecular electron transfer should be. A detailed inspection of the electron transfer kinetic falls in the Hush's theory but is out of the scope of the present study. In the light of our experimental results, there is strong evidence for interligand electron delocalization. Thus, the energy differences δE (see Table 1) arising from the two speculated electron localization scenario were calculated for the [M(Cat-N-BQ)(Cat-N-SQ)] forms, M=Co, Fe.

Table 1.

Complex	GS spin state	Tautomer spin state	ΔE	δE
2	Co(III) S=1/2 (ls)	Co(II) S=3/2 (hs)	3500	
3	Fe(III) S=2 (ls)	Fe(II) S=1/2 (ls)	12400	600
4	Ni(II) S=1 (hs)	Ni(III) S=1/2 (ls)	20100	

For the Ni compound, lowest triplet CAS(2,2)SCF solutions were obtained. The ground state is consistent with a d^8 Ni^{2+} ion, holding two unpaired electrons in the mainly $d_{x^2-y^2}$ and d_{z^2} atomic orbitals in a distorted octahedral environment. The higher lying triplet state exhibits one d-type and a mainly ligand based MOs (see Figure 7).

Figure 7. ((Figure Caption.))

This picture is consistent with a d^7 Ni^{3+} ion, one electron being transferred from the Ni^{2+} to the ligand Cat-N-BQ. At a CASPT2 level of calculation, the energy difference ΔE is 20100 cm^{-1} , thus ruling out the possibility of the coexistence of Ni(II) and Ni(III).

The first excited state is, as expected from Tanabe-Sugano diagram, a Ni^{2+} singlet lying 16000 cm^{-1} above the GS triplet.

Similar strategy was used for the Fe compound which may display either 5 or 6 electrons (i. e. Fe(III) or Fe(II)) mostly localized on the Fe ion. By allowing 6 electrons in 7 MOs in a CAS(6,7)SCF calculations, the active space is flexible enough to allow for the occupations of the 5 Fe d-orbitals and either one of the ligand orbital. The two lowest septuplet (S=3) states solutions were first converged since this particular spin multiplicity forces the single occupation of the active MOs, one of them being a ligand orbital shown in Figure Fe_OM. Starting from this set of MOs, the lowest quintet (S=2) energy was calculated and turned out to be 1600 cm^{-1} lower in energy than the septuplet.

Figure 8. ((Figure Caption.))

From the correlated wavefunction analysis, this spin state arises from the antiferromagnetic coupling between an *hs*-Fe(III) ($s=5/2$) and a Cat-N-SQ radical ($s=1/2$). Interestingly, another quintet lies relatively close in energy ($\delta E = 600$ cm^{-1}) and corresponds to a similar picture, involving the second Cat-N-SQ• radical. The next quintet displays 6 electrons in the d-type MOs of a high-spin Fe(II) center. Clearly, such electronic configuration accounts for the ligand-to-metal intramolecular electron transfer, while the energy difference ΔE is 12400 cm^{-1} disposes the participation of a Fe(II)-Cat-N-BQ configuration. The spectroscopy of complex **2** in the S=2 manifold is summarized in Figure FeCo_spectro. In agreement with our experimental data, **2** is likely to undergo interligand electron transfer at room temperature while VT is unlikely to occur.

Figure 9. ((Figure Caption.))

Finally, the spectroscopy for complex **2** exhibits three competing states that reflect the simultaneous presence of intramolecular and interligand charge transfers. The strategy we used for to evaluate the energy levels ordering in **1**, is very similar (see Figure FeCo_spectro). Starting from a CAS(7,7)SCF, the lowest lying quartet (S=3/2) and two doublets (S=1/2) were determined in order to identify the possible electron hopping phenomena. As expected, at a CASPT2 level the quasi degenerate doublets ($\delta E = ???$ cm^{-1}) consist of a formally d_6 Co ion, leaving one unpaired electron in a mainly Cat-N-SQ• ligand orbital. As experimentally evidenced, the ligand-to-metal charge transfer quartet state (d_7 Co) lies relatively close in energy ($\Delta E = 3500$ cm^{-1}), a reflection of the VT phenomenon in complex **2**. From our ab initio calculation, the ability of one electron to get delocalized over three partners is shown to generate a variety of spin states which competes at room temperature.

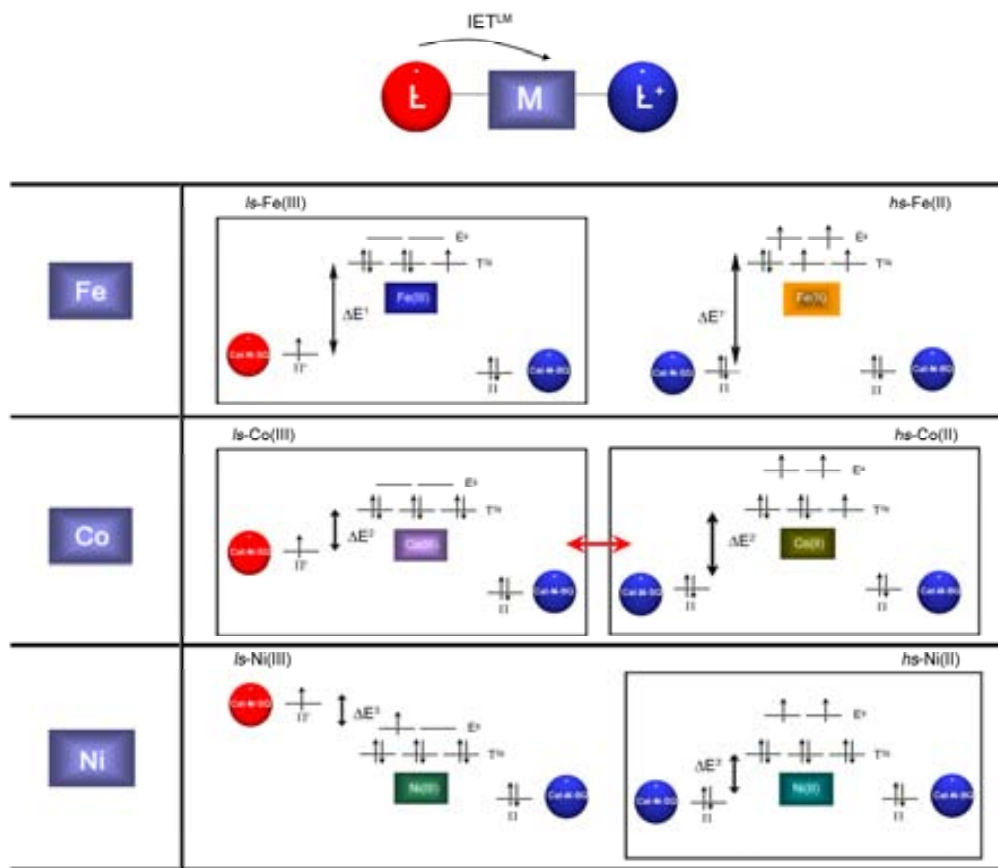


Figure 10. Energy levels of the Atomic orbitals of each part of the iminoquinone-complexes. Top (Fe-complex (3)), the energy between the electroactive ligand and the metal is too high for induce the IET^M. Middle (Co-Complex (2)), the energy levels between metal ion and electroactive ligand are in the range of the temperature applied. Under these conditions the IET^M takes place. Down (Ni-complex (4)), the atomic orbital of the electroactive ligand is in a lowest energy to the metal-ion, without external stimuli, the IET^M takes place, and the second isomer is now the thermodynamically stable.

Discussion

Intramolecular electron transfer in the series of complexes 2-4 has been studied by means of electronic spectroscopy, magnetization measurements, 1H-NMR experiments and quantum chemical calculations. The results have been summarized in the potential energy curves of the three complexes shown in Figure 10.

The experimental results indicate that the energy of the 3,*ls*-Fe(III) tautomer remains much lower in energy than that of the 3,*hs*-Fe(II) tautomer along the temperature range studied, both in solution and in solid state. Therefore, the intramolecular electron transfer between the imino ligand and the metal ion in complex 3, i.e. valence tautomerism, does not take place. In other words, as far as the ligand-to-metal (LM) electron transfer is concerned complex 3 can be considered most likely as a Class I or a Class II with very large activation energy, according to the classification of Robin and Day.^[25] Even if the molecule acquires sufficient activation energy to reach the intersection region, the probability of electron exchange would be null or very small in the temperature range under study due to a rather weak interaction between the imino ligand and the iron ion. On the contrary, the energy gap between the 2,*ls*-Co(III) and 2,*hs*-Co(II) tautomers gets smaller and lies within the same range of the energy applied in the temperature range studied.

Therefore, even though 2,*ls*-Co(III) is energetically more stable, an increase of the temperature promotes an IET from the ligand Cat-N-SQ²⁻ to the Co(III) ion, i.e., the VT interconversion takes place along the temperature range studied. Complex 2 can be then formally considered as a Class II system where the interaction between the redox centres is moderate. Under these circumstances, the electronic interaction has almost no effect on the potential energy curves in the vicinity of the equilibrium geometries but causes mixing in the vicinity of the crossing point. In other words, the electron is vibrationally localized in one of the redox centres due to the presence of an activation energy barrier (ΔG), although such a barrier may be overcome by an external thermal stimulus, to promote an IET process. Finally, in the case of complex 4 the tautomeric form 4,*hs*-Ni(III) remains lower in energy than the 4,*ls*-Ni(III) isomer, reason why only the high-spin Ni(II) isomer is detected in the whole temperature range. The differential VT behaviour along the series of complexes 2-4 can be tentatively assigned to the different ionization potentials of the iron, cobalt and nickel complexes that induce a differential overlapping of the d metal orbitals with the π -orbitals of the iminoquinone ligands. For instance, VT in related iron and nickel complexes that exhibit a good matching between the d and π orbitals have been already reported. In fact, Tanaka et al.^[26] have recently reported complexes with the general formula [Ni(L)-(Bu₂SQ)]·PF₆ as the first examples for the successful control of valence tautomerism between the Ni(II)-SQ and Ni(III)-Cat frameworks whereas Shimazaki et al. have also recently reported that the one-electron oxidized form of a new mononuclear Ni(II)-bis(salicylidene)diamine complex exhibits valence tautomerism. On the other hand, Banerjee et al.^[27] reported a semiquinone-catecholate based mixed valence complex

[Fe(bispicen)(Cl₄Cat)(Cl₄SQ)]•DMF, for which valence tautomerism has been followed by electronic absorption spectroscopy. The tautomer [Fe^{III}(Cl₄Cat)(Cl₄SQ)] is favored at low temperatures while at higher temperatures the [Fe^{II}(Cl₄SQ)₂] tautomer is the predominant form. This fact clearly reflects the interplay between the metal ion and ligand-based orbitals.

Another important question that has been raised within this family of complexes containing mixed-charge ligands Cat-N-BQ and Cat-N-SQ²⁻ concerns the extent to which LL can coexist with LM electron transfer. These compounds may be considered as a reversal of the ligand-bridged mixed-valence metal complexes where redox-active iminoquinone ligands are electronically coupled to an extent that depends upon orbital interactions with the bridge. In this sense, ¹H-NMR experiments indicate that extra electron can not be formally considered localized within one of the ligands Cat-N-SQ²⁻ but rather fully delocalized between both of them. These results were confirmed by quantum chemical calculations. Therefore, according to the classification of Robin and Day,^[25] the LL electron transfer can be considered as a Class III mixed-valence system where the electronic interaction is so intense that the electron is completely delocalized all over the molecule. Then the properties of each isolated unit are lost and the delocalization gives into new properties. Further support for this hypothesis was obtained after revising the X-ray structures of complexes **2** and **3**.^[22] The single-crystal X-ray crystallographic data reported in the literature support charge delocalization over the entire molecule. Indeed, the structural features exhibit C-O and C-N bond lengths which average to 1.305 (7) and 1.362 (7) Å, respectively and do not significantly differ between the two ligands. Previous examples in the related family of catechol-based complexes [M(DTBcat)(DTBSQ)(N[⊖]N)] For instance, Prokofev et al.^[14] have demonstrated the dynamic exchange of charge between ligands on the complexes [where M stands for P, Si and Sn.

The coupling between the (Cat-N-BQ)¹⁻ and (Cat-N-SQ)²⁻ ligands should occur through π-type valence orbitals. Nevertheless, the quasi-orthogonality between the latter rules out the possibility of such interligand electron hopping. This fact, together with the electron delocalization between the mixed-valence ligands independently of the metal ion used, seem to indicate that other mechanisms should be envisaged such as a tunnelling mechanism and/or through the solvent shell. Both mechanisms were already pointed out by Pierpont et al.^[28] in complex [Ga(tmeda)(3,6-DBSQ)(3,6-DBCat)] where no significant π-bonding of the quinone ligands with the metal ion was observed.

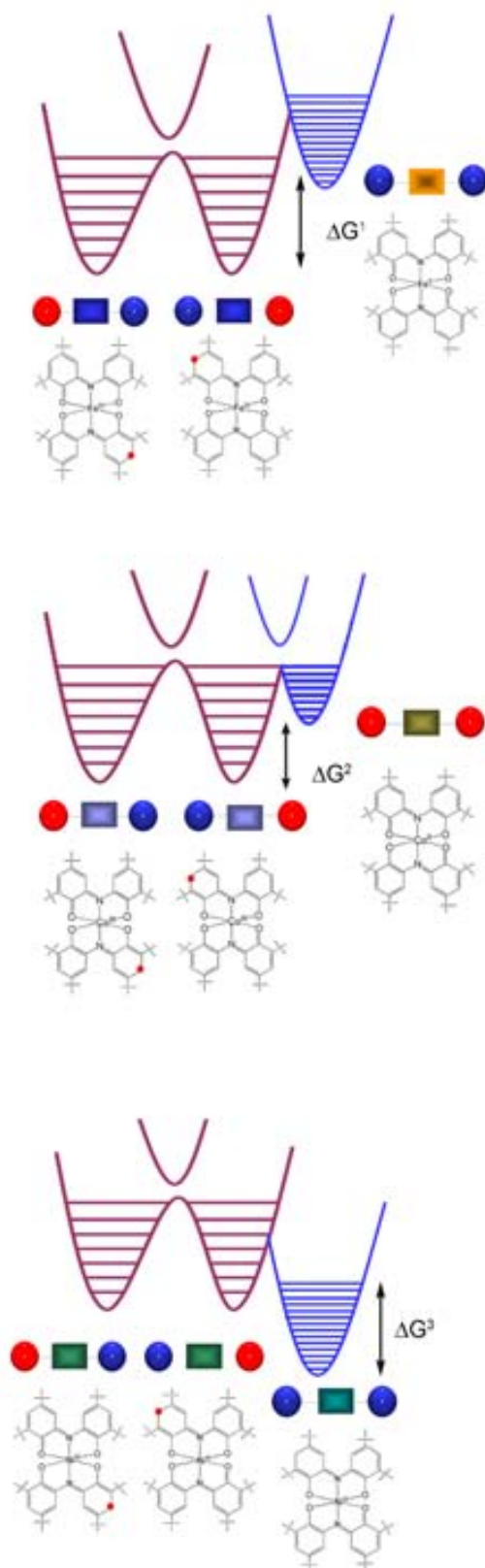


Figure 11. Resulting potential energy curve considering the two different electron transfer mechanisms present in complex **2-4**.

Conclusion

The series of complexes [M(Cat-N-BQ)(Cat-N-SQ)], where M=Co (**2**), Fe (**3**) and Ni (**4**) has been thoroughly revised and the two possible electron transfer mechanisms studied. The results indicate that among them only complex **2** exhibits valence tautomerism whereas complex **3** and **4** remain mainly in their **3**,/s-Fe(III) and **4**,/s-Ni(II) forms, respectively. This fact has been attributed to the different ionization potential of the three metal ions and its influence on the matching between their d orbitals and the π orbitals of the electroactive ligands. Moreover, the low-spin tautomers [M(Cat-N-BQ)(Cat-N-SQ)] of complexes **2** and **3**, formally with mixed-charge ligands Cat-N-BQ¹⁻ and Cat-N-SQ²⁻, have been shown to exhibit a delocalized electronic structure where the additional electron is fully delocalized between the two ligands at least on the time scale of the different experimental techniques used. Such electron delocalization is taking place more likely through a tunnelling mechanism though further experiments for the complete determination of their electronic densities by X-ray means combined with photophysical measurements are being developed nowadays.

Experimental Section

All the reagents used were purchased from Aldrich and Fluka and used as received unless otherwise specified. Complexes 1-3 were synthesized as previously described. [22,23]

Physical measurements. Electronic absorption spectra were recorded with a Varian Cary05e spectrophotometer equipped with a thermostated cell holder that can operate between 280 and 370 K. Temperature stability was better than ± 5 K. Spectra were collected after the sample had been allowed to thermally equilibrate at each temperature for 10 min. T_c , the temperature at which the isomer ratio is 1:1, was deduced from the temperature at which the peaks of the low-spin and the high-spin exhibit similar intensities. The operating temperature window for each solvent does not allow to collect the absorption of the pure low and high-spin species, and therefore, to have an accurate estimation of T_c . Direct current (dc) magnetic susceptibility measurements were carried out on a Quantum Design MPMS SQUID susceptometer with a 55KG magnet and operating in the range of 1.7-320K. All measurements were collected in a field of 10kG. Background correction data were collected from magnetic susceptibility measurements on the holder capsules. Diamagnetic corrections estimated from the Pascal contents were applied to all data for determination of the molar paramagnetic susceptibilities of the compounds. NMR spectra were recorded on a Bruker AV400 spectrometer equipped with a 5 mm triple resonance inverse probe with dedicated 31P channel operating at 500.33 MHz for ¹H equipped with a BVT3000 variable temperature unit. TMS was used as an internal reference.

Evans method. This method is suitable for the calculation of the number of unpaired electrons in solution samples and is based on the frequency shift of the NMR signal of a reference sample by the magnetic field of a co-dissolved paramagnetic species. The relative frequency shift $\Delta\nu/\nu$ with $\Delta\nu = \nu_{\text{TMS(Outer tube)}} - \nu_{\text{TMS(Inner tube)}}$, produced by the presence of the paramagnetic species is used to calculate the magnetic moment according to Equation 1, [29]

$$\chi_g = \chi_0 + [(3 \cdot \Delta\nu) / (2 \cdot \pi \cdot \nu_0 \cdot c)] + [(\chi_0 \cdot (\rho_0 - \rho_s)) / c] \quad (1)$$

where χ_g = mass magnetic susceptibility of the solute (cm³/g); χ_0 = magnetic susceptibility of the solvent (cm³/g); $\Delta\nu$ = separation in paramagnetic chemical shift (Hz); ν_0 = spectrometer radiofrequency; c = concentration (mol/mL); ρ_0 = density of the pure solvent and ρ_s = density of the solution.

Equation 2 can be transformed then to:

$$\chi_m = \chi_0 \cdot M^1 + [(3 \cdot \Delta\delta \cdot 10^6) / (4 \cdot \pi \cdot c)] \quad (2)$$

and subsequently into Equation 3 by taking into account the diamagnetic contribution, which can be estimated as the sum of constants (called Pascal's constants) for each diamagnetic species in the sample.

$$\chi_m^{\text{corr}} = \chi_m - \sum \chi_a$$

$$\chi_m^{\text{corr}} = \chi_0 \cdot M^1 + [(3 \cdot \Delta\delta \cdot 10^6) / (4 \cdot \pi \cdot c)] - \sum \chi_a \quad (3)$$

Finally, the χ_m^{corr} obtained from Equation 3 is used to calculate the effective magnetic moment as shown in Equation 4.

$$\mu_{\text{eff}} = 2,828 \sqrt{(\chi_m^{\text{corr}} \cdot T)} \quad (4)$$

The NMR samples for susceptibility measurements using the Evans Method were prepared by dissolving a weighted amount of complex 1, 2 and 3 in a measured volume of solvent. All the experiments are done in deuterated solvents. The concentration of the paramagnetic solute was in the range of 1-3 mg mL⁻¹. The temperature-dependent density changes of the solvent were corrected using equations and data from the International Critical Tables. [30] The complex solution was transferred into a 5 mm tube containing a 1 mm capillary with the deuterated diamagnetic solvent and one drop of tetramethylsilane (TMS) as a reference. The different signal shifts found for the methyl groups of the TMS was used to determine the susceptibility in solution.

Computational details. Both density functional theory (DFT) based and wavefunction based ab initio quantum chemical approaches have reached a level of accuracy which allows one to give some relevant insights into the electronic phenomena. It is known that explicitly correlated calculations are powerful tools to extract both information upon excitation energies and microscopic representations of the ground and excited states. On the other hand, DFT calculations are very reliable in the determination of equilibrium geometries, understanding of IR and UV spectra, but may suffer from their intrinsic single reference character. Methods that use the exact Hamiltonian do not suffer from the arbitrariness of the multiparametrization of the exchange correlation potential in density functional theory techniques. For those reasons, wavefunction calculations are particularly appealing since the multireference character of the description accounts for both non-dynamical and dynamical correlation effects and gives access to important information with respect to the weights of the different relevant configurations. The efficiency of ab initio techniques has been demonstrated in the study of magnetically coupled molecular were conducted. More recently, spectroscopic accuracy has also been reached and intriguing electronic distributions have been unraveled for the important class of non-innocent ligand-based metal complexes (ref Wieghardt). In the context of this study, wavefunction calculations were preferred since our goal is to look for the microscopic origin of competing spin states which may be attributed to electron transfer phenomena. Not only how effective is the intramolecular electron transfer but also to what extent both Cat-N-BQ ligands are involved in the process remain challenging questions. The one electron basis sets employed to describe the molecular orbitals (MOs) are derived from primitive atomic natural orbitals (ANOs) (17s12p9d4f) for iron, nickel and cobalt, respectively. These basis sets were contracted into [7s6p4d1f]. Regarding the lighter elements C and N, we used (10s6p3d)/[3s2p1d], and O (10s6p3d)/ [3s3p1d] contractions. Finally, hydrogen atoms were described with minimal basis set (3s)/[1s]. The zeroth-order wavefunction is formed by a linear expansion of Slater determinants. Such description is accessible by means of Complete Active Space Self-Consistent Field (CASSCF) calculations which incorporate qualitatively the leading electronic configurations distributing n electrons in m MOs, defining an active space referenced as CAS(n,m). At this level of calculation, the so-called static correlation effects are taken into account variationally provided that the active space is flexible enough. Depending on the number of d electrons for the various systems at hands, the CAS which can be anticipated consists of the mainly d-type orbitals and a mainly ligand type orbital possibly singly-occupied. However such procedure fails to reproduce the correct relative energies since dynamical correlation effects are not incorporated. These predominantly atomic effects can be incorporated within different framework on top of the CASSCF wavefunction. In this respect, complete active space second-order perturbation theory (CASPT2) calculations have proven to be impressive tools to accurately investigate spectroscopy issues (ref). All CASPT2 calculations were performed with an imaginary shift of 0.3 Hartree to avoid the presence of intruder states. All electrons were correlated except those in the core parts. Both CASSCF and CASPT2 procedures are available in the Molcas 6.2 package we used throughout the theoretical analysis.

Acknowledgements

This work was supported from the spanish government under MAT 2006-13765-C02-01 and the Network of Excellence MAGMAnet. E. E. thanks the Spanish Government for a predoctoral grant. M. N. wants also to thank the Spanish Government for kind support for a sabbatical leave.

[1] (a) P. Gütllich, Y. Garcia, T. Woike, T. Coord. Chem. Rev. 2001, 219-221 839. (b) O. Kahn, J. P. Launay, Chemtronics , 1988, 3 140. (c) A. Hauser, Coord. Chem. Rev. 1991, 111, 275.

[2] N. Sutin, Acc. Chem. Res. 1982, 15, 275.

[3] C. Creutz, H. Taube, J. Am. Chem. Soc. 1969, 91, 3988.

- [4] (a) M. D. Ward, *Chem. Ind.* **1996**, 568. (b) R. Ziessel, M. Hissler, A. El-Ghayoury, A. Harriman, *Coord. Chem. Rev.* **1998**, 178-180, 1251. (c) M. N. Paddon-Row, *Acc. Chem. Res.* **1994**, 27, 18. (d) M. R. Wasielewski, *Chem. Rev.* **1992**, 92, 435. (e) J. P. Launay, *Chem. Soc. Rev.* **2001**, 30, 386.
- [5] (a) T. M. Figueira-Duarte, V. Lloveras, J. Vidal-Gancedo, A. Gégout, B. Delavaux-Nicot, R. Welter, J. Veciana, C. Rovira, J.-F. Nierengarten, *Chem. Commun.* **2007**, 42, 4345. (b) S. Barlow, D. O'Hare, *Chem. Rev.* **1997**, 97, 637 and references therein.
- [6] For a general review on pure organic mixed-valence systems, see: D. Ruiz-Molina, J. Sedó, C. Rovira, J. Veciana in *Handbook of Advanced Electronic Materials and Devices* (Ed. H. S. Nalwa), **2001**, 303 and references cited therein.
- [7] (a) S. F. Rak and L. L. J. Miller, *J. Am. Chem. Soc.* **1992**, 114, 1388. (b) L. L. Miller and C. A. Liberko, *Chem. Mater.* **1990**, 2, 339 and references cited therein.
- [8] K. Lahlil, A. Moradpour, C. Bowlas, F. Menou, P. Cassoux, J. Bonvoisin, J. P. Launay, G. Dive, D. Dehareng, *J. Am. Chem. Soc.* **1995**, 117, 9995.
- [9] (a) S. F. Nelsen, H. Q. Tran and M. A. Nagy, *J. Am. Chem. Soc.* **1998**, 120, 298. (b) S. F. Nelsen, R. F. Ismagilov, Y. Teki, *J. Am. Chem. Soc.* **1998**, 120, 2200.
- [10] A. Dei, D. Gatteschi, C. Sangregorio, L. Sorace, *Acc. Chem. Res.* **2004**, 37, 827.
- [11] (a) J. Bonvoisin, J. P. Launay, M. Van der Auweraer and F. C. De Schryver, *J. Phys. Chem.* **1994**, 98, 5052. (b) C. Lambert, G. Nöll, *J. Am. Chem. Soc.* **1999**, 121, 8434. (c) S. Utamapanya, A. Rajca, *J. Am. Chem. Soc.* **1991**, 113, 9242.
- [12] (a) O. Elsner, D. Ruiz-Molina, J. Vidal-Gancedo, C. Rovira, J. Veciana, *Nano Letters*, **2001**, 1, 117. (b) J. Sedo, D. Ruiz, J. Vidal-Gancedo, C. Rovira, J. Bonvoisin, J. P. Launay and J. Veciana, *Adv. Mater.* **1997**, 8, 748.
- [13] E. Evangelio, D. Ruiz-Molina, *Eur. J. Inorg. Chem.* **2005**, 2957.
- [14] (a) S. P. Solodovnikov, N. N. Bubnov, A. I. Prokofev, *Usp. Khim.* **1980**, 49, 1. (b) R. R. Rakhimov, S. P. Solodovnikov, V. S. Pupkov, A. I. Prokofev, *Isv. Akad. Nauk SSSR*, **1990**, 1385. (c) C. W. Lange, B. J. Conklin, C. G. Pierpont, *Inorg. Chem.* **1994**, 33, 1276. (d) D. M. Adams, L. Noodleman, D. N. Hendrickson, *Inorg. Chem.* **1997**, 36, 3966.
- [15] In mixed-valence complexes electron transfer phenomena can be monitored easily by the study of intervalence transitions which usually appear in the near-IR region: C. Creutz, *Prog. Inorg. Chem.* **1993**, 30, 1.
- [16] (a) A. A. Vlcek, *Coord. Chem. Rev.* **1982**, 95, 39. (b) B. K. Ghosh, A. Chakravorty, *Coord. Chem. Rev.* **1989**, 95, 239. (c) A. Juris, V. Balzani, S. Campagna, P. Belser, A. V. Zelewsky, *Coord. Chem. Rev.* **1989**, 95, 239. (d) C. G. Pierpont, C. W. Lange, *Prog. Inorg. Chem.* **1993**, 41, 331.
- [17] (a) D. M. Adams, A. Dei, A. L. Rheingold, D. N. Hendrickson, *Angew. Chem. Int. Ed.*, **1993**, 32, 880-882. (b) D. M. Adams, A. Dei, A. L. Rheingold, D. N. Hendrickson, *J. Am. Chem. Soc.*, **1993**, 115, 8221-8229. (c) O. -S. Jung, D. H. Jo, Y. A. Lee, B. J. Conklin, C. G. Pierpont, *Inorg. Chem.*, **1997**, 36, 19-24. (d) O. -S. Jung, C. G. Pierpont, *J. Am. Chem. Soc.*, **1994**, 116, 2229-2230. (e) O. -S. Jung, D. H. Lee, Y. S. Sohn, C. G. Pierpont, *Inorg. Chem.*, **1998**, 37, 5875-5880. (f) S. Bin-Salamon, S. H. Brewer, E. C. Depperman, S. Franzen, J. W. Kampf, M. L. Kirk, R. K. Kumar, S. Lappi, K. Peariso, K. E. Preuss, D. A. Shultz, *Inorg. Chem.* **2006**, 45, 4461-4467.
- [18] E. Evangelio, D.N. Hendrickson, D. Ruiz-Molina, Intramolecular electron transfer in the mixed-valence [Co(3,5-DTBCCat)(3,5-DTBSQ)(bpy)] complex. Beyond valence tautomerism, *Inorganica Chimica Acta*, **2008**, doi: 10.1016/j.ica.2008.02.069
- [19] (a) O. Hayaishi, M. Nozaki, *Science*, **1969**, 164, 389-396. (b) C. A. Tyson, A. E. Martell, *J. Am. Chem. Soc.*, **1972**, 94, 939-945. (c) A. Y. Girgis, A. L. Balch, *Inorg. Chem.*, **1975**, 14, 2724-2727. (d) L. A. deLaire, R. C. Haltiwanger, C. G. Pierpont, *Inorg. Chem.*, **1989**, 28, 644-650.
- [20] This ligand may exhibit sometimes a more complicated behaviour: P. Chauduri, M. Hess, K. Hildebrand, E. Bill, T. Weyhermüller, K. Wieghardt, *Inorg. Chem.* **1999**, 38, 2781.
- [21] (a) S. K. Larsen, C. G. Pierpont, *J. Am. Chem. Soc.* **1988**, 110, 1827. (b) A. Caneschi, A. Cornia, A. Dei, *Inorg. Chem.* **1998**, 37, 3419.
- [22] C. L. Simpson, S. R. Boone, C. G. Pierpont, *Inorg. Chem.* **1989**, 28, 4379.
- [23] (a) O. Cador, F. Chabre, A. Dei, C. Sangregorio, J. V. Slageren, M. G. F. Vaz, *Inorg. Chem.* **2003**, 42, 6432. (b) P. L. Gentili, L. Bussotti, R. Righini, A. Beni, L. Bogani, A. Dei, *Chem. Phys.* **2005**, 314, 9.
- [24] D. F. Evans, *J. Chem. Soc.* **1959**, 2003-2005.
- [25] M. B. Robin, P. Day, *Adv. Inorg. Chem. Radiochem.* **1967**, 10, 247.
- [26] H. Ohtsu, K. Tanaka, *Angew. Chem. Int. Ed.* **2003**, 43, 6301.
- [27] N. Shaikh, S. Goswami, A. Panja, X.-Y. Wang, S. Gao, R. J. Butcher, P. Banarjee, *Inorg. Chem.* **2004**, 43, 5908.
- [28] C. W. Lange, B. J. Conklin, C. G. Pierpont, *Inorg. Chem.* **1994**, 33, 1276.
- [29] S. K. Sur, *J. Magn. Reson.* **1989**, 82, 169-173.
- [30] Valours obtained from the reviews of *J. Chem. Eng. Data*, **1999**, 44, 411.

Received: ((will be filled in by the editorial staff))
 Revised: ((will be filled in by the editorial staff))
 Published online: ((will be filled in by the editorial staff))

Article VII

Title: Valence Tautomerism: More Actors than Just Electroactive Ligands and Metal Ions

Authors: E. Evangelio, and D. Ruiz-Molina

Publication: Comptes Rendues Chimie. 2008, Submitted

Valence Tautomerism: More Actors than Just Electroactive Ligands and Metal Ions

Emi Evangelio^a, Daniel Ruiz-Molina^{b*}

^a*Institut de Ciència dels Materials de Barcelona (CSIC), Esfera UAB, Campus UAB, 08193, Cerdanyola del Vallès, Catalonia, Spain*

^b*Centro de Investigación en Nanociencia y Nanotecnología (ICN-CSIC), Esfera UAB, Edificio CM7, 08193, Cerdanyola del Vallès, Catalonia, Spain.*

Received (will be filled in by the editorial staff)

Abstract

Valence tautomeric complexes combining electro-active ligands and transition metal ions, are known for exhibit two nearly degenerated electronic states (tautomers) with localized electronic structures. The intramolecular electron transfer (IET) led between both redox active units is activated by an external stimuli such as photons, temperature and/or pressure, brings to a reversible interconversion between the degenerated electronic states, indicating an important sensibility of the charge distribution onto the environment. Moreover, the IET, confers different chemical and physical properties to both tautomers converting these molecules as promise for applications as storage memories and/or devices, for example. Since this phenomena was first discovered in the late 80s, most of valence tautomeric complexes so far reported are based on quinone or quinone-type ligands with a series of transition metal ions such as Cu, Rh and Ir, Ni, Mn and Co, which makes them good candidates for study the role of various parameters governind the IET rates. But, finally, recent studies, foccus the attention on the external centers where the IET is taking place, such as counterligand, the partial oxidation or reduction of the complex and the nature of the matrix in which the molecule is surrounded. These factors, are important for tune and controle the temperature of the electron transfer. In this review we are going to give an overall view of all the five actors that influence in the IET scenario, as the key for construct new molecules enhancing or combining multifunctional properties.

Résumé

* Corresponding author
E-mail address: dani@icmab.es

Keywords: Valence tautomerism, electroactive, intramolecular electron transfer, bistability, switch

Mots-clés : Tautomerisme de Valénce, electroactive, transferé electronique intramoléculaire, bistabilité, interrupteur

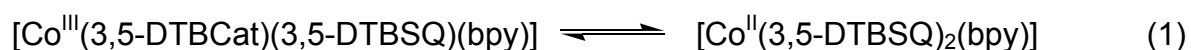
1. Introduction

There is currently active interest in the development of molecular electronic devices that can be used as optical and/or magnetic data storage media. Compounds of specific interest are bistable molecular materials having two nearly degenerated states with different optical and/or magnetic properties [1]. These complexes have an appreciable sensitivity to the environment so an external perturbation, such as temperature or irradiation, may lead to an interconversion between the two degenerated electronic states, settling down the conceptual basis of a molecular device. Examples of electronic labile complexes are mixed-valence,[2] spin-crossover [3] and valence tautomeric complexes [4]. The comprehension and understanding of the characteristic features for all these complexes has been developed in parallel over the last decades, rising out a large interest in the scientific community as demonstrated by the large amount of examples developed for each case.

Valence tautomeric (VT) metal complexes with at least two redox-active centres, the metal ion and an electro-active ligand, are characterized by the existence of two electronic isomers (valence tautomers) with different charge distributions, and consequently, different optical, electric and magnetic properties [5]. The interconversion between the different electronic isomers is accomplished by a reversible intramolecular electron transfer involving the metal ion and the redox active ligand. A schematic representation of valence tautomerism together with the corresponding potential energy curve plotted in function of the nuclear coordinate is shown in Figure 1.

-Insert Figure 1 here-

One of the first descriptions of valence tautomerism and an excellent example of the above mentioned charge distribution sensitivity is exhibited by the cobalt bis(quinone) complex $[\text{Co}^{\text{III}}(3,5\text{-DTBCat})(3,5\text{-DTBSQ})(\text{bpy})]$ (**1**),[6] where 3,5-DTBCat²⁻ and 3,5-DTBSQ⁻ refer, respectively, to the catecholate (DTBCat²⁻) and semiquinonate (DTBSQ⁻) forms of 3,5-di-tert-butyl-*o*-quinone, and bpy is 2,2'-bipyridine. In solution, the equilibrium in Equation 1 can be induced by variations of temperature and monitored by magnetic measurements and spectroscopic techniques such as UV–VIS, NMR and/or EPR.



For instance, the UV-Vis spectrum of a solution of complex **1** in toluene at low temperatures shows a band at 600 nm characteristic of the [Co^{III}(3,5-DTBCat)(3,5-DTBSQ)(bpy)] (**1**,*ls*-Co(III)) tautomer. An increase of temperature promotes an intramolecular electron transfer so the **1**,*ls*-Co(III) converts into the **1**,*hs*-Co(II) as one of the ligands is reduced by one electron from a DTBSQ⁻ to a DTBCat²⁻ ligand. As a consequence, the intensity of the 600 nm band decreases and a band at 770 nm characteristic of the **1**,*hs*-Co(II) tautomer increases in intensity. Accompanying the optical changes, variations of the magnetic response are also observed.

This interconversion is an entropy-driven process, in analogy to the extensively studied low-spin to high-spin crossover phenomena. The large entropy gain arises from: 1) a gain in electronic entropy due to the higher spin state degeneracy of the *hs*-Co(II) form and 2) the higher density of vibrational states of the *hs*-Co(II) form due its longer metal-ligand bond lengths.[7] Thus thermal population of tautomeric states is dictated by the Gibbs free energy expression shown in Equation 2. At low temperatures, TΔS is negligible compared to ΔH, and consequently if ΔH>kT only the *ls*-Co(III) state is populated. An increase of the temperature will increase the TΔS contribution, making it non negligible and favouring the population of the *hs*-Co(II) state, up to a critical temperature T_c where ΔG = 0 and ΔH = TΔS. A further increase of the temperature will change the sign of ΔG.

$$\Delta G = \Delta G_{hs-Co(II)} - \Delta G_{ls-Co(III)} = \Delta H - T\Delta S \quad (2)$$

Moreover, since valence tautomeric complexes are electronically labile, they exhibit significant vibronic interactions and therefore an appreciable sensitivity to the environment. As a consequence, intramolecular electron transfer can be induced not only by temperature variations but also by irradiation or pressure. For instance, Hendrickson *et al.* have reported results of the first picosecond time-resolved optical experiments on valence tautomeric complexes in solution [8] and in the solid state after illumination at low temperatures [9,10,11]. Light-induced VT has also been observed in polynuclear complexes. For instance, Sato *et al.* reported not only photoswitching but also hysteresis effects around room temperature (310 and 297 K) for complex [{Co(tpa)}₂(DHBQ)](PF₆)₃ (**2**), (where DHBQ is the deprotonated 2,5-dihydroxy-1,4benzoquinone), for which intermolecular interactions are enhanced by the presence of significant π-π interactions [12]. Some years before, Dei *et al.*,[13] realised additional femtosecond spectroscopic experiments in a simple cobalt-dioxolene derivative, [Co(Me₄Cyclam)DTBSQ]⁺ Me₄Cyclam

= 1,4,8,11-tetramethyl-1,4,8,11-tetraazacyclotetradecane (**3**) showing the involvement of at least three states in a two-step VT process in solution.

Examples of pressure-induced VT have also been reported although in less extent than thermally-driven or light-induced transitions, mainly due to experimental difficulties [14]. In these experiments, the increase of the molecular size on passing from the low to the high-spin isomer due to the population of antibonding orbitals is used to favour the low-spin isomer after application of pressure as an external stimulus. The first example of a pressure-driven solid state valence tautomeric transformation was reported by Verdagner and Hendrickson,[15] who studied the non-solvated complex $[\text{Co}^{\text{II}}(\text{3,5-DTBSQ})_2(\text{phen})]$ (**4**) and its related solvated form $\mathbf{4} \cdot \text{C}_6\text{H}_5\text{CH}_3$ by EXAFS and XANES. Recently, pressure-induced valence tautomerism has also been monitored by changes on the magnetic response [16]. A nice example is complex $[\text{Co}(\text{cth})(\text{Phendiox})]\text{PF}_6 \cdot \text{H}_2\text{O}$ (**5**), where cth is a macrocycle and phendiox corresponds to the dioxolene neutral form (catecholate) of 9,10-dihydroxyphenanthrene. This complex has been shown by X-ray diffraction experiments to shrink its unit cell volume by more than 4% along the VT process. Systems with these characteristics have potential interest as pressure sensors [17]. A schematic representation of the representative complexes **1**, **2**, **4** and **5** as well as a brief summary of their VT characteristics is shown in Table 1.

-Insert Table 1 here-

In summary, the interest for studying this family of complexes is considerable [18]. First, they are unique model systems which provide insight into the basic factors affecting intramolecular electron transfer in coordination complexes. And second, from an applied perspective, the large changes in the optical, structural, and magnetic properties that often accompany the valence tautomeric interconversion have potential applications in bistable molecular materials and devices. For this reason, since first reported by Pierpont *et al.* in 1980,[6] several new tautomeric complexes especially over the last few years have been described. For most of these cases, observation of valence tautomerism has been traditionally associated almost exclusively to the matching paper of the redox-active ligand and the transition metal ion electronic orbital. However, several other factors (structural or environmental) have also been detected to play a crucial role. For this reason we have structured this review into two main sections. First, we will give a brief revision of the different families of VT complexes so far reported, with special emphasis on the families of complexes derived from catecholate and phenoxylate ligands that are by far the ligands

most often used in VT. In the second section we will revise in detail the different structural and environmental factors that clearly influence VT processes. Even though different reviews have already been reported in the literature that compile several examples of VT organized according to the nature of their redox active ligand and the transition metal ion, this is the first revision that systematically faces the crucial effect of such additional structural and environmental factors on the observation of *valence tautomerism*.

2. Redox-Active Ligands and Transition Metal Ions

The term of non-innocent ligand directly related to their role and the influence on the final electronic distribution of certain transition metal complexes was first pointed out by Jørgensen [19]. This concept can be used when both the metal-centred and ligand-centred electronic frontier orbitals are similar in energies. Within such scenario, the final oxidation state of the complex and the internal electronic distribution may be modulated becoming a great subject of investigation both by theoretical [20] and experimental means [21]. This investigation is of interest not only for the field of valence tautomerism but also for several other fields such as the study of complexes bearing non-innocent ligands that perform physiological functions on biological systems. For instance, transition metal complexes in which one or more of the ligands is present as a phenoxyl radical have attracted much interest due to their broad occurrence in technical processes [22] and enzymatic metalloproteins such as galactose oxidase (GAO) [23] or glyoxal oxidase (GLO) [24]. A schematic representation of the active site of both metalloproteins is shown in Figure 2.

-Insert Figure 2 here-

So far, many different types of redox-active ligands have been described in the literature,[25] among them quinone-type, crown-ethers,[26] ferrocene [27] and tetrathiafulvalene derivatives [28]. A schematic drawing of the different redox active ligands previously mentioned is shown in Scheme 1. π -Conjugated polymers and/or oligomers bearing coordinating sites, such as polyanilines and polythiophenes, have also been successfully used with this aim [29]. However, we must emphasize that even though the number of redox-active ligands is considerable, those exhibiting valence tautomerism are rather limited since they must simultaneously satisfy two conditions: 1) the degree of covalency in the interaction between metal ion and electroactive ligand must be low, and

2) the energy of their frontier orbitals must be similar [7,18]. In other words, it is necessary that these complexes exhibit localized electronic structures, low orbital mixing, and a small energy difference between the two electronic tautomers. Most of the valence tautomeric complexes so far reported are based on quinone or phenoxylate ligands with a series of transition metal ions. Nevertheless, in the last few years the number of electroactive ligands inducing valence tautomerism is being expanded by including new electroactive ligands such as polychlorotriphenylmethyl radicals (PTM) [30] and tetraphenylporphyrin (TTP) [31]. Among them, redox-active catecholate and phenoxyl are by far the ligands most often used in VT, reason why both families are revised next (for a detailed description of the different families of VT complexes so far reported, please see Ref. 4-5).

-Insert Scheme 1 here-

Quinones. Most of the ligands so far shown to exhibit valence tautomerism are quinone or quinone-based ligands with a series of transition metal ions. Thanks to their rich redox activity, *o*-quinone ligands may exist as neutral quinones (Q), radical semiquinones (SQ⁻) or dianionic catecholates (Cat²⁻) (see Scheme 2), although they usually are only found in the SQ⁻ and Cat²⁻ forms due to the limiting binding ability of the quinone ligand [32].

-Insert Scheme 2 here-

As far as the metal ion is concerned, one of the most effective in showing valence tautomerism is the pair Co(II)/Co(III). In other words, cobalt complexes bearing quinone-based ligands have been shown to exhibit not only localized structures but also a good matching between the energy of its frontier orbitals with those of the redox-active ligand. For this reason, several mononuclear complexes exhibiting VT have been described. The simplest cobalt-quinone complexes undergoing valence tautomerism belong to the family of ionic complexes with the general formula [ML(diox)]Y, where L= tetraazamacrocyclic ancillary ligand, diox=9,10-dioxophenanthrene and Y=PF₆, BPh₄, I [16,33]. However, most cobalt complexes shown to exhibit valence tautomerism are of the general formula [Co(DTBQ)₂(N-N)], where N-N is a diazine ligand, DTBQ = 3,5- and 3,6-di-*tert*-butylcatecholato (DTBCat²⁻) or semiquinone (DTBSQ⁻) form [6,17,34]. In addition to monomeric complexes, a further step was done in the synthesis of binuclear cobalt-dioxolene complexes. For instance, the use of a modified (diimine)-bipyridine ligand as electronic coupling of two cobalt centres led to the description of the first dinuclear VT

complex with the three possible tautomeric forms existing below 500 K [35]. Pierpont *et al.* also studied modified catecholate ligands to tune the critical temperature (T_C), defined as the temperature at which there are equal amounts of both electronic isomers, in a related family of dinuclear complexes [36]. Similar results were observed for another cobalt bis(dioxolene) complex by near-IR absorption spectroscopy in a thin amorphous film [37]. Simultaneously, Dei *et al.* reported the binuclear complex $[\{\text{Co}(\text{cth})\}_2(\text{DHBQ})](\text{PF}_6)_3$ (**6**) that undergoes a gradual thermal tautomeric transition at around 175 K as well as a quantitative VT photoconversion [38].

Finally, in addition to mono- and binuclear, different polynuclear (mostly polymeric) tautomeric complexes have also been reported. Pierpont *et al.*, [17] reported the polymer $[\text{Co}(\text{pyz})(3,6\text{-DTBQ})_2]_n$ (**7**) that exhibited a temperature-induced tautomeric interconversion in the solid state that derived in a mechanical process due to variations on the bond lengths. Hysteresis was recently reported by Schultz *et al.*, [39] in the coordination polymer with analytical formula $[\text{Co}(\text{phen})\text{L}] \cdot 0.5\text{CH}_2\text{Cl}_2$ (**8**) where L = 3,5-bis(3',4'-dihydroxy-5'-*tert*-butylphenyl)-1-*tert*-butylbenzene. This cobalt-dioxolene polymer exhibits the necessary cooperative properties that lead to thermal hysteresis in a valence tautomeric equilibrium, even though the transition could be classified as gradual. Finally, very recently a new strategy based on coordination polymerization and precipitation in a poor solvent to produce cross-linked valence tautomeric metal-organic nanospheres has been reported [40]. A schematic representation of the nanospheres formed along the polymerization process is shown in Figure 3.

-Insert Figure 3 here-

In addition to the cobalt ion, valence tautomerism has also been observed for different transition metal complexes such as manganese, nickel and copper. Few years after the first report of VT on a cobalt complex, a similar temperature-dependent equilibrium was observed for a related manganese complex [41]. Complex $[\text{Mn}(\text{py})_2(3,5\text{-DTBCat})_2]$ (**9**) experienced a reversible colour change from the intense purple of the Mn(IV) form to the pale green-brown characteristic of the Mn(II) form. The interconversion takes place through a Mn(III) form, which usually exhibits similar colour than the Mn(IV) form, as confirmed later on in solid state [42] and in solution [43,44]. Valence tautomerism has also been reported in a tetrazaamacrocyclic complex of manganese with a single *o*-benzoquinone ligand [45].

In addition to manganese, copper complexes containing dioxolene ligands may also yield under the right conditions the valence tautomeric interconversion shown in Equation 3 [46].



One of the first examples of valence tautomerism involving the Cu(I)/Cu(II) pair was reported in a copper containing enzyme that catalyzes the oxidation of amines to aldehydes, [47] an important process in relevant biological functions such as growth regulation and tissue maturation. Similar studies have also been done by Speier *et al.*, who described the existence of valence tautomerism for the species $[\text{Cu}(\text{py})_2(\text{PhenQ})_2]$ [48] (**10**) and Kaim *et al.*, who reported the use of a weak π -acceptor thioether in a Cu(I)-semiquinone complex to induce valence tautomerism as a paramagnetic compound associated to amine oxidase enzymes [49].

Finally, very recently, two new examples of nickel and iron-quinone complexes have been reported to exhibit valence tautomerism. Tanaka *et al.*, [50] reported complexes $[\text{Ni}(\text{PyBz}_2)(\text{DTBSQ})]\text{PF}_6$ (**11**) and $[\text{Ni}(\text{MePyBz}_2)(\text{DTBCat})]\text{PF}_6$ (**12**) as the first examples for successful control of valence tautomerism between the Ni(II)-SQ and Ni(III)-Cat frameworks. On the other side, Banerjee *et al.*, [51] have reported a semiquinone-catecholate based mixed valence complex $[\text{Fe}(\text{bispicen})(\text{Cl}_4\text{Cat})(\text{Cl}_4\text{SQ})]\text{-DMF}$ (**13**), where valence tautomerism has been followed by electronic absorption spectroscopy. This is the first example where a mixed valence semiquinone/catecholate iron(III) complex undergoes intramolecular electron transfer.

Phenoxy radicals. Phenoxy radicals are monovalent oxygen radical species that exhibit delocalization of the unpaired electron over the aromatic ring with *ortho* and *para* substituents that give steric protection [52]. For instance, it has been shown that *tert*-butyl substituents at the *ortho* and *para* positions of the phenolates facilitate one-electron oxidation to the corresponding phenoxy radicals, because these substituents decrease the oxidation potential of the phenolates and provide enough steric bulkiness to suppress bimolecular decay reactions of the generated phenoxy radicals [53]. Several groups have prepared metal-phenoxy complexes giving new insights into the chemical factors that govern the generation and stability of this type of radicals, [54] among to them worth to mention Wieghardt *et al.* For instance, they have established that bidentate *O,N*-coordinated *o*-aminophenolato ligands can be found in one of the following different protonation and oxidation levels bounded to a transition metal ion: *o*-imidophenolate(2⁻)

anions, *o*-iminobenzosemiquinonate (1^-) π radical monoanions or even *o*-iminobenzoquinone. All these forms can exist in coordination compounds as confirmed by high quality low-temperature X-ray crystallography [55]. In addition, *o*-iminobenzosemiquinonate (1^-) anions are paramagnetic ($S=1/2$) ligands that couple either ferro or antiferromagnetically when coordinated to a paramagnetic transition metal ion, depending on the reciprocal symmetry of the SOMO ligand orbital of the 3d magnetic orbital of the metal ion. Following this approximation a large number of new complexes bearing non-innocent phenoxyl ligands have been reported, not only in the aminophenolate case (O,N-) [56] or (N,N-) [57] but also with other donor atoms such as S (S,N-, S,S- or S,O-) [58] or with different metal ions (Fe, Cu, Co, Mn, Ni, Rh, Ru, Pt, Pd as representative examples) [59]. However, and in spite of the large number of complexes so far reported, only a few of such examples have been shown to exhibit valence tautomerism. For instance, Wieghardt *et al.*, [60] described a octahedral $\{\text{Fe-NO}\}^7$, $[\text{L}^{\text{Pr}}\text{Fe}(\text{NO})\cdot 2.5\text{CH}_2\text{Cl}_2$ (**14**) ($\text{L}^{\text{Pr}} = 1$ -isopropyl-4,7-(4-*tert*-butyl-2-mercaptobenzyl)-1.4,7-triazacyclononane), with a pentadentate macrocyclic pendent arm ligand exhibiting the first temperature dependent $S=1/2$ to $S= 3/2$ spin equilibrium in the solid state (see Figure 4). The first example of valence tautomeric equilibria for a N,S-coordinated *o*-aminothiophenolate cobalt and S,S-coordinated *o*-dithiolate iron-complexes in solution was also recently reported [61]. Almost simultaneously, Shimazaki *et al.* reported the one-electron oxidized form of a new mononuclear nickel(II)-bis-(salicylidene)diamine complex (**15**), derived from $\text{H}_2\text{tert-Bu-salcn}$ ligand, that exhibits valence tautomerism, [62] and a few years later a similar complex (**16**) but now with the $\text{H}_2\text{tert-Bu-salen}$ was shown to exhibit a structurally-induced (VT) transition on the translation from a square planar to a octahedral geometry [63]. Finally, Yamauchi *et al.*, [64] have recently shown additional studies based on VT for mononuclear nickel(II) complex with same ligand-type and complexes where the metal is replaced by platinum and palladium (II).

-Insert Figure 4 here-

A further step has been the study and characterization of *O,N,O*-coordinated type ligands containing two phenolate donor groups such as ligand BQ-N-SQ (also termed 2-[(3,5-bis(1,1-dimethylethyl)-6-hydroxyl-2,4-cyclohexadien-1-ylidene)amino]-4,6-bis(1,1-dimethylethyl)-phenol) [65]. These ligands, in addition to producing phenoxyl radicals in the presence of air, exhibit better chelating capabilities and good π -donor atoms that

stabilize higher oxidation states [66]. The synthesis and mechanical features for the obtaining of the ligand BQ-N-SQ was first described in 1975 by Girgis and Balch, [65c] treating the 3,5-di-tert-butyl-catechol with aqueous ammonia in the presence of a divalent metal ion under aerobic conditions. Since then, a considerable interest has increased in the scientific community for this family of complexes. Thanks to their rich redox activity, these ligands may exist at least in four different oxidation states (see Scheme 2) although structural and magnetic characterization of the complexes bearing this ligand suggest that they can be mostly found as $M^{IV}(\text{Cat-N-SQ})_2$, $M^{III}(\text{Cat-N-SQ})(\text{Cat-N-BQ})$ and $M^{II}(\text{Cat-N-BQ})_2$. Other unusual interesting trends of the electronic distribution along different members of this family of complexes have also been found [65c,d,67]. Recently, Wieghardt *et al.*, [68] showed the stabilization of the trianionic $(\text{Cat-N-Cat})^{3-}$ form in a Cu(II) metal complex. Moreover, on the quest for dinuclear M^{II} -phenoxyl radical complexes playing an active role on the aerobic catalysis of alcohols, two new zinc-complexes [69] $[\text{Zn}(\text{Cat-N-BQ})_2]$ (**17**) and its isomeric red and paramagnetic form $[\text{Zn}(\text{Cat-N-SQ})(\text{BQ-N-SQ})]$ (**18**) have been published. The last complex represents the first example where the oxidation levels of the two coordinated ligands differ formally by two electrons although the stability of this product is relatively low.

As far valence tautomerism is concerned, the first complex of this family to be shown to exhibit VT was complex $[\text{Co}^{III}(\text{Cat-N-BQ})(\text{Cat-N-SQ})]$ (**19**). Although first reported in 1988 by Pierpont *et al.*, no evidence for tautomeric interconversion was shown to take place at that time [67a] Ten years later, the temperature dependence of the spectral and magnetic properties of solutions of this compound in nonpolar solvents suggested the existence of the valence tautomeric equilibrium shown in Equation 4 [67d]. A few years later the interconversion was also shown to take place in solid state [82] though at much higher temperatures.



Afterwards, valence tautomerism has also been reported for the related manganese complex $[\text{Mn}^{IV}(\text{Cat-N-SQ})_2]$ (**20**) [70]. Whereas its solid-state structural features are in agreement with the electronic distribution that involves the manganese atom in its oxidation state (IV), its solution temperature-dependence shows that this complex exhibits valence tautomerism involving three different tautomeric isomers associated to the three different oxidation states of the manganese ion: Mn(IV), Mn(III) and Mn(II) [67a,b].

The advantages of valence tautomeric Schiff base complexes over transition metal complexes with *o*-quinone ligands are considerable. First, valence tautomeric Schiff base complexes display higher stabilities relative to atmospheric oxygen atmosphere in solution and solid state. Second, the differences between the optical properties of isomers involved in the valence tautomerism of the cobalt Schiff base complex are enhanced when compared to those observed for cobalt complexes with *o*-quinone ligands. Third, the Schiff base ligand exhibits a richer electrochemical behavior since it can exist in different oxidation forms, ranging from +1 to -3 (see scheme 2b), which may lead to stable coordination complexes with several metal ions in a variety of oxidation states [69].

3. Valence Tautomerism: Beyond Electroactive Ligands and Metal Ions

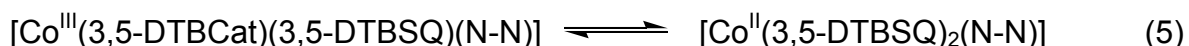
As shown in the previous chapter, the presence of VT in a given complex has been traditionally associated almost exclusively to the role played by the the redox-active ligand and the transition metal ion. More specifically to the degree of covalency in the interaction between them, which must be low, and the matching between the energy of their frontier orbitals, which must be similar [18]. However, the existence of several other factors that can modulate the observation of VT has also been detected along all these years of research in the field. In other words, the same complex may exhibit or not, or the VT process can be shifted to much higher temperatures, depending on other structural and environmental parameters such as those schematized in Figure 5. Such factors can be grouped into three main areas of influence that are counter-ligand, charge-induced and environmental effects. It is the aim of the following section to revise more in detail such factors, which must be taken seriously into consideration for a proper evaluation of potential VT candidates.

-Insert Figure 5 here-

3.1. Counter-ligand effect.

Most of the work devoted to elucidate the role played by the counter ligand has been done on the family of complexes with the general formula $[\text{Co}^{\text{III}}(3,5\text{-DTBCat})(3,5\text{-DTBSQ})(\text{N-N})]$. Even though the N-N diazine ligand is not directly involved in the electron transfer process, Hendrickson *et al.*, [71] Pierpont *et al.*, [17,72] and Dei *et al.*, [73] have concluded that it

can be used to systematically shift the T_C for the equilibrium shown in Equation 5 by changing its donor abilities.



For instance, the systematic variation on the series of complexes with the general formula $[\text{Co}(\text{py}_2\text{X})(3,5\text{-DTBSQ})_2]$ ($\text{X} = \text{O}, \text{S}, \text{Se}$ and Te) has been shown to clearly influence T_C , inducing in some of the cases even a large hysteresis effect [72a]. Sato *et al.*, [74] reported complex $[\text{Co}^{\text{III}}(3,5\text{-DTBSQ})(3,5\text{-DTBCat})(\text{dpa})]$ ($\text{dpa} = \text{N,N-bis}(2\text{-pyridylmethyl})\text{amine}$) (**21**) with one of the highest T_C values (around 380 K) so far reported for a VT complex, fact that was attributed to the strong coordination field of the counterligand used (dpa) (see Figure 6). Another interesting example of the counterligand effect on the valence tautomeric processes has been described by Awaga *et al.*, [75] who reported valence tautomerism in the spin-labeled complex $[\text{Co}(\text{nnbpy})(3,5\text{-DTBSQ})_2]$ (**22**), where nnbpy is a bipyridine substituted nitronyl nitroxide radical. Even though the temperature dependence of the magnetic susceptibility indicates a tautomeric interconversion above 250 K as is indicated in Figure 6b, the ligand radical behaves as a Curie spin over the whole temperature region. Finally, interesting results were obtained for a series of complexes $[\text{Co}(\text{Cnbpy})(3,5\text{-DTBQ})_2]$ (**23**) (Figure 6c) where the bipy coligand modified with alkyl groups ranging from 0 to 13 alkyl chain has been shown to tune the VT by favouring the presence of crystal phase transitions (cooperativeness) [76]. All these studies have demonstrated that the charge distribution in metal-quinone complexes is sensitive to the balance of metal and quinone orbital energies, tuned by the appropriate choice of the counterligand. Of special relevance is the possibility to use such modulation for the development of VT complexes that show hysteresis if a future molecular switching device based on these complexes is to be realized.

-Insert Figure 6 here-

the donor The acceptor characteristics of the counterligand in a series of copper-quinone synthetic model with the general formula $[(\text{Q}^{\text{n-}})\text{Cu}^{\text{n+}}\text{L}]$ have been studied due to their relevance not only for VT purposes but also on other biological or commercial processes. Strong π acceptor ligands such as $\text{L}=\text{CO}$, CNR , PR_3 or AsR_3 stabilize the $\text{Cu}(\text{I})$ -semiquinone form whereas the use of non- π -acceptor ligands, such as amine ligands,

favour the Cu(II)-semiquinone form [77]. For instance, Buchanan *et al.*, [78] have demonstrated the possibility to modulate the charge distribution between the two electronic isomers $[L_2Cu^{II}(3,5-DTBCat)]$ and $[L_2Cu^I(3,5-DTBSQ)]$ by changing the nature of the counter-ligand from a strong nitrogen donor to a soft phosphine donor. On the other side, Kaim *et al.*, [79] have also reported the use of a weak π -acceptor thioether to induce sensitive valence tautomerism in paramagnetic copper complexes related to amine oxidase enzymes. In a more recent study, the comparison between two thioether ligands that differ on their π -acceptor capacity and structural rigidity has been used to have a comparative study of both effects [80].

Finally, another example of the relevance of VT systems beyond its potential use for molecular based devices is their influence on the catalytic center of cytochrome c oxidase (CcO). The substitution of the tyrosinate cross-linked for a semiquinone group have generated a long-lived imidazolyl-phenoxy radical [81]. The resulting complexes with the general formula (Cu-imidazolyl-phenoxy) are created to mimic the Cu_B^{II} -histidine-tyrosinate center in an attempt to study its catalytic potential on biological processes. A nice example of the formation of such mimic models is complex $[(tpa)Cu(lm-hq^*H_2)](OTs)_2$ complex (**24**). The study of its double deprotonation show the evidence of the free radical anion ($lm-sq^*$) and the presence of a valence tautomerism on the coordinative labile copper(I) intermediate.

3.2. Charge-induced effects

3.2.1. Counter-ion effect. One of the few examples where the nature of the counterion has been shown to modify valence tautomerism is that of the ionic (charged) cobalt-quinone complexes with the general formula $[ML(diox)]Y$, where L is a tetraazamacrocyclic ancillary ligand, $diox=9,10$ -dioxophenanthrene and $Y=PF_6, BPh_4, I$ [16,33]. Such complexes undergo a temperature and pressure-induced VT equilibrium with a transition temperature that varies with the volume and columbic interaction of the counterion Y. Another example of the counterion effect was reported by Cador *et al.*, [82] on the series of complexes $[M(tpy)L]Y$, where $M = Ni$ or Co , $tpy = 2,2':6',2''$ -terpyridine, $L = Cat-N-SQ$ or $Cat-N-BQ$ and $Y = PF_6, BPh_4$. It is found that the critical temperature for the interconversion in the cobalt case is strongly affected by the counterion. Whereas no VT transition was detected for the tetraphenylborate compound, the related hexafluorophosphate complex exhibits a VT interconversion in solid state around 500 K, as confirmed by magnetic measurements,

whereas in solution it takes place at lower temperatures, as shown by spectrophotometric measurements.

3.2.2. Redox activity. The redox activity of the ligands not only allows for the existence of valence tautomerism but also for additional switching capacities resulting from an electrochemical process. Such a strategy has been shown to be very useful for the systematic tuning of the critical temperature at which there are equal amounts of both tautomers, as well as to establish arrays of four or six members depending on the redox possibilities of the metal ion involved in the array (Figures 7 and 8).

The first example of redox-tuned valence tautomerism was based on the reduction of complex $[\text{Co}^{\text{III}}(3,5\text{-DTBCat})(3,5\text{-DTBSQ})(\text{bpy})]$ (**1**) [83]. Interestingly, the resulting reduced complex also exhibited a temperature-dependence consistent with the existence of a valence-tautomeric equilibrium. This fact allowed for the first time to establish an array of four states (Figure 7) showing different optical and magnetic ground states controlled by two temperature-controlled valence tautomeric equilibria and two reversible redox processes. The possibility of entering the cycle at each state and advancing through the square array in a clockwise and counter-clockwise direction was also established.

-Insert Figure 7 here-

Following this approach, Rovira *et al.*, [84] also established an array of four states (see Figure 7) based on the oxidation of the tautomeric complex $[\text{Co}^{\text{III}}(\text{Cat-N-BQ})(\text{Cat-N-SQ})]$ (**19**). The charged species $[\text{Co}^{\text{III}}(\text{Cat-N-BQ})_2]^+$ formed by partial oxidation was generated chemically. Interestingly, its variable-temperature absorption spectra showed the existence of an equilibrium consistent with the existence of a temperature-induced valence tautomerism shown in Equation 6. This fact allowed the establishing of an array of four states showing different optical and magnetic ground states by using a reversible oxidation process as additional stimulus.



Later on, three different oxidation states where the manganese metal ion can be most frequently found on a given complex, Mn(IV)-Mn(III)-Mn(II) allowed us to expand the array from four to six members using complex **20** (see Figure 8) [**Error! Marcador no definido.**]. The principal parameters of the VT processes involved in the four and six-member arrays shown in Figures 7 and 8 are summarized in Table 2.

-Insert Figure 8 here-

-Insert Table 2 here-

3.3. Environmental effects

In this section, matrix factors (i.e., depending whether if the VT interconversion takes place in solution, solid state or embedded in a polymeric matrix) will be analyzed. As far as the study of VT phenomena in solution is concerned, the influence of the nature of the solvent on the VT equilibrium for the family of complexes $[\text{Co}^{\text{III}}(\text{Cat})(\text{SQ})(\text{N-N})]$ has already been shown [71-73]. By choosing the appropriate solvent and by controlling the temperature of the solution, the tautomeric equilibrium of this family of complexes can be modulated and one of the two isomers can be made to be the dominant species in solution. Moreover, there is no a direct correlation between the T_c values obtained experimentally for each solvent and their corresponding dielectric constant values. This fact evidences that the displacement of the tautomeric equilibrium most probably is not only controlled by ϵ but also by other solute-solvent interactions. As is shown, tautomeric interconversion brings changes in the Co-L bond lengths, consequently the endoergic term (Ω) probably has also a reasonable influence. This term, characteristic of each solvent, measures the required work for separating the solvent molecules in order to accommodate them and provide a suitable sized and shaped enclosure.

These complexes can interconvert between the VT isomers also in the solid state though with significant differences. Indeed, whereas in solution the interconversion takes place over a large temperature range, in a crystalline matrix they can interconvert cooperatively on a narrow temperature range. For instance, it was shown that for complex $4\cdot\text{C}_6\text{H}_5\text{CH}_3$, [8,71] the tautomeric interconversion between the $4,ls\text{-Co(III)}$ and $4,hs\text{-Co(II)}$ isomers can be reversibly driven with temperature and monitored by large changes in the magnetic susceptibilities, with an interconversion that occurs abruptly within a narrow temperature range of $\sim 30^\circ$. Similar observations for the differential behaviour of VT complexes in solution and in solid state were found for complex $[\text{Co}^{\text{III}}(\text{Cat-N-BQ})(\text{Cat-N-SQ})]$ (**19**). In a preliminary work, the UV-Vis temperature dependence of a toluene solution of this

complex in solution suggested the existence of a valence tautomeric equilibrium close to 300 K, [67d] as deduced by the ratio between the enthalpy and the entropy changes in solution. However, no tautomerism was observed in the solid state, as evidenced by the lack of changes in the variable-temperature magnetic susceptibility data up to 300 K. However, in a subsequent work, [82] the same authors showed that indeed this complex exhibits a tautomeric interconversion in the solid state but at higher temperatures, with a transition that starts at approximately 370-380 K, i.e., at least 150 K higher than in solution. The variations found for the behaviour of these complexes in solution and in solid state are not atypical. In fact, it is important to emphasize that whereas most of the valence tautomeric complexes thus far reported exhibit a temperature-dependent interconversion in solution, the number of examples exhibiting a valence-tautomeric interconversion in the solid state is rather limited. Such variations between the behaviour in solution and solid state have been attributed by Dei *et al.* to variations of the entropy factor, as deduced by comparison of the thermodynamic quantities obtained for the same VT process in a toluene solution and in solid state. And this is not surprising at all. The valence tautomeric interconversion from the *ls*-Co(III) to the *hs*-Co(II) leads to a gain in electronic entropy (ΔS_{elec}) due to the higher spin state degeneracy of the *hs*-Co(II) form and the longer metal-ligand bond lengths of the *hs*-Co(II) tautomer, which results in lower energy vibrations and a higher density of vibrational states. The spin state degeneracy is not expected to vary on the different solvents under study. However, the variations on the metal-ligand bond lengths, i.e. the density of vibrational states, are expected to be strongly dependent on the surrounding matrix.

Finally, a remarked influence of the solvent nature has been found not only for measurements in solution but also when acting as guest molecules within a given crystalline network (in solid state). This fact was initially attributed to the effect of solvate molecules that are assumed to impart softness to the lattice, and therefore, to influence any possible phonon relaxation mechanism. For instance, whereas complex $[\text{Co}^{\text{III}}(3,5\text{-DTBSQ})(3,5\text{-DTBCAT})(\text{phen})] \cdot \text{C}_6\text{H}_5\text{CH}_3$ (**4**·**C₆H₅CH₃**) interconverts abruptly within a narrow temperature range of $\sim 30^\circ$, a polycrystalline sample recrystallized from ethanol has a μ_{eff} value essentially independent of the temperature and close to the value of $1.7 \mu_{\text{B}}$ expected for the low-spin isomer [85]. In between, for samples recrystallized from acetonitrile and methylene chloride, incomplete transitions were observed. The two paradigms or extremes are the toluene and ethanol solvates. Whereas in the first of the cases the solvate molecules are favouring a strong cooperative effect that induces an abrupt transition over a short range of temperatures, the ethanol guest molecules are

either suppressing or shifting to much higher temperatures the interconversion. The obtaining of a systematic correlation between T_c and the nature of the solvent remains elusive. However, the correlation of T_c found in the different solvate crystallographic forms differs from that observed for the solutions of the same solvent. This is once more not surprising at all. Whereas in solution the target molecules are mostly surrounded by solvent molecules, in the crystalline network they are surrounded by other neighbour molecules. All the attempts to obtain different crystallographic phases of complex **19** by recrystallization from different solvents to give more light on this topic were unsuccessful, obtaining the same crystallographic phase in all the cases as confirmed by X-ray powder diffraction. However, the obtaining of an amorphous phase showed that the disorder introduced within the network in this case did not suppress or shift the VT to much higher temperatures, as previously observed for complex **4**. For comparison purposes, the X-ray diffraction data obtained for the different crystalline phases of complexes **4** and **19** and the corresponding VT characteristics are shown in Figure 9.

-Insert Figure 9-

Other examples of the solvent guest molecule effects on the VT interconversion have been reported by Dei *et al.* on the family of complexes of general formula $[\text{Co}(\text{CTH})(\text{Phendiox})]\text{Y}\cdot\text{solv}$, where CTH stands for tetraazamacrocyclic and Phendiox for the catecholato or semiquinonato form of 9,10-dioxophenanthrene. The critical interconversion temperature was found to depend not only in the nature of the counterion Y but also in the nature of the solvent trapped [86] in the lattice. Moreover, significant hysteresis effects were detected by substituting the solvent guest molecules found within the lattice by its deuterated analogue. Within this scenario, the differential “softness” that the solvent molecules are giving to the crystalline network is clearly affecting the vibrational relaxation of the molecules.

4. Conclusions

The observation of valence tautomerism has been traditionally associated almost exclusively to the role played by two main actors, the redox-active ligand and the transition metal ion. In other words, requirements of potential candidates to exhibit VT were always seek to fulfil the following requirements: 1) the degree of covalency in the interaction

between metal ion and electroactive ligand must be low, and 2) the energy of their frontier orbitals must be similar. However, the occurrence of several other factors that can modulate the observation of VT have also been detected along all these years of research on the field. In other words, the same complex may exhibit or not, or the VT process be shifted to much higher temperatures, depending on other structural and environmental parameters. Such factors have been divided into three main categories (counter-ligand, charge and environmental effects) and thoroughly revised in this review. These results summarized are very important for future investigations on the field. Among others, they reveal the necessity to use a very systematic approach when identifying new VT candidates since the use of an inappropriate solvent may mask the VT interconversion.

Acknowledgments

Authors would like to thank Prof. A. Dei and Prof. D. N. Hendrickson for fruitful discussions and share of knowledge. We also acknowledge financial support of the Ministerio de Educación y Ciencia under grant (MAT2006-13765-C02) and the network of Excellence Magmanet. E. E. thanks the Ministerio de Educación y Ciencia for a predoctoral grant.

References

- [1] a) N. Sutin, *Acc. Chem. Res.* 15 (1982) 275. b) O. Kahn, J. P. Launay, *Chemtronics*, 3 (1988) 140. c) A. Hauser, *Coord. Chem. Rev.* 111 (1991) 275. d) P. Gütllich, Y. Garcia, T. Woike, *T. Coord. Chem. Rev.* 219-221 (2001) 839.
- [2] P. Day, *Int. Rev. Phys. Chem* 1 (1981) 149. b) J. R. Reimers, B. B. Wallace, N. S. Hush, *Phil. Trans. R. Soc. A* 366 (2008) 15.
- [3] P. Gütllich, *Topics in Current Chemistry, Spin Crossover in Transition Metal Complexes I, II, and III*. ISBN: 978-3-540-40394-4 (I), 978-3-540-40396-8 (II), 978-3-540-40395-1 (III) and references cited therein
- [4] E. Evangelio, D. Ruiz-Molina, *Eur. J. Inorg. Chem.*, 15 (2005) 2957 and references cited therein.
- [5] a) D. N. Hendrickson, C. G. Pierpont, *Top. Curr. Chem.* 234 (2004) 63. b) O. Sato, J. Tao, Y. –Z. Zhang, *Angew. Chem. Int. Ed.* 46 (2007) 2152. c) D. A. Shultz in *Magnetism: Molecules to Materials, Vol. II* (Eds.: J. S. Miller, M. Drillon), Wiley-VCH, Weinheim, 2001, 81-306.
- [6] R. M. Buchanan, C. G. Pierpont, *J. Am. Chem. Soc.* 102 (1980) 4951.
- [7] P. Gütllich, A. Dei, *Angew. Chem. Int. Ed. Engl.* 36 (1997) 2734.
- [8] a) D. M. Adams, B. Li, J. D. Simon, D. N. Hendrickson, *Angew. Chem. Int. Ed. Engl.* 34 (1995) 1481. b) D. M. Adams, D. N. Hendrickson, *J. Am. Chem. Soc.* 118 (1996) 11515.
- [9] a) O. Sato, S. Hayami, Z. –Z. Gu, R. Saki, R. Nakajima, A. Fujishima, *Chem. Lett.* (2001) 874. b) O. Sato, S. Hayami, Z. –Z. Gu, K. Takahashi, R. Nakajima, A. Fujishima, *Chem. Phys. Lett.* 355 (2002) 169.
- [10] A. Cui, K. Takahashi, A. Fujishima, O. Sato, *J. Photochem. Photobiol. A: Chem.* 167 (2004) 69-73.
- [11] a) S. Decurtins, P. Gütllich, C. P. Khöler, H. Spiering, A. Hauser, *Chem. Phys. Lett.* 105 (1984) 1. b) O. Sato, S. Hayami, Z. –Z. Gu, K. Takahashi, R. Nakajima, K. Seki, A. Fujishima, *J. Photochem. Photobiol. A Chem.* 149 (2002) 111. c) O. Sato, S. Hayami, Y. Einaga, Z. –Z. Gu, *Bull. Chem. Soc. Jpn*, 76 (2003) 443. d) O. Sato, S. Hayami, Z. –Z. Gu, K. Takahashi, R. Nakajima, A. Fujishima, *Phase Transitions* 75 (2003) 779.
- [12] J. Tao, H. Maruyama, O. Sato, *J. Am. Chem. Soc.* 128 (2006) 1790.
- [13] F. V. R. Neuwahl, R. Righini, A. Dei, *Chemical Physics Letters* 352 (2002) 408.
- [14] For the analogous spin crossover systems, studies using hydrostatic cells adapted to magnetic susceptibility, Mössbauer, optical absorption and reflectivity methods in conjunction with methods of detection such as IR, EXAFS and X-ray diffraction techniques, have been successfully used in the last years: P. Gütllich, A. B. Gaspar, V. Ksenofontov, Y. Garcia, *J. Phys. Condens. Matter.* 16 (2004) S1087.
- [15] C. Roux, D. M. Adams, J. P. Itié, A. Polian, D. N. Hendrickson, M. Verdager, *Inorg. Chem.* 35 (1996) 2846.
- [16] A. Caneschi, A. Dei, F. F. De Biani, P. Gütllich, V. Ksenofontov, G. Levchenko, A. Hofer, F. Renz, *Chem. Eur. J.* 7 (2001) 3926.
- [17] O. –S. Jung, C. G. Pierpont, *J. Am. Chem. Soc.* 116 (1994) 2229.
- [18] a) A. Vlcek, *Comments Inorg. Chem.* 16 (1994) 207. b) C. G. Pierpont, *Coord. Chem. Rev.* 216 (2001) 99–125.
- [19] C. K. Jørgensen, *Coord. Chem. Rev.* 1 (1966) 164.
- [20] S. Messaoudi, V. Robert, N. Guihéry, D. Maynau, *Inorg. Chem.* 45 (2006) 3212 and references cited therein.

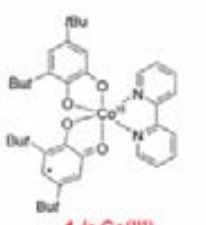
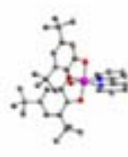

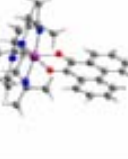
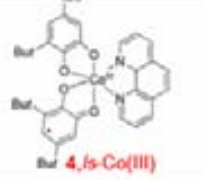
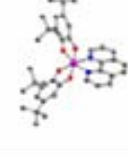
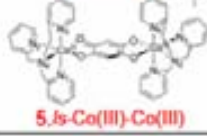
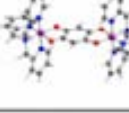
-
- [21] W. Kaim, B. Schwederski, *Pure Appl. Chem.* 76 (2004) 351 and references cited therein.
- [22] B. A. Jazdzewski, W. B. Tolman, *Coord. Chem. Rev.* 200-262 (2000) 633.
- [23] J. W. Whittaker, *Chem. Rev.* 103 (2003) 2347.
- [24] M. M. Whittaker, P. J. Kersten, D. Cullen, J. W. Whittaker, *J. Biol. Chem.* 274 (1999) 36226.
- [25] a) C. G. Pierpont, C. W. Lange, *Prog. Inorg. Chem.* 41 (1994) 331. b) A. M. Costero, C. Andreu, R. Martínez-Mañez, J. Soto, L. E. Ochando, J. M. Amigó, *Tetrahedron* 54 (1998) 8159. c) T. Hirao, *Coord. Chem. Rev.* 226 (2002) 81. d) C. Rovira, *Chem. Rev.* 104 (2004) 5289. e) T. Hirao, *Macromolecules Containing Metal and Metal-Like Elements* 5 (2005) (Metal-Coordination Polymers) 209.
- [26] F. Le Derf, M. Mazari, N. Mercier, E. Levillain, G. Trippe, A. Riou, P. Richomme, J. Becher, J. Garin, J. Orduna, N. Gallego-Planas, A. Gorgues, M. Salle, *Marc. Chem. Eur. Journal* 7 (2001) 447.
- [27] W. R. Cullen, J. D. Woollins, *Coord. Chem. Rev.* 39 (1981) 1.
- [28] K. S. Gavrilenko, Y. Le Gal, O. Cador, S. Golhen, L. Ouahab, *Chem. Commun.* 3 (2007) 280.
- [29] J. L. Reddinger, J. R. Reynolds, *Macromolecules* 30 (1997) 673.
- [30] I. Ratera, D. Ruiz-Molina, F. Renz, J. Ensling, K. Wurst, C. Rovira, P. Gülich, J. Veciana, *J. Am. Chem. Soc.*, 125 (2003) 1462.
- [31] a) D. Chang, T. Malinski, A. Ulman, K. M. Kadish, *Inorg. Chem.* 23 (1984) 817. b) J. Seth, V. Palaniappan, D. F. Bocian, *Inorg. Chem.* 34 (1995) 2201.
- [32] C. G. Pierpont, R. M. Buchanan, *Coord. Chem. Rev.* 38 (1981) 45.
- [33] A. Bencini, A. Caneschi, C. Carbonera, A. Dei, D. Gatteschi, R. Righini, C. Sangregorio, J. VanSlageren, *J. Mol. Struct.* 656 (2003) 141.
- [34] a) G. A. Abakumov, V. I. Nevodchikov, V. K. Cherkasov, *Dokl. Akad. Nauk SSSR* 278 (1984) 641. b) G. A. Abakumov, G. A. Razuvaev, V. I. Nevodchikov, V. K. Cherkasov, *J. Organomet. Chem.* 341 (1988) 485.
- [35] S. Bin-salamon, S. H. Brewer, E. C. Depperman, S. Franzen, J. W. Kampf, M. L. Kirk, R. K. Kumar, S. Lappi, K. Peariso, K. E. Preuss, D. A. Shultz, *Inorg. Chem.* 45 (2006) 4461-4467.
- [36] Y. Suenaga, C. G. Pierpont, *Inorg. Chem.* 44 (2005) 6183.
- [37] N. G. R. Hearn, J. L. Kořcok, M. M. Paquette, K. E. Preuss, *Inorg. Chem.* 45 (2006) 8817.
- [38] C. Carbonera, A. Dei, J. -F. Letard, C. Sangregorio, L. Sorace, *Angew. Chem. Int. Ed.* 43 (2004) 3136.
- [39] S. H. Bodnar, A. Caneschi, D. A. Shultz, L. Sorace, *Chem. Commun.* (2001) 2150.
- [40] I. Imaz, D. Maspocho, C. Rodríguez-Blanco, J. M. Pérez-Falcón, J. Campo, D. Ruiz-Molina, *Angew. Chem. Int. Ed.* 47 (2008) 1857.
- [41] M. W. Lynch, D. N. Hendrickson, B. J. Fitzgerald, C. G. Pierpont, *J. Am. Chem. Soc.* 103 (1981) 3961.
- [42] A. S. Attia, O. -S. Jung, C. G. Pierpont, *Inorg. Chim. Acta* 226 (1994) 91.
- [43] A. S. Attia, C. G. Pierpont, *Inorg. Chem.* 36 (1997) 6184.
- [44] A. S. Attia, C. G. Pierpont, *Inorg. Chem.* 35 (1998) 3051.
- [45] A. Caneschi, A. Dei, *Angew. Chem. Int. Ed.* 37 (1988) 3005.
- [46] W. Kaim, *Dalton. Trans.* (2003) 761.

- [47] M. S. Dooley, M. A. McGuirl, D. E. Brown, P. N. Turowski, W. S. McIntire, P. F. Knowles, *Nature* 349 (1991) 262.
- [48] G. Speier, Z. Tyeklar, P. Toth, E. Speier, S. Tisza, A. Rothenbauer, A. M. Whalen, N. Alkire, C. G. Pierpont, *Inorg. Chem.* 40 (2001) 5653.
- [49] a) J. Rall, M. Wanner, M. Albrecht, F. M. Hornung, W. Kaim, *Chem. Eur. J.* 5 (1999) 2802. b) W. Kaim, M. Wanner, A. Knödler, S. Zalis, *Inorg. Chim. Acta* 337 (2002) 163.
- [50] H. Ohtsu, K. Tanaka, *Angew. Chem. Int. Ed.* 43 (2004) 6301.
- [51] N. Shaikh, S. Goswami, A. Panja, X.-Y. Wang, S. Gao, R. J. Butcher, P. Banarjee, *Inorg. Chem.* 43 (2004) 5908.
- [52] E. R. Altvicker, *Chem. Rev.* 67 (1967) 475.
- [53] P. Chaudhuri, K. Wieghardt, *Prog. Inorg. Chem.* 50 (2002) 151.
- [54] A. K. Nairn, R. Bhalla, S. P. Foxon, X. Liu, L. J. Yellowlees, B. C. Gilbert, P. H. Walton, *J. Chem. Soc. Dalton. Trans.* (2002) 1253 and references cited therein.
- [55] K. S. Min, T. Weyhermüller, K. Wieghardt, *Dalton Trans.* (2004) 178 and references cited therein.
- [56] a) R. Schnepf, A. Sokolowski, J. Müller, V. Bachler, K. Wieghardt, P. Hildebrandt, *J. Am. Chem. Soc.* 120 (1998) 2352. b) P. Chaudhuri, M. Hess, J. Müller, K. Hildenbrandt, E. Bill, T. Weyhermüller, K. Wieghardt, *J. Am. Chem. Soc.* 121 (1999) 9599. c) P. Chaudhuri, C. N. Verani, E. Bill, E. Bothe, T. Weyhenmüller, K. Wieghardt, *J. Am. Chem. Soc.* 123 (2001) 2213. d) H. Chun, P. Chaudhuri, T. Weyhermüller, K. Wieghardt, *Inorg. Chem.* 41 (2002) 790. e) A. K. Nairn, R. Bhalla, S. P. Foxon, X. Liu, L. J. Yellowlees, B. C. Gilbert, P. H. Walton, *J. Chem. Soc. Dalton Trans.* (2002) 1253. f) H. Chun, E. Bill, E. Bothe, T. Weyhermüller, K. Wieghardt, *Inorg. Chem.* 41 (2002) 5091. g) S. Mukherjee, T. Weyhermüller, E. Bothe, K. Wieghardt, P. Chaudhuri, *Eur. J. Inorg. Chem.* (2003) 863. h) K. S. Min, T. Weyhermüller, K. Wieghardt, *Dalton Trans.* (2003) 1126. i) S. Mukherjee, E. Rentschler, T. Weyhenmüller, K. Wieghardt, P. Chaudhuri, *Chem. Commun.* (2003) 1828. j) S. Mukherjee, T. Weyhenmüller, K. Wieghardt, P. Chaudhuri, *Dalton Trans.* (2003) 3483. k) H. Chun, E. Bill, T. Weyhenmüller, K. Wieghardt, *Inorg. Chem.* 42 (2003) 5612. l) K. S. Min, T. Weyhenmüller, E. Bothe, K. Wieghardt, *Inorg. Chem.* 43 (2004) 2922. m) S. Ye, B. Sarkar, F. Lissner, T. Scleid, J. Van Slageren, J. Fiedler, W. Kaim, *Angew. Chem. Int. Ed.* 44 (2005) 2 as only some of the examples.
- [57] J. Rall, A. F. Stange, K. Hübler, W. Kaim, *Angew. Chem. Int. Ed.* 37 (1998) 2681. b) F. N. Penkert, T. Weyhermüller, E. Bill, P. Hildebrandt, S. Lecomte, K. Wieghardt, *J. Am. Chem. Soc.* 122 (2000) 9663. c) P. Ghosh, A. Begum, D. Herebian, E. Bothe, K. Hildebrandt, T. Weyhermüller, K. Wieghardt, *Angew. Chem. Int. Ed.* 42 (2003) 563. d) D. Herebian, E. Bothe, F. Neese, T. Weyhenmüller, K. Wieghardt, *J. Am. Chem. Soc.* 125 (2003) 9116. e) U. Beckmann, E. Bill, T. Weyhermüller, K. Wieghardt, *Inorg. Chem.* 42 (2003) 1045.
- [58] a) P. Ghosh, E. Bill, T. Weyhermüller, K. Wieghardt, *J. Am. Chem. Soc.* 125 (2003) 3967. b) P. Ghosh, A. Begum, E. Bill, T. Weyhenmüller, K. Wieghardt, *Inorg. Chem.* 42 (2003) 3208. c) K. Ray, T. Weyhermüller, A. Goossens, M. W. J. Crajé, K. Wieghardt, *Inorg. Chem.* 42 (2003) 4082.
- [59] a) V. Bachler, G. Olbrich, F. Neese, K. Wieghardt, *Inorg. Chem.* 41 (2002) 4179. b) S. Patra, B. Sarkar, S. M. Mobin, W. Kaim, G. K. Lahiri, *Inorg. Chem.* 42 (2003) 6469. c) P. Ghosh, A. Begum, D. Herebian, E. Bothe, K. Hildebrandt, T. Weyhermüller, K. Wieghardt, *Angew. Chem. Int. Ed.* 42 (2003) 563.
- [60] M. Li, D. Bonnet, E. Bill, F. Neese, T. Weyhenmüller, N. Blum, D. Sellmann, K. Wieghardt, *Inorg. Chem.*, 2002, 41, 3444.
- [61] a) D. Herebian, P. Ghosh, H. Chun, E. Bothe, T. Weyhenmüller, K. Wieghardt, *Eur. J. Inorg. Chem.* (2002) 1957. b) K. Ray, E. Bill, T. Weyhenmüller, K. Wieghardt, *J. Am. Chem. Soc.* 127 (2005) 5641.
- [62] Y. Shimazaki, F. Tani, K. Fukui, Y. Naruta, O. Yamauchi, *J. Am. Chem. Soc.* 125 (2003) 10512.
- [63] O. Rotthaus, F. Thomas, O. Jarjayes, C. Philouze, E. Saint-Aman, J. -L. Pierre, *Chem. Eur. J.* 12 (2006) 6953.

-
- [64] Y. Shimazaki, T. Yajima, F. Tani, S. Karasawa, K. Fukui, Y. Naruta, O. Yamauchi, *J. Am. Chem. Soc.* 129 (2007) 2559.
- [65] a) O. Hayaishi, M. Nozaki, *Science* 164 (1969) 389. b) C. A. Tyson, A. E. Martell, *J. Am. Chem. Soc.* 94 (1972) 939. c) A. Y. Girgis, A. L. Balch, *Inorg. Chem.* 14 (1975) 2724. d) L. A. deLaire, R. C. Haltiwanger, C. G. Pierpont, *Inorg. Chem.* 28 (1989) 644.
- [66] T. K. Paine, T. Weyhermüller, L. D. Slep, F. Neewe, E. Bill, E. Bothe, K. Wieghardt, P. Chaudhuri, *Inorg. Chem.* 43 (2004) 7324.
- [67] a) S. K. Larsen, C. G. Pierpont, *J. Am. Chem. Soc.* 110 (1988) 1827. b) C. L. Simpson, S. R. Boone, C. G. Pierpont, *Inorg. Chem.* 28 (1989) 4379. c) S. Bruni, A. Caneschi, F. Cariati, C. Delfs, A. Dei, D. Gatteschi, *J. Am. Chem. Soc.* 116 (1994) 1388. d) A. Caneschi, A. Cornia, A. Dei, *Inorg. Chem.* 37 (1998) 3419.
- [68] P. Chaudhuri, M. Hess, T. Weyhermüller, K. Wieghardt, *Angew. Chem. Int. Ed.* 38 (1999) 1095.
- [69] This ligand may exhibit sometimes a more complicated behaviour: P. Chaudhuri, M. Hess, K. Hildebrand, E. Bill, T. Weyhermüller, K. Wieghardt, *Inorg. Chem.* 38 (1999) 2781.
- [70] D. Ruiz-Molina, K. Wurst, D. Hendrickson, C. Rovira, J. Veciana, *Adv. Funct. Mater.* 12 (2002) 347.
- [71] a) D. M. Adams, A. Dei, A. L. Rheingold, D. N. Hendrickson, *Angew. Chem. Int. Ed. Engl.* 32 (1993) 880. b) D. M. Adams, A. Dei, A. L. Rheingold, D. N. Hendrickson, *J. Am. Chem. Soc.* 115 (1993) 8221. c) D. M. Adams, L. Noodleman, D. N. Hendrickson, *Inorg. Chem.* 36 (1997) 3966.
- [72] a) O. -S. Jung, D. H. Jo, Y. A. Lee, B. J. Conklin, C. G. Pierpont, *Inorg. Chem.* 36 (1997) 19. b) O. -S. Jung, D. H. Lee, Y. S. Sohn, C. G. Pierpont, *Inorg. Chem.* 37 (1998) 5875.
- [73] a) C. Benelli, A. Dei, D. Gatteschi, L. Pardi, *Inorg. Chim. Acta* 163 (1989) 99. b) A. Caneschi, A. Dei, D. Gatteschi, V. [Tangoulis](#), *Inorg. Chem.* 41 (2002) 3508.
- [74] A. Cui, K. Takahashi, A. Fujishima, O. Sato. *J. Photochem. and Photobiol. A: Chem* 161 (2004) 243.
- [75] A. Yamaguchi, K. Awaga, *J. Mater. Chem.* 11 (2001) 2142.
- [76] D. Kiriya, H. -C. Chang, A. Kamata, S. Kitagawa, *Dalton Trans.* (2006) 1377.
- [77] a) J. Rall, W. Kaim, *J. Chem. Soc. Faraday Trans.* 90 (1994) 2905. b) G. Speier, S. Tisza, Z. Tyeklar, C. W. Lange, C. G. Pierpont *Inorg. Chem.* 33 (1994) 2041.
- [78] R. M. Buchanan, C. Wilson-Blumenberg, C. Trapp, S. K. Larsen, D. L. Green, C. G. Pierpont, *Inorg. Chem.* 25 (1986) 3070.
- [79] W. Kaim, M. Wanner, A. Knödler, S. Zalis, *Inorg. Chim. Acta* 337 (2002) 163.
- [80] S. Ye, B. Sarkar, M. Niemeyer, W. Kaim, *Eur. J. Inorg. Chem.* (2005) 4735.
- [81] D. G. Lonnon, S. T. Lee, S. B. Colbran, *J. Am. Chem. Soc.* 129 (2007) 5800.
- [82] O. Cador, F. Chabre, A. Dei, C. Sangregorio, J. V. Slagereen, M. G. F. Vaz, *Inorg. Chem.* 42 (2003) 6432.
- [83] a) D. Ruiz-Molina, J. Yoo, I. Guzei, A. L. Rheingold, D. N. Hendrickson, *Chem. Commun.* (1998) 2089. b) D. Ruiz-Molina, L. N. Zakharov, A.L. Rheingold, D.N. Hendrickson, *J. Phys. Chem. Sol* 65 (2004) 831.
- [84] D. Ruiz-Molina, J. Veciana, K. Wurst, D. N. Hendrickson, C. Rovira, *Inorg. Chem.* 39 (2000) 617.
- [85] The solvent dependence of the VT for [Co(DBSQ)(DBCAT)(NN)] (NN = bipy and Phen) and [Co(Cat-N-SQ)(Cat-N-BQ)] complexes has already been revised. E. Evangelio, C. Rodriguez-Blanco, Y. Coppel, D. N. Hendrickson, J. P. Sutter, J. Campo, D. Ruiz-Molina, doi:10.1016/j.solidstatesciences.2007.11.039 .

[86] O. Cador, A. Dei, C. Sangregorio, *Chem. Commun.* (2004) 652.

Table 1: Representative examples of valence tautomeric complexes induced by different external stimuli applied and their interconversion characteristics.

Ext. Stimuli	Representative Compounds	Matrix	Charact. Techniques	T_c/P_c or Temperature Range	Reference		
TEMPERATURE INDUCED	 1,1s-Co(III)		Solid	Magnetism EPR X-Ray Diffraction	310 K	6	
			Liquid	Electronic Spectra ¹ H-NMR Magnetism EPR	273 K	17 71a	
LIGHT INDUCED	 2,1s-Co(III)		Solid	Irrad. at 532 nm (5 K and 30 min) Magnet. Charact.	310 $T_c \uparrow$ · 297 $T_c \downarrow$ Thermal Hysteresis 13 K	12	
PRESSURE INDUCED	 4,1s-Co(III)		Solid	Diamond Cell XANES EXAFS	4	240 K 0.37 GPa	15
					4-C ₆ H ₅ CH ₃	— K 1.1 GPa	
	 5,1s-Co(III)-Co(III)		Solid	Magnetic charac. Hydrostatic Pressure Cell.	150-340 K $T_c \uparrow$ as $P \uparrow$	16	

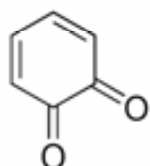
* T_c (critical temperature) and P_c (critical pressure), in VT are defined as the temperature and Pressure at which there are equal amounts of both electronic isomers at atm. pressure or room temperature. When we refer to range temperature is due that the T_c (which is the term more used in these cases is not calculated in the reference. For strictly obtain this value is required the thermodynamic parameters ΔH and ΔS .

Table 2: Redox-tuned valence tautomeric systems in solution at different temperatures for complexes **1**, **19** and **20**. (**1**) Ref. 71b. (**1⁺**) Ref. 83. (**19**) Ref 67d. (**19⁺**) Ref 84. (**20**) Ref. 67b. (**20⁺**) Ref. 70.

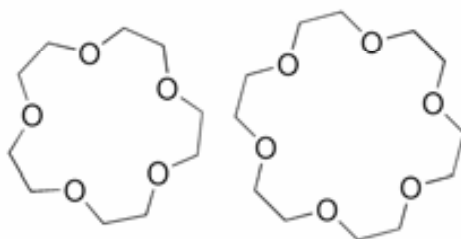
Compound	Neutral		Ionic	
	VT isomer	Working Temp.	VT isomer	Working Temp.
1	1 , <i>ls</i> -Co(III)	< 273 K	1⁺ , <i>ls</i> -Co(III)	< 200 K
	1 , <i>hs</i> -Co(II)	> 273 K	1⁺ , <i>hs</i> -Co(II)	> 305 K
19	19 , <i>ls</i> -Co(III)	< 300 K	19⁺ , <i>ls</i> -Co(III)	< 328 K
	19 , <i>hs</i> -Co(II)	> 300 K	19⁺ , <i>hs</i> -Co(II)	> 328 K
20	20 -Mn(IV)	< 5 K	20⁺ -Mn(IV)	< 5 K
	20 -Mn(III)	5 K<T>270 K	20⁺ -Mn(III)	5 K<T>130 K
	20 -Mn(II)	> 360 K	20⁺ -Mn(II)	> 360 K

Redox-Active-type ligands

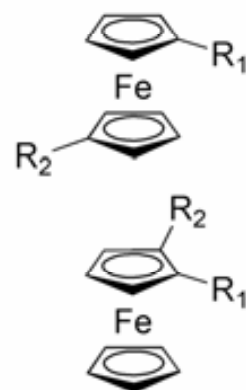
1) quinones



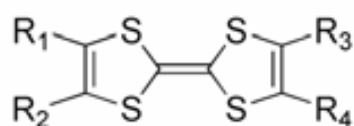
2) crown-ethers



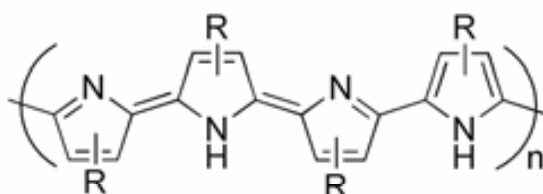
3) ferrocene



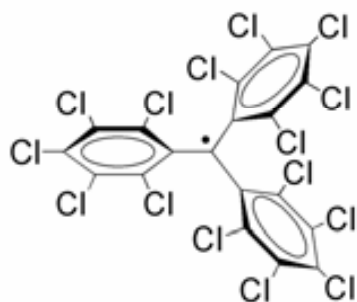
4) TTF



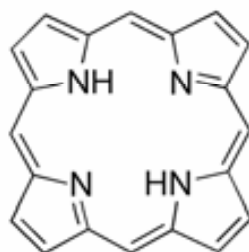
5) polymers



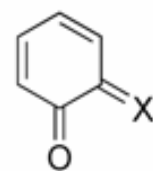
6) PTM



7) tetraphenylporphyrine



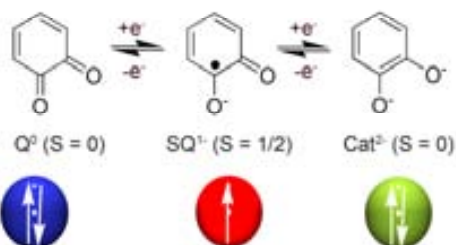
8) phenoxyate



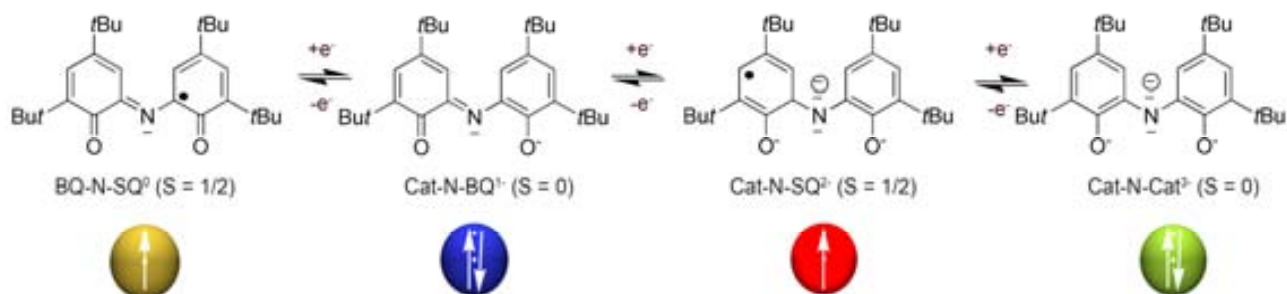
X = S, N, Se...

Scheme 1

a) oxidation levels quinone ligand



b) oxidation levels bis-phenolate ligand



Scheme 2

Figure Captions

Figure 1: Schematic representation of valence tautomerism involving a redox active ligand and a transition metal-ion together with the corresponding potential energy curve plotted in function of the nuclear coordinate.

Figure 2: Representation of the phenoxyl radical acting as an active site in enzymatic metalloproteins as galactose oxidase (GAO) and glyoxal oxidase (GLO). Pictures of the proteins were extracted from personal scientific web page of Prof. Mike McPherson: www.astbury.leeds.ac.uk/gallery/leedspix.html (GAO) and Int. Microbiol. 8 (2005) 195 (GLO) rights authorised by ©International Microbiology.

Figure 3: Coordination polymerization technique used to obtain valence tautomeric nano-scale metal-organic particles with general formula $[\text{Co}(3,5\text{-DBSQ})(\text{DBCat})(\text{N-N})]$ where N-N stands for the 1,4-bis(imidazol-1-ylmethyl)benzene ligand. Representation of the χT values as function of temperature for the amorphous nanosphere, showing the transition between both electronic isomers. Ref. 40.

Figure 4: a) Schematic representation of the valence tautomerism transition in the octahedral $\{\text{FeNO}\}_7$ nitrosyl complex **14** (from $S=1/2$ to $S = 3/2$). b) Mössbauer spectra at different temperatures and fields (Ref. 60).

Figure 5: Schematic representation of the different factors that have been shown to modulate valence tautomerism represented as casual ordered/disordered puzzles. Such representation is intended to emphasize the need for a good understanding of the effect of such parameters to fully understand and predict VT (i.e., the need for a proper connection of all the puzzles pieces).

Figure 6: Representative examples of the counterligand effect on the VT for complexes with the general formula $[\text{Co}(3,5\text{-DTBCat})(3,5\text{-DTBSQ})(\text{N-N})]$. A variation of such counterligand may induce the obtaining of a high interconversion temperature (Figure 6a, Ref. 74), a considerable shift (Figure 6b, Ref. 75) or even modifications of the fraction of both electronic isomers induced by a crystal phase transition (Figure 6c, Ref. 76).

Figure 7: Array of four states showing different optical and magnetic ground states controlled by two temperature-controlled valence tautomeric equilibria and two reversible redox processes for complex $[\text{Co}(3,5\text{-DTBSQ})(3,5\text{-DTBCat})(\text{bpy})]$ (**1**) (top) and complex $[\text{Co}(\text{Cat-N-SQ})(\text{Cat-N-BQ})]$ (**19**) (bottom).

Figure 8: Array of six states showing different optical and magnetic ground states controlled by two temperature and a reversible redox process for complex $[\text{Mn}(\text{Cat-N-SQ})(\text{Cat-N-BQ})]$ (**20**).

Figure 9: Influence of the crystalline phase on the VT interconversion found for complexes **4** (a) and **19** (b). The different VT parameters found for each of the cases are summarized in the table (c). Ref. 85.

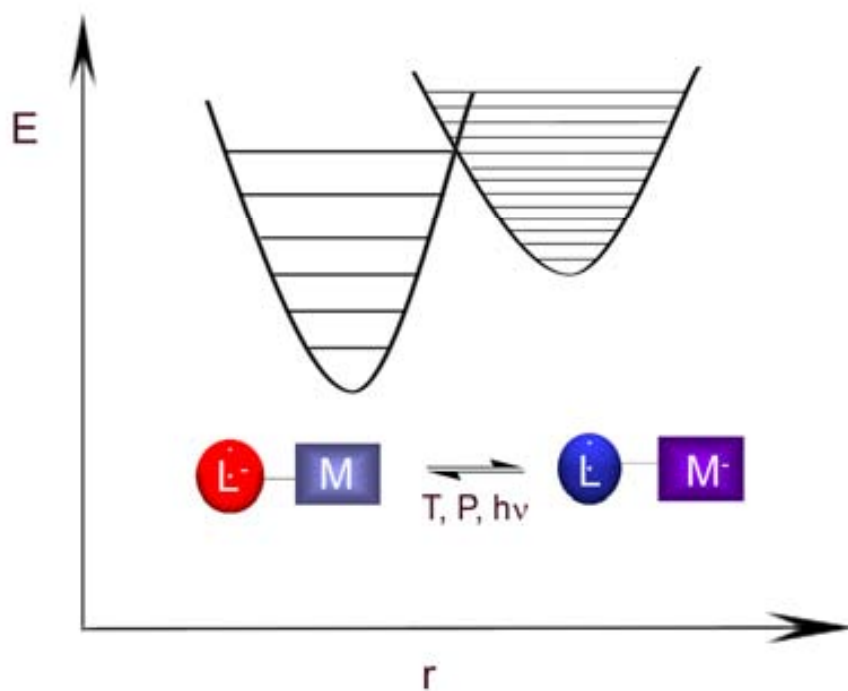


Figure 1

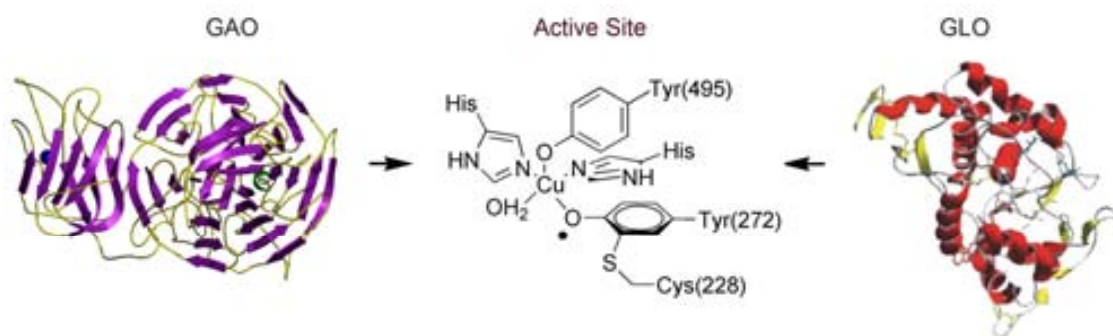


Figure 2

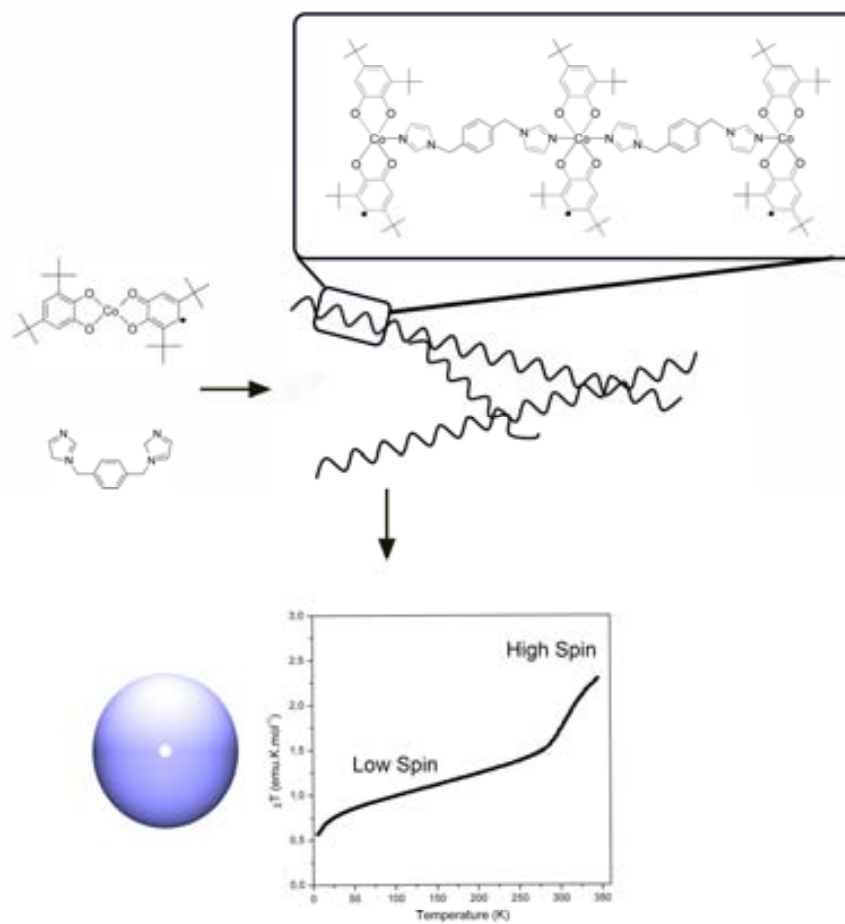


Figure 3

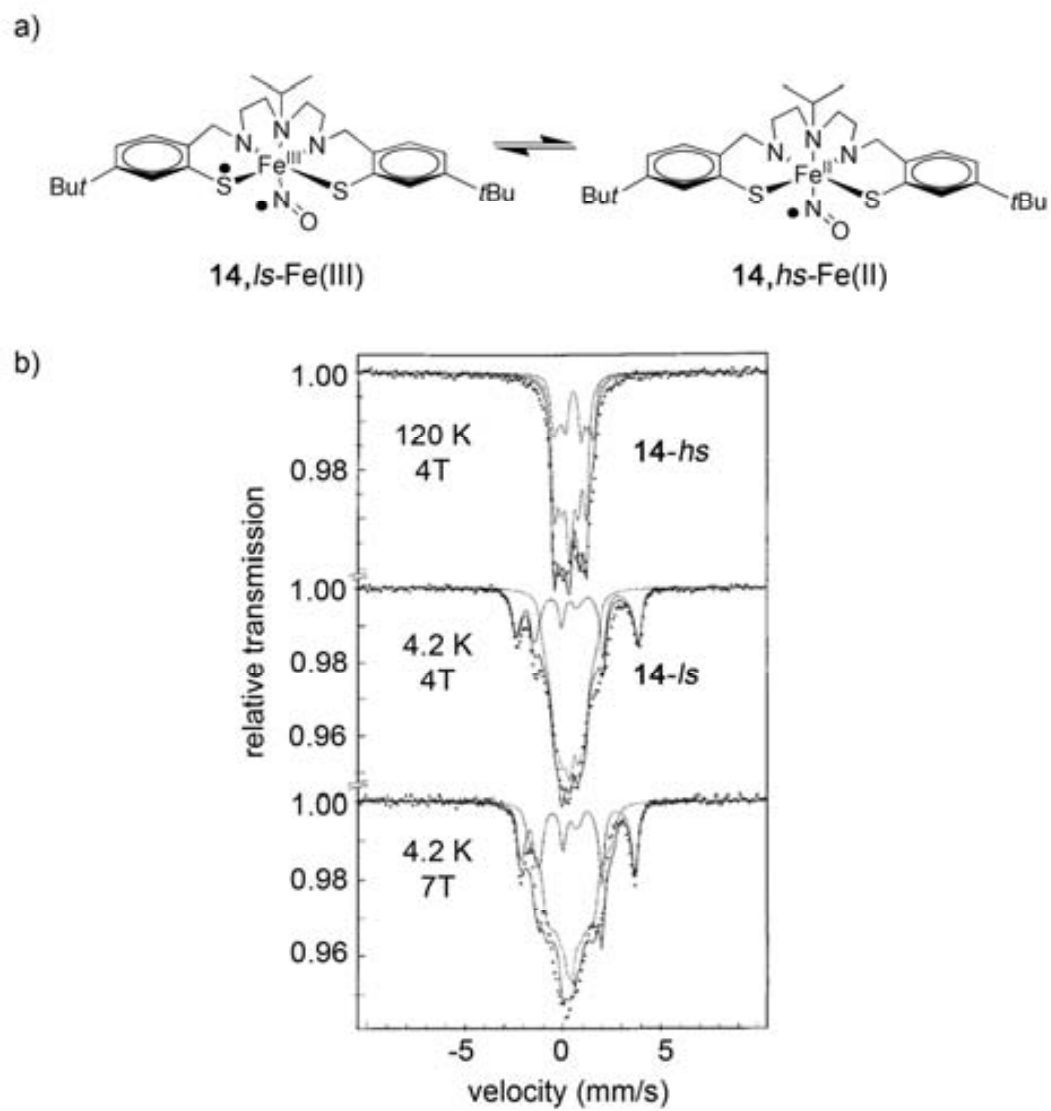


Figure 4

**Figure 5**

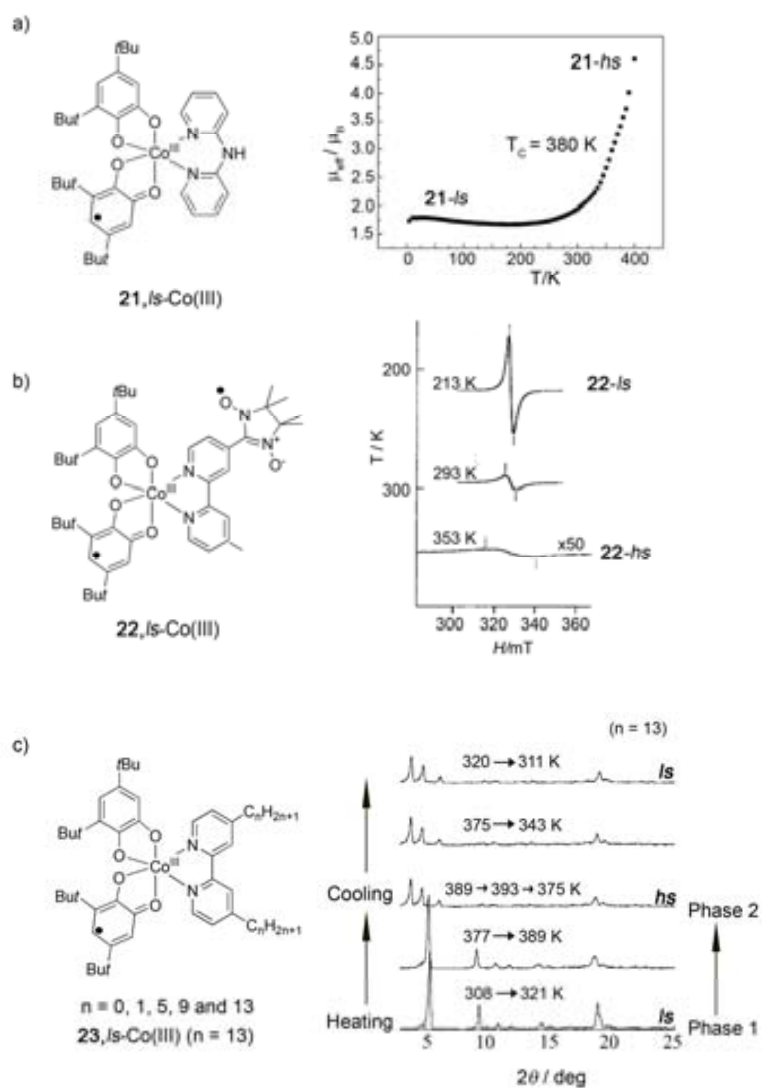


Figure 6

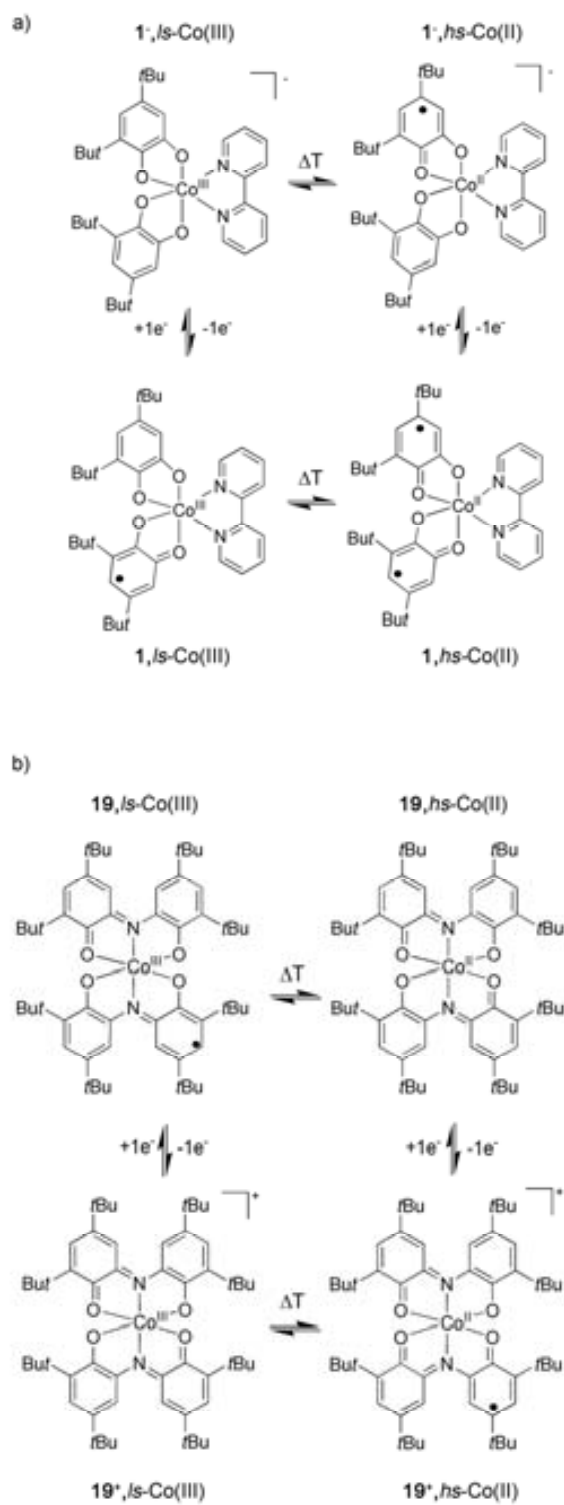


Figure 7

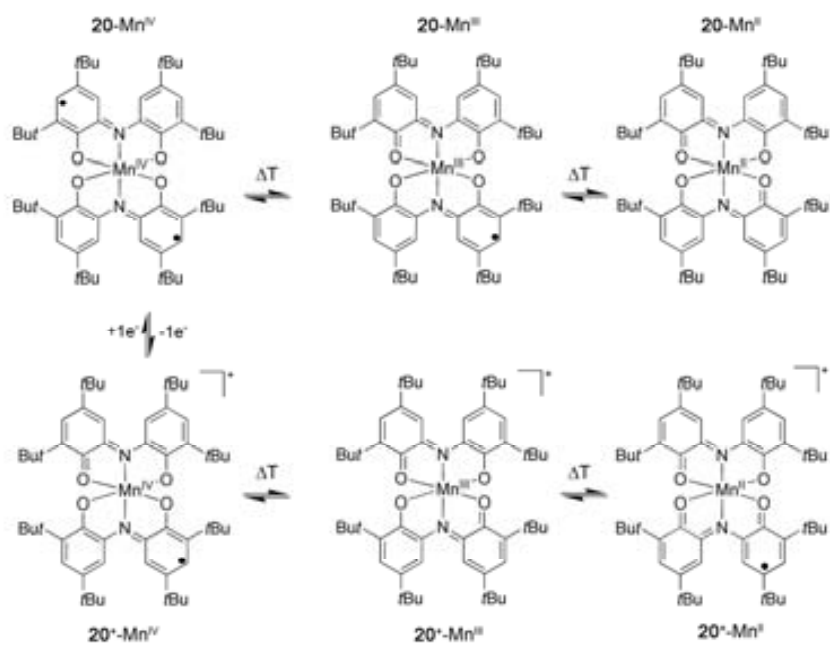
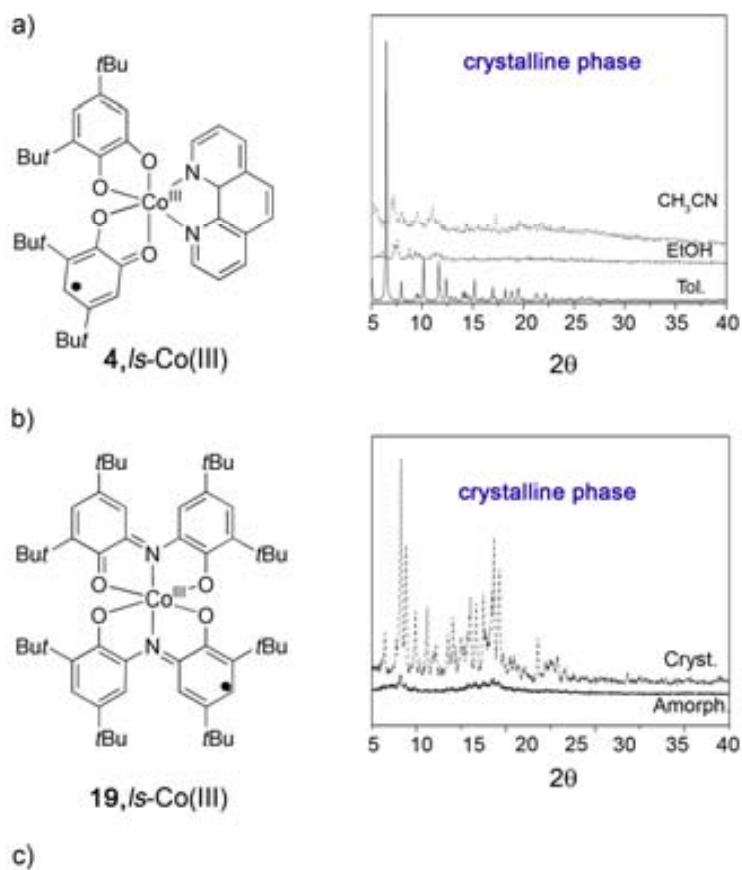


Figure 8



Magnetic measurements in solid matrix				
Crystalline Phase		Temperature Range		
Compound	Phase	<i>ls</i>	<i>ls</i> to <i>hs</i>	<i>hs</i>
4	4·C ₆ H ₅ CH ₃	< 225 K	230-360 K abrupt increase	> 300 K
	4·EtOH	< 300 K	-	-
	4·CH ₃ CN	< 225 K	250-300 K gradual increase	> 300 K
19	crystalline	< 360 K	360-500 K gradual increase	> 500 K decomp.
	amorph	< 360 K	360-500 K gradual increase	> 500 K decomp.

Figure 9

Graphical Abstract

